FATIGUE, BOND AND CRACKING CHARACTERISTICS OF REINFORCED CONCRETE TENSION MEMBERS

by

Ploutarchos John Yannopoulos

B.Sc.(Eng.), A.C.G.I., M.Sc.(Eng.), D.I.C.

a thesis submitted for the degree of
Doctor of Philosophy
in the Faculty of Engineering
of the University of London

Department of Civil Engineering
Imperial College of Science and Technology
London

January 1976

ABSTRACT

This thesis describes an investigation of the fatigue, bond and cracking characteristics of reinforced concrete tension members.

To improve the state of knowledge on the behaviour of reinforced concrete beams under fatigue loading, an experimental investigation of the fatigue life of hot rolled deformed bars, as affected by their embedment in concrete, their test length in air and identification marks within their length, was carried out. An extensive number of statistically planned fatigue tests were performed on a large proportion of the hot rolled deformed bar types marketed in the United Kingdom, which were either free in air or embedded axially in concrete tension members. The fatigue test results were analysed and compared statistically and curves of stress range against number of cycles to failure were determined by regression analyses, for different probabilities of survival.

Extensive numbers of tests were also carried out to determine the bond stress-slip relations for hot rolled dedeformed bars and mild steel plain bars, from specimens with a concrete embedment length of 38 mm. The effect of bar back load, bar pull relative to the settlement of concrete, concrete cover to bar and different intensity repeated loading on the bond stress-slip relationships was also statistically determined.

Load-crack width and load-end slip data determined

by testing concrete tension and long pull-out members respectively, reinforced with a hot rolled deformed bar, were compared with the results of a finite element computer program developed for the analysis of axi-symmetric reinforced concrete members. The non-linear bond stress-slip characteristics between steel and concrete determined from the short pull-out specimens were incorporated into the program by using special bond linkage elements. The non-linear reponse of the members under load and the formation and propagation of cracks in the concrete matrix were handled by specially adapted non-linear finite element techniques.

ACKNOWLEDGEMENTS

The author wishes to express his gratitude to the following persons and associations that helped in carrying out this research project :

Professor A.J. Harris, head of the Concrete Structures and Technology section of the Civil Engineering Department of Imperial College of Science and Technology, for his general supervision of the project.

Dr.A.D. Edwards, who supervised this work, for his valuable advice, guidance and help during the research period and during the preparation of the thesis.

The Road Research Laboratory of the Department of the Environment under whose sponsorship the research was carried.

The technical staff of the Concrete Structures and Technology Laboratories without whose experience and technical expertise the experimental part of the project would not have been possible. Special mention must be made in this context of Mr.J. Baulch for his skilled and continuous assistance during the laboratory work, Mr. R. Loveday for his technical advice and Messrs. C. Mortlock, J. Turner and H. Wilson for their general help.

CONTENTS

ABSTRACT 2

ACKNOWLEDGEMENTS 4

CONTENTS 5

LIST OF TABLES, FIGURES AND PLATES. 15

NOTATION 24

CHAPTER 1 : INTRODUCTION

1.1. Introduction 26

1.2. Object and scope of present investigation . . . 29

CHAPTER 2 : CRITICAL REVIEW OF PAST WORK

2.1. Critical review of past work on fatigue 30

2.1.1. Fatigue behaviour of steel. 30

2.1.2. Fatigue properties of hot-rolled deformed reinforcing steel bars 31

2.1.2.1. General 31

2.1.2.2. Factors affecting fatigue strength 33

2.1.3. Type of fatigue specimen 39

2.1.3.1. Fatigue behaviour of deformed bars as affected by their embedment in concrete 39

2.1.3.2. Gripping arrangement of bars tested free in air . . . 44

2.2. Critical review of past work on bond and cracking 46

2.2.1. General 46

2.2.2. Nature of bond and mechanism of bond failure 47

2.2.3. Measurement of anchorage and flexural bond strengths 49

2.2.4. Experimental determination of bond stress and slip between concrete and reinforcing bars 50

2.2.4.1. Average bond stress 50

2.2.4.2. Bond stress distribution . . 52

2.2.4.3. Slip between concrete and a reinforcing bar 54

2.2.4.4. Bond stress - slip relationships 56

2.2.5. Investigations related to cracking . . 62

2.2.5.1. General 62

2.2.5.2. Empirical studies on cracking 63

2.2.5.3. Classical analytical methods on cracking 65

2.2.5.4. Finite element studies on cracking 66

2.2.6. Investigations on the effect of repeated loading on bond 73

CHAPTER 3 : EXPERIMENTAL TECHNIQUES AND PROCEDURE

3.1. Materials and their properties 94

3.1.1. Concrete 94

3.1.2. Hot rolled deformed bars 96

3.1.3. Hot rolled mild steel plain bars . . . 97

3.2. Details of specimens 97

3.2.1. Specimens for fatigue tests 97

3.2.1.1. Specimens free in air 97

3.2.1.2. Specimens embedded in concrete 99

3.2.2. Specimens for bond tests 99

3.2.2.1. Specimens details 99

3.2.2.2. Casting and curing 101

3.3. Description of test rig 102

3.4. Static tests on hot rolled deformed bars and mild steel plain bars 103

3.5. Fatigue tests on hot rolled deformed bars free in air and on hot rolled deformed bars embedded in concrete 104

3.5.1. Loading equipment 104

3.5.2. Static and dynamic calibration of loading equipment 106

3.5.3. Testing procedure 109

3.6. Bond tests on hot rolled deformed bars and mild steel plain bars 111

3.6.1. Loading equipment 111

3.6.2. Instrumentation and testing procedure 111

CHAPTER 4 : TECHNIQUES OF STATISTICAL ANALYSIS OF FATIGUE DATA

4.1. Introduction 139

4.2. Fatigue life frequency distribution 139

4.2.1. Choice of life distribution shape and point estimates of parameters . . . 140

4.2.2. The normal distribution 141

4.2.3. Level of significance of a statistical hypothesis 144

4.2.4. X^2 - test for goodness of fit 144

4.3. Confidence intervals for the mean and the variance 147

4.4. Tests of significance for normal populations 148

4.4.1. Test for the equality of the variances of k populations 148

4.4.2. Test for the equality of the variances of two populations 150

4.4.3. Test for the equality of the means of k populations 150

4.4.4. Test for the equality of the means of two populations 152

4.4.4.1. Variances not significantly different . . . 152

4.4.4.2. Variances significantly different 153

4.5. Regression analysis 154

4.5.1. Hypothesis underlying regression analysis 154

4.5.2. Linear regression analysis 156

4.5.2.1. Estimates of parameters a, b, and σ^2 of linear regression analysis 157

4.5.2.2. Testing of linearity of regression curve and confidence limits 158

4.5.2.3. Blom's test 161

4.5.3. Comparison of two regression lines . . 161

4.5.3.1. Comparison of two regression lines of not significantly different variances 162

4.5.3.2. Comparison of two regression lines of significantly different variances 164

4.5.4. Linear regression for fatigue data . . 166

4.6. Probability curves 167

4.7. Computer programs 168

CHAPTER 5 : EXPERIMENTAL INVESTIGATION OF THE FATIGUE PROPERTIES OF HOT-ROLLED DEFORMED BARS AND STATISTICAL ANALYSIS OF THE RESULTS

5.1. Object and scope of tests 169

5.2. Definitions and notation 170

5.3. Static tests on hot rolled deformed bars . . . 171

5.4. Fatigue tests on hot rolled deformed bars . . . 172

5.4.1. General 172

5.4.2. Fatigue tests on bars free in air test series WEL-F-900-NI 174

5.4.3. Fatigue tests on bars embedded in concrete. Test series WEL-C-900-NI. . . 175

5.4.4. Fatigue tests on bars free in air. Test series WEL-F-400-WI, JON-F-400-WI, SHE-F-400-WI, UNI-F-400-WI and WEL-F-400-NI, JON-F-400-NI, SHE-F-400-NI 176

5.5. Description of static and fatigue failures of hot rolled deformed bars 177

5.6. Statistical analysis of fatigue test data . . . 180

5.6.1. χ^2 - test for goodness of fit 182

5.6.2. Regression analysis, Blom's test and comparison of regression lines . . 183

5.6.2.1. Regression analysis 183

5.6.2.2. Blom's test 184

5.6.2.3. Comparison of regression lines 185

5.7. Interpretation of results of statistical analysis and conclusions 187

CHAPTER 6 : EXPERIMENTAL INVESTIGATION OF THE BOND PROPERTIES OF HOT ROLLED DEFORMED BARS AND MILD STEEL PLAIN BARS

6.1. General 237

6.2. Bond-slip relation for hot-rolled deformed bars and mild steel plain bars 238

6.2.1. Test results 238

6.2.2. Statistical analysis of Welbond deformed bar bond-slip data and discussion of results 241

6.2.2.1. Bond-slip curves for Welbond deformed bar 241

6.2.2.2. χ^2 - test for goodness of fit 243

6.2.2.3. Effect of bar back load on maximum bond stress . . . 244

6.2.2.4. Effect of concrete cover on maximum bond stress . . . 245

6.2.2.5. Effect of direction of bar pull relative to that of casting 246

6.2.3. Comparison of plain bar bond-slip data and discussion of results 247

6.3. Effect of repeated loading on the bond-slip relations for hot-rolled deformed bars 248

6.3.1. Test results 248

6.3.2. Discussion of test results 250

6.4. Tensile bond tests on specimens with an 800 mm deformed bar length embedded in concrete. Tests results and discussion 252

6.5. Pull-out tests on concrete specimens reinforced with a deformed bar. Test results and discussion 255

CHAPTER 7 : FINITE ELEMENT ANALYSIS OF REINFORCED CONCRETE

7.1. Statement of the problem 312

7.2. General description of finite element method 313

7.3. Axi-symmetric finite element analysis of members 314

7.3.1. Basis of analysis and structural idealisation 314

7.3.2. Element characteristics 316

7.4. Isoparametric, rectangular, numerically integrated finite element properties 320

7.4.1. Co-ordinate definition 320

7.4.2. Isoparametric shape functions 321

7.4.3. Evaluation of element matrices in curvilinear co-ordinates 322

7.4.4. Satisfaction of convergence criteria 324

7.4.5. Numerical integration 325

7.5. Representation of bond and linkage element stiffness 326

7.6. Assembly of structural stiffness matrix 330

7.7. Introduction of boundary conditions 332

7.8. Solution of equilibrium equations 334

7.9. Material properties 338

7.9.1. Concrete stress-strain relations . . . 338

7.9.2. Strength criteria for concrete 339

7.9.3. Steel stress-strain relations 341

7.10. Non-linear solution methods 341

7.10.1. General 341

7.10.2. Basic non-linear iterative solution methods 342

7.10.2.1. General equations 342

7.10.2.2. "Variable stiffness" methods 344

7.10.2.3. "Initial strain" method . . . 345

7.10.2.4. "Initial stress" method . . . 345

7.10.2.5. Combination of variable and constant stiffness methods 347

7.10.3. Non-linear solution method adopted in this work 348

7.11. Cracking of concrete elements 348

7.11.1. Crack formation 348

7.11.2. Shear on open cracks 349

7.11.3. Axi-symmetric conditions 350

7.11.4. Constitutive relations 351

7.11.5. Release of tensile stresses in cracked elements 355

7.11.6. Cracking procedure 357

CHAPTER 8 : DESCRIPTION OF COMPUTER PROGRAM AND ANALYSIS OF REINFORCED CONCRETE TENSION MEMBER AND PULL-OUT SPECIMEN

8.1. General 372

8.2. Description of non-linear finite element program 372

8.2.1. Introduction to computer program . . . 372

8.2.2. Structure of program 374

8.2.2.1. Modules 374

8.2.2.2. Control of the modules . . . 377

8.2.2.3. Description of subroutines. . 378

8.3. Analysis of reinforced concrete tension member and pull-out specimen and comparison with experimental data 385

8.3.1. Basis of the analysis 385

8.3.2. Analysis of reinforced concrete tension member and comparison with experimental data 386

8.3.2.1. Description of model and finite element idealisation . 386

8.3.2.2. Analytical results and comparison with experimental data 388

8.3.3. Analysis of concrete pull-out specimen and comparison with experimental data 393

CHAPTER 9 : MAIN CONCLUSIONS OF PRESENT INVESTIGATION AND SUGGESTIONS FOR FUTURE RESEARCH

9.1. Main conclusions of the fatigue investigations 415

9.2. Main conclusions of the bond and cracking investigation 416

9.3. Suggestion for future research 418

REFERENCES. 420

APPENDIX A : Statistical tables 437

APPENDIX B : Fatigue data 445

APPENDIX C : Typical comparison of two regression lines 483

LIST OF TABLES, FIGURES AND PLATES

A. LIST OF TABLES

5.1	Results of static tests on hot-rolled deformed bars	194
5.2	Summary of the results of fatigue tests on 16 mm diameter hot-rolled deformed bars	195
5.3	χ^2- test for goodness of fit Test series: WEL-F-400-WI	196
5.4	χ^2- test for goodness of fit Test series: JON-F-400-WI	197
5.5	Summary of all χ^2 - tests for goodness of fit	198
5.6	Blom's test Test series: SHE-F-400-WI	199
5.7	Results of linear regression analysis	200
5.8	Results of comparisons of regression lines	201
6.1	Summary of the results of basic bond-slip tests for 16 mm diameter hot rolled Welbond deformed bar Group SL-PD	257
6.2	Summary of the results of basic bond-slip tests for 16 mm diameter hot rolled Welbond deformed bar Group SL-ND	258
6.3	Summary of the results of basic bond-slip tests for 16 mm diameter hot rolled Welbond deformed bar Group BG-PD	259
6.4	Summary of the results of basic bond-slip tests for 16 mm diameter hot rolled Welbond deformed bar Group BG-ND	260
6.5	Summary of χ^2- tests for goodness of fit of u_{max} values to normal distribution	261
6.6	Results of comparisons of six bond test series of each test group	261

6.7	Results of comparisons of pairs of bond test groups	262
6.8	Summary of the results of basic bond-slip tests for 16 mm diameter mild steel plain bar	263
7.1	The finite element analysis procedure	358

B. LIST OF FIGURES

2.1	S - N curves for reinforcing bars	78
2.2	Marking of deformed bars specified by BS 4449 : 1969	78
2.3	Rehm's specimen for testing embedded bars	79
2.4	The effect of concrete embedment on fatigue strength	80
2.5	Tensile principal stresses at steel - concrete interface	81
2.6	Internal crack and secondary crack with 19 mm bar, longitudinal splitting face and cross section	81
2.7	Wedging action in resisting pull-out	82
2.8	Tension pull-out specimens, schematic	82
2.9	Bond-slip curve for 28.5 mm dia. deformed bar	83
2.10	Bond-slip curves at different distances from end face for 25 mm dia. deformed bar	84
2.11	Rehm's bond test arrangement	85
2.12	The influence of casting positions on bond performance	85
2.13	Morita's and Kaku's bond specimen	86
2.14	Bond-slip curves for 25 mm dia. deformed bar	86
2.15	Edwards' and Picard's bond specimen	87
2.16	Experimental bond-slip curves for strand	88
2.17	Ratio of crack widths at steel surface to crack widths at concrete exterior surface versus steel stress	88

2.18	Assumed bond distribution by various investigators and resulting concrete and steel stresses	89
2.19	Linkage element representing bond	90
2.20	Representation of aggregate interlock	91
2.21	Representation of a crack with finite element geometry	92
2.22	Loov's proposed analytical method of following crack propagation	93
3.1	Stress-strain curves for concrete	116
3.2	Basic specimens for bond tests	117
3.3	Tensile specimen for fatigue and bond tests	118
3.4	Pull out specimen for bond tests	118
3.5	Fluctuation stress test	119
3.6	Basic bond tests load system	120
3.7	Calibrated bars connected to rigid frame for measurement of bond forces	121
3.8	Displacement transducer assembly used in measuring end slip	122
5.1	Stress-strain diagrams for hot-rolled deformed Welbond bar	202
5.2	Blom's test. Test series: SHE-F-400-WI. Cumulative frequency distribution of residuals	203
5.3	Mean fatigue life and 95 % confidence limits Test series WEL-F-900-NI	204
5.4	Probability curves for fatigue failure Test series WEL-F-900-NI	205
5.5	Mean fatigue life and 95 % confidence limits Test series WEL-C-900-NI	206
5.6	Probability curves for fatigue failure Test series WEL-C-900-NI	207
5.7	Mean fatigue life and 95 % confidence limits Test series WEL-F-400-WI	208
5.8	Probability curves for fatigue failure Test series WEL-F-400-WI	209

5.9	Mean fatigue life and 95 % confidence limits Test series WEL-F-400-NI	210
5.10	Probability curves for fatigue failure Test series WEL-F-400-NI	211
5.11	Mean fatigue life and 95 % confidence limits Test series JON-F-400-WI	212
5.12	Probability curves for fatigue failure Test series JON-F-400-WI	213
5.13	Mean fatigue life and 95 % confidence limits Test series JON-F-400-NI	214
5.14	Probability curves for fatigue failure Test series JON-F-400-NI	215
5.15	Mean fatigue life and 95 % confidence limits Test series SHE-F-400-WI	216
5.16	Probability curves for fatigue failure Test series SHE-F-400-WI	217
5.17	Mean fatigue life and 95 % confidence limits Test series SHE-F-400-NI	218
5.18	Probability curves for fatigue failure Test series SHE-F-400-NI	219
5.19	Mean fatigue life and 95 % confidence limits Test series UNI-F-400-WI	220
5.20	Probability curves for fatigue failure Test series UNI-F-400-WI	221
5.21	Comparison of mean fatigue life Different manufacturers' deformed bars with identification marks	222
5.22	Comparison of mean fatigue life Different manufacturers' deformed bars with no identification marks	223
5.23	Comparison of mean fatigue life Welbond deformed bars with and with no identification marks	224
5.24	Comparison of mean fatigue life Jones deformed bars with and with no identification marks	225
5.25	Comparison of mean fatigue life Sheerness deformed bars with and with no identification marks	226

5.26 Comparison of mean fatigue life Welbond deformed bars of different test length 227

5.27 Welbond deformed bars tested free in air and embedded in concrete 228

Experimental bond-slip curves for 16 mm dia. hot rolled high yield (410) deformed bar :

6.1 Test series SL-L0-PD 264

6.2 Test series SL-L1-PD 265

6.3 Test series SL-L2-PD 266

6.4 Test series SL-L3-PD 267

6.5 Test series SL-L4-PD 268

6.6 Test series SL-L5-PD 269

6.7 Test series SL-L0-ND 270

6.8 Test series SL-L1-ND 271

6.9 Test series SL-L2-ND 272

6.10 Test series SL-L3-ND 273

6.11 Test series SL-L4-ND 274

6.12 Test series SL-L5-ND 275

6.13 Test series BG-L0-PD 276

6.14 Test series BG-L1-PD 277

6.15 Test series BG-L2-PD 278

6.16 Test series BG-L3-PD 279

6.17 Test series BG-L4-PD 280

6.18 Test series BG-L5-PD 281

6.19 Test series BG-L0-ND 282

6.20 Test series BG-L1-ND 283

6.21 Test series BG-L2-ND 284

6.22 Test series BG-L3-ND 285

6.23 Test series BG-L4-ND 286

6.24 Test series BG-L5-ND 287

Experimental bond-slip curves for 16 mm dia. mild steel (250) plain bar :

6.25 Test series SL-L0-ND 288

6.26 Test series SL-L1-ND 289

6.27 Test series BG-L0-ND 290

6.28 Test series BG-L1-ND 291

Experimental bond-slip curves for 16 mm dia. hot rolled high yield (410) deformed bar under :

6.29 repeated loading (0 - 2.0 N/sq.mm) Concrete cover = 25 mm 292

6.30 repeated loading (0 - 2.0 N/sq.mm) Concrete cover = 35 mm 293

6.31 repeated loading (0 - 3.9 N/sq.mm) Concrete cover = 25 mm 294

6.32 repeated loading (0 - 3.9 N/sq.mm) Concrete cover = 35 mm 295

6.33 repeated loading (0 - 5.6 N/sq.mm) Concrete cover = 25 mm 296

6.34 repeated loading (0 - 5.6 N/sq.mm) Concrete cover = 35 mm 297

6.35 Magnified experimental bond-slip curve for 16 mm dia. hot-rolled high yield (410) deformed bar under repeated loading (0 - 3.9 N/sq.mm) Concrete cover = 35 mm 298

6.36 Steel stress - average concrete surface strain 299

6.37 Relation between steel stress and average crack spacing for reinforced concrete tension specimens 300

6.38 Mean relation between steel stress and average crack spacing from reiforced concrete tension specimens 301

6.39 Steel stress - crack width. Specimen 1 302

6.40 Steel stress - crack width. Specimen 2 303

6.41 Steel stress - crack width. Specimen 3 304

6.42 Steel stress - crack width. Specimen 4 305

6.43	Steel stress - crack width. Specimen 5	306
6.44	Steel stress - crack width. All specimens	307
6.45	Load versus end slip curves of 100 mm long pull-out specimens	308
6.46	Load versus end slip curves of 200 mm long pull-out specimens	309
6.47	Load versus end slip curves of 100 and 200 mm long pull-out specimens	310
7.1	Element of an axi-symmetric solid	359
7.2	Strains and stresses involved in the analysis of axi-symmetric solids	359
7.3	Curvilinear co-ordinates for a rectangular element	360
7.4	Bond representation	361
7.5	Finite element idealisation of a reinforced concrete member	362
7.6	Bond linkage element	363
7.7	Schematic representation of storage matrix for banded solution	364
7.8	Schematic storage arrangement in Choleski method	364
7.9	Idealised stress-strain relations	365
7.10	Variable stiffness methods for non-linear constitutive laws	366
7.11	Constant stiffness solution methods for non-linear constitutive laws	367
7.12	Non-linear solution methods	368
7.13	Assumed concrete tensile elastic-fracture model	369
7.14	Cracking model	369
7.15	Types of cracks	370
7.16	Global and local axes	371
8.1	Program modules and subroutines	397
8.2	Flowchart for CONCMEB	398

8.3	Determination of external crack width	399
8.4	Axi-symmetric finite element idealisation of a reinforced concrete tension member	400
8.5	Bond-slip curves used in the finite element analysis of reinforced concrete tension members	401
8.6	Formation and propagation of internal cracks in reinforced concrete tension specimens	
	(a) Free bar stress = 99 N/mm^2	402
	(b) Free bar stress = 149 N/mm^2	403
	(c) Free bar stress = 249 N/mm^2	404
	(d) Free bar stress = 348 N/mm^2	405
8.7	Variation of steel stress with distance along bar embedded in concrete tension member	406
8.8	Variation of bond stress with distance along bar embedded in concrete tension member	407
8.9	Free bar steel stress - average embedded steel strain	408
8.10	Displacement of end face of reinforced concrete tension member	409
8.11	Steel stress - crack width	410
8.12	Axi-symmetric finite element idealisation of a reinforced concrete pull-out member	411
8.13	Bond-slip curves used in the finite element analysis of reinforced concrete pull-out members	412
8.14	Theoretical and experimental load versus loaded end slip curves for 100 mm long pull-out specimens	413
8.15	Theoretical and experimental load versus free end slip curves for 100 mm long pull-out specimens	414

C. LIST OF PLATES

3.1	Hot rolled deformed bars - 16 mm diameter	123
3.2	Specimen free in air held in between test rig's gripping devices	124
3.3	Grip preparation	125

3.4	Test rig's gripping device	126
3.5	Specimen embedded in concrete held in between test rig's gripping devices	127
3.6	General view of the rig for fatigue tests	128
3.7	Mould and basic specimen for bond tests	129
3.8	Mould and tensile specimen for fatigue and bond tests	130
3.9	Static calibration of test rig and loading equipment	131
3.10	Dynamic calibration of test rig and loading equipment	132
3.11	Dynamic strain outputs on oscilloscope	133
3.12	Instrumentation for basic bond tests	134
3.13	Measurement of bond and slip	135
3.14	Prestressing jack and accumulator system	136
3.15	Tensile bond specimen	137
3.16	Pull-out specimen in test rig	138
5.1	Profiles of static bar fractures	229
5.2	Static bar fractures	230
5.3	Profiles of fatigue bar fractures	231
5.4	Fatigue fractures of Welbond bar	232
5.5	Fatigue fractures of Jones bar	233
5.6	Fatigue fractures of Sheerness bar	234
5.7	Fatigue fractures of Unisteel bar	235
5.8	Fatigue fracture of specimen embedded in concrete	236
6.1	Failure patterns of basic specimens for bond tests	311

NOTATION

The following list contains symbols used in the theory of statistics and fatigue. Any other symbols used than those below are defined where they appear in the text :

A.1. LIST OF SYMBOLS RELATED TO STATISTICS

A.1.1. General

C_v	:	Coefficient of variation
n_i	:	Number of observations in the ith sample
P,p	:	Probability of survival of N load cycles
s^2	:	Sample variance
s^2_{am}	:	Variance among samples
s^2_w	:	Average variance within samples
x_{ij}	:	j^{th} value of x of ith sample
$\bar{x}$	:	Sample mean
α	:	Level of significance
γ	:	Confidence level
μ	:	Population mean
σ^2	:	Population variance

A.1.2. Regression Analysis

a	:	Parameter (constant) of the linear regression equation
b	:	Slope of regression line
s^2_a	:	Variance of parameter a of linear regression equation

s_b^2 : Variance of parameter b of linear regression equation

s_i^2 : Variance of the ith sample

s_m^2 : Variance of sample means about the regression line

s_r^2 : Variance about the regression line

s_{rr}^2 : Average variance of two regression lines

$s_{y_r}^2$: Variance of y_r

x : Independent variable in regression analysis

x_i : Value of the ith sample of the independent variable

y : Dependent variable in regression analysis

$\bar{y}_i$: Mean of the ith sample of the dependent variable

y_{ij} : j^{th} value of the ith sample of the dependent variable

y_{r_i} : Value of the dependent variable calculated from the linear regression equation and corresponding to x_i

μ_y : Population mean value of the dependent variable

CHAPTER 1

INTRODUCTION

1.1. INTRODUCTION

The need to ensure that concrete structures have adequate strength to resist failure due to the effects of fluctuations in loading is becoming more important. The stress level in the steel is gradually being increased, the factors of safety eroded by more precise calculations, and, in concrete bridges, the number of stress cycles increased due to heavier traffic flows. In general, the possible fatigue failure of structures subject to fluctuating loads should be considered carefully because of the brittle nature of the failure.

The fatigue strength of reinforced concrete structures depends upon the individual properties of the constituent materials, on the way they are put together and on their particular conditions of use. If the effect of the last two factors and the actual distribution of stresses could be known accurately, it would be possible to calculate the behaviour of a structure from the behaviour of the constituent materials. But the parameters involved have not been studied sufficiently because they are numerous, they may interact with each other and a large number of tests are needed to obtain a reliable estimate of each parameter due to the inherent scatter of fatigue data.

Attempts have been made to correlate the fatigue life

of a reinforced concrete beam to the fatigue properties of the reinforcement when tested free in air, but there has been a contradiction in the technical literature as to whether a bar has a higher fatigue strength in air or embedded in concrete. This difference in behaviour has been attributed mainly to cracks and the length of bond breakdown between steel and concrete; nevertheless no researcher has investigated the effect of test length on the fatigue properties of deformed bars tested free in air.

One of the most important prerequisites of reinforced concrete construction is the bond between the reinforcement and the concrete, which is necessary for the continuous co-operation of the two materials. In deriving equations for the design of reinforced concrete structures it is assumed that this cooperation is adequately ensured, without relative displacement between the steel and the concrete. This represents an ideal case which cannot be attained with the usual kinds of reinforcement. The implications with regards to width and spacing of tensile cracks in the concrete do not correlate with observed behaviour, and so empirical crack width equations are used, which are based on tests of members of conventional size and shape. But the disadvantage of empirical studies is that their findings cannot be extrapolated safely to member shapes and sizes other than those from which they were derived and large expenditures are required in testing complex concrete members and structures.

The advent of digital computers and modern methods of numerical analysis, such as the finite element method,

provide the necessary tools to develop analytical solutions which can replace much of the empirical testing carried out in the past, both for the purpose of formulating design rules, and in treating special design problem which fall outside the normal range of member size and proportion. However, such analytical solutions must still be checked by a selected, but smaller number of experimental tests to varify their accuracy.

Although notable progress has been made in applying the finite element method to reinforced concrete, efforts have been handicapped by lack of reliable knowledge of the bond stress-slip relation governing behaviour at the concrete-steel interface. This relation is analogous to the stress-strain law for the steel or concrete. It has a direct influence on the width and spacing of tensile cracks, and on the distribution of concrete stress in partially cracked beams. Unfortunately there have not been a sufficient number of reliable bond stress-slip relations obtained so far. Difficulties have been experienced in measuring accurately bond slip, both because of its small magnitude and because the measuring devices interfere with the bond distribution. A relatively small number of bond stress-slip curves have been obtained either indirectly from long lengths of steel embedded in concrete prisms, or from small length pull out specimens. No statistically dependable curves have been developed to take account of the large scatter observed in the data, neither has the effect of steel stress, concrete cover to steel or repeated loading been investigated thoroughly.

1.2. OBJECT AND SCOPE OF PRESENT INVESTIGATION

In fatigue, the main object is to carry out experimental investigations to provide quantitative information on the fatigue life of hot rolled deformed bars, as affected by their embedment in concrete tension members and their test length in air, and to employ statistical techniques for the treatment and comparisons of the test results.

In bond, the first object is to determine statistically dependable bond stress-slip relations for hot rolled deformed bars and mild steel bars and to determine how these relations are affected by the bar back load, bar pull relative to the settlement of concrete, concrete cover to bar and intensity of repeated loading. The second object is to develop a non-linear finite element program, incorporating the determined non-linear bond stress-slip relations, to predict the load-crack width and load-end slip response of concrete tension and pull-out members respectively and carry out tests on such members to verify their predicted response.

CHAPTER 2

CRITICAL REVIEW OF PAST WORK

2.1. CRITICAL REVIEW OF PAST WORK ON FATIGUE

2.1.1. FATIGUE BEHAVIOUR OF STEEL

Fatigue may be defined as the progressive fracture of a material under conditions of fluctuating / alternating stresses having a maximum value less - and usually well below - than the static strength. The fatigue behaviour of steel, relevant to the present work, may be summarised (1, 2, 3, 4) as follows :

a) The sequences by which fatigue failure occurs are three : crack initiation, crack propagation and final failure.

b) A fracture surface due to fatigue shows two distinct zones : a fatigue zone where the crack propagates and a rupture zone where final failure occurs after the fatigue crack has weakened the section.

c) The fatigue zone is crescent shaped, generally having a smooth, dull and rubbed appearance and focuses on the point where the fatigue crack initiates. The rupture zone generally has a rough, crystalline appearance.

d) Fatigue fracture, whether the material is ductile or brittle, follows that of a brittle fracture, characterised by lack of necking-down.

e) Fatigue failures are in most cases due to stress raisers, which can be in the form of an inclusion or notch.

Fatigue failures originating from an inclusion are extremely rare; most fatigue failures initiate from surface notch effects like weak points, flaws and surface defects.

f) Fretting corrosion resulting from periodic relative movement between two surfaces in close contact, acts as an initiating source of fatigue cracks and may reduce the fatigue strength by 25 to 50 % depending on the loading conditions. Fretting corrosion increases with the magnitude of the relative movement, number of load cycles, contact pressure and an increase of oxygen in the environment. Motions with amplitudes as low as 125×10^{-9} mm have been reported (1) to have produced fretting damage.

g) Fatigue properties vary with the size of a material. Large structural members can have very much reduced fatigue strength compared to small notched specimens which are machined from the same material.

h) The fatigue lives of specimens tested at the same stress levels show a large scatter because the flaws are randomly distributed and are of random severity.

2.1.2. FATIGUE PROPERTIES OF HOT ROLLED DEFORMED REINFORCING STEEL BARS

2.1.2.1. GENERAL

Quite a number of laboratory investigations of the fatigue strength of reinforcing bars have been reported in recent years from Europe (5-11), the United States (12-17), Canada (19-22) and Japan (23-26). In most of these investigations, the relationship between applied stress range, σ_r, and

fatigue life, N, was determined from a series of repeated load tests on bars which were either tested in air or embedded in concrete. There is a large variation between the σ_r - N, or more commonly denoted by S - N, curves reported from these investigations.

There have been no comprehensive series of fatigue tests on British-made reinforcement either in air or embedded in concrete. Bannister (9) has tested under fluctuating loads only 25 beams reinforced with one type of British-made deformed high-tensile steel bar or with mild steel bars. Also some increasing amplitude tests have been carried out by Snowdon (10) on concrete beams reinforced with different types of bar, but only one test was carried per bar.

A number of S - N curves obtained from tests on concrete beams containing straight deformed bars made in North America are shown in Figure 2.1 (taken from (18)). These curves include the highest and the lowest reported fatigue strengths and are for bars varying in size from 16 mm to 35 mm diameter, with minimum stress levels ranging from -10 % to 43 % of the static yield strength of the bars. The varying characteristics of these curves suggest that there are many variables affecting the fatigue strength of deformed reinforcing bars apart from the stress range.

Most published S - N curves exhibit a transition from a steeper - finite life - to a flatter - long life - slope in the vicinity of one million cycles, indicating that deformed bars exhibit a practical fatigue limit. Because of the lack of sufficient data in the long life region, it is

noted that many of the S - N curves in this region are conjectural.

All S - N curves are mean curves of data which exhibit a large scatter. This indicates that fatigue phenomena should be treated in probabilistic terms, using appropriate statistical techniques.

A literature review of the factors influencing the fatigue strength of concrete structures has been recently published by ACI Committee 215 (18). A review of the main factors affecting the fatigue behaviour of hot rolled deformed reinforcing steel bars, which are relevant to the present work, is reported in section 2.1.2.2 and the type of fatigue specimens used is reported in section 2.1.3. The fatigue of concrete is outside the scope of this report. This is justified by the fact that the commonest form of fatigue failure in both reinforced and prestressed concrete members is by fracture of the steel reinforcement. Compressive failure of the concrete is restricted to over-reinforced beams or high levels of repeated loads.

2.1.2.2. FACTORS AFFECTING FATIGUE STRENGTH

a) Minimum Stress Level

Several investigators (5, 12) have suggested that the fatigue strength of hot rolled deformed bars is relatively insensitive to the minimum stress level. However, in two recent investigations (16, 20), it was found that fatigue strength decreases with increasing minimum stress level in proportion

to the ratio of the change in the minimum stress level to the tensile strength of the reinforcing bars.

b) Bar Diameter

In metal fatigue literature, it is generally concluded that the fatigue of small specimens with significant stress gradients due to notching or flexural loading is affected by size (2). The size effect tends to disappear, however, in specimens comparable in size to most reinforcing bars, which are predominantly in axial tension or compression and where the stress gradients tend to be small.

In three investigations (7, 20, 23) on hot rolled deformed bars a small decrease was observed in the fatigue strength with an increase in bar diameter. This decrease was of the order of 5 to 10 % between 16 mm and 25 mm diameter bars. However, in another investigation (16) although the overall trend was similar to the previous investigations there was a corresponding decrease of 15 to 20 %.

c) Yield Stress and Tensile Strength

Research on machine parts has indicated the dependance of fatigue strength on yield stress and tensile strength (3). However, findings from three projects in the United States and Canada (12, 16, 20), two projects in Europe (7, 11) and one in Japan (26) suggest that the fatigue strength of deformed reinforcing bars is relatively insensitive to the steel yield stress or tensile strength. Contrary to these findings tests by Lash (19), on only 19 beams containing 16 mm diameter bars, indicated that fatigue strength may be predicted for a grade of steel as a function of the yield stress. Jhamb and MacGregor

(22) showed by a multiple regression analysis that there is an interaction between the effects of stress concentrations and the grade of steel. Thus although the fatigue strength of the bar metal improves with an increase in grade, this is offset by a greater susceptibility to stress concentrations.

d) Bending

Rehm (5) and Pfister and Hognestad (12) have reported tests on bent hot rolled deformed bars in concrete beams. In both projects a severe reduction in fatigue strength was observed due to bends. The fatigue strength of deformed bars bent through an angle of 45° around a mandrel having diameters ranging from 6 to 8 times the nominal bar diameter were found to be about 50 % of that of straight bars. The reduction due to a bend probably decreases as the diameter of the bend increases. This has been confirmed by Wascheidt (7) who found that the reduction was about 18 % for 26 mm bars when the diameter of the bend was 15 times the bar diameter and was about 55 % when the diameter of the bend was only 5 times the bar diameter.

e) Geometry of Deformations

There is a wide variety of deformations used in different reinforcing bars but most consist of transverse lugs between longitudinal ribs that are hot rolled on to the bar. These deformations provide the means of obtaining good bond between the reinforcing steel bars and the concrete. However, these same deformations produce stress concentration at their bases, and it is well known that any stress concentration is a point of fatigue weakness. Particularly high stress concentrations exist :

(i) along the base of the transverse lugs,

(ii) along the base of the longitudinal ribs,
(iii) at the base of a transverse lug at the point of intersection with a longitudinal rib, and
(iv) at the base of a transverse lug at the point of intersection with another transverse lug.
These places of high stress concentration are where fatigue fractures have been observed to initiate.

The base of a transverse lug at the point of intersection with a longitudinal rib was considered so critical that some manufacturers produced bars in which the transverse lugs are discontinued before reaching the longitudinal ribs, and in some cases no longitudinal ribs are rolled on to the bar. Tests in Europe (5, 6, 7) have shown that fatigue strengths are actually improved by terminating the transverse lugs before reaching the longitudinal ribs. However, tests in the United States on hot rolled deformed bars in concrete beams did not support this conclusion (15). Bars with terminated transverse lugs did not necessarily perform better in fatigue than bars with lugs merging into the longitudinal ribs.

The effect of the geometry of deformations on bar fatigue behaviour has been studied analytically by Jhamb and MacGregor (22). The most significant variable affecting the magnitude of stress concentration was found to be the lug base radius. Tests on bars having a base radius varying from 0.1 to 10 times the height of the deformation (15, 16, 20, 21, 23) have indicated that when the base radius is increased from 0.1 to about 1 or 2 times the height of the deformation, the fatigue strength is increased appreciably. An increase in base radius

beyond 1 or 2 times the height of the deformation does not show much effect on fatigue strength.

It has also been demonstrated that the fatigue strength of a reinforcing bar is influenced by the orientation of the longitudinal ribs. In one investigation by Burton (13) on beams reinforced with deformed bars having transverse lugs merging into the longitudinal ribs, a decrease of 5 to 7 % in fatigue strength was obtained when the longitudinal ribs were in a vertical plane as opposed to when the ribs were in the horizontal plane. However, in another investigation by Hanson, Burton and Hognestad (15) on bars having transverse lugs not merging into the longitudinal ribs, the orientation of the ribs in a reinforced concrete beam produced a very small increase in fatigue strength. The above phenomenon is apparently associated with the location at which the fatigue crack initiates, i.e. if there is a particular location on the surface of a bar which is more critical for fatigue than other locations, then the positioning of that location in the beam will influence the fatigue strength due to the stress gradient across the depth of the bar.

f) Identification Marks

Identification marks are often rolled by manufacturers on to the surface of reinforcing steel bars for the purpose of identifying the bar size, type of steel, mill that rolled the steel and yield strength. The most commonly used identification marks are in the form of dots, short lines or even letters.

Wascheidt (7) carried out fatigue tests on smooth bars and obtained a 17 % reduction in fatigue strength with

smooth bars having two dots and a line rolled on to their surface. Fractures occured at the base of one of the identification marks. He also found from other tests a decrease of approximately the same amount in deformed bars as compared to smooth bars. Thus it seems that deformed bars with identification marks rolled on to their surface do not behave worse than those with no identification marks.

In fatigue tests by Hanson, Burton and Hognestad (15) on 26 concrete beams reinforced with a deformed bar containing identification marks, no fatigue fractures occurred at one of these marks. All fractures originated at the base of one of the transverse lugs.

In another fatigue investigation by Hanson, Somes and Helgason (16) on 236 concrete beams with a deformed bar embedded in them only 5 fatigue fractures occurred at the base of one of the identification marks, although these were present in all bars. 228 fractures occurred at the base of one of the transverse lugs and 3 beams failed due to fatigue of the concrete in compression.

Jhamb and MacGregor (20, 21) carried out fatigue tests in air on 88 deformed bars, 25 mm in diameter and all failures originated at the base of one of the transverse lugs. No specimen failed at the identification marks despite the fact that such marks were present on 21 % of the specimens. They also tested 72 concrete beams reinforced with the same manufacturer's deformed bars. Again no failure occurred at the identification marks.

Clause 23 of BS 4449 : 1969 (79) on hot rolled bars

for the reinforcement of concrete, specifies that for the purpose of identifying the grade of steel of any bar rolled from any other than mild steel, manufacturers must roll on to the surface of such bars at regular intervals a legible mark in one or other of the styles in Figure 2.2. Any other marks rolled on to the steel must, by their position or character, be such that they cannot be mistaken for an identification mark. If necessary, transverse ribs intersecting these marks may be omitted.

2.1.3. TYPE OF FATIGUE SPECIMEN

2.1.3.1. FATIGUE BEHAVIOUR OF DEFORMED BARS AS AFFECTED BY THEIR EMBEDMENT IN CONCRETE

The selection of a proper fatigue specimen to simulate the fatigue behaviour of reinforcing steel bars in concrete structures is important. Most of the previous investigators tested bars embedded in concrete beams, since this type of fatigue specimen has been considered necessary to represent the most critical of field conditions.

The pioneer fatigue tests on deformed reinforcing bars by Rehm (5) at the Technical University of Munich were performed on special concrete beams having a bent reinforcing bar as tension reinforcement (Figure 2.3). Cracks in the concrete were preformed by metal sheets located either in the zone where the bars were straight or at the bend. Fractures in steel appeared mostly at the preformed cracks. The special beams were designed to ensure a constant stress along the whole length of the bar. This was achieved in spite of the individual

load acting in the centre of the beam by a variable effective depth, decreasing from the midspan of the beam towards the ends approximately as the bending moment decreased. The application of Rehm's special beams for testing reinforcing bars was later discontinued, because of the unfavourable effects of the radius of the bend, of shearing forces and of inclined force components acting on the bar.

Most other investigators have used one or more straight reinforcing bars as tensile reinforcement in concrete beam specimens of rectangular or tee cross-section. Some investigators (16, 26) used beam specimens with different effective depths, but the beam cross-section or shape was found to have no effect on the fatigue strength of the reinforcing bars.

In some projects it was attempted to simplify the fatigue test specimen by testing reinforcing bars in air, under pulsating tension, since it is easier, less time consuming and more economical to test a reinforcing bar in air than in a concrete beam. However, there is a disagreement in the technical literature on the effect of concrete embedment on the fatigue strength of bars.

Rehm (5) conducted fatigue tests on smooth and deformed bars using both of the above described specimens. The test results showed that the fatigue strength of an embedded bar in a beam test was 20 % lower than that of the same bar tested in air.

In another investigation by Ravello (cited in (29)) on pretensioned and post-tensioned beams, containing cables and strands, of different bond efficiencies it was found that

the better the bond the worse was the fatigue behaviour of a cracked member. This was explained by the different distribution of stresses along poorly bonded and strongly bonded tendons. For strongly bonded tendons the stresses vary greatly and suddenly between the cracked sections, where the bond is locally destroyed, and the neighbouring sections, where the steel remains embedded in the concrete. For less well bonded tendons, there are zones adjacent to the cracks where the bond is destroyed. In these zones- the weaker the bond, the more extensive they are- the stresses and stress variations are practically uniform such that the differences between the condition of the cracked sections and the neighbouring sections are less pronounced and less abrupt than in the case of strong bond. However, these explanations should be treated with scepticism since the obtained reduced fatigue resistance with increasing bond could not be necessarily due to the bond but possibly due to the actual fatigue behaviour of the steel, as it is known that improvement in bond is often obtained at the expense of poorer fatigue properties.

Contrary to the above findings, however, tests on 20 beams reinforced with ribbed Tor-stahl bars reported by Soretz (6), showed that embedded bars had a fatigue strength at least 10 % higher than similar bars tested in air. He attributed this to the large influence of the efficiency of bond on the fatigue strength of the reinforcement. He stated that the fatigue strength of steel decreases in proportion to the increasing deficiency of bond. This was explained as being caused by the size effect. In a bar tested in air, the weakest

section determines failure, whereas in a beam with good bond the failure always occurs at a crack. Since there is little probability that the occurrence of a crack and the weakest part of the bar should coincide, the fatigue life of well-bonded bars is increased by as much as 10 to 20 %. But when the bond is poor, the reverse may be the case because if the length of bond breakdown is longer than the length of bar tested free in air, the probability of finding a weak point or surface flaw is increased.

A more recent extensive investigation on the influence of concrete embedment on the fatigue strength of bars was carried out by Wascheidt (7). He tested plain bars and a variety of deformed bars in air and embedded in concrete prisms and beams. The length of the specimens tested free in air was 200 mm, while the length of the specimens embedded in prisms and the constant moment region of beams was 500 mm. The relative rib area (f_R), of the bars was found to be a significant variable in these tests. This parameter is defined as

$$f_R = \frac{\text{lug area projected on a cross-section of bar}}{(\text{bar diameter})\ (\text{rib spacing})}$$

Figure 2.4 shows that there was a reduction of up to 17 % in the fatigue strength of smooth bars ($f_R = 0$) when embedded in concrete prisms, and no difference in the fatigue strength of commercially available deformed bars ($f_R \geqslant 0.060$). This was attributed to the fact that in poorly-bonded bars the slip between concrete and steel in the vicinity of a crack produces

an abrasion phenomenon which after a while makes the steel surface layers chemically active. The oxygen in the air in the cracks induces frictional oxidation which can penetrate into the material and thus reduce the fatigue strength, especially under the accelerating influence of increased temperature which was measured in the crack areas around smooth bars.

Wascheidt's beam tests showed an increase of 6 % in fatigue strength due to concrete embedment for a bar having relative rib area f_R equal to 0.069. A more recent experimental investigation by Jhamb and MacGregor (21) supports Wascheidt's and Soretz's test results. The fatigue strength of 25 mm diameter deformed bars, having f_R equal to 0.071, embedded in a beam was 8 % higher than those tested in air. A similar result was found for Soretz's tests, as shown in Figure 2.4. Results reported by Rehm, and Ravello could not be compared with the others since the f_R values could not be obtained.

The general comments about testing fatigue beams under fatigue loading are that (i) the steel stresses in beams calculated on the assumption of the fully cracked state results in stresses which are a little higher than the existing ones; (ii) Few investigators have carried out associated independent fatigue tests on deformed bars in order that their fatigue properties may be related to the prediction of their behaviour in a beam; (iii) In most cases the number of beams tested is too small so that statistical comparisons could be made; And (iv) although the length of bond breakdown seems to affect fatigue performance of a beam, no investigator has considered

the effect of test length on the fatigue properties of deformed bars tested free in air.

2.1.3.2. GRIPPING ARRANGEMENT OF BARS TESTED FREE IN AIR

Although testing reinforcing bars in air, under pulsating tension is easier and more economical than testing reinforced concrete beams, a lot of difficulty was experienced in developing suitable grips so that fatigue failures would not occur in them but within the test length.

Wascheidt (7) cast an enveloping layer of synthetic resin around the gripping points of the fatigue specimens, and after hardening of the resin it was machined down to the correct diameter of the gripping jaws.

Gorodnickij and Konevskij (8) carried out fatigue test in the USSR on ribbed steel bars, whose ends were coated with glass-fibre resin. Failure occurred at the grips in 20 % of the specimens tested.

Jhamb and MacGregor (21) tested deformed and plain bars in air, which were cemented into conical end grips using an epoxy resin. No slip was observed between the deformed bars and the end grips because of adequate bond. But in the case of plain bars approximately 70 mm of the bars had to be knurled on both ends of each specimen to stop it slipping in the grips.

Warner and Hulsbos (27) used a gripping arrangement, for testing strand in air, in which the pulsating force in the specimen was transmitted partly through a 600 mm long cement grout bond anchorage and partly through a steel anchorage at the ends of the test piece.

Bennett and Boga (28) investigated the fatigue properties of large diameter plain and deformed hard drawn wires, testing them in an Amsler Vibrophone. The specimens were surface hardened at the gripped ends by a special hardening roller applying a pressure-force up to 125 kg. This proved successful and slip of the wire in the grips was avoided by increasing the friction of the bar ends using fine carborundum powder. But it seems doubtful whether ribbed bars, which are rather more heavily deformed than indented wires, and held in machine jaws which are not as special as those provided in the Amsler Vibrophones, could be tested successfully only by surface hardening their gripped ends. Nevertheless surface hardening when used in combination with a resin type of grip could possibly give less failures at the grips than using a resin coat only.

In one investigation by Edwards and Price (30) on strand tested under fatigue loading in air, the grips consisted of a piece of plastic, 1 mm thick, wrapped around the ends of the strand and two 3 mm thick soft aluminium angles placed on top of the plastic. These grips were 100 mm long and load was transferred from the machine's jaws to the strand without creating a notch effect on its surface, so that only 12 % of all specimens failed at the grips. This type of grip is simpler, quicker as well as more economical to make than the cement grout bond anchorage or epoxy resin type of grips. But although it proved very successful for testing strand, which is rather smooth, it seems doubtful whether it can be effective with commercially available ribbed bars which are comparatively heavily deformed.

2.2. CRITICAL REVIEW OF PAST WORK ON BOND AND CRACKING

2.2.1. GENERAL

In the early part of this century a number of bond tests were reported. However, these tests were conducted using a variety of test specimens and test procedures and in almost all tests only the maximum bond values were reported. Duff Abrams (cited in (32)) was the first to employ both pull-out and beam specimens and measured slip as well as bond strength. Numerous investigations have followed but the subject is not yet fully understood. It is still one of the most complicated in the concrete field for the following reasons :

(i) There are many factors influencing bond and it is not always possible to isolate them in tests.

(ii) Measurement of bond distribution and especially slip between concrete and steel, along their interface, is complicated.

(iii) Bond in practice exists under a wide variety of complex stress conditions which influence its behaviour. The simulation of conditions in practice by tests on simple specimens is never assured.

Most research studies on bond and cracking in reinforced concrete members are empirical. Comparatively few analytical studies have been developed. Classical methods of analysis, based on two-dimensional elasticity and plasticity, are limited in application to cases so idealised as to bear little relation to the member under study. With the recent development of the finite element method for analysis of structural continua a new powerful tool has become available for use in understanding the behaviour of reinforced concrete.

2.2.2. NATURE OF BOND AND MECHANISM OF BOND FAILURE

Bond between plain bars and concrete is generally considered to be basically due to adhesion and friction between concrete and steel. Adhesion bond develops first and after a small slip it is destroyed and for larger slips frictional bond develops between the concrete and steel sliding surfaces. Mikhailov (cited in (32)) studied experimentally the relative values of adhesion and frictional bond with plain bars using pull-out and beam specimens, and found that :

(i) The adhesive forces between steel and concrete are not large and amount only to 0.5 - 0.7 N/mm^2; thus adhesion itself is of no significance in the resistance to slipping of the reinforcement.

(ii) Adhesion and frictional resistances resulting from shrinkage account for 25 to 30 % of the bond strength.

(iii) 70 to 75 % of the total bond resistance of plain bars depends primarily on the degree of roughness of its surface and the change in the lateral dimension of the bars along their embedded length.

With deformed bars the mechanism of bond failure is radically different. Adhesion and friction are still operative but bond strength primarily relies on the bearing of lugs and the strength of concrete between lugs. There is also a fundamental change in the manner of failure. With plain bars embedded either in a pull-out or a beam specimen failure usually occurs by slip of the bar as a whole which may be pulled completely out of the concrete leaving a smooth bore in the specimen. With deformed bars failure is almost always associated with longitudinal

splitting along the surface nearest the reinforcing bar. Splitting of the concrete is due to the wedging action of the bar lugs against the concrete and occurs in both pull-out test specimens, where the concrete is in compression longitudinally, and beams, where the concrete surrounding the bars is in tension longitudinally.

Additional insight into the nature of bond strength can be obtained from recent studies on internal cracking associated with the development of bond stresses in concrete tension prisms. Experiments carried out by Broms and Lutz (33 - 36) established the existence of radial cracks originating at the steel-concrete interface and terminating within the prism, i.e. not extending to the concrete surface and therefore not visible to the outside observer. Further studies by Bresler and Bertero (37) showed that at low steel stress levels principal tensile stresses at the steel-concrete interface are inclined at an angle of about 60° with the longitudinal axis at the cracked face and decreasing with distance from it, as shown in Figure 2.5. Goto's (38,39) experimental investigations also showed that cracks develop within the concrete prism, inclined at an angle of 45° to 80° to the bar axis, as shown in the photograph of Figure 2.6.

Based on these investigations the mechanism of bond development with increasing loads has been described by Watstein and Bresler (32) as follows. At low steel load levels high principal stresses develop only next to the reinforcement adjacent to the full transverse cracks. This results in local inclined cracking which relieves the high tension near the transverse

crack face and shifts the zone of maximum principal stresses inward from the crack face. With increasing load these principal stresses become equal to the tensile strength of the concrete generating additional internal cracking. As the load is further increased the process of internal cracking and of shifting the peak stresses continues. At a very high steel stress level the internal cracks propagate through most of the prism and a bounding layer of teeth-like concrete segments is formed around the steel which resist the pull-out forces by wedging action, as shown in Figure 2.7. At intermediate steel stress levels, because of cracking, there is a continuous softening of this bounding layer. This loss of stiffness results externally in a local relative slip between steel and concrete. The deformation characteristics of the boundary layer have not as yet been defined quantitatively in a realistic manner.

2.2.3. MEASUREMENT OF ANCHORAGE AND FLEXURAL BOND STRENGTHS

It is virtually impossible to devise a sngle type of test specimen, and test it under such conditions that the results would be applicable to all bond conditions in practice. In general bond exists under a wide variety of stress combinations where concrete and steel are stressed diversely in different directions. In the past primary interest has been concentrated in anchorage bond and in flexural bond and these have been measured by means of tests on pull-out and beam specimens respectively.

Bond values derived from pull-out tests cannot in general be applied to the design of reinforced concrete beams.

Beam tests are necessary to develop design criteria. The differences between bond values obtained from pull-outs and from beams are due mainly to the different crack patterns which develop in the two types of specimens. As the applied load increases on beams, there are transverse and longitudinal cracks formed. In pull-out specimens there are no transverse cracks formed and cracking is confined, in the case of deformed bars, to longitudinal splitting. In addition friction at the base of a pull-out specimen restrains longitudinal splitting. Modifications of this specimen, called the tensile pull-out specimen, have also been used (Figure 2.8). These eliminate the compression of the concrete and are an improvement; but each introduces some of the special problems of spaced splices and any crack pattern is influenced by this interaction.

Nevertheless, pull-out tests are satisfactory, because of their simplicity, for measuring the relative bond values of bars with different deformations. Also pull-out test data can be used to predict the behaviour of the anchorage zone in a reinforced concrete beam, since in this zone the concrete surrounding the steel is in compression.

2.2.4. EXPERIMENTAL DETERMINATION OF BOND STRESS AND SLIP BETWEEN CONCRETE AND REINFORCING BARS

2.2.4.1. AVERAGE BOND STRESS

Traditionally, specifications have treated bond stress in terms of average values. For pull-out tests, this is calculated by dividing the bar load by the embedded bar surface :

$$f_{bs} = \frac{F}{\left(\sum u\right).l}$$

where f_{bs} = average bond stress

F = applied tensile bar force

$\sum u$ = bar perimeter

l = embedded length

For beams, average local bond stress at any point along the bar axis is calculated by dividing the change in tensile bar force, over a differential length dx, by the bar surface of the embedded length of bar dx :

$$f_{bs} = \frac{dF}{\left(\sum u\right).dx}$$

where dF = change in bar force in differential length dx.

An average value for bond stress does not show how the bond stress in distributed along the length of a bar embedded in concrete. In the case of a pull-out specimen it reaches a maximum value close to the loaded face and reduces to zero at some distance from that face. In the case of a beam specimen, maximum bond stress is found close to flexural cracks. As the bond load is increased, the maximum bond stress moves progressively inwards away from the loaded face of a pull-out specimen or from the crack face in a beam. These local bond stress values are accompanied by slip between the reinforcement and concrete, as was explained in section 2.2.2.

Different techniques have been developed by different

investigators for measuring the distribution of bond stress and relative slip, between a reinforcing bar and concrete, along their interface. These are briefly described in sections 2.2.4.2 and 2.2.4.3 respectively. Local bond-slip relationships can then be dirived either using these distributions or by taking direct measurements on short embedded bar lengths, as explained in section 2.2.4.4.

2.2.4.2. BOND STRESS DISTRIBUTION

The local bond stress at any point on the interface between an embedded bar and the surrounding concrete can be found using Equation (2.1.) :

$$f_{bs} = \frac{dF}{\left(\sum u\right).dx}$$

or

$$f_{bs} = \frac{A_s.df_s}{\left(\sum u\right).dx} \qquad (2.1)$$

where

f_{bs} = average bond stress at point considered

$\sum u$ = bar perimeter

A_s = bar cross sectional area

df_s = change in steel stress in the bar infinitesimal length dx

The bond stress is thus directly proportional to the slope df_s/dx of the steel stress distribution curve. Equation (2.1)

can be rewritten in terms of the steel strain, by :

$$f_{bs} = \frac{A_s . E_s}{\sum_u} \cdot \frac{d\varepsilon_s}{dx} \qquad (2.2)$$

where

ε_s = strain in the bar at the point considered

E_s = elastic modulus of steel bar

Thus at any load, the bond stress at any point along a bar embedded in concrete in proportional to the slope of the steel strain distribution curve at the point considered.

A number of investigators have used many different techniques for obtaining the distribution of bond stress through measurements of the steel tensile strain distribution along bars embedded in concrete. Watstein (40, 41) measured steel strains at intervals along embedded bars using external dial gauges in combination with access slots through the concrete permitting access to circular holes in the surface of the steel bar. This method is not satisfactory because the distribution of bond is modified around the circular holes.

Electrical resistance strain gauges have been used extensively on the surface of bars but this is objectionable because the presence of properly waterproofed gauges at the desired close spacing modifies the distribution of steel strain and bond.

Some investigators have fixed electrical resistance strain gauges on either side of a small slot cut into the bar. The volume of the bar is thus not much reduced, but it is rather difficult to make the slots and fix the strain gauges and the

wires which must cross the concrete section may induce premature cracks.

To eliminate these difficulties, Mains (42) used electrical resistance strain gauges mounted internally in a hollow core formed by sawing the bar longitudinally in a diametrical plane, milling a slot along the centreline of each cut surface, and tack welding the bar together in its original position after fixing the gauges in the slots. This method has the disadvantage that the volume of the bar is considerably reduced compared with a solid bar of the same surface area. This means that for similar loads the hollowed bar has a larger extension; therefore the strain in the concrete next to the bar is greater and the bond breaks down more quickly than in the solid bar.

2.2.4.3. SLIP BETWEEN CONCRETE AND A REINFORCING BAR

The measurement of local slip along the steel-concrete interface is a very difficult problem. Evans and Williams (43, 44) used a radiographic technique in which thin strips of lead were inserted into slots 0.125 mm wide allowing a small projection into the concrete. When slip took place, the lead sheared and an X-ray photograph indicated the amount of relative movement or slip. Besides the reduction in cross sectional area of the bar and non-uniform stress distribution, there is the restriction on specimen size due to the degree of penetration of the rays and the expensive equipment and safety precautions required.

Moore and Lewis (cited in (45)) used an air gauge consisting of a plastic cube which acted as a valve, and the

flow of air was dependent on the relative displacement between steel and concrete. But this method did not prove satisfactory due to lack of sensitivity and accuracy.

More recent attempts to measure directly the slip between steel and concrete in realistic specimens were initiated at Cornell University by Ruiz (cited in (45)). He developed a slip gauge using a standard electric resistance strain gauge installed with the central portion unbonded. One end of the gauge was bonded to the reinforcing bar, the other bonded to a small cube of mortar later to be embedded in the concrete. The gauges were placed parallel to the axis of the bar, and after pretensioning and calibrating were waterproofed and completely encased by the poured concrete. Encouraging results were claimed to have been obtained. This technique was further refined by Wahla (46). But these specially-adapted electrical resistance strain gauges required great care in their placement and calibration and, most important of all, their presence interferred with the bonding surface to a possibly significant degree.

Wahla also used miniaturized linear differential transducers to measure slip directly at internal locations in several types of reinforced concrete specimens. But the fixing pin attached to the transducer casing and placed in a positioning hole drilled into the reinforcing bar was affecting the bond distribution. The work by Wahla was extended by Tanner (cited in (45)) who used recently developed internal strain gauges for concrete. These consisted of a wire resistance strain gauge cemented between two thin polyester resin blocks. The outside surface of the resin was coated with a coarse grit material to

provide good bonding with the concrete. Such concrete strain gauges were embedded in the concrete along the length of the specimen, about 10 mm from the surface of the reinforcement. The advantage of these gauges is that they do not interfere with the normal distribution of bond stresses. They can be regarded as the equivalent of pieces of aggregate. The variation of slip along the steel-concrete interface was obtained indirectly from the internal measurements of concrete strain and steel strain, by integrating the steel and concrete strains along the length of the bar. The weakness of this method lies in that (i) concrete strains were not measured next to the bar, but at a distance of 10 mm from it, (ii) slip was indirectly obtained from concrete and steel strain measurements which were both subject to experimental error, and (iii) the calculations required are tedious, since strain, displacement, and slip functions must be determined at each increment of applied load.

2.2.4.4. BOND STRESS - SLIP RELATIONSHIPS

In a finite element analysis of reinforced concrete, carried out by Nilson (47, 48), a third degree polynomial was used to represent the bond-slip characteristics between the reinforcement and concrete. These were derived indirectly from data obtained by Bresler and Bertero (49) in tests on concentrically reinforced concrete cylinders. Tensile load was applied axially on both ends of the steel bar and the strain along the embedded bar length was measured by electrical resistance strain gauges fixed into the hollowed bar.

Slip between steel and concrete was measured only at

the end faces, being 406 mm apart. Nilson calculated the variation of slip between these two points indirectly. He assumed a parabolic variation of the concrete displacement between two cracks. The obtained bond-slip characteristics are shown in Figure 2.9, as well as their simplified forms that Nilson used in his finite element program. For an element of the bar surface near a crack face the bond stress was assumed to drop to zero after reaching its maximum value, because of a longitudinal crack forming along the bar. But for an element well removed from a crack, bond stress was assumed to remain constant after reaching its maximum value.

The reliability of the bond-slip curve that Nilson derived is questionable, because (i) a simplifying assumption was made about the variation of concrete displacement between two cracks, and (ii) the bond-slip curve was obtained indirectly. More recently he tried to establish bond-slip relationships in reinforced concrete by carrying out direct measurements (45). He used concentric tensile pull-out specimens reinforced with a 25 mm deformed bar. The variation of steel strain along the length of the embedded reinforcing bar was measured using the technique developed by Mains and described in section 2.2.4.2. The slip between steel and concrete was measured using the technique developed by Tanner and described in section 2.2.4.3. The test results required tedious calculations for obtaining values to be used for plotting bond-slip curves. Nilson found that both the peak local bond stress and the initial slope of the bond-slip curves vary with distance from the loaded end of the specimens tested (and, by analogy, with distance from a crack

face in a typical member). Average bond-slip curves are shown in Figure 2.10.

The above method of obtaining bond-slip curves is an improvement on the indirect method that Nilson first used. But even this improved method has serious disadvantages; the main one being the laborious and not strictly exact way of obtaining slip values, as pointed out in section 2.2.4.3. (Tanner's method).

Rehm (50) was the first to get directly the relationship between bond stress and the associated displacement on a localised basis. He carried out pull-out tests on a "bar differential", i.e. on very short embedded lengths. The bars were embedded centrally in 100 mm and 200 mm concrete cubes and the test arrangement is shown in Figure 2.11. He tested mainly plain bars and bars with a single rib, machined on a lathe from plain bars, and experimented with different shapes. The length of embedment used varied between 3 mm and 67 mm.

With this testing arrangement bond-slip curves were obtained directly from the load indication of the testing machine and the measured displacements. These curves constitute what Rehm termed a "fundamental law for bond", just as stress-strain diagrams do for the strength behaviour of steel or concrete. With the aid of them the bond stress can be deduced directly from the local displacement at any point of the reinforcement. Similarly, if the boundary values (stress, displacement) are known, the stress distribution over any desired length of a bar can be calculated by integration.

Rehm also investigated the influence of bar casting positions on bond performance. He found that horizontally cast

bars behaved much worse than bars cast vertically, even though both tended towards the development of the same ultimate load, as shown in Figure 2.12 for three different positions of casting. He attributed this different performance to the reduction of the deformation resistance of the concrete just below the bar surface, because of local settlement and pore formation in the freshly placed concrete.

The applicability of Rehm's results to real bar reinforcement is opened to question for the following reasons :

(i) Rehm used highly idealised specimens with a single rib. These could not possibly represent all the different types of ribs rolled on commercially available deformed bars.

(ii) Specimens with just a single rib are under different lateral restraint conditions compared to specimens with a number of consecutive ribs.

(iii) The results obtained from tests on a single rib are more affected than tests on multiple ribs by imperfections which occur during casting, handling and testing, as well as those due to the non-homogeneous nature of the concrete.

(iv) Rehm's results cannot be used for design purposes, because the bond-slip curves produced are not statistically dependable. Only two or three replications of a test were carried out even though there was a scatter in the results of the order of $\pm$ 20 % from the mean.

(v) Rehm embedded the single ribs of his test bars at the centre of 100 and 200 mm cubes of concrete, thus using much bigger concrete covers to the reinforcement than used in practice. These large covers are known to affect bond strength values

appreciably; he actually found for similar test bars a decrease of 35 % in the bond resistance when they were embedded in the 200 mm cubes as compared to the 100 mm cubes. No tests were carried with covers comparable to those used in normal practice.

Further studies of a localised nature were conducted by Lutz and Gergely (51, 52) on bars with single ribs embedded in concrete prisms, 230 x 230 mm in cross-section and 255 mm long. The same comments as for Rehm's specimens apply in this case as well.

Stocker and Sozen (53) carried out an extensive series of pull-out tests on strands with a short length of embedment. They used a concrete specimen, 100 x 230 mm in cross-section and 200 mm long, similar to the one used by Rehm. The tests were designed to provide information on the relationship between bond and slip and to study the effect of the following variables on the bond strength of strand : length of embedment, concrete cover, size of strand, lateral confining pressure, concrete strength and curing conditions.

Tests with length of embedment of 12.7, 25.4, 38.1 and 50.8 mm showed that there was a relatively large scatter of the individual tests with bonded lengths of 12.7 mm. The shortest length giving reliable and consistent test results was found to be the 25.4 mm one, and this was chosen as the standard bonded length for all further pull-out tests. The tests on the effect of concrete cover showed that the bond strength of strand held in a horizontal position during casting decreased rapidly with increasing depth of concrete below the strand due to settlement of the fresh concrete. A depth of

concrete of 152 mm below the strand caused the bond strength to drop by as much as 30 % with respect to that obtained for a concrete depth of 51 mm.

Morita and Kaku (54) carried out pull-out tests on deformed bars embedded in a short reinforced concrete beam. The bars were cast vertical and at right angles with the beam's axis, as shown in Figure 2.13. Deformed bars of 19 mm and 25 mm diameter were used in the tests, embedded in concrete along a short length of 48 mm and 66 mm respectively. The beam was properly held down, while each of the bars was pulled out of the beam and measurements of free bar end slips were taken. The influence of the bar cover and longitudinal splitting can be seen in the bond-slip curves that they obtained, shown in Figure 2.14, for a 25 mm diameter bar embedded near the beam end face and one in the beam middle.

Edwards and Picard (56, 57) developed a pull-out specimen for obtaining bond-slip curves for a 12.7 mm diameter strand. They used a length of embedment of 38.1 mm and three covers of 12.7, 25.4 and 38.1 mm, as shown in Figure 2.15. The load in the bar was accurately measured by calibrated measuring bars passing through holes provided in the specimen and both loaded and unloaded end slips were measured by linear displacement transducers. These measurements were used to produce bond-slip curves showing an elastic-plastic behaviour (Figure 2.16) and the results showed that the average value of the maximum bond strength decreased when the concrete cover increased. Although only 12 tests were carried out, the specimen that they developed and the testing arrangement are much simpler than any of the ones

used by the previous investigators. This sort of specimen thus seems suitable for performing a large number of parametric studies so that reliable bond-slip curves can be obtained for analytical or design calculations.

2.2.5. INVESTIGATIONS RELATED TO CRACKING

2.2.5.1. GENERAL

Extensive research studies on the cracking behaviour of reinforced concrete have been conducted over the last fifty years. The effect on cracking of various parameters such as the ratio of reinforcement, the diameter of bars, and the dimensions of cross-sections of concrete members, has been investigated by taking innumerable measurements of crack spacing and crack width. Comparatively very few investigators have attempted to tackle the problem analytically because of its complexity and because of the many factors involved. In most cases the experimental results have been summarised by an empirical formula.

The disadvantage of empirical studies is that any derived formulae are in general only applicable to the type and size of specimens, as well as test conditions used. Application of the results to other cases is not guarranteed to be accurate.

An extensive review of the knowledge prior to 1957 concerning various aspects of cracking was presented at a RILEM Symposium on 'Bond and Crack Formation in Reinforced Concrete' (31). A thorough review of research, prior to 1965, on the causes and control of cracking in concrete reinforced with

high-strength steel bars was published by Reis et al (58) at Illinois University. A more recent review of the control of cracking in concrete structures was published by ACI Committee 224 (59), associated with a bibliography (60) of reports published between 1911 - 1970.

It is not intended in the present study to go into the details of all derived formulae or different analytical methods. Only the factors found to affect cracking in empirical studies will be given and the assumptions and limitations in analytical studies. The literature review will be concentrated in the suitability of the finite element method to predict the cracking behaviour of reinforced concrete members.

2.2.5.2. EMPIRICAL STUDIES ON CRACKING

Watstein and Bresler (32) carried out a comprehensive review of empirical formulae derived from studies on flexural cracking in reinforced concrete elements, and suggested that the crack width w under service load conditions can be expressed in general terms by the equation given below, from which all existing formulae can be generated :

$$w = \frac{k_1 \, k_f \, R \, t_i \, f_s}{E_s} = K \, R \, t_i \, f_s$$

where

f_s = tensile stress in the steel reinforcement

k_f = stress reduction coefficient which depends on surface bond characteristics and bond effectiveness

of steel reinforcement, on tensile strength, modulus, and creep properties of concrete, as well as on stresses due to temperature and humidity conditions

k_1 = numerical coefficient depending on loading and boundary conditions of the structural element

t_i = geometric index having dimensions of length and sometimes expressed as effective thickness of concrete surrounding each bar (this is related to the shape and size of the member, area and arrangement of tensile steel reinforcement, spacing of reinforcing steel bars across the width of the structural element, concrete cover measured from the surface to the centre of the nearest bar, and bar diameter)

E_s = modulus of elasticity of reinforcing steel

K = a coefficient, equal to $(k_1.k_f)/ E_s$

R = ratio of the distance between the neutral axis and the level where the crack is located to the distance between the neutral axis and the centroid of the reinforcing steel

Precise definition of the coefficients k_1, k_f, and of the geometric index t_i is difficult and a large number of empirical equations for crack widths has been proposed.

The common primary variable in all of these expressions is the tensile stress or strain in the reinforcement and the second major variable in determining crack width w is the effective thickness t of concrete surrounding the bar.

Watstein and Mathey (61) found, from tests on axially loaded members, that especially at high loads the crack width at the surface of a deformed bar was significantly less than the crack width at the exterior surface of concrete, as shown in Figure 2.17. These crack widths were estimated by comparing the over-all extension of the embedded bar with the extension of concrete adjacent to the bar. For plain bars this extension of concrete was negligible, while for deformed bars it was a significant fraction of the total extension of the reinforcement.

2.2.5.3. CLASSICAL ANALYTICAL METHODS ON CRACKING

Most previous analytical studies on cracking of reinforced concrete have been founded on closely similar basic concepts, differing essentially in the assumptions concerning the bond stress distribution between two cracks. General equations were given by Watstein and Parsons in 1943 (62) for cracking of axially loaded members. Commission IVa on Cracking of CEB (63), has attempted a synthesis of the varies theories, both for axial tension and flexural members. The basic assumptions used by CEB, which are common to most individual theories, are as follows :

(i) The elastic strain of the concrete is negligible.

(ii) The bond stress distribution has a zero value in the middle between two cracks and changes sign on either side of it.

(iii) At this point the tension in the concrete reaches its maximum value and the maximum crack spacing occurs when this tension is equal to, but not exceeding, the ultimate tensile strength of concrete.

Some of the widely different bond stress distributions in between two cracks, assumed by various investigators along with the resulting steel and concrete stresses are shown in Figure 2.18.

It should be noted that these theories do not take into account the effect of the concrete cover on crack width and crack spacing, which was found to be of importance in empirical studies. It is obvious that simplified equations cannot possibly account for all the parameters affecting cracking in reinforced concrete members. The many different theoretical cracking formulae that have been proposed in the past are not in general applicable to beams that are different from those considered by each particular investigator.

2.2.5.4. FINITE ELEMENT STUDIES ON CRACKING

Relatively recently the problem of cracking was approached in a different way from the classical analytical methods. The finite element method has been used to obtain the stresses and deformations around bars embedded in concrete and to study the initiation and propagation of cracks.

Lutz (52, 64) and Gergely (52) used an elastic finite element technique to analyse the stresses in concrete near a reinforcing bar due to bond and transverse cracking. They found that due to bond between the concrete and the reinforcing bar, while the outer concrete surface remained essentially unstressed, the concrete adjacent to the bar was highly stressed. This was followed by primary transverse cracks which decreased in size from the concrete outer surface to the bar. Assuming perfect

bond after the formation of transverse cracks, it was shown that the concrete would separate from the steel due to the very high interfacial tensile stresses developed between the steel and concrete near a transverse crack. In the case of a plain bar all bond transfer capabilities would be lost for the extent of this separation and thus it was concluded that the crack width at the bar-concrete interface would be the same as that at the surface of the concrete member. However, with a deformed bar, bond continued to exist in the region of separation by bearing of the concrete against the bar ribs, and the crack width at the bar surface would thus be a small fraction, of the order of one-fourth, of that at the concrete outer surface.

Bond deterioration as a consequence of inelastic deformation and fracture in the concrete boundary layer adjacent to the steel-concrete interface, as described in length in section 2.2.2, was incorporated into an axisymmetric finite element program developed by Bresler and Bertero (37). They analysed a 150 mm diameter tensile cylindrical concrete specimen, reinforced with a 29 mm diameter plain steel bar, and they distinguished two regions in the concrete continuum. The first region was bounded by the steel-concrete interface and a surface located 11 mm from it. This boundary layer was used to model bond by assigning to it reduced elastic constants, i.e. $E_c = 1.9 \times 10^3$ N/mm^2 and $\nu_c = 0.495$, as compared to the outside layer where normal concrete elastic constants were used, i.e. $E_c = 33 \times 10^3$ N/mm^2 and $\nu_c = 0.2$. However no slip was allowed between steel and concrete at their interface.

From the above analysis, which was rather of a qualitative nature, Bresler and Bertero found high local stresses at the steel-concrete interface near the end of the concrete prism, which were of such magnitude that local fracture should occur even at a low level of steel stress.

In 1962 Clough (cited in (65)) tackled the cracking problem using the finite element method. He used an elastic analysis to determine the stress distribution in a dam which had cracked during construction. The cracks were assumed to be free boundaries which remained open until compressive forces acted across them.

The concept of predefining the position and extent of cracks by calling on previous practical experience, has been employed by Ngo and Scordelis (66) for the analysis of cracked reinforced concrete beams. Concrete and steel were represented by two dimensional triangular finite elements and the two materials were assumed to behave linearly elastically. Bond slip was taken into account by using finite spring linkage elements spaced along the steel bar length and connecting the bar to the adjacent concrete, as shown in Figure 2.19. Each linkage contained two springs, one acting parallel to the bar, representing bond, and one acting perpendicular to it, representing the normal forces between bar and concrete. The force-displacement, or bond-slip, characteristics of the longitudinal springs were taken as linear for simplicity and their slope given a value calculated from load-slip measurements on axially reinforced concrete tension specimens. The vertical springs were arbitrarily given a very large stiffness value assuming that

the steel and concrete are almost rigidly connected in the vertical direction.

Several singly reinforced concrete beams on simple supports, with different predefined idealised crack patterns, were analysed under third-point loading. The distribution of concrete stresses through the depth of the cracked concrete beams, as well as steel and bond stresses, were found to be non-linear, particularly in the vicinity of a crack. Although no general conclusions regarding the behaviour of the reinforced concrete beams under load were attempted, the potential of the finite element method as an analytical tool was clearly demonstrated. As the variables affecting cracking are experimentally determined, they can be incorporated into the analytical model resulting in better predictions of reinforced concrete members' response under load.

Ngo, Franklin and Scordelis (67), in another study of reinforced concrete beams, used cracks predefined in shape and location, the two sides of which were initially held rigidly together by very stiff springs, joining opposite nodes, as shown in Figure 2.20. When the tensile limit was exceeded across the crack, the spring normal to the crack was released, while the spring parallel to the crack, which represented aggregate interlock, was assigned a constant value.

The research initiated by Ngo and Scordelis was taken a step further by Nilson (47, 48) who analysed reinforced concrete tension members by including the changing topology of the members due to progressive cracking. Concrete and steel were represented by two-dimensional rectangular finite elements.

The biaxially loaded concrete was treated as an orthotropic material, assuming that the stresses and strains in the principal directions not to be affected by each other. A stress-strain equation proposed by Saenz was used to described the non-linear behaviour of concrete under compression in each direction, while the behaviour in tension was assumed to be linearly elastic. The behaviour of steel was assumed to be linearly elastic up to the yield point. Bond was modelled by using discrete, closely spaced spring elements similar to those employed by Ngo and Scordelis. The non-linear bond-slip characteristics used were obtained indirectly as described in section 2.2.4.4 and shown in Figure 2.9. Account of the non-linearity in the bond-slip and stress-strain curves was taken by adopting an incremental loading procedure and adjusting the slope of the curves during each increment.

The member to be analysed was loaded incrementally until the principal tensile stress exceeded the tensile strength of the concrete at one or more locations. Execution was temporarily terminated, and the computer output subjected to a visual inspection. If the average value of the principal tensile stress in two adjacent elements exceeded the tensile strength, then a crack was assumed to form between the two elements along their common edge. This was done by disconnecting the elements at one of their common nodes in the case of an exterior crack, and at both of their common nodes in the case of an interior crack, as shown in Figure 2.21. Nilson recognized that this overestimated the length of an internal crack, but considered the error to be small for a refined mesh. Successive

extensions of a crack were simulated by disconnecting single nodal points.

The newly-defined member, with cracks and partial bond failure, was then re-loaded from zero in a second loading stage, also incrementally applied. Once again execution was terminated if failure criteria were exceeded, and the member redefined accordingly. This procedure was repeated until eventual failure was obtained by yielding of the reinforcing bar. Nilson realised that complete unloading of the member, after a crack has formed, does not correspond to what would actually occur, but he was forced to adopt the above procedure because of the complications of the problem. Results thus obtained compared favourably with the observations by Broms (33) on tests of concentrically, as well as eccentrically, reinforced concrete tensile members.

Another approach developed for solving the cracking problem is by changing the material properties and/or allowing for the effect of a crack by redistributing the released stress to the surrounding material. A non-tension model was suggested by Zienkiewicz et al (68) in order to analyse rock structures. The rock material was assumed to be incapable of sustaining tensile stresses because of the inherent flaws and fissures. First an elastic analysis was performed from which the principal stresses were computed and all tensile principal stresses were eliminated. An iterative technique was used to redistribute the eliminated stresses. This was done by applying nodal loads equal and opposite to the tension during the next increment of load and iterating until finally an almost pure compressive

field was obtained. Areas where tension had occurred were considered to be fissured regions. Four rock structures were analysed elastically, taking no account of material or geometric non-linearities and consequently the same stiffness matrix was used throughout the analysis.

A similar analysis applied to reinforced concrete was presented by Valliappan and Nath (69). The load was applied incrementally, and cracks were considered to form when the principal tensile stress exceeded the allowable value. No individual cracks were defined, but cracked zones composed of cracks at infinitesimal spacing from each other were given.

The investigation was extended by Valliappan and Doolan (70) to include the non-linear material properties of concrete and steel. The stress-strain curves for both materials were assumed to be elasto-plastic and the bond between concrete and steel was taken to be perfect, i.e. no slip was allowed between concrete and steel. An 'initial stress' method proposed by Zienkiewicz et al (71) was used, which uses the same initial elastic stiffness matrix but redistributes any additional stresses beyond the limited values. Two reinforced concrete beams and one reinforced concrete haunch were analysed and the extent of cracked, as well as plastic, zones were obtained. The authors emphasized the necessity to use a refined mesh to achieve a good representation of the extent of cracking.

In order to predict more accurately the propagation of a crack once it has initiated Loov (72) employed a small sensor element ahead of the crack which was assumed to have a finite width. Guide lines for choosing the size of the sensor

element were given in order to maintain numerical accuracy. But the required narrow triangular elements joining the sides of the sensor element to the original mesh (see Figure 2.22) are likely to result in ill-conditioned matrices. The automatic introduction of nodes and elements during the analysis required a considerable programming effort. Although the time spent in computation of a crack is small, for real members having a large number of cracks the computational effort would make this technique impractical.

2.2.6. INVESTIGATIONS ON THE EFFECT OF REPEATED LOADING ON BOND

While bond and cracking in reinforced concrete elements have been studied by numerous investigators, as already discussed in length in section 2.2.5, studies of bond and cracking under repeated loading have received comparatively little attention so far.

Mühlenbrunch (73) carried out pull-out tests on concrete specimens, 127 x 127 mm in cross-section, with a length varying from 127 to 255 mm, and reinforced with a 16 mm diameter deformed bar. The effect of repeated loading on the static pull-out strength was determined by testing the specimens statically after subjecting them to a certain number of load cycles. The higher the ratio of the repeated load to the static pull-out load, the lower was the static bond strength after the same number of load cycles. The reduction in strength was found to be highly dependent upon the embedment length; the highest reduction was obtained with the shortest length. A reduction of as much as 50 % was obtained with the 127 mm embedment

length under a repeated load equal to 50 % of the static pull-out load.

Perry and Jundi (74) tested sixteen eccentric pull-out specimens, reinforced with a 19 mm diameter bar, under repeated loading. The bars were hollowed and electrical strain gauges were mounted on the inside, so that the distribution of steel stress could be obtained along the embedded length. The test results showed that the peak bond stress was shifting away from the loaded end of the specimen to the unloaded end, as the number of cycles of loading and unloading increased. This redistribution of bond stresses tended to become stabilised after several hundred of cycles. From the limited number of tests performed in this study there was no evidence that failure of a specimen would occur by increasing the number of cycles of loading unless the applied load was at least 80 % of the ultimate load.

Bresler and Bertero (49) carried out an experimental investigation of strains, stresses, and crack widths in an axially reinforced concrete prism subjected to repeated tension loads. Four cylindral specimens, 152 mm in diameter and 406 mm long, were reinforced with a 29 mm diameter deformed steel bar, specially instrumented with electrical strain gauges to define the strain distribution along the length of the bar. The steel bar was sectioned longitudinally, grooved for installation of 30 strain gauges along the length, and after wiring the gauges the sections were rewelded to form an instrumented bar with effectively undisturbed exterior. After casting and curing the specimens, a circumferential notch was cut in the mid-height

of the concrete cylinder to induce formation of a crack at the notched section during loading. The specimens were subjected to repeated loads at different stress levels, with the total number of load cycles varying from 14 to 65. Crack widths at mid-length, end slips, and strains in the steel bar and concrete cylinder were recorded.

The test results showed that under a variable stress history, the effectiveness of bond between concrete and steel depends primarily on the magnitude of the previous maximum load. The greater the magnitude of the previous load, the lesser is the effectiveness of bond at subsequent lower stress levels. Overstress, even below the yield stress of the reinforcement, may reduce bond effectiveness at service stress level by 60 to 90 %.

Ismail and Jirsa (75) carried out a similar experimental investigation on the influence of load history on the deterioration of bond along bars subjected to elastic stresses. They used axially reinforced concrete prisms, having the same dimensions as those used by Bresler and Bertero, except that they were square in cross-section. Two of the specimens were subjected to cyclic tensile loads and two to cyclic tensile and compressive loads. The load was increased in steps up to yielding of the reinforcement and at each step there was cycling of the load applied. The amplitude of the compressive steel stresses was the same in all cycles and equal to 40 % of the concrete compressive strength. The total number of cycles varied from 11 to 22. The test results showed the following trends, which were similar to those obtained by Bresler and Bertero :

(i) The most important factor affecting bond is the peak stress reached in preceeding cycles. If the peak stress was increased, the bond at lower stresses was reduced in subsequent cycles. The most significant reduction was at stress levels well below the peak stress.

(ii) A small number of repetitions of load cycles with constant peak stress produced a gradual deterioration of bond, but the reduction was minimal in comparison with the reduction associated with increases in peak stress.

(iii) The bond stresses, after cyclic loading was applied, were higher in those specimens in which compressive load, as compared to those that only tensile load, was applied. This was attributed to the reversal of slip along the bar and reduction of residual effects which tended to accumulate when tensile load only was applied.

Thus it was concluded that in structures where replications of service loads or some overloads are expected, it may be necessary to make special provisions for bond at low stress levels, since the effectiveness of bars in bond is reduced substantially in some cases.

Singh, Gerstle and Tulin (76) tested pull-out specimens, having a 76 mm embedment length, under monotonic and cyclic loadings in order to determine load-slip characteristics under both types of loading. The results of their tests revealed a small increase in slip and a small reduction in strength due to cyclic loading.

Morita and Kaku (54) studied experimentally the effect of repeated loading on the local bond stress-slip relationship.

They applied repeated loading in one direction and cyclic reversed loading between constant load or constant slip limits, on the short length of embedment pull-out specimens described in section 2.2.4.4. The results that they obtained showed that a small number of repetitions within a limited slip range did not significantly affect the bond-slip behaviour at a larger slip than the peak slip in the previous cycles; on the other hand once the peak slip was increased, a considerable reduction in bond was produced at a lower slip in the subsequent load history.

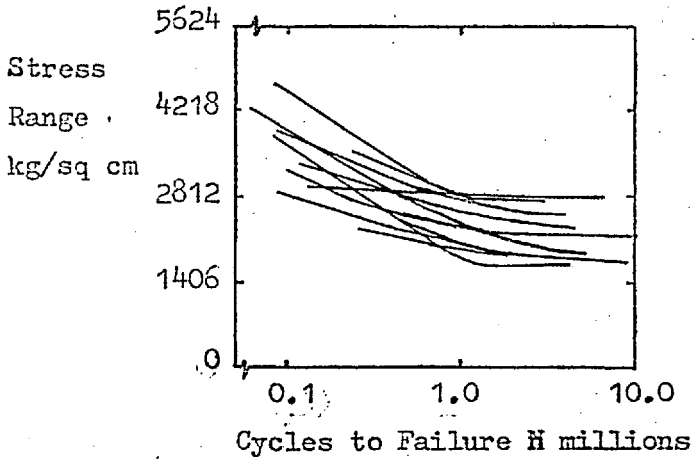
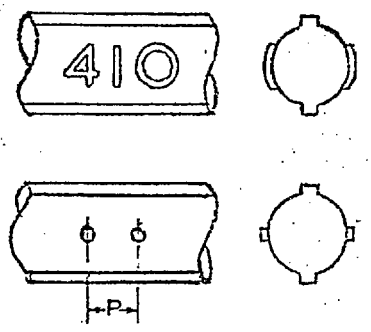


FIGURE 2.1 S - N CURVES FOR REINFORCING BARS

(From ACI Committee 215 - Ref. 18)



P = spacing of transverse lugs

FIGURE 2.2 MARKING OF DEFORMED BARS SPECIFIED BY BS 4449 : 1969

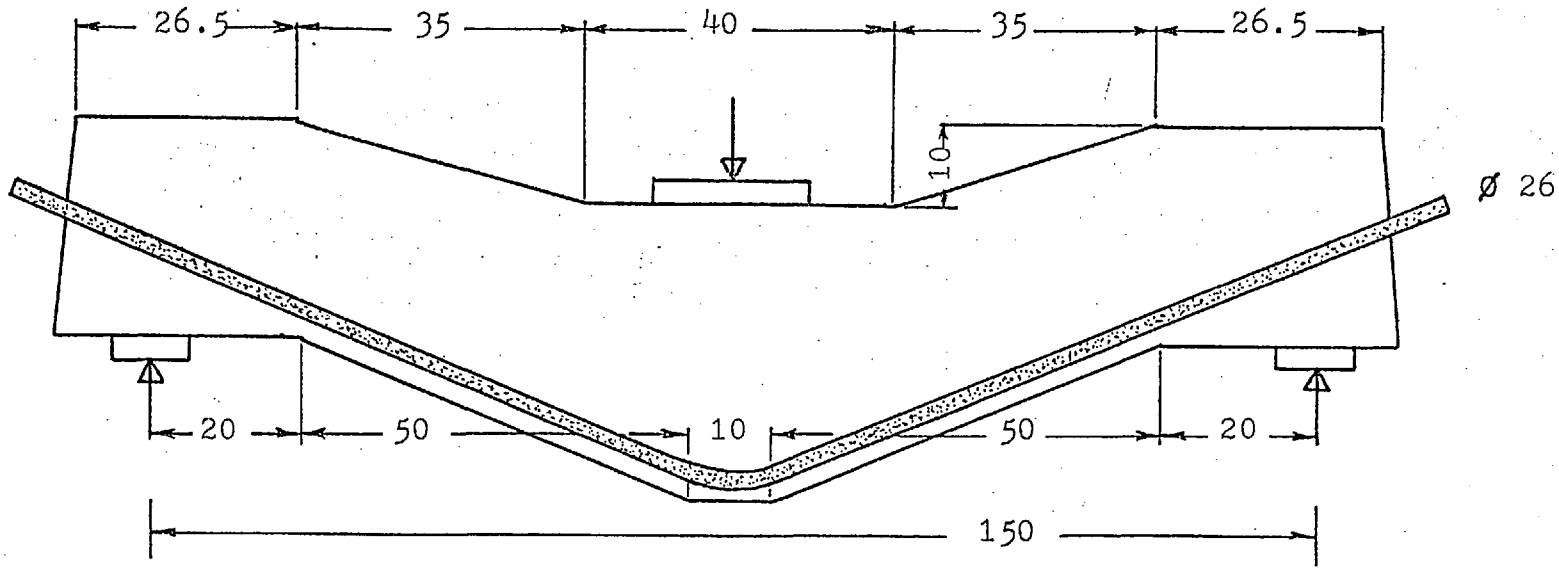


FIGURE 2.3 REHM'S SPECIMEN FOR TESTING EMBEDDED BARS

(Ref. 5)

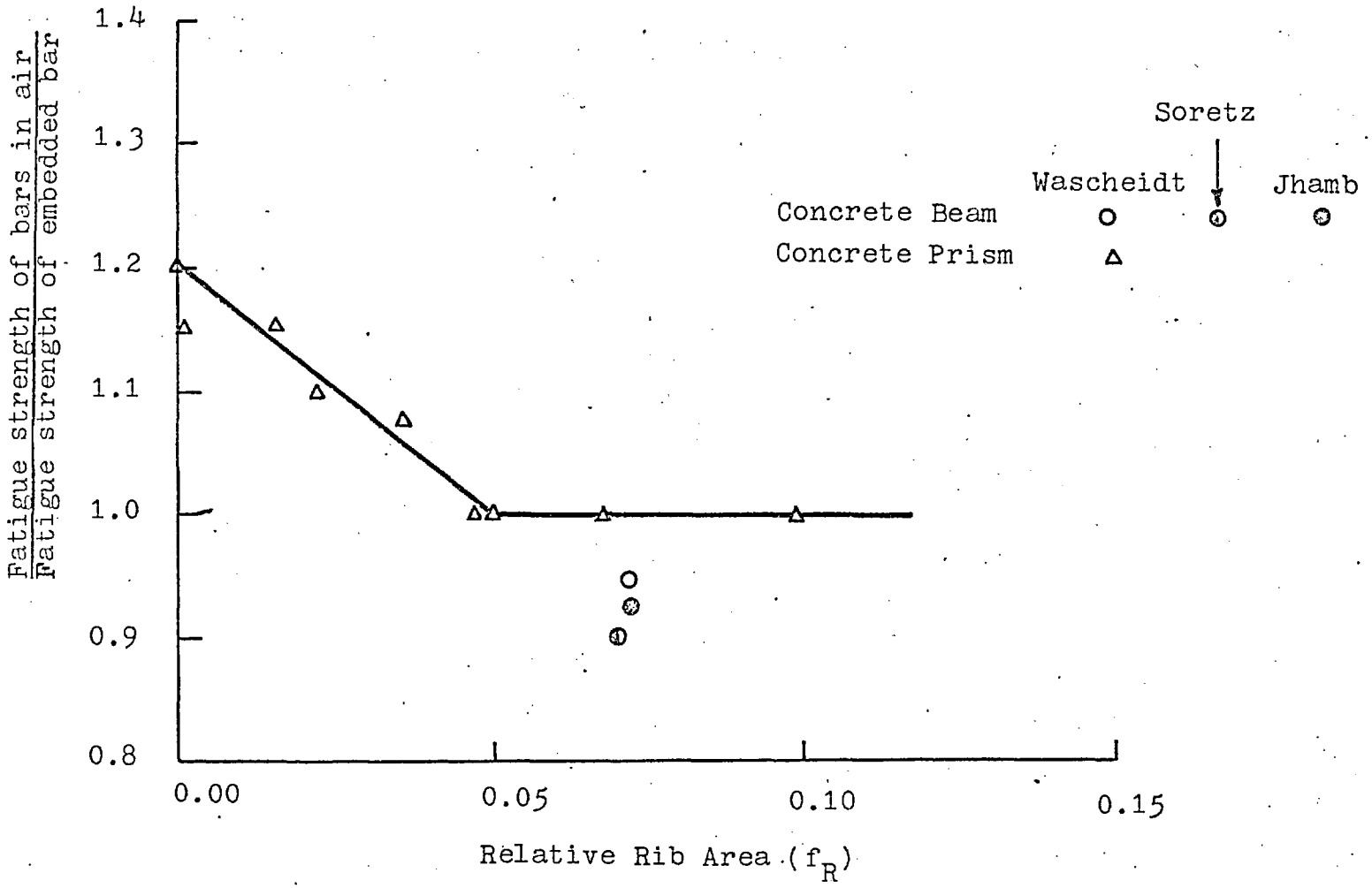


FIGURE 2.4 THE EFFECT OF CONCRETE EMBEDMENT ON FATIGUE STRENGTH

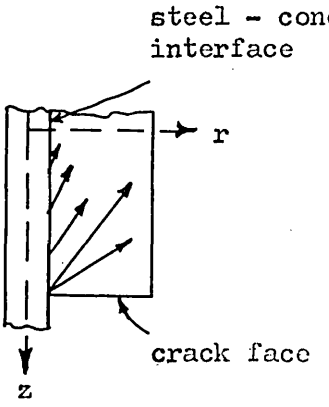
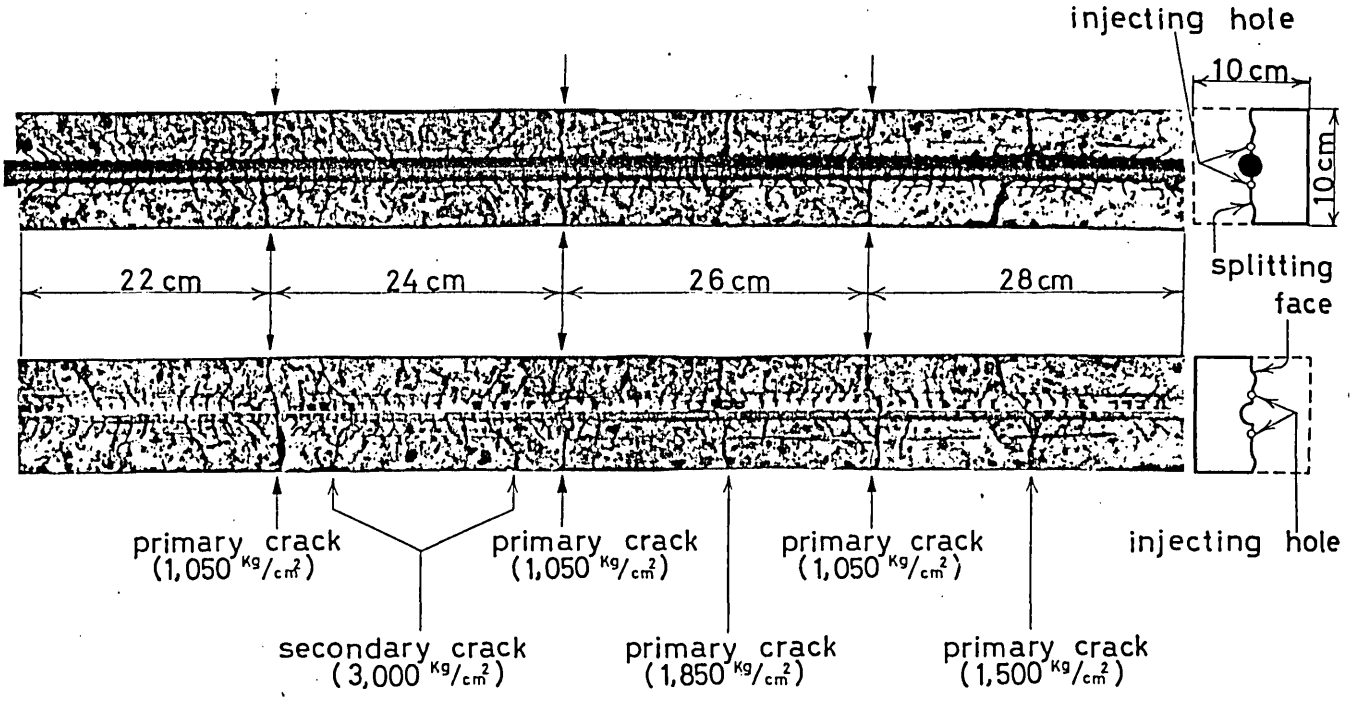


FIGURE 2.5 TENSILE PRINCIPAL STRESSES AT STEEL - CONCRETE INTERFACE
(From Bresler & Bertero - Ref. 37)



location of notch

( ) values in parentheses indicate steel stress at formation of cracks

FIGURE 2.6 INTERNAL CRACK AND SECONDARY CRACK WITH 19 MM BAR, LONGITUDINAL SPLITTING FACE AND CROSS SECTION.
(From Goto - Ref. 39)

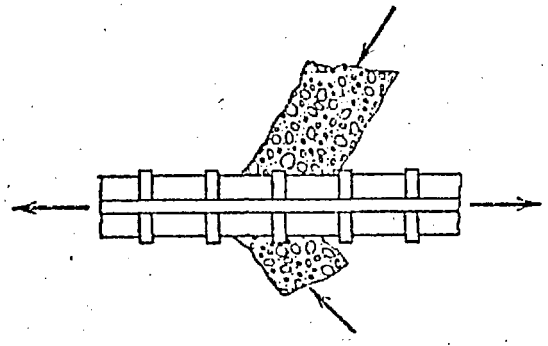


FIGURE 2.7 WEDGING ACTION IN RESISTING PULL-OUT

(From Watstein and Bresler - Ref. 33)

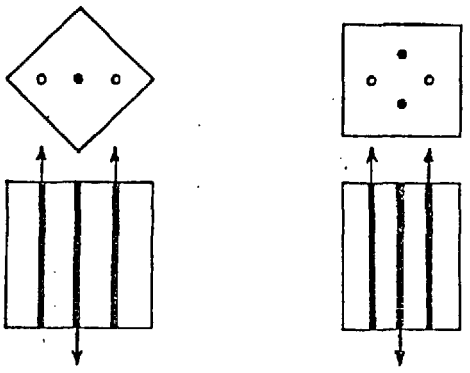


FIGURE 2.8 TENSION PULL-OUT SPECIMENS, SCHEMATIC

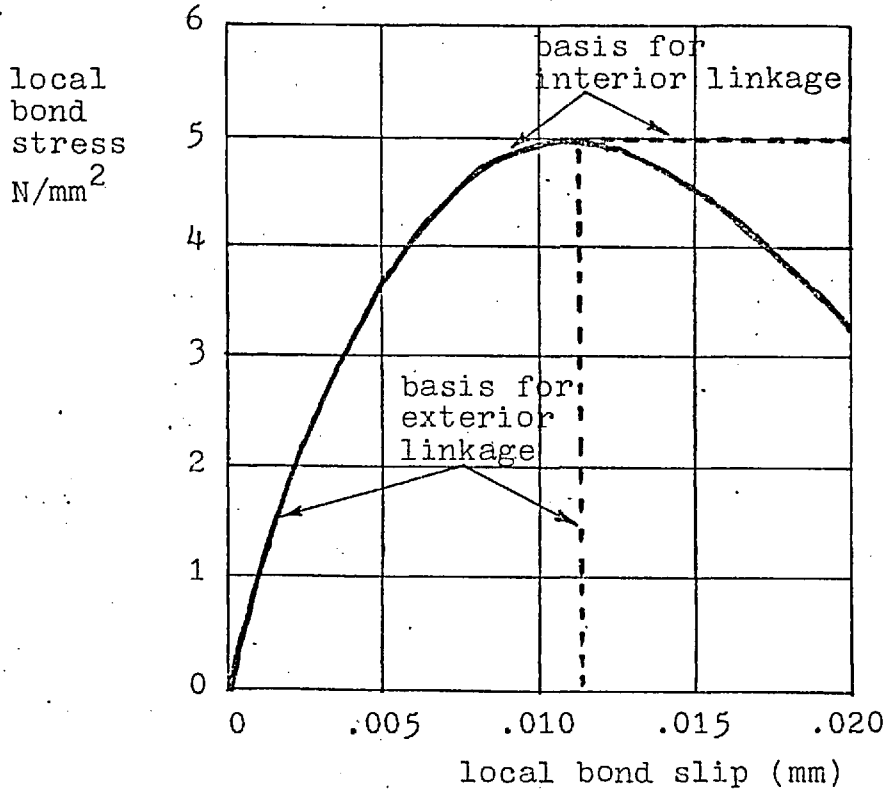


FIGURE 2.9 BOND-SLIP CURVE FOR 28.5 MM DIA. DEFORMED BAR

(From Nilson - Ref. 47, 48)

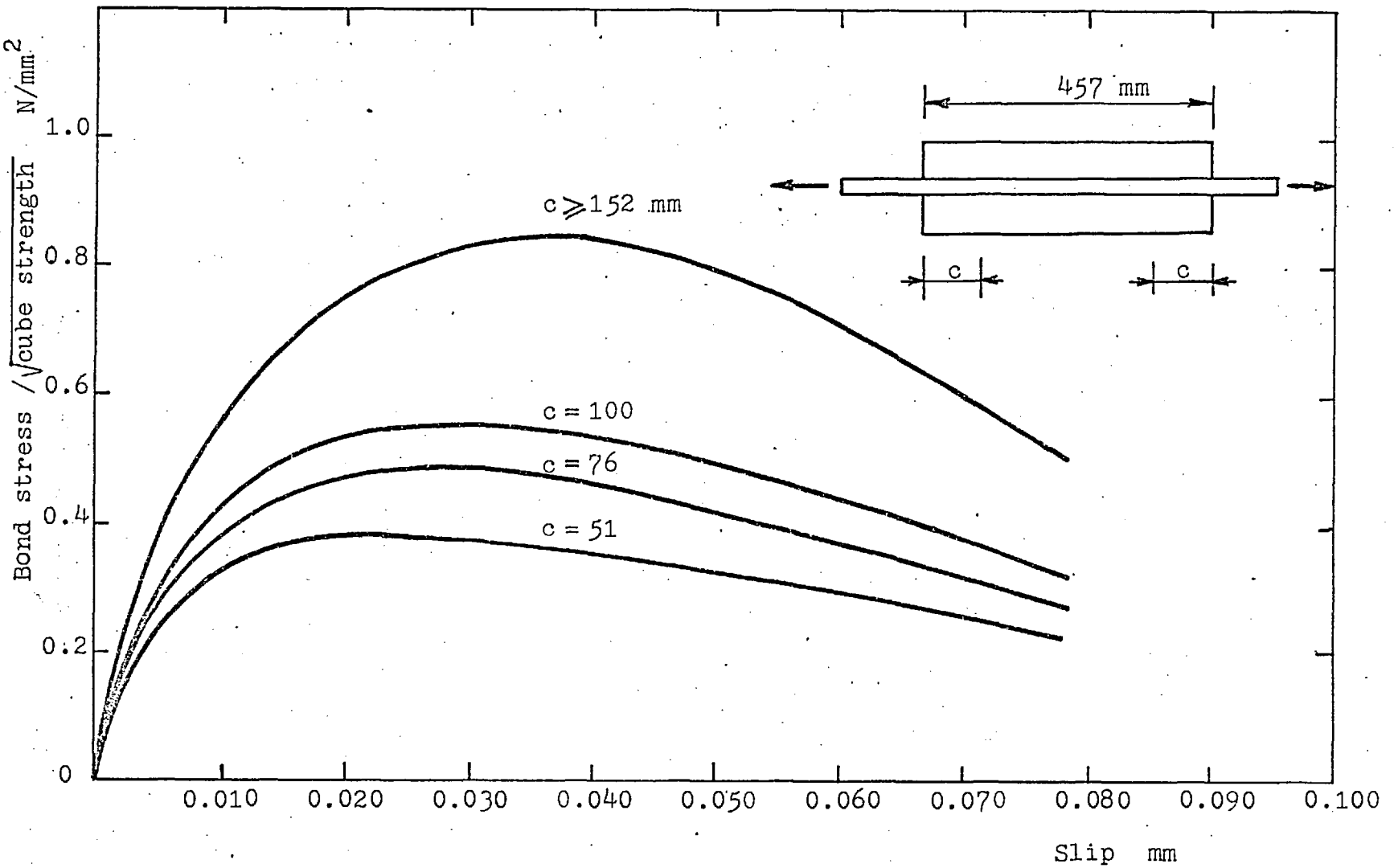


FIGURE 2.10 BOND-SLIP CURVES AT DIFFERENT DISTANCES FROM END FACE FOR 25 MM DIA. DEFORMED BAR

(From Nilson - Ref. 45)

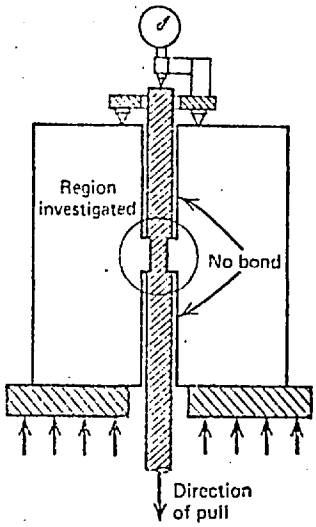


FIGURE 2.11 REHM'S BOND TEST ARRANGEMENT

(Ref. 50)

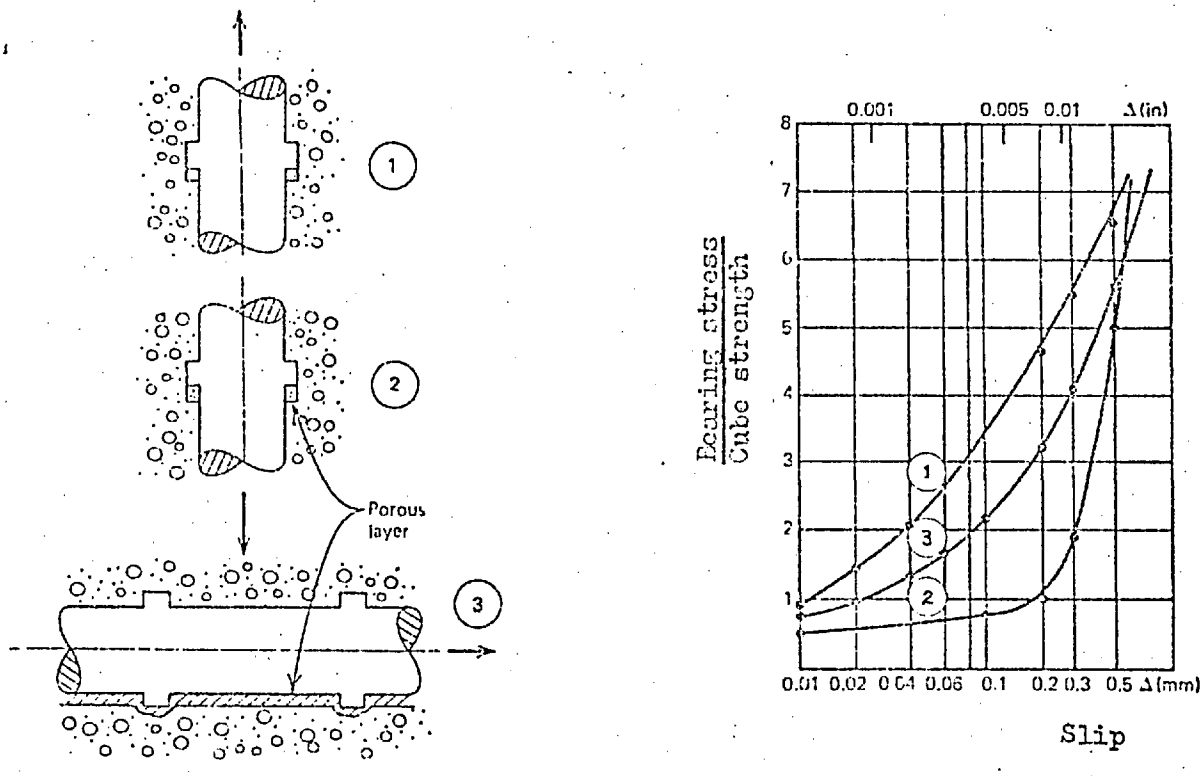


FIGURE 2.12 THE INFLUENCE OF CASTING POSITIONS ON BOND PERFORMANCE (From Rehm - Ref. 50)

1. Vertical bar pulled against slump direction
2. Vertical bar pulled in slump direction
3. Horizontal bar

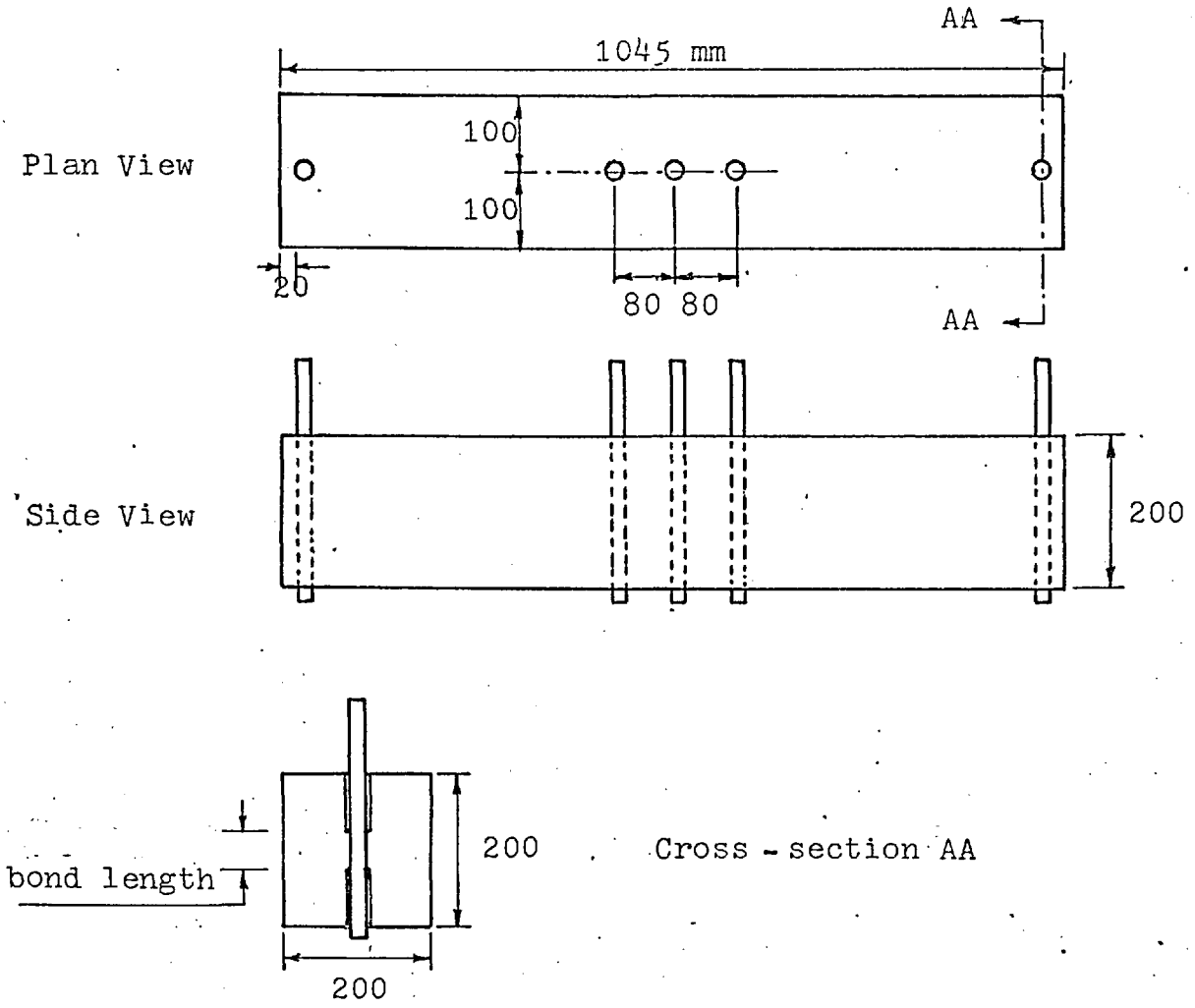


FIGURE 2.13 MORITA'S AND KAKU'S BOND SPECIMEN

(Ref. 54)

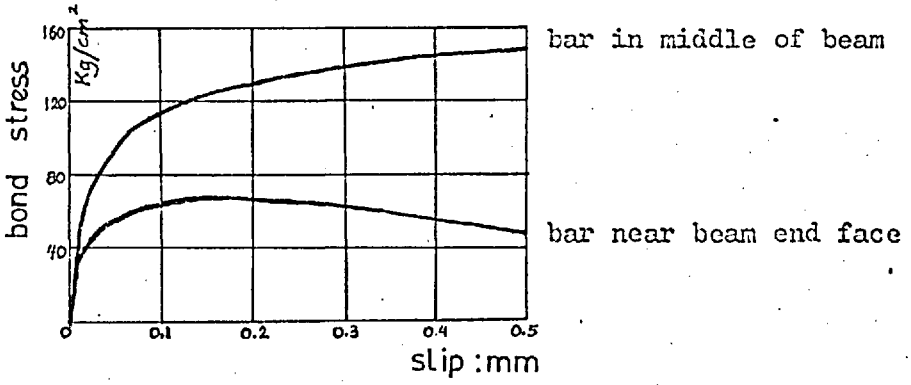
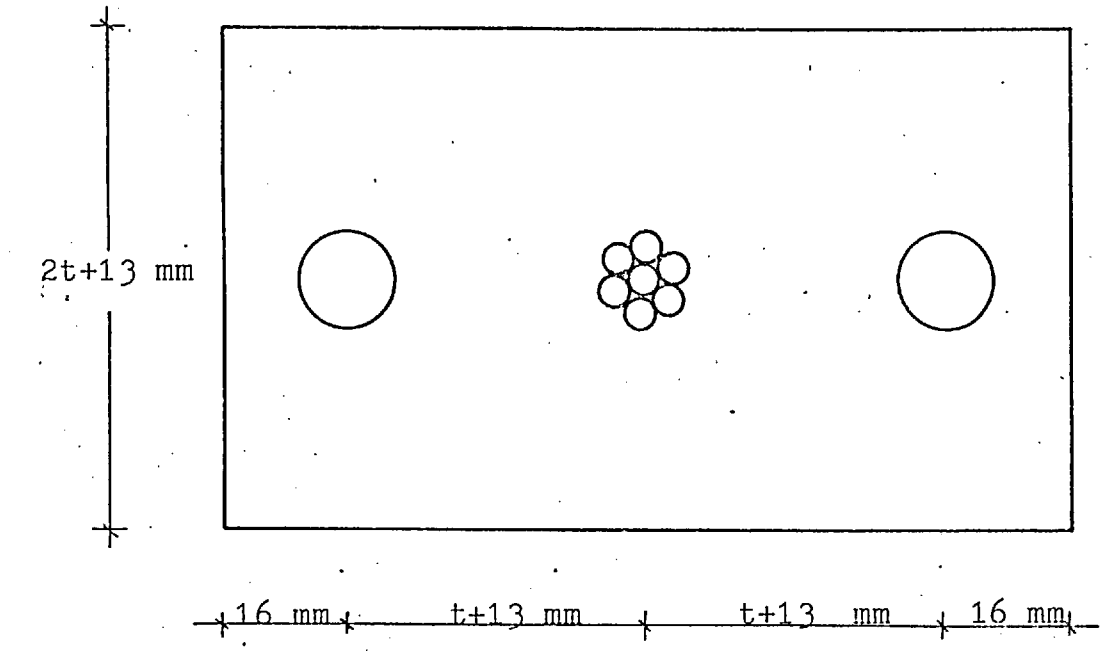


FIGURE 2.14 BOND-SLIP CURVES FOR 25 MM DIA. DEFORMED BAR

(Ref. 54)



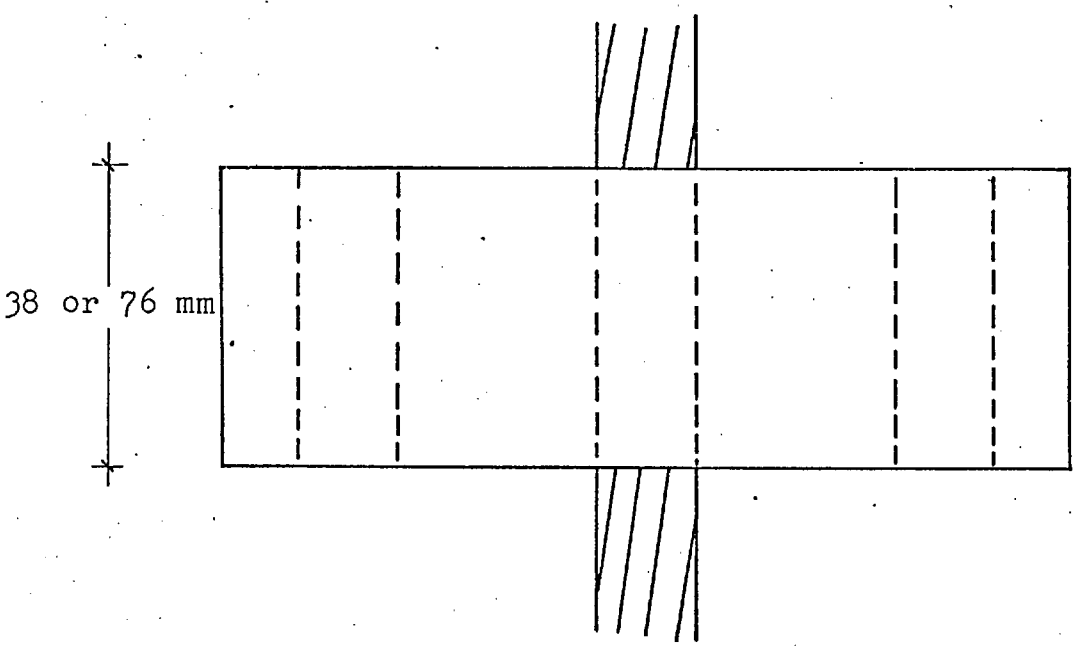


FIGURE 2.15 EDWARDS' & PICARD'S BOND SPECIMEN

(Ref. 56,57)

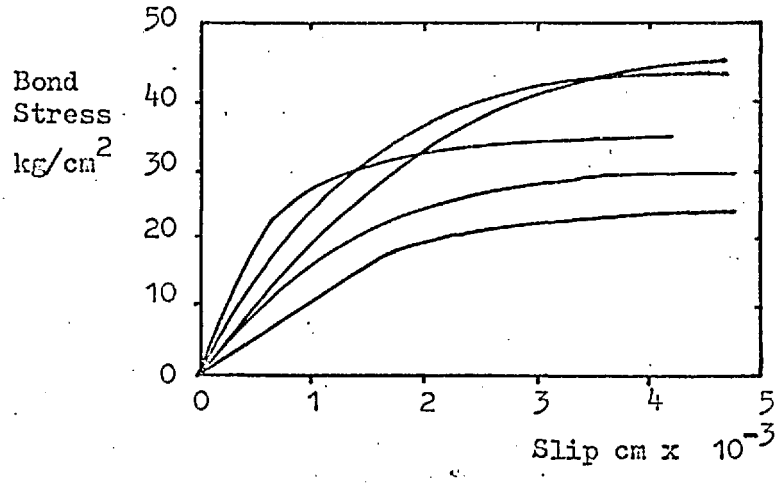


FIGURE 2.16 EXPERIMENTAL BOND-SLIP CURVES FOR STRAND

(From Edwards & Picard - Ref. 56,57)

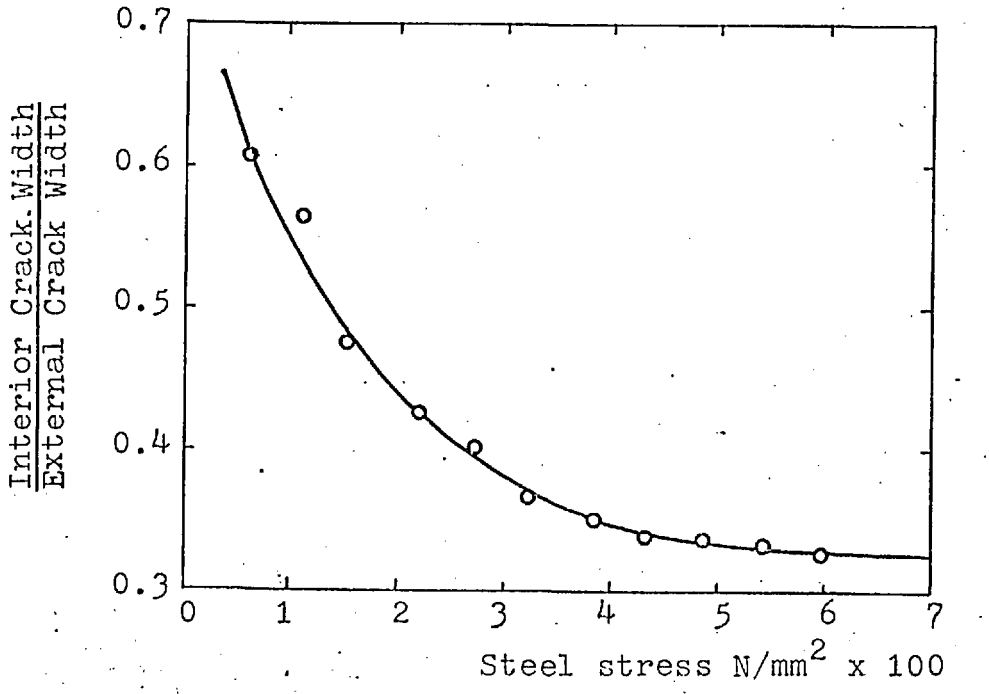


FIGURE 2.17 RATIO OF CRACK WIDTHS AT STEEL SURFACE TO CRACK WIDTHS AT CONCRETE EXTERIOR SURFACE VERSUS STEEL STRESS

(From Watstein and Mathey - Ref. 61)

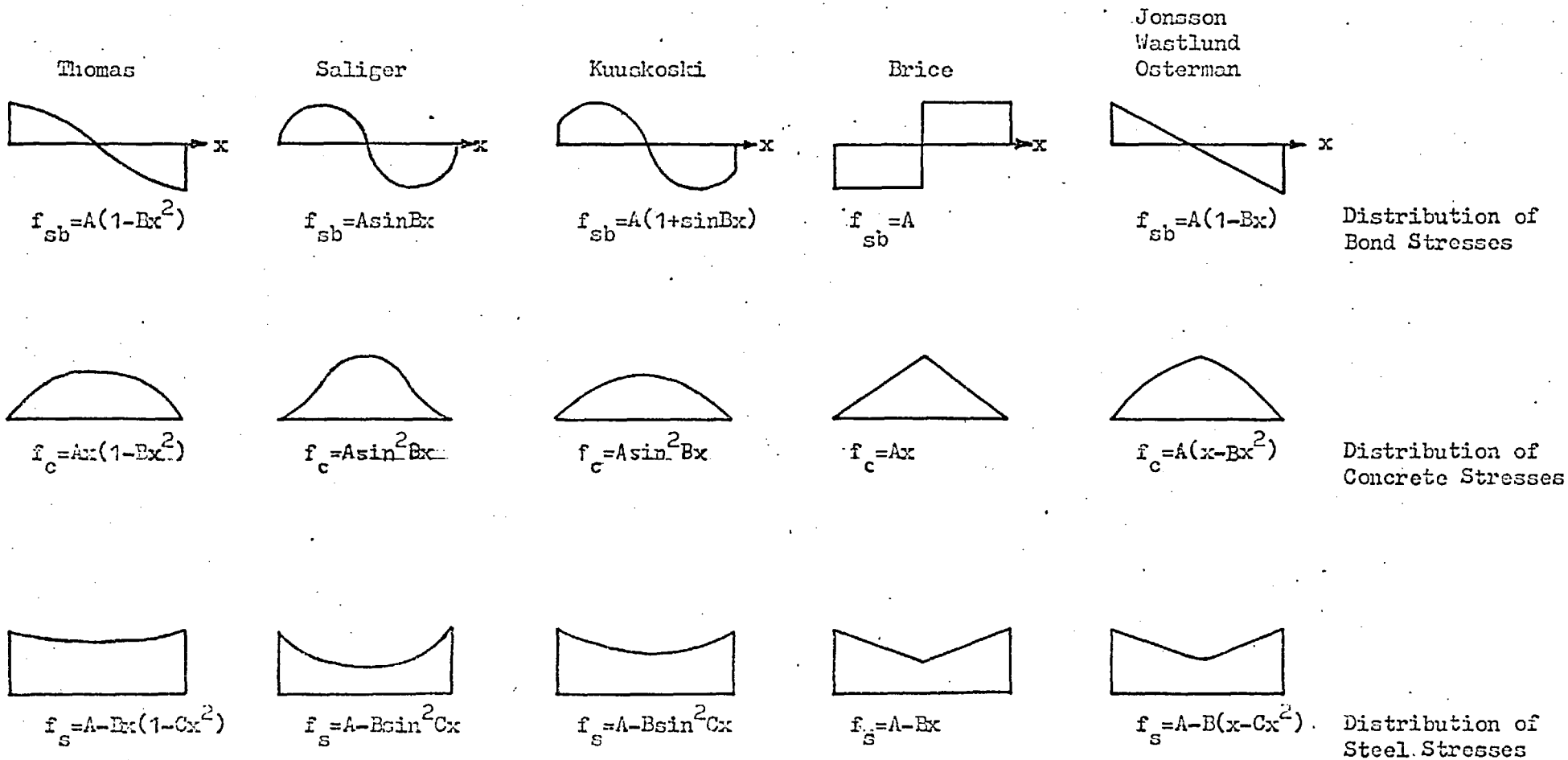


FIGURE 2.18 ASSUMED BOND DISTRIBUTION BY VARIOUS INVESTIGATORS AND RESULTING CONCRETE AND STEEL STRESSES

(From Ref. 58)

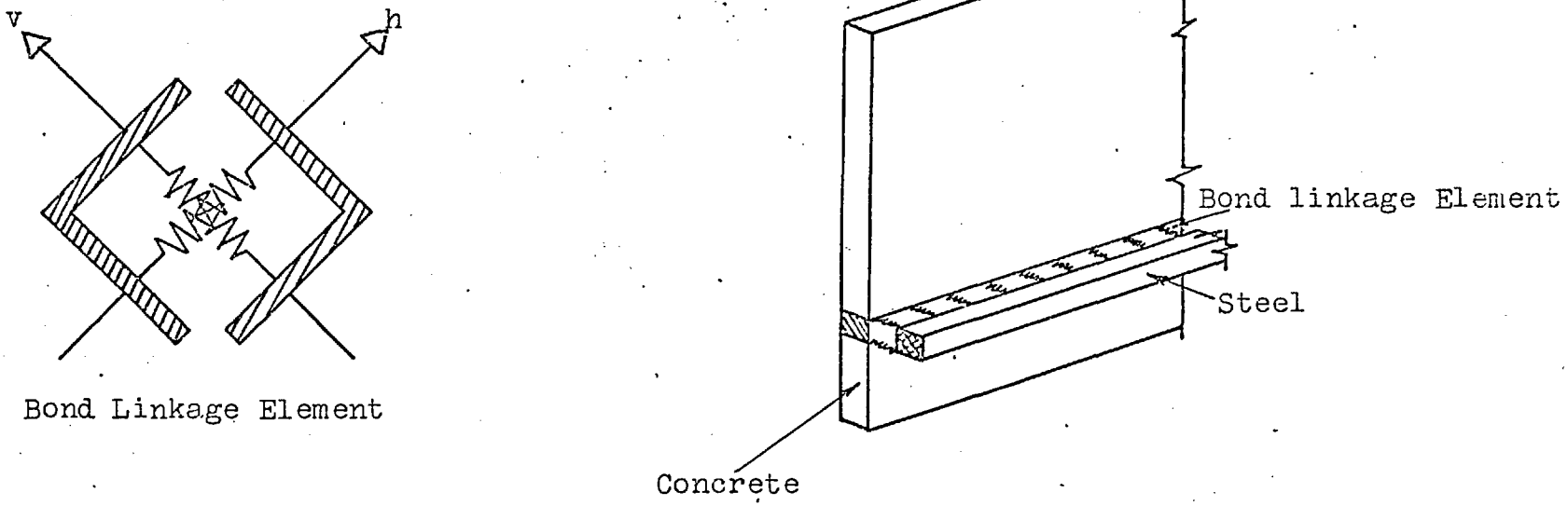


FIGURE 2.19 LINKAGE ELEMENT REPRESENTING BOND

(Ngo and Scordelis - Ref. 66)

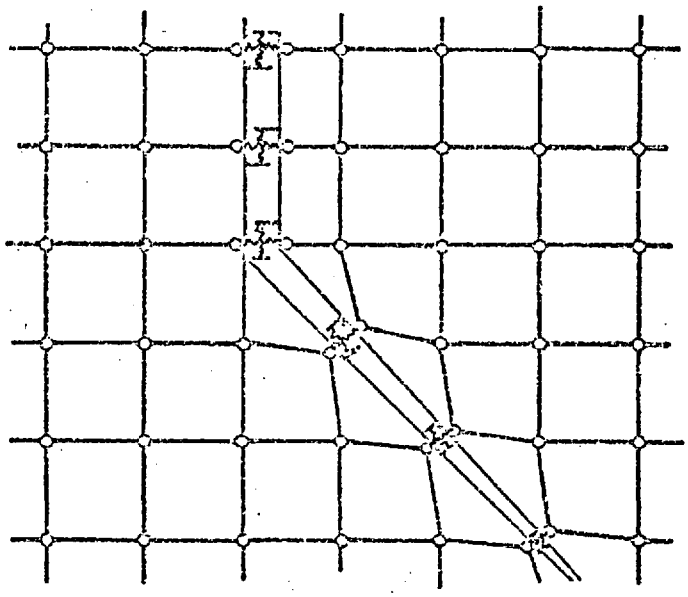
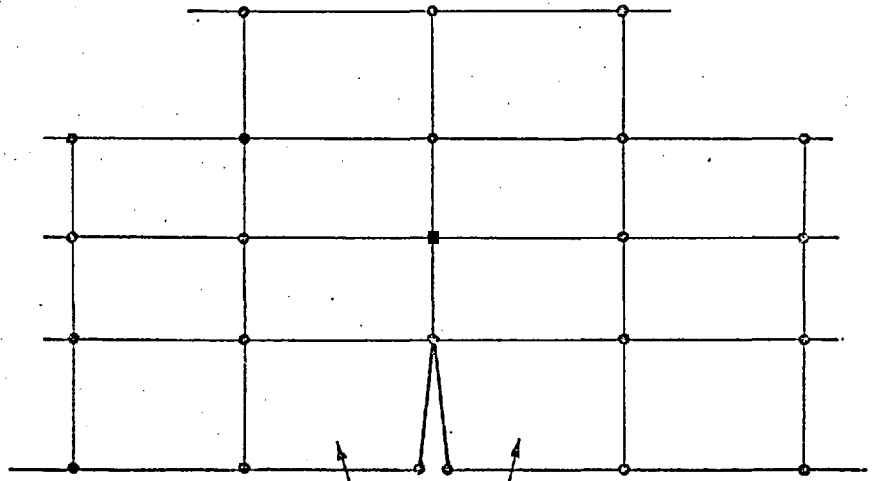
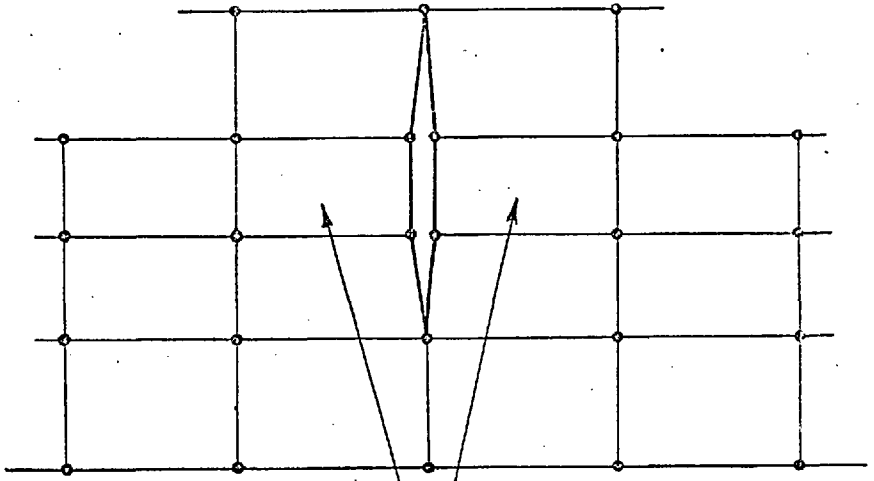


FIGURE 2.20 REPRESENTATION OF AGGREGATE INTERLOCK

(Ngo, Franklin and Scordelis - Ref 67)



Exterior Crack



Interior Crack

FIGURE 2.21 REPRESENTATION OF A CRACK WITH FINITE ELEMENT GEOMETRY

(From Nilson - Ref. 47,48)

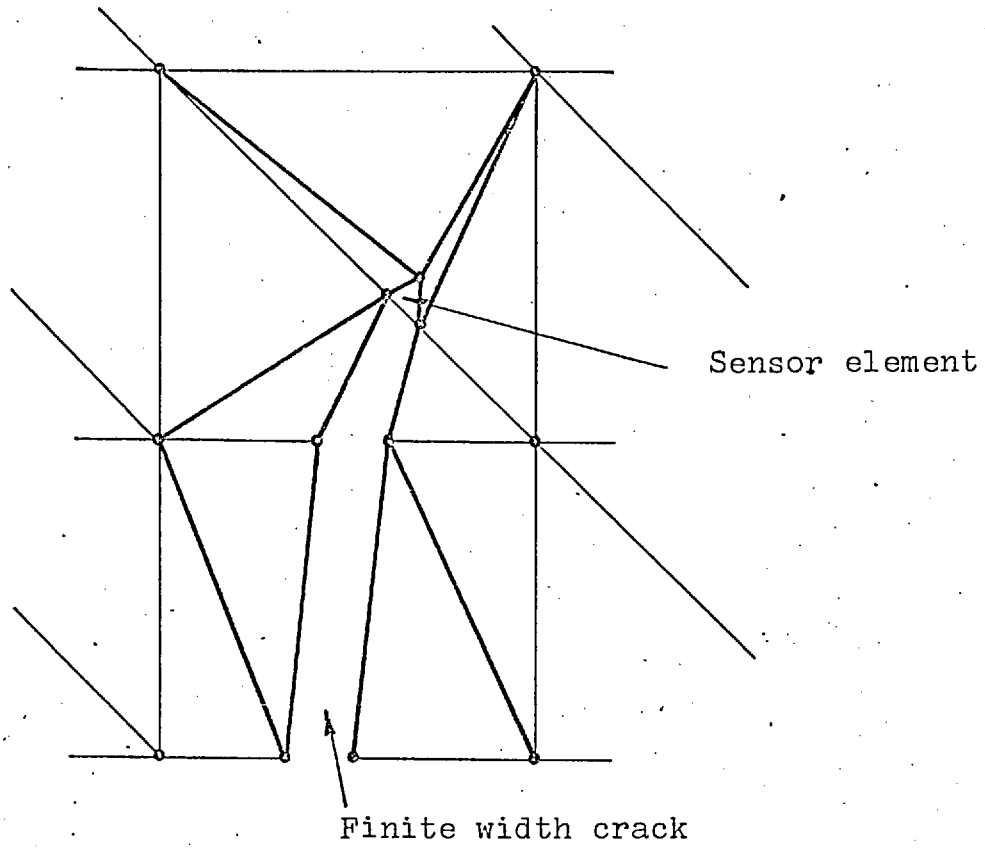


FIGURE 2.22 LOOV'S PROPOSED ANALYTICAL METHOD OF FOLLOWING CRACK PROPAGATION

(Ref. 72)

CHAPTER 3

EXPERIMENTAL TECHNIQUES AND PROCEDURE

3.1. MATERIALS AND THEIR PROPERTIES

3.1.1. CONCRETE

An ordinary structural concrete, of approximately 40 N/mm^2 characteristic strength, suitable for reinforced as well as pretensioned and post-tensioned construction, was adopted in the investigations. A trial mix was designed using D.S.I.R. Road Note 4 (77) and McIntosh's Design of Concrete Mixes (78). This was tested and modified until a desirable mix was obtained. The following mix proportions were used for all specimens :

Actual Water / Cement Ratio = 0.60
Effective Water / Cement Ratio = 0.48
Total Aggregate / Cement Ratio = 5.00

Ordinary Portland cement and Thames valley river aggregates were used, in the following proportions and sizes :

Fine sand : 12.2 % by weight
Coarse sand : 31.3 % by weight
3/8" aggregate : 25.5 % by weight
3/4" aggregate : 31.0 % by weight

Fine sand : that passing No.25 but retained on No.100 B.S.S.
Coarse sand : that passing 3/16" but retained on No.25 B.S.S.
3/8" aggregate : that passing 3/8" but retained on 3/16" B.S.S.
3/4" aggregate : that passing 3/4" but retained on 3/8" B.S.S.

The properties of the fresh concrete mix were as follows :-

Slump value ≑ 30 mm
Compacting factor = 0.98

Nearly fifty batches of concrete, about $1\frac{3}{4}$ cubic yards each, were mixed. The control specimens for each batch consisted of nine 4" (102 mm) cubes and three 9"x 6" (229 x 152 mm) diameter cylinders. Three cubes were tested in compression at 7 days and six cubes at 28 days. The three cylinders were used for splitting tests. The properties of the hardened concrete mix are given below :

	7 - day Compressive Strength	28 - day Compressive Stength	28 - day Splitting Strength
Average Value N/mm^2	26.7	43.4	3.3
C_v	8.9 %	5.4 %	6.5 %

Three cylinders were used to determine the stress-strain curve of concrete. The strains were measured by four electrical resistance strain gauges. These were manufactured by Tokyo Sokki Kenkyujo Co. Ltd., were 60 mm long, had a resistance of 120 $\pm$ 0.3 ohms and a gauge factor very nearly equal to 2.0. The four gauges were cemented at the mid-height of each cylinder and equally distributed around its periphery. Two of the gauges were parallel to the axis of the cylinder and the other two at 90° to that. Thus both axial and transverse strains could be measured. The gauges of each pair were connected in series and formed one resistance arm opposite to a 240 ohm dummy gauge arm of a Wheatstone bridge. The strain readings were read on a Peekel Strain Indicator. The obtained stress-strain curves for concrete are shown in Figure 3.1. The average Poisson's ratio value of concrete was found to be 0.15.

3.1.2. HOT ROLLED DEFORMED BARS

Four different, 16 mm diameter, hot rolled deformed bars were used in the bond and fatigue programmes. All four bars were made to BS 4449 : 1969 (79) with a specified characteristic strength of 410 N/mm^2, but having different deformation patterns rolled on them. The names of the bars are: Welbond, Jones, Sheerness and Unisteel (BSC), see Plate 3.1. The identification marks, as specified by clause 23 of BS 4449, are also seen on the bars of the same Plate.

The yield stress of the hot rolled deformed bars is:

Welbond	: 440 N/mm^2
Jones	: 420 N/mm^2
Sheerness	: 448 N/mm^2
Unisteel (BSC)	: 454 N/mm^2

A stress-strain diagram for a typical 16 mm diameter hot rolled Welbond bar is shown in Figure 5.1a. The modulus of elasticity, E, of all deformed bars was found to be 200,000 N/mm^2. The method of testing and all results obtained are given in sections 3.4 and 5.3.

All bars were free from rust when used in the bond and fatigue programmes.

3.1.3. HOT ROLLED MILD STEEL PLAIN BARS

Hot rolled mild steel plain bars, of 16 mm diameter, were used in the bond programme. They were manufactured by BSC to BS 4449 : 1969(79) with a specified characteristic strength of 250 N/mm^2. The modulus of elasticity, E, of the mild steel bars was found to be 200,000 N/mm^2, and their yield stress 297 N/mm^2. The method of testing is described in section 3.4.

All bars were free from rust when used in the bond programme.

3.2. DETAILS OF SPECIMENS

3.2.1. SPECIMENS FOR FATIGUE TESTS

3.2.1.1. SPECIMENS FREE IN AIR

Hot rolled deformed bars were received in 6 metre lengths from the rolling mill. Specimens were cut fromm these lengths and given a number which was used for randomising

their test allocation. Bars of 800 and 1300 mm length were cut for use as specimens free in air with 400 and 900 mm test lengths respectively. Any identification marks present in the test length were removed by filing and the corresponding area of the bar polished. A specimen held in between the test rig's gripping devices is shown in Plate 3.2.

Special grips were developed for the specimens so that fatigue failures did not occur within the grips. These were of a type enabling load to be applied approximately uniformly to the specimen over the length gripped into the four wedges described in section 3.3. These grips consisted of a 5 mm thick half round piece of leather and two pairs of 1.5 mm thick soft aluminium pieces, shown in Plate 3.3b. The piece of leather was shaped round the bar by force. The aluminium pieces were formed by cutting a 30 mm diameter tubing into lengths and splitting them in half. Coarse carborundum powder was glued on the inside face of the aluminium pieces to reduce slipping over each other and over the leather.

The end of a specimen held in the gripping device is shown in Plate 3.4a. With this arrangement approximately 85 % of the fatigue failures occurred within the test length. A further improvement was achieved by work hardening the bar ends to be gripped using the peening apparatus shown in Plate 3.3a. At each end approximately 100 mm of the bar length was surface treated, 90 mm of which was within the grips and the rest in the test length. This increased the fatigue resistance of the bar ends and approximately 95 % of all failures occurred

within the test length.

3.2.1.2. SPECIMENS EMBEDDED IN CONCRETE

To investigate the effect of concrete cracking on the fatigue strength of hot rolled deformed bar, concrete cylindrical tension specimens of 76 mm diameter were used with a 16 mm deformed, Welbond bar cast along their axis (Figure 3.3). Accurate steel moulds were made and the deformed bar was held in position by locating plates at the top and bottom ends of the mould, as shown in Plate 3.8. The length of the bar was 1300 mm, while the test length was 900 mm long, with the central 800 mm embedded in concrete. Any identification marks present in the test length were removed before casting. The two 50 mm lengths on either side of the concrete, as well as the bar lengths to be held in the grips, were surface treated, before casting, with the peening apparatus, so that failures would occur in the length embedded in concrete. A specimen held in between the test rig's gripping devices is shown in Plate 3.5. A general view of the test rig is shown in Plate 3.6.

The casting and curing procedure was the same for all specimens and is fully described in section 3.2.2.2.

3.2.2. SPECIMENS FOR BOND TESTS

3.2.2.1. SPECIMENS DETAILS

Basic specimens were cast in moulds of two sizes, depending on the concrete cover required to the bar (Figure 3.2 and Plate 3.7). Welbond deformed and plain 16 mm bars were

used. The larger specimens had a concrete cover of 35 mm, while the smaller specimens had one of 25 mm. The length of embedment was chosen to be 38 mm long or four times the deformed bar lug spacing. The ideal would have been to use an infinitesimally small bonded length, so that the basic law of bond would be determined directly in the form of a relationship between local bond stress and local slip. However there are limits to the chosen length depending on the uniformity of the steel surface, the maximum aggregate size and the relative effect of boundary conditions on total length. Also practical considerations suggest that the bonded length must not be too short because imperfections in the specimens which occur during casting and handling are likely to produce relatively large scatter in the test results.

The steel moulds of the basic specimens were accurately made and two circular bars were placed into them with the reinforcing bar to obtain 16 mm diameter holes in the basic concrete specimens. These holes were used to connect two calibrated bars which measured the bond stress as explained in section 3.6.2.

Tensile specimens, 76 mm in diameter and 800 mm long, reinforced with a 16 mm diameter Welbond deformed bar embedded along their axis (Figure 3.3 and Plate 3.8), were used for obtaining crack width data when tested in tension. These specimens were the same as the corresponding ones used for the fatigue tests, except that the identification marks present in the test length were not removed and the ends of the bar on either side of the concrete were not surface treated.

Pull-out specimens, 76 mm in diameter and of lengths of 100 or 200 mm, reinforced with a 16 mm diameter Welbond deformed bar along their axis (Figure 3.4), were cast using the same moulds as those used for the tensile specimens, except that only part of the moulds was used, the rest being suitably plugged out.

3.2.2.2. CASTING AND CURING

Nearly fifty batches of concrete, about $1\frac{3}{4}$ cubic yards each, were mixed. Each batch of concrete was enough for casting eight basic specimens, three tensile specimens, three pull-out specimens and a number of control specimens as given in section 3.1.1.

Dry aggregates and water were placed in the mixer and the cement added after they had been thoroughly mixed. The same mixing procedure was followed for all batches.

Febstrike releasing agent was applied to the inside of all the moulds prior to casting. Concrete in the moulds was vibrated by suitably attaching the moulds to a 'V-B' (Vebe) vibrating table.

The specimens were left in the moulds under wet hessian and polythene sheeting for 24 hours. The specimens were then removed from the moulds and put into a tank filled with water for six days. Then they were taken out of the water, Febstrike was applied on them and were stored in the laboratory atmosphere (approximately 20° C and 65 % R.H.) for three weeks until testing.

3.3. DESCRIPTION OF TEST RIG

A general view of the rig used in all fatigue tests is shown in Plate 3.6.

The rig was designed with a safety factor of 3.0. The two rectangular reinforced concrete columns are 610 x 380 mm in cross-section, and the two mild steel rectangular box beams 305 x 203 x 13 mm. The two columns and the bottom beam were stressed to the floor by means of 35 mm diameter Macalloy bars. One end of the top beam was fixed to the jack and the other end was completely free to rotate in the plane of the rig. This end of the top beam was bolted to a plate with two protruding shafts which were free to rotate within Skefko self-aligning roller bearings.

Each gripping device had one end fixed to one of the box beams and the other end used to grip the specimen. The gripping devices were both completely free to rotate in the plane of the rig and in a vertical plane perpendicular to the plane of the rig. The gripping devices were made of mild steel plates and Skefko self-aligning spherical roller bearings.

Each bar specimen was gripped by means of four wedges which fitted into a tapered opening drilled in a steel block 100 mm thick, as shown in Plate 3.4b. To reduce slipping of the specimen in the grips, especially during the early stages of the test, the inside of the wedges was serated and an anchorage with a plate were put on the bar just behind the four wedges. High grade tool steel was used for the making of the block and the wedges, having an angle of inclination

of nine degrees, were specially heat hardened, after machining.

The length between the top and bottom grips was approximately 890 mm. Mild steel extension plates were added to the top and bottom grips, when a reduced test length was required.

Suitable load ranges could be obtained by using different capacity hydraulic jacks. The Amsler jack used in the test rig was connected by rigid steel pipe to a distributor which was in the turn connected to the pulsator, as shown in Plate 3.6. The pulsator was operated by an Amsler programme control unit.

3.4. STATIC TESTS ON HOT ROLLED DEFORMED BARS AND MILD STEEL PLAIN BARS

Static tests on 16 mm diameter hot rolled deformed bars and mild steel plain bars were carried out in a 35-ton Amsler universal testing machine. This was calibrated using a proving ring, before starting the tests. Load could be applied with a sensitivity better than $\pm$ 100 Newtons.

Load was transferred from the machine to the specimen through specially shaped Amsler grips, allowing practically no slip of the bar in the machine jaws. A test length of 400 mm of bar was used in all tests.

Load was applied by means of an Amsler hydro-pacer unit, connected to the testing machine, at a rate of 20,000 Newtons / minute throughout each test to failure. The yield point and modulus of elasticity of the reinforcement were determined from

a plot of an electronic extensometer fixed to the test piece.

3.5. FATIGUE TESTS ON HOT ROLLED DEFORMED BARS FREE IN AIR AND ON HOT ROLLED DEFORMED BARS EMBEDDED IN CONCRETE

3.5.1. LOADING EQUIPMENT

The load was applied by means of an Amsler hydraulic pulsator through an Amsler hydraulic jack. The jack used in the fatigue programme had a 10 ton static and 5 ton dynamic load capacity. The load in the specimens was twice the jack load, since these were gripped halfway between the beam supports.

The testing machine was capable of applying a sinusoidal load cycle varying between two limits. These were measured with an electronic pressure transducer fixed directly to the jack. The minimum and maximum loads were set on two separate precision potentiometers on the Amsler programme control unit, which were calibrated in divisions representing 1 % of the static load capacity of the jack. Additionally the output from the pressure transducer fixed to the jack could be read on an externally connected voltameter, thus making possible to apply the loads with a sensitivity of $\pm$ 0.1 % of the jack static capacity or $\pm$ 100 Newtons.

The range of frequencies available of application of the oscillating load was 200 to 800 cycles/minute. A reset counter on the Amsler control unit indicated the number of loadings, to the nearest 1000 cycles, applied to the specimens. The machine could be stopped automatically when it reached a preset number of cycles or when a preset

decrease in minimum load or increase in maximum load occurred. If the machine or the test specimen started to vibrate significantly or the specimen fractured, the machine was stopped automatically by means of a seismic cut-out fixed to the top beam of the test rig.

The minimum and maximum loads indicated by the potentiometers on the control desk corresponded to the fluctuating hydraulic pressure within the cylinder of the jack, and consequently to the load applied to the test specimen by the pressure oil only. However, the effective forces acting on the specimen were greater/smaller than the ones corresponding to the hydraulic pressure, the factor being due to the acceleration of the oscillating heavy top beam of the test rig and the oscillating parts of the jack. The sinusoidal load cycle produced by the pulsator on the jack ram, as well as the effective load cycle, are shown in Figure 3.5. Knowing the weights of the moving parts, the testing speed and the elongation of the specimen for a given stress range, the accelerating force was calculated from formulae provided in an Amsler Instruction Manual (80), and is given by:

$$P_b = w^2 s \frac{W}{g}$$

where P_b = accelerating force on specimen due to inertia of moving masses

w = angular velocity

s = elongation of specimen in a load cycle

W = effective weight of moving masses(top beam and moving parts of jack)

g = acceleration due to gravity

The accelerating force, P_b, was calculated for each load range to be applied to the specimen and the pulsator adjusted to produce the desired effective loads, i.e. the maximum presure gauge indicated a load which was smaller by P_b than the desired maximum load and the minimum pressure gauge indicated a load which was bigger by P_b than the desired minimum load. The maximum correction applied, in the case of the maximum stress range used in the tests, was found to be 0.4 % of the characteristic strength of deformed bar, for a 400 mm specimen test length.

3.5.2. STATIC AND DYNAMIC CALIBRATION OF LOADING EQUIPMENT

The test rig and its loading equipment used in the fatigue programme were statically calibrated using a 10-ton proving ring. The proving ring was held in between the gripping ends of the test rig by means of high yield steel bars, as shown in Plate 3.9 and load was applied to it through the hydraulic jack at the right hand end of the top beam.

The recommendations of BS 1610 : 1964 on "Methods For The Load Verification of Testing Machines" (81) were followed for the calibration of the test rig by means of a proving ring. This was loaded three times to its maximum test load which was maintained for one-and-a-half minutes, before starting any calibration. The constant true load procedure of verification was followed for the calibration of the test

rig, i.e. the machine was operated to balance a given applied load as indicated by the proving ring and the reading on the pressure gauge of the machine was then taken. Five series of eight test loads were applied.

The greatest difference between the indicated loads corresponding to the five repeated applications of the true load was less than 0.5 % of the true load specified for the repeatability of class A_1 machines in BS 1610 : 1964.

Dynamic calibration of the test rig was carried out following the guiding principles of DD2 : 1971 Draft British Standard (82) on dynamic force calibration of axial load fatigue testing machines by means of a strain gauge technique. A calibration bar was used in between the test rig's gripping ends and connected to a Peekel electronic strain indicator and an oscilloscope, as shown in Plate 3.10. The strain recording instrument was suitable for both static and dynamic strain measurements. The middle 50 mm of the calibration bar was waisted down to a diameter of 20.8 mm, suitable for the load ranges to be checked. Four electrical resistance foil strain gauges, of 1 million cycles fatigue resistance, were attached to this portion of the bar, two being parallel to the bar axis and the other two transversely to it and equally distributed around the periphery of the bar. The four gauges were connected to form a full Wheatstone bridge, fully compensated against temperature changes, and the calibration bar was calibrated statically in an Amsler universal testing machine, of known accuracy. The calibration bar was then used for the calibration of the fatigue testing rig, assuming

identical performance under static and dynamic conditions.

For the dynamic calibration a sinusoidally varying strain, Plate 3.11a, was applied by the pulsator to the calibration bar. This picture was obtained on the screen of an oscilloscope connected to the dynamic strain recording instrument. Then the strain recording instrument was used to balance the strain gauges at the instant of maximum strain and further at the instant of minimum strain. The system employed in this strain gauge apparatus is the carrier-frequency method. Alternating current at a carrier frequency of 1000 cycles/second was applied to an adjustable bridge circuit and by means of a phase sensitive demodulating circuit and a low pass filter the carrier frequency was modulated with the fatigue force waveform and the output observed on an oscilloscope. The figures of Plates 3.11b and 3.11c appeared on the screen of the scope when there was a capacitive unbalance or an unadjusted phase of the oscillator voltage on the strain gauges respectively. When both were correctly adjusted, by turning the slide wire scale on the strain recording instrument the line AA was made horizontal, as in Plate 3.11d, which corresponded to the peak value of the vibrating strain. By turning further the slide wire scale the reverse picture was obtained with the line AA again being horizontal, as in Plate 3.11e. This corresponded to the other peak valve of the vibrating strain. By reading the two positions off the slide wire scale the maximum and minimum values of the vibrating strain were obtained. All photographs were obtained by means of a special Polaroid camera mounted on the

screen of the oscilloscope and shown in Plate 3.10.

The above procedure was followed for other stress ranges and each calibration was repeated four times. The greatest difference between the indicated strains corresponding to the five repeated applications of the vibrating stress was less than 1.0 % of the average strain at maximum stress, as specified in DD2 : 1971.

The values obtained from the dynamic calibration of the test rig were compared with those obtained from the calculation of the accelerating forces, given in section 3.5.1, and were found to be in good agreement.

3.5.3. TESTING PROCEDURE

The recommendations of BS 3518 : Part 3 : 1963 on "Methods of fatigue testing——Direct stress fatigue tests" (83) were followed in the fatigue testing programme.

Every specimen before being tested was visually examined and if any surface faults were observed or the specimen was not straight, it was rejected. Then a specimen was inserted into the test rig and gripped at each end by means of four wedges which fitted into a tapered opening in the test rig's gripping devices. These were of a type enabling the load to be transmitted axially to the whole of the test piece (section 3.3). The wedges were coated with wax prior to insrting them into the gripping devices, so that after fracture of the specimen the broken bar pieces could be easily forced out of the grips. Load to the bar was applied through the special grips, described in section 3.2.1,

which ensured a nearly uniform distribution of force in the area of contact between the test piece and the grips. Slipping of the bar in the grips, especially during the early stages of the test, was avoided by putting a plate and an anchorage on the bar just behind the four wedges. A specimen mounted into the test rig is shown in Plate 3.6.

The minimum desired test load was first applied to the specimen and the load amplitude was then continuously increased, as rapidly as possible but without jerking, until the maximum desired load was reached. The same procedure was followed for attaining full load running conditions for each specimen.

After starting the pulsations and for the whole of the test, the maximum and minimum loads were periodically checked to ensure that the required conditions were maintained. This was particularly necessary during the first hour or so of testing.

All fatigue tests were carried out without interruption to failure or terminated at one and a half million cycles of loading in case of no failure. When the specimen failed under the fatigue loading the machine stopped automatically. The number of cycles to failure were recorded and the pieces of the fractured bar were taken out of the grips, properly identified and preserved for examination of the fracture surfaces and their location on the bar.

3.6. BOND TESTS ON HOT ROLLED DEFORMED BARS AND MILD STEEL PLAIN BARS

3.6.1. LOADING EQUIPMENT

The bond tests were carried out in the same rig as the fatigue tests. Load was applied by means of an Amsler pendulum dynamometer and an Amsler hydropacer unit through the 10-ton jack as shown in Plate 3.12. A suitable load range was used on the spring dynamometer which gave a sensitivity of $\pm$ 0.1 % of the jack static capacity or $\pm$ 100 Newtons. The load was controlled and kept constant at any level by the hydropacer unit. Before starting the bond tests the rig and loading equipment were calibrated using a proving ring as described in section 3.5.2. The repeatability of application of load was better than 0.5 % of the true load specified for class A_1 machines in BS 1610 : 1964 (81).

3.6.2. INSTRUMENTATION AND TESTING PROCEDURE

For the basic bond tests, on specimens with a short length of embedment, a mild steel plate, 25 mm thick, was placed on top of the specimen before holding the bar into the rig's top gripping device by means of an anchorage. Then two calibrated bars, which measured directly the bond forces, were fixed into a rigid frame and connected to the specimen by means of two nuts which were carefully tightened so that no forces were read in the calibrated bars before loading. Two induction type linear displacement transducers were then attached to the top of the specimen and two at the bottom of it to measure the top and bottom slip between the steel bar

and concrete block as shown in Plate 3.13. The transducers were attached to the reinforcing bar at a short distance from the concrete surface; the top transducers at 35 mm from the the 25 mm thick steel plate and the bottom transducers at 35 mm from the 25 mm thick perspex blocks stuck on the bottom concrete surface. Due to the elongation of the reinforcing bar between the concrete surface and the point where the transducers were attached, it was necessary to correct the measured slips, as explained in section 6.2.1.

Two types of basic bond tests were carried out : (a) tests with the bottom end of the steel bar free and (b) tests with a back load applied to the bottom end of the bar. These two types of loading are shown schematically in Figure 3.6.

The loading procedure described above was that for tests with no back load. For tests with a back load, the two calibrated bars were not attached to the specimen until the back load was applied to the bar by means of a prestressing jack and anchorage as shown in Plate 3.12. The jack was operated by a hand pump and the back load, measured by a load cell, was held constant throughout the test by putting a hydro-pneumatic accumulator into the jack oil system as shown in Plate 3.14. The accumulator had a synthetic compound bag filled with nitrogen fed from a N_2 bottle. The oil pressure acting around the bag was equilibrated by the nitrogen within the bag, when the accumulator was functioning. The operation of the system depended on the small compressibility of the oil as compared to the large one of the nitrogen gas. During

the test oil presure was thus kept practically constant with this arrangement.

In the basic bond tests, under monotonically increasing loading, both the slips and the load in the calibrated bars were measured at different load stages until fracture of the specimen. In the case of basic bond tests, under repeated loading, a sufficient number of load stages were employed to define the loading and unloading paths of each load cycle, as well as the final path to failure. The strains in the calibrated bars were read on a Peekel Strain Indicator and slips were recorded by a Sogenique linear displacement measuring unit. The load in the bars was measured with a sensitivity of $\pm$ 7 Newtons and the slips with a sensitivity of $\pm$ 0.00001 mm. All the instrumentation is shown in Plate 3.12.

To avoid bending in the calibrated bars, due to twisting of the steel bar, which would have affected the readings, the bars were connected to a rigid frame incorporating axial thrust ball bearings as shown in Figure 3.7. All parts of this frame were designed so that their deformations were negligible compared to the measured slips. The rigid frame was bolted to the top of the test rig's bottom gripping device as shown in Plate 3.13. With this arrangement, the basic bond specimens were free to rotate in an horizontal plane and any twisting of the steel bar did not affect the calibrated bar readings.

Tensile bond tests were carried out on specimens with an 800 mm length of steel bar embedded in concrete. Load was applied to the specimen through the bar ends held by means

of anchorages into the test rig's gripping devices as shown in Plate 3.15a. Load was measured with a load cell put next to the bottom anchorage. Crack widths on the concrete surface were measured by means of a microscope, along four lines running parallel to the bar axis and equally spaced around the periphery of the concrete member. The microscope had a magnification power of 50 and was fitted with a graticule marked in 0.02 mm divisions. Demec points were fixed every 100 mm on the four lines on the specimen and a 100 mm (4") demec gauge was used to take readings of the concrete surface strain.

All the above readings were taken at a number of load stages. Also every crack appearing on the concrete surface was marked with ink and its extend at each load stage was denoted by a number as shown in Plate 3.15b.

Pull-out tests were carried out on specimens with a concrete length of 100 or 200 mm. The smooth end face of the concrete member was held against a 25 mm thick steel plate, fixed in the test rig's top gripping device, and which had a central hole through which the reinforcing bar could just pass. The loaded end of the reinforcing bar was held by an anchorage and a steel plate in the test rig's bottom gripping device as shown in Plate 3.16.

Load was applied through the 10-ton Amsler hydraulic jack and the top gripping device and it was measured with a load cell put next to the bottom anchorage. Slips between the reinforcing bar and the concrete were measured both at the loaded end and free end of the specimen. This was done by

using a special assemblage of displacement transducers shown in Plate 3.16 and Figure 3.8. Three induction type linear displacement transducers were clamped at 120° spacing around the perimeter of the bar a short distance from the concrete face. At the loaded end of the specimen these transducers contacted the fixed plate against which the concrete member was bearing. At the free end of the specimen the three transducers contacted a smooth steel plate with a 19 mm inside diameter and 1.5 mm thick sleeve which was glued to the concrete surface.

The load cell microstrain was read on a Peekel Strain Indicator and the loaded-end and free-end slips recorded by the Sogenique linear displacement measuring unit used in the basic bond tests. All these readings were taken at a number of load stages in the linear stress-strain range of the material of the steel reinforcing bar.

STRESS-STRAIN CURVES FOR CONCRETE

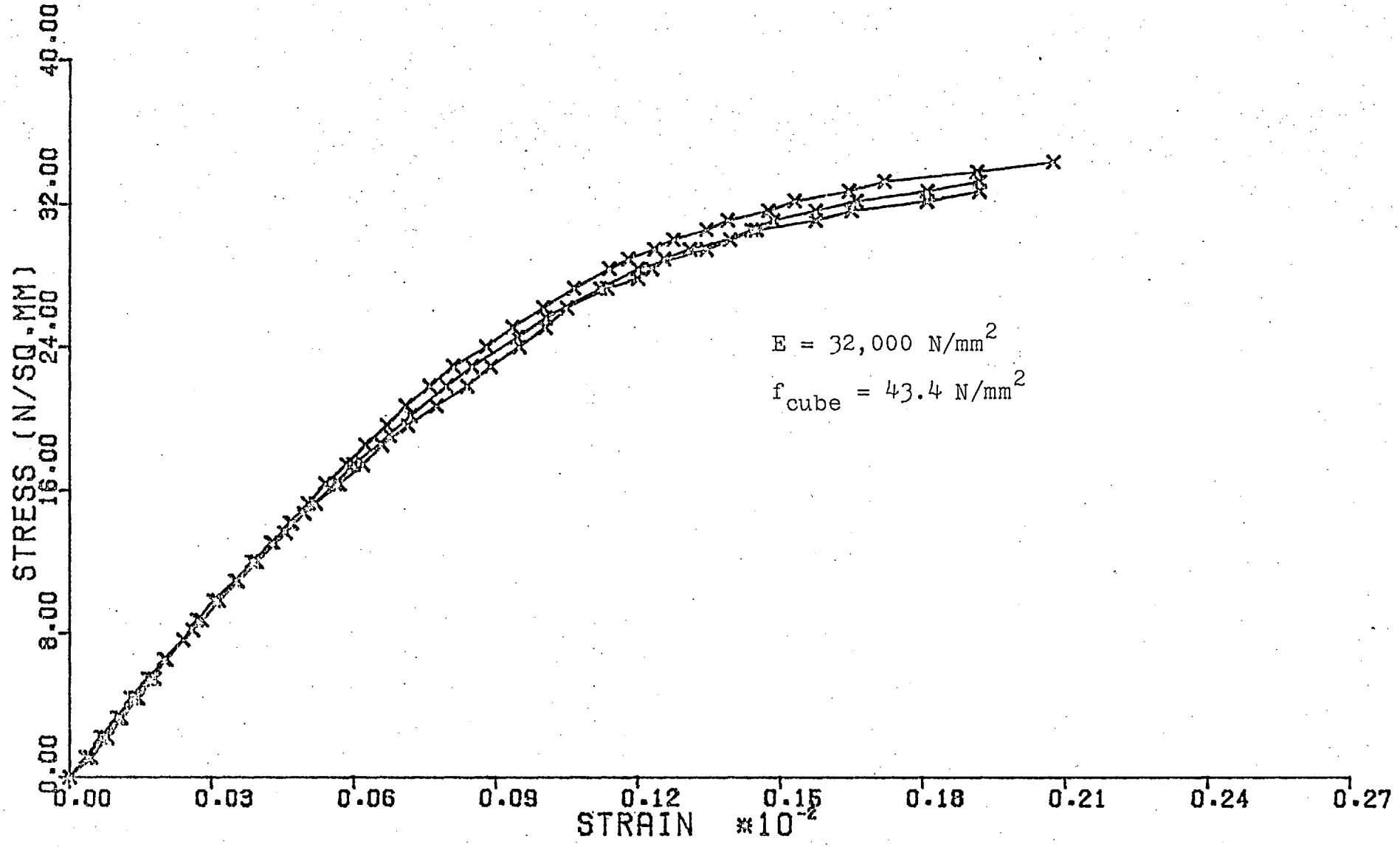


FIGURE 3.1

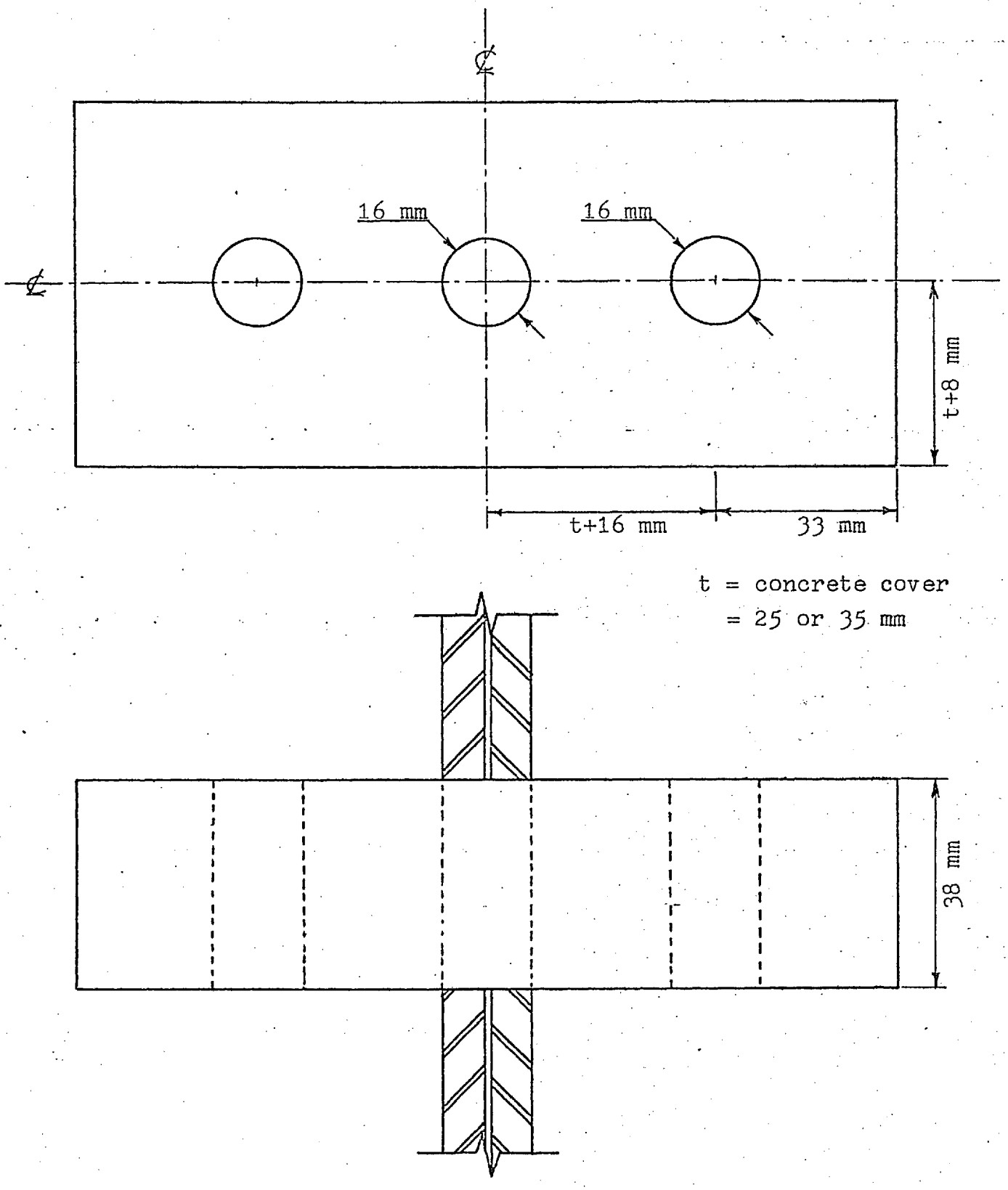


FIGURE 3.2 BASIC SPECIMENS FOR BOND TESTS

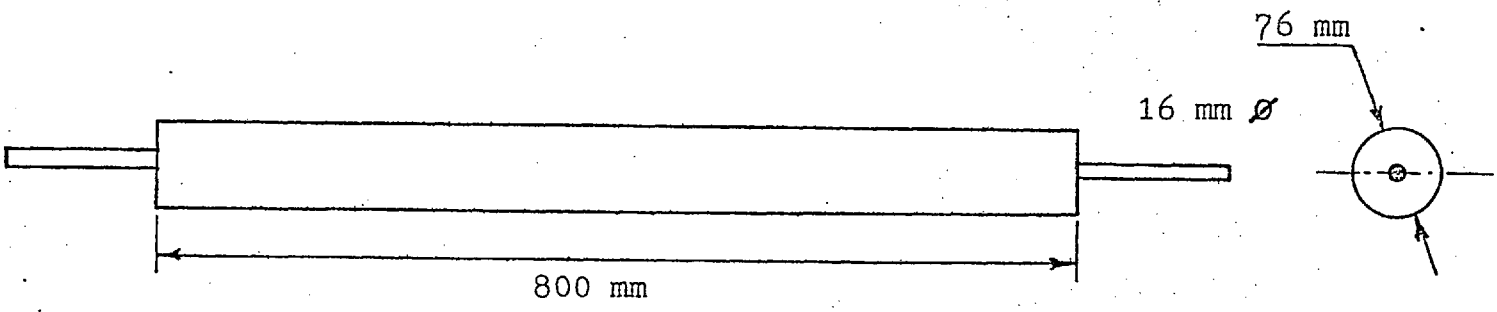
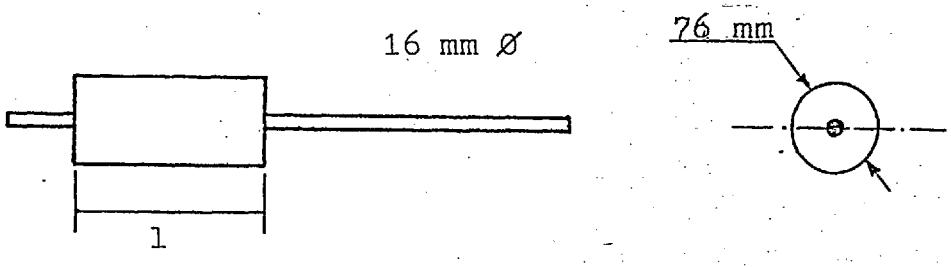
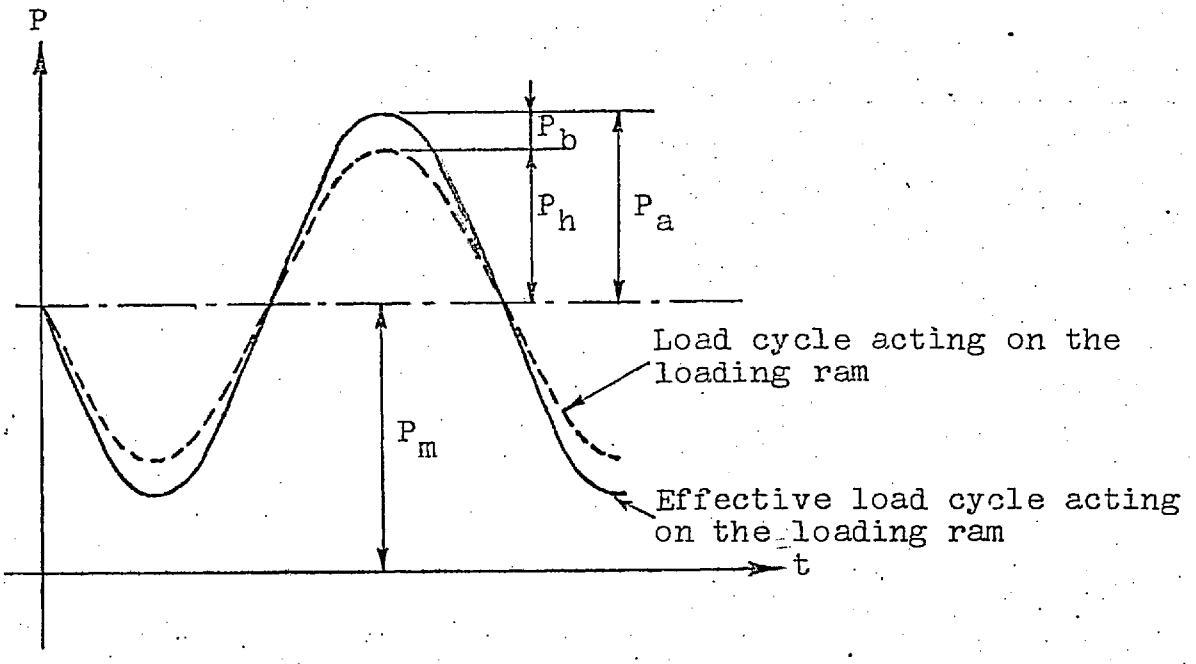


FIGURE 3.3 TENSILE SPECIMEN FOR FATIGUE AND BOND TESTS



l = 100 or 200

FIGURE 3.4 PULL - OUT SPECIMEN FOR BOND TESTS



P_m = Mean load

P_h = Load amplitude acting on the loading ram

P_a = Load amplitude acting on the specimen

P_b = Accelerating force due to the inertia of the moving masses

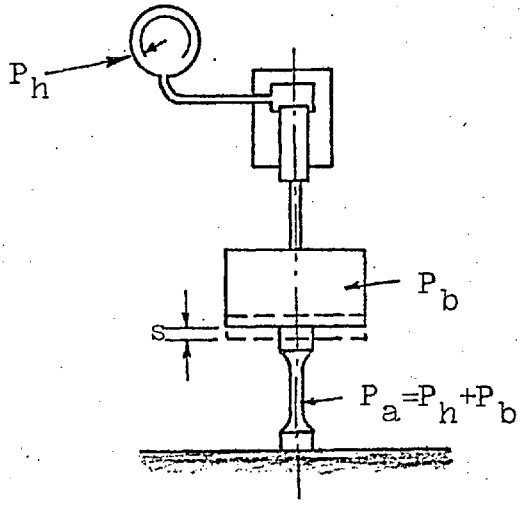
2s = Stroke of the moving masses

C = Elastic constant of the specimen

w = Angular velocity

W = Effective weight of moving masses

g = Acceleration due to gravity



$$P_b = w^2 \, s \, \frac{W}{g}$$

$$s = \frac{P_a}{C}$$

$$\therefore P_b = \frac{w^2 \, W}{C \, g} P_a$$

FIGURE 3.5 FLUCTUATION STRESS TEST

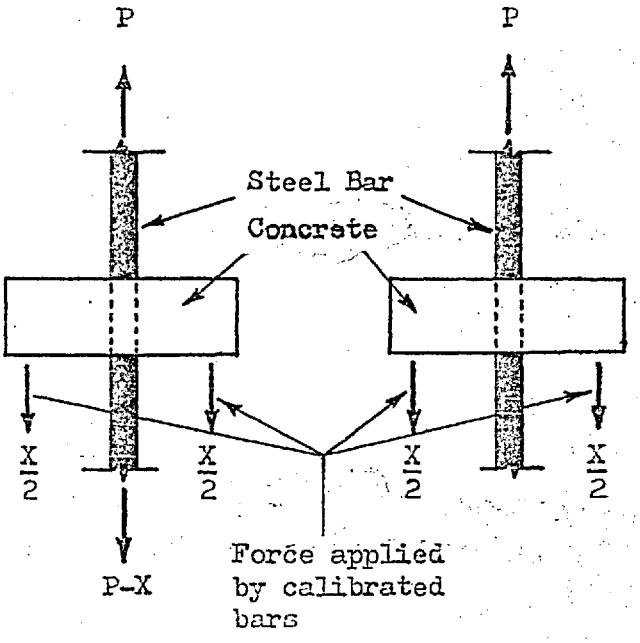


FIGURE 3.6 BASIC BOND TESTS LOAD SYSTEM

(a) With back load

(b) No back load

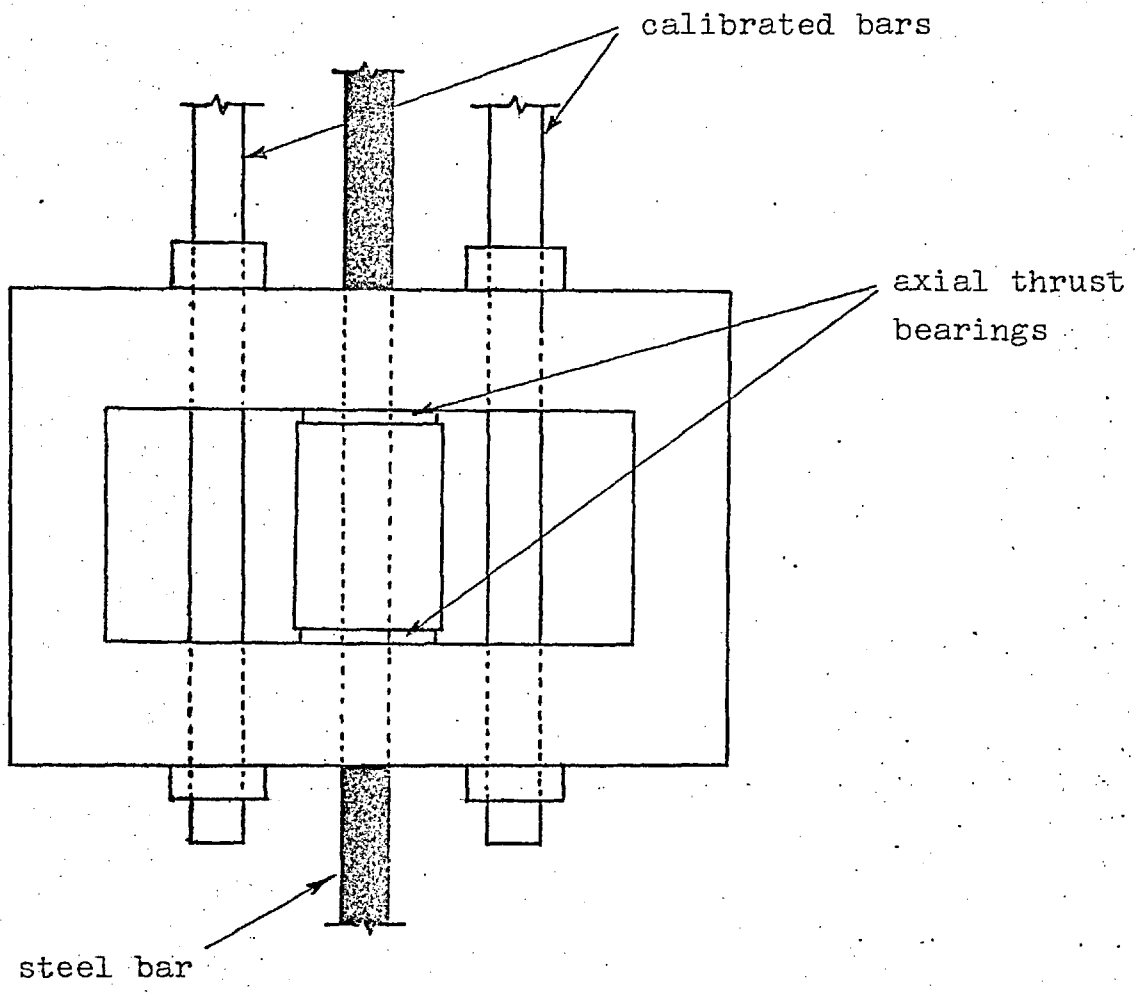


FIGURE 3.7 CALIBRATED BARS CONNECTED TO RIGID FRAME FOR MEASUREMENT OF BOND FORCES

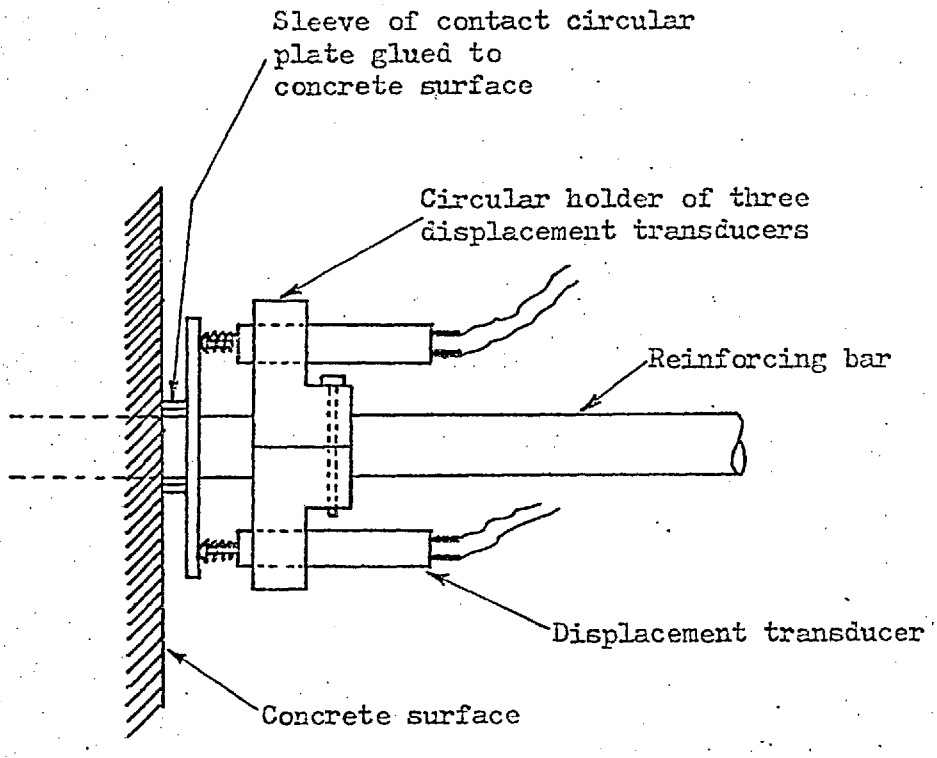


FIGURE 3.8 DISPLACEMENT TRANSDUCER ASSEMBLY USED IN MEASURING END SLIP

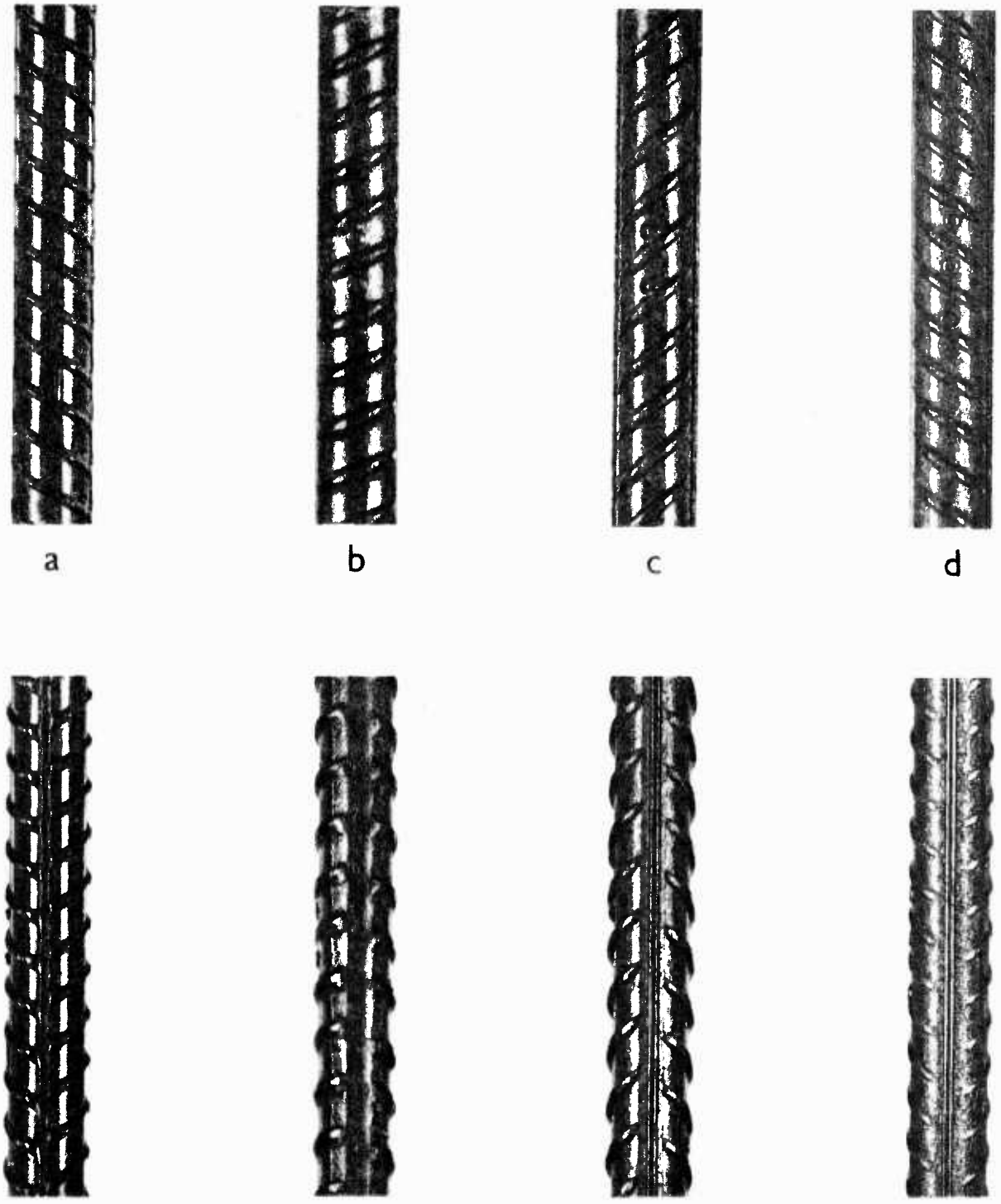


PLATE 3.1 HOT ROLLED DEFORMED BARS - 16 MM DIAMETER

Two views at 90° orientation

(a) Welbond

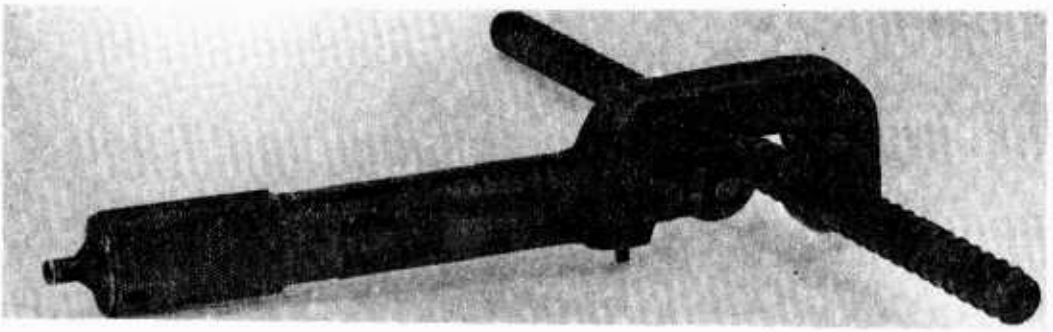
(b) Unisteel (BSC)

(c) Jones

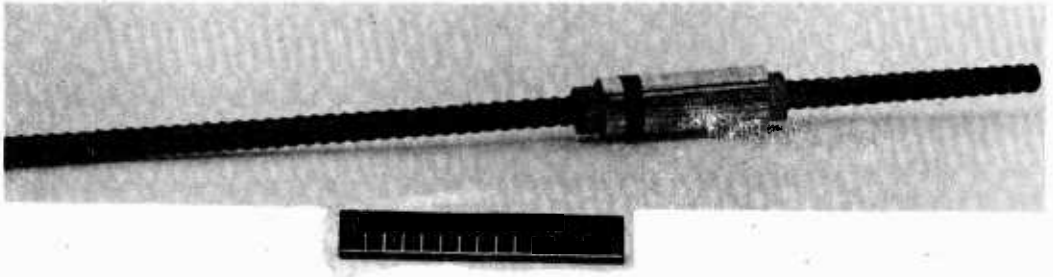
(d) Sheerness



PLATE 3.2 SPECIMEN FREE IN AIR HELD IN BETWEEN TEST RIG'S GRIPPING DEVICES



a

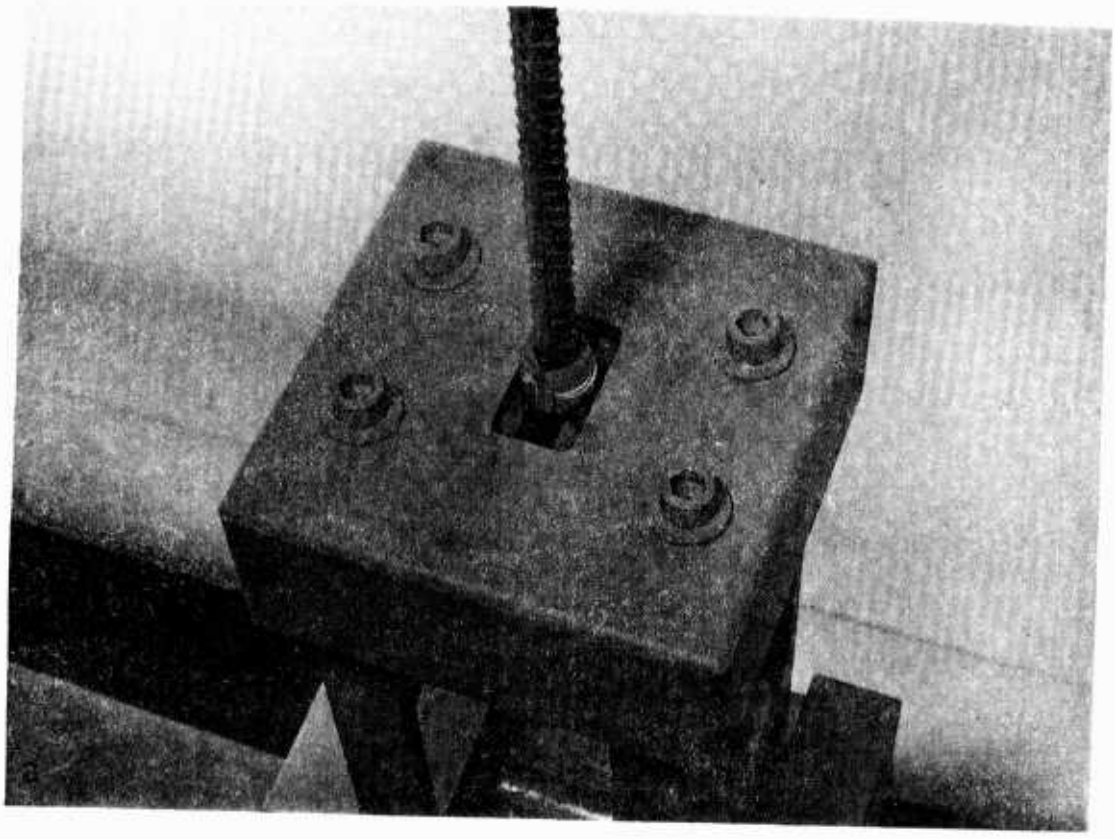


b

PLATE 3.3 GRIP PREPARATION

(a) Peening apparatus attached to bar

(b) Bar with end grip on it



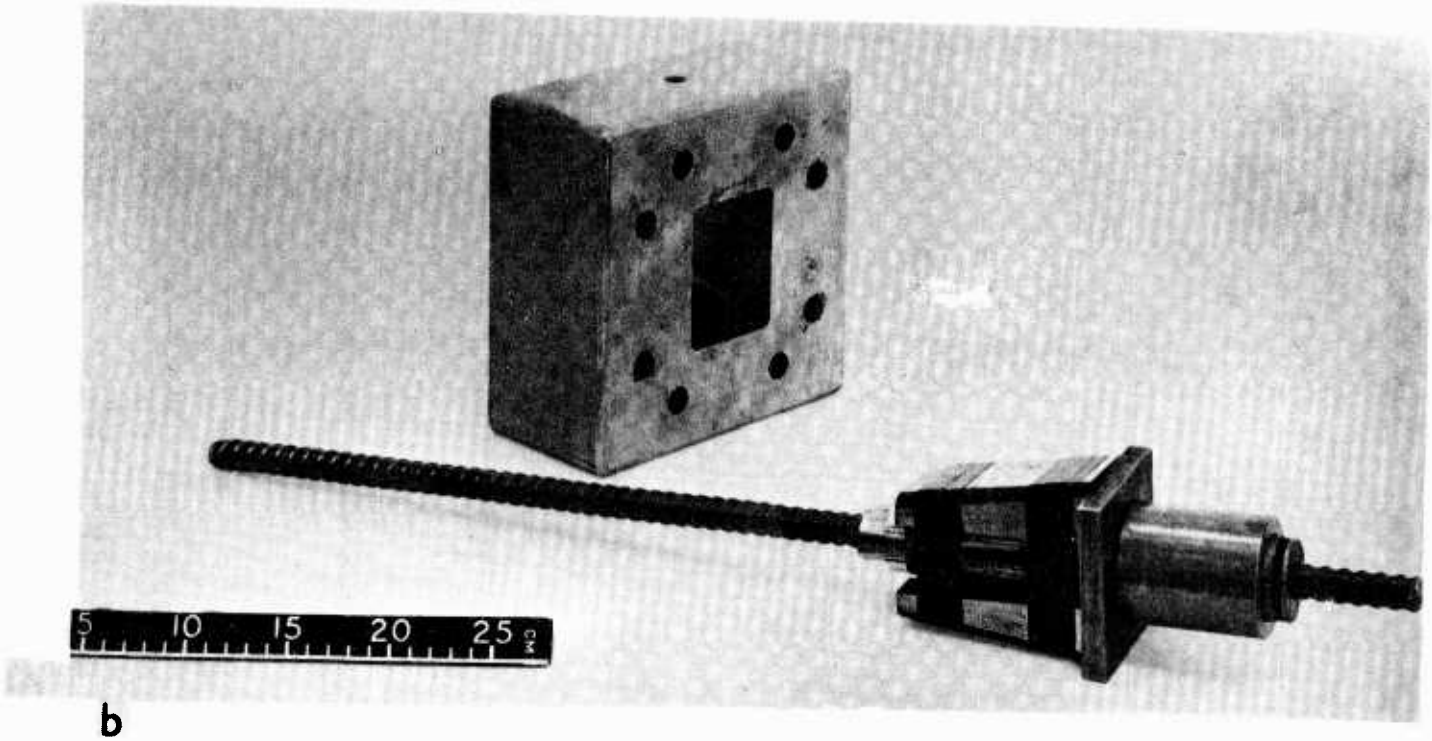


PLATE 3.4 TEST RIG'S GRIPPING DEVICE

(a) End of specimen held in gripping device

(b) Specimen's grips and gripping device's end block



PLATE 3.5 SPECIMEN EMBEDDED IN CONCRETE HELD IN BETWEEN TEST RIG'S GRIPPING DEVICES

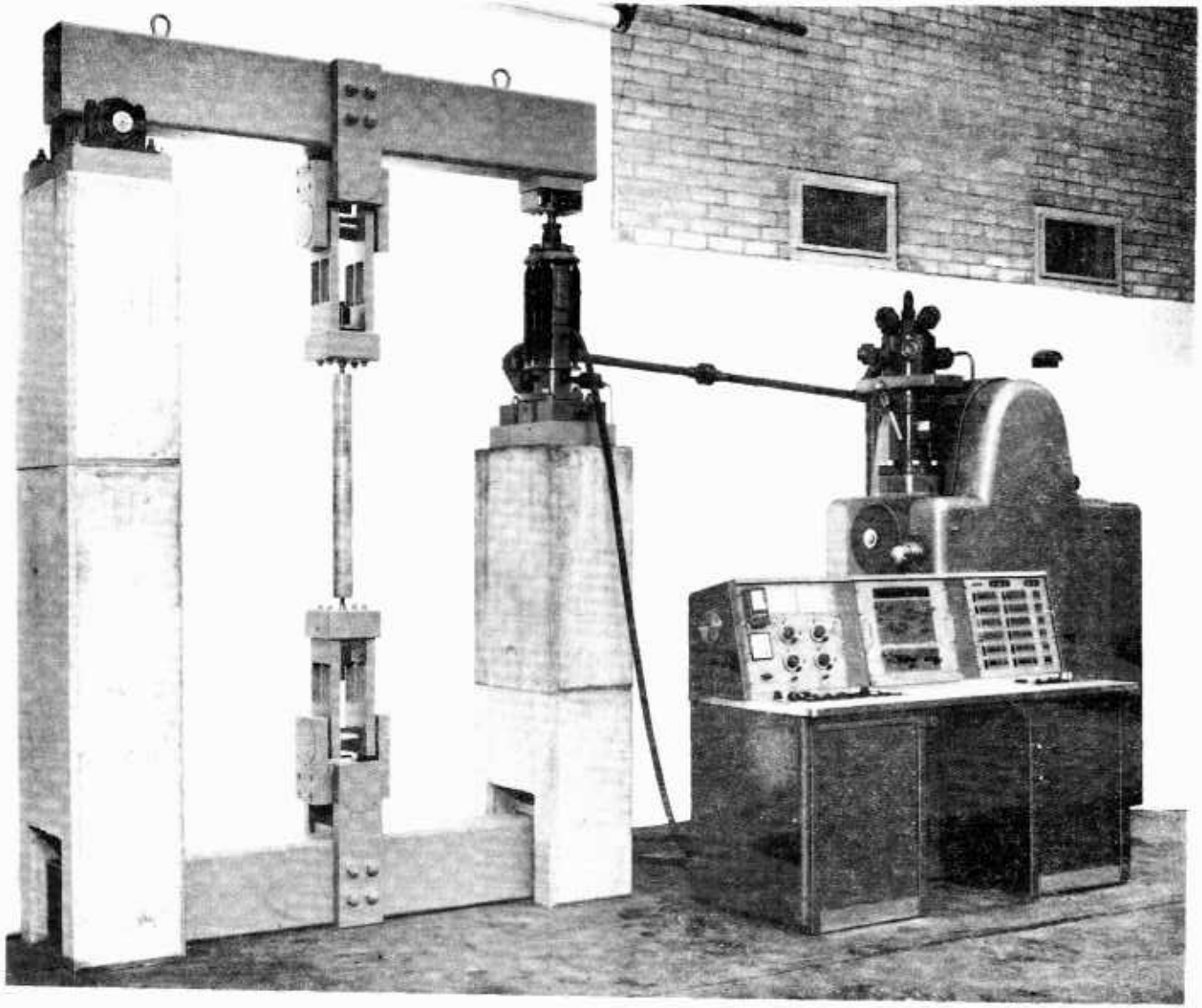


PLATE 3.6 GENERAL VIEW OF THE RIG FOR FATIGUE TESTS

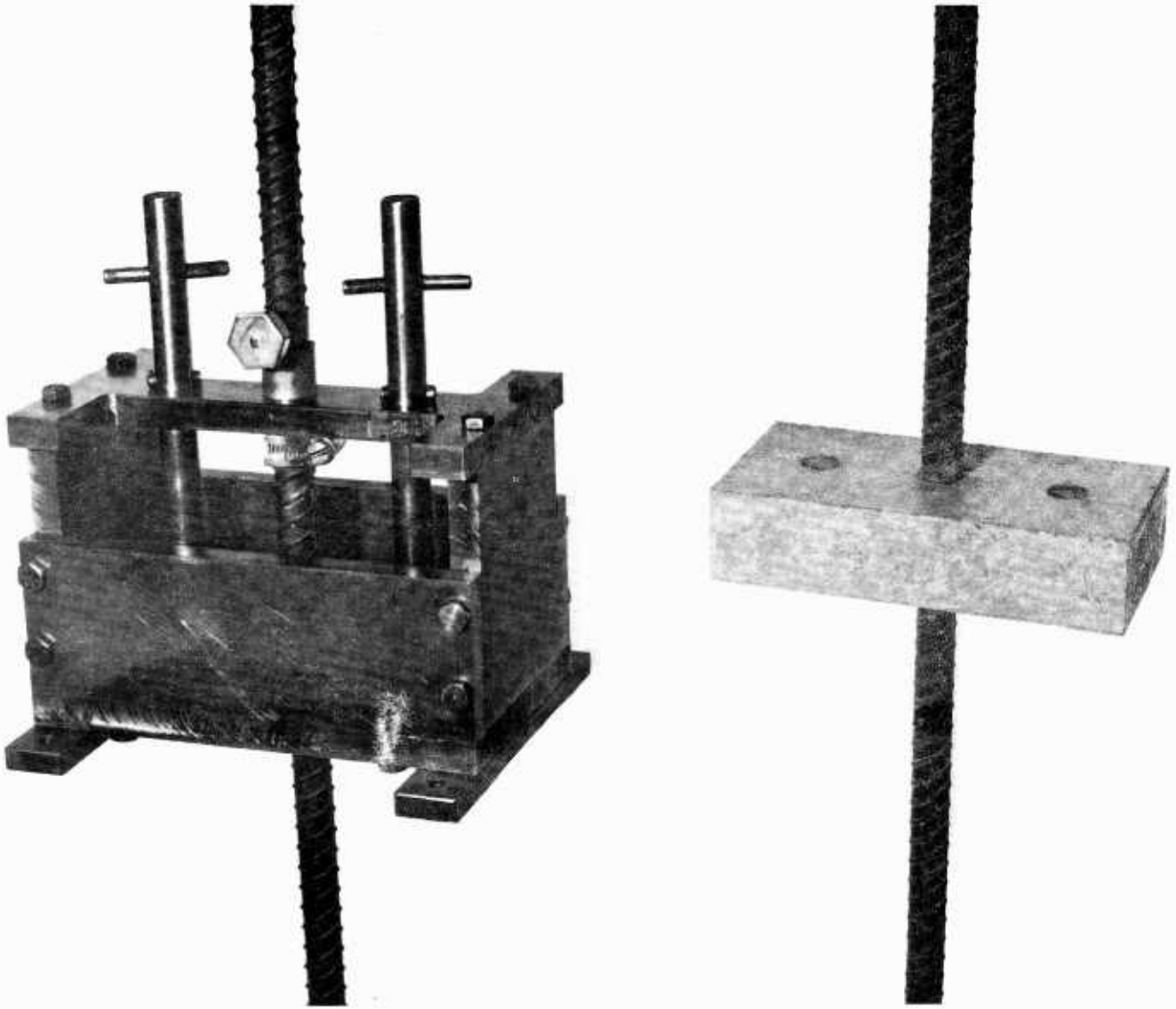


PLATE 3.7 MOULD AND BASIC SPECIMEN FOR BOND TESTS

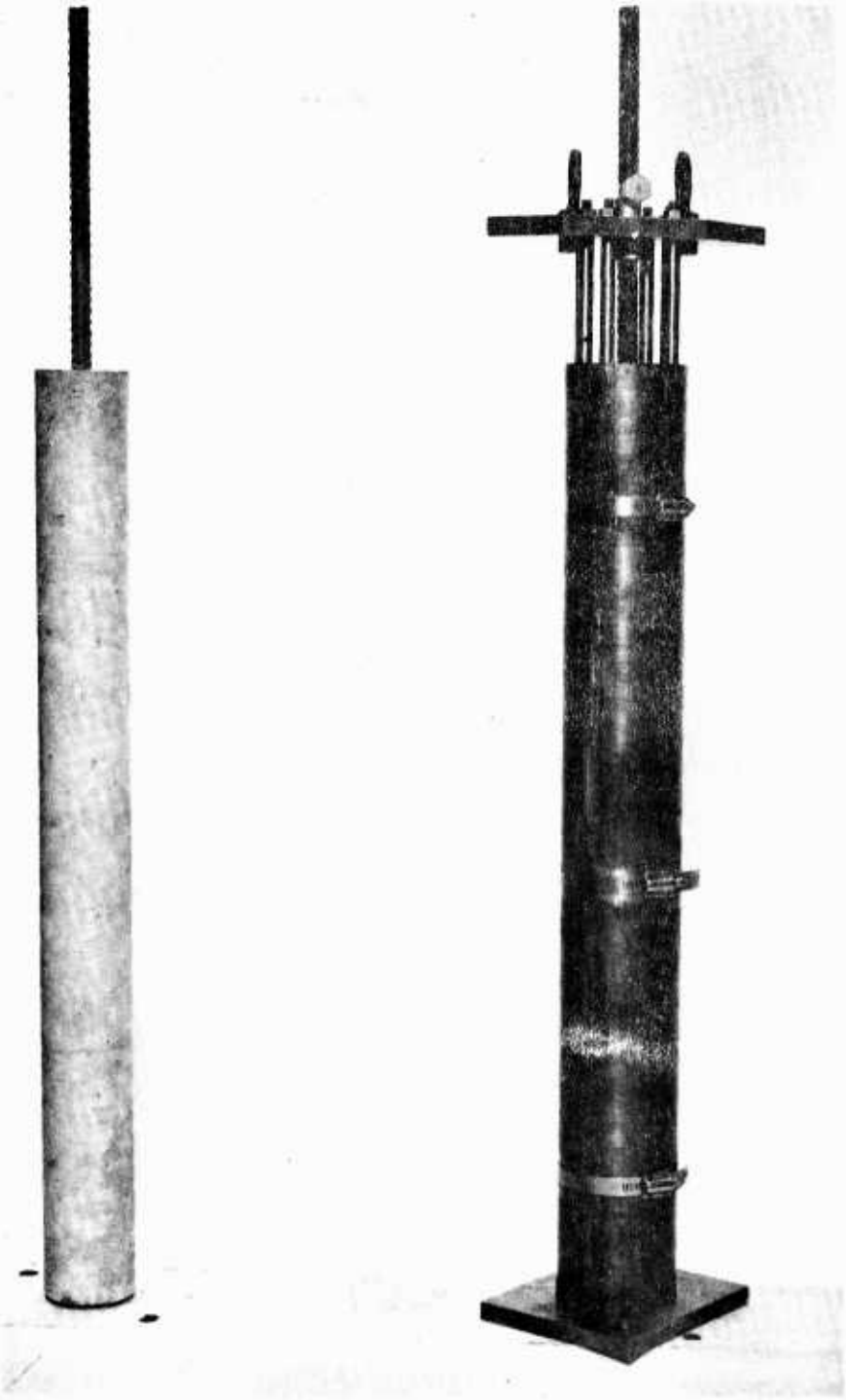


PLATE 3.8 MOULD AND TENSILE SPECIMEN FOR FATIGUE AND BOND TESTS

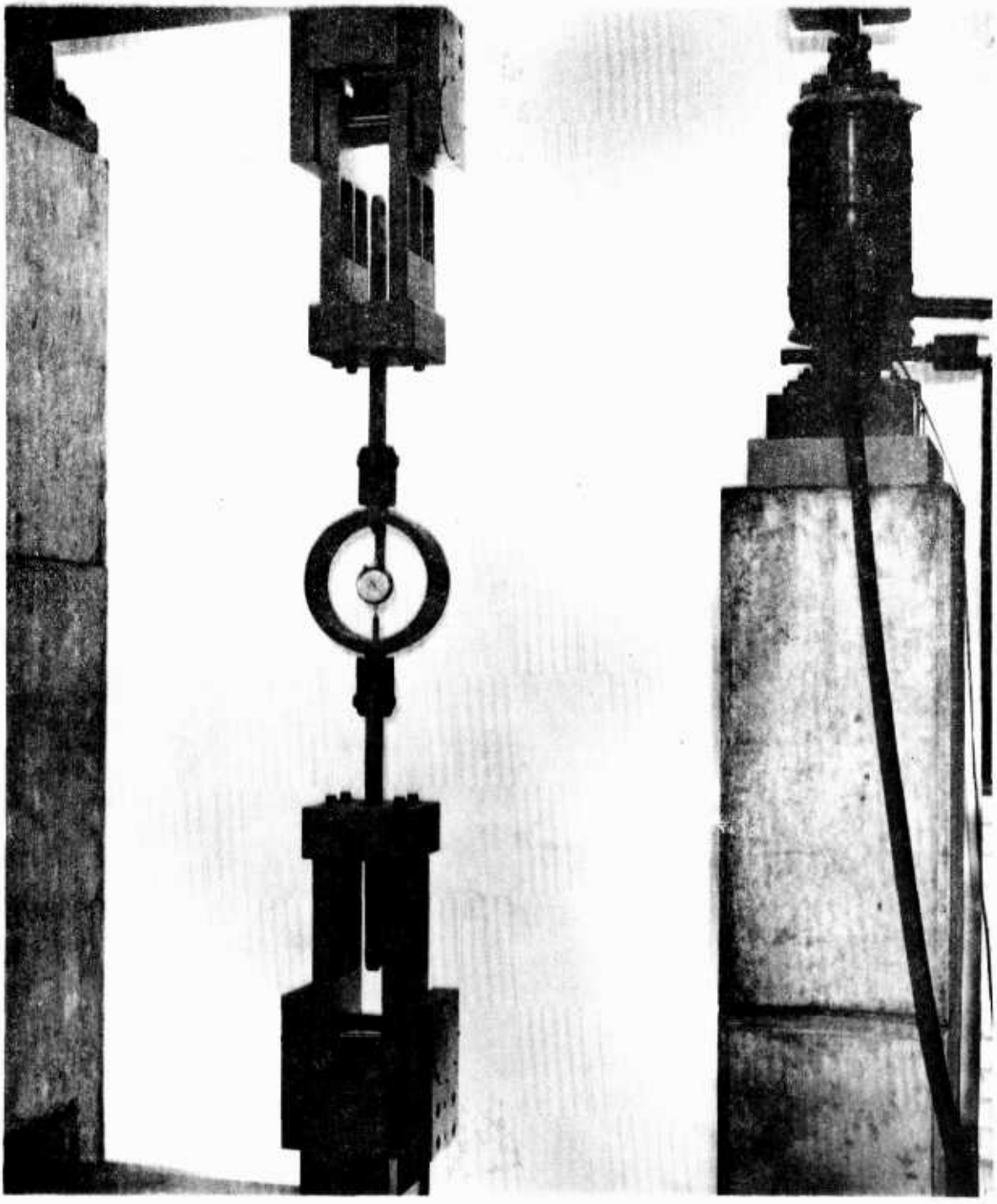


PLATE 3.9 STATIC CALIBRATION OF TEST RIG AND LOADING EQUIPMENT

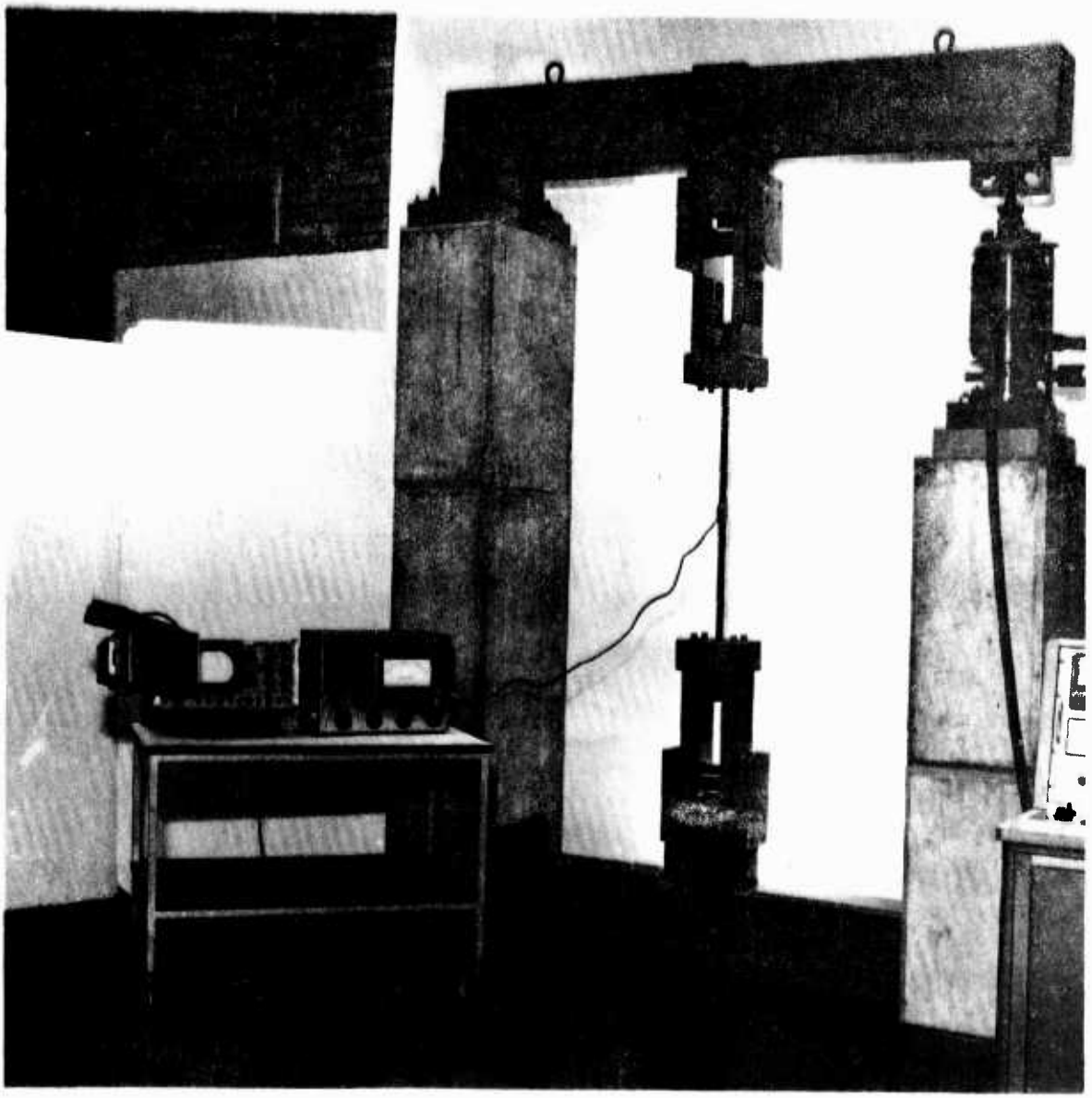
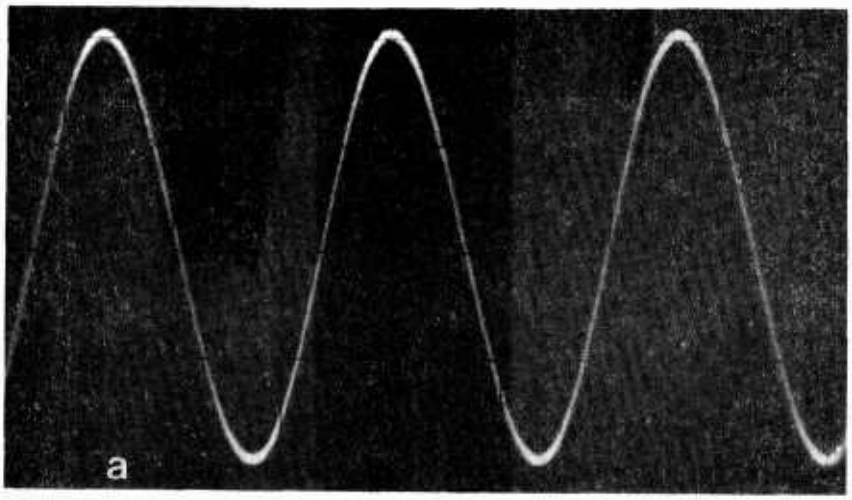
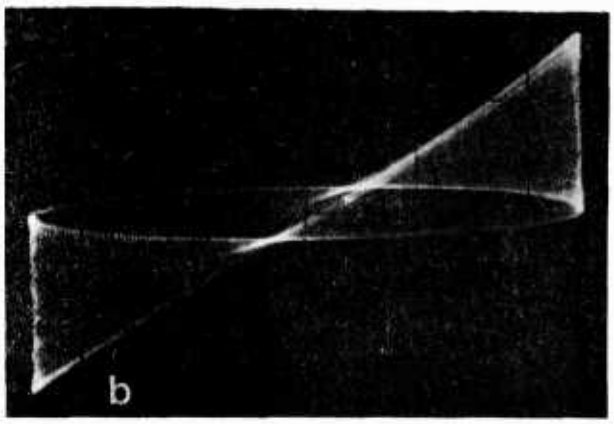
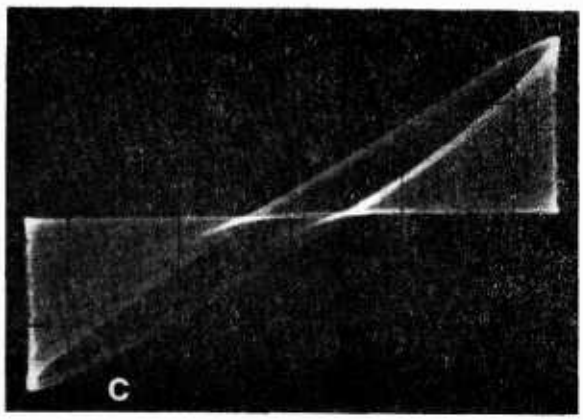
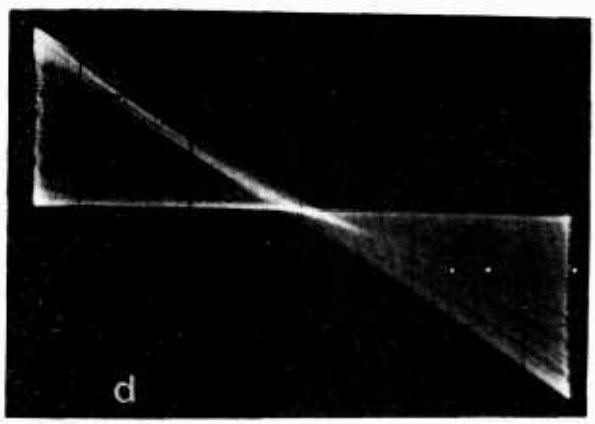


PLATE 3.10 DYNAMIC CALIBRATION OF TEST RIG AND LOADING EQUIPMENT









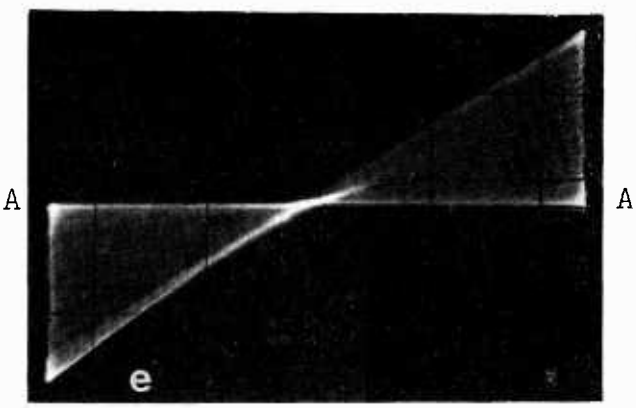


PLATE 3.11 DYNAMIC STRAIN OUTPUTS ON OSCILLOSCOPE

(a) Sinusoidally varying strain applied by pulsator

(b) Capacitive unbalance in dynamic strain output

(c) Unadjusted phase of oscillator voltage in dynamic strain output

(d) Peak value of dynamic strain output

(e) Other peak value of dynamic strain output

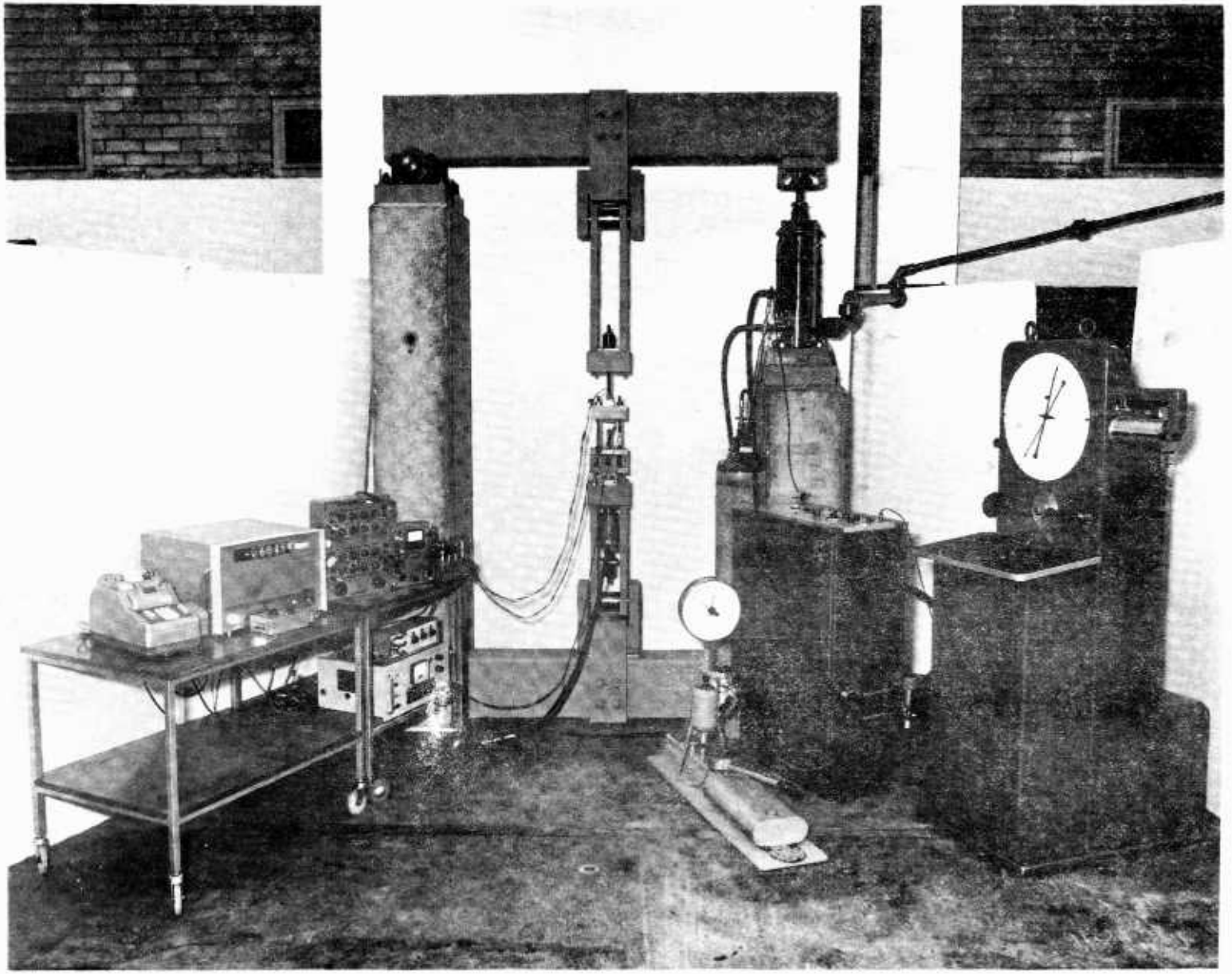


PLATE 3.12 INSTRUMENTATION FOR BASIC BOND TESTS

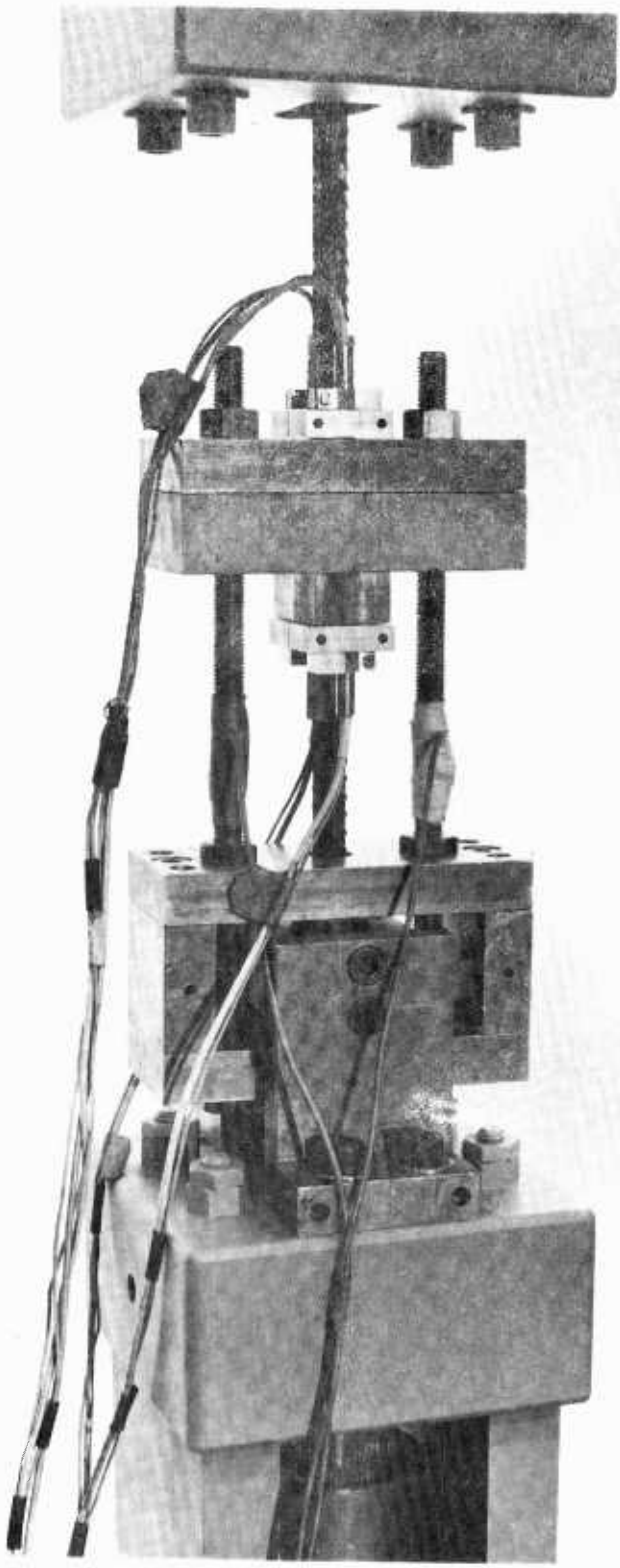


PLATE 3.13 MEASUREMENT OF BOND AND SLIP

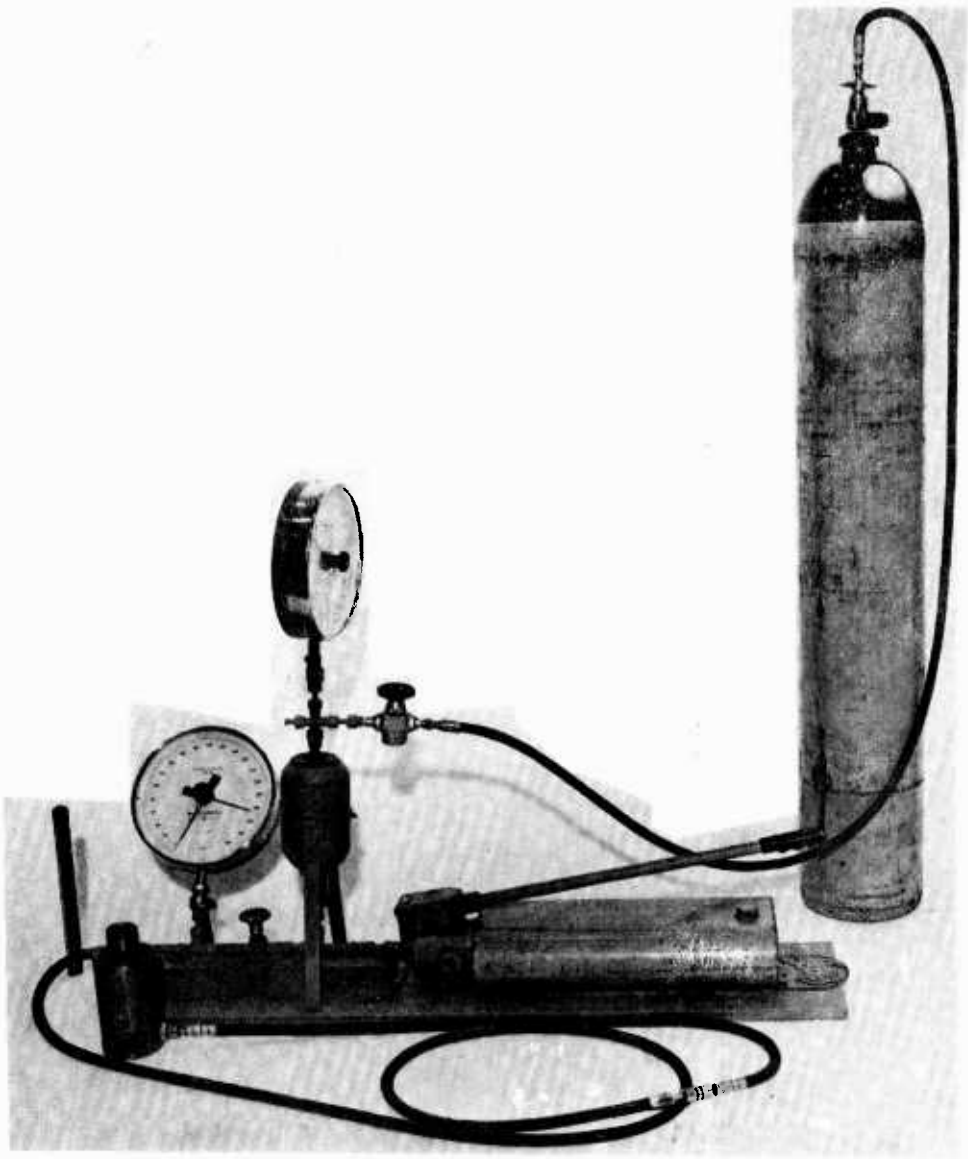


PLATE 3.14 PRESTRESSING JACK AND ACCUMULATOR SYSTEM

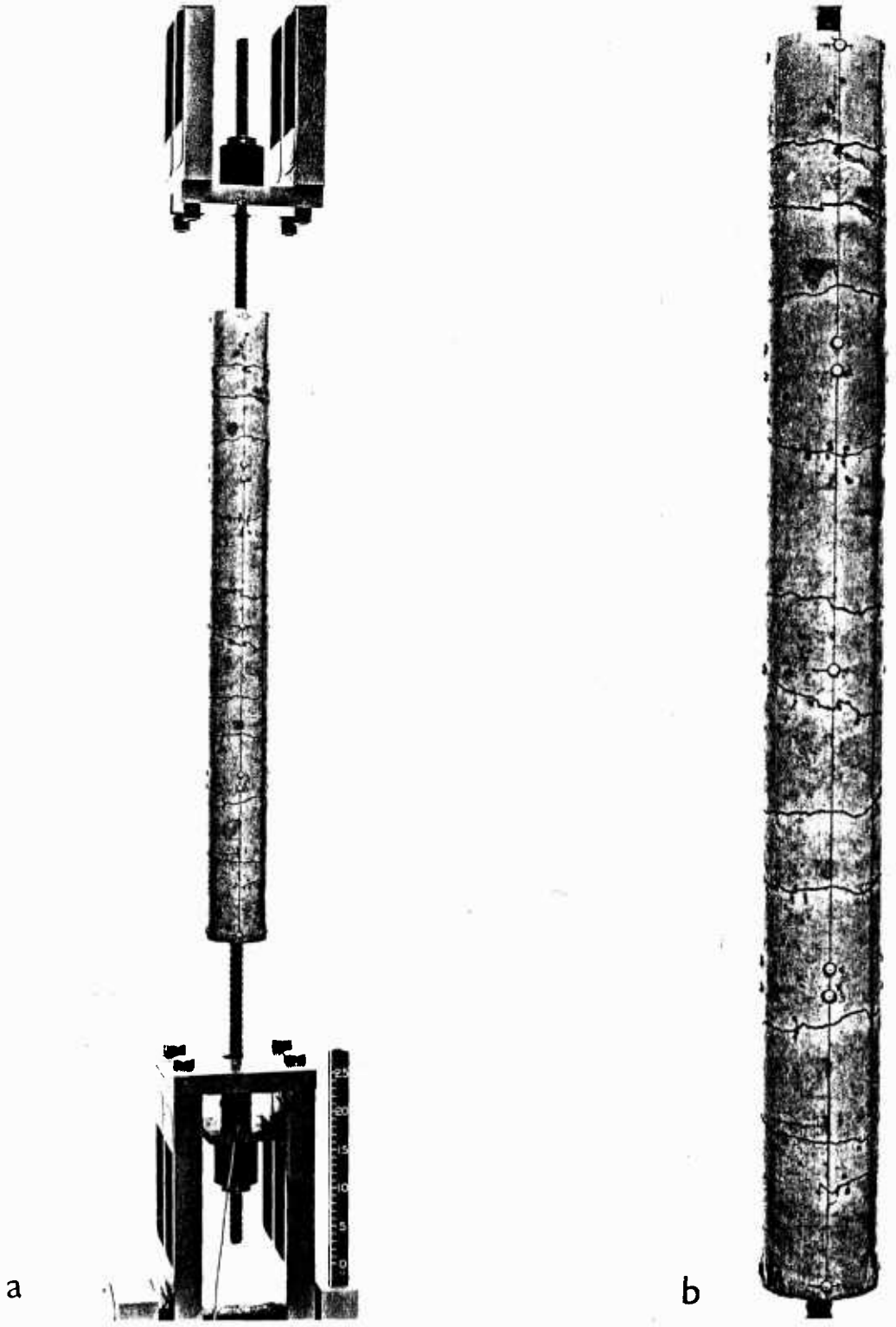


PLATE 3.15 TENSILE BOND SPECIMEN

(a) Specimen mounted in test rig

(b) Close up of specimen

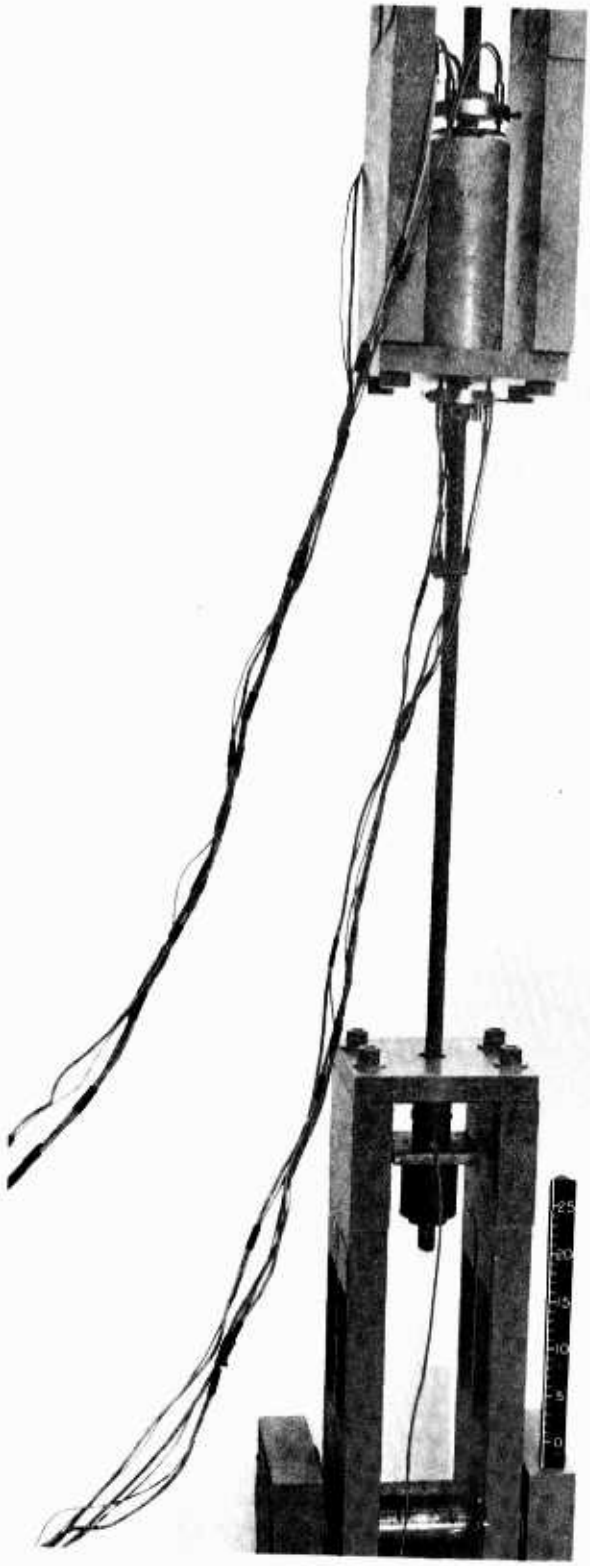


PLATE 3.16 PULL-OUT SPECIMEN IN TEST RIG

CHAPTER 4

TECHNIQUES OF STATISTICAL ANALYSIS OF FATIGUE DATA

4.1. INTRODUCTION

Statistical methods are essential for the analysis of fatigue test results because of their considerable scatter. The primary purposes of this statistical analysis are : (a) to estimate the fatigue life of the material (together with measures of the reliability) from a given set of fatigue data, obtained by testing a sample of fatigue specimens, (b) to provide objective procedures for comparing two or more sets of fatigue data and (c) to make estimates of the fatigue life for different probabilities of failure.

A detailed description of the statistical tests used in the analysis of the fatigue test data, obtained in this investigation, is given in this chapter. Only enough of the basic concepts of statistics are included to make the statistical methods used understandable; theory is left to the references (86 to 91).

4.2. FATIGUE LIFE FREQUENCY DISTRIBUTION

A basic concept of statistics is that a group of one or more specimens is a sample taken from a larger body or population. Such a sample is considered to be just one of a number, often very large, of samples that could have been taken. The results obtained from tests on a random sample

from the population, implicitly assumed to be representative of the population, can be used to estimate the characteristics of the whole population and to measure the precision of the estimates.

In fatigue tests the lives of specimens tested between given stress limits vary from specimen to specimen, and this is best described by a frequency distribution. The graphical presentation of the distribution of fatigue lives, for the population of specimens considered, is known as a frequency distribution curve. Such a distribution curve may be estimated from the raw test data or from transformed test data, that is either from values of fatigue life, N, or from values of logN, log(logN), $N^{\frac{1}{2}}$, and so forth.

4.2.1. CHOICE OF LIFE DISTRIBUTION SHAPE AND POINT ESTIMATES OF PARAMETERS

Different theoretical distributions have been used for forecasting fatigue life. However, empirical evidence gathered to date has not allowed a clear-cut choice to be made amongst them. When a form is chosen for the fatigue life distribution there should be satisfatory agreement between the data gathered and the results predicted by the theoretical distribution. Also it is advantageous for the distribution chosen to be mathematically tractable or, at worst, one on which extensive studies have been made so that laborious computations can be kept to a minimum.

The above two conditions can be fulfilled by finding a transformation, which when applied to a set of fatigue life

data, results in new data which closely follow the Normal or Gaussian distribution. Once this has been done, all the results of Normal distribution theory are available to analyse the transformed data.

The most important parameters of a population are the arithmetic mean denoted by μ and the variance denoted by σ^2. The information from a random sample of the population can be used to obtain estimates of these parameters.

The sample mean is defined as the sum of the observed values divided by their number, n :

$$\bar{x} = \frac{\sum_{i=1}^{n} x_i}{n} \qquad (4.1)$$

The sample variance is defined as the sum of squares of the deviations of the observed values from the sample mean, divided by one less than the number of observations :

$$s^2 = \frac{\sum_{i=1}^{n} (x_i - \bar{x})^2}{n - 1} \qquad (4.2)$$

The positive square root of the variance is called the standard deviation s. The ratio of standard deviation to mean is called the coefficient of variation C_v and is often used as a measure of dispersion.

4.2.2. THE NORMAL DISTRIBUTION

The normal distribution function with parameters

(μ, σ^2) is defined by

$$f(x) = \frac{1}{\sigma\sqrt{2\pi}} e^{-\frac{(x-\mu)^2}{2\sigma^2}} \qquad (4.3)$$

where $-\infty < x < \infty$. This distribution has a particular kind of bell shape, as shown in Figure 4.1, and is extensively used in statistical work.

The probability that the variable x is less than or equal to any specified value x_1, is given by the cumulative normal distribution function. This is equal to the area under the normal distribution curve from $-\infty$ to x_1, and is given by

$$P(x \leqslant x_1) = \frac{1}{\sigma\sqrt{2\pi}} \int_{-\infty}^{x_1} e^{-\frac{(x-\mu)^2}{2\sigma^2}} dx \qquad (4.4)$$

The probability that the variable x is between two points x_1 and x_2, where $x_2 > x_1$, is the area under the curve between these two points; this is equal to the area from $-\infty$ to x_2 minus the area from $-\infty$ to x_1, i.e.

$$P(x_1 \leqslant x \leqslant x_2) = P(x \leqslant x_2) - P(x \leqslant x_1) \qquad (4.5)$$

A normal distribution with $\mu=0$ and $\sigma^2=1$ is called a standardised normal distribution. Any normal distribution can be standardised by the following transformation of variables

$$z = \frac{x - \mu}{\sigma}$$

and the standardised curve is given by

$$f(z) = \frac{1}{\sqrt{2\pi}} e^{-\frac{z^2}{2}} \qquad (4.6)$$

The values of the area under this curve from $-\infty$ to z are given in Table A.1.

The fatigue life distribution is not in general normally distributed. It has been found that by replacing the observed fatigue life, N, by $\log_{10}N$ will often result in a distribution which is approximately normal. This will be referred to as a log normal distribution and the results of normal distribution theory can be used to analyse the transformed fatigue life data.

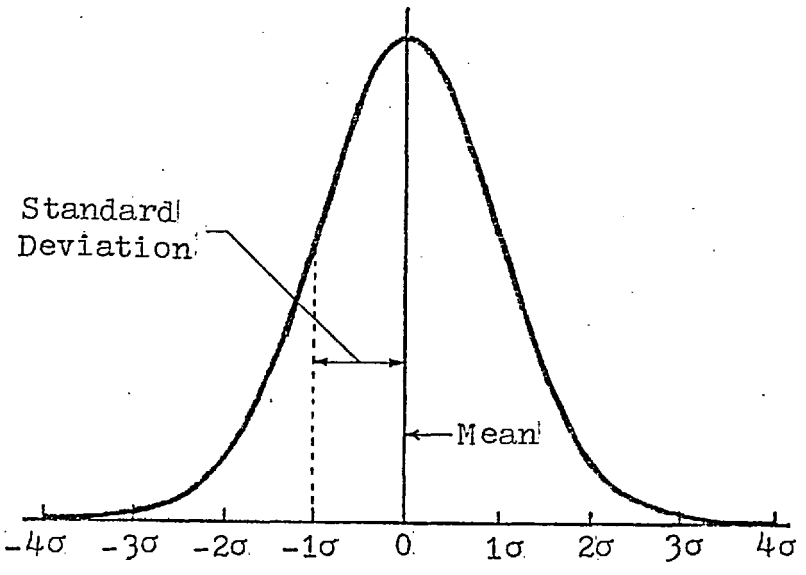


FIGURE 4.1 NORMAL DISTRIBUTION CURVE

4.2.3. LEVEL OF SIGNIFICANCE OF A STATISTICAL HYPOTHESIS

The procedure for testing a statistical hypothesis is based on the calculation from the sample values of an appropriate test-statistic with known sampling distribution, by means of which it is possible to determine a region such that the hypothesis is rejected if the value of the test-statistic belongs to it.

There is, of course, always a finite probability of making an error. There are two types of error either of which may be made :

(i) type I error, i.e. rejecting as false a hypothesis which in fact is true, and

(ii) type II error, i.e. accepting as true a hypothesis which in fact is false.

The frequency with which mistakes are made is, of course, very important. The probability of making a type II error depends on the probability of a type I error. The probability of a type II error increases as the probability of a type I error decreases. A small value of the probability of a type I error is certainly desirable, but making it too small may result in a probability of a type II error so large that we seldom recognize the hypothesis to be false when it is false. The probability of type I error is called the level of significance α. The most commonly used values for α are 0.05 and 0.10.

4.2.4. χ^2 - TEST FOR GOODNESS OF FIT

The cumulative normal distribution curve when plotted

on arithmetic probability paper takes the shape of a straight line. If fatigue life test data are plotted on probability paper and found to approximate satisfactorily to a straight line then they are normally distributed.

Instead of relying on a visual inspection of the fatigue life data plotted on probability paper, it is possible to carry a χ^2 - goodness of fit test (90) by comparing the plotted points against the normal straight line at a chosen significance level.

To carry out this test, the sample values from an experiment should be arranged into r categories. To decide at the significance level α whether the data constitute a sample from a population with a normal distribution, the expected number of observations that could fall in each category is computed as predicted by the normal distribution. The grouping is arranged so that this theoretical frequency is at least five for each category. The number of categories, which is an integer, is then given by

$$r \leqslant \frac{n}{5}$$

where n is the total number of data

The test-statistic is given by

$$\chi^2 = \sum_{i=1}^{r} \frac{(p_{o_i} - p_{t_i})^2}{p_{t_i}} \qquad (4.7)$$

where p_{o_i} is the observed frequency and p_{t_i} the theoretical frequency for the ith category.

If the calculated value of χ^2 is smaller than the theoretical value of $\chi^2_{1-\alpha}(r-1-g)$ given in Table A.2 for $(r-1-g)$ degrees of freedom, the hypothesis that the data are normally distributed cannot be rejected at the $100\,\alpha$ percent level of significance.

The value of g stands for the number of quantities necessary to specify completely the population distribution function. These quantities must be obtained as estimates from the experimental data themselves. In the case of the normal distribution, g=2 since two quantities are necessary for specifying the distribution, i.e. the sample mean as an estimate of μ and the sample variance as an estimate of σ^2.

In fatigue tests, the number of results at each stress level is often too small to test that the data at a given stress level are normally distributed. However, the data from different stress levels can be grouped together by making a change of variable from $\log_{10}N$ to z, where

$$z = \frac{\log_{10}N - \overline{\log_{10}N}}{s_{\log_{10}N}} \qquad (4.8)$$

and $\overline{\log_{10}N}$ and $s_{\log_{10}N}$ are the mean and standard deviation respectively of the corresponding set of data. Thus each set of data is reduced to one with a mean of zero and a standard deviation of unity. The z-values calculated for each stress level can then be used to check if they are normally distributed by means of the χ^2-test.

4.3. CONFIDENCE INTERVALS FOR THE MEAN AND THE VARIANCE

Estimates of a population's parameters can be obtained using the information from a random sample of it. In many cases it is sufficient to obtain point estimates of these parameters; more meaningful estimates can be obtained by the use of confidence intervals. Exact values would require that the total population to be tested.

A confidence interval of a population parameter can be constructed so that it contains this parameter for a stated proportion of time, γ $(0 < \gamma < 1)$, called the confidence level. The greater the confidence, the wider the interval will be. There is a risk of $(1 - \gamma)$ that the interval being constructed will not contain the parameter.

For a population which is normally distributed the confidence interval for the mean is given by :

$$\bar{x} + \frac{s}{\sqrt{n}} t_{\beta_1}(\varphi) \leqslant \mu \leqslant \bar{x} + \frac{s}{\sqrt{n}} t_{\beta_2}(\varphi) \qquad (4.9)$$

where $\beta_1 = (1-\gamma)/2$, $\beta_2 = (1+\gamma)/2$ and n the sample size. The value of $t_\beta(\varphi)$ for $\varphi = n-1$ degrees of freedom can be read from Table A.3.

The confidence interval for the variance of a normal population has the following confidence limits :

$$\frac{s^2}{\left(\frac{\chi^2}{d.f.}\right)_2} \leqslant \sigma^2 \leqslant \frac{s^2}{\left(\frac{\chi^2}{d.f.}\right)_1} \qquad (4.10)$$

The values of $(\chi^2/d.f.)_1$ and $(\chi^2/d.f.)_2$ can be read from

Table A.4 using the percentages $100\beta_1$ and $100\beta_2$ respectively, with (n-1) degrees of freedom.

4.4. TESTS OF SIGNIFICANCE FOR NORMAL POPULATIONS

A certain amount of scatter is present in the results of experimental work. In fatigue tests there is a considerable scatter in the obtained fatigue lives, and thus a statistical analysis of the fatigue results is essential.

The basis of different statistical techniques required for the comparison of different fatigue life distributions resulting from different parameters, are given in this section. Different normal populations can thus be tested to see if they are identical or not by comparing their sample variances and means.

4.4.1. TEST FOR THE EQUALITY OF THE VARIANCES OF k POPULATIONS

Before testing whether or not the means of k populations are significantly different it is important to investigate whether their standard deviations are significantly different or not.

If the test hypothesis

$$s_1^2 = s_2^2 = \ldots = s_k^2$$

is correct, then the k variances can be combined to form the average variance within the samples, s_w^2 , given by

$$s_w^2 = \frac{\sum_{i=1}^{k} f_i s_i^2}{\sum_{i=1}^{k} f_i} \qquad (4.11)$$

where $f_i = n_i - 1$ and n_i and s_i^2 are the size and variance of the ith sample.

To test the hypothesis of equal variances, Bartlett's test (86) can be used, i.e. χ^2 as calculated from Equation (4.12) can be compared with the theoretical value of $\chi^2_{1-\alpha}(k-1)$ given in Table A.2 for (k-1) degrees of freedom.

$$\chi^2 = \frac{2.3026}{C}\left(f \log_{10} s_w^2 - \sum_{i=1}^{k} f_i \log_{10} s_i^2\right) \qquad (4.12)$$

in which

$$f = \sum_{i=1}^{k} f_i$$

$$C = 1 + \frac{1}{3(k-1)} \sum_{i=1}^{k} \frac{1}{f_i} - \frac{1}{f}$$

If $\chi^2 \leqslant \chi^2_{1-\alpha}(k-1)$, then the hypothesis that the variances are equal cannot be rejected at the 100α percent level of significance. If $\chi^2 > \chi^2_{1-\alpha}(k-1)$, the variances are considered to be significantly different.

4.4.2. TEST FOR THE EQUALITY OF THE VARIANCES OF TWO POPULATIONS

To test the hypothesis of common variance of two populations the two-sided F test can be used. The computed value of F is given by

$$F = \frac{s_1^2}{s_2^2} \qquad (4.13)$$

where s_1^2 is the variance of the first sample of size n_1

s_2^2 is the variance of the second sample of size n_2

and $s_1^2 > s_2^2$

If $F \leqslant F_\beta(\varphi_1, \varphi_2)$, where $\beta = 1-(\alpha/2)$, the hypothesis that the variances are equal cannot be rejected at the 100α percent level of significance. Values of $F_\beta(\varphi_1, \varphi_2)$ are given in Tables A.5, A.6 and A.7,

for $\varphi_1 = n_1-1$ degrees of freedom of the numerator

$\varphi_2 = n_2-1$ degrees of freedom of the denominator.

If $F > F_\beta(\varphi_1, \varphi_2)$ the variances are considered to be significantly different.

4.4.3. TEST FOR THE EQUALITY OF THE MEANS OF k POPULATIONS

Let x_{ij} be the jth observation from the ith sample, $\bar{x}_i$ be the mean of the ith sample, and n_i be the size of the ith sample. If the k variances are not significantly different, the average variance within the samples, s_w^2, is given by Equation (4.11). The variance among the samples, s_{am}^2, is given by

$$s_{am}^2 = \frac{\sum_{i=1}^{k} n_i (\bar{x}_i - \bar{x})^2}{k - 1} \qquad (4.14)$$

where $\bar{x}$ is the mean of the numbers x_{ij} and given by

$$\bar{x} = \frac{\sum_{i=1}^{k} \sum_{j=1}^{n_i} x_{ij}}{\sum_{i=1}^{k} n_i} \qquad (4.15)$$

The test-statistic is given by

$$F = \frac{s_{am}^2}{s_w^2} \qquad (4.16)$$

If $F \leqslant F_\beta(\varphi_1,\varphi_2)$, where $\beta = 1- \alpha$, the hypothesis that the k means are equal cannot be rejected at the $100\,\alpha$ percent level of significance. Values of $F_\beta(\varphi_1,\varphi_2)$ are given in Tables A.5, A.6, and A.7,

for φ_1 = k-1 degrees of freedom of numerator, and

φ_2 = N-k degrees of freedom of denominator, where

$$N = \sum_{i=1}^{k} n_i$$

If $F > F_\beta(\varphi_1,\varphi_2)$ the k means are considered to be significantly different.

4.4.4. TEST FOR THE EQUALITY OF THE MEANS OF TWO POPULATIONS

The means of two samples can be compared by using the t-test. Values of the t-distribution are given in Table A.3 for different degrees of freedom and different levels of significance, α.

4.4.4.1. VARIANCES NOT SIGNIFICANTLY DIFFERENT

If the two sample variances are not significantly different the test-statistic is given by

$$t = \frac{\bar{x}_1 - \bar{x}_2}{s_w \left[\frac{1}{n_1} + \frac{1}{n_2}\right]^{\frac{1}{2}}} \qquad (4.17)$$

where $\bar{x}_1$ and $\bar{x}_2$ are the sample means for the first and second samples respectively, and

$$s_w = \left[\frac{(n_1 - 1)s_1^2 + (n_2 - 1)s_2^2}{n_1 + n_2 - 2}\right]^{\frac{1}{2}}$$

If $|t| \leqslant t_\beta(\varphi)$, where $\beta = 1-(\alpha/2)$ and $\varphi = n_1+n_2-2$ degrees of freedom, the hypothesis that the means are equal cannot be rejected at the $100\,\alpha$ percent level of significance.

If $|t| > t_\beta(\varphi)$, then the two populations are significantly different in mean or in variance or both. On the average identical populations will be erroneously judged to be different about $100\,\alpha$ percent of the time. If the samples are large enough so that the test difference between the standard deviations would have probably detected any important diffe-

rence in the variances, a value of $|t| > t_\beta(\varphi)$ can be attributed to different population means.

4.4.4.2. VARIANCES SIGNIFICANTLY DIFFERENT

If the two sample variances are significantly different, the hypothesis that the populations means are equal may be tested by using the following test-statistic

$$t = \frac{\bar{x}_1 - \bar{x}_2}{\left[\frac{s_1^2}{n_1} + \frac{s_2^2}{n_2}\right]^{\frac{1}{2}}} \qquad (4.18)$$

This test is approximate and only if both n_1 and n_2 are larger than 30 a good approximation is possible.

If $|t| \leqslant t_\beta(\varphi)$, where $\beta = 1-(\alpha/2)$, the hypothesis that the population means are equal cannot be rejected at the $100\,\alpha$ percent level of significance, while if $|t| > t_\beta(\varphi)$ they are considered to be significantly different. The number of degrees of freedom, φ, is given by

$$\varphi = \left[\frac{C^2}{n_1 - 1} + \frac{(1 - C)^2}{n_2 - 1}\right]^{-1} \qquad (4.19)$$

where

$$C = \frac{\frac{s_1^2}{n_1}}{\frac{s_1^2}{n_1} + \frac{s_2^2}{n_2}}$$

4.5. REGRESSION ANALYSIS

Regression analysis is a statistical technique for obtaining a mathematical description of the relationship between two or more variables with a specified accuracy.

Regression analysis could be used, for example, to determine the association between two variables in experiments where one of the variables is a non-stochastic variable, the values of which are pre-determined when the experiments are planned. Such a case arises in fatigue experiments, when the fatigue life of specimens is determined for certain values of the stress range.

4.5.1. HYPOTHESIS UNDERLYING REGRESSION ANALYSIS

In regression analysis one variable, x, is denoted the independent variable and the other variable, y, the dependent variable.

In what follows it is assumed that

(i) Corresponding to each value of x, y is normally distributed with parameters (μ_y, σ^2).

(ii) The mean value of y is a function of x,

$$\mu_y = f(x) = f(x; a, b, c, \ldots) \qquad (4.20)$$

which includes certain unknown constants or parameters, a, b, c, ...The type of the function is known, and the function is linear as regards the parameters, i.e. the function for example may take the form

$$f(x) = a + bx + cx^2$$

or $$f(x) = a + bx + c\log_{10}x$$

The graphical representation of the function $\mu_y = f(x)$ is called the theoretical regression curve.

(iii) The variance of y is constant or proportional to a known function of x.

In regression analysis we determine estimates of the parameters a, b, c, ...

Let us assume that the data is given in the form shown in Table 4.1, the observations being stochastically independent.

Independent variable	Dependent variable	Sample mean	Sample variance
x_1	$y_{11}, y_{12}, \cdots, y_{1n_1}$	$\bar{y}_1$	s_1^2
x_2	$y_{21}, y_{22}, \cdots, y_{2n_2}$	$\bar{y}_2$	s_2^2
$\vdots$	$\vdots \quad \vdots \quad \vdots \quad \vdots$	$\vdots$	$\vdots$
x_k	$y_{k1}, y_{k2}, \cdots, y_{kn_k}$	$\bar{y}_k$	s_k^2

TABLE 4.1

An estimate of the type of function $\mu_y = f(x)$ may be obtained by plotting the k pairs of numbers $(x_i, \bar{y}_i)$, $i = 1,2,...k$, in a coordinate system. Based on this diagram and experience, a hypothesis regarding the type of the function $\mu_y = f(x)$ can be set up.

It can be proved that the best estimates of the parameters in the equation of the regression curve are obtained by application of the method of least squares, i.e. by determining the values of a, b, c, ... which minimize the sum of squares

$$\sum_{i=1}^{k} \sum_{j=1}^{n_i} (y_{ij} - f(x_i; a, b, c, ...))^2$$

By this method the determination of the empirical regression curve is such that the sum of squares of the deviations between the observed values of y and the corresponding values on the curve takes the least possible value.

In the following the theory of linear regression analysis with only one independent variable is given.

4.5.2. LINEAR REGRESSION ANALYSIS

In the linear regression analysis all hypotheses mentioned in the previous section hold, and the mean value of y is now a linear function of x. This is given by

$$\mu_y = a + b(x - \bar{x}) \qquad (4.21)$$

where $\bar{x}$ denotes the weighted mean of the x-values, i.e.,

$$\bar{x} = \frac{\sum_{i=1}^{k} n_i x_i}{\sum_{i=1}^{k} n_i} \qquad (4.22)$$

Only the particular case of the variance of y being independent of x will be considered.

Estimates of the three parameters a, b and σ^2 will now be calculated from the observations given in Table 4.1.

4.5.2.1. ESTIMATES OF PARAMETERS a, b and σ^2 OF LINEAR REGRESSION ANALYSIS

From the method of least squares estimates of the parameters can be obtained and are given by

$$a = \frac{\sum_{i=1}^{k} n_i \bar{y}_i}{\sum_{i=1}^{k} n_i} \qquad (4.23)$$

$$b = \frac{\sum_{i=1}^{k} n_i (x_i - \bar{x})\, \bar{y}_i}{\sum_{i=1}^{k} n_i (x_i - \bar{x})^2} \qquad (4.24)$$

where

$$\bar{y}_i = \frac{1}{n_i} \sum_{j=1}^{n_i} y_{ij} \qquad (4.25)$$

The estimates of a and b can be used to obtain values of y_{r_i} for different values of x_i using the following empirical regression line

$$y_{r_i} = a + b(x_i - \bar{x}) \qquad (4.26)$$

The hypothesis of a constant variance, σ^2, within the samples can be tested by comparing s_1^2, s_2^2, ..., s_k^2, as given in section 4.4.1. If they are found to be not significantly different they can be combined to form an average variance within the samples, s_w^2, as given by Equation (4.11), which is an estimate of σ^2.

4.5.2.2. TESTING OF LINEARITY OF REGRESSION CURVE AND CONFIDENCE LIMITS

The linearity of a regression curve can be tested by comparing the average variance within the samples, s_w^2, (Equation 4.11) with the variance of the deviations of the means about the regression line, s_m^2 :

$$s_m^2 = \frac{\sum_{i=1}^{k} n_i(\bar{y}_i - y_{r_i})^2}{k - 2} \qquad (4.27)$$

The F-test can be used for this comparison. F is calculated as a ratio of the two variances

$$F = \frac{s_m^2}{s_w^2} \qquad (4.28)$$

and compared with the theoretical value of $F_{1-\alpha}(\varphi_1,\varphi_2)$, given in Tables A.5, A.6 and A.7,

for φ_1 = k-2 degrees of freedom of the numerator, and

φ_2 = N-k degrees of freedom of the denominator, where

$$N = \sum_{i=1}^{k} n_i$$

If $F > F_{1-\alpha}(\varphi_1,\varphi_2)$ the hypothesis of linearity is rejected at the $100\,\alpha$ percent level of significance. If $F \leqslant F_{1-\alpha}(\varphi_1,\varphi_2)$ the hypothesis of linearity cannot be rejected at $100\,\alpha$ percent level of significance, i.e. the regression curve is accepted as linear and a pooled estimate of the variance about the regression line is given by :

$$s_r^2 = \frac{\sum_{i=1}^{k} \sum_{j=1}^{n_i} (y_{ij} - y_{r_i})^2}{N - 2} \qquad (4.29)$$

The positive square root of s_r^2 is called the standard error of estimate.

The variances of parameters a and b are given by:

$$s_a^2 = \frac{s_r^2}{\sum_{i=1}^{k} n_i} \qquad (4.30)$$

$$s_b^2 = \frac{s_r^2}{\sum_{i=1}^{k} n_i (x_i - \bar{x})^2} \qquad (4.31)$$

The variance of y_r is given by:

$$s_{y_r}^2 = s_a^2 + s_b^2 (x - \bar{x})^2 \qquad (4.32)$$

Confidence limits for y_r can be determined with the aid of the t-distribution for (N-2) degrees of freedom and a chosen confidence level, γ. Then

lower limit = $y_r + t_{\beta_1}(\varphi)\ s_{y_r}$

upper limit = $y_r + t_{\beta_2}(\varphi)\ s_{y_r}$

and

$$\beta_1 = (1-\gamma)/2$$

$$\beta_2 = (1+\gamma)/2$$

It should be noted that the limits depend on s_{y_r} which in turn depends on x. Thus the limits are variable and are closest at $x = \bar{x}$ and the distance between them increases as x diverges from $\bar{x}$.

4.5.2.3. BLOM'S TEST

Blom's test can be used to check visually whether the obtained fatigue lives are log normally distributed.

The results of the linear regression analysis are used to plot, on normal probability paper, the cumulative percent of observations versus regression residuals, ($\log N_{obs.} - \log N_{pred.}$), where $\log N_{obs.}$ is the log value of the observed fatigue life and $\log N_{pred.}$ the log value of the fatigue life predicted by the linear regression analysis. In order to minimize bias, the residuals are plotted against the percent of survivals, (100 - P), where

$$P = \frac{i - \frac{3}{8}}{n + \frac{1}{4}} \qquad (4.33)$$

as suggested by Blom (92) and Kimball (93) for the normal distribution. If the plot fits satisfactorily to a straight line this indicates that the fatigue data are log normally distributed.

4.5.3. COMPARISON OF TWO REGRESSION LINES

Two sets of observational data are considered, which have each formed the basis of a regression analysis according to the principles given in section 4.5.2. For each regression line, five quantities have been calculated (a, b, s_r^2, N, $\bar{x}$). The identity of two regression lines can be tested by comparing first their variances by means of a F-test and second their slopes by means of a t-test.

The hypothesis of equal variances about the two regression lines can be tested as explained in section 4.4.2. by means of a two-sided F-test.

4.5.3.1. COMPARISON OF TWO REGRESSION LINES OF NOT SIGNIFICANTLY DIFFERENT VARIANCES

In this case a pooled estimate s^2_{rr} of the theoretical variance σ^2 can be calculated from the two variances $s^2_{r_1}$ and $s^2_{r_2}$:

$$s^2_{rr} = \frac{(N_1 - 2)s^2_{r_1} + (N_2 - 2)s^2_{r_2}}{N_1 + N_2 - 4} \qquad (4.34)$$

The slopes of the two lines can be compared by means of the following test-statistic :

$$t = \frac{b_1 - b_2}{s_{rr}\left[\frac{1}{h_1} + \frac{1}{h_2}\right]^{\frac{1}{2}}} \qquad (4.35)$$

where

$$h_1 = \sum_{i=1}^{k} n_i(x_i - \bar{x}_1)^2$$

$$h_2 = \sum_{i=1}^{k} n_i(x_i - \bar{x}_2)^2$$

If $|t| > t_{\beta}(\varphi)$, where $\beta = 1-(\alpha/2)$ and $\varphi = N_1+N_2-4$ degrees of freedom, the slopes are considered significantly different at the 100α percent level of significance, and thus the two regression lines are significantly different. If $|t| \leqslant t_{\beta}(\varphi)$, then the hypothesis of equal slopes cannot be rejected at the 100α percent level of significance, and the two regression lines would be parallel or identical.

The identity of the two lines, can be tested using the following test-statistic :

$$t' = \frac{B - \bar{b}}{s \left[\frac{1}{(\bar{x}_1 - \bar{x}_2)^2} \left(\frac{1}{N_1} + \frac{1}{N_2} \right) + \frac{1}{h_1 + h_2} \right]^{\frac{1}{2}}} \qquad (4.36)$$

where

$$B = \frac{a_1 - a_2}{\bar{x}_1 - \bar{x}_2}$$

$$\bar{b} = \frac{b_1 h_1 + b_2 h_2}{h_1 + h_2}$$

$$s = \left[\frac{(N_1 - 2)s_{r_1}^2 + (N_2 - 2)s_{r_2}^2 + \frac{(b_1 - b_2)^2}{\frac{1}{h_1} + \frac{1}{h_2}}}{N_1 + N_2 - 3} \right]^{\frac{1}{2}}$$

If $|t| > t_{\beta}(\varphi)$, where $\beta = 1-(\alpha/2)$ and $\varphi = N_1+N_2-3$ degrees of freedom, the lines are not identical, but parallel to each other. If $|t| \leqslant t_{\beta}(\varphi)$ then the hypothesis of identity of the two lines cannot be rejected at the $100\,\alpha$ percent level of significance.

4.5.3.2. COMPARISON OF TWO REGRESSION LINES OF SIGNIFICANTLY DIFFERENT VARIANCES

The following test-statistic can be used to check if the regression lines are parallel :

$$t = \frac{b_1 - b_2}{\left[\frac{s^2_{r_1}}{h_1} + \frac{s^2_{r_2}}{h_2}\right]^{\frac{1}{2}}} \qquad (4.37)$$

This can be compared with $t_{\beta}(\varphi)$ given in Table A.3 for $\beta = 1-(\alpha/2)$ and for φ degrees of freedom given by

$$\varphi = \left[\frac{C^2}{N_1 - 1} + \frac{(1 - C)^2}{N_2 - 1}\right]^{-1} \qquad (4.38)$$

$$C = \frac{\frac{s^2_{r_1}}{N_1}}{\frac{s^2_{r_1}}{N_1} + \frac{s^2_{r_2}}{N_2}}$$

The test is approximate and only if both N_1 and N_2 are larger than 30 a good approximation is possible.

If $|t| > t_{\beta}(\varphi)$, the slopes of the regression lines are significantly different at the 100α percent level of significance; this means that the two regression lines are significantly different. If $|t| \leqslant t_{\beta}(\varphi)$, the hypothesis of equal slopes cannot be rejected at the 100α percent level of significance, and the lines would be parallel or coinciding.

Their coincidence can be tested by

$$t = \frac{B - \bar{b}}{\left[\frac{1}{(\bar{x}_1 - \bar{x}_2)^2}\left(\frac{s^2_{r_1}}{N_1} + \frac{s^2_{r_2}}{N_2}\right) + \frac{1}{\frac{h_1}{s^2_{r_1}} + \frac{h_2}{s^2_{r_2}}}\right]^{\frac{1}{2}}} \qquad (4.39)$$

where

$$B = \frac{a_1 - a_2}{\bar{x}_1 - \bar{x}_2}$$

$$\bar{b} = \frac{\frac{b_1 h_1}{s^2_{r_1}} + \frac{b_2 h_2}{s^2_{r_2}}}{\frac{h_1}{s^2_{r_1}} + \frac{h_2}{s^2_{r_2}}}$$

If $|t| > t_{\beta}(\varphi)$, where $\beta = 1-(\alpha/2)$ and $\varphi = N_1+N_2-3$ degrees of freedom, the lines are not coinciding, but are parallel to each other. If $|t| \leqslant t_{\beta}(\varphi)$, then the hypothesis of coincidence of the lines cannot be rejected at the 100α level of significance.

4.5.4. LINEAR REGRESSION FOR FATIGUE DATA

In fatigue testing, the logarithm of the fatigue life ($\log_{10}N$) is often normally distributed at each stress level. An estimate of the type of function $\sigma_r = f(\log_{10}N)$, connecting the stress range σ_r and $\log_{10}N$, can be obtained by plotting all pairs of (σ_r, $\log_{10}N$) in a coordinate system. Based on this diagram and experience, a hypothesis regarding the type of the function $\sigma_r = f(\log_{10}N)$ can be set up.

Using the obtained results of the fatigue test programme the following type of function was chosen :

$$\sigma_r = C_1 \, e^{C_2 \log_{10}N} \qquad (4.40)$$

where C_1 and C_2 are experimental constants. This curve is, of course, not linear, but by a logarithmic transformation of the variables a linear relation was obtained between the transformed variables. This is given by :

$$\log_{10}N = a + b(\log_{10}\sigma_r - \overline{\log_{10}\sigma_r}) \qquad (4.41)$$

where $\log_{10}\sigma_r$ is the independent variable, $\overline{\log_{10}\sigma_r}$ the weighted mean of the $\log_{10}\sigma_r$ values and $\log_{10}N$ the dependent variable.

It can be shown that the coefficients C_1 and C_2 are given by :

$$C_1 = \log^{-1}(\overline{\log_{10}\sigma_r} - \frac{a}{b}) \qquad (4.42)$$

$$C_2 = \frac{1}{0.4343\ b} \qquad (4.43)$$

4.6. PROBABILITY CURVES

The regression equation (4.41) :

$$\log_{10}N = a + b(\log_{10}\sigma_r - \overline{\log_{10}\sigma_r})$$

represents a mean S-N curve, i.e. it provides an estimate of the relationship between applied stress and the number of cycles -to-failure that 50 % of the population would survive.

Assuming that at each stress level the fatigue test data are log-normally distributed, then for each stress level, the probability that a specimen will survive a number of cycles equal to N_1 is P and this is given by the cumulative normal distribution function :

$$P(y>y_1) = \frac{1}{s_r\sqrt{2\pi}} \int_{y_1}^{\infty} e^{-\frac{(y - y_r)^2}{2\ s_r^2}}\ dy \qquad (4.44)$$

where

$y = \log_{10}N$

$y_1 = \log_{10}N_1$

y_r = value predicted by the regression line

s_r^2 = variance about the regression line

Equation (4.44) can be used to determine the proba-

bility of survival for any particular value of $\log_{10}N_1$, and vice versa. Thus plots of σ_r versus $\log_{10}N$ can be drawn for various probabilities of survival.

4.7. COMPUTER PROGRAMS

Computer programs were written for the statistical analysis of fatigue data and automatic plotting of S-N and probability curves for fatigue failure. The results are given and discussed in Chapter 5.

CHAPTER 5

EXPERIMENTAL INVESTIGATION OF THE FATIGUE PROPERTIES OF HOT ROLLED DEFORMED BARS AND STATISTICAL ANALYSIS OF THE RESULTS

5.1. OBJECT AND SCOPE OF TESTS

The object of the test programme was to investigate the fatigue life of hot rolled deformed bars as affected by their embedment in concrete and their test length in air. All the tests were carried out for one minimum stress. The results were used to obtain a relationship between the stress-range and the fatigue life.

Preliminary tests carried out on one manufacturer's hot rolled deformed bar to determine the stress ranges to be used in the main programme revealed that bars with BS 4449 identification marks within their test length failed at these marks and there was a substantial reduction in the fatigue life. A survey of different manufacturer's bars marketed in the United Kingdom showed that different shapes of identification marks were used, some were more pronounced than others and thus it was to be expected that the fatigue life was affected to a different extent. Hence it was decided to undertake additional tests to investigate the effect of the identification marks upon the fatigue life of deformed bars.

The first series of tests was carried out to obtain the fatigue properties of a manufacturer's deformed bars tested free in air. The identification marks appearing in the test

length were removed by filing. The second series of tests was conducted on concrete tension members reiforced with the same hot rolled deformed bar, having the same test length as the specimens tested free in air and with identification marks removed.

Further series of tests were carried out to determine the effect of test length and identification marks upon the fatigue life of deformed bars tested free in air. Four different manufacturers' bars were used, all marketed in the United Kingdom; the test length was nearly half of that used in the first series of tests.

5.2. DEFINITIONS AND NOTATION

The fatigue life, N, of a specimen is defined as the number of load cycles of a specified character that the specimen sustains before failure occurs. Terminology and notation in this work follows, in so far as possible, the recommendations of BS 3518 : Part 1 (83).

The fatigue tests consisted of submitting specimens to a tensile sinusodial pulsation between two stress levels described as the maximum stress, σ_{max}, and the minimum stress, σ_{min}. The stress range, σ_r, is considered as the difference between the maximum and minimum stresses in one cycle.

The test was terminated either by fracture of the test piece, or by completion of up to one and a half million cycles of loading. Those specimens which did not rupture are termed runouts and are indicated as such when plotted.

In the description of the fatigue tests and in the analysis of the results, stress ranges and maximum and minimum

stress levels are all stated as percentages of the characteristic strength of the bars.

A plot of stress range, σ_r, against the number of cycles, N, to failure will be refered to as an S-N diagram. The diagram indicates the S-N relationship for a specified probability of survival. If the probability of survival is 50 % then the corresponding curve will be a mean S-N curve. Throughout this work the failure life is assumed to be at the 50 % probability of survival unless stated otherwise. A curve fitted to the fatigue life for p % survival values at each of several stress levels will be termed a P-S-N curve. It is an estimate of the relationship between applied stress range and the number of cycles-to-failure that p % of the population would survive; p may be any number, such as 1, 10, 90, etc.

For convenience, each series of tests was identified by four groups of alphanumeric characters separated by dashes; for example WEL-F-400-WI. The first group is the name of the bar manufacturer, i.e. WEL stands for Welbond, JON for Jones, SHE for Sheerness, and UNI for Unisteel (BSC) bars. The second character is either F for specimens tested free in air, or C for bars tested embedded in concrete. The third group of characters stands for the test length used, being either 400 mm or 900 mm, while the fourth group stands for the identification marks, i.e. WI if with identification marks in the test length or NI if no identification marks are present in the test length.

5.3. STATIC TESTS ON HOT ROLLED DEFORMED BARS

These tests were carried out to determine the charac-

teristic strength from 6 replications of the four different, 16 mm diameter, hot rolled deformed bars used in the fatigue programme. All four bars were made to BS 4449 : 1969, with a specified characteristic strength of 410 N/mm^2, but having different deformation patterns rolled on them. The names of the bars are : Welbond, Jones, Sheerness and Unisteel (BSC), see Plate 3.1.

The results of all static tests are given in Table 5.1. All specimens failed in the test length of the bar and none in the grips. Examples of profiles of fractured bars are shown in Plate 5.1 and the necking of the bars around the fracture surface is readily seen. Close-ups of static bar fractures are shown in Plate 5.2.

A full stress-strain diagram for a typical 16 mm diameter hot rolled deformed Welbond bar is shown in Figure 5.1a. The normal method of plotting this stress-strain diagram is shown in Figure 5.1b where the elongation scale is magnified and readings stop after 1 % elongation when the electronic extensometer used in plotting the curve was taken off to avoid damage as the test piece fails.

5.4. FATIGUE TESTS ON HOT ROLLED DEFORMED BARS

5.4.1. GENERAL

Hot rolled deformed bars conforming to BS 4449 : 1969, with a specified characteristic strength of 410 N/mm^2 and of 16 mm diameter were used in all fatigue tests.

There is a considerable scatter in fatigue life, and hence there is the need for replications and for a statistically

designed experiment. The test allocation of all specimens was randomised, in the way described in section 3.2.1.1. Thus the influence of all the variability inherent in the material and testing procedures was given a fair chance of being reflected in the test data.

The frequency adopted in the fatigue programme was 400 cycles/minute. This was the frequency at which the test rig operated best, and is within the limits of 200 to 600 cycles/minute recommended by the FIP Commission on Steel for Pretressing (85).

The effect of the minimum stress level on the fatigue life has been studied experimentally by others, as discussed in section 2.1.2.2, and it was decided not to investigate this parameter. Guided by published test results, mainly on American bars, and a small number of preliminary tests, a minimum stress level of 20 % of the characteristic strength was chosen so that suitable stress ranges could be established for obtaining fatigue failures varying between approximately 100,000 cycles and 1,000,000 cycles.

As pointed out in section 2.1.2.1, most S-N curves exhibit a transition from a steeper - finite life - to a flatter - long life - slope in the vicinity of one million cycles, indicating that deformed bars exhibit a practical fatigue limit. Because the scatter in fatigue life is very much higher in the long life region than in the finite life, any test programme in the long life region would require a large number of tests of long duration which would limit the number of possible replications. Furthermore the sensitivity of the load

measurement is such as to cause a large variation in fatigue life in the long life range. Thus it was decided to concentrate on the finite life region.

The minimum number of tests required for the determination of Probability-Stress-Cycle (P-S-N) curves for deformed bars depends on the dispersion of the results and on the confidence level desired. The Recommendations of ASTM Committee E-9 on fatigue (84) were followed in the selection of the number of stress levels and the minimum number of specimens required at each stress level for the determination of P-S-N curves. Thus four or five stress ranges were used and five or six specimens tested at each stress range in most fatigue test series.

The result of any specimen that failed in the grips was not taken into account in the statistical analysis, and the test was repeated.

5.4.2. FATIGUE TESTS ON BARS FREE IN AIR

TEST SERIES WEL-F-900-NI

These tests were carried out to obtain an empirical relationship between the stress range and the probable fatigue life of 16 mm diameter, hot rolled Welbond deformed bar tested free in air.

The test length used was 900 mm and the identification marks within this length were removed and the corresponding area of the bar polished.

The stress ranges used for obtaining failures between approximately 100,000 and 1,000,000 cycles were 0.70 σ_{char},

0.65 σ_{char}, 0.63 σ_{char} and 0.60 σ_{char} with a minimum stress level of 0.20 σ_{char}. A total of twenty-four specimens was tested.

The results of this series of tests are given in Table B.1 to B.4 and summarised in Table 5.2. In approximately 95 % of all tests, fractures occurred at random positions along the test length of the specimens, the remainder failing within the grips. No fracture occurred at the filed identification marks.

A description of the statistical analysis carried out is given in section 5.6. As a result of the regression analysis the mean fatigue life with its 95 % confidence limits was obtained and is shown in Figure 5.3 and the mean fatigue life with various probabilities of survival is shown in Figure 5.4.

5.4.3. FATIGUE TESTS ON BARS EMBEDDED IN CONCRETE

TEST SERIES WEL-C-900-NI.

These tests were carried out to investigate the fatigue life of 16 mm diameter, hot rolled Welbond deformed bar as affected by its embedment in concrete and the associated concrete cracking.

The test length of the bars was 900 mm long, with the central 800 mm embedded in concrete, as shown in Plate 3.5. Twenty-four of these specimens were tested using stress ranges of 0.70 σ_{char}, 0.65 σ_{char}, 0.63 σ_{char} and 0.60 σ_{char}.

The two 50 mm lengths of the bar on either side of the concrete were surface treated and all failures occurred in the length embedded in concrete. In the first cycle transverse cracks formed in the concrete, as shown in Plate 3.5 at an

average spacing of 87 mm. For the range of stresses used, these cracks traversed the whole section of the concrete cylindrical member. Fatigue fractures in the steel always occurred at one of these cracks and were remote from the filed identification marks.

The results of this series of tests are given in Tables B.5 to B.8 and summarised in Table 5.2.

A statistical treatment of the test results is carried out in section 5.6. The mean fatigue life with its 95 % confidence limits, obtained from a regression analysis of the test data, is shown in Figure 5.5 and the mean fatigue life with various probabilities of survival is shown in Figure 5.6. The regression lines from this series of tests and from those tested free in air are compared in section 5.6.2.3.

5.4.4. FATIGUE TESTS ON BARS FREE IN AIR

TEST SERIES WEL-F-400-WI, JON-F-400-WI, SHE-F-400-WI, UNI-F-400-WI AND WEL-F-400-NI, JON-F-400-NI, SHE-F-400-NI

These tests were carried out to provide stress versus cycles to fatigue failure (S-N) curves for four different hot rolled deformed bars marketed in the United Kingdom. Each manufacturer's bar was tested with identification marks and with no identification marks included in the test length. The effect on the fatigue behaviour of deformed bars of test length was established by comparing results of these tests with the corresponding ones obtained in an earlier series.

A test length of 400 mm was chosen for the whole series so that no identification marks would be present between

the grips. Approximately half of the number of tests were on bars with identification marks randomly placed in their test length, and the other half on bars with no identification marks. A total of 161 tests was carried out; 53 on Welbond bars, 44 on Jones, 43 on Sheerness and 21 on Unisteel (BSC).

Only approximately 5 % of the specimens tested failed in the grips. The results of these tests were ignored and the tests were repeated. Those bars with identification marks included in their test length all failed at these marks except for the Unisteel bars. Thus it was decided to abandon the series of tests on Unisteel bars with no identification marks in their test length. In all the series of tests where no identification marks were present fractures occurred at random positions along the test length.

The results are given in Tables B.9 to B.37 and summarised in Table 5.2. A regression analysis was carried out on each of the seven series of test results. The mean fatigue lives with 95 % confidence limits are shown in Figures 5.7, 5.9, 5.11, 5.13, 5.15, 5.17 and 5.19, and the mean fatigue lives with various probabilities of survival are shown in Figures 5.8, 5.10, 5.12, 5.14, 5.16, 5.18, and 5.20.

The results obtained from these seven series of tests and those from the previous series are compared in section 5.6.2.3.

5.5. DESCRIPTION OF STATIC AND FATIGUE FAILURES OF HOT ROLLED DEFORMED BARS

Following the fatigue fracture of each specimen, the

detail of the fracture surface and its location on the bar were visually examined and recorded. The present investigation of fatigue fractures was at the phenomenological level. In most cases, the bar fracture surfaces had two distinct zones, a familiar feature of fatigue failures (1). These zones can be seen in Plates 5.4, 5.5, 5.6 and 5.7. The zone associated with the fatigue crack was crescent shaped, generally having a smooth, dull and rubbed appearance. The remainder of the fracture surface had a rough, crystalline appearance. This zone is the part that finally fractured in tension after the fatigue crack had weakened the bar.

Ductile failures under static overload exhibit a necking-down portion. This can be seen in the bars of Plate 5.1 which were statically tested in tension to failure. A brittle material under static overload will not show any evidence of necking-down. A fatigue fracture, whether the material is ductile or brittle, follows that of a brittle fracture, as shown in the bars of Plate 5.3 which were tested under a tensile cycling load to failure.

In general, a fairly good determination of the point where the fatigue crack started could be made by visual examination of the fracture surface. This was based largely on the observation that there was, in general, an increase in roughness away from the apparent nucleus of the fatigue crack, and that the crescent shaped transition from the crack to the static fracture surface appeared generally to focus on the point where the fatigue crack began.

All deformed bars tested in fatigue with identification

marks present in their test length failed at a cross section which contained one of these marks, e.g. as shown in Plate 5.4c and 5.5c. The only exceptions were the Unisteel bars. Examination of the identification marks showed that in most cases they were not uniformly rolled along the length of the deformed bars, and one of their sides was steeper than the other. The fatigue crack originated at the base of the steeper side of the most pronounced identification mark within the test length. The Unisteel bars had identification marks which were rather smooth, compared to those used in the other bars, as can be seen in Plate 3.1.

All fatigue failures in bars with no identification marks occurred either at the base of the transverse lugs, or at the base of the longitudinal ribs, or at the point of intersection of the transverse lugs and the longitudinal ribs. In the Jones and Sheerness bars the transverse lugs were terminated so that they did not intersect the longitudinal ribs, while in the Unisteel bars no longitudinal ribs were present, as shown in Plate 3.1.

The reinforcing bar specimens tested in air were uniformly stressed along the length of the bar under the applied fatigue loading. Thus the probability of failure of the specimen was essentially the same at each deformation along the length of the specimen. Fatigue failures, in the case of Welbond bars, originated at the base of one of the transverse lugs at the point of intersection of one of the longitudinal ribs, as shown in Plate 5.4; this point must therefore be the weakest region in the bar under cyclic loading. Though the

Welbond bars embedded in concrete cylindrical members were most highly stressed in only a short length adjacent to each crack, and there were only 8 or 9 cracks present in the 800 mm of concrete length, failure always occurred at one of these cracks and originated at the same spot as for the Welbond bars tested in air, see Plate 5.8. The similar failure origin of the Welbond bars tested in air or embedded in concrete can be attributed to the close spacings of the deformations which ensured that a deformation occurred within the highly stressed region in a reinforced concrete tension member.

In the Jones bars the fatigue crack always originated at the base of one of the transverse lugs (Plate 5.5). In the Sheerness bars 30 % of the failures had fatigue cracks originating at the base of the longitudinal ribs and the remaining 70 % at the base of one of the transverse lugs (Plate 5.6). In the Unisteel bars all failures had a fatigue crack originating at the base of one of the transverse lugs (Plate 5.7).

5.6. STATISTICAL ANALYSIS OF FATIGUE TEST DATA

A certain amount of scatter is present in the results of all experimental work and is caused by the inherent variability of the material properties due to flaws and other variations in addition to the scatter caused by inexact methods of measurement and testing. When the scatter is small compared with the quantity being measured, the mean may be taken to represent the quantity adequately, as in the case of the static ultimate strength of Welbond hot rolled deformed bar, where the coefficient of variation of the results was only 2.2 %.

However, in fatigue life data, scatter is considerable, and in the tests on Welbond bars - Free in Air - 400 mm long - with no identification marks, with a stress range of 63 % of the characteristic strength, the coefficient of variation of the fatigue life was 22 %. Consequently because of this large scatter a statistical analysis of the fatigue results is essential. The present analysis includes the following tests :

(i) χ^2 - goodness of fit test and Blom's test to investigate the suitability of the log-normal distribution.

(ii) χ^2 - test to check the hypothesis of common variance of the linear regression analysis.

(iii) F - test to check the hypothesis of linearity of the linear regression analysis.

(iv) t - test to compare the slopes and identity of two regression lines.

To test a statistical hypothesis, a level of significance, α, must be chosen. As explained in section 4.2.3, the most commonly used values of α are 5 % and 10 %.

When the χ^2 - test is used to test if the data is normally distributed or to check the hypothesis of common variance of the linear regression analysis, the most critical value of χ^2 is at a level of significance $\alpha = 10$ %, since $\chi^2_{0.90}$ is smaller than $\chi^2_{0.95}$.

When the F - test is used to check the hypothesis of equality of two variances or the linearity of the linear regression analysis, again the value of F at $\alpha = 10$ % is more critical than at $\alpha = 5$ %.

When two slopes are compared, they have less chance to be significantly different at $\alpha = 5$ % than $\alpha = 10$ %, since the theorectical valve of t corresponding to a 5 % probability is higher than the value corresponding to a 10 % probability. Consequently, when the calculated value of t is larger than the theoretical value $t_{0.975}$, the slopes are considered as significantly different. When the calculated value of t is smaller than the theoretical value $t_{0.95}$, the slopes are considered not significantly different. If the value of t were near $t_{0.975}$ the slopes are probably significantly different, while if the value of t were near $t_{0.95}$ they are probably not significantly different. When the value of t is midway between $t_{0.95}$ and $t_{0.975}$ it is uncertain that the slopes are significantly different or not. Calculated values of t between $t_{0.95}$ and $t_{0.975}$ are considered to be in a zone of uncertainty.

5.6.1. χ^2 - TEST FOR GOODNESS OF FIT

Before a statistical analysis of fatigue data can be made, the frequency distribution must be known. Several investigations have been carried out to determine the shape of the frequency distributions obtained for the fatigue life of test specimens. It has been found that the logarithm of the fatigue life is very nearly normally distributed. In the analysis of the fatigue data obtained in the present study, the suitability of a log-normal distribution to fatigue lives was investigated. Nine χ^2 - tests were carried out covering all series of fatigue test data.

Examples of the χ^2 - test are given in Tables 5.3

and 5.4. The results of all the χ^2 - tests are summarised in Table 5.5.

In all the series of tests, the χ^2 - test was passed at the 10 % level of significance. Therefore, it can be assumed that the data obtained in the fatigue tests is log-normally distributed.

Another verification of the log-normal distribution of the fatigue data is given in section 5.6.2.2 by means of Blom's test, where a visual inspection is made.

Thus it can be concluded that, for each stress level, the probability that failure will occur at a number of cycles equal to or less than N, is given by the cumulative normal distribution function.

5.6.2. REGRESSION ANALYSIS, BLOM'S TEST AND COMPARISON OF REGRESSION LINES

5.6.2.1. REGRESSION ANALYSIS

A linear regression analysis was performed on the nine series of fatigue data. The results are shown in Table 5.7 where it can be seen that, in all the series of tests, the hypothesis of common variance and linearity of the linear regression analysis are true at the 10 % level of significance.

For each series of tests the following curves, resulting from the linear regression analysis, were plotted :

(i) the mean fatigue life and its 95 % confidence limits, and

(ii) the mean fatigue life as well as the 1 %, 10 %, 90 % and 99 % probabilities of survival.

All these curves and their equations are shown in Figures 5.3 to 5.20 and compared graphically in Figures 5.21 to 5.27. All these curves are strictly correct within the range in which experimental data were obtained, but they have been extended to 10^6 cycles for uniformity of presentation.

It should be mentioned that the confidence limits of a regression line depend upon the number of observations used to calculate the regression line. The smaller is the number of observations, the bigger is the confidence interval for a given confidence level. The confidence interval is variable along a regression line, being narrowest at $x = \bar{x}$ and becoming larger as x moves from $\bar{x}$, where $x = \log_{10} \sigma_r$ and $\bar{x}$ is the weighted mean of the x - values. Outside the range of observations the confidence interval becomes very wide.

5.6.2.2. BLOM'S TEST

This test can be used to check graphically whether the observed fatigue lives, when transformed logarithmically are normally distributed.

With Blom's test a comparison is made of a plot, on normal probability paper, of cumulative percent of observations versus regression residuals to a straight line.

All nine series of fatigue test data have been analysed using Blom's test. In order to minimise bias, the residuals are plotted against the cumulative frequency equal to $(i - \frac{3}{8})/(n + \frac{1}{4})$ as suggested by Blom (92) and Kimball (93) for the normal distribution. All plots fitted satisfactorily to straight lines, indicating that the fatigue lives, when transformed logarithmi-

cally, are normally distributed.

A typical calculation on one of the series of fatigue test data is given in Table 5.6 with the corresponding plot on normal probability paper shown in Figure 5.2.

5.6.2.3. COMPARISON OF REGRESSION LINES

Any comparison between regression lines must be done statistically at a chosen significance level, since these lines are best fit lines to fatigue data exhibiting considerable scatter.

Fourteen comparisons of regression lines were carried out, each comparison being between two lines. All statistical comparisons of variances, slopes and identity of regression lines were performed at the 5 % and 10 % significance levels as explained in section 5.6. A typical comparison of two regression lines is given in Appendix C. The results of all comparisons are summarised in Table 5.8.

In three of the above fourteen comparisons of the regression lines the variances were found to be significantly different and one case was in the zone of uncertainty. The results of these four comparisons should then be treated with caution, since, as it was pointed out in section 4.5.3.2, the test of identity of two regression lines is only approximate for 30 or less degrees of freedom, if their variances are significantly different.

Although the slopes of six of the fourteen pairs of regression lines were not significantly different, the lines of only one pair were found to be identical, and those of the other five pairs were just parallel to each other.

Different manufacturers' bars with identification marks included in their test length were compared using the results of series WEL-F-400-WI, JON-F-400-WI and SHE-F-400-WI. In addition to the above analysis, their S-N curves are shown in Figure 5.21. The results of test series WEL-F-400-NI, JON-F-400-NI, SHE-F-400-NI and UNI-F-400-WI were used to compare different bars with no identification marks in their test length. The Unisteel bar results are included in this comparison, since these bars did not fail at the identification marks. In addition to the above statistical analysis, the corresponding four S-N curves are shown in Figure 5.22.

The effect of identification marks upon the fatigue life of hot rolled deformed bars was investigated by comparing the test results of series WEL-F-400-WI to WEL-F-400-NI, JON-F-400-WI to JON-F-400-NI and SHE-F-400-WI to SHE-F-400-NI. Their S-N curves are compared in Figures 5.23, 5.24 and 5.25 respectively, and statistical comparisons are given in Table 5.8.

Series WEL-F-400-NI and WEL-F-900-NI were compared for assessing the effect on the fatigue life of deformed bars of their test length. Their S-N curves are compared in Figure 5.26 and statistical comparisons are given in Table 5.8.

The effect on the fatigue life of deformed bars of their embedment in concrete was assessed by comparing the test results of series WEL-F-900-NI and WEL-C-900-NI. Their S-N curves are shown in Figure 5.27 and statistical comparisons are given in Table 5.8.

5.7. INTERPRETATION OF RESULTS OF STATISTICAL ANALYSIS AND CONCLUSIONS

(a) General

The gripping arrangement developed for the testing of bars in air or embedded in axial tension members, under pulsating load, proved very successful. There was approximately only 5 % of the specimens that failed into the grips, as compared to 20 % obtained by the epoxy resin type of grips, which were reported in section 2.1.3.2. Also the type of grip employed in this fatigue programme is simpler, quicker as well as more economical to make than the cement grout bond anchorage or resin type of grips.

Nine series of fatigue tests were carried out on four different manufacturers', 16 mm diameter, hot rolled deformed bars, tested free in air or embedded in concrete. Identification marks, as well as no identification marks, were included in the bars test length. The observed fatigue lives in all series of tests, when transformed logarithmically, were found to be normally distributed.

The data from each of the above fatigue test series were plotted on log(stress) and log (number of cycles to failure) axes and the equations of best fit lines were derived by linear regression analysis. In all cases the hypothesis of common variance and linearity of the regression lines were verified at the 10 % level of signicance. Also 95 % confidence limits were found for each mean S-N curve, as well as a number of S-N curves of different probabilities of survival.

(b) Different Manufacturers' Deformed Bars

There was a wide variation found between the S-N curves of the four different bars, with identification marks, as well as with no identification marks, included in their test length. This variation was both in slopes as well as in relative values, of the obtained S-N curves. All bars with identification marks included in their test length failed at a cross-section which contained one of these marks, except for the Unisteel bar.

Statistical comparisons of the S-N curves, as given in Table 5.8, showed that the slopes of the curves of the Welbond and Jones bars, with identification marks, were not significantly different, while the slope of the Sheerness bar was significantly different to that of the other two bars. In addition, the regression lines of the three bars were found to be significantly different statistically. Visual inspection of the S-N curves of Figure 5.21 was in agreement with the above statistical comparisons. With identification marks in the test length, the bar with the largest fatigue life was found to be the Sheerness bar and the one with the shortest fatigue life was the Welbond bar. At a stress range of 63 % of the characteristic strength of the bar there is a 50 % probability that failure would occur at 1,000,000 cycles for the Sheerness bar and 240,000 cycles for the Welbond bar.

With no identification marks included in the test length, Welbond, Jones, Sheerness and Unisteel bars were compared statistically. The Unisteel bar results were included in this comparison, since these bars did not fail at the iden-

tification marks. All bars were found to have significantly different regression lines statistically, although some of the statistical tests were approximate because of non-common variances. Nevertheless visual inspection of the S-N curves of the four deformed bars, given in Figure 5.22, also revealed large differences between the bars. For example, at a stress range of 64.5 % of the characteristic strength of the bar there is a 50 % probability that failure would occur at 1,000,000 cycles for the Sheerness bar and 470,000 cycles for the Unisteel bar. These were correspondingly the bars with the longest and shortest fatigue lives when no identification marks were present within their test length, or, in the case of the Unisteel bar failure occurred remote from the marks.

(c) Effect Of Identification Marks

Identification marks on deformed bars were found to produce a statistically significant reduction in their fatigue lives. This was true for the Welbond, Jones and Sheerness bar, as can be seen from Figures 5.23 to 5.25. To access the magnitude of this reduction, the stress range at which, there is a 50 % probability that bars, with no identification marks in their test length, will fail at one million cycles is taken as reference. The percentage reductions in fatigue lives of the above deformed bars, containing identification marks in their test length, under each bar's reference stress range are given below :

	Reference Stress Range σ_{ref} % char. strength	Reduction in fatigue life under σ_{ref}
Welbond	59	70 %
Jones	57	47 %
Sheerness	64	20 %

The variation in the magnitude of the above percentage reductions can be attributed to the different stress concentration factors of the identification marks rolled onto the surface of the three deformed bars. Visual examination revealed that the identification marks on the Welbond bars had the sharpest profile of all marks used, while the profile of the marks on the Unisteel bars was rather smooth compared to the others and no failure occurred at these marks.

Thus it is recommended that bar manufacturers should pay more attention to the design of identification marks and develop suitable profiles which would not act as fatigue crack initiators. The Unisteel bar manufacturers achieved this by using identification marks with smooth base radii.

(d) Effect Of Test Length

S-N curves for Welbond deformed bars, of 400 and 900 mm test lengths, were found to be significantly different statistically and to have significantly different slopes, as shown in Table 5.8. This is also clearly seen in the curves of Figure

5.26. At a stress range of 59 % of the characteristic strength of the bar there is a 50 % probability that failure would occur at 1,000,000 cycles for the 400 mm test length and 600,000 cycles for the 900 mm one, i.e. there is a reduction of 40 % in fatigue life. This reduction can be attributed to the fact that increasing the test length, the probability of including a critical flaw increases and thus the fatigue life decreases. Edwards and Picard (56) obtained a similar decrease in fatigue life when testing strand with test lengths of 255 and 890 mm.

In the above fatigue test series on Welbond bars, there were no identification marks included in the 400 mm test lengths; in the 900 mm test lengths the identification marks were removed by filing and no failure occurred at these positions. This shows that the detrimental effect of identification marks upon the fatigue life of deformed bars, is only a surface effect.

(e) Effect Of Embedment In Concrete

Welbond deformed bars, of 900 mm test length, tested in air were compared with Welbond bars, of the same test length, but embedded centrally in concrete cylindrical tension members. In both types of tests the identification marks present in the test length were filed away. The statistical comparison of the derived regression lines, given in Table 5.8, revealed no significant difference between the lines, but caution should be exercised because the statistical tests were approximate due to the non-common variances of the two regression lines. Also visual inspection of the two S-N curves, shown in Figure 5.27,

indicates a small but non-significant increase in fatigue life of the bars embedded in concrete as compared to those free in air.

The following factors can influence the fatigue behaviour of deformed bars embedded in concrete :

(i) The cracks may not close after removal of the load, because small grains of material can lodge between the faces of cracks. Thus minimum stress in the bar may be higher than that calculated from the minimum applied load.

(ii) The bars tested in air were uniformly stressed along their length, however for the same load the stress in the bars embedded in the concrete could have obtained similar values only at and adjacent to the transverse cracks and must have been lower elsewhere.

Thus in the case of an embedded bar the following factors arise, which appear in this case to be nearly self cancelling : the length of the specimen subjected to the maximum stress, the stress concentration at a crack, and local fretting between steel and concrete adjacent to a crack. All these factors lead to the fatigue fracture occurring at a crack and this was confirmed by the experimental results. Assuming a critical length of 10 mm adjacent to each crack, where fatigue failure can take place, then since 8 or 9 cracks were formed in the 800 mm concrete length, it could be argued that the corresponding length for the test in air should be of the order of 100 mm. It has already been shown that the fatigue life of a deformed bar in air increases with decreasing length and thus it is to be expected that the fatigue life of a 100 mm bar test

length should be higher than that of a 400 mm one. But at a stress range of 59 % of the characteristic strength of the bar, it was found that there is a 50 % probability that failure would occur at 1,000,000 cycles for the 400 mm test length in air and 710,000 cycles for the bar in concrete with an assumed uniform stress length of 100 mm. Thus instead of an increase in fatigue life there is a reduction of 29 %. This marked reduction in fatigue life could be attributed to the stress concentration at a crack and the local fretting between steel and concrete in the vicinity of a crack. But it is felt that more fatigue tests are required to be carried out on a number of different test lengths, before drawing firm conclusions.

TABLE 5.1

RESULTS OF STATIC TESTS ON HOT-ROLLED DEFORMED BARS

	Yield Load (Newtons)			
	Welbond	Jones	Sheerness	Unisteel
	84950	82700	89050	90200
	88050	83700	89550	90500
	88500	84300	89550	90700
	88750	85400	90050	91500
	89650	85500	91000	92300
	90500	85700	91500	92600
Mean Yield Load N	88400	84550	90100	91300
Mean Yield Stress N/mm^2	440	420	448	454
C_v	2.2 %	1.4 %	1.1 %	1.1 %

TABLE 5.2

SUMMARY OF THE RESULTS OF FATIGUE TESTS ON 16 MM DIAMETER HOT-ROLLED DEFORMED BARS

Test Series	% $\sigma_{r\ char}$	Sample Size	$\overline{\log N}$	$\bar{N}_{\log}$	$S_{\log N}$
WEL-F-500-NI	70	6	5.446	279000	0.03292
	65	7	5.595	395000	0.05914
	63	6	5.620	417000	0.07400
	60	5	5.767	585000	0.04380
WEL-C-500-NI	70	6	5.463	291000	0.10632
	65	6	5.620	417000	0.06610
	63	6	5.640	437000	0.06958
	60	6	5.846	702000	0.10856
WEL-F-400-NI	70	6	5.234	171000	0.03839
	57	5	5.504	319000	0.03162
	53	3	5.605	402000	0.07444
	50	6	5.707	510000	0.08835
	49	7	5.783	606000	0.06891
WEL-F-400-NI	70	7	5.531	340000	0.05232
	67	6	5.611	408000	0.03544
	65	6	5.753	566000	0.04799
	63	7	5.806	640000	0.09262
JON-F-400-NI	70	6	5.411	258000	0.04803
	60	6	5.667	464000	0.04144
	57	6	5.715	518000	0.04922
	55	6	5.776	597000	0.10563
JON-F-400-NI	70	5	5.646	443000	0.09514
	68	5	5.647	444000	0.06666
	65	5	5.796	625000	0.12765
	60	5	5.892	780000	0.06599
SHE-F-400-NI	73	5	5.447	280000	0.06465
	70	5	5.580	380000	0.10439
	68	6	5.692	492000	0.04710
	65	6	5.893	782000	0.06732
SHE-F-400-NI	73	6	5.521	332000	0.09826
	70	5	5.657	454000	0.07643
	69	4	5.740	550000	0.08184
	68	6	5.796	626000	0.06668
UNI-F-400-NI	68	6	5.535	343000	0.03134
	67	5	5.602	400000	0.03851
	65	5	5.650	446000	0.04026
	64	5	5.692	492000	0.05883

$$\overline{\log N} = \frac{\sum_{i=1}^{n} \log N}{n} \qquad \bar{N} = \log^{-1}(\overline{\log N})$$

TABLE 5.3

χ^2 TEST FOR GOODNESS OF FIT

TEST SERIES: WEL-F-400-WI

Total number of data = 27

Number of categories : $r \leq \frac{27}{5} = 5.4$ $\therefore$ $r = 5$

Theoretical relative frequency : $\frac{1}{r} = 0.200$

Theoretical frequency : $p_{t_i} = \frac{27}{r} = 5.40$

Categories	Theor. Rel. Frequency	Theoretical Frequency (p_{t_i})	Observed Frequency (p_{o_i})	$\frac{(p_{o_i}-p_{t_i})^2}{p_{t_i}}$
$-\infty < z < -0.842$	0.200	5.40	7	0.474
$-0.842 \leq z < -0.253$	0.200	5.40	3	1.067
$-0.253 \leq z < 0.253$	0.200	5.40	4	0.363
$0.253 \leq z < 0.842$	0.200	5.40	6	0.067
$0.842 \leq z < \infty$	0.200	5.40	7	0.474
$\sum$	1.000	27.00	27	2.450

d.f. = r-1-g = 5-1-2 = 2

$\chi^2_{.90}(2) = 4.61$

$\chi^2_{.95}(2) = 5.99$

$2.45 < \chi^2_{.90}(2) < \chi^2_{.95}(2)$

TABLE 5.4

χ^2-TEST FOR GOODNESS OF FIT

TEST SERIES: JON-F-400-WI

Total number of data = 24

Number of categories : $r \leq \frac{24}{5} = 4.8$ $\therefore$ $r = 4$

Theoretical relative frequency : $\frac{1}{r} = 0.250$

Theoretical frequency : $p_{t_i} = \frac{24}{r} = 6.00$

Categories	Theor. Rel. Frequency	Theoretical Frequency (p_{t_i})	Observed Frequency (p_{o_i})	$\frac{(p_{o_i}-p_{t_i})^2}{p_{t_i}}$
$-\infty < z < -0.675$	0.250	6.00	7	0.167
$-0.675 \leq z < 0.000$	0.250	6.00	7	0.167
$0.000 \leq z < 0.675$	0.250	6.00	4	0.667
$0.675 \leq z < \infty$	0.250	6.00	6	0.000
$\sum$	1.000	24.00	24	1.001

d.f. = r-1-g = 4-1-2 = 1

$\chi^2_{.90}(1) = 2.71$

$\chi^2_{.95}(1) = 3.84$

$1.001 < \chi^2_{.90}(1) < \chi^2_{.95}(1)$

TABLE 5.5

SUMMARY OF ALL χ^2 - TESTS FOR GOODNESS OF FIT

Test Series	Series Size	d.f.	χ^2	$\chi^2_{.90}$	$\chi^2_{.95}$
WEL-F-400-WI	27	2	2.45	4.61	5.99
WEL-F-400-NI	26	2	1.31	4.61	5.99
WEL-F-900-NI	24	1	2.33	2.71	3.84
WEL-C-900-NI	24	1	0.66	2.71	3.84
JON-F-400-WI	24	1	1.00	2.71	3.84
JON-F-400-NI	20	1	2.40	2.71	3.84
SHE-F-400-WI	22	1	0.18	2.71	3.84
SHE-F-400-NI	21	1	1.67	2.71	3.84
UNI-F-400-WI	21	1	0.91	2.71	3.84

TABLE 5.6

BLOM'S TEST

TEST SERIES: SHE-F-400-WI n = 22

i	$p = \frac{(i - \frac{3}{8})}{(n + \frac{1}{4})} \times 100\%$	Percent Survivals (1-p) x 100%	$(\log N_{obs.} - \log N_{pred.}) \times 10^{-3}$
1	3	97	-138
2	7	93	- 84
3	12	88	- 72
4	16	84	- 62
5	21	79	- 53
6	25	75	- 51
7	30	70	- 43
8	34	66	- 28
9	39	61	- 26
10	43	57	- 17
11	48	52	- 7
12	52	48	0
13	57	43	1
14	61	39	7
15	66	34	22
16	70	30	39
17	75	25	46
18	79	21	57
19	84	16	68
20	88	12	98
21	93	7	112
22	97	3	143

TABLE 5.7

RESULTS OF LINEAR REGRESSION ANALYSIS

Test Series	Series Size	$\bar{x} = \log_{10}\sigma_r$	a	b	s_r^2	C_1	C_2	Test Of Common Variance			Test Of Linearity		
								χ^2	$\chi^2_{.90}$	$\chi^2_{.95}$	F	$F_{.90}$	$F_{.95}$
WEL-F-400-WI	27	1.743	5.573	- 3.420	0.00417	2355.6	- 0.673	5.43	7.78	9.49	1.17	2.36	3.08
WEL-F-400-NI	26	1.821	5.675	- 6.314	0.00404	524.5	- 0.365	5.26	6.25	7.81	1.45	2.57	3.46
WEL-F-900-NI	24	1.810	5.600	- 4.573	0.00317	1084.1	- 0.504	3.16	6.25	7.81	1.34	2.59	3.49
WEL-C-900-NI	24	1.809	5.642	- 5.427	0.00860	705.5	- 0.424	1.91	6.25	7.81	1.71	2.59	3.49
JON-F-400-WI	24	1.780	5.642	- 3.465	0.00414	2560.1	- 0.665	5.79	6.25	7.81	0.34	2.59	3.49
JON-F-400-NI	20	1.817	5.745	- 3.996	0.00829	1798.7	- 0.576	2.36	6.25	7.81	0.81	2.69	3.66
SHE-F-400-WI	22	1.837	5.666	- 8.902	0.00492	297.5	- 0.259	2.70	6.25	7.81	0.41	2.63	3.57
SHE-F-400-NI	21	1.846	5.674	- 8.934	0.00614	302.4	- 0.258	0.71	6.25	7.81	0.20	2.66	3.60
UNI-F-400-WI	21	1.820	5.616	- 5.565	0.00180	674.8	- 0.414	1.75	6.25	7.81	0.82	2.66	3.60

TABLE 5.8

RESULTS OF COMPARISONS OF REGRESSION LINES

Test Series Compared	Test Of Common Variance Of Regression Lines			Test Of Common Slopes Of Regression Lines			Test Of Identity Of Regression Lines		
	F	$F_{.95}$	$F_{.975}$	|t|	$t_{.95}$	$t_{.975}$	|t|	$t_{.95}$	$t_{.975}$
WEL-F-400-WI and JON-F-400-WI	1.01	2.01	2.38	0.116	1.679	2.014	10.300^{oo}	1.679	2.013
WEL-F-400-WI and SHE-F-400-WI	1.18	2.00	2.29	6.765^{++}	1.681	2.016	16.340^{oo}	1.680	2.015
JON-F-400-WI and SHE-F-400-WI	1.19	2.05	2.37	6.372^{++}	1.683	2.019	7.340^{oo}	1.682	2.018
WEL-F-400-NI and JON-F-400-NI	2.05	2.05	2.36	2.115^{++}	1.683	2.019	23.740^{oo}	1.682	2.018
WEL-F-400-NI and SHE-F-400-NI	1.52	2.03	2.33	1.754^{+}	1.682	2.018	6.430^{oo}	1.681	2.017
WEL-F-400-NI and UNI-F-400-WI	2.24^{*}	2.08	2.41	0.660	1.701	2.049	4.190^{oo}	1.681	2.017
JON-F-400-NI and SHE-F-400-NI	1.35	2.14	2.49	2.910^{++}	1.688	2.027	2.030^{oo}	1.687	2.025
JON-F-400-NI and UNI-F-400-WI	4.61^{**}	2.14	2.49	1.316	1.706	2.056	5.120^{oo}	1.687	2.025
SHE-F-400-NI and UNI-F-400-WI	3.41^{**}	2.12	2.46	2.030^{++}	1.688	2.027	8.280^{oo}	1.685	2.023
WEL-F-400-WI and WEL-F-400-NI	1.03	1.97	2.26	3.856^{++}	1.678	2.012	14.540^{oo}	1.677	2.010
JON-F-400-WI and JON-F-400-NI	2.00	2.09	2.41	0.662	1.684	2.021	8.910^{oo}	1.683	2.020
SHE-F-400-WI and SHE-F-400-NI	1.25	2.10	2.43	0.020	1.685	2.023	3.710^{oo}	1.684	2.021
WEL-F-400-NI and WEL-F-900-NI	1.27	2.03	2.32	2.033^{++}	1.680	2.015	6.960^{oo}	1.679	2.014
WEL-F-900-NI and WEL-C-900-NI	2.71^{**}	2.04	2.35	0.928	1.684	2.021	1.680	1.681	2.016

** Variances significantly different

* Variances in the zone of uncertainty

++ Slopes of regression lines significantly different

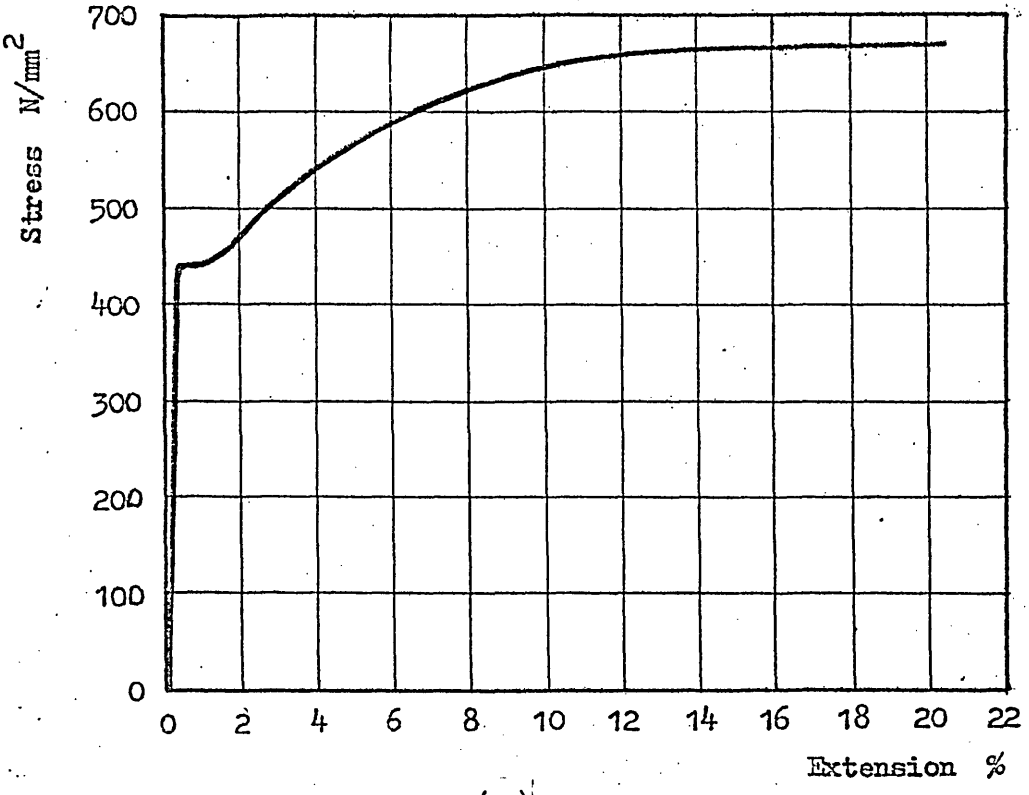
+ Slopes of regression lines in the zone of uncertainty

oo Regression lines significantly different

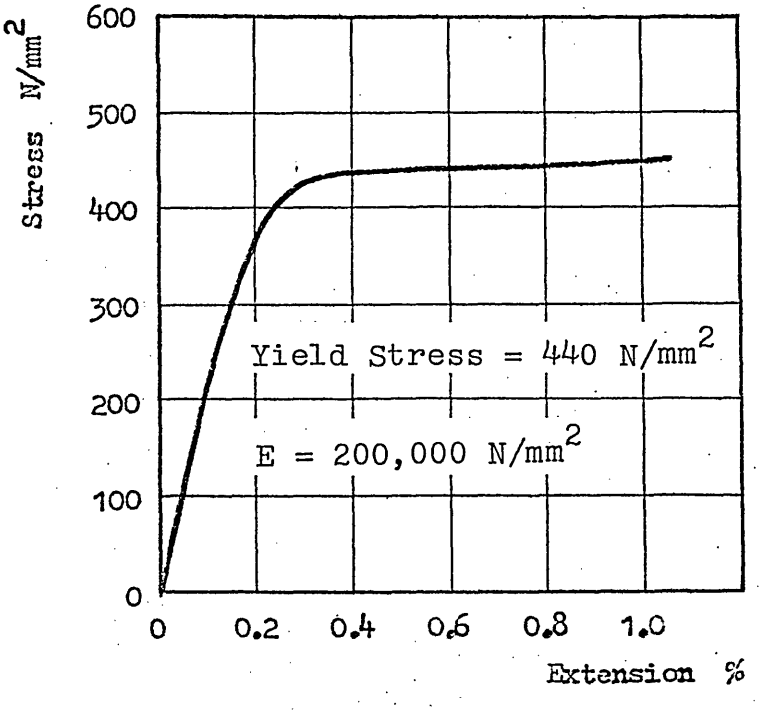
o Regression lines in the zone of uncertainty

STRESS-STRAIN DIAGRAMS FOR

HOT-ROLLED DEFORMED WELBOND BAR



(a)



(b)

FIGURE 5.1

BLOM'S TEST

Test Series: SHE-F-400-WI

Cumulative Frequency Distribution Of Residuals

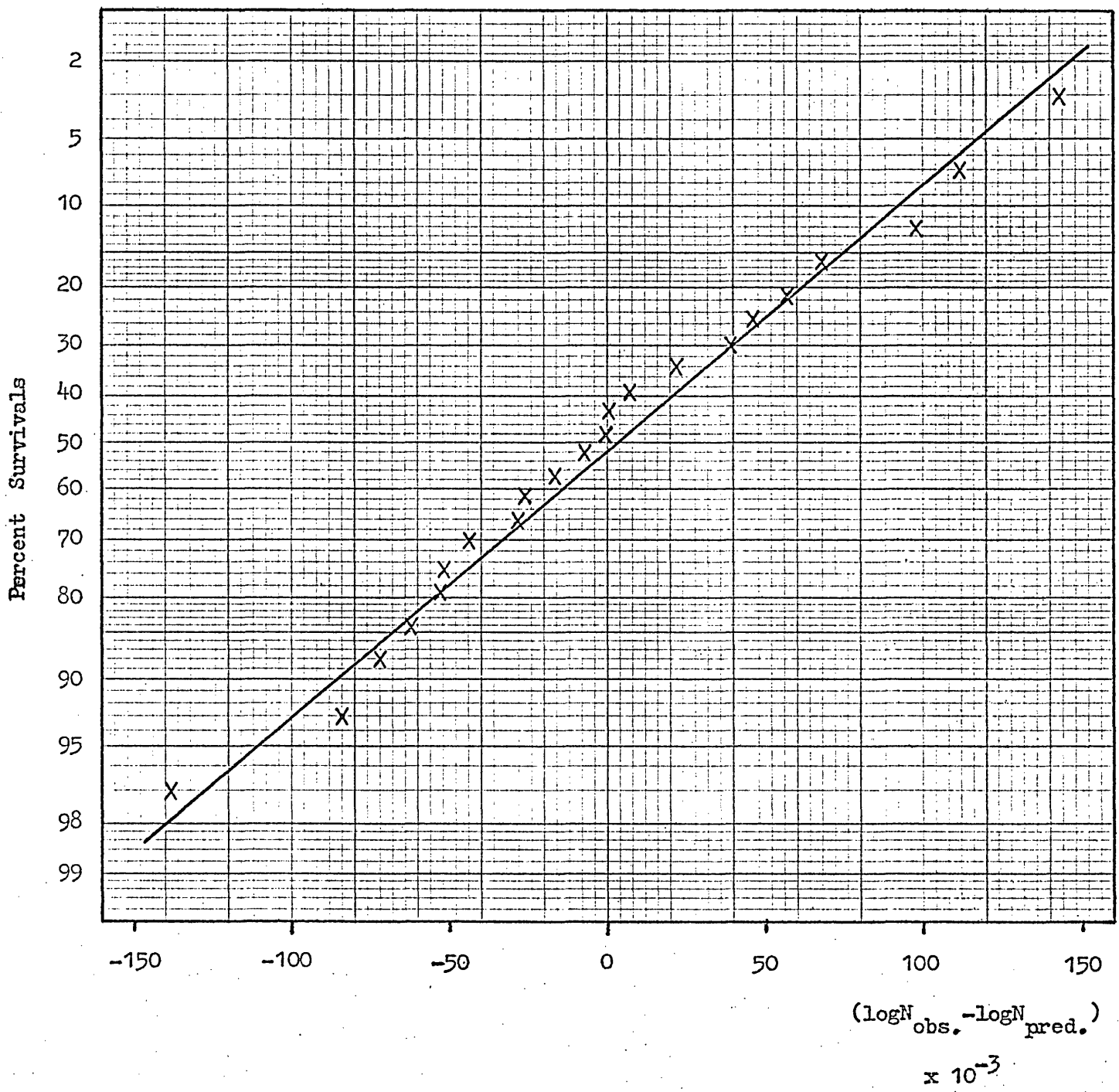


FIGURE 5.2

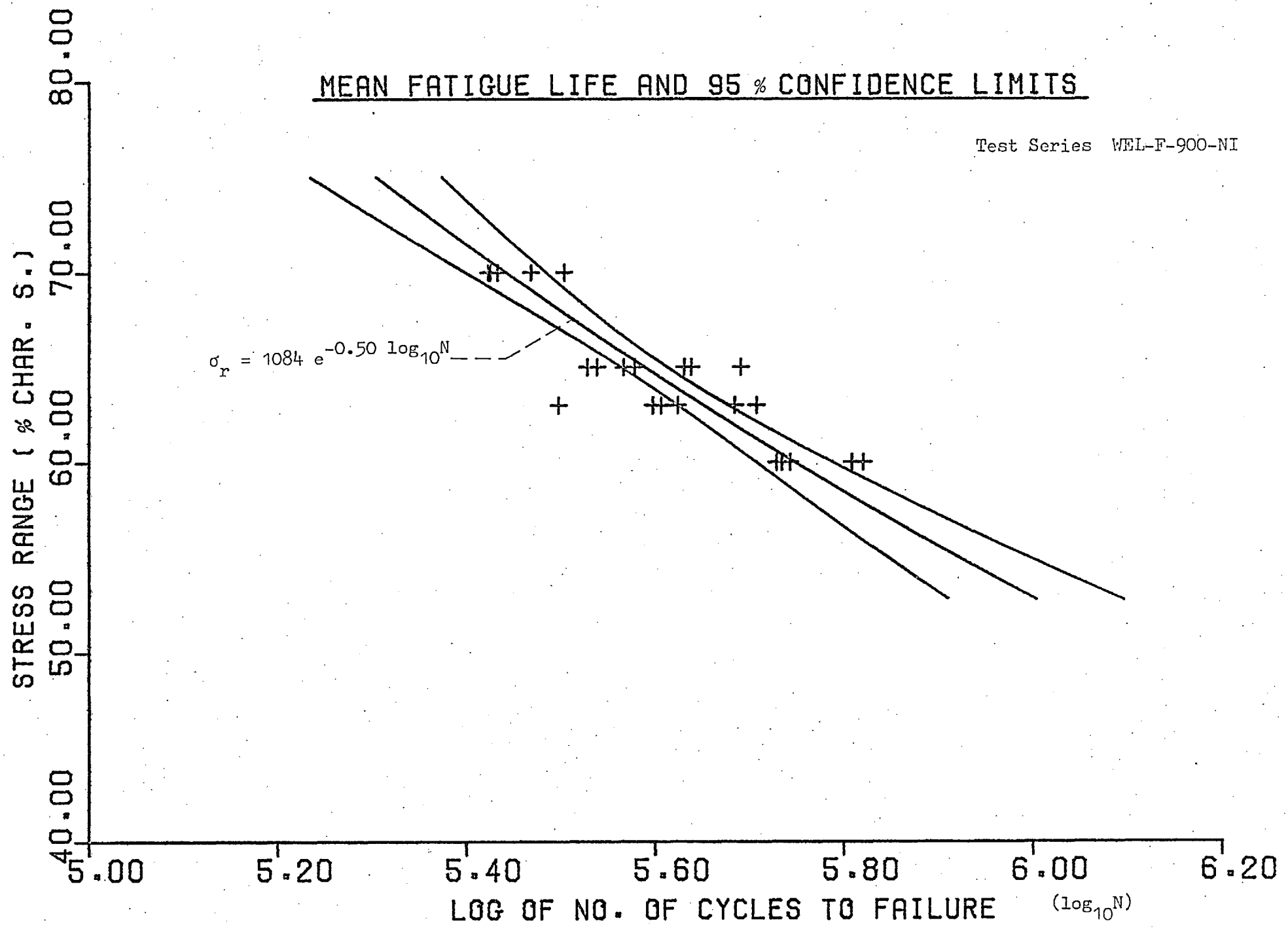

MEAN FATIGUE LIFE AND 95 % CONFIDENCE LIMITS
Test Series WEL-F-900-NI
$\sigma_r = 1084\ e^{-0.50 \log_{10} N}$
STRESS RANGE (% CHAR. S.)
80.00
70.00
60.00
50.00
40.00
5.00
5.20
5.40
5.60
5.80
6.00
6.20
LOG OF NO. OF CYCLES TO FAILURE ($\log_{10} N$)

FIGURE 5.3

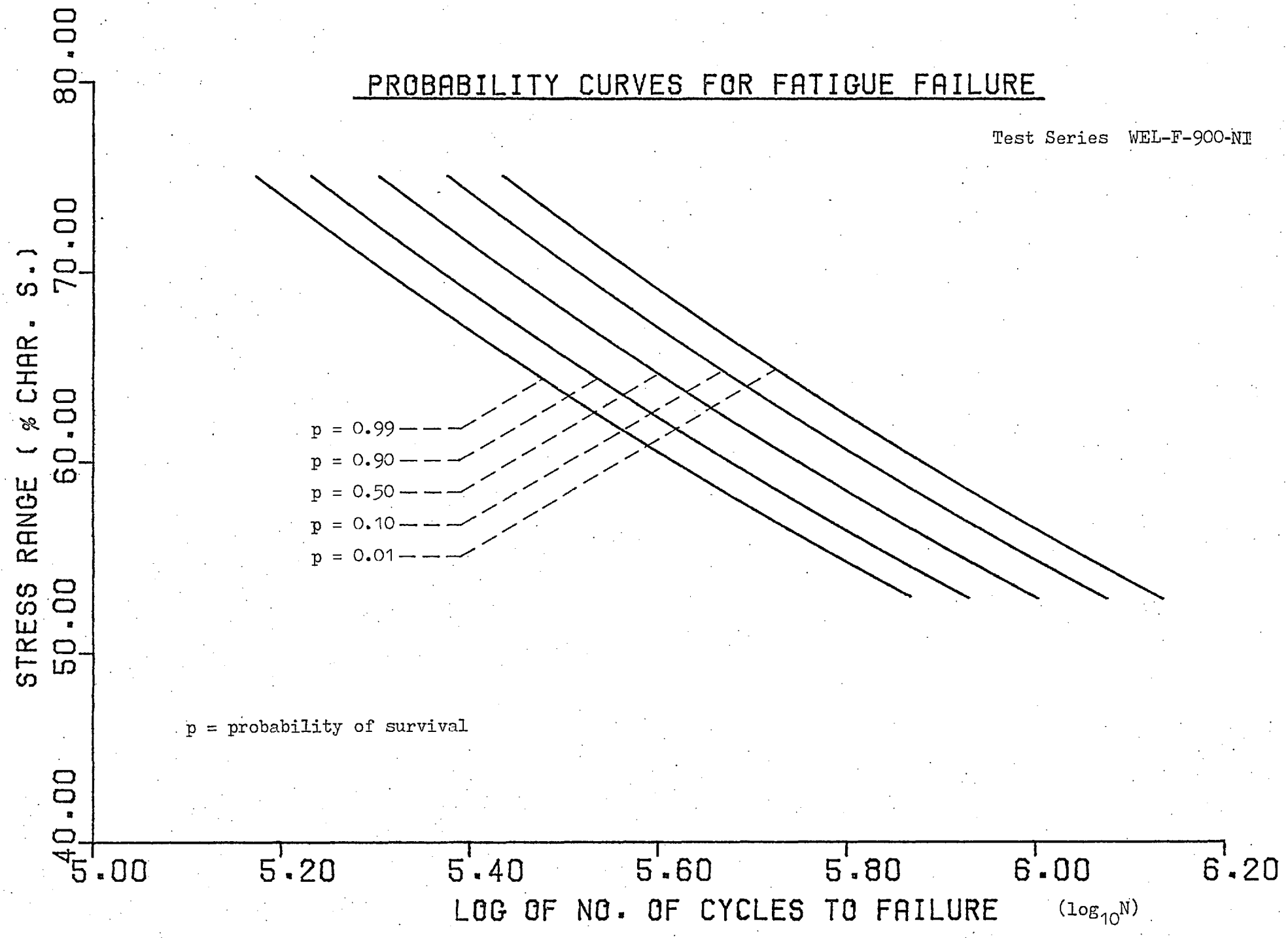

PROBABILITY CURVES FOR FATIGUE FAILURE
Test Series WEL-F-900-NI
STRESS RANGE (% CHAR. S.)
80.00
70.00
60.00
50.00
40.00
p = 0.99
p = 0.90
p = 0.50
p = 0.10
p = 0.01
p = probability of survival
5.00
5.20
5.40
5.60
5.80
6.00
6.20
LOG OF NO. OF CYCLES TO FAILURE (log10N)

FIGURE 5.4

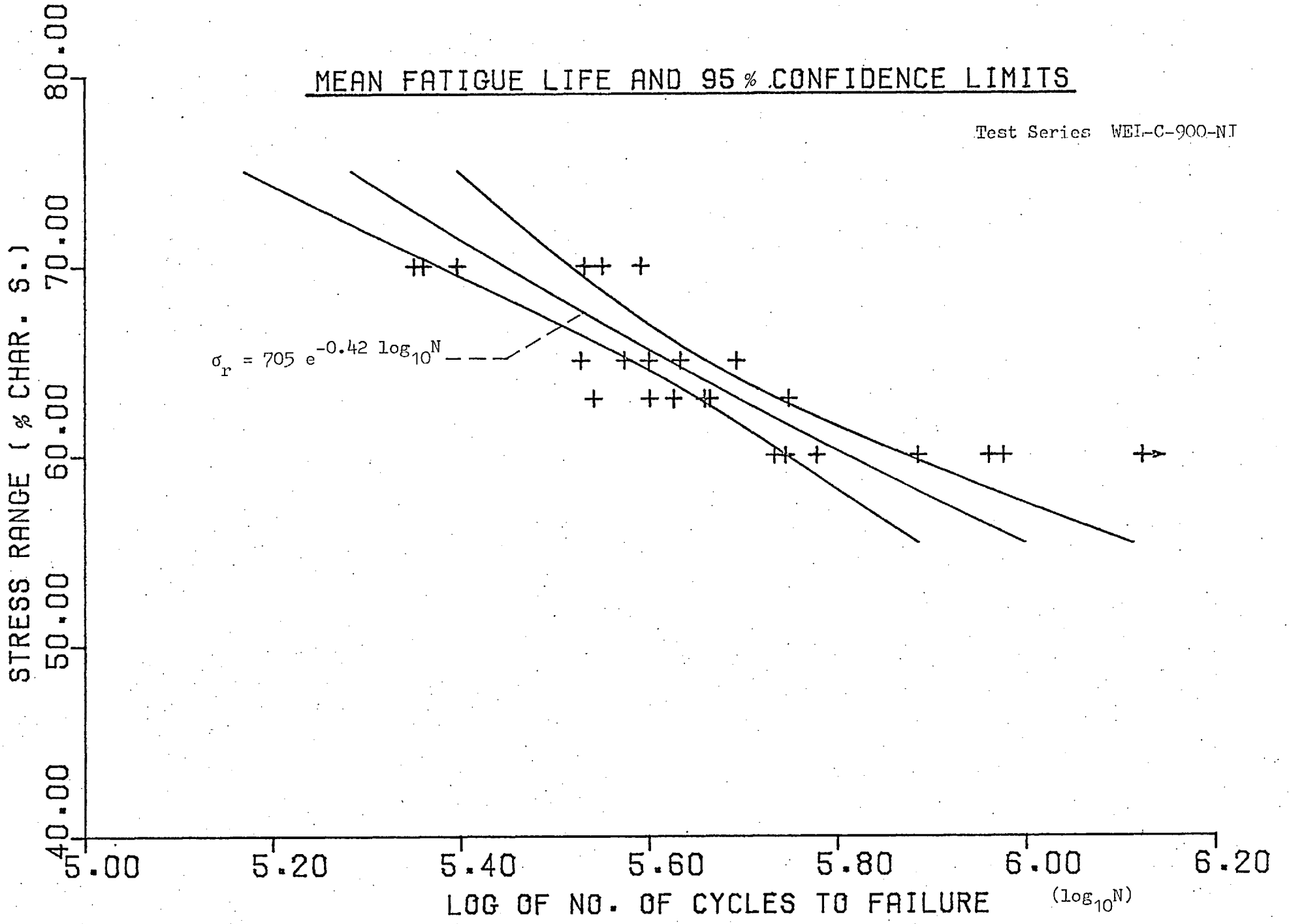

MEAN FATIGUE LIFE AND 95% CONFIDENCE LIMITS
Test Series WEI-C-900-NI
$\sigma_r = 705\ e^{-0.42 \log_{10} N}$
STRESS RANGE (% CHAR. S.)
80.00
70.00
60.00
50.00
40.00
5.00
5.20
5.40
5.60
5.80
6.00
6.20
LOG OF NO. OF CYCLES TO FAILURE ($\log_{10} N$)

FIGURE 5.5

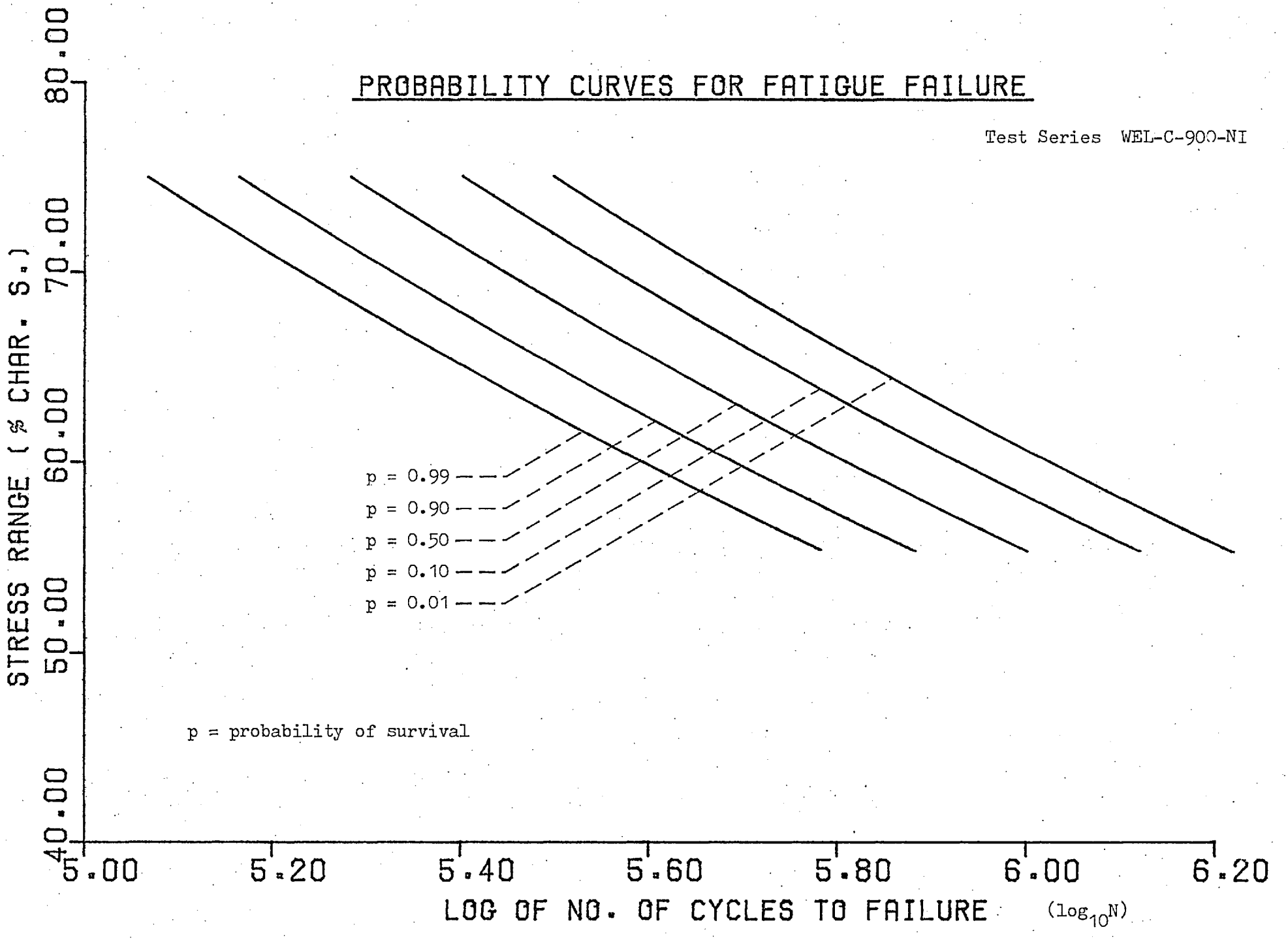

PROBABILITY CURVES FOR FATIGUE FAILURE
Test Series WEL-C-900-NI
STRESS RANGE (% CHAR. S.)
80.00
70.00
60.00
50.00
40.00
p = 0.99
p = 0.90
p = 0.50
p = 0.10
p = 0.01
p = probability of survival
5.00
5.20
5.40
5.60
5.80
6.00
6.20
LOG OF NO. OF CYCLES TO FAILURE (log10N)

FIGURE 5.6

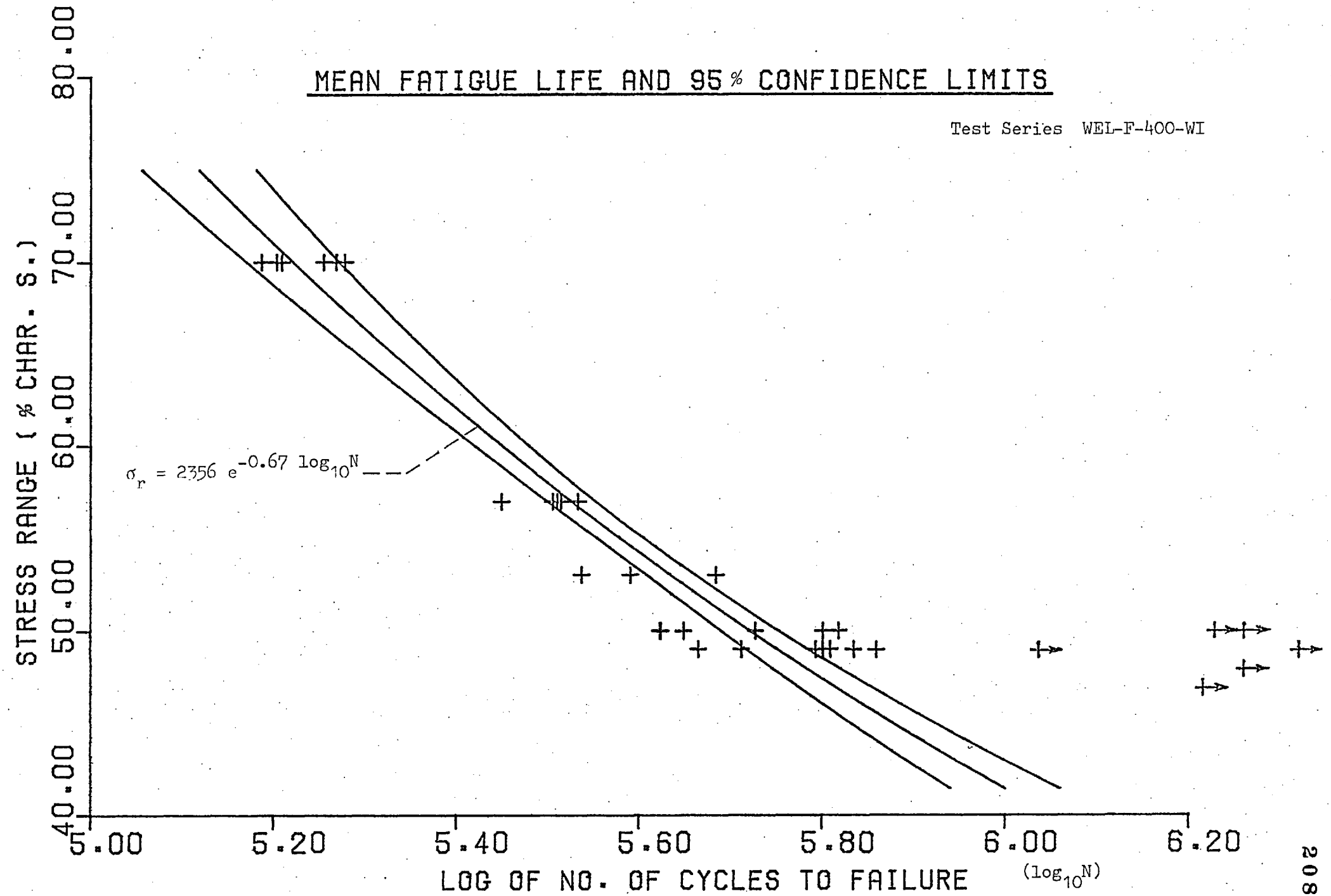

MEAN FATIGUE LIFE AND 95% CONFIDENCE LIMITS
Test Series WEL-F-400-WI
$\sigma_r = 2356\ e^{-0.67 \log_{10} N}$
STRESS RANGE (% CHAR. S.)
80.00
70.00
60.00
50.00
40.00
5.00
5.20
5.40
5.60
5.80
6.00
6.20
LOG OF NO. OF CYCLES TO FAILURE ($\log_{10} N$)

FIGURE 5.7

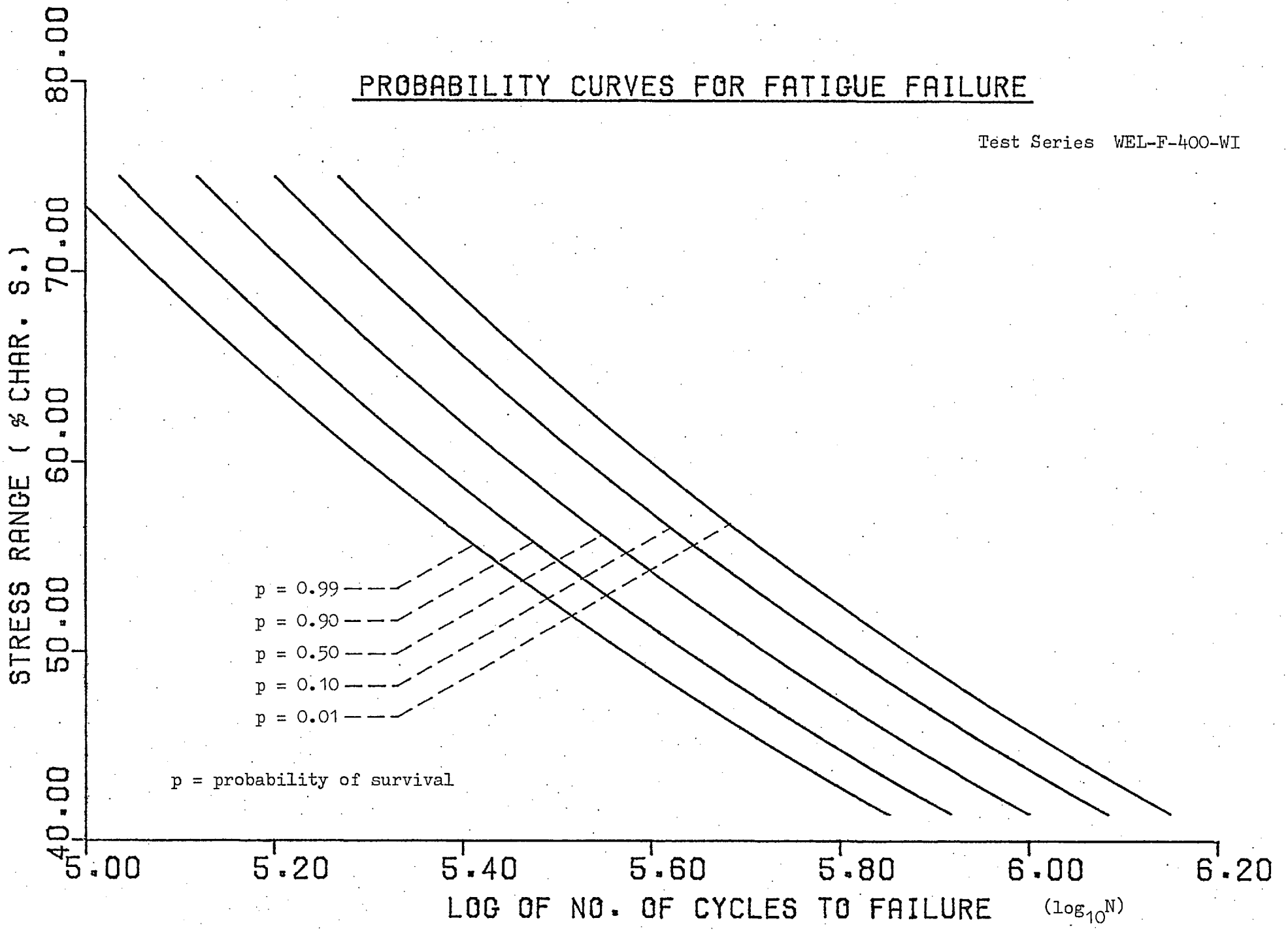

PROBABILITY CURVES FOR FATIGUE FAILURE
Test Series WEL-F-400-WI
STRESS RANGE (% CHAR. S.)
80.00
70.00
60.00
50.00
40.00
p = 0.99
p = 0.90
p = 0.50
p = 0.10
p = 0.01
p = probability of survival
5.00
5.20
5.40
5.60
5.80
6.00
6.20
LOG OF NO. OF CYCLES TO FAILURE (log10N)

FIGURE 5.8

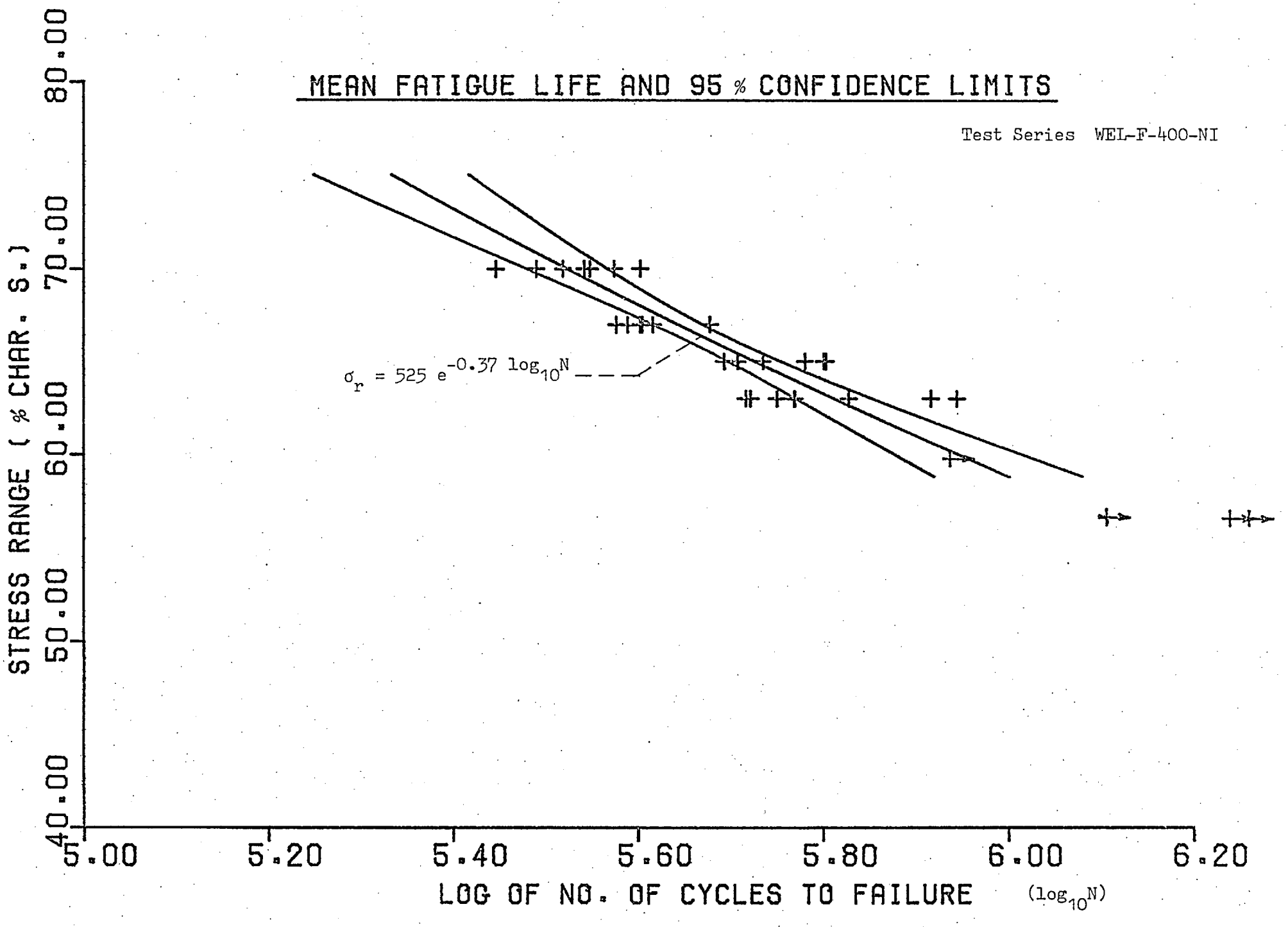

MEAN FATIGUE LIFE AND 95 % CONFIDENCE LIMITS
Test Series WEL-F-400-NI
$\sigma_r = 525\ e^{-0.37 \log_{10} N}$
STRESS RANGE (% CHAR. S.)
80.00
70.00
60.00
50.00
40.00
5.00
5.20
5.40
5.60
5.80
6.00
6.20
LOG OF NO. OF CYCLES TO FAILURE ($\log_{10} N$)

FIGURE 5.9

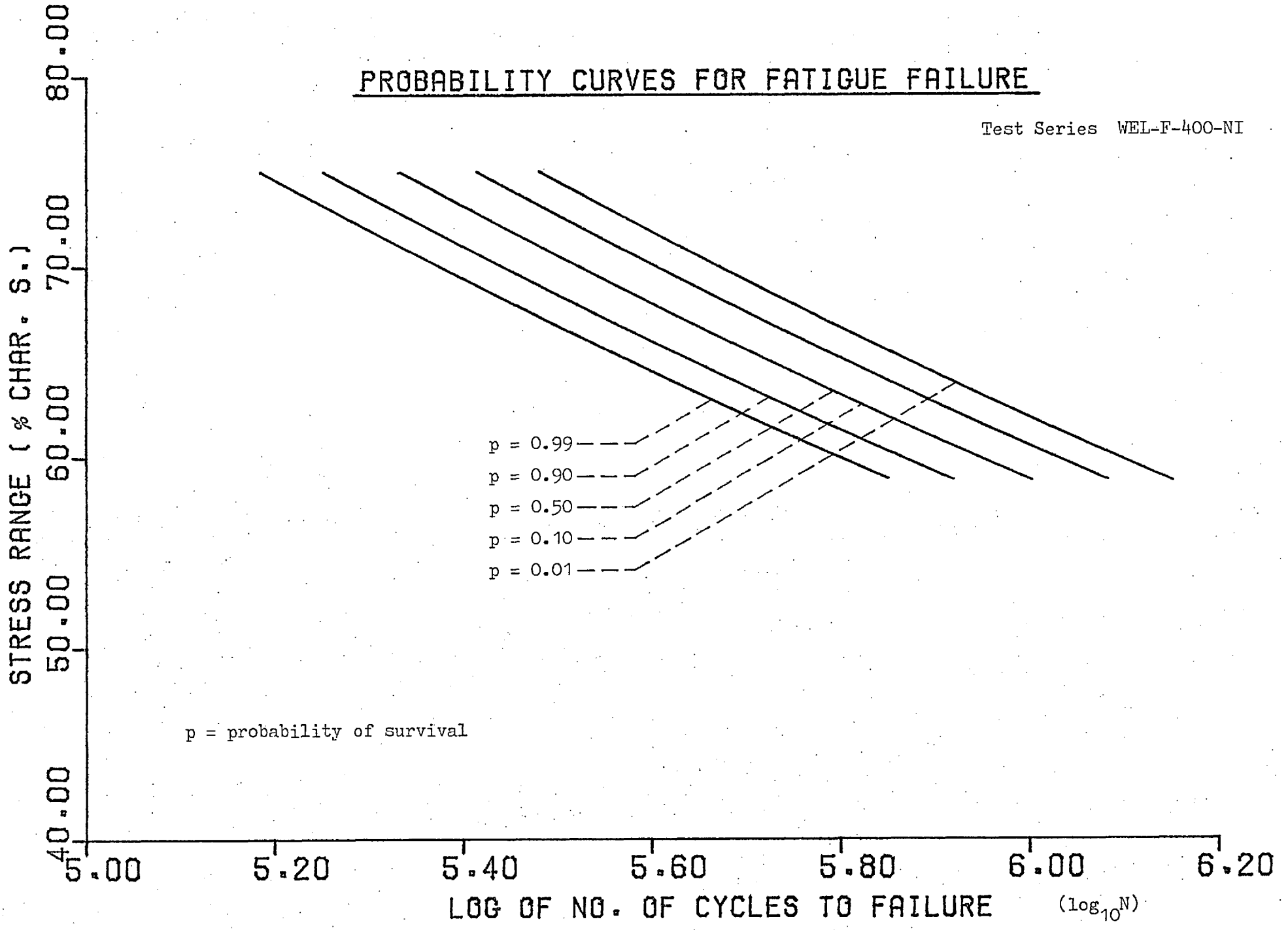

PROBABILITY CURVES FOR FATIGUE FAILURE
Test Series WEL-F-400-NI
STRESS RANGE (% CHAR. S.)
80.00
70.00
60.00
50.00
40.00
p = 0.99
p = 0.90
p = 0.50
p = 0.10
p = 0.01
p = probability of survival
5.00
5.20
5.40
5.60
5.80
6.00
6.20
LOG OF NO. OF CYCLES TO FAILURE (log10N)

FIGURE 5.10

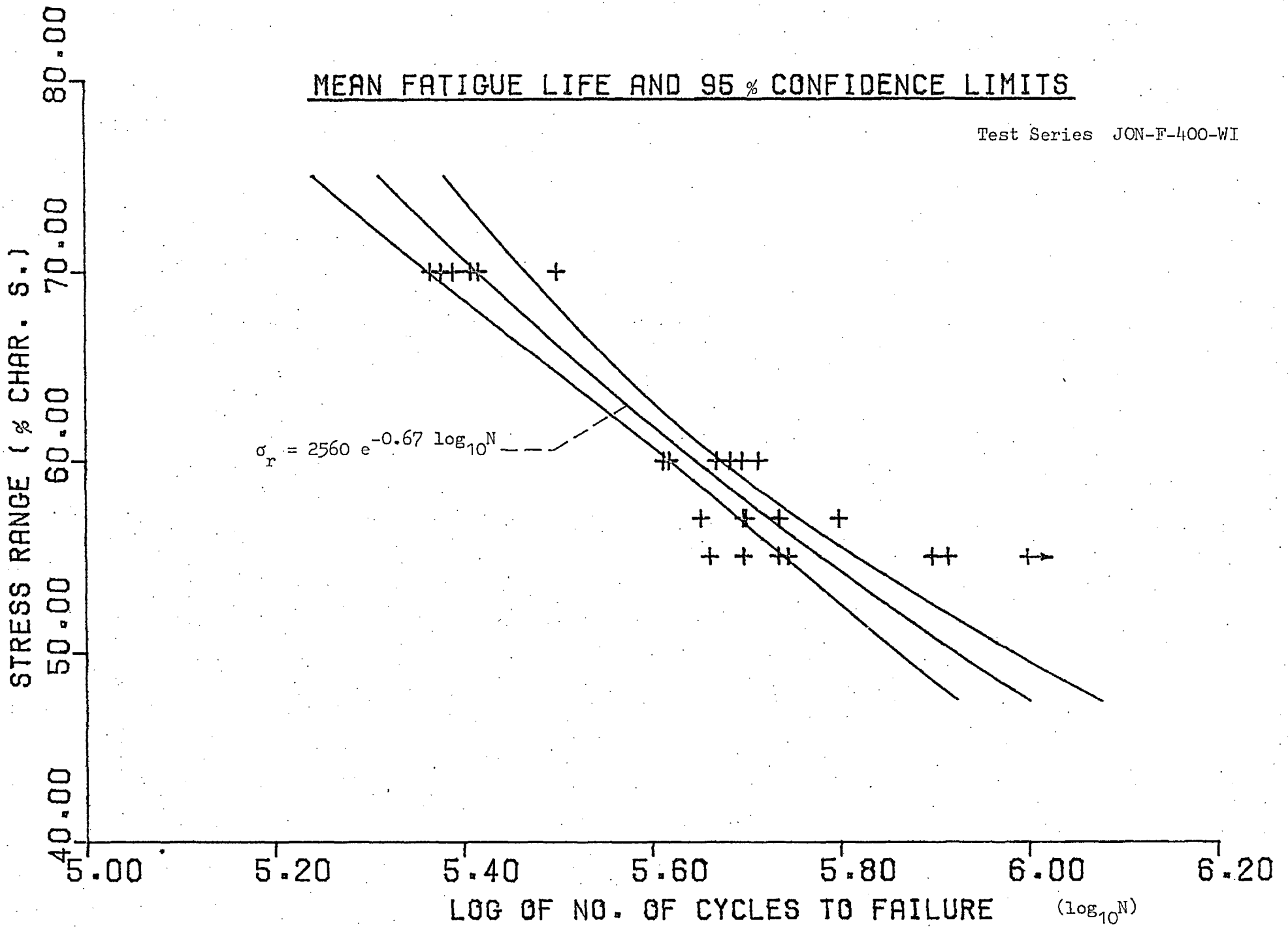

MEAN FATIGUE LIFE AND 95 % CONFIDENCE LIMITS
Test Series JON-F-400-WI
$\sigma_r = 2560\ e^{-0.67 \log_{10} N}$
STRESS RANGE (% CHAR. S.)
80.00
70.00
60.00
50.00
40.00
5.00
5.20
5.40
5.60
5.80
6.00
6.20
LOG OF NO. OF CYCLES TO FAILURE ($\log_{10} N$)

FIGURE 5.11

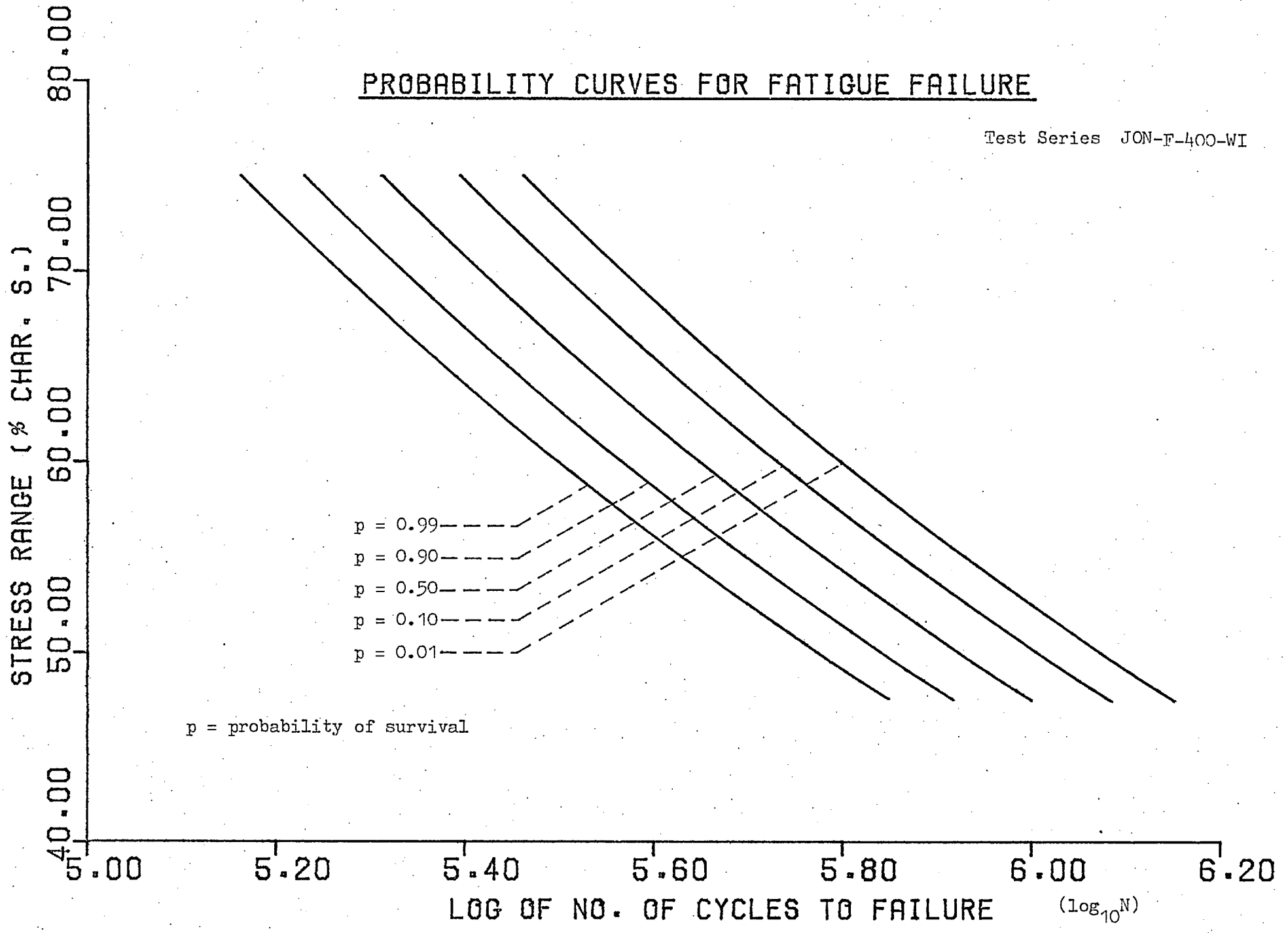

PROBABILITY CURVES FOR FATIGUE FAILURE
Test Series JON-F-400-WI
STRESS RANGE (% CHAR. S.)
80.00
70.00
60.00
50.00
40.00
p = 0.99
p = 0.90
p = 0.50
p = 0.10
p = 0.01
p = probability of survival
5.00
5.20
5.40
5.60
5.80
6.00
6.20
LOG OF NO. OF CYCLES TO FAILURE (log10N)

FIGURE 5.12

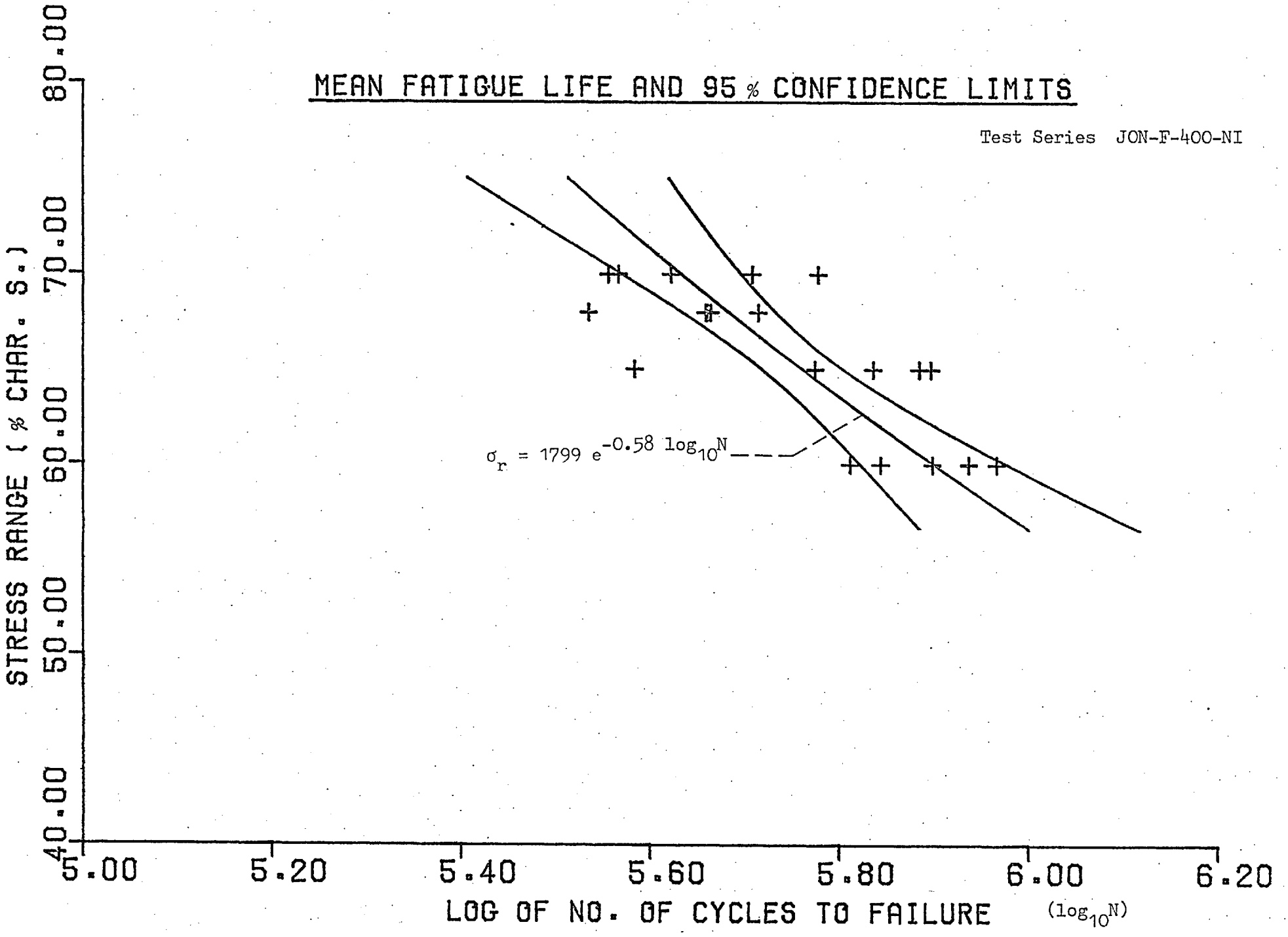

MEAN FATIGUE LIFE AND 95 % CONFIDENCE LIMITS
Test Series JON-F-400-NI
$\sigma_r = 1799\ e^{-0.58 \log_{10} N}$
STRESS RANGE (% CHAR. S.)
80.00
70.00
60.00
50.00
40.00
5.00
5.20
5.40
5.60
5.80
6.00
6.20
LOG OF NO. OF CYCLES TO FAILURE ($\log_{10} N$)

FIGURE 5.13

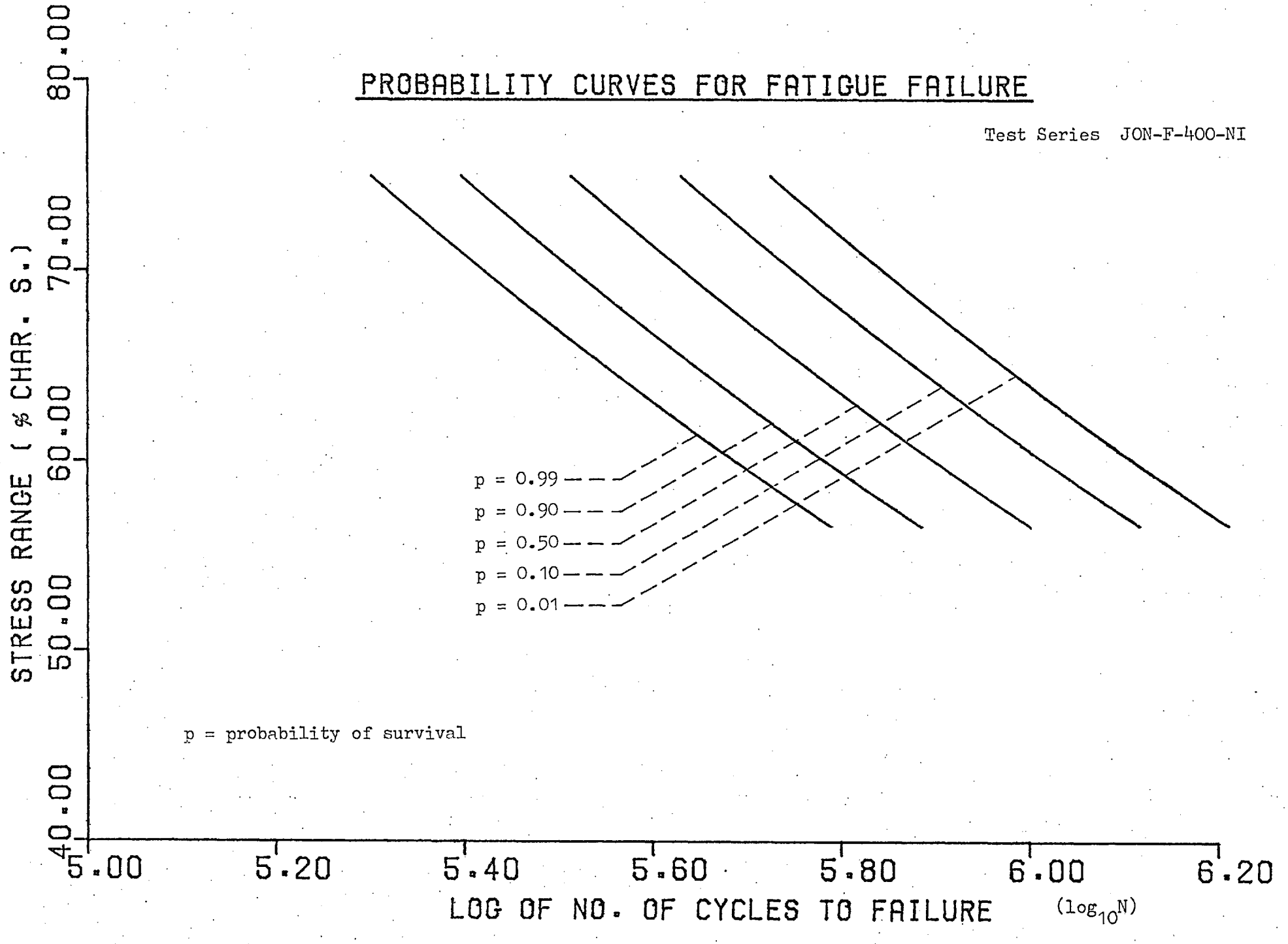

PROBABILITY CURVES FOR FATIGUE FAILURE
Test Series JON-F-400-NI
STRESS RANGE (% CHAR. S.)
80.00
70.00
60.00
50.00
40.00
p = 0.99
p = 0.90
p = 0.50
p = 0.10
p = 0.01
p = probability of survival
5.00
5.20
5.40
5.60
5.80
6.00
6.20
LOG OF NO. OF CYCLES TO FAILURE (log10N)

FIGURE 5.14

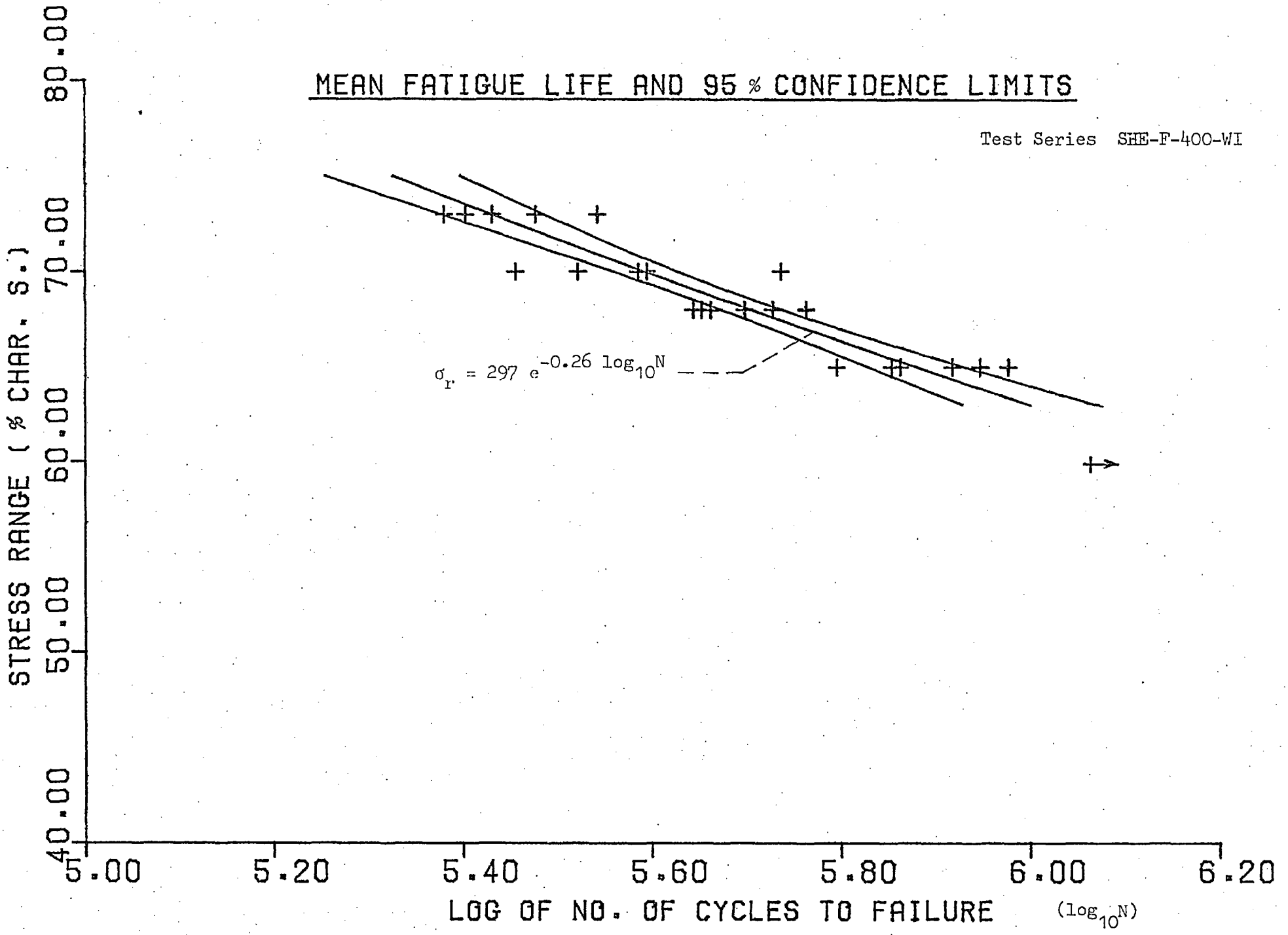

MEAN FATIGUE LIFE AND 95 % CONFIDENCE LIMITS
Test Series SHE-F-400-WI
$\sigma_r = 297\ e^{-0.26 \log_{10} N}$
STRESS RANGE (% CHAR. S.)
80.00
70.00
60.00
50.00
40.00
5.00
5.20
5.40
5.60
5.80
6.00
6.20
LOG OF NO. OF CYCLES TO FAILURE ($\log_{10} N$)

FIGURE 5.15

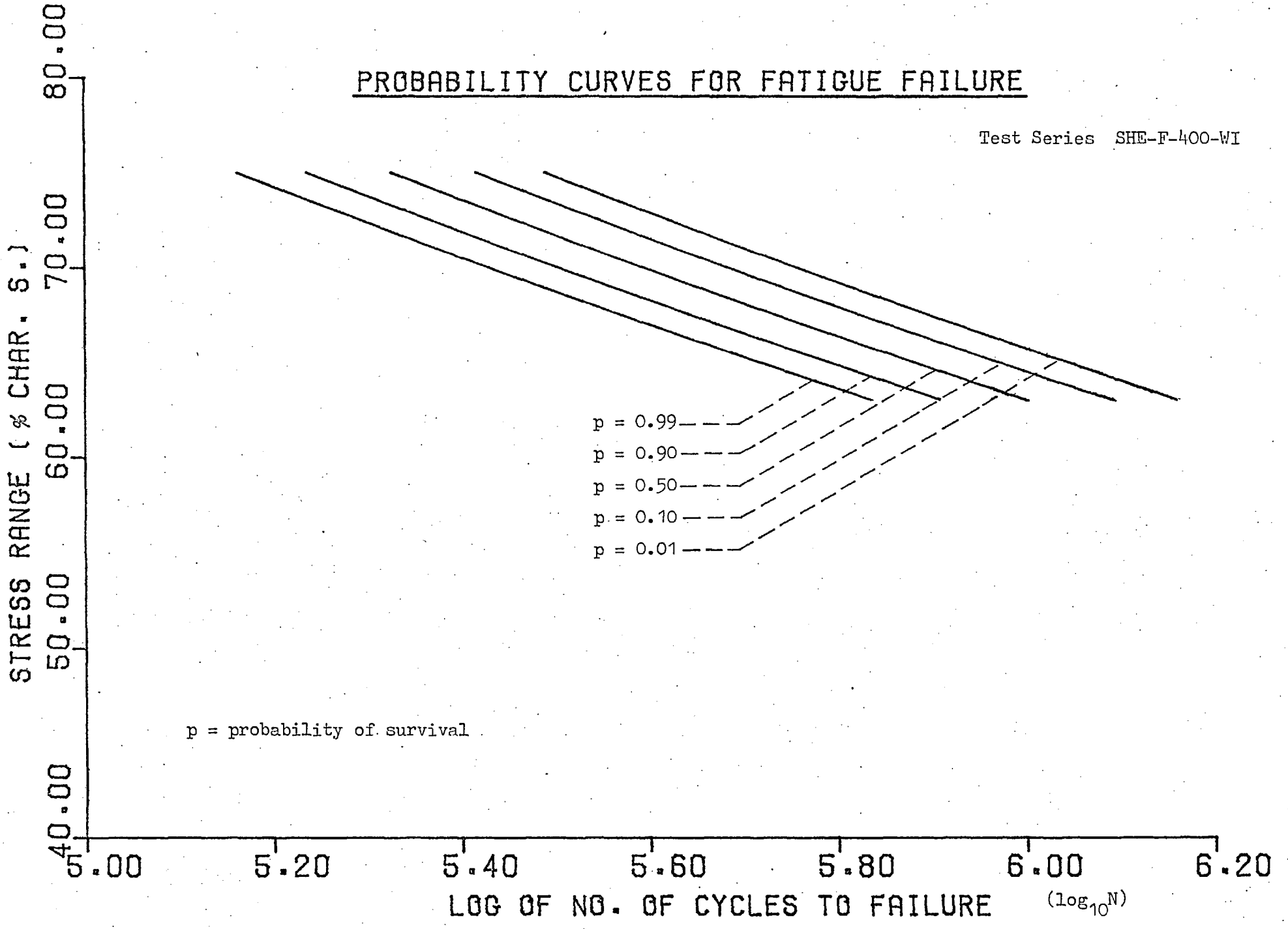

PROBABILITY CURVES FOR FATIGUE FAILURE
Test Series SHE-F-400-WI
STRESS RANGE (% CHAR. S.)
80.00
70.00
60.00
50.00
40.00
p = 0.99
p = 0.90
p = 0.50
p = 0.10
p = 0.01
p = probability of survival
5.00
5.20
5.40
5.60
5.80
6.00
6.20
LOG OF NO. OF CYCLES TO FAILURE (log10N)

FIGURE 5.16

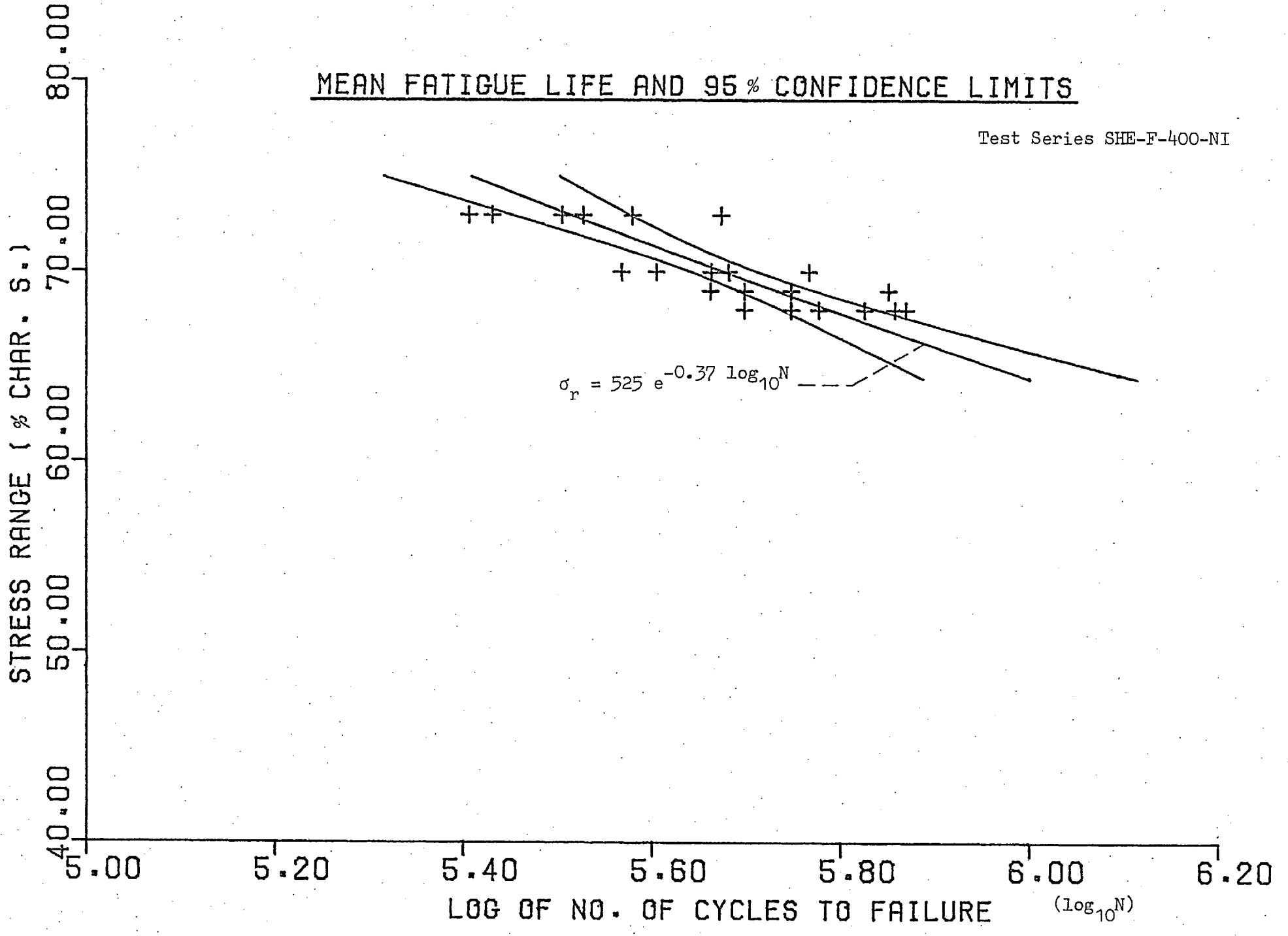

MEAN FATIGUE LIFE AND 95% CONFIDENCE LIMITS
Test Series SHE-F-400-NI
$\sigma_r = 525\ e^{-0.37 \log_{10} N}$
STRESS RANGE (% CHAR. S.)
80.00
70.00
60.00
50.00
40.00
5.00
5.20
5.40
5.60
5.80
6.00
6.20
LOG OF NO. OF CYCLES TO FAILURE ($\log_{10} N$)

FIGURE 5.17

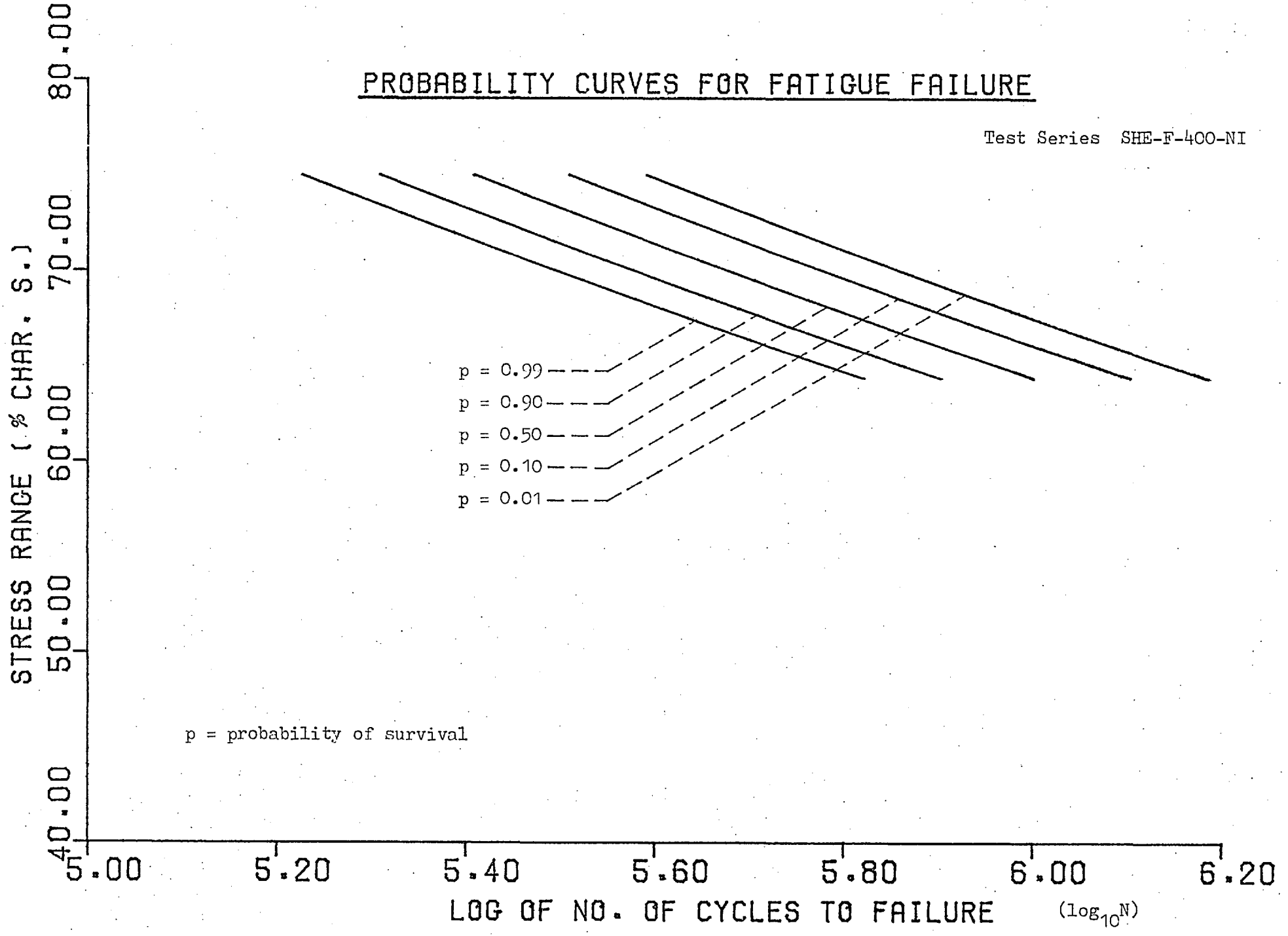

PROBABILITY CURVES FOR FATIGUE FAILURE
Test Series SHE-F-400-NI
p = 0.99
p = 0.90
p = 0.50
p = 0.10
p = 0.01
p = probability of survival
STRESS RANGE (% CHAR. S.)
80.00
70.00
60.00
50.00
40.00
5.00
5.20
5.40
5.60
5.80
6.00
6.20
LOG OF NO. OF CYCLES TO FAILURE (log10N)

FIGURE 5.18

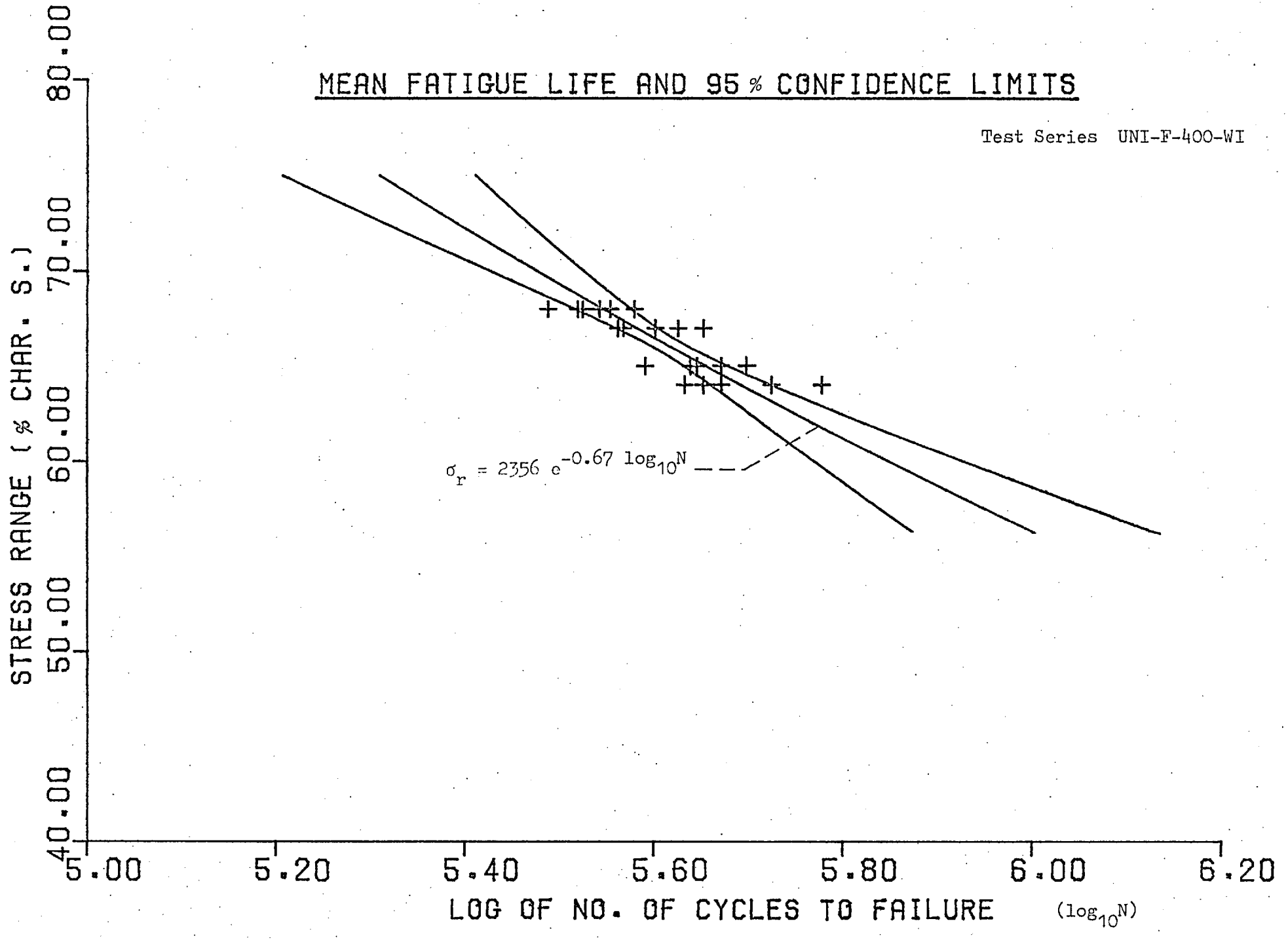

MEAN FATIGUE LIFE AND 95% CONFIDENCE LIMITS
Test Series UNI-F-400-WI
$\sigma_r = 2356\ e^{-0.67 \log_{10} N}$
STRESS RANGE (% CHAR. S.)
80.00
70.00
60.00
50.00
40.00
5.00
5.20
5.40
5.60
5.80
6.00
6.20
LOG OF NO. OF CYCLES TO FAILURE ($\log_{10} N$)

FIGURE 5.19

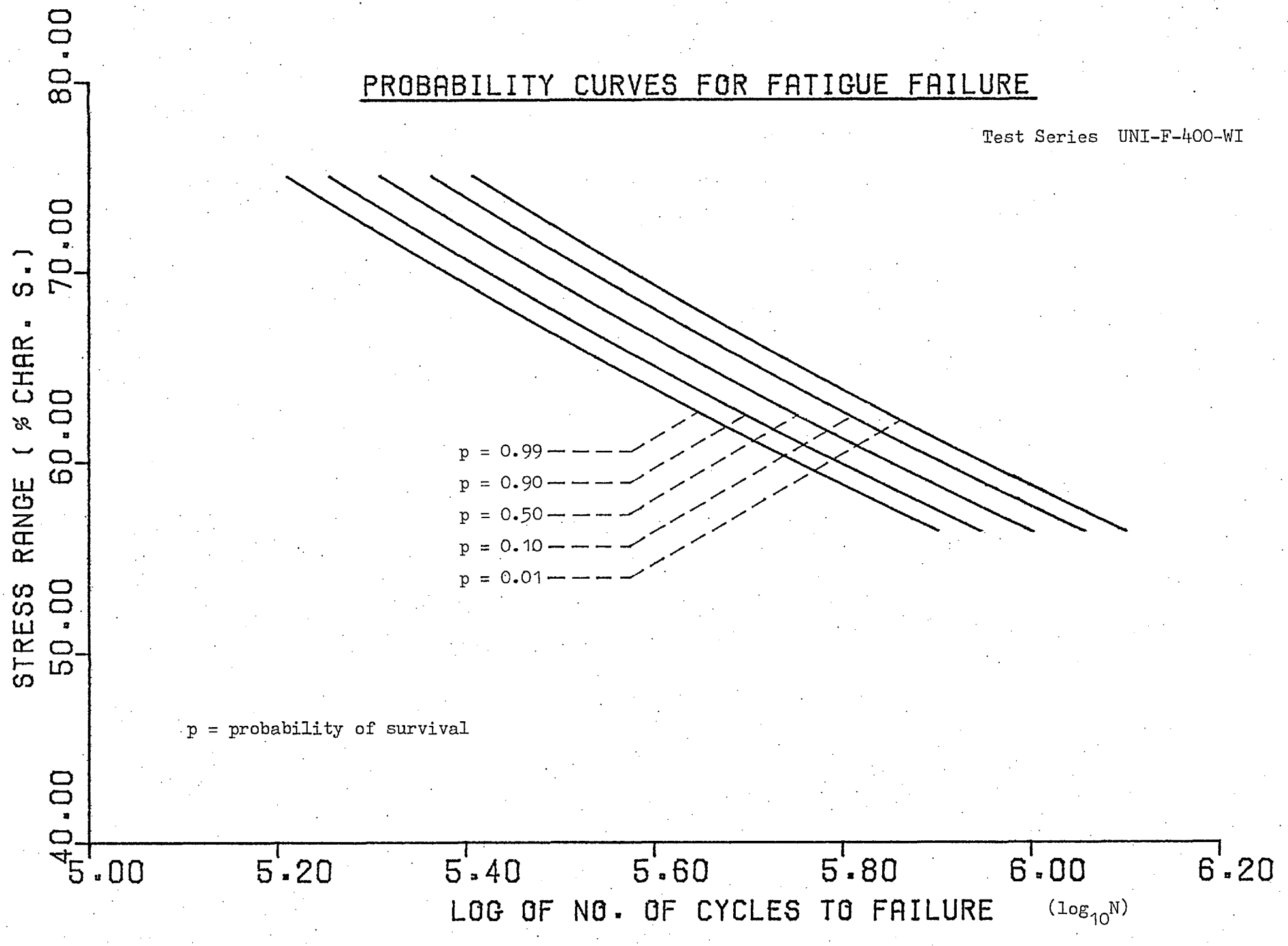

PROBABILITY CURVES FOR FATIGUE FAILURE
Test Series UNI-F-400-WI
STRESS RANGE (% CHAR. S.)
80.00
70.00
60.00
50.00
40.00
p = 0.99
p = 0.90
p = 0.50
p = 0.10
p = 0.01
p = probability of survival
5.00
5.20
5.40
5.60
5.80
6.00
6.20
LOG OF NO. OF CYCLES TO FAILURE (log10N)

FIGURE 5.20

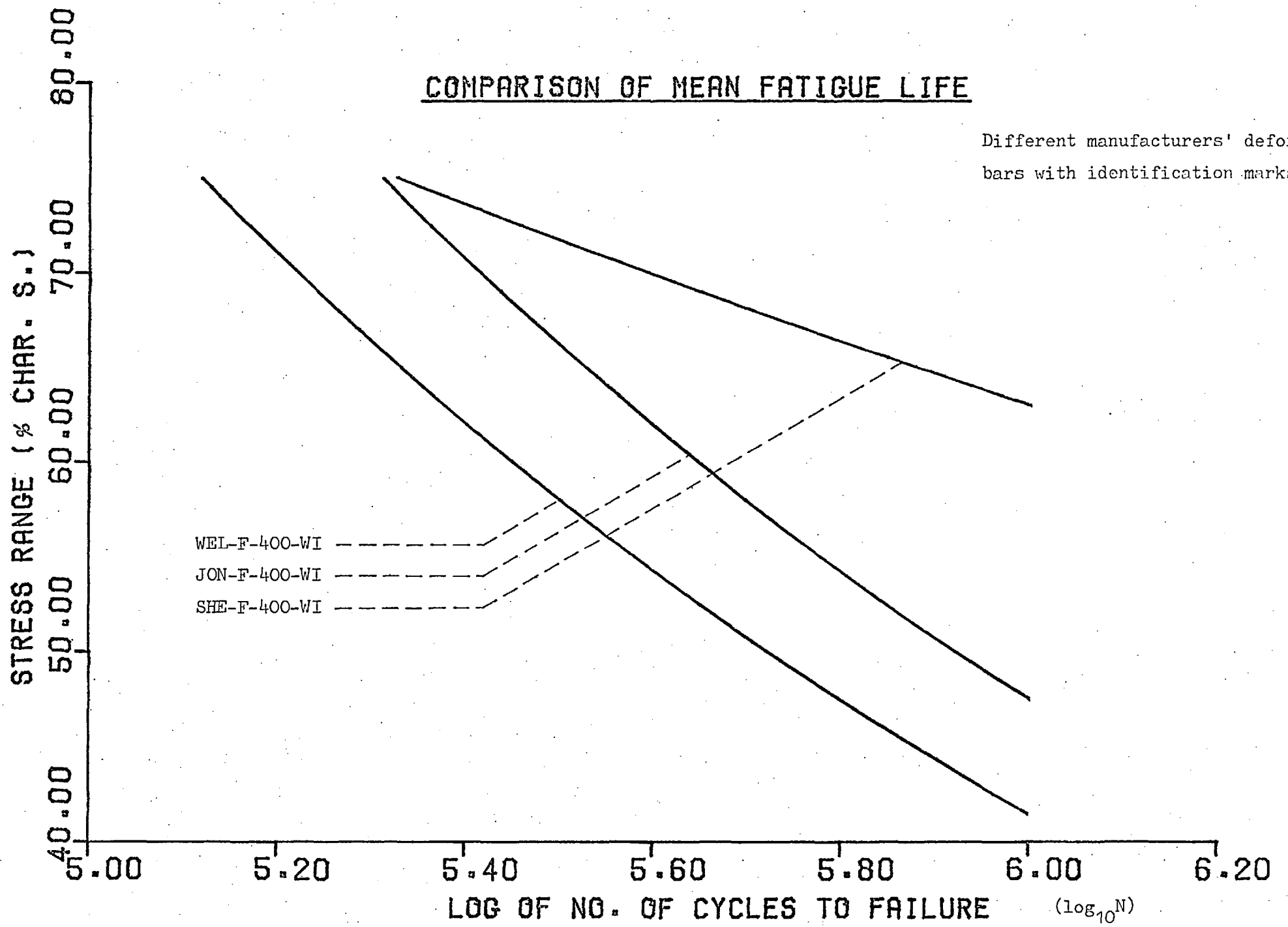

COMPARISON OF MEAN FATIGUE LIFE
Different manufacturers' deformed bars with identification marks
STRESS RANGE (% CHAR. S.)
80.00
70.00
60.00
50.00
40.00
WEL-F-400-WI
JON-F-400-WI
SHE-F-400-WI
5.00
5.20
5.40
5.60
5.80
6.00
6.20
LOG OF NO. OF CYCLES TO FAILURE (log10N)

FIGURE 5.21

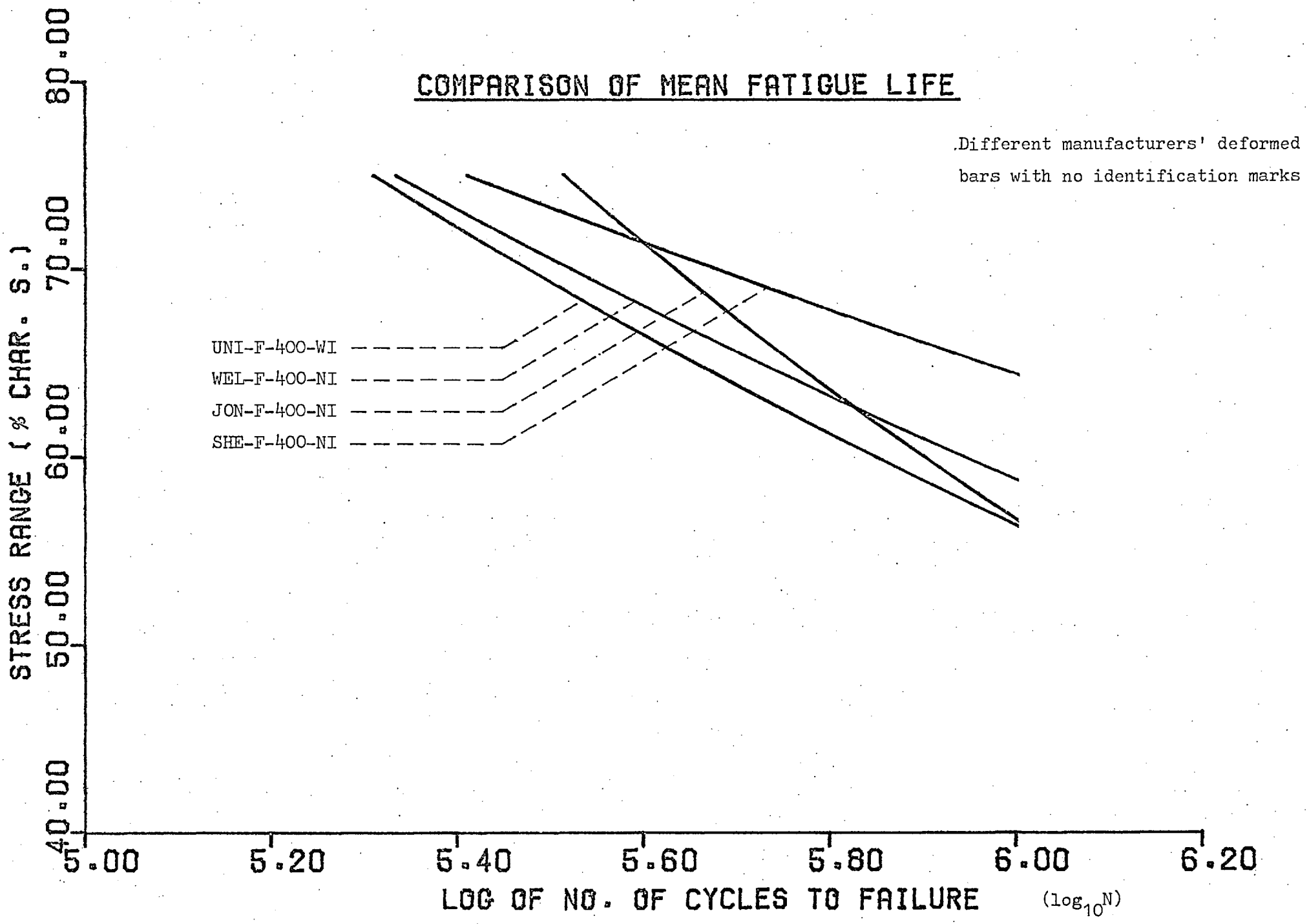

COMPARISON OF MEAN FATIGUE LIFE
Different manufacturers' deformed bars with no identification marks
UNI-F-400-WI
WEL-F-400-NI
JON-F-400-NI
SHE-F-400-NI
STRESS RANGE (% CHAR. S.)
80.00
70.00
60.00
50.00
40.00
5.00
5.20
5.40
5.60
5.80
6.00
6.20
LOG OF NO. OF CYCLES TO FAILURE (log10N)

FIGURE 5.22

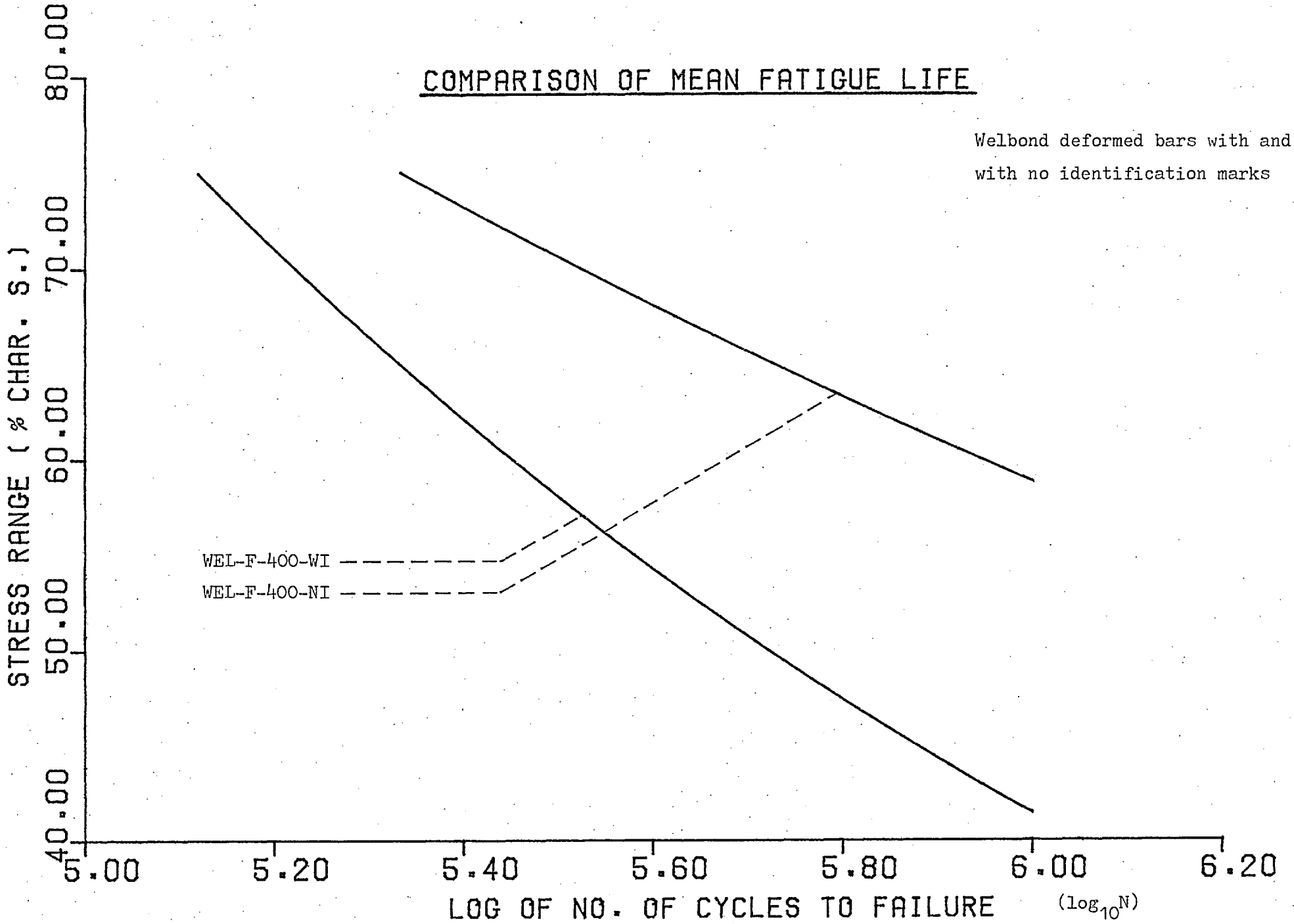

COMPARISON OF MEAN FATIGUE LIFE
Welbond deformed bars with and
with no identification marks
WEL-F-400-WI
WEL-F-400-NI
STRESS RANGE (% CHAR. S.)
80.00
70.00
60.00
50.00
40.00
5.00
5.20
5.40
5.60
5.80
6.00
6.20
LOG OF NO. OF CYCLES TO FAILURE (log10N)

FIGURE 5.23

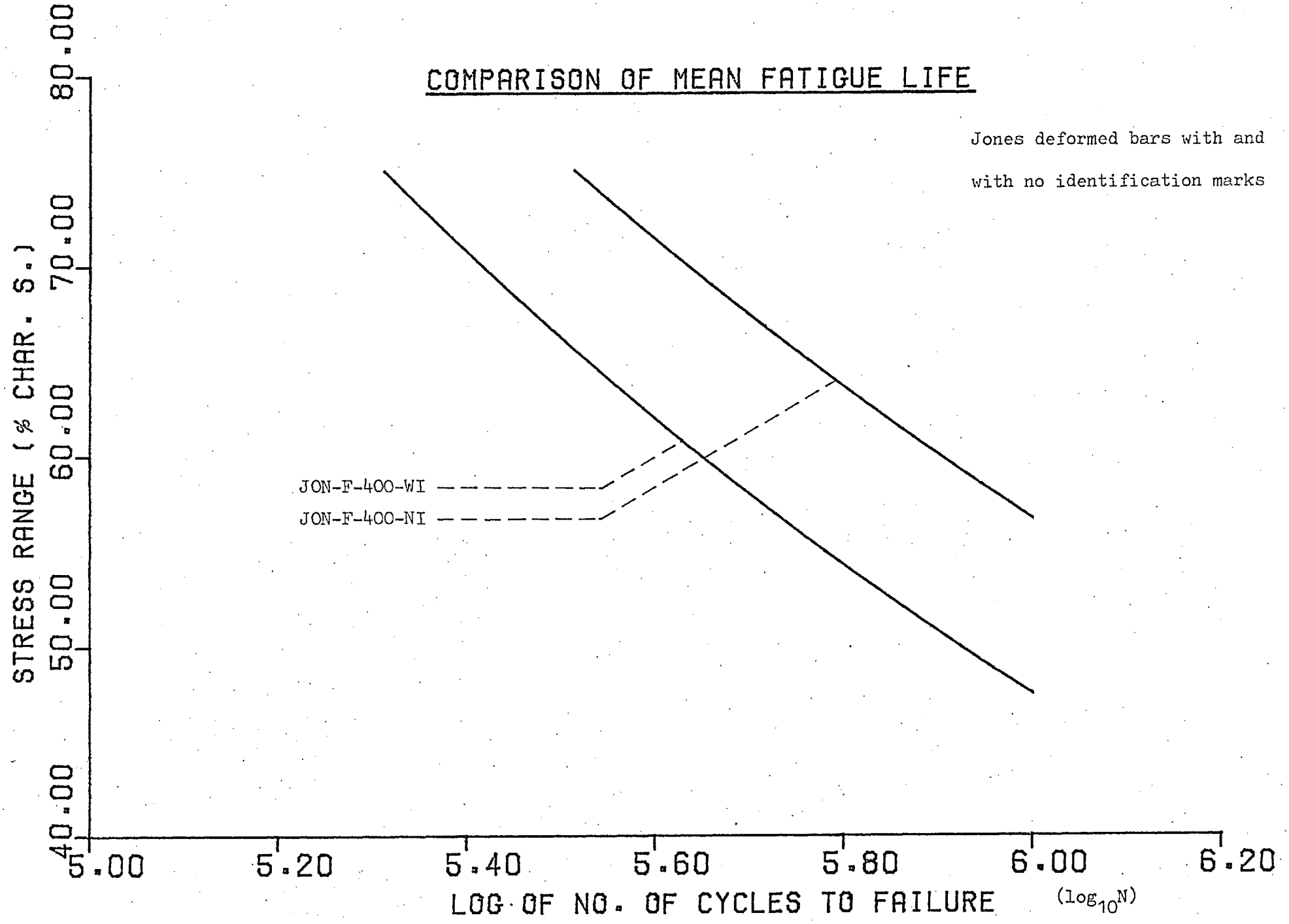

COMPARISON OF MEAN FATIGUE LIFE
Jones deformed bars with and
with no identification marks
JON-F-400-WI
JON-F-400-NI
STRESS RANGE (% CHAR. S.)
80.00
70.00
60.00
50.00
40.00
5.00
5.20
5.40
5.60
5.80
6.00
6.20
LOG OF NO. OF CYCLES TO FAILURE (log10N)

FIGURE 5.24

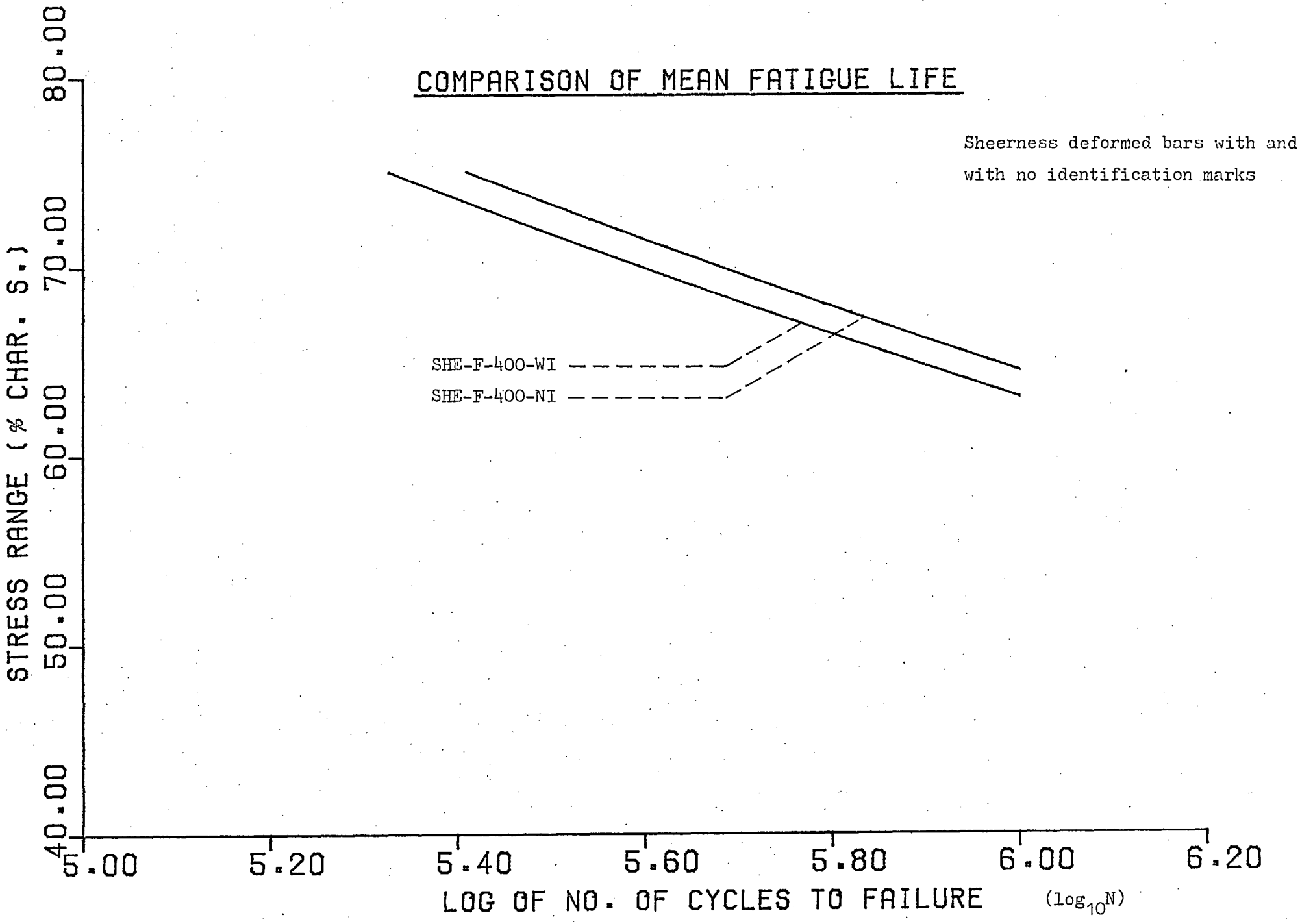

COMPARISON OF MEAN FATIGUE LIFE
Sheerness deformed bars with and
with no identification marks
SHE-F-400-WI
SHE-F-400-NI
STRESS RANGE (% CHAR. S.)
80.00
70.00
60.00
50.00
40.00
5.00
5.20
5.40
5.60
5.80
6.00
6.20
LOG OF NO. OF CYCLES TO FAILURE (log10N)

FIGURE 5.25

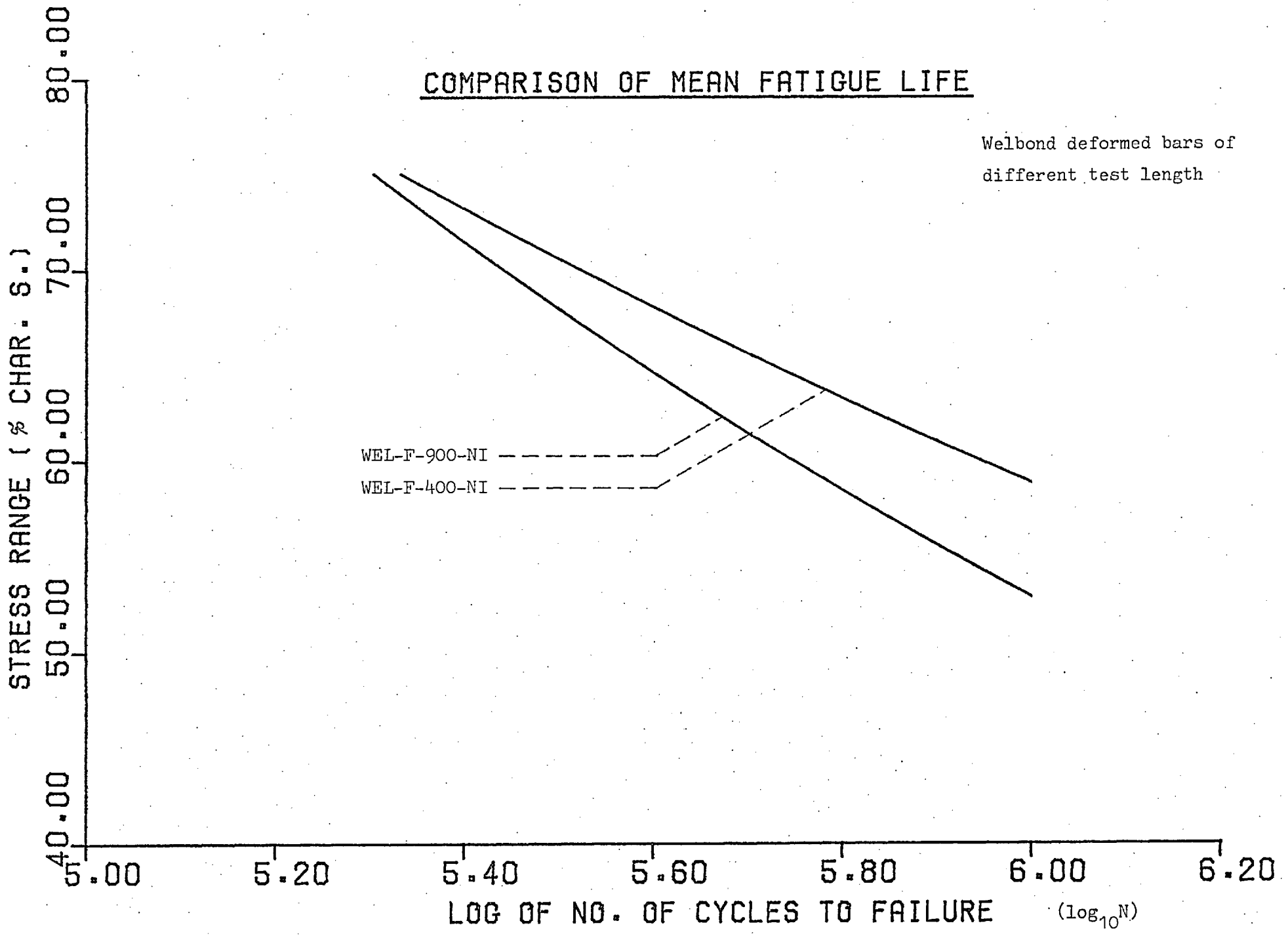

COMPARISON OF MEAN FATIGUE LIFE
Welbond deformed bars of different test length
WEL-F-900-NI
WEL-F-400-NI
STRESS RANGE (% CHAR. S.)
80.00
70.00
60.00
50.00
40.00
5.00
5.20
5.40
5.60
5.80
6.00
6.20
LOG OF NO. OF CYCLES TO FAILURE (log10N)

FIGURE 5.26

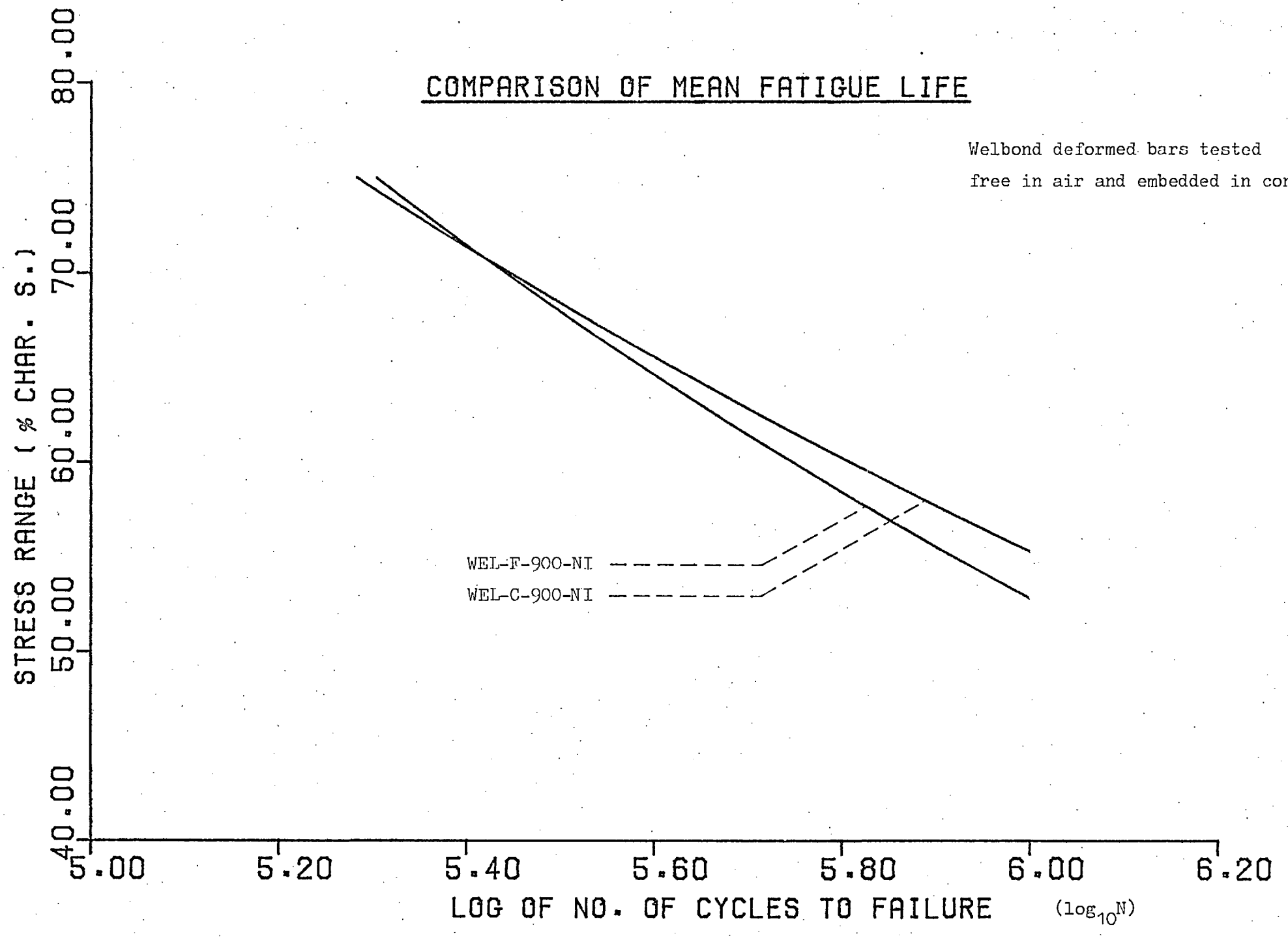

COMPARISON OF MEAN FATIGUE LIFE
Welbond deformed bars tested
free in air and embedded in concrete
WEL-F-900-NI
WEL-C-900-NI
STRESS RANGE (% CHAR. S.)
80.00
70.00
60.00
50.00
40.00
5.00
5.20
5.40
5.60
5.80
6.00
6.20
LOG OF NO. OF CYCLES TO FAILURE (log10N)

FIGURE 5.27

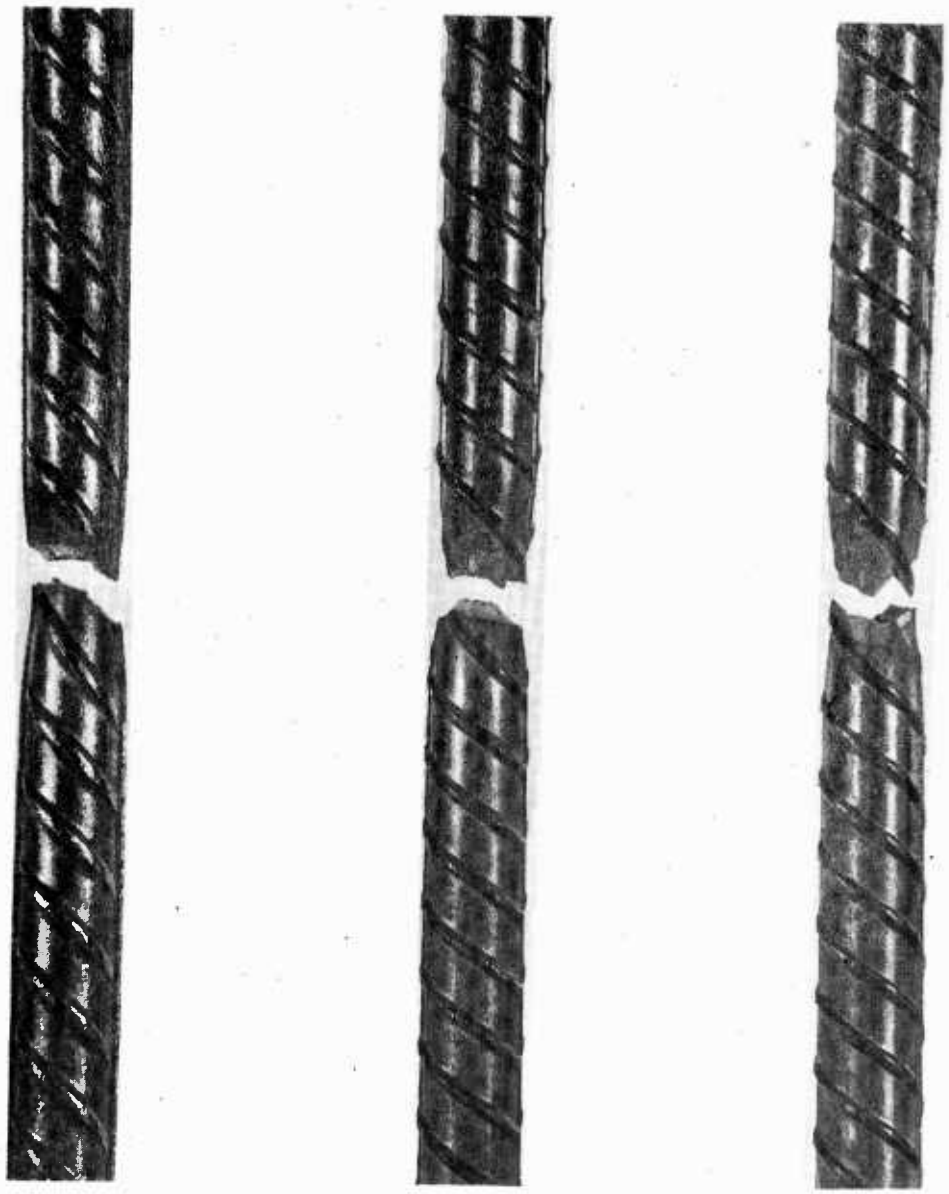


PLATE 5.1 PROFILES OF STATIC BAR FRACTURES

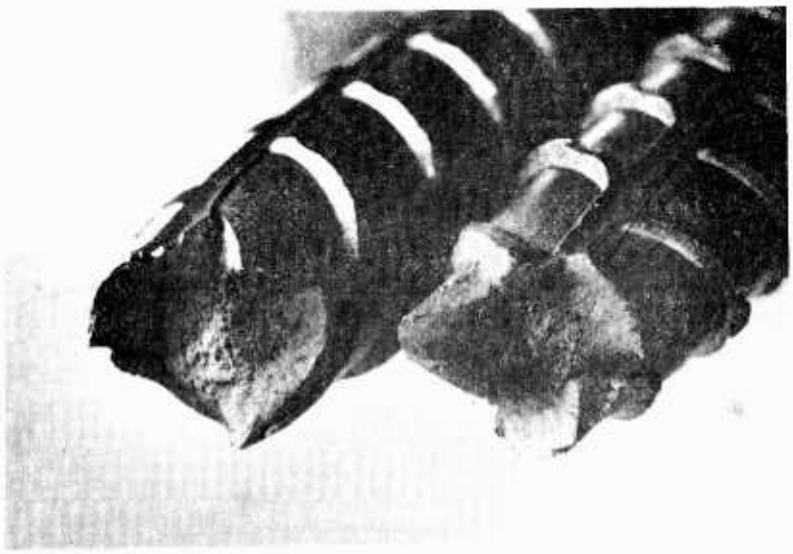


PLATE 5.2 STATIC BAR FRACTURES



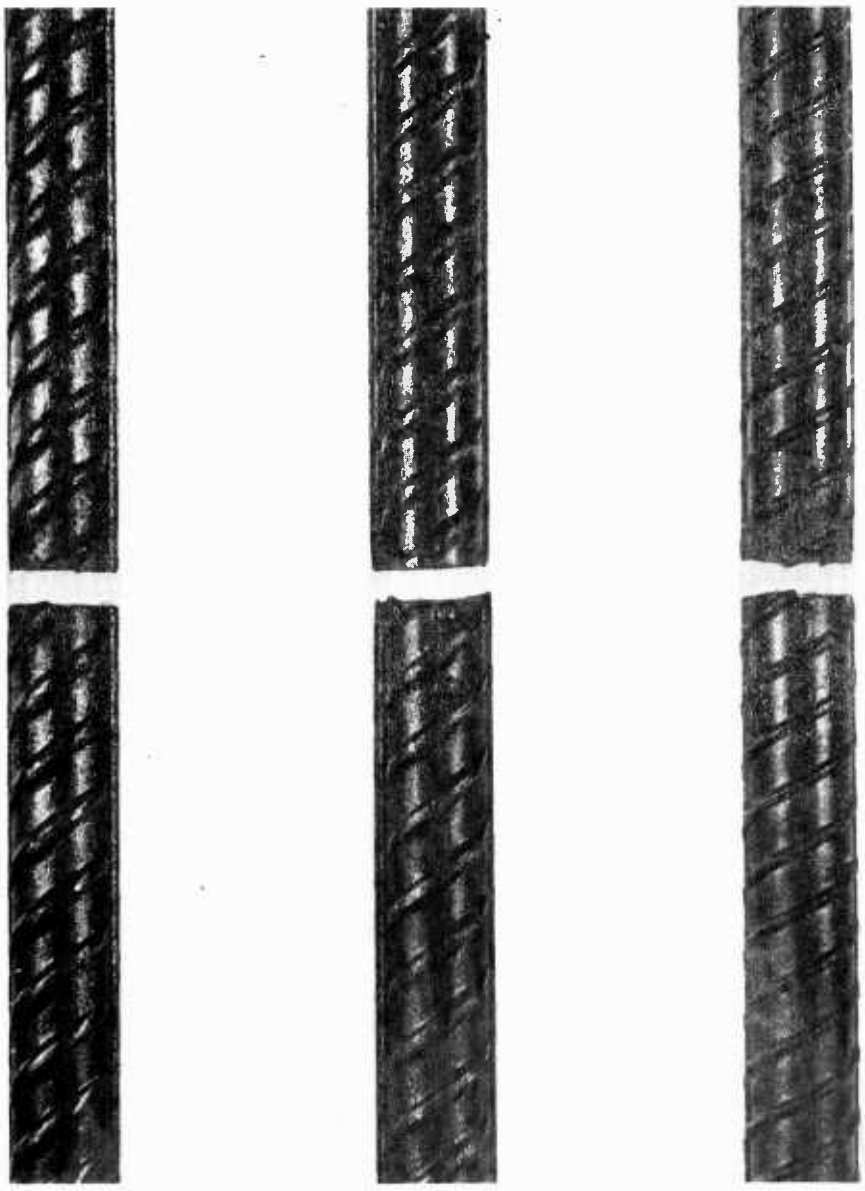
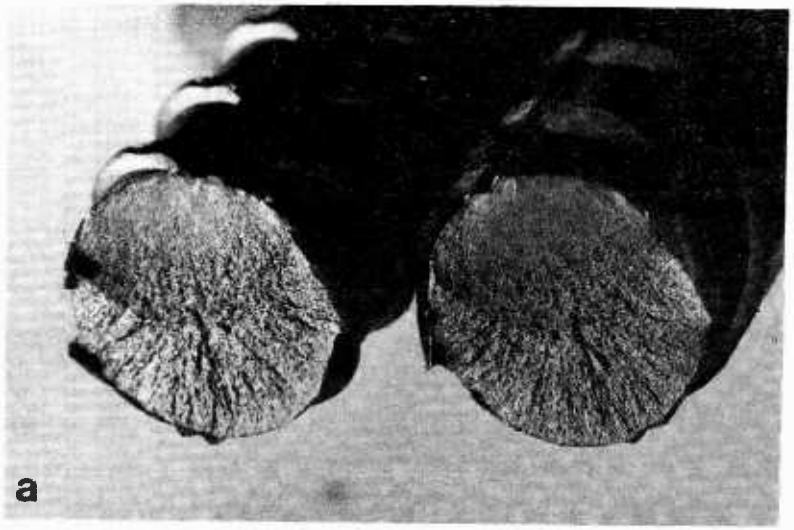
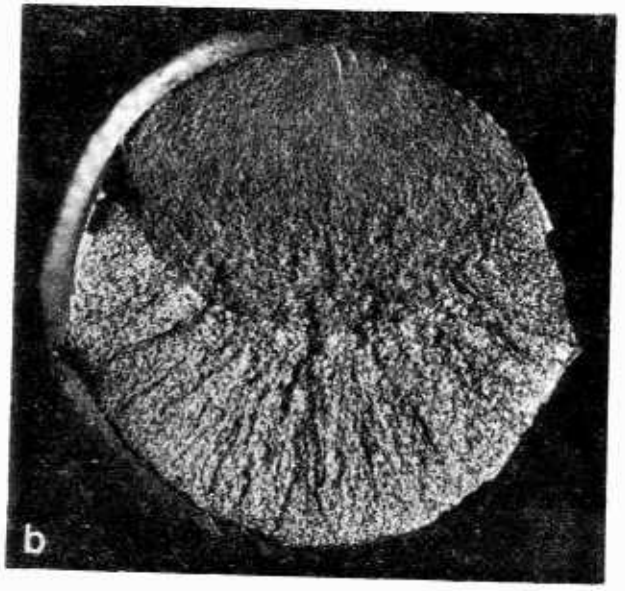


PLATE 5.3 PROFILES OF FATIGUE BAR FRACTURES





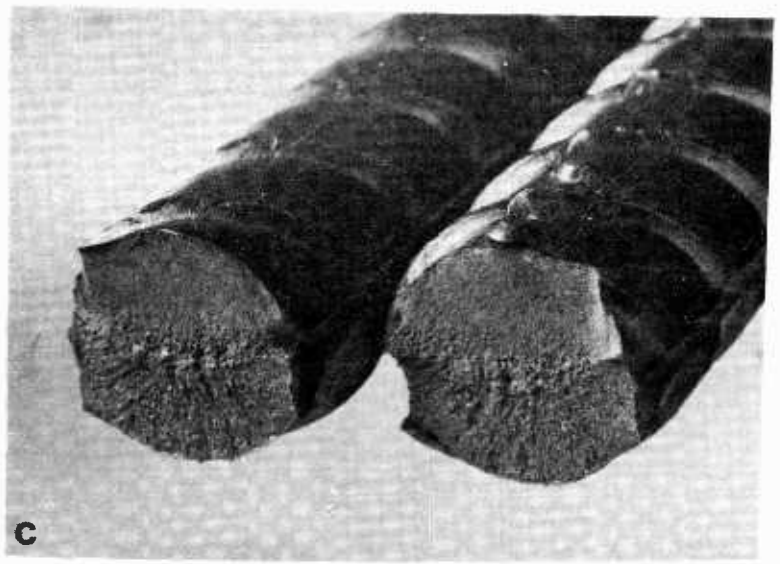
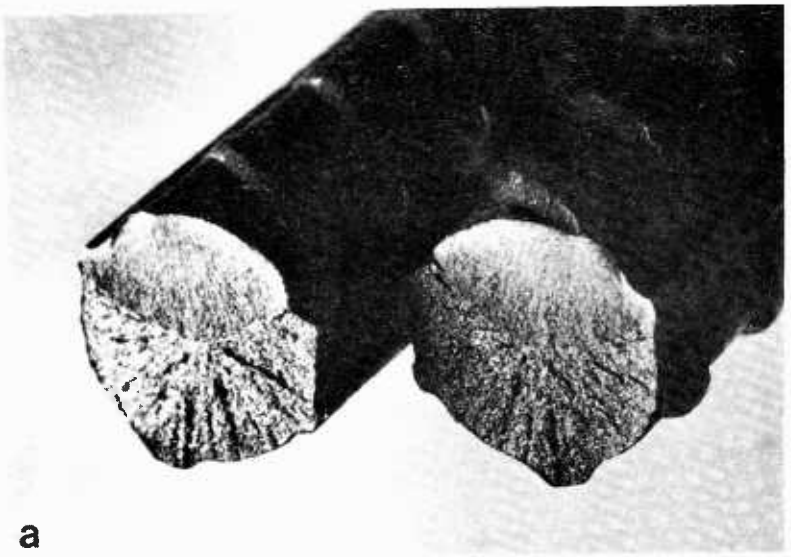


PLATE 5.4 FATIGUE FRACTURES OF WELBOND BAR

Fatigue crack originating at the base of
(a)&(b) a transverse lug at the point of intersection of one of the longitudinal ribs
(c) an identification mark



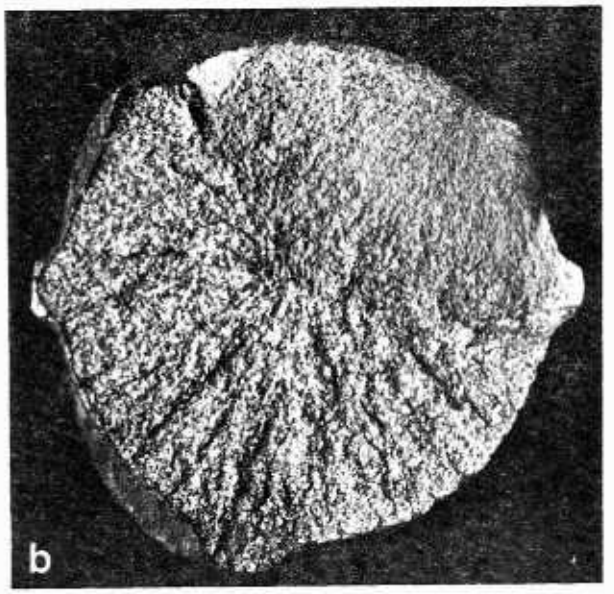


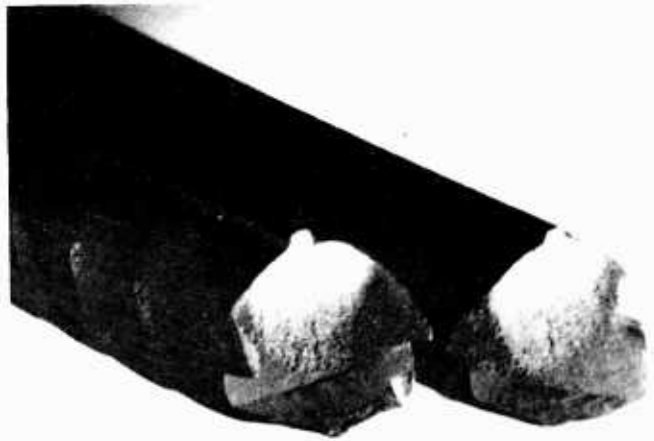


PLATE 5.5 FATIGUE FRACTURES OF JONES BAR

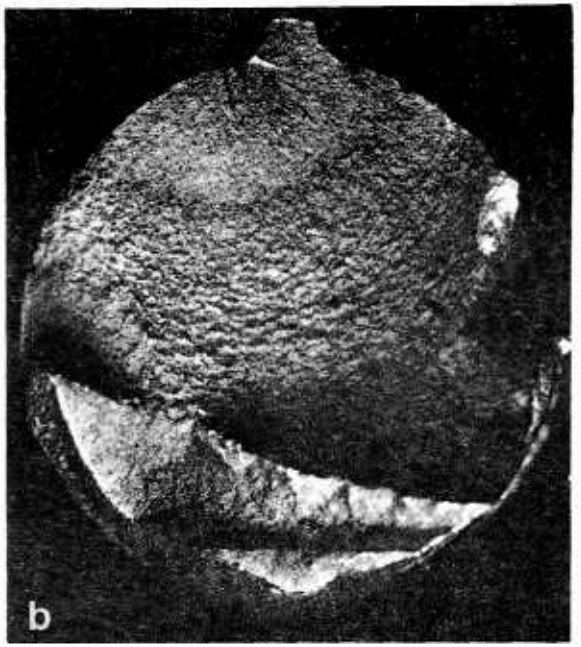
Fatigue crack originating at the base of

(a)&(b) a transverse lug

(c) an identification mark



a



b



c

PLATE 5.6 FATIGUE FRACTURES OF SHEERNESS BAR

Fatigue crack originating at the base of
(a)&(b) one of the longitudinal ribs
(c) a transverse lug



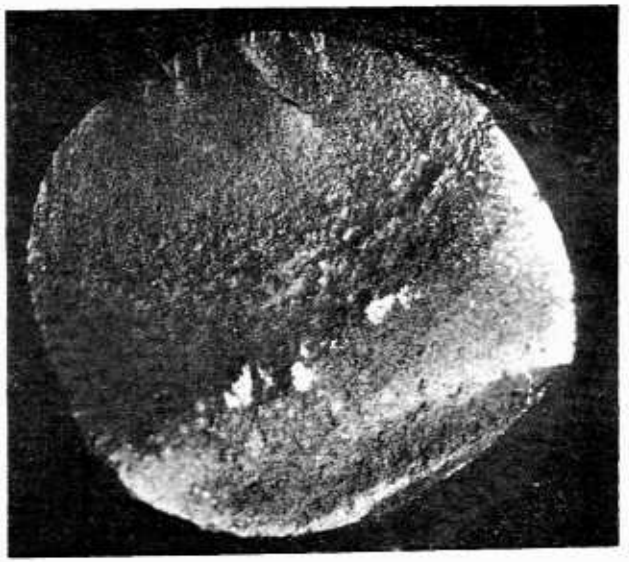


PLATE 5.7 FATIGUE FRACTURES OF UNISTEEL BAR
Fatigue crack originating at the base of a transverse lug

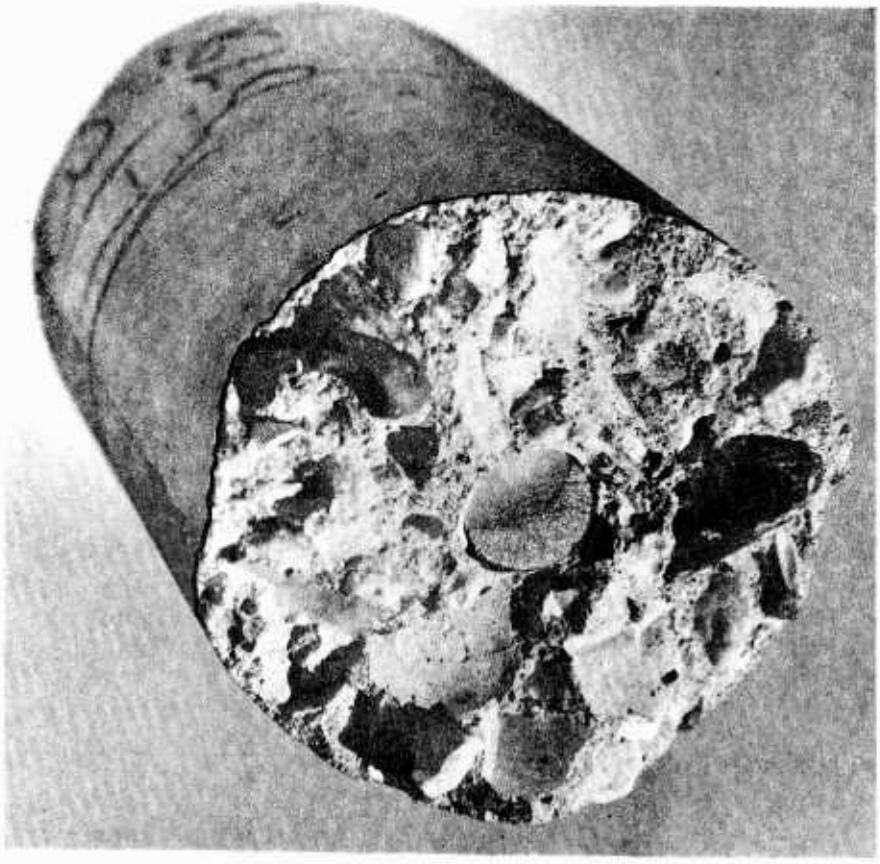
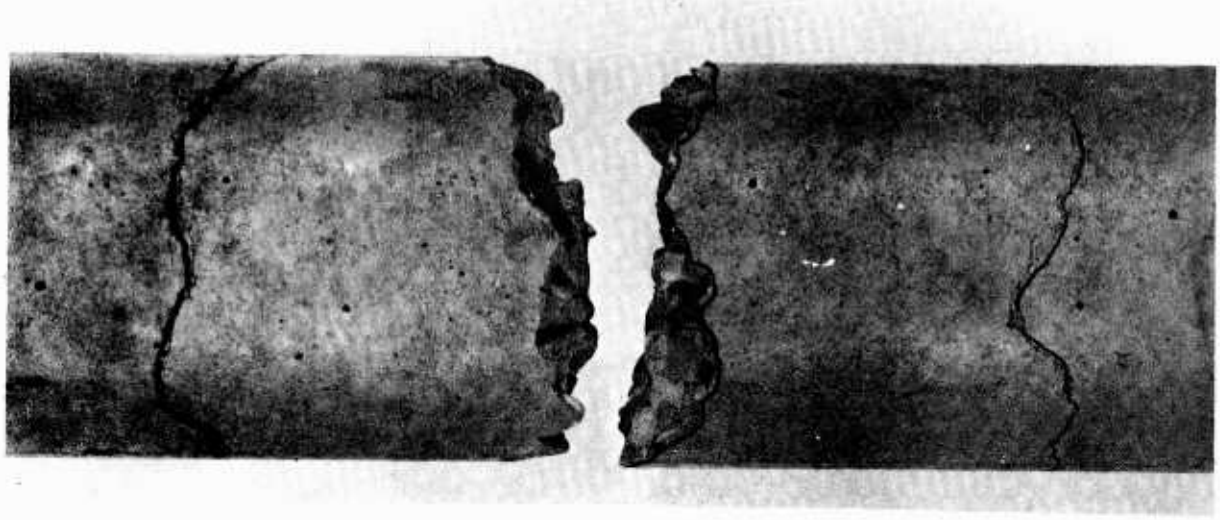


PLATE 5.8 FATIGUE FRACTURE OF SPECIMEN EMBEDDED IN CONCRETE



CHAPTER 6

EXPERIMENTAL INVESTIGATION OF THE BOND PROPERTIES OF HOT ROLLED DEFORMED BARS AND MILD STEEL PLAIN BARS

6.1 GENERAL

Four series of tests are reported in this chapter. The first series was carried out to determine bond-slip relations for hot rolled deformed bars and mild steel plain bars, from specimens with a concrete embedment length of 38 mm. The second series of tests was carried out to determine the effect of repeated loading on the bond-slip relations for deformed bars. The third series was carried out to obtain crack width data from 800 mm long tensile concrete specimens, reinforced with a deformed bar, while the fourth series was to obtain the free end slip and the loaded end slip data from 100 and 200 mm long pull-out specimens. The crack width and end slip data were to be used to verify the theoretical results of finite element analyses of long tensile and pull-out concrete specimens, given in chapters 7 and 8.

The type of specimen used in the first two series is similar to the one used by Edwards and Picard (56,57) for testing strand, and its details are given in section 3.2.2.1.

6.2. BOND-SLIP RELATIONS FOR HOT-ROLLED DEFORMED BARS AND MILD STEEL PLAIN BARS

6.2.1. TEST RESULTS

Basic specimens were tested statically under monotonically increasing load, following the testing procedure described in section 3.6.2, to determine bond-slip relations for 16 mm diameter hot-rolled Welbond deformed bars and mild steel plain bars. Two sizes of basic specimens, two directions of bar pull and an embedment length of 38 mm was used in this investigation. Also different magnitudes of back load were applied to the specimens (section 3.6.2) to find its effect on the bond-slip curves. This is important because reinforcing bars embedded in concrete members are subjected to different stress conditions along their length and these may influence their bond-slip characteristics due to Poisson's effects. The details of the different parameters considered in this series of tests and the notation adopted for their representation, are described below.

For convenience, each test was identified by three groups of alphanumeric characters separated by dashes; for example BG-L2-PD. The first group is either BG for specimens with a big concrete cover (35 mm) or SL for specimens with a small one (25 mm). The second group denotes the magnitude of the back load, i.e. L0 stands for zero back load, while L1-L5 stand for the following :

(i) Welbond hot-rolled deformed bars

L1 = 15 % of design load of Welbond deformed bar

L2 = 30 % of design load of Welbond deformed bar

L3 = 45 % of design load of Welbond deformed bar

L4 = 60 % of design load of Welbond deformed bar

L5 = 75 % of design load of Welbond deformed bar

Design load of Welbond deformed bar = $\frac{\text{characteristic load}}{1.15}$

= 77,000 N

(ii) Mild steel plain bars

L1 = 57 % of design load of mild steel plain bar

Design load of mild steel plain bar = $\frac{\text{characteristic load}}{1.15}$

= 52,000 N

The third group of characters stands for the direction of pull relative to the direction of settlement of concrete when being fresh. The direction of pull is positive (PD) if both are in the same direction, and negative (ND) if in opposite directions. In the case of specimens reinforced with a plain bar, the direction of pull was, in all tests, in the opposite direction to that of concrete settlement.

Eight basic specimens were cast from the same batch of concrete, and tested within the three day period of 27th-29th day after casting. In general the tests were repeated six times in the case of Welbond deformed bars, and four times in the case of plain bars, A total of 129 Welbond deformed bar, and 14 plain bar, basic specimens were tested. Their test allocation and sequence was randomised, to take account of the variability of the materials and load testing and thus have statistically unbiased test results suitable for statistical treatment.

All Welbond deformed bar basic specimens failed by splitting along the bar axis. Two typical failure patterns are shown in Plate 6.1. In contrast to this mode of failure all plain bar basic specimens did not fail by cracking of the concrete, but by the bar pulling out of the concrete block.

As it was mentioned in section 3.6.2 the two top and two bottom transducers to measure slip between steel and concrete were attached to the steel bar at a short distance (35mm) from the concrete face (Plate 3.13). It was thus necessary to correct the measured slip due to the elongation of the two 35 mm lengths of steel. It can be shown that the correction to the average slip which is the mean of four readings is proportional to the bond force.

The experimentally obtained load and slip readings for every test were used for calculating the bond stress and the corresponding slip values. These were used as data in suitably written computer programs to draw automatically bond-slip curves by means of a Kingmatic computer plotting machine. The obtained bond-slip curves for Welbond deformed bar are shown in Figures 6.1 to 6.24, while those for plain bar are shown in Figures 6.25 to 6.28. These include all the different parameters mentioned earlier on in this section. All replications of the same test are shown on the same figure for ease of comparison.

The test results for the Welbond bar and the plain bar are summarised in Tables 6.1 to 6.4 and Table 6.8 respectively, where u_{max} is the maximum bond stress reached with a mean value denoted by $\bar{u}_{max}$ and a standard deviation by $s_{u_{max}}$.

6.2.2. STATISTICAL ANALYSIS OF WELBOND DEFORMED BAR BOND-SLIP DATA AND DISCUSSION OF RESULTS

6.2.2.1. BOND-SLIP CURVES FOR WELBOND DEFORMED BAR

The obtained bond-slip curves for Welbond deformed bar, shown in Figures 6.1 to 6.24, have in general the same shape. While considerable scatter is in evidence between the curves of replicated tests, this is not surprising, considering (a) the heterogeneous nature of concrete, (b) the variable bonding conditions between the deformed bar and the concrete matrix, which depend on some uncontrollable factors like local settlement and shrinkage, and (c) the formation of internal concrete cracking.

All the bond-slip curves show that the bond stress increases with increasing slip until a maximum bond stress value is reached. This occurs at a slip varying from 0.10 to 0.30 mm in different curves. The slope of the curves decreases with increasing slip, having a maximum value at zero slip and approaching zero at the maximum bond stress. For larger values of slip the bond stress is almost constant and equal to its maximum value. No experimental data could be obtained beyond those shown in the plotted bond-slip curves because a further small increase in the bar load was quickly followed by a sudden fracture of the specimen.

The bond-slip curves of Figures 6.1 to 6.24 do not indicate that there is a relation between the stiffness of a curve (being proportional to its tangent modulus) and its maximum bond stress. Therefore high stiffness at small bond stress levels does not necessarily mean a high maximum bond

stress and vice versa. The differences between the bond-slip curves of replications of a test are getting larger at higher bond stress levels, while their initial slope, referred to hereafter as the slip modulus, is in the majority of tests not much different. Also the average slip modulus values of bond-slip curves obtained from basic specimens of different size, different back load values or different direction of bar pull relative to that of casting, do not appear to be significantly different, neither is any relation between them evident. An average slip modulus value for all tests is 500 $N/mm^2/mm$.

Visual inspection of the bond-slip curves of Figures 6.1 to 6.24, and reference to the summarised test results given in Tables 6.1 to 6.4, reveals a small increase in the maximum bond stress (u_{max}) for the basic specimens with a 35 mm concrete cover as compared to those with a 25 mm one, under the same test conditions. However, because of the large scatter in u_{max}, comparison of mean u_{max} values is not reliable unless it is done employing statistical techniques. The random test allocation and sequence, and the six replications of almost every test, renders the obtained bond-slip data suitable for statistical treatment.

The effect of the following parameters on u_{max} was determined statistically :

(a) Bar back load

(b) Concrete cover to bar

(c) Direction of bar pull relative to that of casting.

Some of the statistical techniques given in Chapter 4, which were used for the analysis of fatigue data, were also used for

the analysis of the bond (u_{max}) data.

The obtained u_{max} values were first checked whether they were normally distributed, so that significance tests could be carried out, as described in section 4.4. The effect of the above mentioned parameters on u_{max} was then determined by carrying out statistical comparisons between the corresponding sample variances and means. These statistical tests are given and discussed in the following sections.

6.2.2.2. χ^2 - TEST FOR GOODNESS OF FIT

The up to six replications of each test were too small to test whether the u_{max} values were normally distributed. However, the bond-slip tests were sorted out into four groups, each group consisting of six test series and all series of the same group corresponded to the same concrete cover to bar and the same direction of bar pull relative to that of casting, but to different magnitudes of bar back load. The test results of every group, shown in Tables 6.1 to 6.4, were combined by making a change of variable (section 4.2.4) from u_{max} to z, where :

$$z = \frac{u_{max} - \bar{u}_{max}}{s_{u_{max}}}$$

and $\bar{u}_{max}$ and $s_{u_{max}}$ are the mean and the standard deviation respectively of the u_{max} values at each level of bar back load used. The results of the χ^2 - tests for the four groups of tests are summarised in Table 6.5.

In all four groups of series of tests, the χ^2 - test

was passed at the 10 % level of significance. Therefore it can be concluded that the experimentally determined maximum bond stress values are normally distributed.

6.2.2.3. EFFECT OF BAR BACK LOAD ON MAXIMUM BOND STRESS

The test results of each of the four groups of series of tests described in the previous section were also used to assess the effect of bar back load on u_{max}. This was done by comparing first the variances and then the means of each of the six test series that makes up each group. All comparisons were done statistically at the 5 % and 10 % significance levels using the statistical tests described in sections 4.4.1 and 4.4.3 for k variances and k means. The results of all statistical tests are summarised in Table 6.6.

Since the hypothesis of equality of six variances was passed in three cases at the 10 % level of significance and in one case at the 5 % level and equality of the corresponding means was passed at the 10 % level of significance, the magnitude of the bar back load has no statistically significant effect on the maximum bond stress. This would mean that the maximum bond stress value would not vary with distance from a loaded end, or a crack face, in a concrete member. This is in contradiction to Nilson's conclusions (45), which were derived from (a) a limited number of tests and thus not taking into account the large scatter observed in the bond-slip curves obtained in the present investigation, and (b) tests subject to inaccuracies because of the not strictly exact way of obtaining slip and bond values.

Since the back load was found to have no significant effect on u_{max}, the test results of each of the four groups of series of tests were combined together when used in further statistical tests and an overall average value and standard deviation were calculated.

6.2.2.4. EFFECT OF CONCRETE COVER ON MAXIMUM BOND STRESS

The effect of concrete cover on u_{max} was determined by comparing statistically the results of :

(a) test groups SL-PD and BG-PD, both with a positive bar pull, i.e. in the same direction to that of casting

(b) test groups SL-ND and BG-ND, both with a negative bar pull, i.e. in the opposite direction to that of casting

The equality of each pair of variances and means was checked using the statistical tests described in sections 4.4.2 and 4.4.4 respectively.

The results of the statistical comparisons, given in Table 6.7, show that for both directions of bar pull the variances are not significantly different, while the means are. Thus the size of the concrete cover has a statistically significant effect on u_{max}. Comparison of corresponding group mean u_{max} values, given in Tables 6.1 to 6.4, showed that they were of the order of 20 % higher in the groups with the larger concrete cover as compared to those with the smaller one. This increase in maximum bond stress with increasing concrete cover can be attributed to the increase in confinement to the deformed bar with increasing concrete cover.

6.2.2.5. EFFECT OF DIRECTION OF BAR PULL RELATIVE TO THAT OF CASTING

The effect of direction of bar pull, being in the same or in opposite direction to that of casting, was determined by comparing statistically the results of :

(a) test groups SL-PD and SL-ND, both on small size basic specimens (small concrete cover)

(b) test groups BG-PD and BG-ND, both on big size basic specimens (big concrete cover).

The results of statistical comparisons of each pair of variances and means are given in Table 6.7. These show that for both concrete covers the variances are not significantly different statistically. But the means, while for the small concrete cover are significantly different statistically, for the big concrete cover they are not. Comparison of corresponding group mean u_{max} values, given in Tables 6.1 to 6.4, showed that for the small concrete cover there is an increase of 11 %, while for the big cover only one of 1 %, when the bar pull is in the opposite direction to that of casting as compared to that in the same one. Because of settlement and pore formation in the fresh concrete below every bar deformation, it is to be expected that pulling the bar in the opposite direction to that of casting will give a bigger u_{max} value than pulling it in the same direction. This was indeed observed in basic pull out tests carried out by Rehm(50). The smaller percentage increase in u_{max} for the big concrete cover compared to the one for the small cover, can be attributed to the more unrestricted plastic flow and better compaction obtained when casting a big specimen

as compared to a small one.

6.2.3. COMPARISON OF PLAIN BAR BOND-SLIP DATA AND DISCUSSION OF RESULTS

The obtained bond-slip curves for plain bar, shown in Figures 6.25 to 6.28, have in general the same shape as that for the Welbond deformed bar. There is again softening of the curves for increasing slip values, until a maximum bond stress is reached. Thereafter the bond stress remains constant at its maximum value while the slip increases. No slips bigger than those shown in the curves could be obtained, because just after the u_{max} was reached the slip started increasing very quickly, as the bar was pulling continuously out of the concrete block with no splitting occurring.

The bond-slip curves for deformed and plain bars, shown in Figures 6.1 to 6.28, show that the maximum bond stress developed by plain bars is of the order of 50 to 35 % of that of deformed bars and is reached at a slip of 0.01 to 0.06 mm, as compared to the one for deformed bar at a slip of 0.10 to 0.30 mm. This is explained by the different bond mechanism of plain and deformed bars. In plain bars bond relies mainly on adhesion and friction. Adhesion is lost after a small slip occurs between the plain bar and concrete and does not contribute much to the bond strength. For further increase in slip bond relies mainly on friction between the steel and concrete sliding surfaces. Initially the concrete sliding surface is rough and slipping requires an increase in bar pull. But with increasing slip the concrete interface continuously

wears down and quickly it becomes rather smooth with an almost constant value of the coefficient of friction. This corresponds to the horizontal part of the bond-slip curve, which starts at a slip of 0.01 to 0.06 mm.

In contrast to the above bond mechanism, bond failure with deformed bars is radically different. Adhesion and bond are still operative but bond strength mainly relies on the bearing of bar deformations and the strength of concrete between them. As the bar load is increased, the bar deformations produce high concrete tensile stresses within the concrete matrix next to the bar and associated internal cracking. The process is continuous for increasing loads and results in softening of the concrete next to the bar and local relative slip between the steel and concrete. Eventually high splitting stresses are produced within the concrete and the concrete block fails by splitting, instead of the bar pulling out of the concrete as with plain bars.

Few bond tests were carried out with plain bars, so statistical comparisons were not possible. Visual inspection of the values of Table 6.8, nevertheless shows slightly bigger u_{max} values for the big concrete cover basic specimens, as compared to the small ones.

6.3. EFFECT OF REPEATED LOADING ON THE BOND-SLIP RELATIONS FOR HOT-ROLLED DEFORMED BARS

6.3.1. TEST RESULTS

Basic specimens were tested under repeated loading, following the testing procedure described in section 3.6.2,

to determine its effect on the bond-slip relations for 16 mm diameter hot-rolled Welbond deformed bars. The different test parameters considered were kept to a minimum and attention was focused on repeated loading. Thus two series of basic specimens were tested under only one direction of bar pull, i.e. that opposite to the direction of casting. No back load was applied and each test was repeated in most cases four times. Each specimen was subjected to ten slow load cycles of constant amplitude, before being loaded to failure. The minimum value of all load amplitudes was approximately equal to zero. Three different load amplitudes were employed in order to find the influence of different magnitude repeated loading on bond deterioration. The maximum value of these load amplitudes corresponded to bond stress values of 2.0, 3.9 and 5.6 N/mm^2. Throughout the loading and unloading parts of each load cycle, as well as during the final loading to failure, slip and load readings were taken at close intervals, as explained in section 3.6.2.

All eight basic specimens cast from the same batch of concrete, were tested within the three day period of 27th-29th day after casting. A total of 23 basic specimens reinforced with a Welbond deformed bar were tested. The specimens' test allocation and sequence was randomised to take account of the variability of the materials and load testing. All measured slips were suitably corrected, as described in section 6.2.1, to take account of the elongation of the reinforcing bar between the concrete surface and the point where the displacement transducers were attached.

Bond stress and corresponding slip values were calculated for every test, using the experimentally obtained load and slip readings. These values were used as data in suitably written computer programs to draw automatically bond-slip curves by means of a Calcomp computer plotting mechine. The obtained bond-slip curves, for the three different load amplitudes are shown in Figures 6.29, 6.31 and 6.33 for the small basic specimens and in Figures 6.30, 6.32 and 6.34 for the big basic specimens. All replications of the same test are shown on the same figure for ease of comparison.

All basic specimens in this series of tests, reinforced with a Welbond deformed bar, failed by splitting of the concrete along the bar axis, as described in section 6.2.1.

6.3.2. DISCUSSION OF TEST RESULTS

Comparison of the bond-slip curves of Figures 6.29 to 6.34 shows that although all have the same general shape, there is a relatively large scatter present even in between replications of the same test. This scatter is of the same order as that obtained in the bond-slip curves of basic specimens under monotonically increasing load. Statistical conclusions cannot be drawn from only four replications of each test, but nevertheless general trends can be obtained, which are invaluable in improving the state of knowledge of bond deterioration under repeated loading.

Comparing the bond-slip curves of Figures 6.29 to 6.30, 6.31 with 6.32 and 6.33 with 6.34, there is no evidence of a significant difference between the bond-slip curves of

small and big basic specimens subjected to the same magnitude of load cycling. Thus corresponding bond-slip curves for the two specimen sizes were considered to be replications of the same test. In this way only three groups of bond-slip curves had to be compared for assessing the effect of different load cycle amplitudes on bond deterioration.

A common characteristic of the obtained bond-slip curves under repeated loading, is the presence of residual slip at zero load level and the loading and unloading paths not coinciding, but forming hysteresis loops. This was the case in all tests except four, in which there was practically no residual slip produced. Three of these four tests corresponded to the lowest applied load amplitude.

The characteristics of the hysteresis loops in the experimentally obtained bond-slip curves can be studied better by considering a typical one, corresponding to medium load amplitude. This is shown magnified for clarity in Figure 6.35, and the ten hysteresis loops are relatively clearly distinguishable. As load cycling is applied the hysteresis loops shift by a small amount to the right, producing additional residual slip at zero load level, as well as additional slip at any other load level. The shifting of the hysteresis loops is such that the slopes of the loading and unloading paths of any loop are approximately equal to the corresponding ones of all other loops. The amount of shifting tends to diminish as the number of cycles in increased and the hysteresis loops become more congested.

The bond-slip curves of Figures 6.29 to 6.34 also

show that the amount of additional slip produced between the first and tenth load cycles in general depends on the load amplitude. The trend is that the higher the load amplitude, the bigger the additional slip which means that the rate of bond deterioration is larger at higher load amplitudes.

Although every load cycle produces additional slip at any load level this is comparatively small compared to the slip produced during the first cycle. The first cycle seems to be the one causing most of the bond destruction. With increasing load amplitudes the amount of bond destruction increases. For example, it can be seen from Figures 6.29 to 6.34 that, the residual slip at zero load level is on the average biggest for the highest load amplitude (i.e. bond stress = 5.6 N/mm^2). Also slip at any load level, less than the peak load reached in preceeding cycles, is increased as compared to the slip obtained before cycling at the same load level. This increase in slip was biggest at load levels well below the peak load. This is in agreement with the findings of Bresler and Bertero (37), as well as Ismail and Jirsa (75).

6.4. TENSILE BOND TESTS ON SPECIMENS WITH AN 800 MM DEFORMED BAR LENGTH EMBEDDED IN CONCRETE

TEST RESULTS AND DISCUSSION

In this series of tests, five tensile specimens, 76 mm in diameter and 800 mm long, concentrically reinforced with a 16 mm diameter Welbond deformed bar, were tested statically, under monotonically increasing load, for obtaining crack width data at different load levels, to be used for

verifying the theoretical results of finite element analysis of the members.

Each of the tensile specimens was cast from different batches of the same concrete, i.e. that used for the basic bond specimens, and tested at 28 days from casting. The concrete surface strain and crack widths were measured at a number of load stages up to a maximum load of approximately 80 % of the yield load of the bar, as described in section 3.6.2.

The concrete surface strain values from all tensile specimens were combined and used to plot steel stress against average concrete surface strain, shown in Figure 6.36. For comparative purposes, a dashed line is also plotted, which represents the stress-strain curve of the steel bar with no concrete embedment. The steel stress-average concrete surface strain curve exhibits a linear initial part, up to approximately 25 N/mm^2, having a slope equal to nearly four times that of the steel stress-strain line. But for higher steel stresses the slope of the curve decreases until at approximately 50 N/mm^2 it becomes nearly equal to the slope of the steel stress-strain curve, and for higher stresses it remains unchanged and the two curves are parallel to each other. The initial slope can be attributed to the near monolithic action of steel and concrete and the subsequent slope to the formation of internal cracks and external cracks with increasing steel stresses. Actually the first external cracks were noticed at a steel stress of approximately 60 N/mm^2. Similar results have been obtained experimentally by Broms (35). The measured average concrete surface strain is approximately 15 % less than the

strain of a bar free in air at a steel stress of 100 N/mm^2, and 5 % less than that at a steel stress of 350 N/mm^2.

Cracks were formed in the length of the specimen, under increasing tensile load. A typical crack pattern is shown in Plate 3.15b. Cracks formed transverse to the bar axis, but at high stress levels some longitudinal cracks appeared starting from the faces of the transverse ones and extended for a short distance along the concrete surface.

At each load stage the number of cracks, n, between the two specimens' ends, that were crossing four lines running parallel to the bar axis and equally spaced around the periphery of the concrete member, was counted. This was used to calculate the average crack spacing for a given steel stress by dividing the effective total length of the specimen (4 x 800 mm) by n + 4. Corresponding values of steel stress and average crack spacing, for each specimen, are shown plotted against each other in Figure 6.37. The crack spacing data from all specimens were combined to get a mean steel stress-average crack spacing curve shown in Figure 6.38. These figures show that at zero load, crack spacing tends to be infinite, while as the load increases, cracks are produced and crack spacing tends to a limiting value of 87 mm. At this load stage and for any higher ones the tensile forces transferred from steel to concrete by bond are insufficient to produce additional cracks transversing the whole cross-section of the member and thus visible on its surface.

The width of each crack crossing the above mentioned four lines, was measured at each load stage. These measurements

were used to plot steel stress against crack width for each specimen, as shown in Figures 6.39 to 6.43. The average crack width was calculated at each load level and is also shown on these figures. The crack width data from all tensile specimens were combined and are shown plotted against steel stress in Figure 6.44. The relations between average crack width and the corresponding applied stress at the ends of the reinforcing deformed bar are seen from Figures 6.39 to 6.44 to be nearly linearly related within the applied stress range. In looking at these results it should be remembered that the sensitivity of the crack measuring device was 0.02 mm/division and cracks were estimated to the nearest $\frac{1}{2}$ division.

6.5. PULL-OUT TESTS ON CONCRETE SPECIMENS REINFORCED WITH A DEFORMED BAR

TEST RESULTS AND DISCUSSION

Pull-out specimens, 76 mm in diameter and 100 or 200 mm long, concentrically reinforced with a 16 mm diameter Welbond deformed bar, were tested statically under monotonically increasing load. Three specimens of each length were tested to obtain their load - slip characteristics, to be used for verifying the theoretical results of the finite element analysis.

Each of the pull-out specimens was cast from different batches of the concrete used for the basic specimens, and tested at 28 days from casting. The slips between the deformed bar and the concrete were measured both at the loaded end and free end of the specimens at a number of load stages in the linear stress - strain range of the steel bar. The instrumen-

tation and testing procedure used are described in section 3.6.2.

The experimentally obtained load and slip data were used to plot load versus free end, as well as loaded end slip, for each concrete length, as shown in Figures 6.45 and 6.46. All the curves show that up to a certain load level, load is linearly related to both free end and loaded end slips, and the free end slip is a very small fraction of the loaded end slip. For higher load levels, the slope of both loaded and free ends decreases continuously, indicating the gradual slipping of the bar embedded in concrete, and the free end slip becomes a continuously bigger fraction of the loaded end slip. Eventually bursting stresses develop in the concrete which split the concrete specimen. The load - slip curves for both concrete lengths are shown plotted together in Figure 6.47 for ease of comparison, and indicate that they are not significantly different within their linear parts.

TABLE 6.1

SUMMARY OF THE RESULTS OF BASIC BOND-SLIP TESTS FOR 16 MM DIAMETER HOT ROLLED WELBOND DEFORMED BAR GROUP SL-PD

Test Series	u_{max} (N/mm^2)	$\bar{u}_{max}$ (N/mm^2)	$S_{u_{max}}$ (N/mm^2)
SL-L0-PD	6.5 7.2 7.3 8.2 8.3 8.5	7.7	0.78655
SL-L1-PD	7.4 8.2 8.3 8.8 9.1 9.9	8.6	0.85654
SL-L2-PD	6.2 7.3 8.4 9.1	7.8	1.27148
SL-L3-PD	6.2 6.8 8.3 8.7 10.1	8.0	1.55467
SL-L4-PD	7.6 7.6 7.8 8.3 9.9	8.2	0.97108
SL-L5-PD	7.1 7.8 7.9 8.0 8.3 10.3	8.2	1.08751

Results of all test series combined together :

$\bar{u}_{max} = 8.1 \quad N/mm^2$ $\qquad$ $S_{u_{max}} = 1.05370 \quad N/mm^2$

TABLE 6.2

SUMMARY OF THE RESULTS OF BASIC BOND-SLIP TESTS FOR 16 MM DIAMETER HOT ROLLED WELBOND DEFORMED BAR GROUP SL-ND

Test Series	u_{max} (N/mm^2)	$\bar{u}_{max}$ (N/mm^2)	$S_{u_{max}}$ (N/mm^2)
SL-L0-ND	7.3 8.4 8.5 9.2 10.2	8.7	1.07098
SL-L1-ND	7.3 7.4 9.8 10.3 11.2	9.2	1.76210
SL-L2-ND	6.5 7.5 8.3 9.2 10.6	8.4	1.57385
SL-L3-ND	8.3 8.8 9.1 9.2 9.3 9.9	9.1	0.53292
SL-L4-ND	8.4 8.7 9.0 9.4 10.3 10.5	9.4	0.85654
SL-L5-ND	8.7 9.1 9.4 9.5 9.8	9.3	0.41833

Results of all test series combined together :

$\bar{u}_{max}$ = 9.0 N/mm^2 $S_{u_{max}}$ = 1.08259 N/mm^2

TABLE 6.3

SUMMARY OF THE RESULTS OF BASIC BOND-SLIP TESTS FOR 16 MM DIAMETER HOT ROLLED WELBOND DEFORMED BAR GROUP BG-PD

Test Series	u_{max} (N/mm^2)	$\bar{u}_{max}$ (N/mm^2)	$S_{u_{max}}$ (N/mm^2)
BG-L0-PD	10.2 10.7 12.0 12.1 13.1	11.6	1.16490
BG-L1-PD	9.8 10.3 10.7 11.0 12.2 12.2	11.0	0.98928
BG-L2-PD	8.6 9.0 10.3 10.4 11.7	10.0	1.23491
BG-L3-PD	8.3 9.0 10.3 10.4 10.5	9.7	0.99247
BG-L4-PD	9.3 9.5 10.6 10.7 11.0 11.2	10.4	0.79352
BG-L5-PD	9.1 9.2 9.5 10.5 10.7	9.8	0.74833

Results of all test series combined together :

$\bar{u}_{max} = 10.4 \quad N/mm^2 \qquad S_{u_{max}} = 1.14437 \quad N/mm^2$

TABLE 6.4

SUMMARY OF THE RESULTS OF BASIC BOND-SLIP TESTS FOR 16 MM DIAMETER HOT ROLLED WELBOND DEFORMED BAR GROUP BG-ND

Test Series	u_{max} (N/mm^2)	$\bar{u}_{max}$ (N/mm^2)	$S_{u_{max}}$ (N/mm^2)
BG-L0-ND	8.3 8.6 10.4 10.7 11.2	9.8	1.30499
BG-L1-ND	8.5 10.3 10.4 10.8 11.7	10.3	1.16748
BG-L2-ND	9.3 10.0 10.3 10.5 11.0 11.4	10.4	0.74140
BG-L3-ND	11.0 11.2 11.3 11.6 12.9	11.6	0.75829
BG-L4-ND	7.8 9.8 10.2 11.0 11.2 12.8	10.5	1.67382
BG-L5-ND	9.2 9.5 10.1 10.4 11.3 11.5	10.3	0.93095

Results of all test series combined together :

$\bar{u}_{max} = 10.5 \quad N/mm^2$ $\qquad$ $S_{u_{max}} = 1.17403 \quad N/mm^2$

TABLE 6.5

SUMMARY OF x^2 - TESTS FOR GOODNESS OF FIT OF u_{max} VALUES TO NORMAL DISTRIBUTION

Group Of Series Of Tests	Series Size	d.f.	x^2	$x^2_{.90}$	$x^2_{.95}$
SL-PD	32	3	4.38	6.25	7.81
SL-ND	32	3	5.88	6.25	7.81
BG-PD	32	3	3.25	6.25	7.81
BG-ND	33	3	5.73	6.25	7.81

TABLE 6.6

RESULTS OF COMPARISONS OF SIX BOND TEST SERIES OF EACH TEST GROUP

(k = 6)

Group Of Series Of Tests	Test Of Equality Of Six Variances			Test Of Equality Of Six Means		
	x^2	$x^2_{.90}$	$x^2_{.95}$	F	$F_{.90}$	$F_{.95}$
SL-PD	2.67	9.24	11.07	0.58	2.08	2.59
SL-ND	11.06	9.24	11.07	0.59	2.08	2.59
BG-PD	2.07	9.24	11.07	1.69	2.08	2.59
BG-ND	4.51	9.24	11.07	1.30	2.07	2.57

TABLE 6.7

RESULTS OF COMPARISONS OF PAIRS OF BOND TEST GROUPS

Groups Of Series Of Tests	Test Of Equality Of Two Variances			Test Of Equality Of Two Means			
	F	$F_{.95}$	$F_{.975}$	t	$t_{.95}$	$t_{.975}$	
SL-PD and BG-PD	1.18	1.83	2.05	11.983^{oo}	1.670	1.999	A
SL-ND and BG-ND	1.18	1.82	2.04	5.208^{oo}	1.670	1.999	A
SL-PD and SL-ND	1.06	1.83	2.05	3.445^{oo}	1.670	1.999	B
BG-PD and BG-ND	1.05	1.82	2.04	0.700	1.670	1.999	B

oo Means significantly different

o Means in the zone of uncertainty

(A) Effect of Concrete cover

(B) Effect of bar pull

TABLE 6.8

SUMMARY OF THE RESULTS OF BASIC BOND-SLIP TESTS FOR 16 MM DIAMETER MILD STEEL PLAIN BAR

Test Series	u_{max} (N/mm^2)	$\bar{u}_{max}$ (N/mm^2)
SL-L0-ND	3.1 3.8 3.9 4.0	3.7
SL-L1-ND	3.0 3.3 3.8	3.4
BG-L0-ND	3.8 4.2 4.3 4.4	4.2
BG-L1-ND	4.0 4.1 6.1	4.7

EXPERIMENTAL BOND-SLIP CURVES FOR 16MM DIA. HOT ROLLED HIGH YIELD (410) DEFORMED BAR

Test Series SL-LO-PD

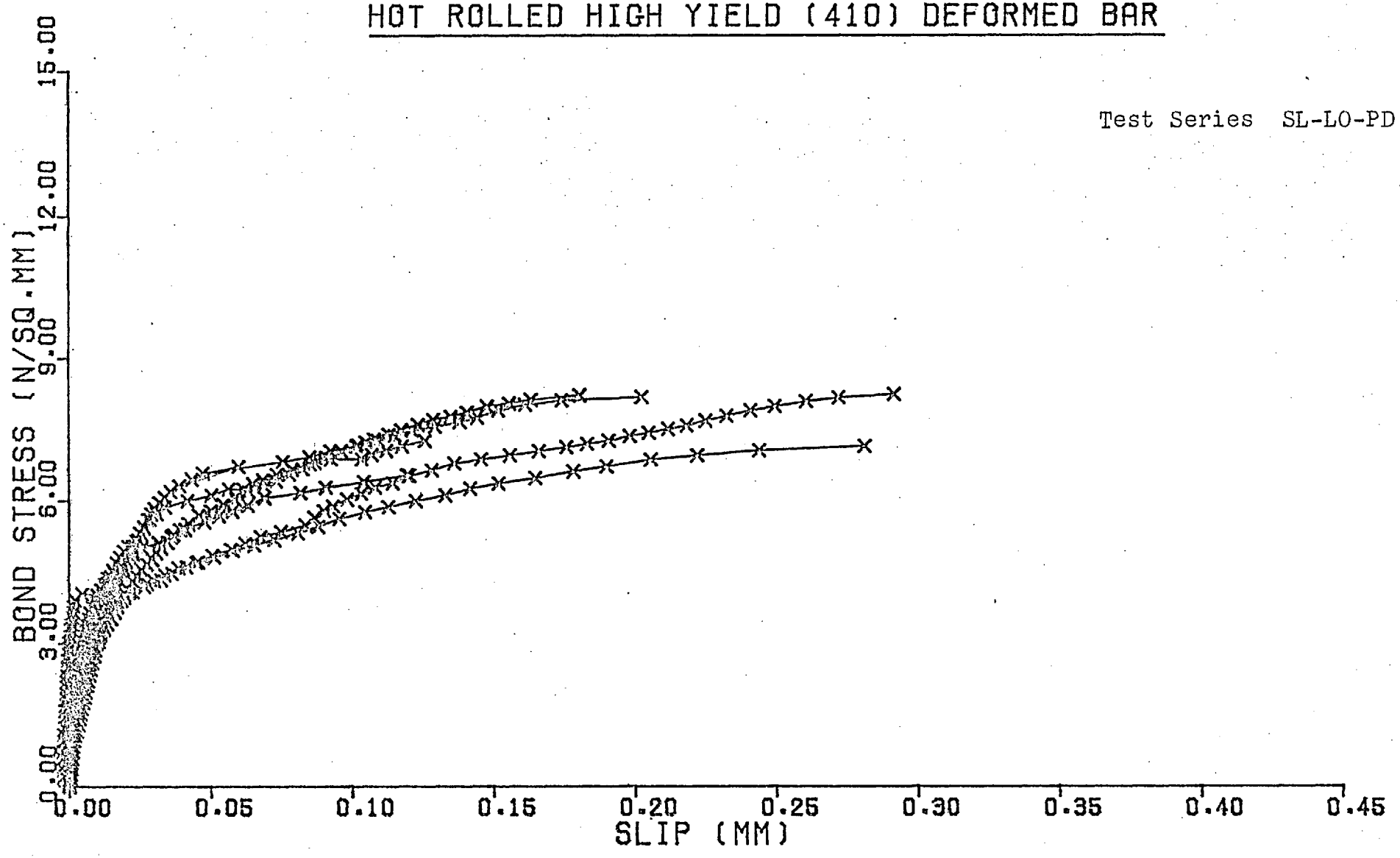


FIGURE 6.1

EXPERIMENTAL BOND-SLIP CURVES FOR 16MM DIA. HOT ROLLED HIGH YIELD (410) DEFORMED BAR

Test Series SL-L1-PD

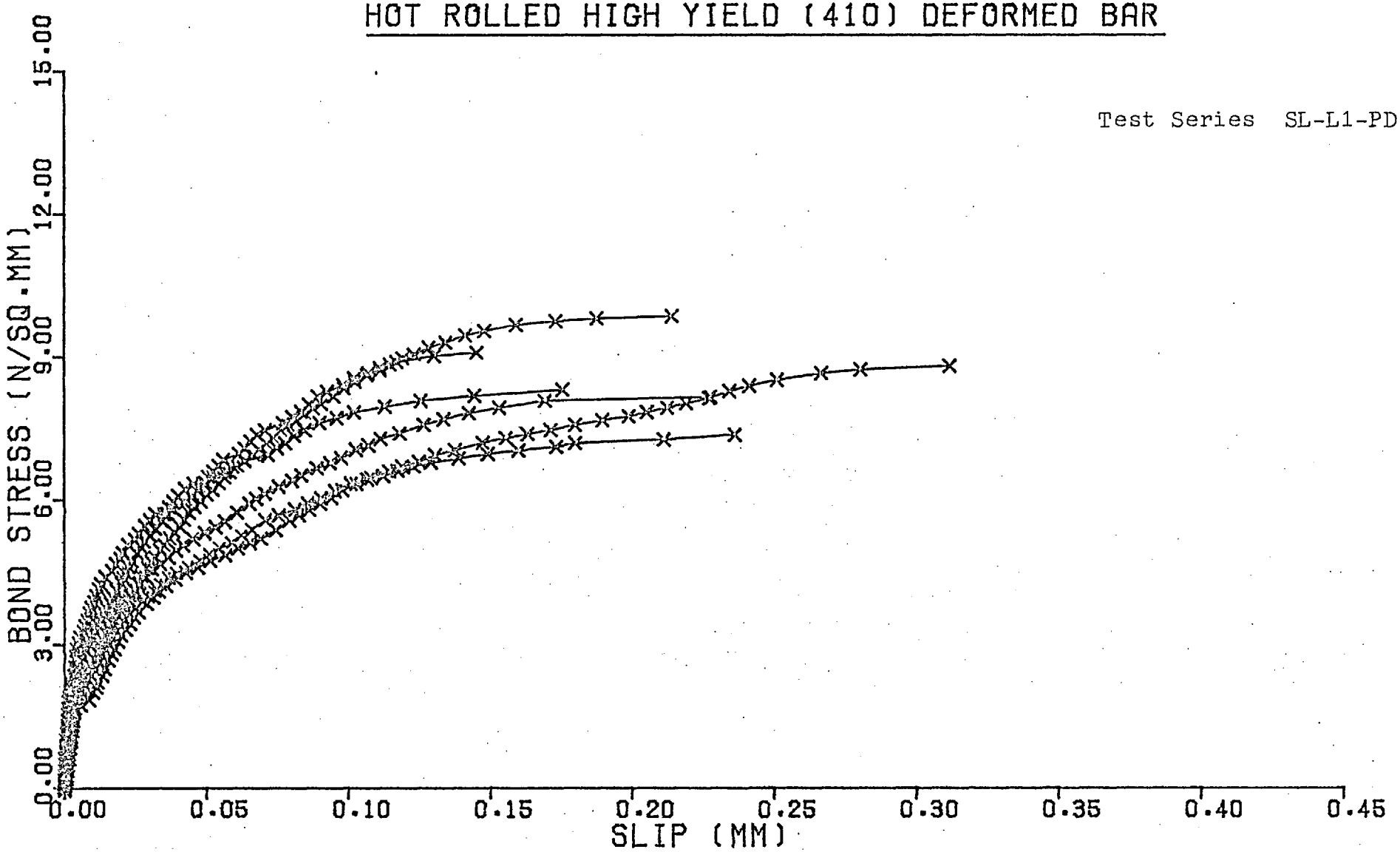


FIGURE 6.2

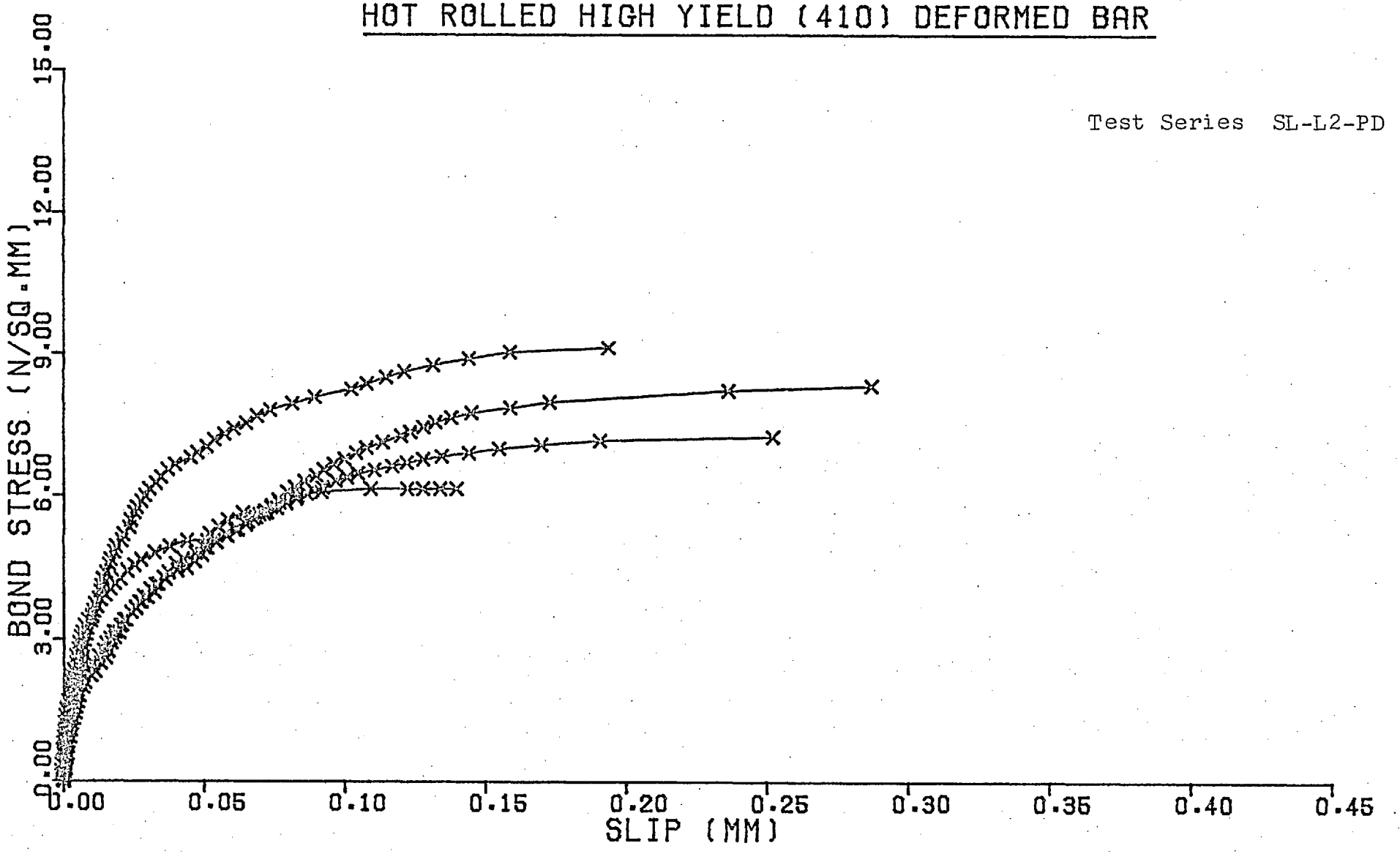

EXPERIMENTAL BOND-SLIP CURVES FOR 16MM DIA.
HOT ROLLED HIGH YIELD (410) DEFORMED BAR
Test Series SL-L2-PD
BOND STRESS (N/SQ.MM)
0.00
3.00
6.00
9.00
12.00
15.00
0.00
0.05
0.10
0.15
0.20
0.25
0.30
0.35
0.40
0.45
SLIP (MM)

FIGURE 6.3

EXPERIMENTAL BOND-SLIP CURVES FOR 16MM DIA. HOT ROLLED HIGH YIELD (410) DEFORMED BAR

Test Series SL-L3-PD

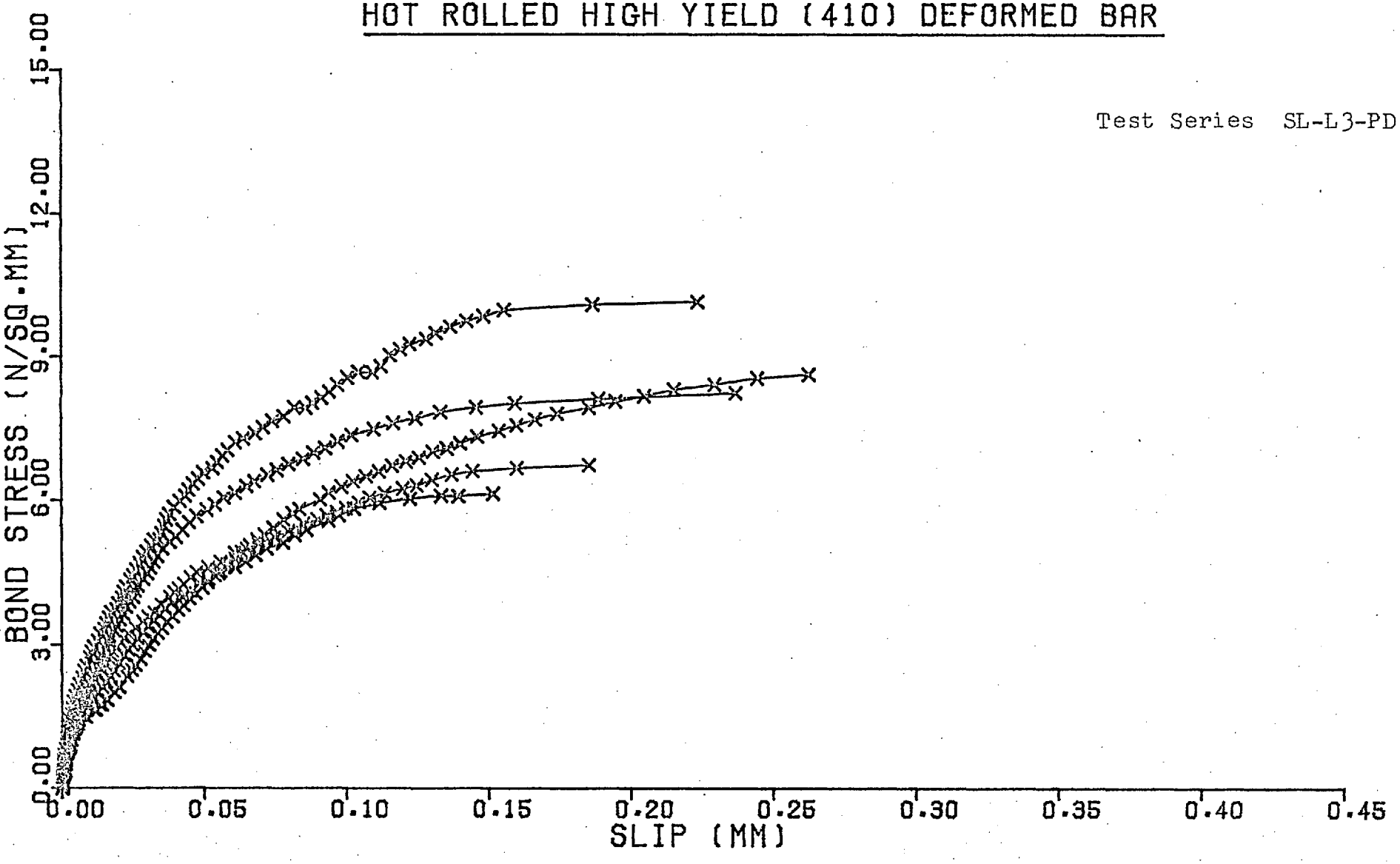


FIGURE 6.4

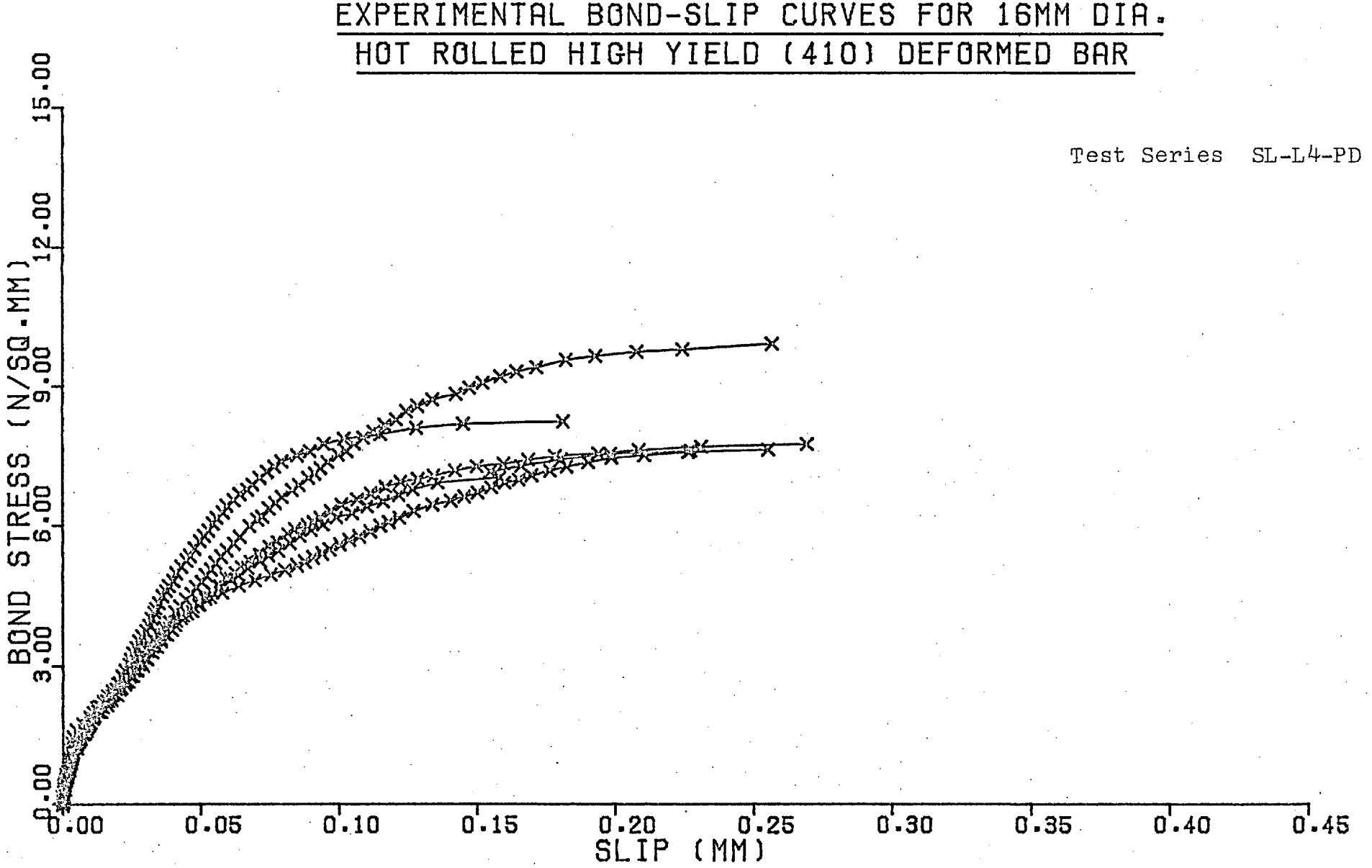

EXPERIMENTAL BOND-SLIP CURVES FOR 16MM DIA.
HOT ROLLED HIGH YIELD (410) DEFORMED BAR
Test Series SL-L4-PD
BOND STRESS (N/SQ.MM)
0.00
3.00
6.00
9.00
12.00
15.00
0.00
0.05
0.10
0.15
0.20
0.25
0.30
0.35
0.40
0.45
SLIP (MM)

FIGURE 6.5

EXPERIMENTAL BOND-SLIP CURVES FOR 16MM DIA. HOT ROLLED HIGH YIELD (410) DEFORMED BAR

Test Series SL-L5-PD

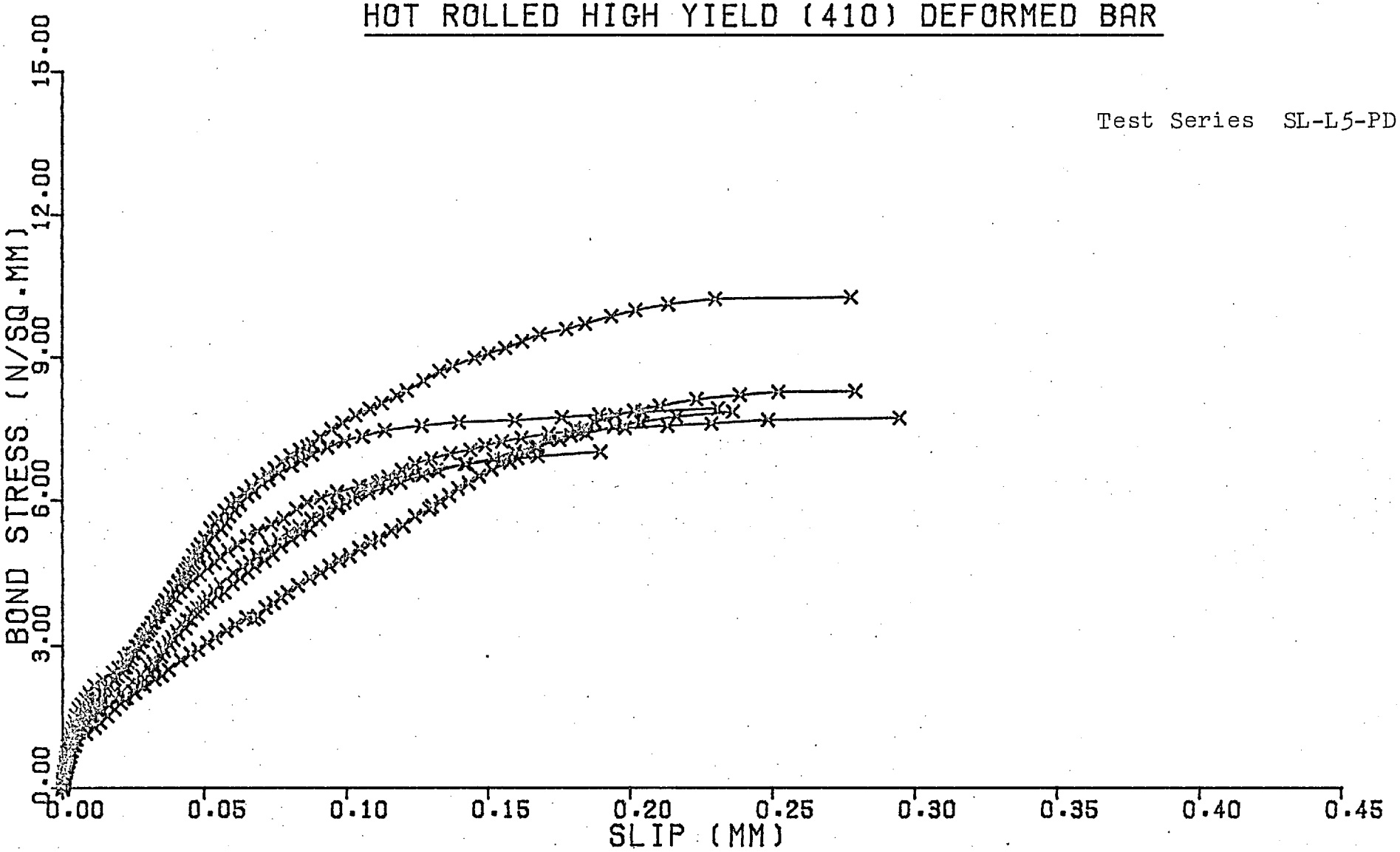


FIGURE 6.6

EXPERIMENTAL BOND-SLIP CURVES FOR 16MM DIA. HOT ROLLED HIGH YIELD (410) DEFORMED BAR

Test Series SL-L0-ND

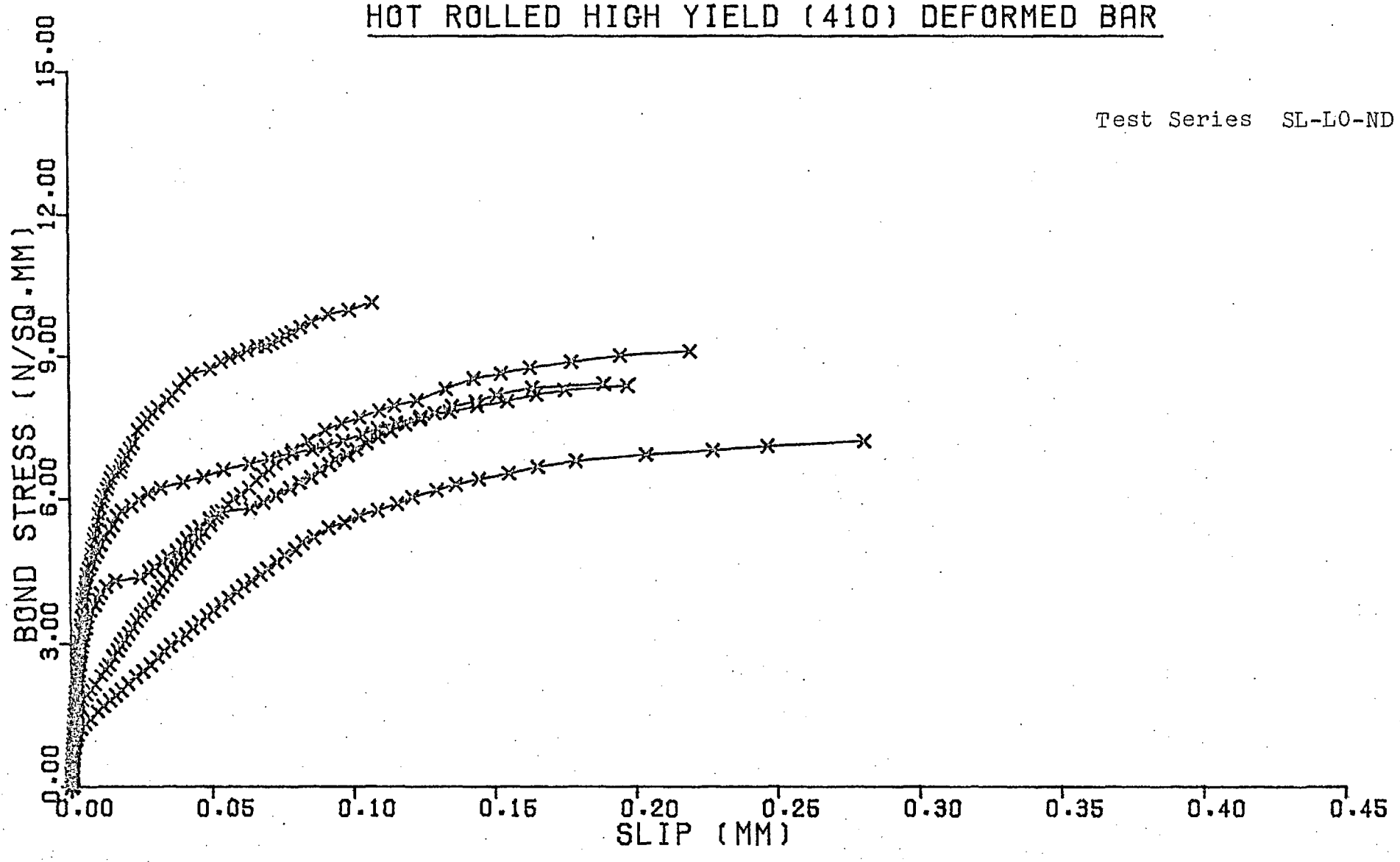


FIGURE 6.7

EXPERIMENTAL BOND-SLIP CURVES FOR 16MM DIA. HOT ROLLED HIGH YIELD (410) DEFORMED BAR

Test Series SL-L1-ND

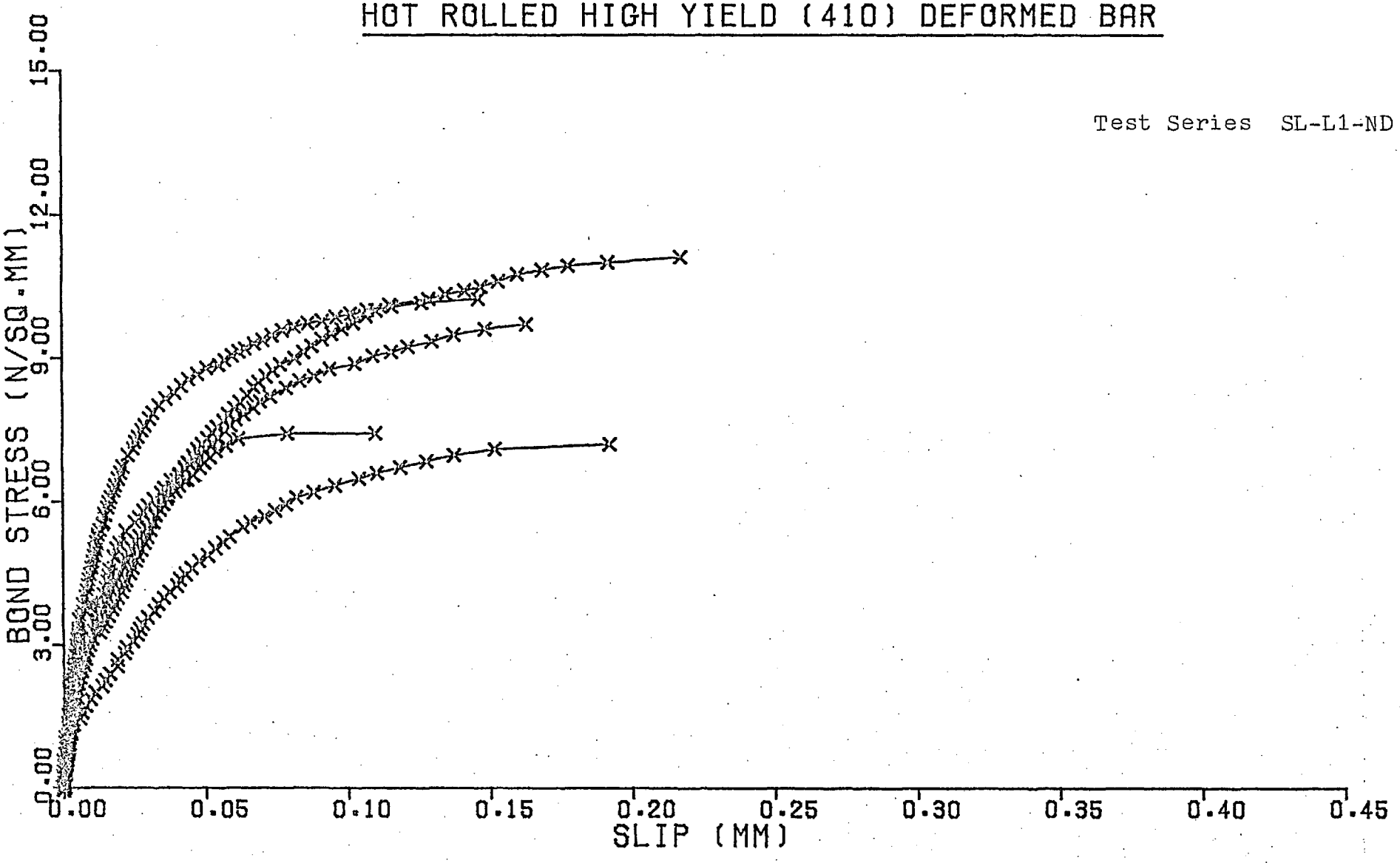


FIGURE 6.8

EXPERIMENTAL BOND-SLIP CURVES FOR 16MM DIA. HOT ROLLED HIGH YIELD (410) DEFORMED BAR

Test Series SL-L2-ND

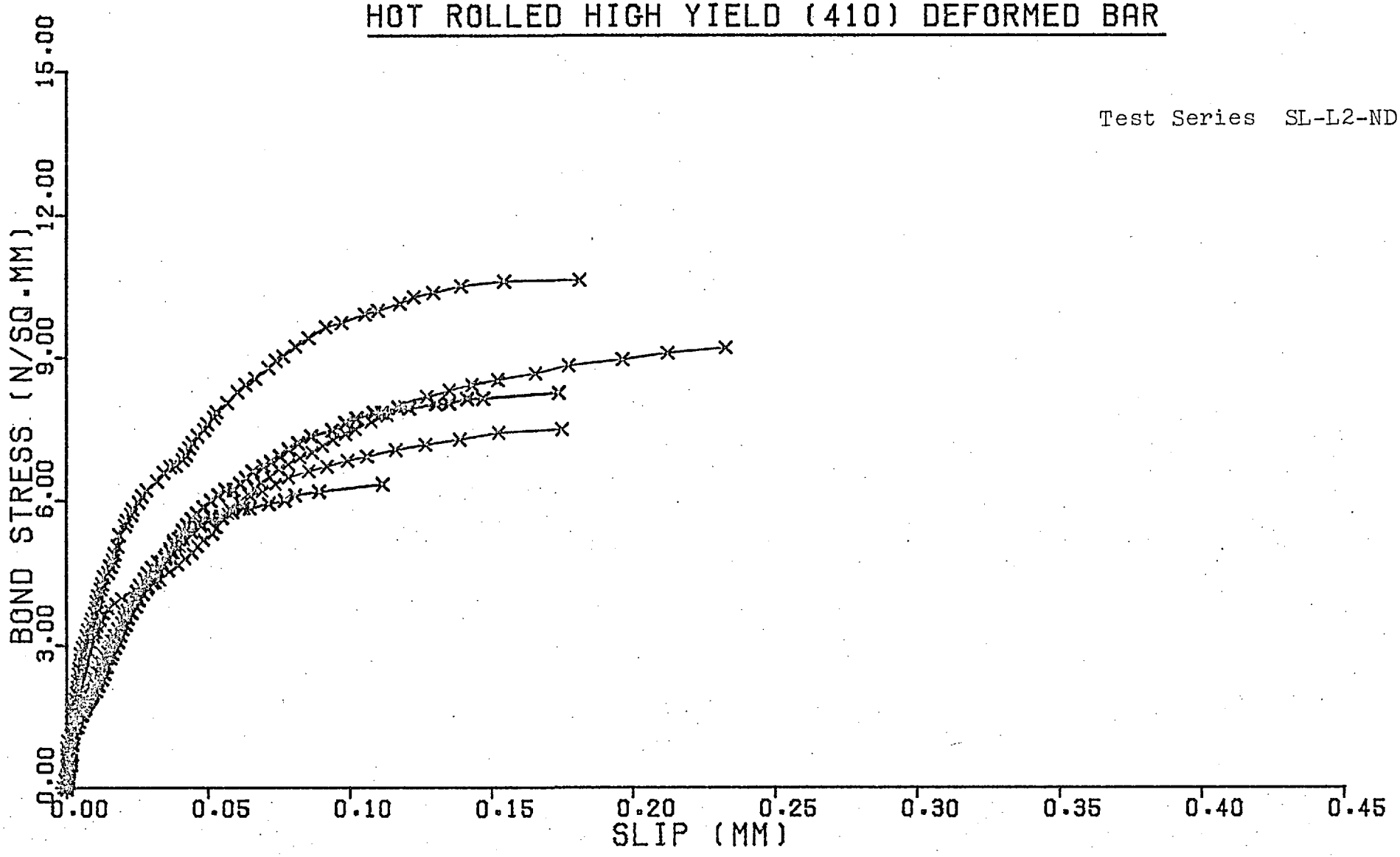


FIGURE 6.9

EXPERIMENTAL BOND-SLIP CURVES FOR 16MM DIA. HOT ROLLED HIGH YIELD (410) DEFORMED BAR

Test Series SL-L3-ND

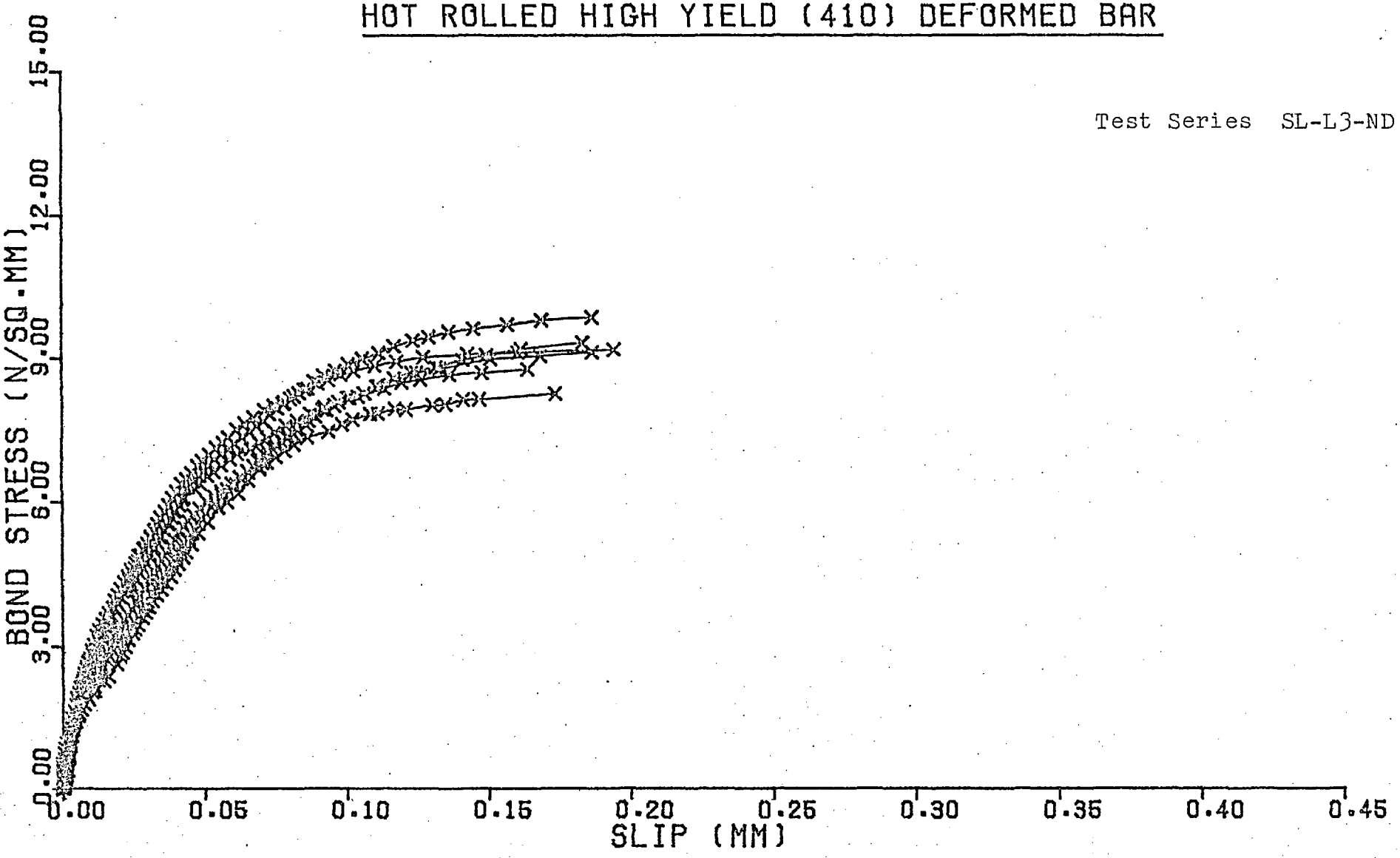


FIGURE 6.10

EXPERIMENTAL BOND-SLIP CURVES FOR 16MM DIA HOT ROLLED HIGH YIELD (410) DEFORMED BAR

Test Series SL-L4-ND

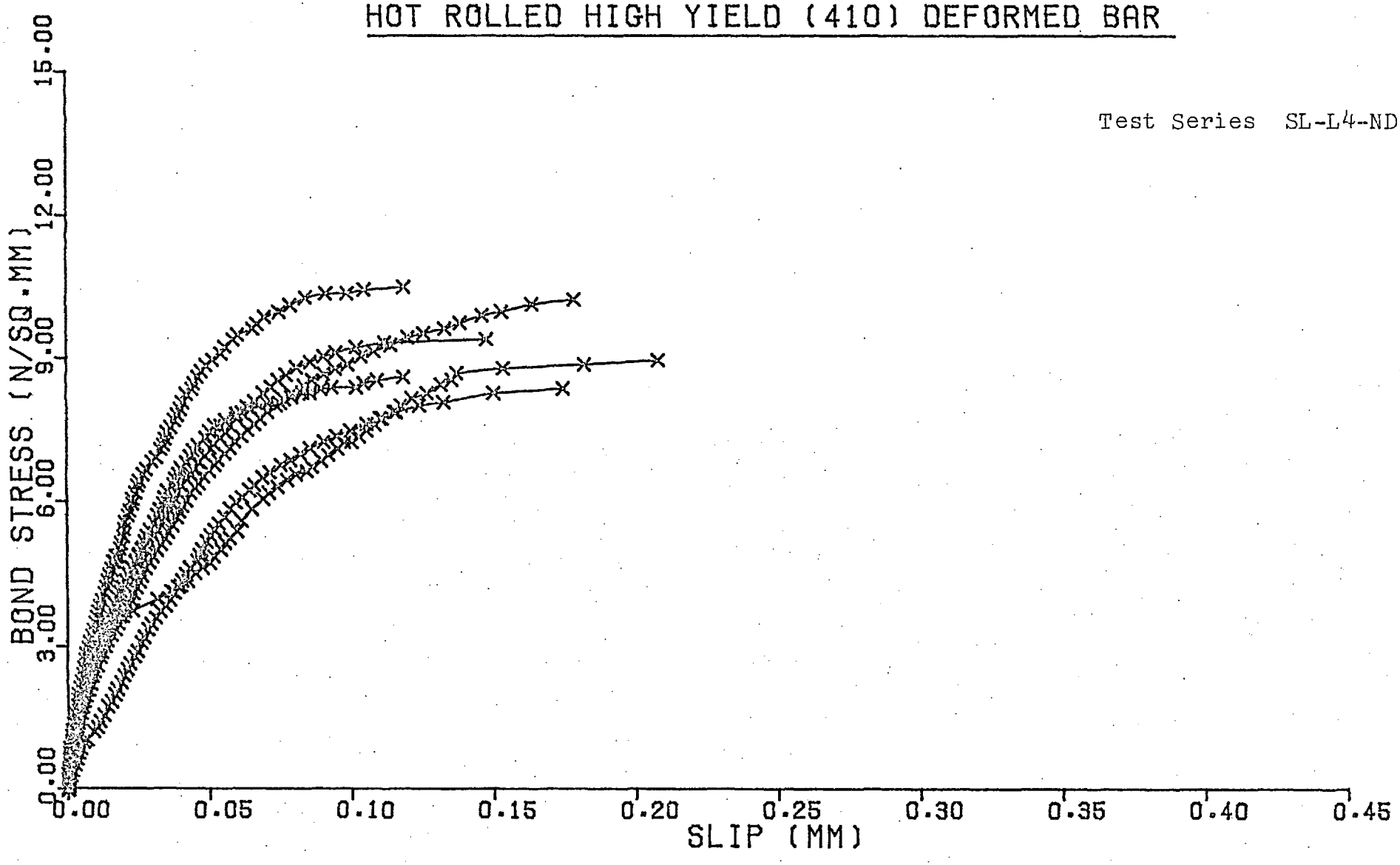


FIGURE 6.11

EXPERIMENTAL BOND-SLIP CURVES FOR 16MM DIA. HOT ROLLED HIGH YIELD (410) DEFORMED BAR

Test Series SL-L5-ND

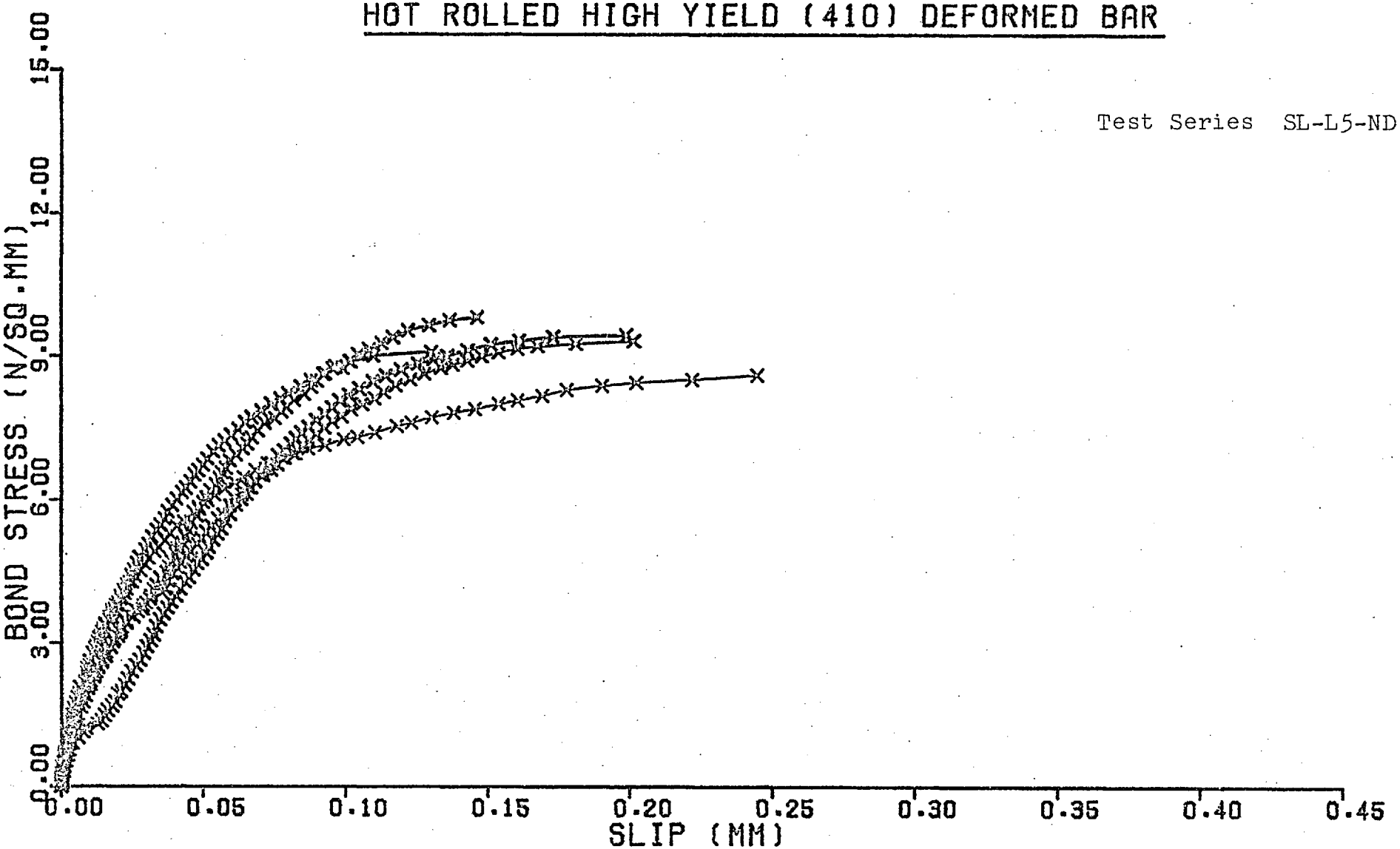


FIGURE 6.12

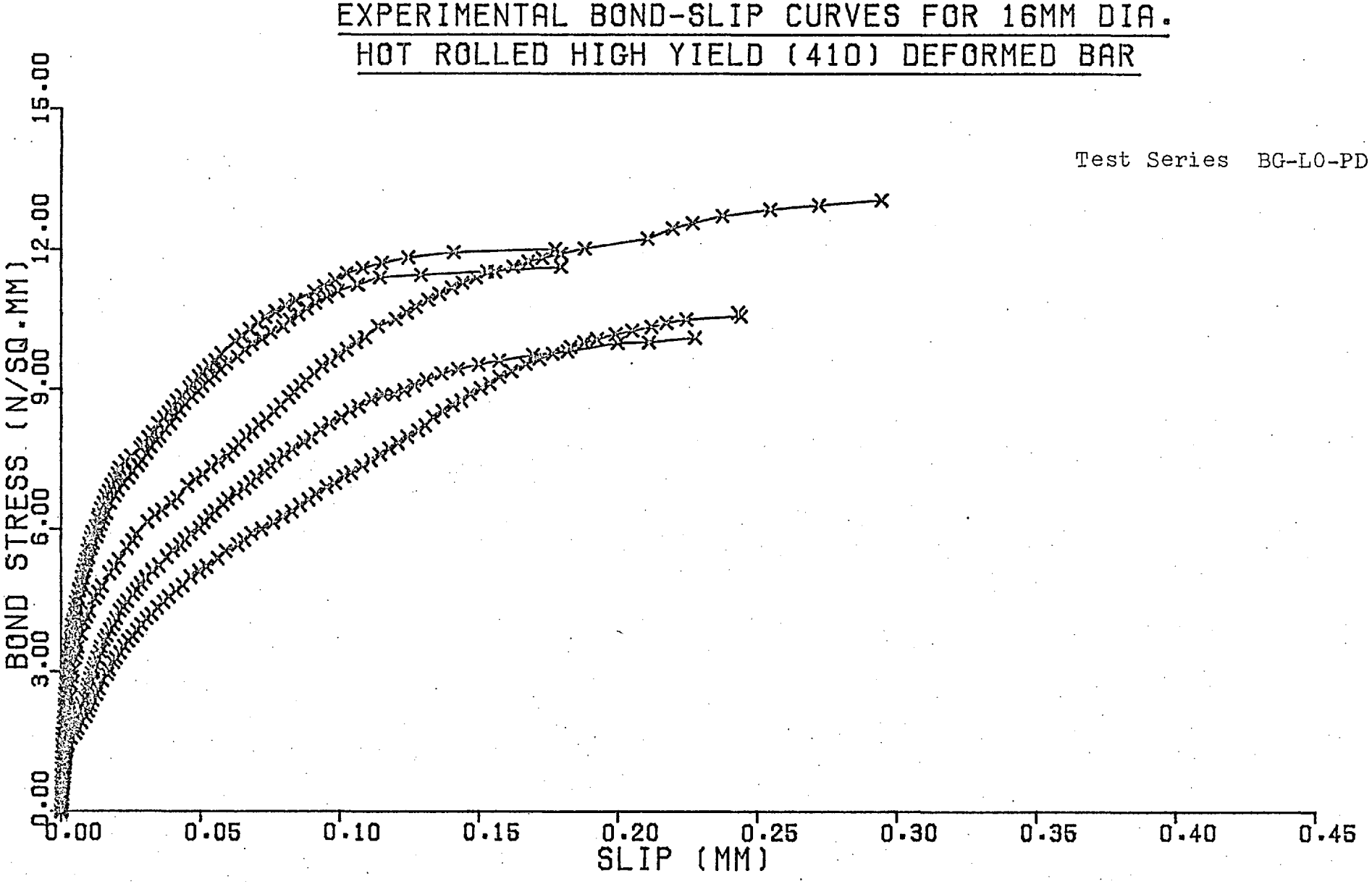

EXPERIMENTAL BOND-SLIP CURVES FOR 16MM DIA.
HOT ROLLED HIGH YIELD (410) DEFORMED BAR
Test Series BG-L0-PD
BOND STRESS (N/SQ.MM)
0.00
3.00
6.00
9.00
12.00
15.00
0.00
0.05
0.10
0.15
0.20
0.25
0.30
0.35
0.40
0.45
SLIP (MM)

FIGURE 6.13

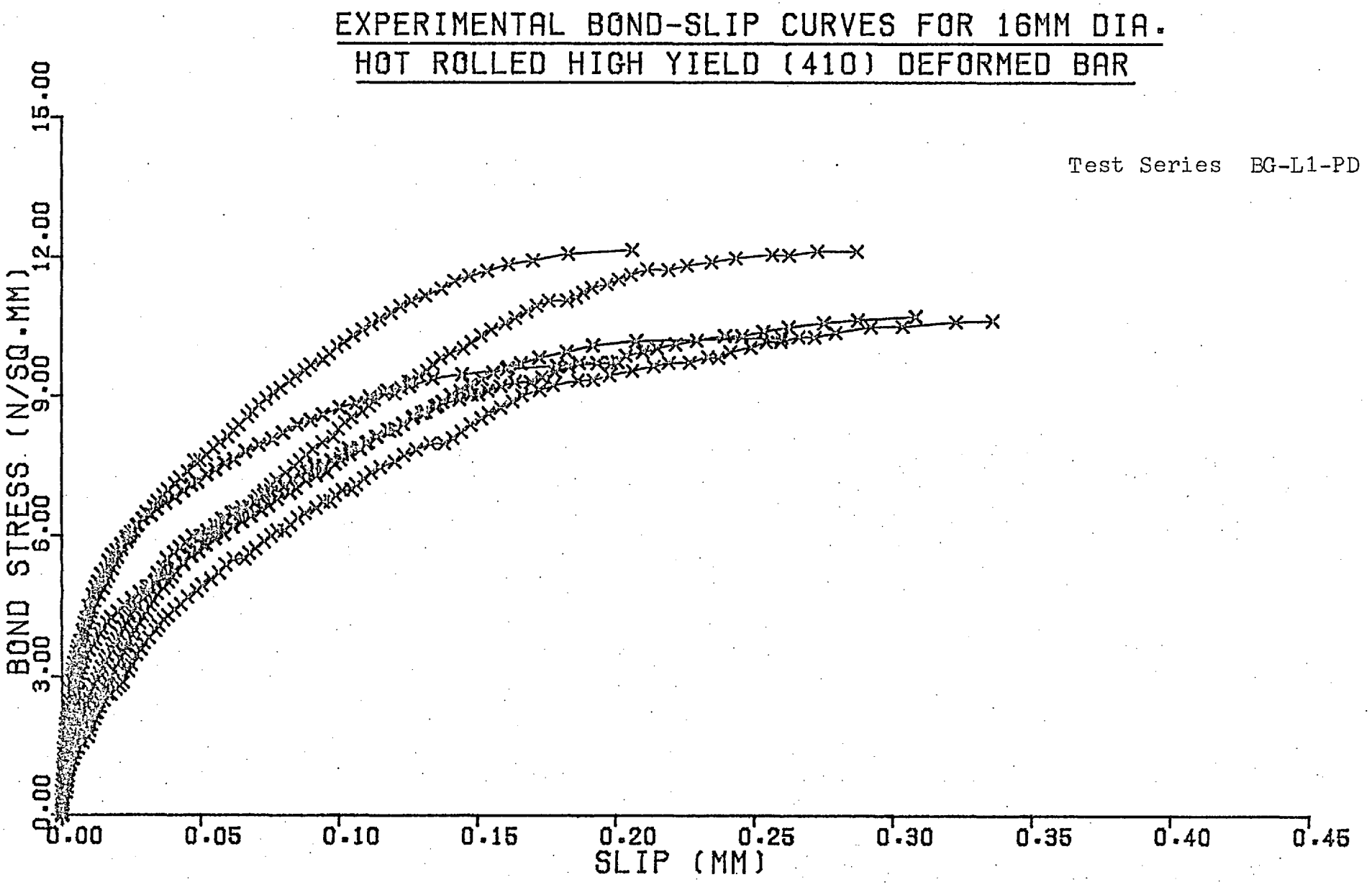

EXPERIMENTAL BOND-SLIP CURVES FOR 16MM DIA.
HOT ROLLED HIGH YIELD (410) DEFORMED BAR
Test Series BG-L1-PD
BOND STRESS (N/SQ.MM)
0.00
3.00
6.00
9.00
12.00
15.00
0.00
0.05
0.10
0.15
0.20
0.25
0.30
0.35
0.40
0.45
SLIP (MM)

FIGURE 6.14

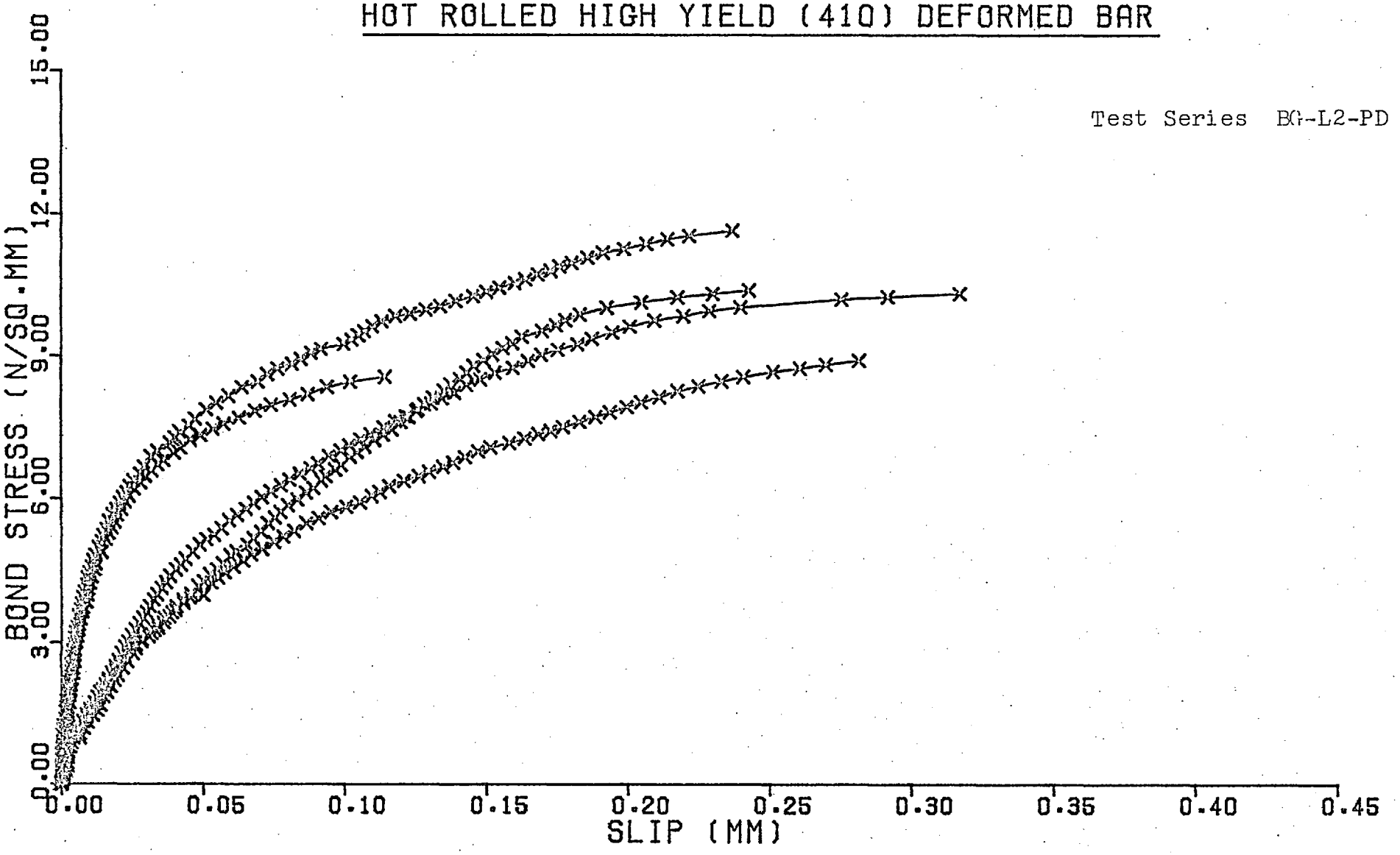

EXPERIMENTAL BOND-SLIP CURVES FOR 16MM DIA.
HOT ROLLED HIGH YIELD (410) DEFORMED BAR
Test Series BG-L2-PD
BOND STRESS (N/SQ.MM)
0.00
3.00
6.00
9.00
12.00
15.00
0.00
0.05
0.10
0.15
0.20
0.25
0.30
0.35
0.40
0.45
SLIP (MM)

FIGURE 6.15

EXPERIMENTAL BOND-SLIP CURVES FOR 16MM DIA. HOT ROLLED HIGH YIELD (410) DEFORMED BAR

Test Series BG-L3-PD

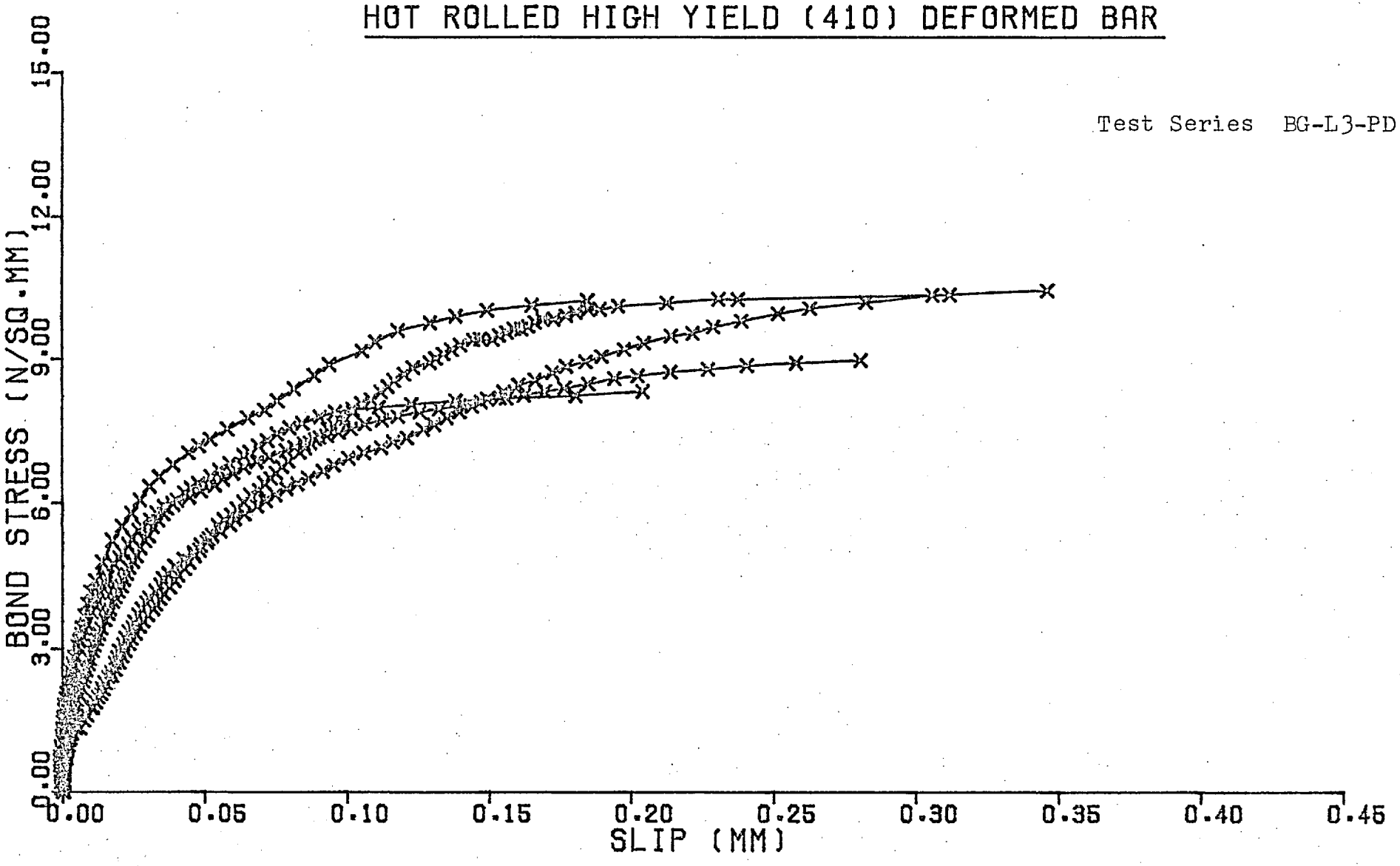


FIGURE 6.16

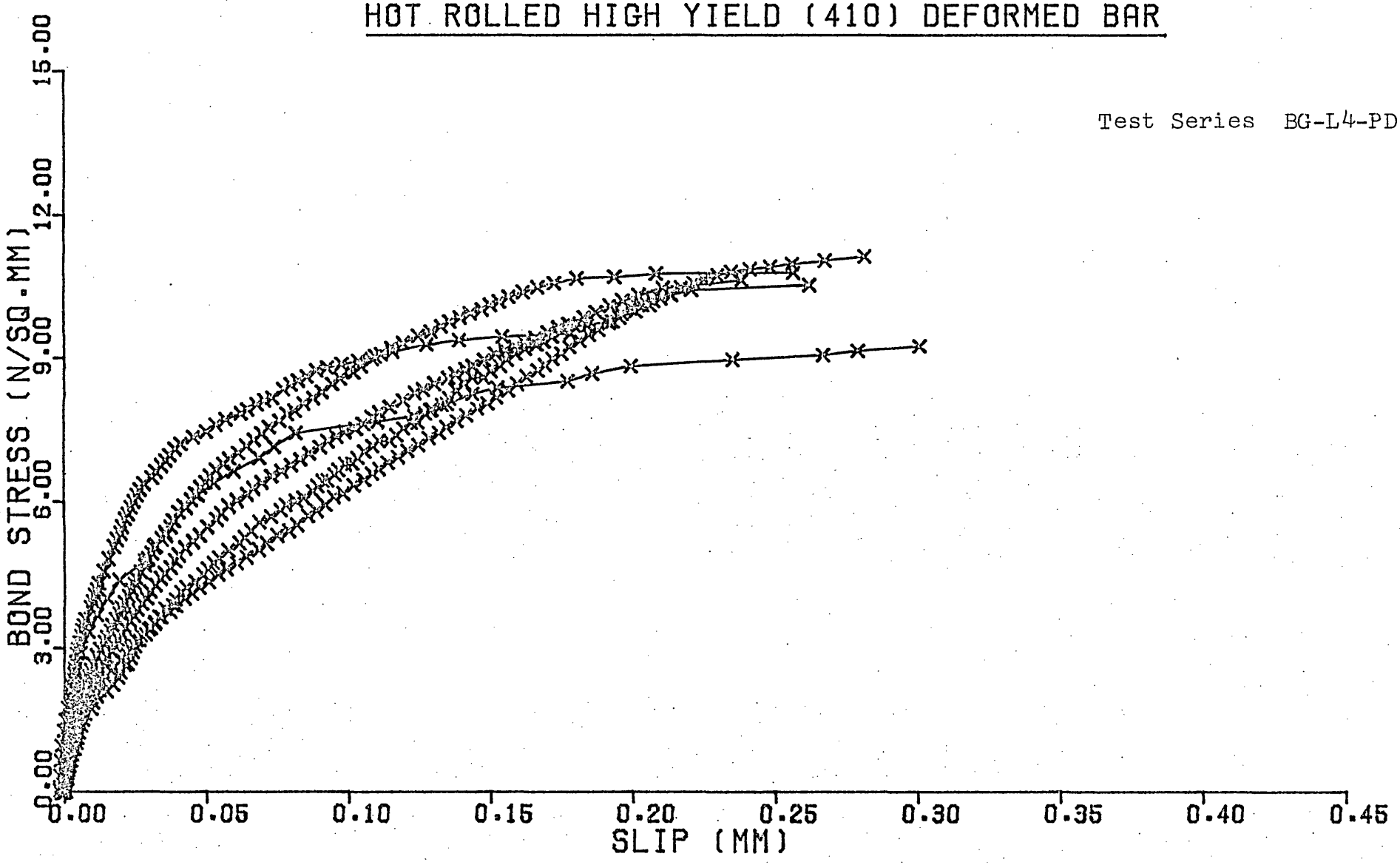

EXPERIMENTAL BOND-SLIP CURVES FOR 16MM DIA.
HOT ROLLED HIGH YIELD (410) DEFORMED BAR
Test Series BG-L4-PD
BOND STRESS (N/SQ.MM)
0.00
3.00
6.00
9.00
12.00
15.00
0.00
0.05
0.10
0.15
0.20
0.25
0.30
0.35
0.40
0.45
SLIP (MM)

FIGURE 6.17

EXPERIMENTAL BOND-SLIP CURVES FOR 16MM DIA. HOT ROLLED HIGH YIELD (410) DEFORMED BAR

Test Series BG-L5-PD

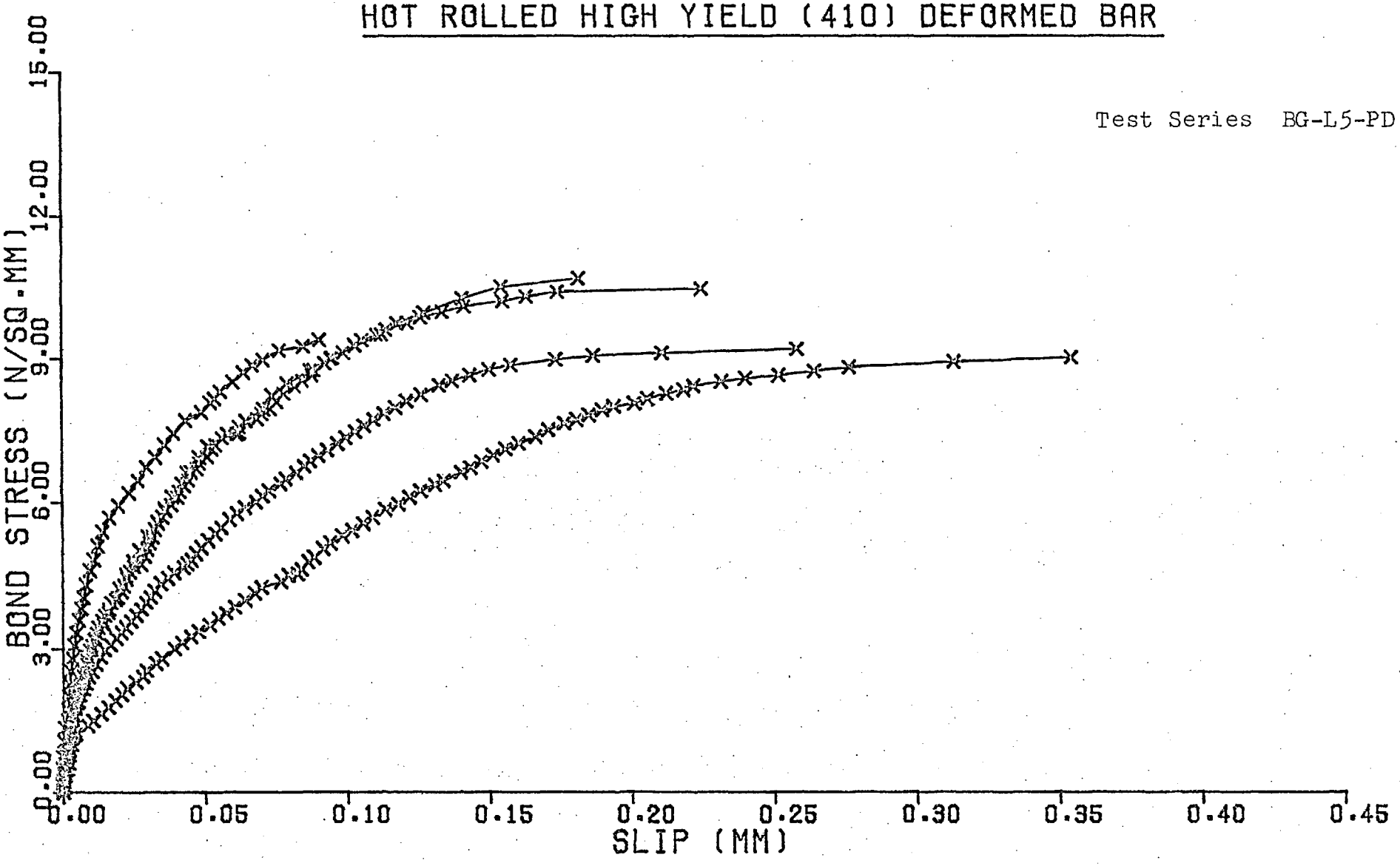


FIGURE 6.18

EXPERIMENTAL BOND-SLIP CURVES FOR 16MM DIA. HOT ROLLED HIGH YIELD (410) DEFORMED BAR

Test Series BG-L0-ND

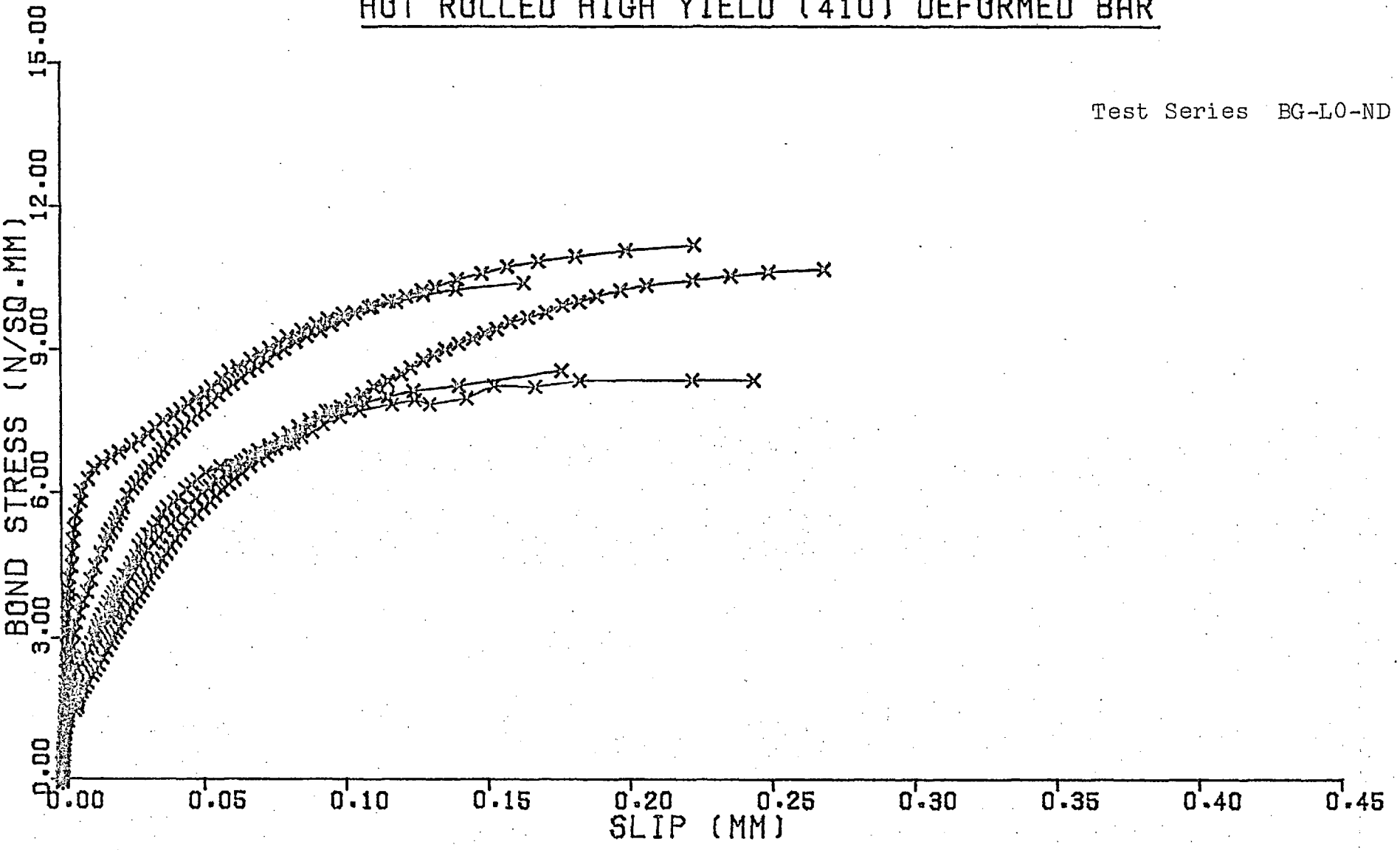


FIGURE 6.12

EXPERIMENTAL BOND-SLIP CURVES FOR 16MM DIA. HOT ROLLED HIGH YIELD (410) DEFORMED BAR

Test Series BG-L1-ND

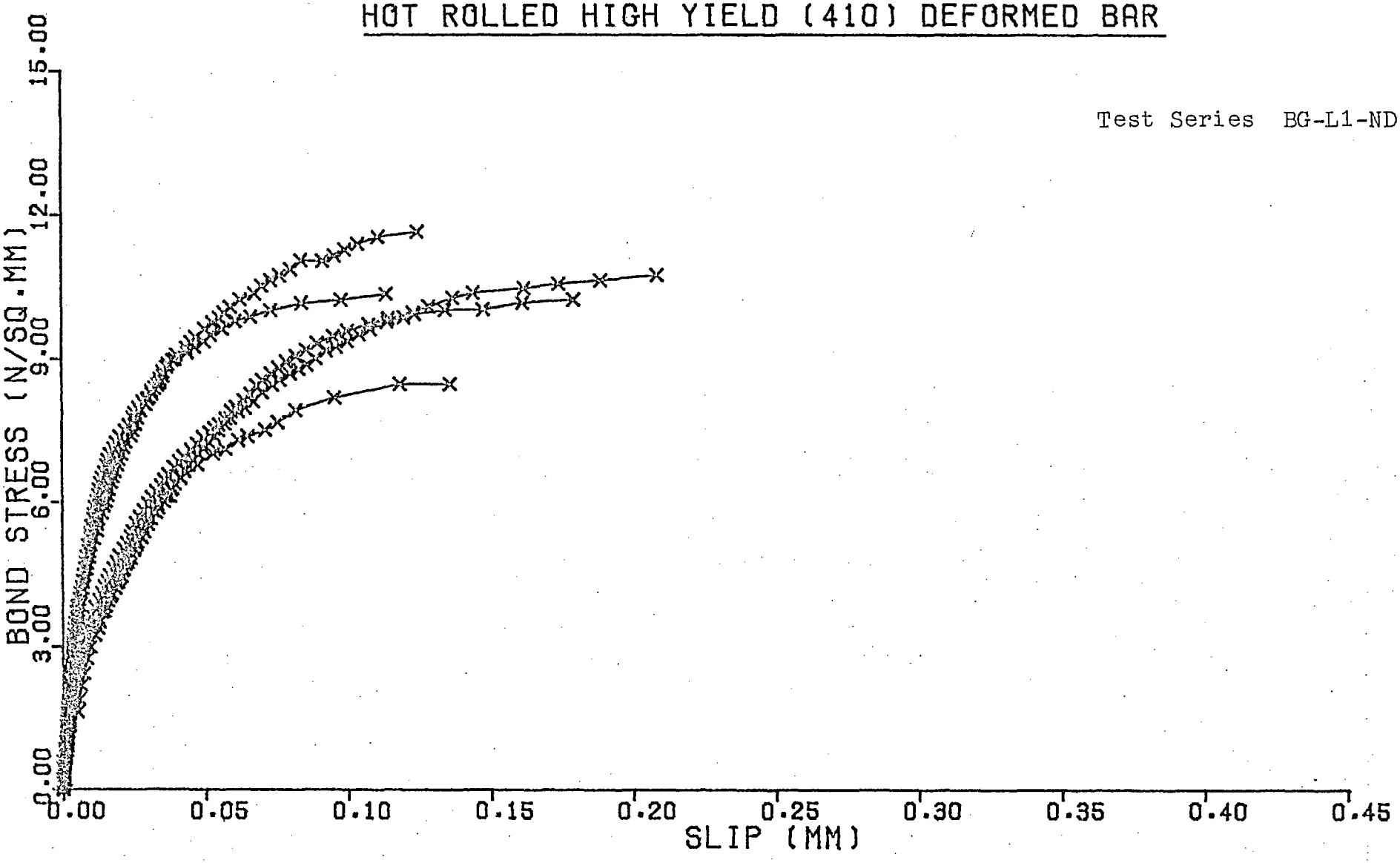


FIGURE 6.20

EXPERIMENTAL BOND-SLIP CURVES FOR 16MM DIA. HOT ROLLED HIGH YIELD (410) DEFORMED BAR

Test Series BG-L2-ND

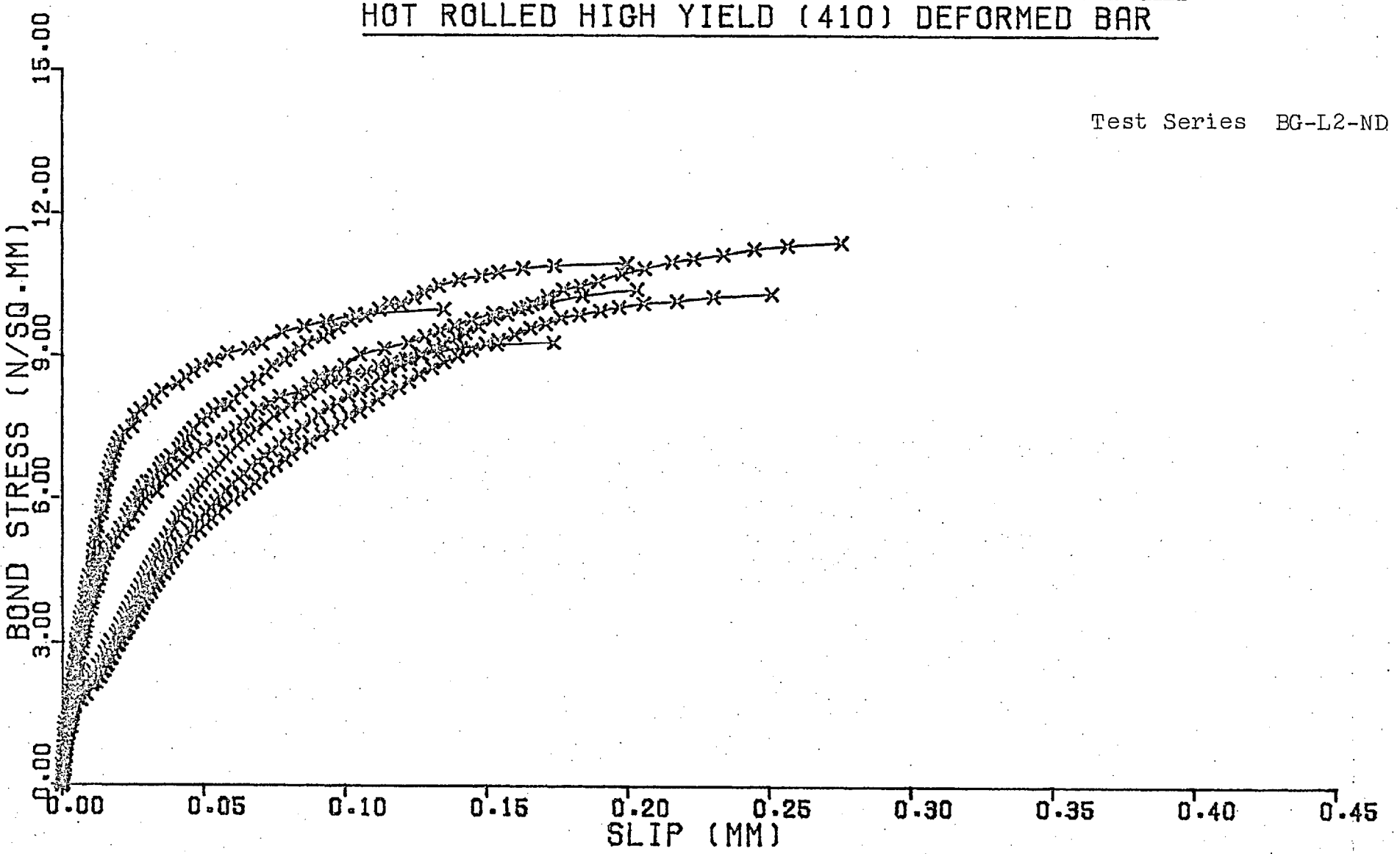


FIGURE 6.21

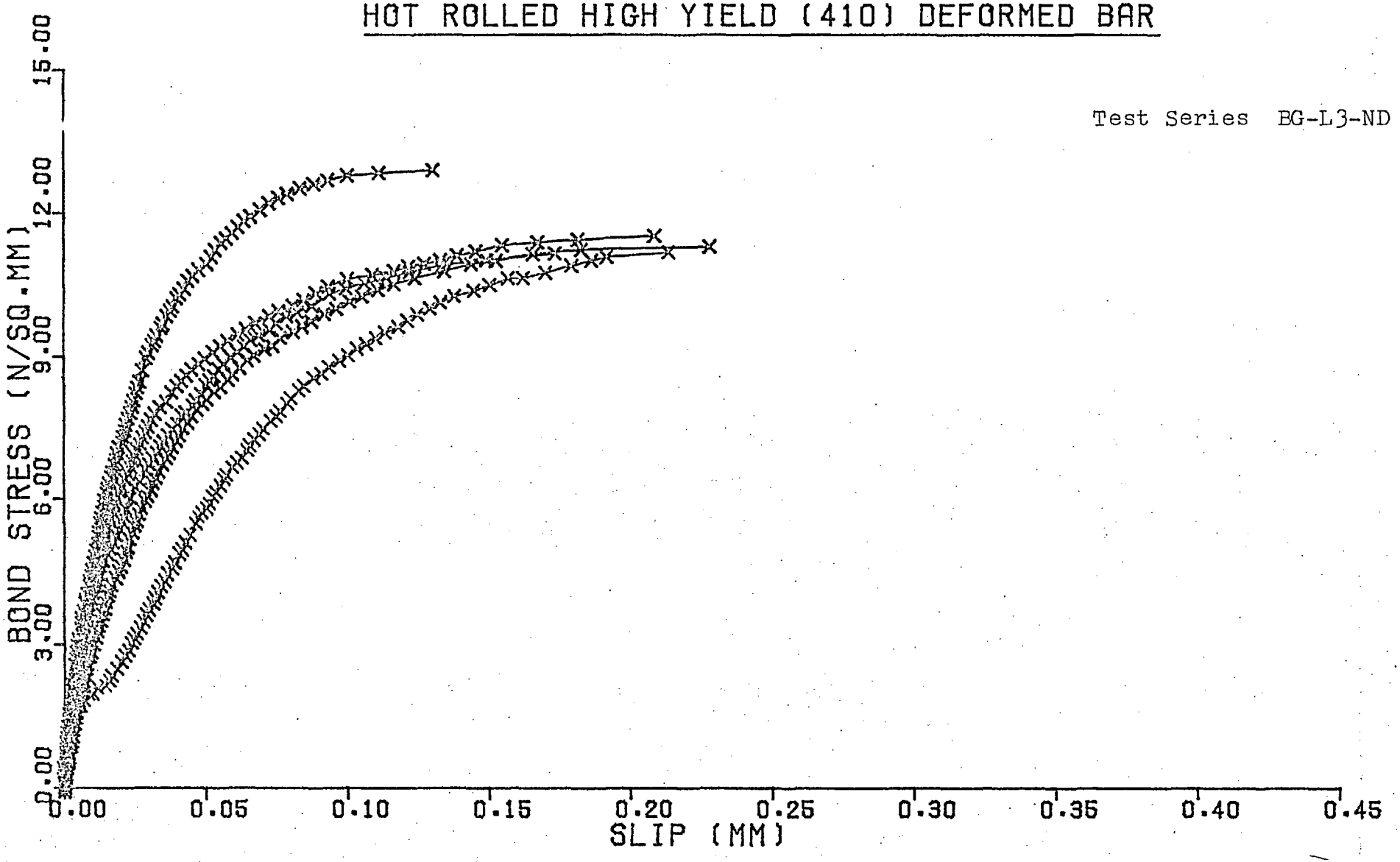

EXPERIMENTAL BOND-SLIP CURVES FOR 16MM DIA.
HOT ROLLED HIGH YIELD (410) DEFORMED BAR
Test Series BG-L3-ND
BOND STRESS (N/SQ.MM)
0.00
3.00
6.00
9.00
12.00
15.00
0.00
0.05
0.10
0.15
0.20
0.25
0.30
0.35
0.40
0.45
SLIP (MM)

FIGURE 6.22

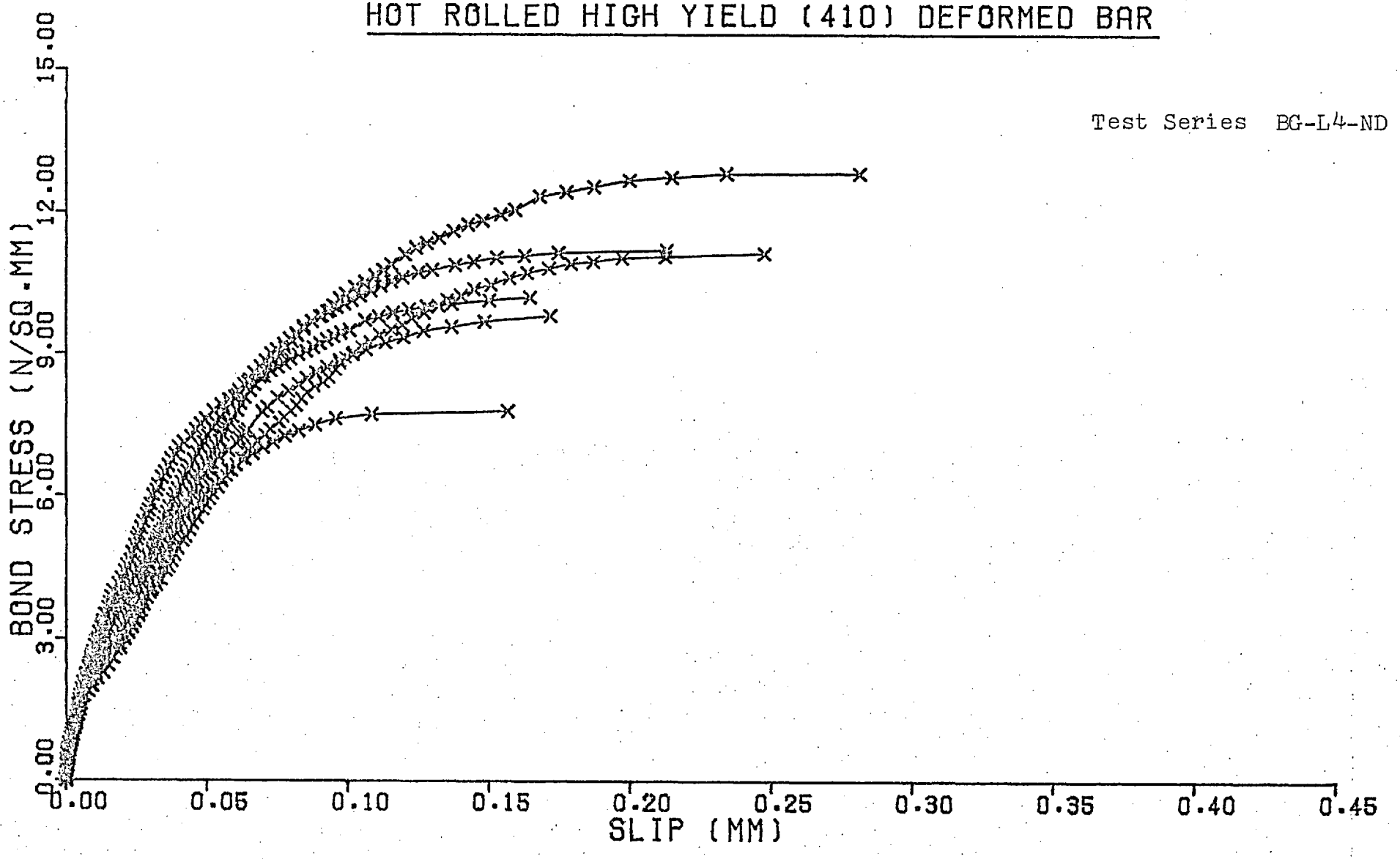

EXPERIMENTAL BOND-SLIP CURVES FOR 16MM DIA.
HOT ROLLED HIGH YIELD (410) DEFORMED BAR
Test Series BG-L4-ND
BOND STRESS (N/SQ.MM)
0.00
3.00
6.00
9.00
12.00
15.00
0.00
0.05
0.10
0.15
0.20
0.25
0.30
0.35
0.40
0.45
SLIP (MM)

FIGURE 6.23

EXPERIMENTAL BOND-SLIP CURVES FOR 16MM DIA. HOT ROLLED HIGH YIELD (410) DEFORMED BAR

Test Series BG-L5-ND

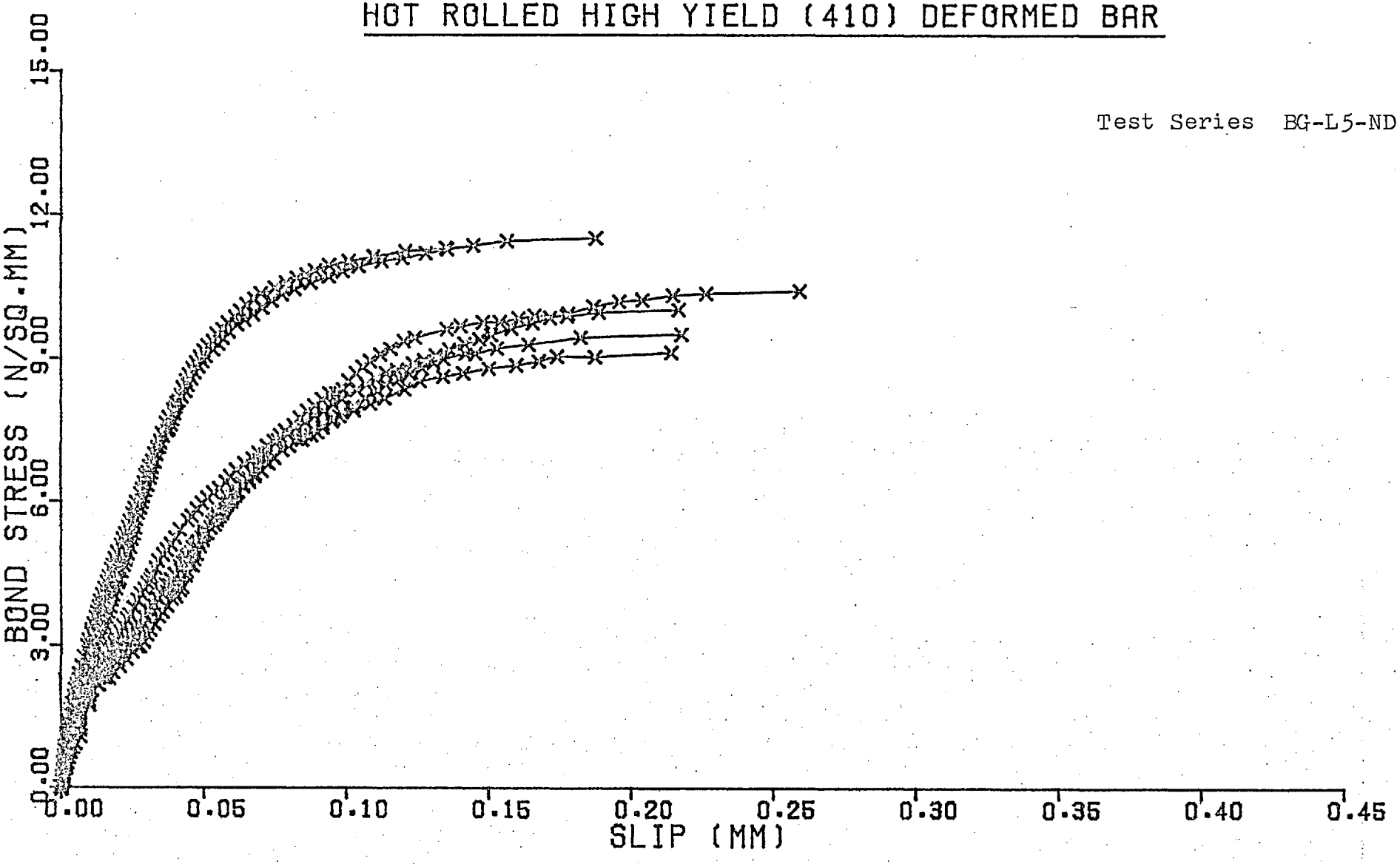


FIGURE 6.24

EXPERIMENTAL BOND-SLIP CURVES FOR 16MM DIA. MILD STEEL (250) PLAIN BAR

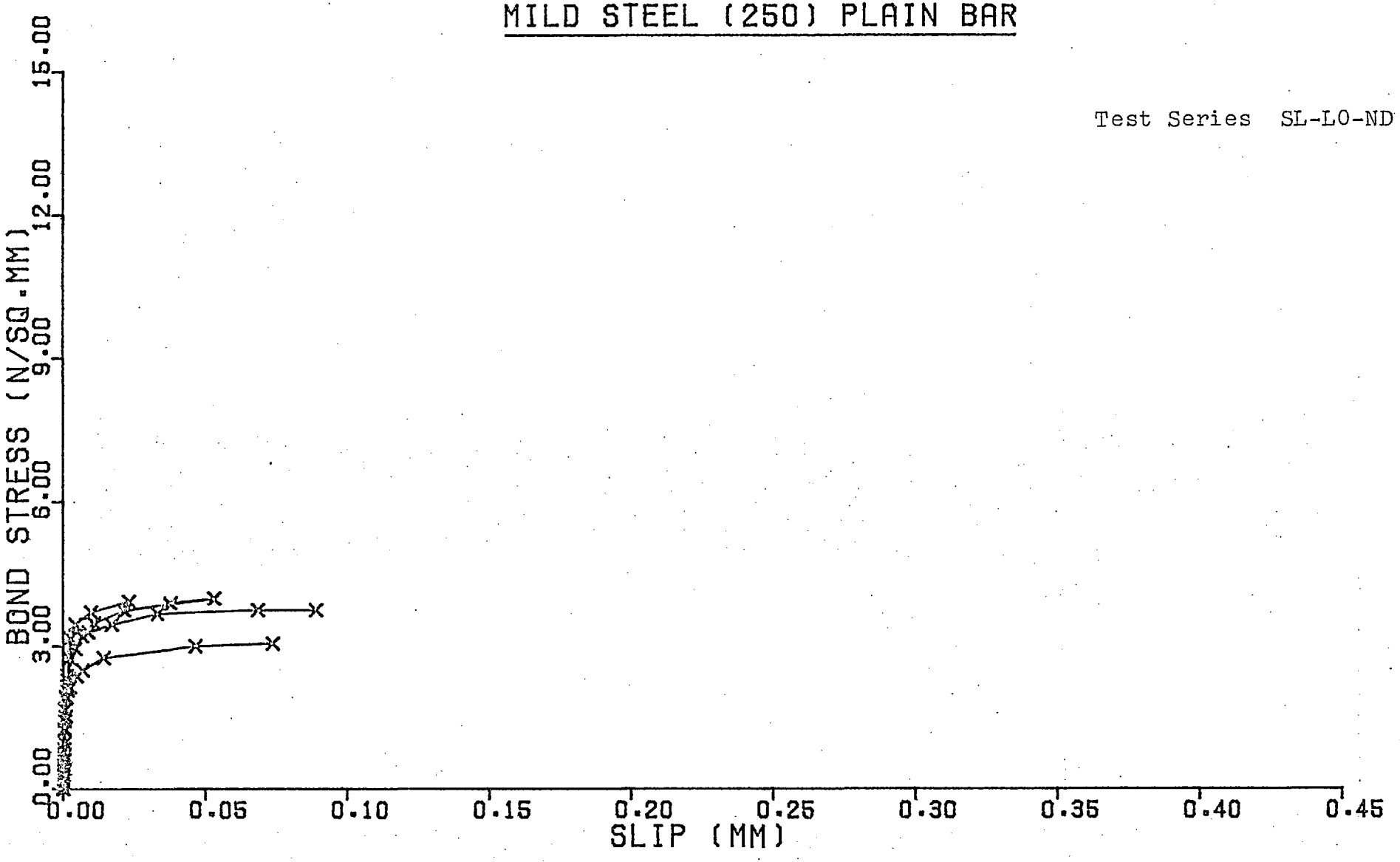


FIGURE 6.25

EXPERIMENTAL BOND-SLIP CURVES FOR 16MM DIA. MILD STEEL (250) PLAIN BAR

Test Series SL-L1-ND

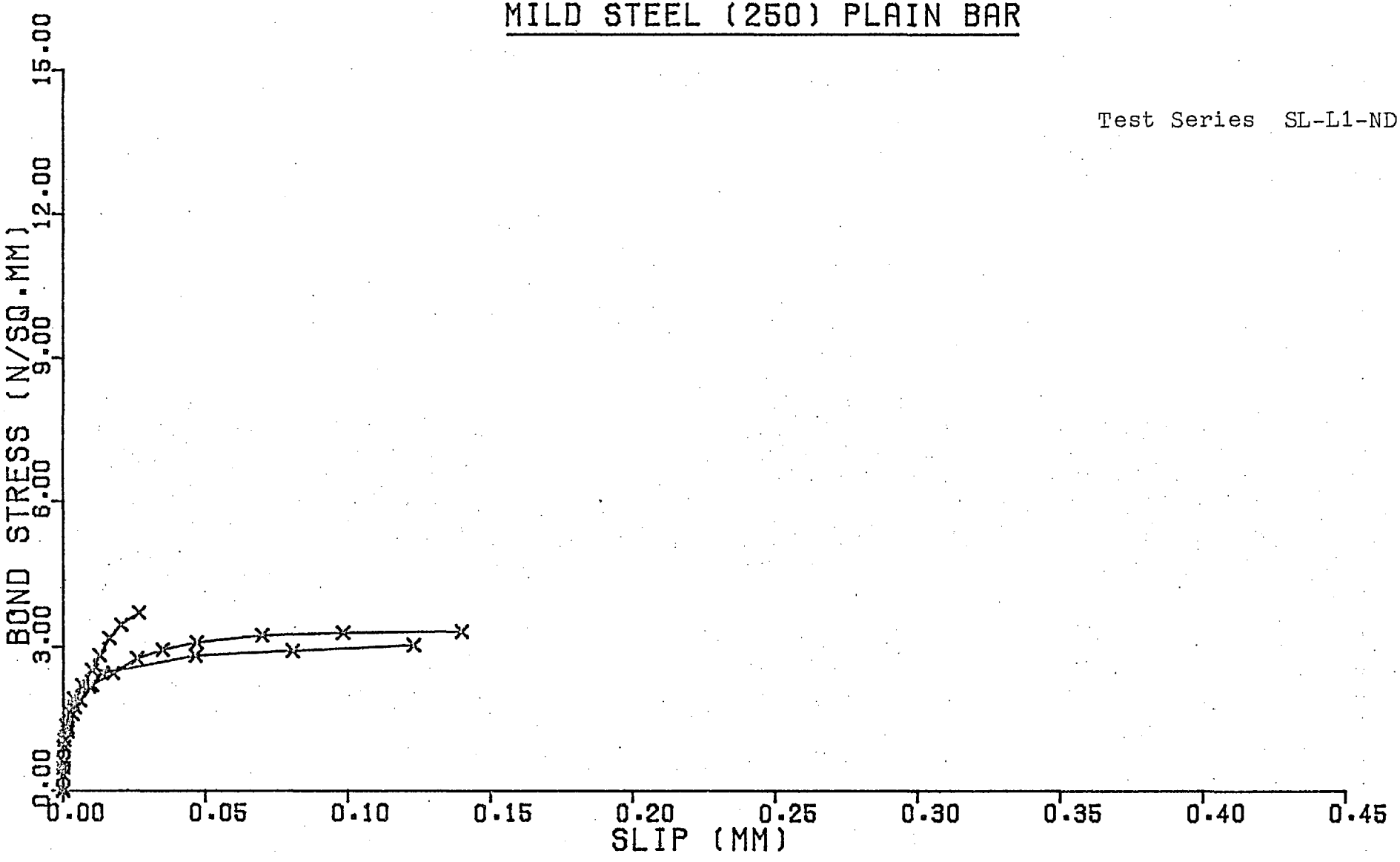


FIGURE 6.26

EXPERIMENTAL BOND-SLIP CURVES FOR 16MM DIA. MILD STEEL (250) PLAIN BAR

Test Series BG-L0-ND

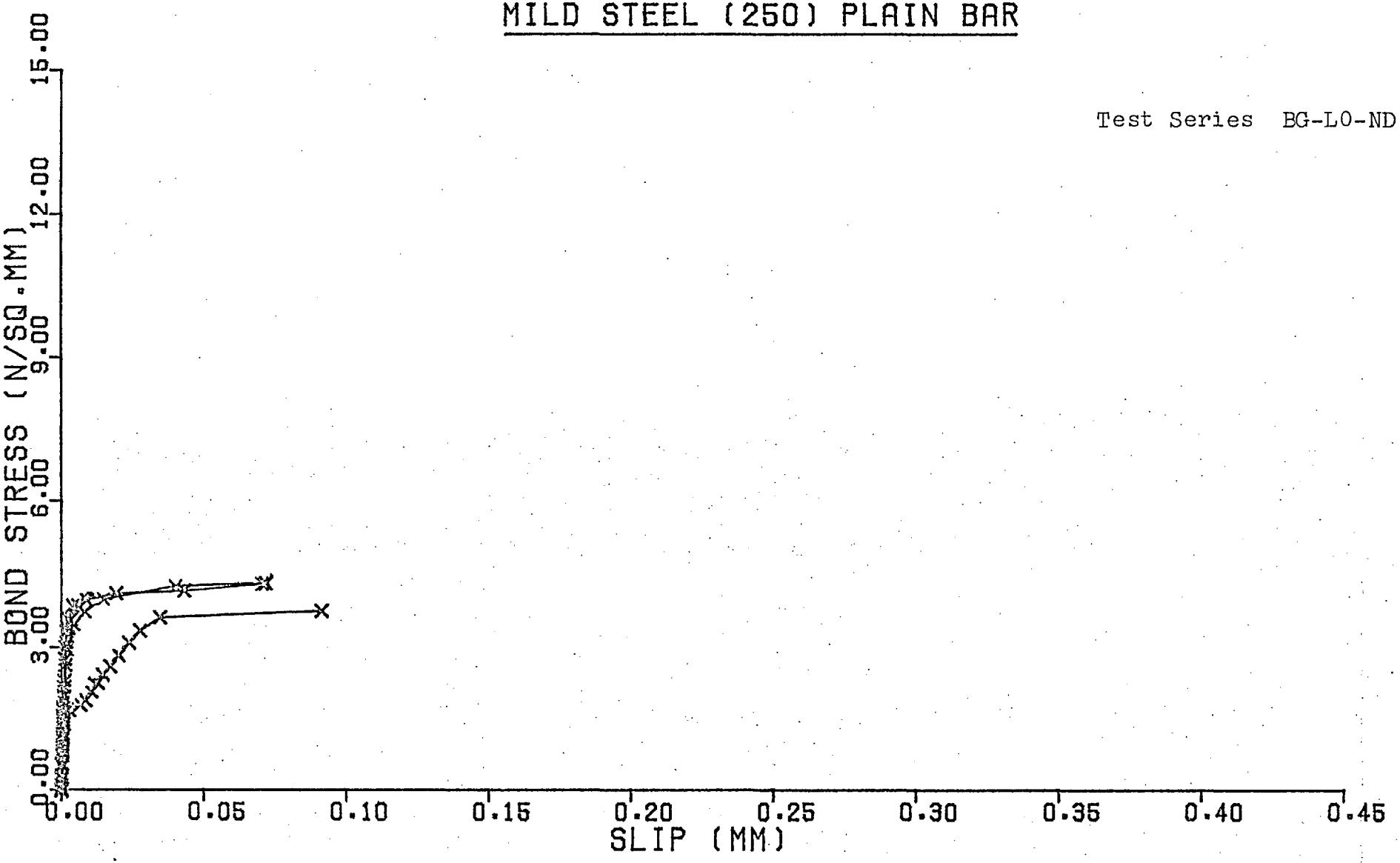


FIGURE 6.27

EXPERIMENTAL BOND-SLIP CURVES FOR 16MM DIA. MILD STEEL (250) PLAIN BAR

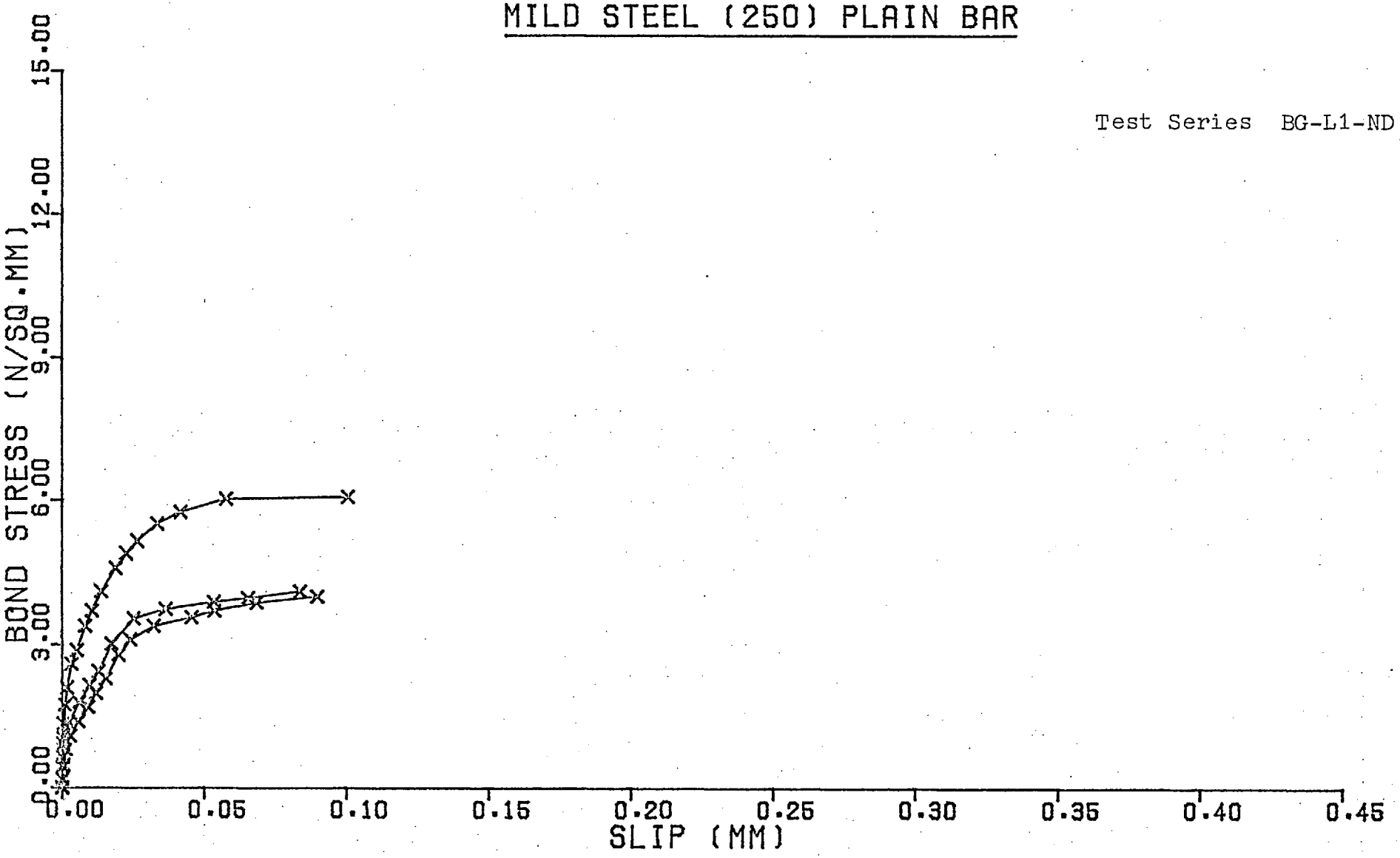
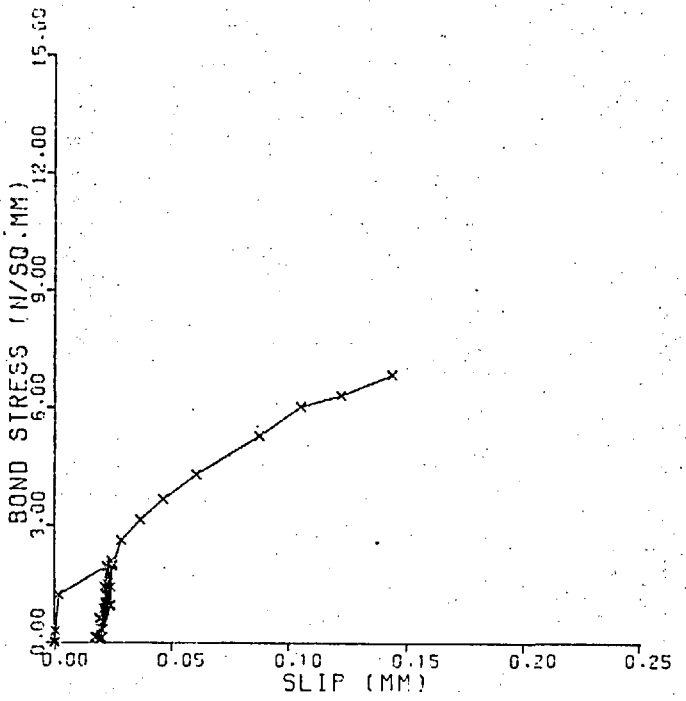
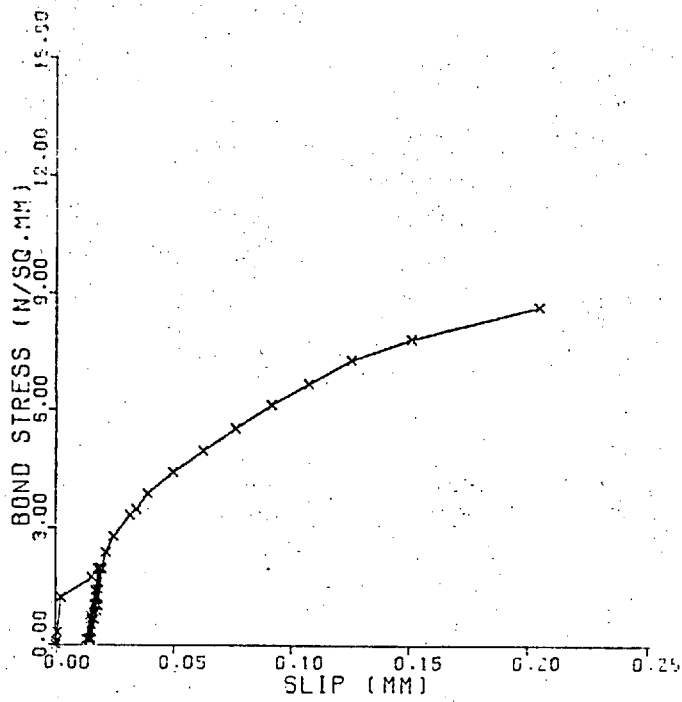
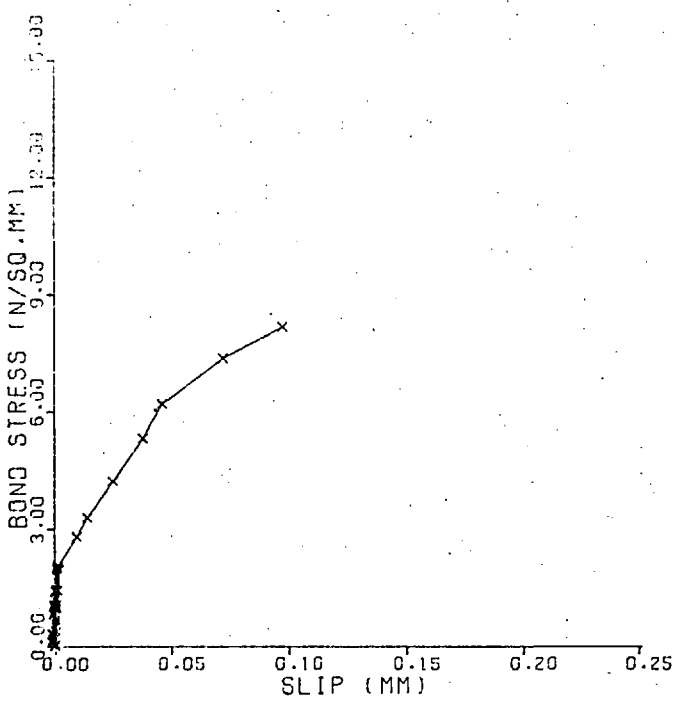


FIGURE 6.28







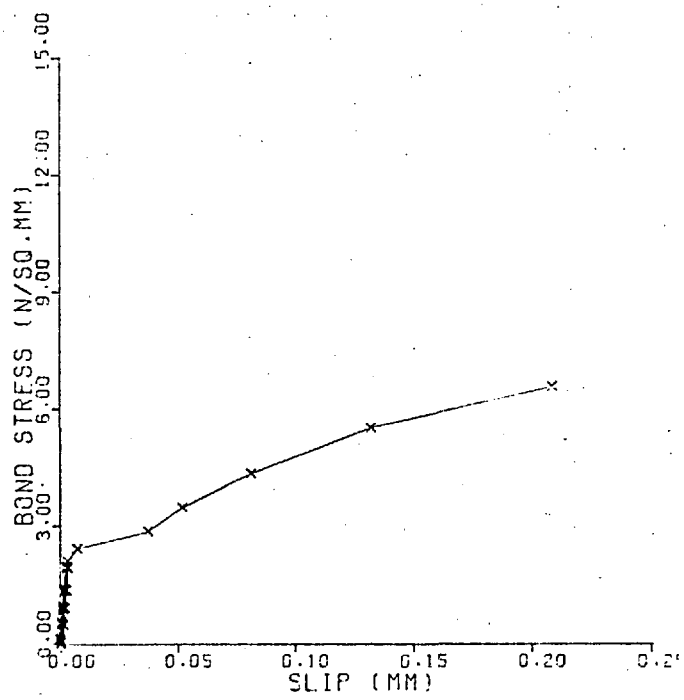


FIGURE 6.29 EXPERIMENTAL BOND-SLIP CURVES FOR 16 MM DIA. HOT-ROLLED HIGH YIELD (410) DEFORMED BAR UNDER REPEATED LOADING (0 - 2.0 N/SQ.MM)

Concrete Cover = 25 mm

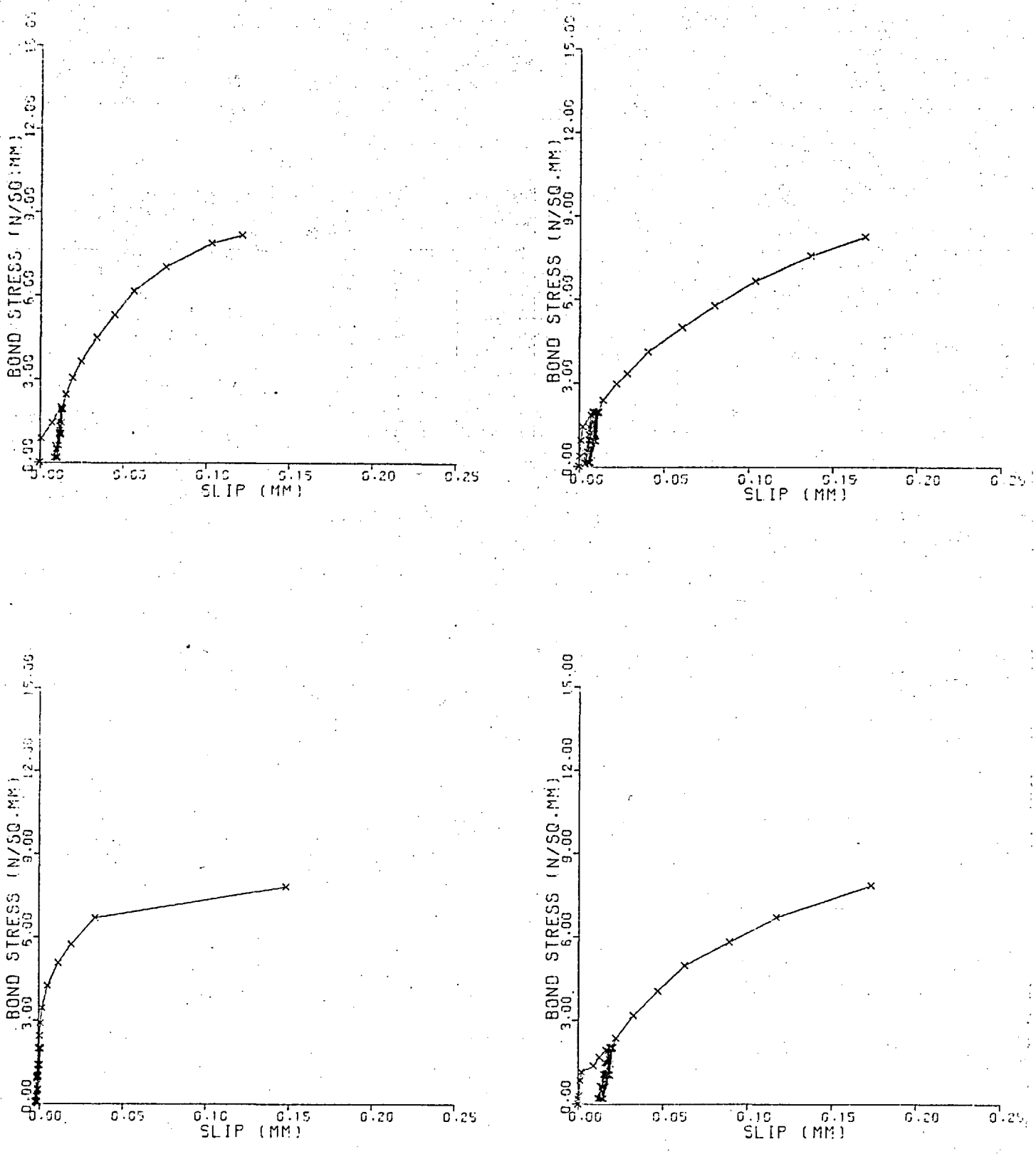
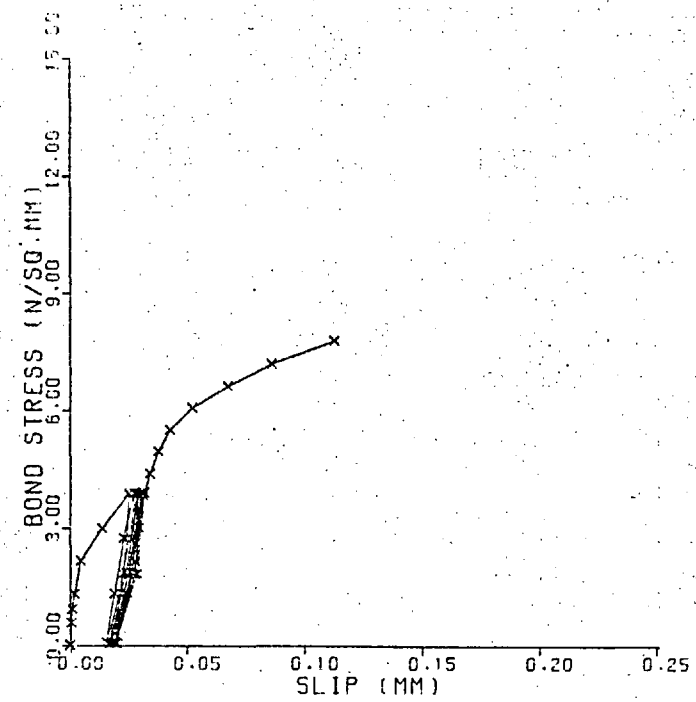
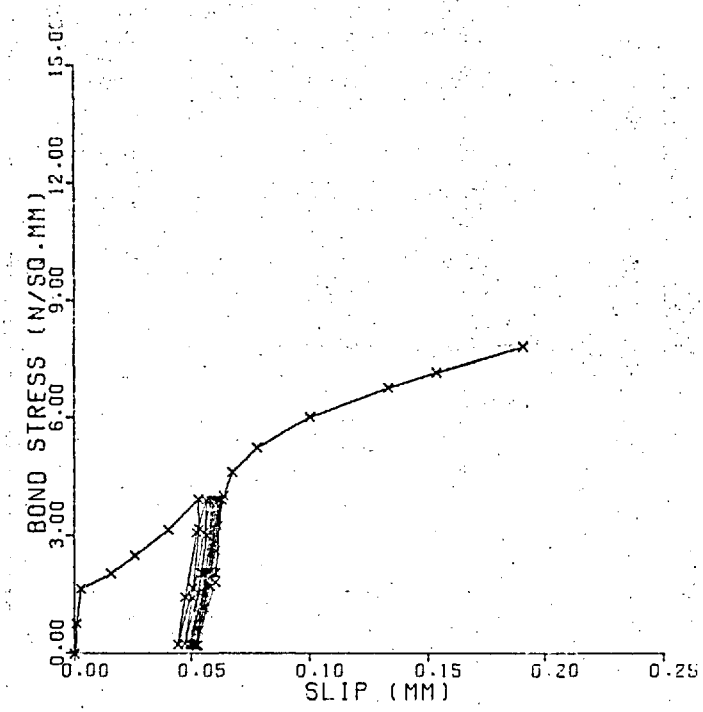
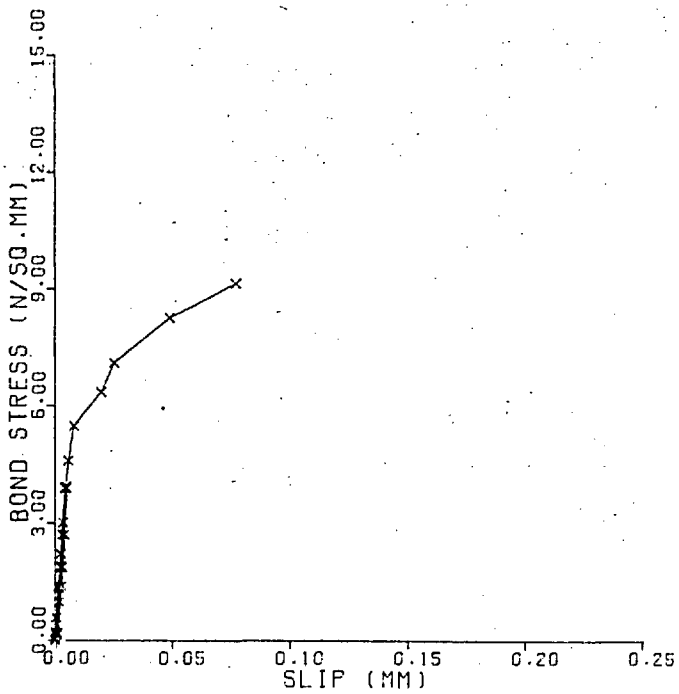


FIGURE 6.30 EXPERIMENTAL BOND-SLIP CURVES FOR 16 MM DIA. HOT-ROLLED HIGH YIELD (410) DEFORMED BAR UNDER REPEATED LOADING (0 - 2.0 N/SQ.MM)

Concrete Cover = 35 mm







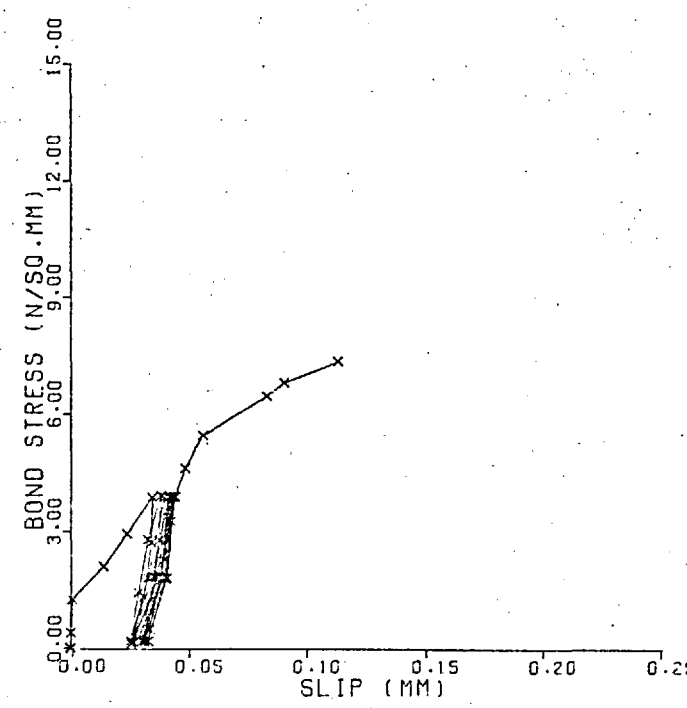
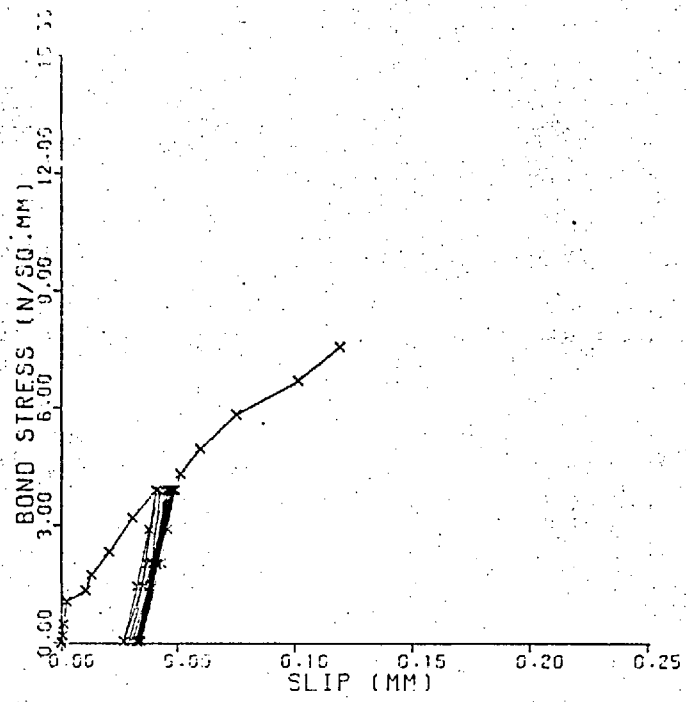
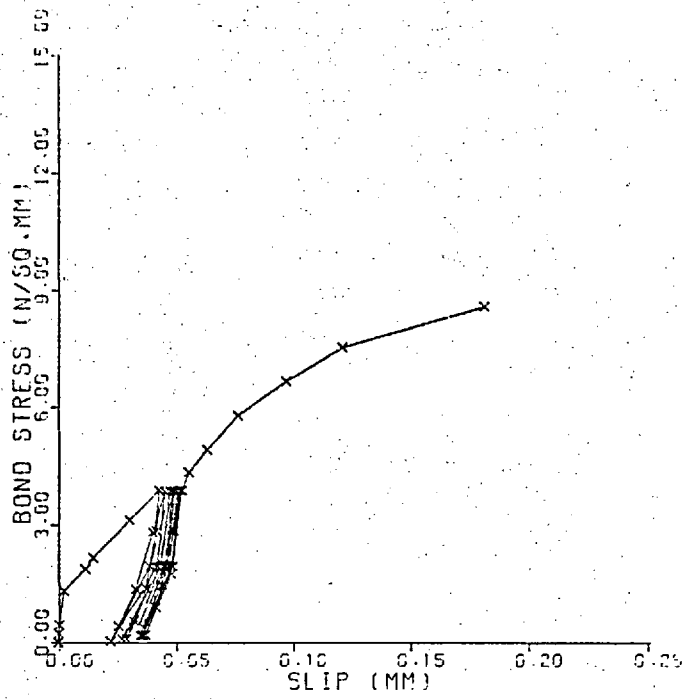
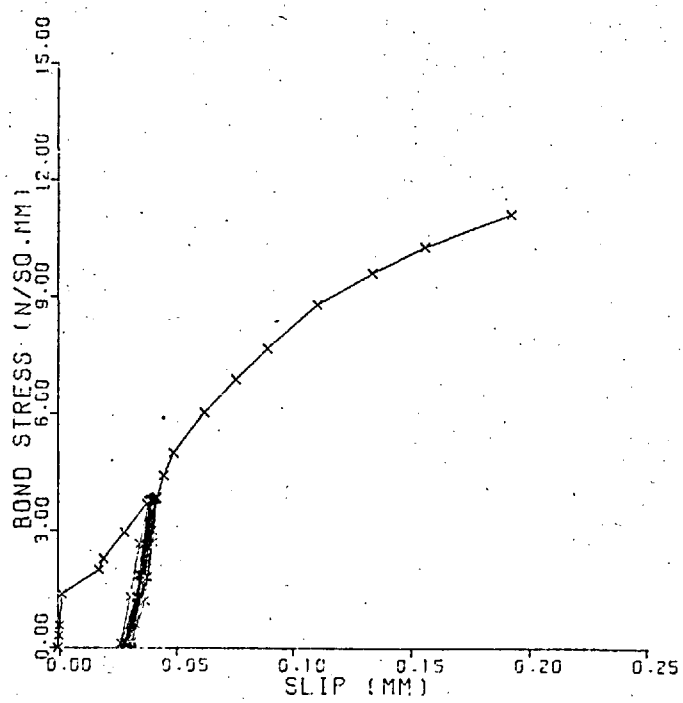


FIGURE 6.31 EXPERIMENTAL BOND-SLIP CURVES FOR 16 MM DIA. HOT-ROLLED HIGH YIELD (410) DEFORMED BAR UNDER REPEATED LOADING (0 - 3.9 N/SQ.MM)

Concrete Cover = 25 mm







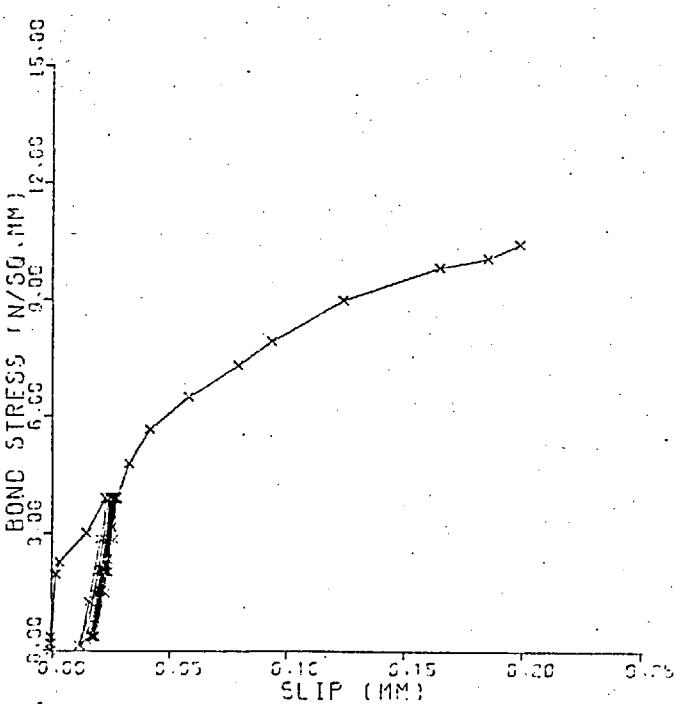
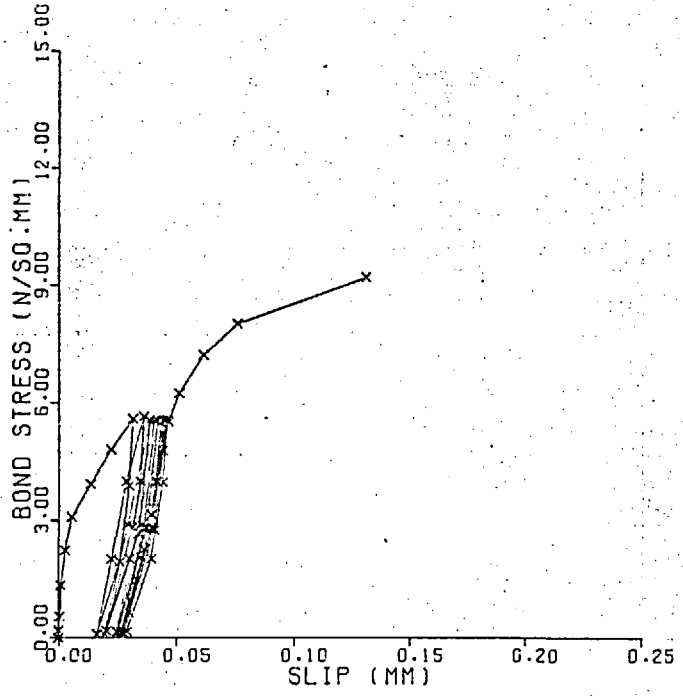
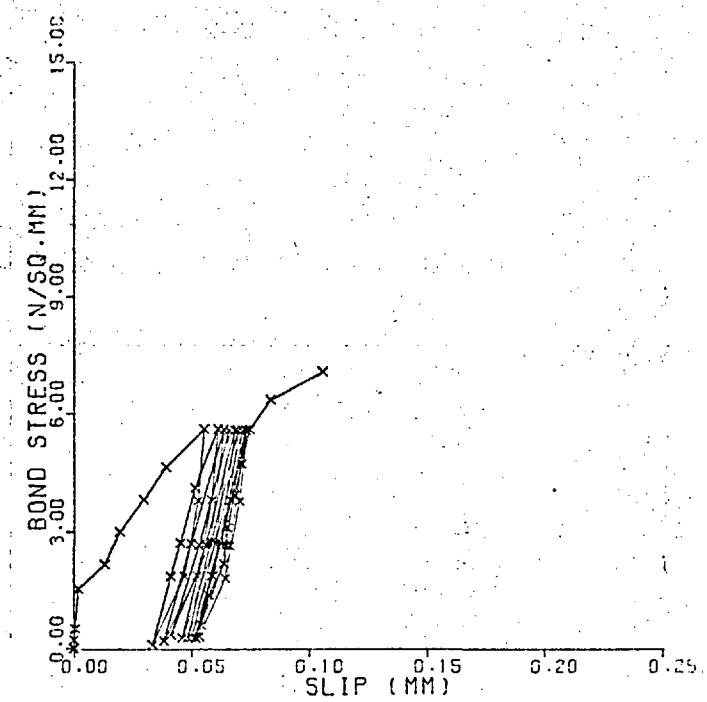
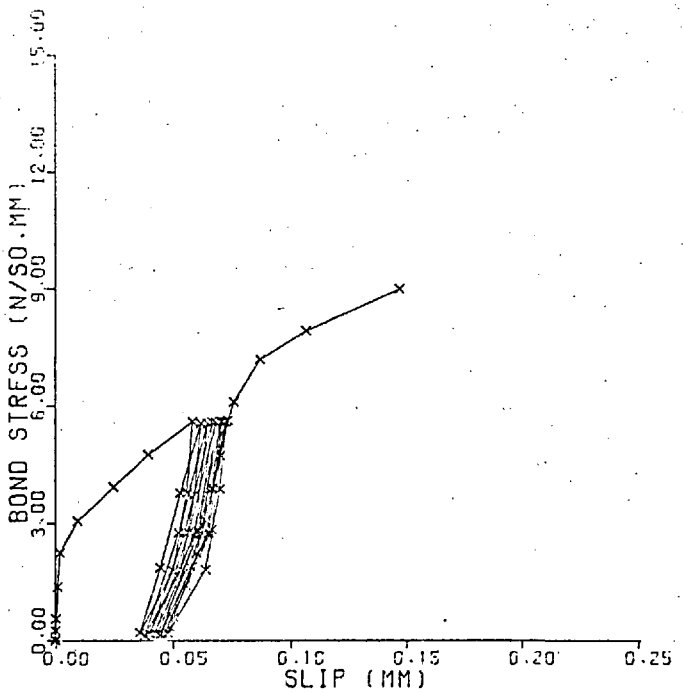


FIGURE 6.32 EXPERIMENTAL BOND-SLIP CURVES FOR 16 MM DIA. HOT-ROLLED HIGH YIELD (410) DEFORMED BAR UNDER REPEATED LOADING (0 - 3.9 N/SQ.MM)

Concrete Cover = 35 mm







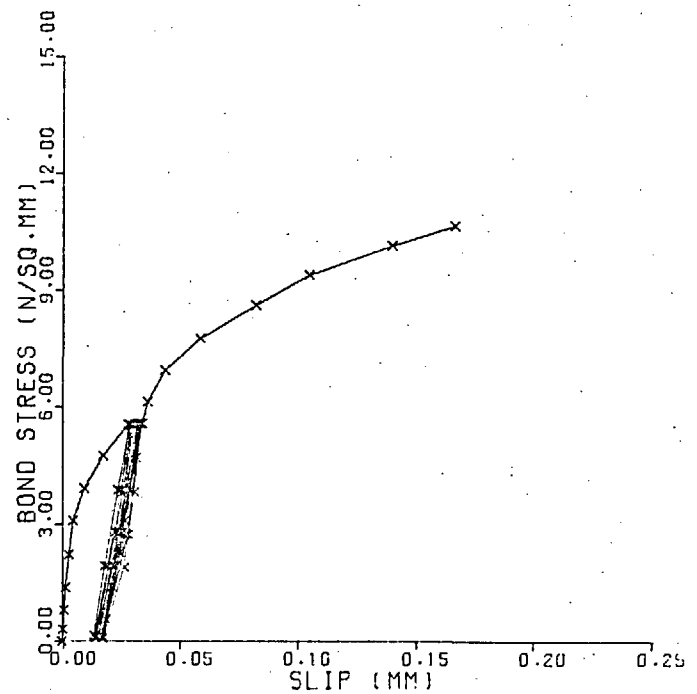
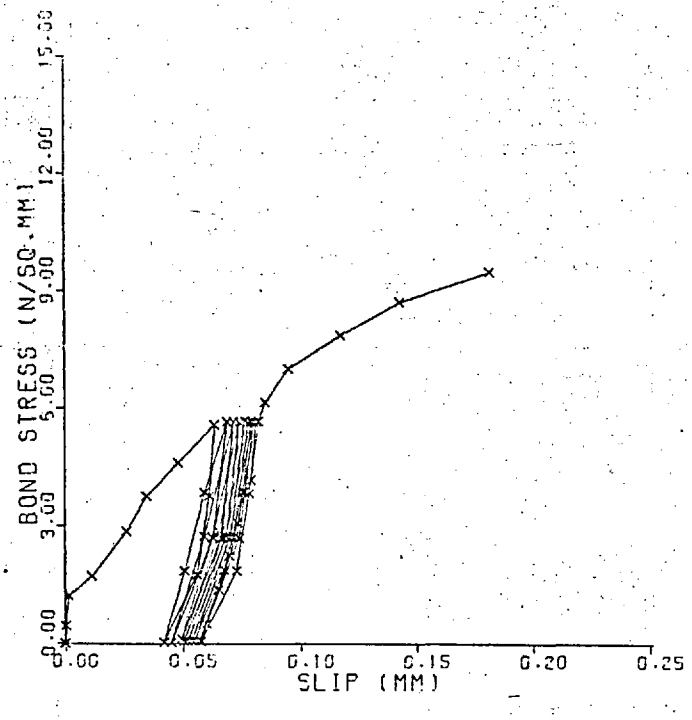
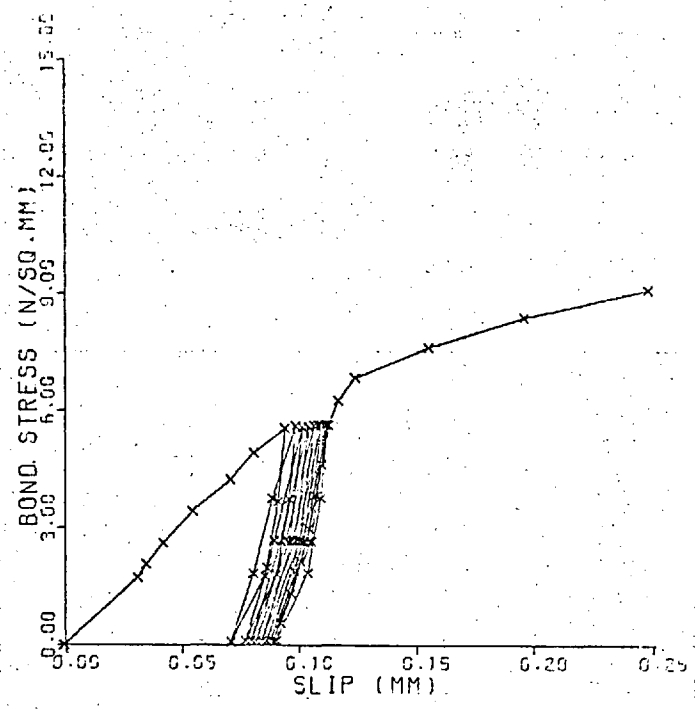


FIGURE 6.33 EXPERIMENTAL BOND-SLIP CURVES FOR 16 MM DIA. HOT-ROLLED HIGH YIELD (410) DEFORMED BAR UNDER REPEATED LOADING (0 - 5.6 N/SQ.MM)

Concrete Cover = 25 mm





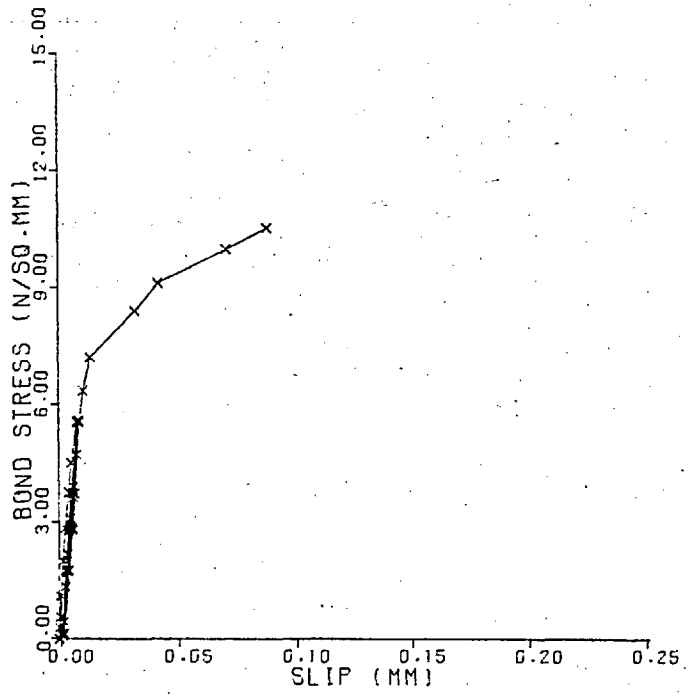


FIGURE 6.34 EXPERIMENTAL BOND-SLIP CURVES FOR 16 MM DIA. HOT-ROLLED HIGH YIELD (410) DEFORMED BAR UNDER REPEATED LOADING (0 - 5.6 N/SQ.MM)

Concrete Cover = 35 mm

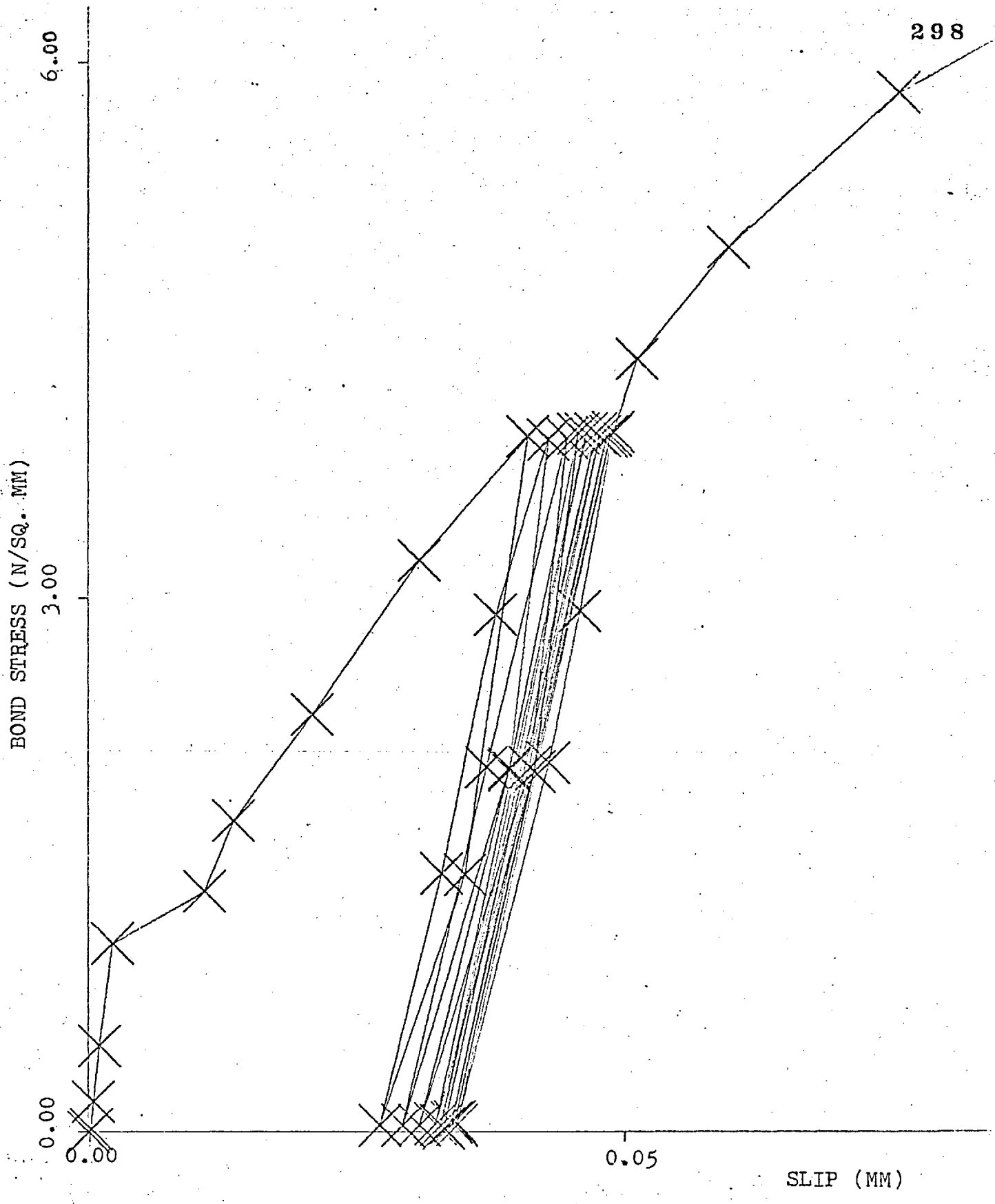


FIGURE 6.35 MAGNIFIED EXPERIMENTAL BOND-SLIP CURVE FOR 16 MM DIA. HOT-ROLLED HIGH YIELD (410) DEFORMED BAR UNDER REPEATED LOADING (0 - 3.9 N/SQ MM)

Concrete Cover = 35 mm

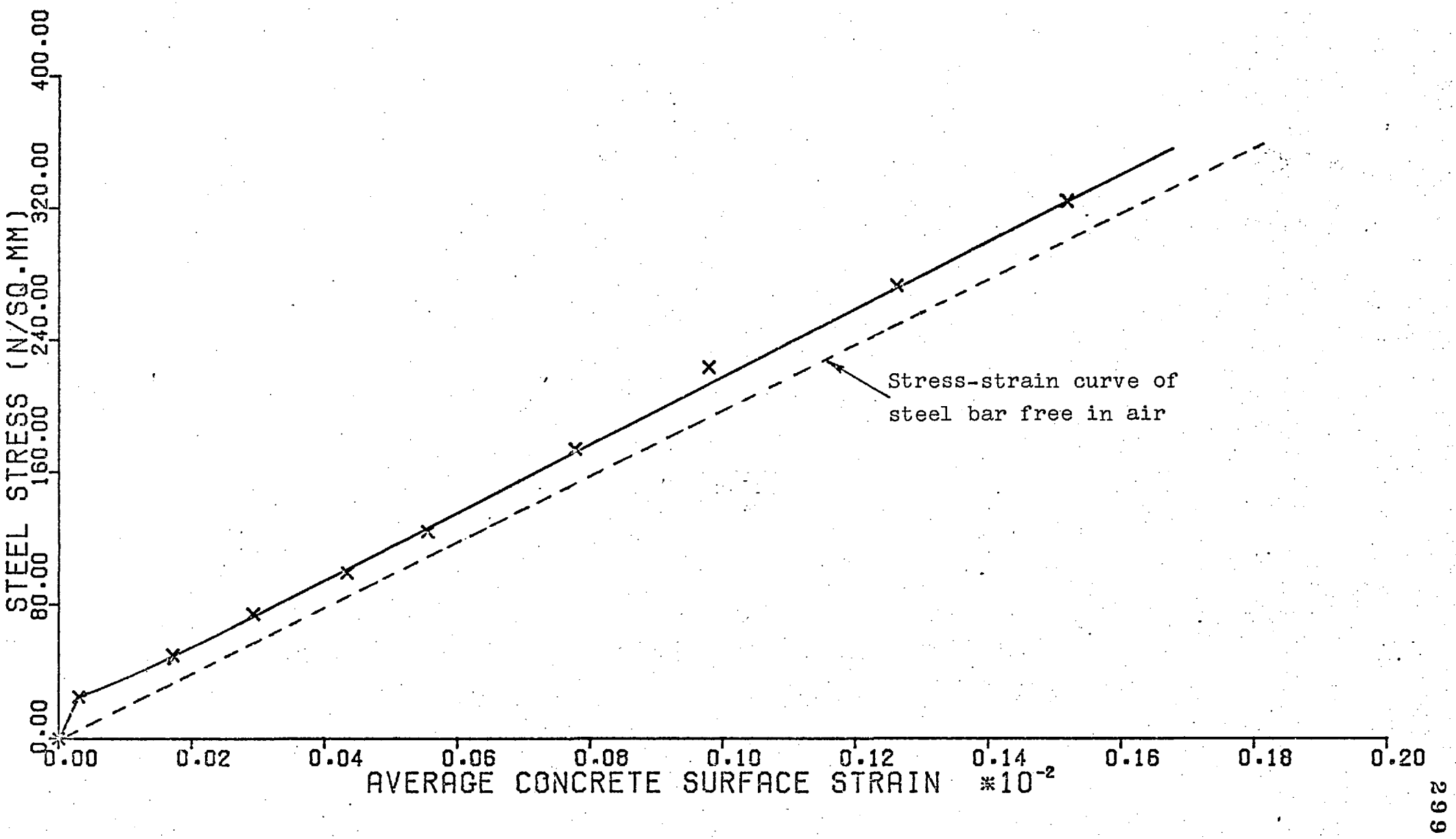
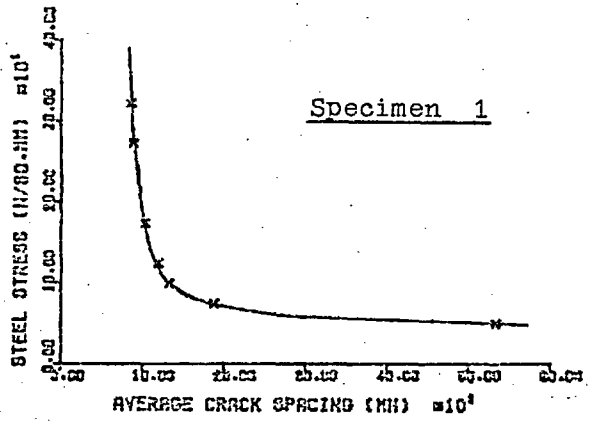
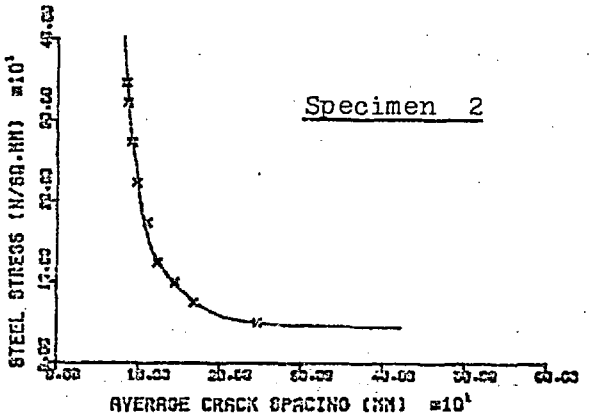
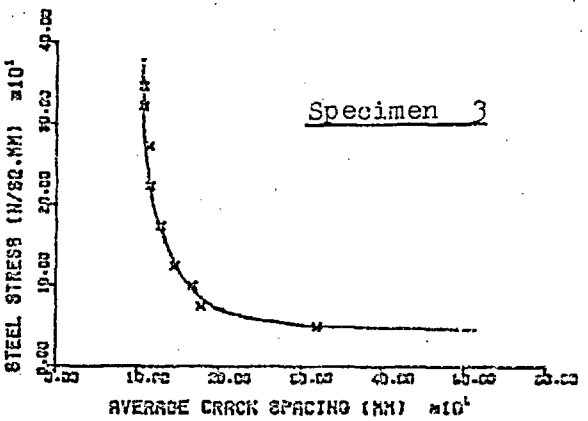
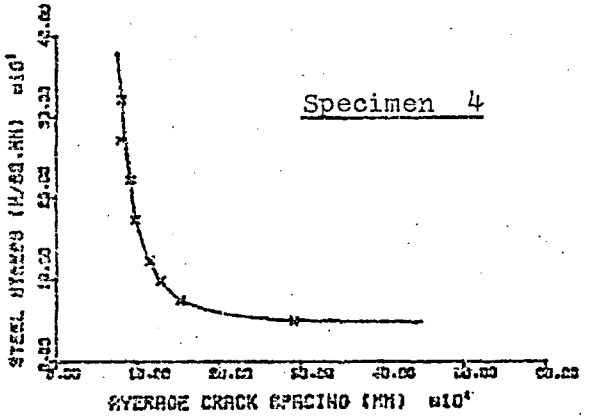

STEEL STRESS - AVERAGE CONCRETE SURFACE STRAIN
STEEL STRESS (N/SQ.MM)
0.00
80.00
160.00
240.00
320.00
400.00
0.00
0.02
0.04
0.06
0.08
0.10
0.12
0.14
0.16
0.18
0.20
AVERAGE CONCRETE SURFACE STRAIN *10^-2
Stress-strain curve of
steel bar free in air

FIGURE 6.36









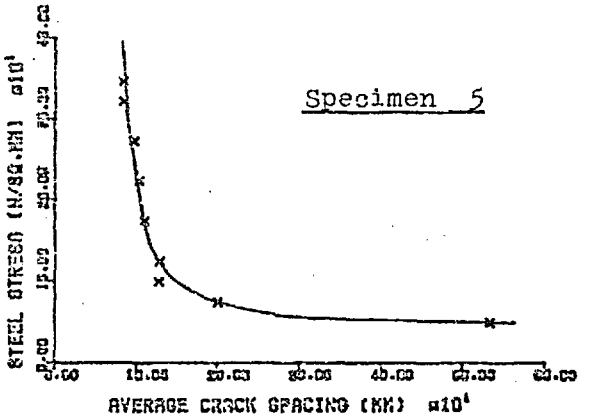


FIGURE 6.37 RELATION BETWEEN STEEL STRESS AND AVERAGE CRACK SPACING FOR REINFORCED CONCRETE TENSION SPECIMENS

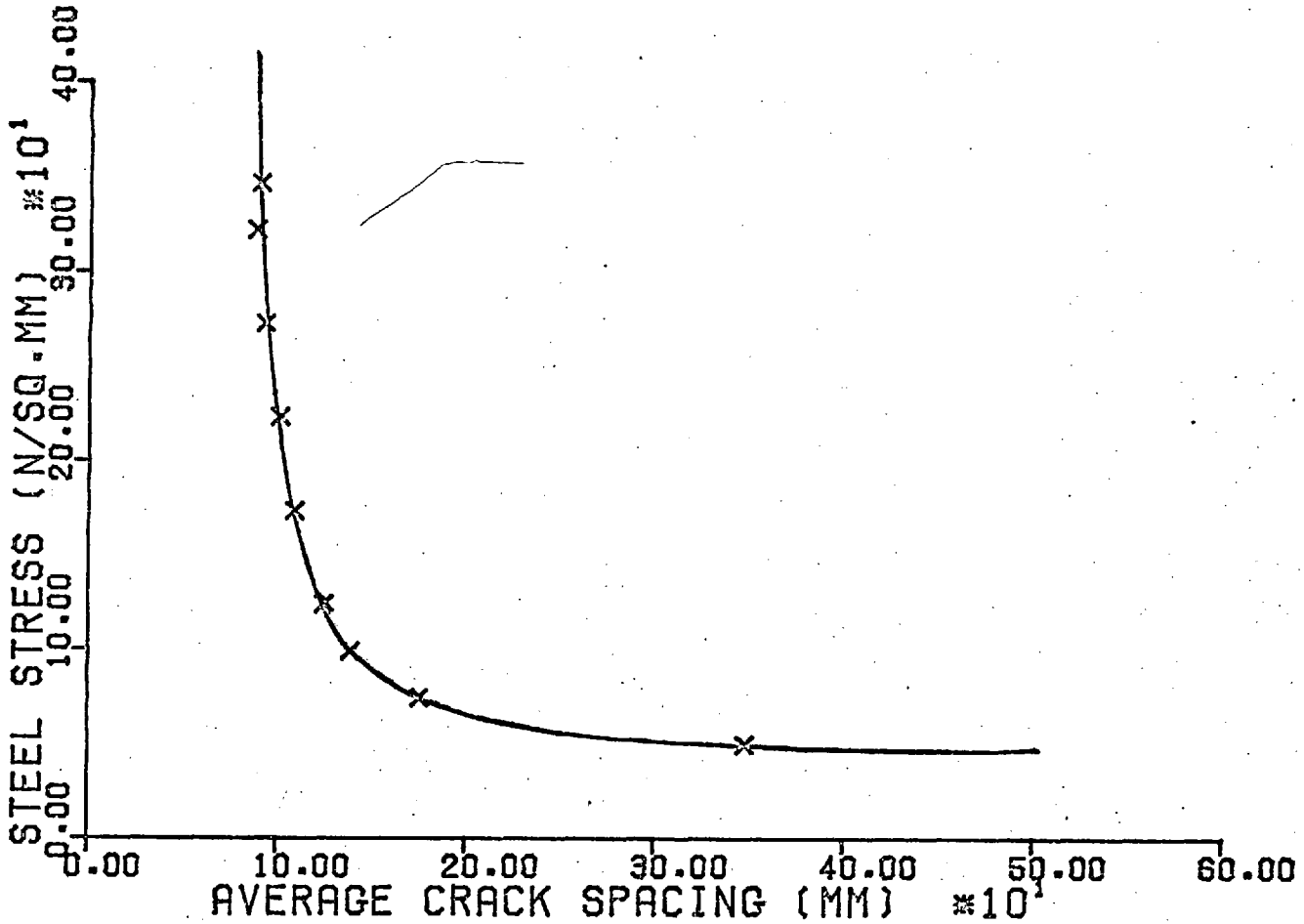


FIGURE 6.38 MEAN RELATION BETWEEN STEEL STRESS AND AVERAGE CRACK SPACING FROM REINFORCED CONCRETE TENSION SPECIMENS

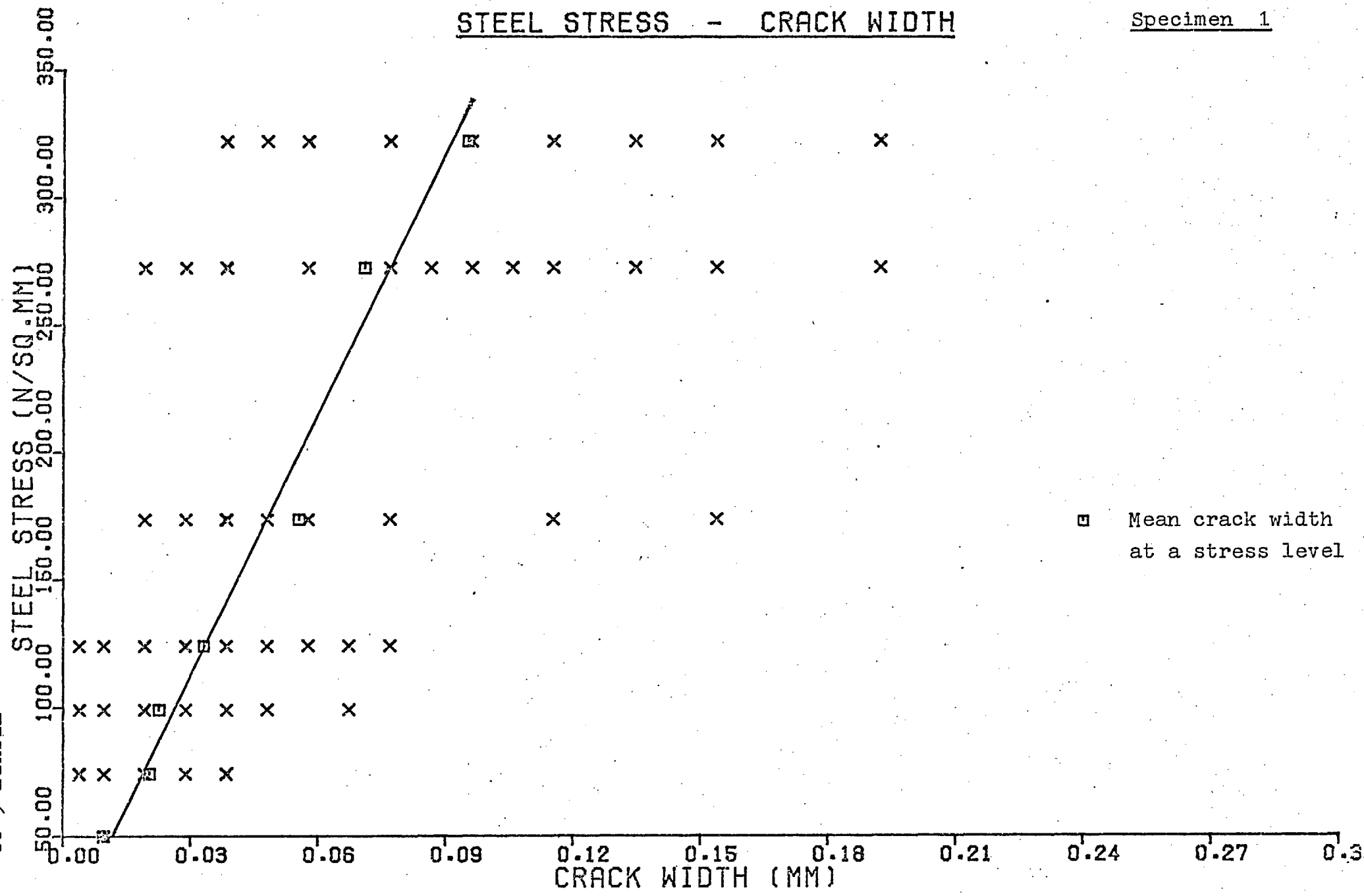

STEEL STRESS - CRACK WIDTH
Specimen 1
STEEL STRESS (N/SQ.MM)
350.00
300.00
250.00
200.00
150.00
100.00
50.00
0.00
0.03
0.06
0.09
0.12
0.15
0.18
0.21
0.24
0.27
0.30
CRACK WIDTH (MM)
Mean crack width
at a stress level

FIGURE 6.39

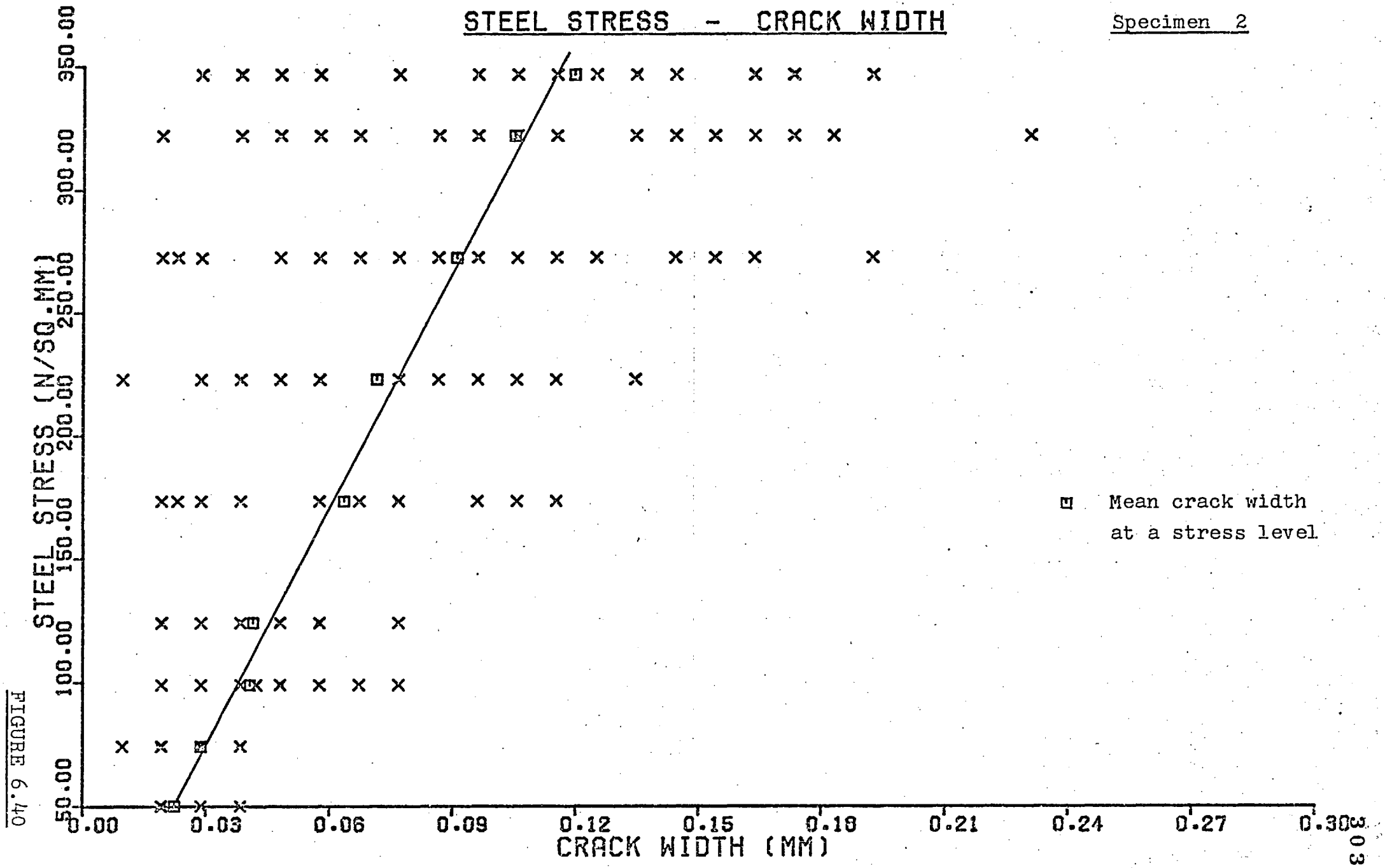

STEEL STRESS - CRACK WIDTH
Specimen 2
STEEL STRESS (N/SQ.MM)
350.00
300.00
250.00
200.00
150.00
100.00
50.00
0.00
0.03
0.06
0.09
0.12
0.15
0.18
0.21
0.24
0.27
0.30
CRACK WIDTH (MM)
Mean crack width at a stress level

FIGURE 6.40

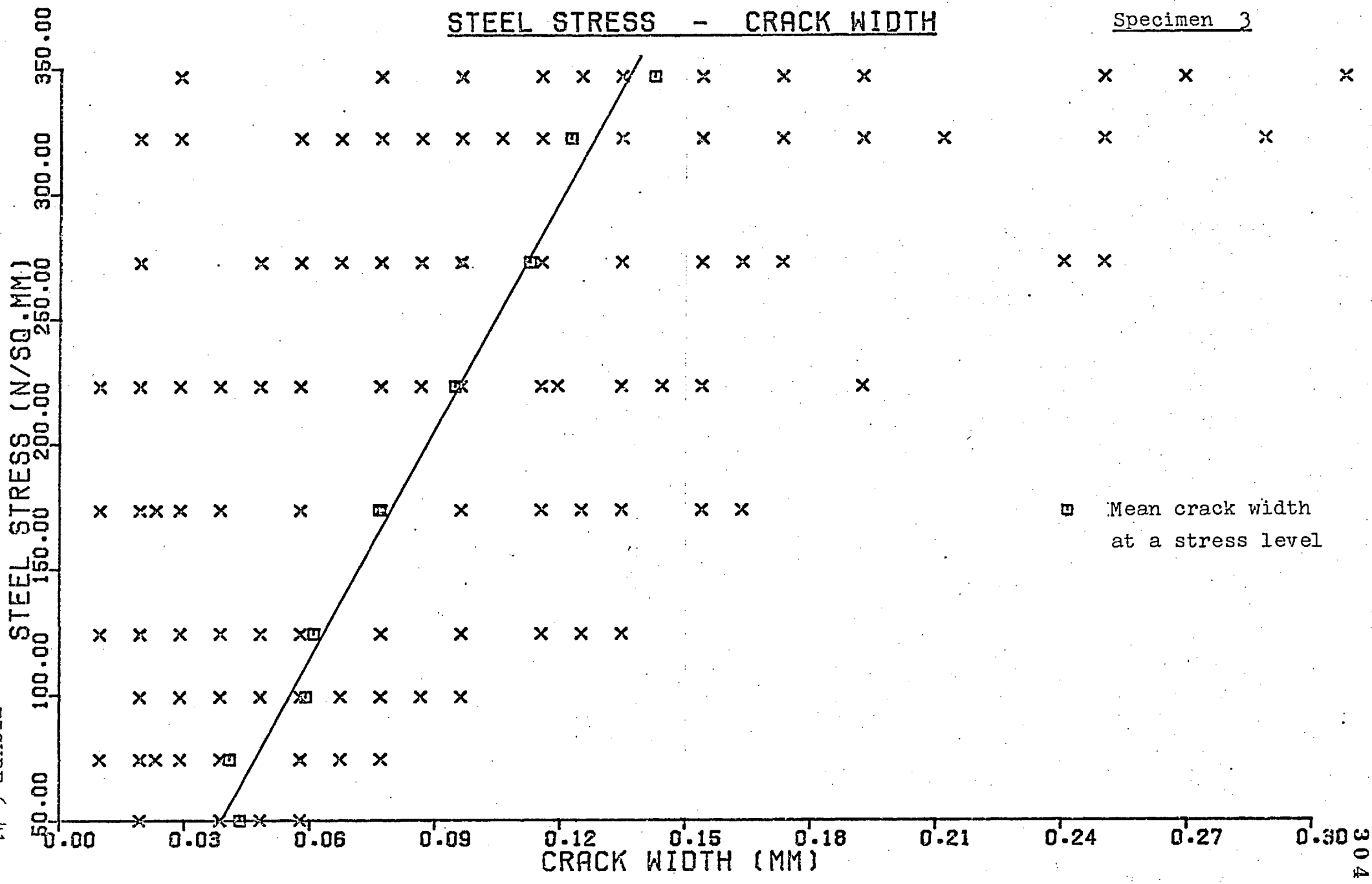

STEEL STRESS - CRACK WIDTH
Specimen 3
STEEL STRESS (N/SQ.MM)
350.00
300.00
250.00
200.00
150.00
100.00
50.00
0.00
0.03
0.06
0.09
0.12
0.15
0.18
0.21
0.24
0.27
0.30
CRACK WIDTH (MM)
Mean crack width
at a stress level

FIGURE 6.41

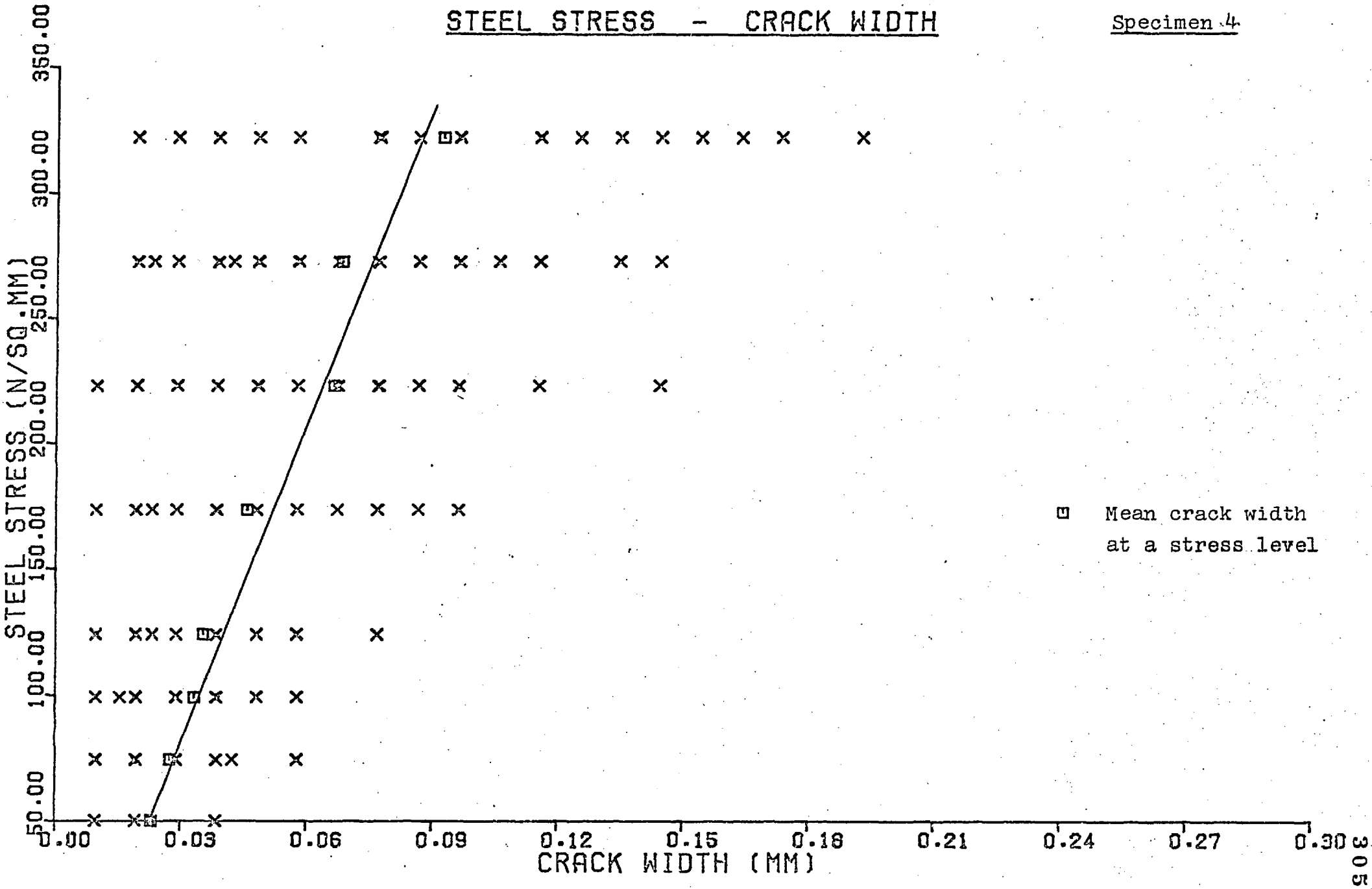

STEEL STRESS - CRACK WIDTH
Specimen 4
STEEL STRESS (N/SQ.MM)
350.00
300.00
250.00
200.00
150.00
100.00
50.00
0.00
0.03
0.06
0.09
0.12
0.15
0.18
0.21
0.24
0.27
0.30
CRACK WIDTH (MM)
Mean crack width
at a stress level

FIGURE 6.42

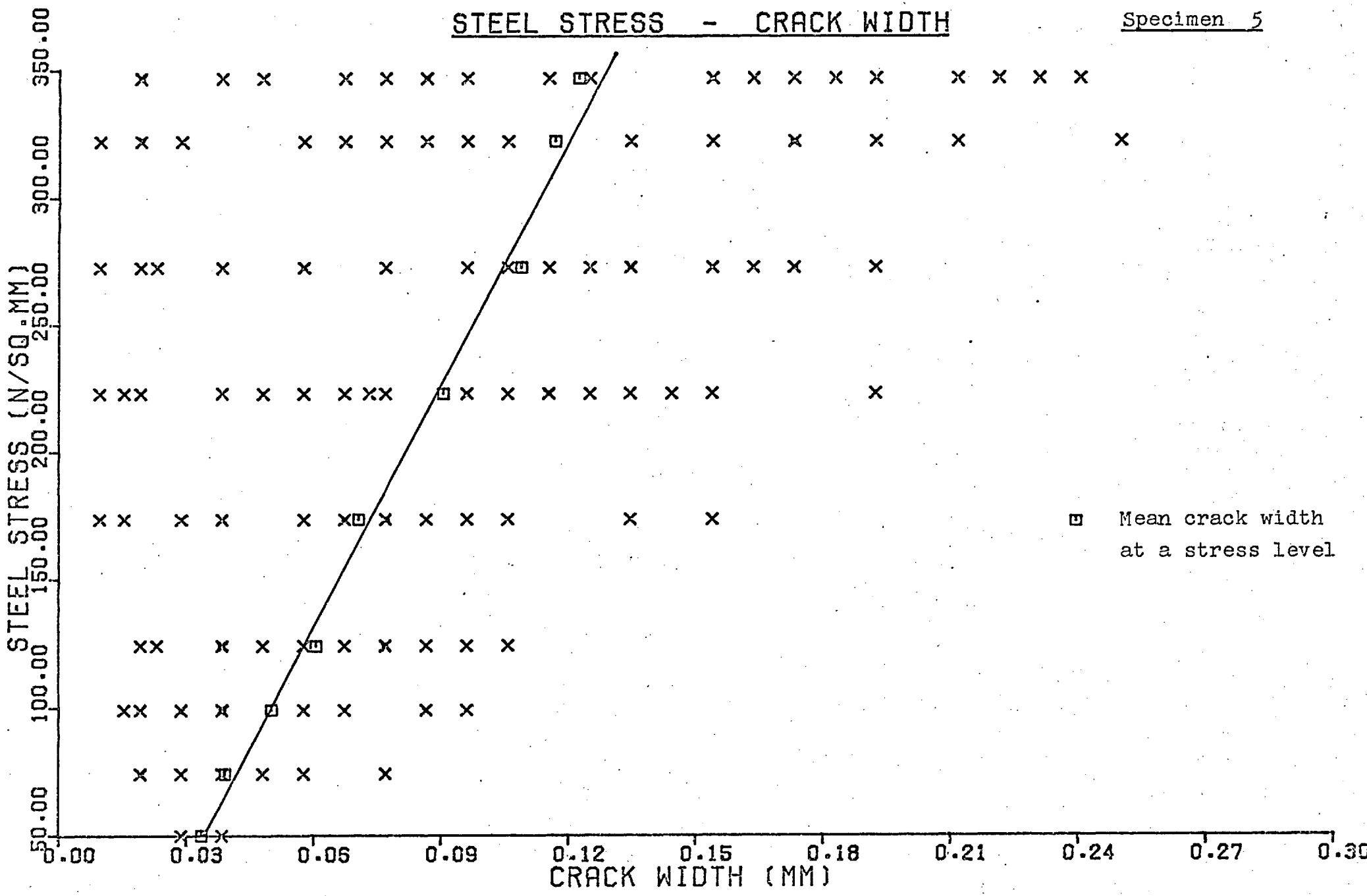

STEEL STRESS - CRACK WIDTH
Specimen 5
STEEL STRESS (N/SQ.MM)
350.00
300.00
250.00
200.00
150.00
100.00
50.00
0.00
0.03
0.06
0.09
0.12
0.15
0.18
0.21
0.24
0.27
0.30
CRACK WIDTH (MM)
Mean crack width
at a stress level

FIGURE 6.43

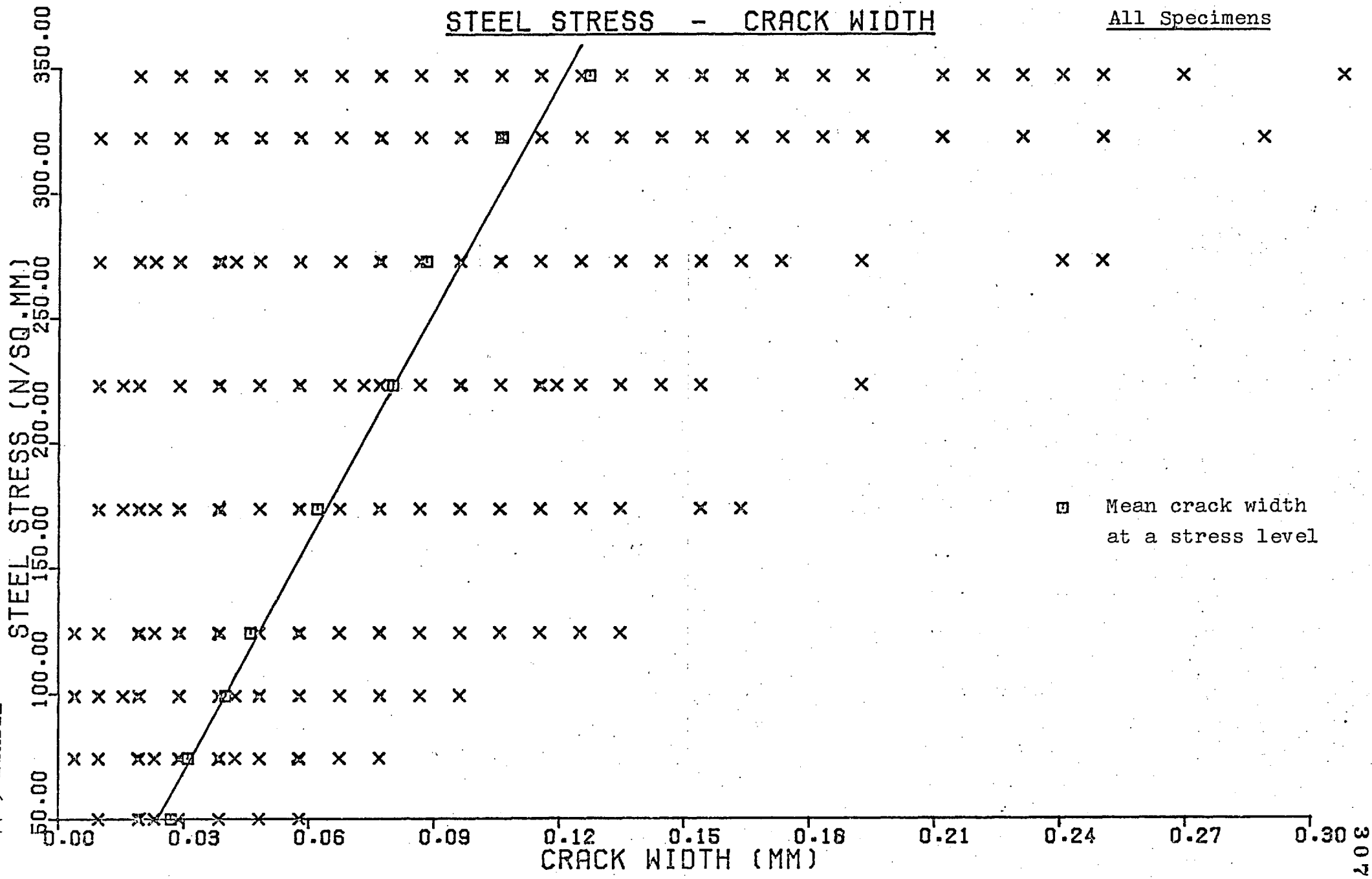

STEEL STRESS - CRACK WIDTH
All Specimens
STEEL STRESS (N/SQ.MM)
350.00
300.00
250.00
200.00
150.00
100.00
50.00
0.00
0.03
0.06
0.09
0.12
0.15
0.18
0.21
0.24
0.27
0.30
CRACK WIDTH (MM)
Mean crack width
at a stress level

FIGURE 6.44

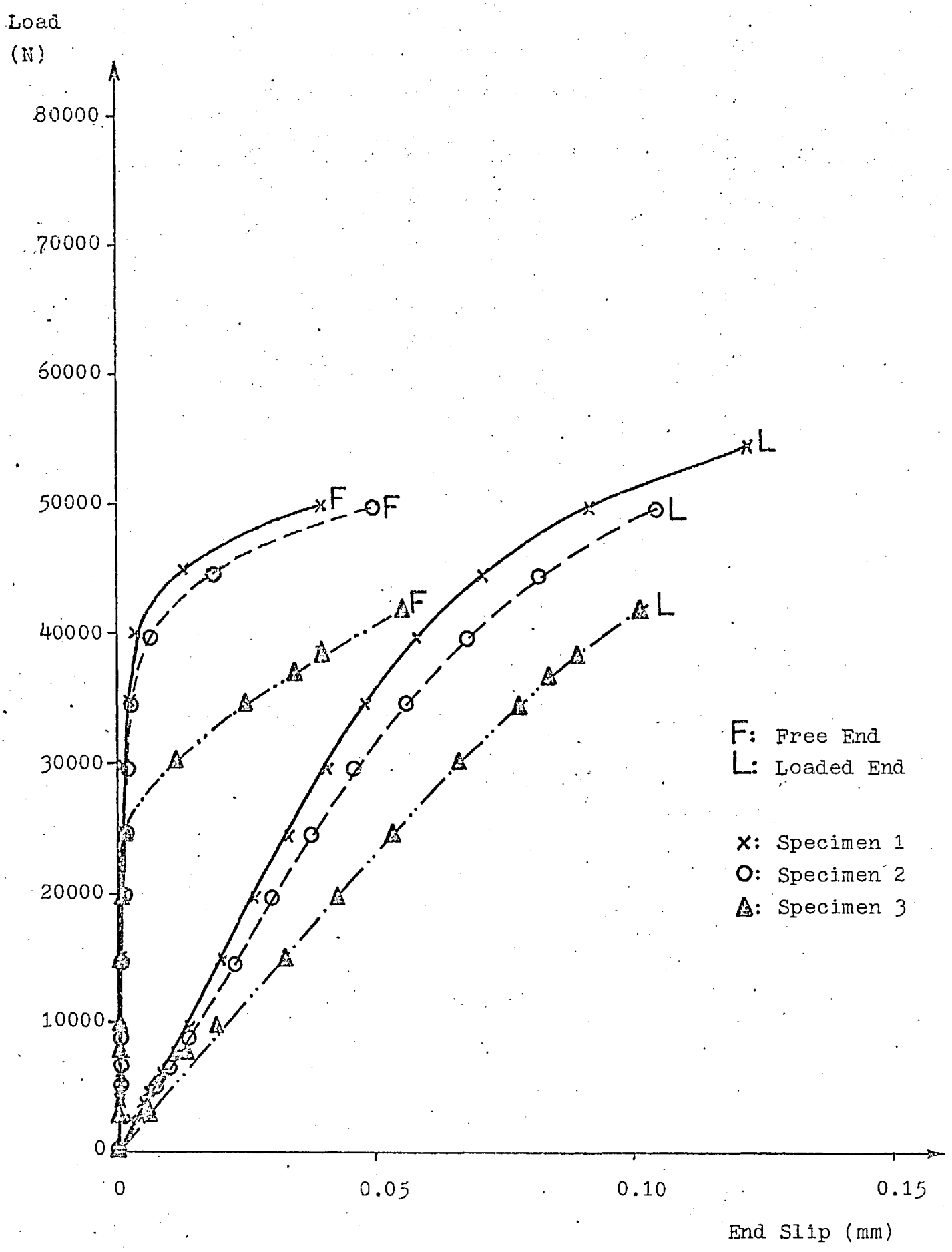


FIGURE 6.45 LOAD VERSUS END SLIP CURVES OF 100 MM LONG PULL-OUT SPECIMENS

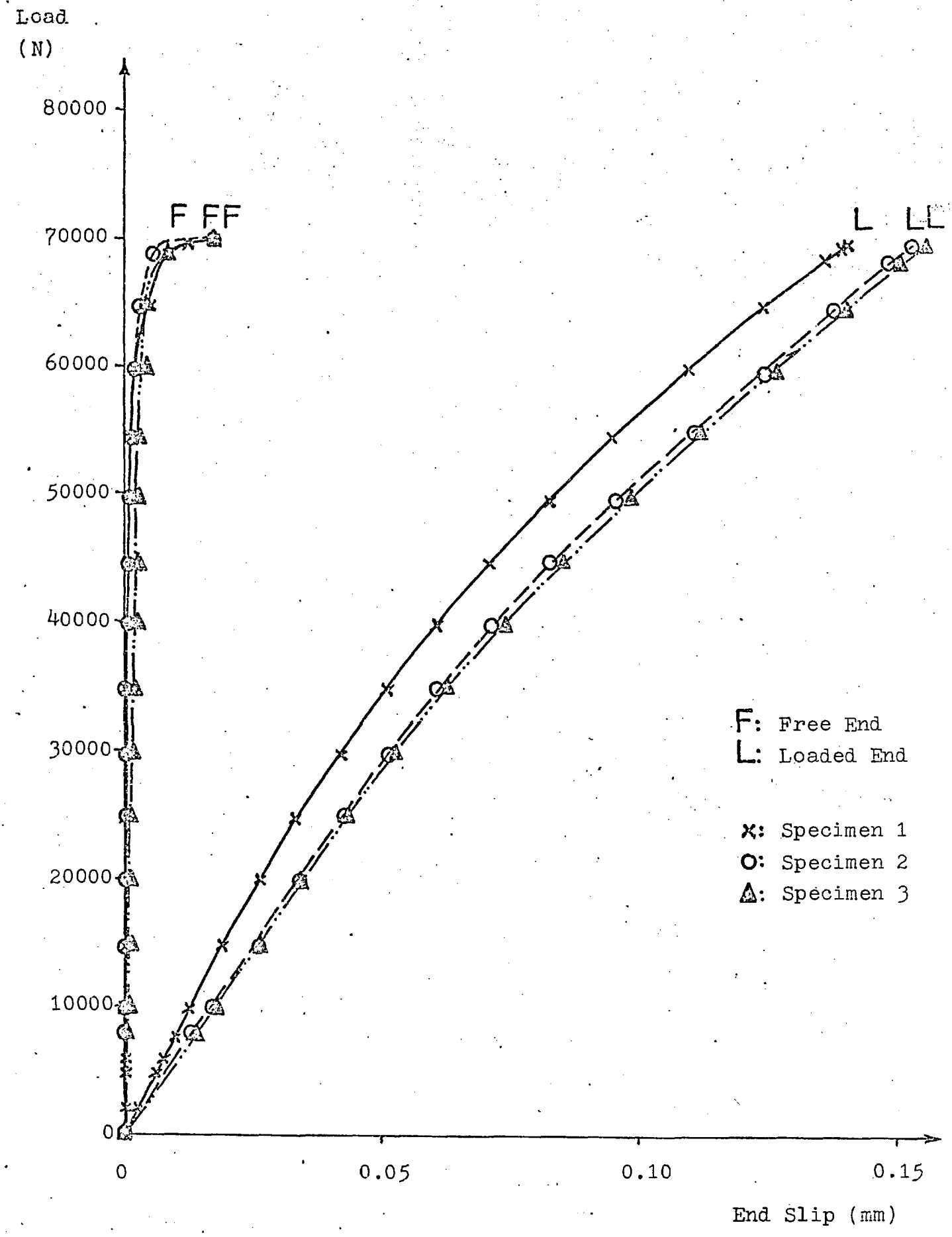


FIGURE 6.46 LOAD VERSUS END SLIP CURVES OF 200 MM LONG PULL-OUT SPECIMENS

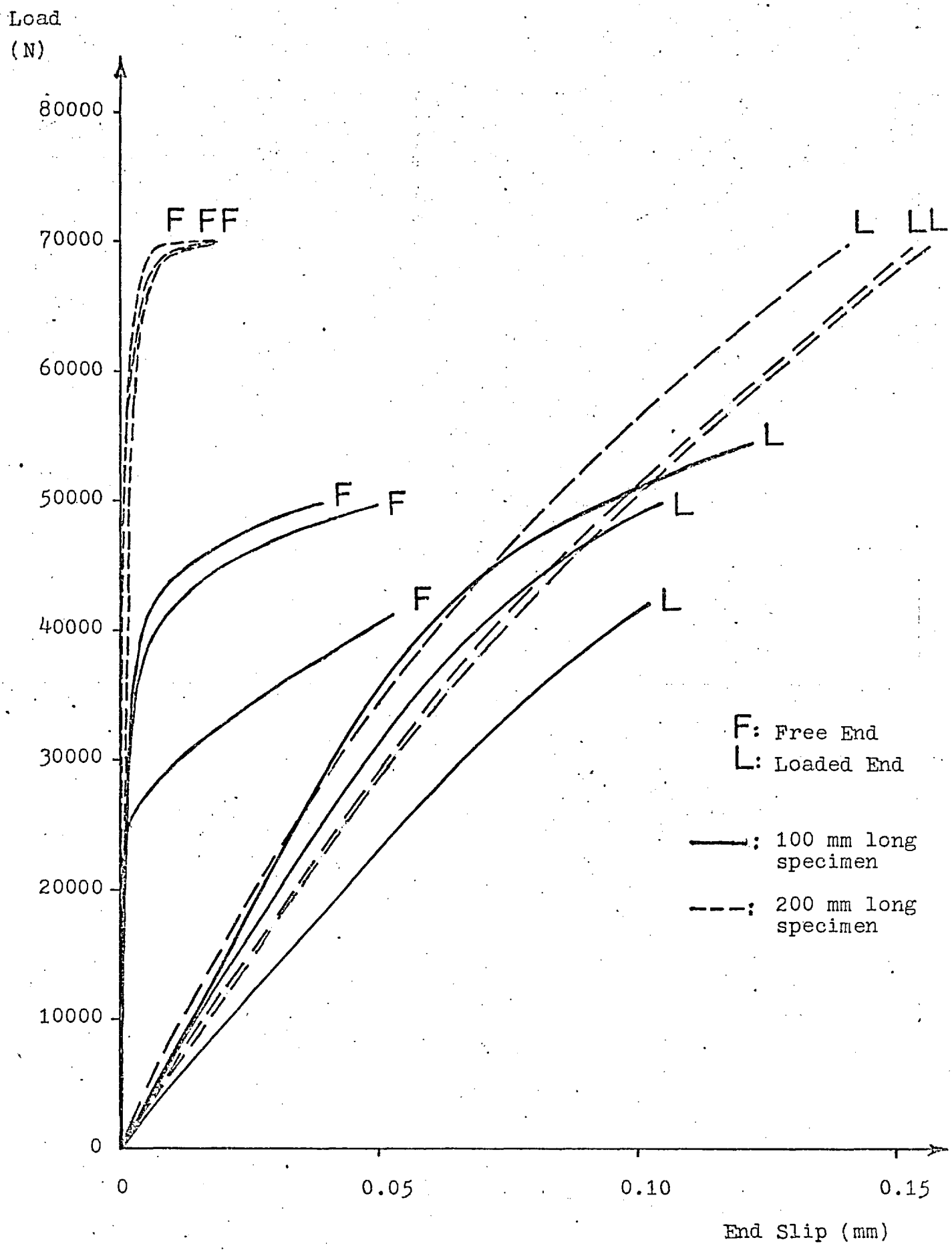


FIGURE 6.47 LOAD VERSUS END SLIP CURVES OF 100 AND 200 MM LONG PULL-OUT SPECIMENS

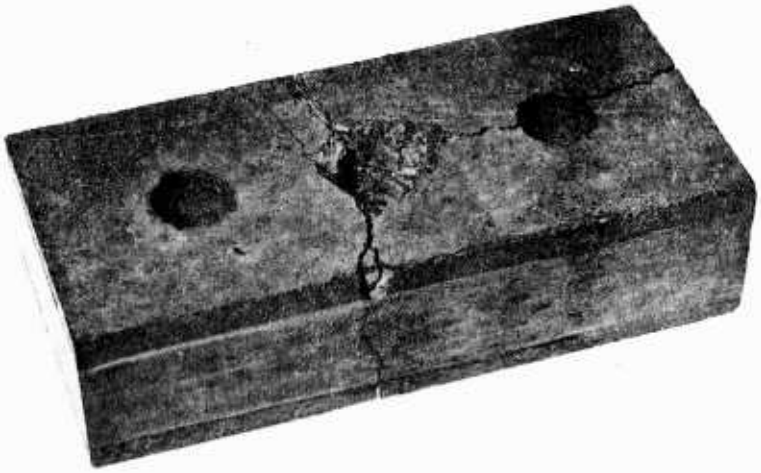


PLATE 6.1 FAILURE PATTERNS OF BASIC SPECIMENS FOR BOND TESTS



CHAPTER 7

FINITE ELEMENT ANALYSIS OF REINFORCED CONCRETE

7.1. STATEMENT OF THE PROBLEM

Conventional axi-symmetric finite element analysis provides the basis for the development of an analytical model of a reinforced concrete member. The concrete mass is considered homogeneous; similarly the steel is also taken as homogeneous. The combination of the two materials, considered through the full range of loads, introduces a number of problems. These are as follows:

(a) As a reinforced concrete member is loaded, small but significant movement occurs between steel and concrete. This response is non-linear.

(b) Progressive destruction of bond occurs as load is applied.

(c) Concrete is subject to cracking under load. In effect, the cracks redefine the member which is to be analysed.

(d) Although steel response to load is nearly linear up to the yield point, concrete response is distinctly non-linear.

(e) The response of concrete to load is dependent upon prior load history of the concrete.

A valid analytical model of reinforced concrete should take these characteristics into account.

7.2. GENERAL DESCRIPTION OF FINITE ELEMENT METHOD

The finite element method today presents a powerful tool in the analysis of complex structural and continuum problems. The virtue of the method lies in its versatility. The same general technique applies to any type of continuum, and loading as well as boundary conditions may be completely arbitrary. Static linear analysis of two and three dimensional complex continuum problems, as well as non-linear effects such as plasticity and creep can be treated. A comprehensive representation of the method together with a large number of applications is given by Zienkiewicz (94).

The finite element method is essentially a generalisation of the standard structural analysis procedures used in the analysis of ordinary framed structures (95). The elastic continuum, is idealized as an assemblage of a finite number of appropriately shaped elements interconnected at a finite number of nodal points or nodes and the behaviour of each element is approximated by assumed displacement and/or stress pattern within the element. The nodal values of displacements or stresses or both are taken as the unknown generalised parameters of the problem.

The finite element displacement method is based on assumed displacement functions which ensure compatibility of deformation both within the elements and across the boundaries. The nodal displacements are the generalised co-ordinates and the method of analysis is generally considered as an application of the minimum potential energy principle and the Ritz method (96). The method will yield solutions which are converging to

the exact solutions when the sizes of the finite elements are progressively reduced if the chosen displacement functions (a) are continuous over each element and across their boundaries, and (b) can reproduce any necessary state of constant strain (or curvature) (97, 98). The second criterion in fact includes any rigid body movement - a state of zero strain.

A second approach, the finite element equilibrium method, assumes stress functions which satisfy internal equilibrium and continuity of stresses between the elements. This method is based on the principle of minimum complementary energy (96). A mixed formulation has also been developed.

In general the displacement method has been most widely used. The mothod is well documented, but since it will be used in this report to obtain the non-linear response of reinforced concrete members under load, a brief summary of the finite element procedure is considered necessary for continuity of presentation.

The finite element displacement method of analysis may logically be divided into the steps shown in Table 7.1. Its adaptation and formulation to analyse axi-symmetric reinforced concrete members under load and include anisotropy, non-linearity, formation and propagation of cracks will be given in the following sections.

7.3. AXI-SYMMETRIC FINITE ELEMENT ANALYSIS OF MEMBERS

7.3.1. BASIS OF ANALYSIS AND STRUCTURAL IDEALISATION

The reinforced concrete members to be analysed in this work were cylindrical and there was symmetric loading

applied to the reinforcing bar. The best finite element representation of these members was an axi-symmetric one. In a cylindrical co-ordinate system, displacement in such a representation may occur only in the radial direction and in the direction parallel with the axis; tangential displacements do not exist because of symmetry. If r and z denote respectively the radial and axial co-ordinates of a point, with u and v being the corresponding displacements, then u and v define completely the state of stress and strain in any plane section of the body along its axis of symmetry. Such a section is shown in Figure 7.1.

In plain stress or strain problems internal work is associated with three strain components in the co-ordinate plane, the strain component normal to this plane not being involve due to zero value of either the stress or the strain. In axi-symmetric problems any radial displacement automatically induces a strain in the circumferential direction, and as the stresses in this direction are certainly non-zero, this fourth component of strain and of the associated stress has to be considered. This is the only and essential difference between plain stress or strain and axi-symmetric analysis.

An axi-symmetric analysis of pull-out and reinforced concrete tension members is reported. The members were modelled by rectangular concrete elements and rectangular steel elements. Bond between steel and concrete was modelled by linkage elements, of variable stiffness, connected between corresponding concrete and steel nodes. The stiffness properties of the rectangular and linkage elements are developed in sections 7.4 and 7.5 respectively. The essentials of axi-symmetric element charac-

teristics are given in next section; a full treatment is given in standard texts (94, 99).

7.3.2. ELEMENT CHARACTERISTICS

(a) Displacement Function

A typical finite element, e, is defined by nodes 1, 2, 3, etc. numbered in an anti-clockwise order, and straight line boundaries. In the standard notation introduced by Zienkiewicz and Cheung (100) the displacement of node-i is defined by its two components by

$$\{\delta_i\} = \begin{Bmatrix} u_i \\ v_i \end{Bmatrix} \qquad (7.1)$$

and the element displacements by the vector

$$\{\delta^e\} = \begin{Bmatrix} \delta_1 \\ \delta_2 \\ \delta_3 \\ \vdots \end{Bmatrix} \qquad (7.2)$$

The displacements at any point within the element are defined by the column vector

$$f(r,z) = \begin{Bmatrix} u(r,z) \\ v(r,z) \end{Bmatrix}$$

$$\{f\} = \begin{Bmatrix} u \\ v \end{Bmatrix} = [N]\{\delta\}^e = [N_1, N_2, N_3, \ldots] \begin{Bmatrix} \delta_1 \\ \delta_2 \\ \delta_3 \\ \vdots \end{Bmatrix} \qquad (7.3)$$

in which the components of $[N]$ are functions of position. The functions N_1, N_2, N_3,... have to be so chosen as to give appropriate nodal displacements when the coordinates of the appropriate nodes are inserted in Equation (7.3). The functions $[N]$ are called Shape Functions.

(b) Strains

For the axi-symmetric case the total strain at any point within the element can be defined by its four components which contribute to internal work. These are all the non-zero strain components possible in an axi-symmetric deformation. Figure 7.2 illustrates and defines these strains and the associated stresses. The strain vector defined below lists the strain components involved and defines them in terms of the displacement of a point by well-known relations (101) -

$$\{\varepsilon\} = \begin{Bmatrix} \varepsilon_r \\ \varepsilon_z \\ \gamma_{rz} \\ \varepsilon_\theta \end{Bmatrix} = \begin{Bmatrix} \frac{\partial u}{\partial r} \\ \frac{\partial v}{\partial z} \\ \frac{\partial u}{\partial z} + \frac{\partial v}{\partial r} \\ \frac{u}{r} \end{Bmatrix} \qquad (7.4)$$

Using Equations (7.3) and (7.4) we have

$$\left\{\varepsilon\right\} = \left[B\right]\left\{\delta\right\}^e = \left[B_1, B_2, B_3, \ldots\right]\left\{\delta\right\}^e \qquad (7.5)$$

in which the element strain matrix is given by

$$\left\{B_i\right\} = \begin{Bmatrix} \frac{\partial N_i}{\partial r} & 0 \\ 0 & \frac{\partial N_i}{\partial z} \\ \frac{\partial N_i}{\partial z} & \frac{\partial N_i}{\partial r} \\ \frac{N_i}{x} & 0 \end{Bmatrix} \qquad (7.6)$$

(c) Stresses

The stresses $\left\{\sigma\right\}$ and strains $\left\{\varepsilon\right\}$ are linked by

$$\left\{\sigma\right\} = \left[D\right]\left(\left\{\varepsilon\right\} - \left\{\varepsilon_o\right\}\right) + \left\{\sigma_o\right\} \qquad (7.7)$$

where $\left[D\right]$ is the elasticity matrix containing the appropriate material properties.

$\left\{\varepsilon_o\right\}$ is the initial strain vector, and

$\left\{\sigma_o\right\}$ is the initial stress vector.

Stresses and nodal displacements are connected by the following relationship derived from Equations (7.5) and (7.7)

$$\{\sigma\} = [D][B]\{\delta\}^e - [D]\{\varepsilon_o\} + \{\sigma_o\} \qquad (7.8)$$

where $[DB] = [D][B]$ is called the element stress matrix. The elasticity matrix in an isotropic material is given by

$$[D] = \frac{E(1-\nu)}{(1+\nu)(1-2\nu)} \begin{bmatrix} 1 & \frac{\nu}{1-\nu} & 0 & \frac{\nu}{1-\nu} \\ \frac{\nu}{1-\nu} & 1 & 0 & \frac{\nu}{1-\nu} \\ 0 & 0 & \frac{1-2\nu}{2(1-\nu)} & 0 \\ \frac{\nu}{1-\nu} & \frac{\nu}{1-\nu} & 0 & 1 \end{bmatrix} \qquad (7.9)$$

(d) The Stiffness Matrix

By virtual work method or from energy considerations, the stiffness $[k]^e$ of the element may be obtained as

$$[k]^e = 2\pi \int\int [B]^T [D][B]\, r\, dr\, dz \qquad (7.10)$$

with $[B]$ given by Equation (7.6) and $[D]$ by Equation (7.9).

The above integration is usually not easy to perform, except for the simplest elements, and numerical integration has to be resorted to. This, as will be seen from later sections, is not a severe penalty and has the advantage that algebraic errors are more easily avoided.

(e) Nodal Forces Due to Initial Strain and Stress

These are given by

$$\left\{F\right\}^e_{\varepsilon_o} = 2\pi \int\int \left[B\right]^T \left[D\right] \left\{\varepsilon_o\right\} r \, dr \, dz \qquad (7.11)$$

and

$$\left\{F\right\}^e_{\sigma_o} = 2\pi \int\int \left[B\right]^T \left\{\sigma_o\right\} r \, dr \, dz \qquad (7.12)$$

where $\left\{F\right\}^e_{\varepsilon_o}$ is nodal force vector due to initial strain and

$\left\{F\right\}^e_{\sigma_o}$ is nodal force vector due to initial stress.

The above integrations can again be performed by numerical techniques.

7.4. ISOPARAMETRIC, RECTANGULAR, NUMERICALLY INTEGRATED FINITE ELEMENT PROPERTIES

7.4.1. CO-ORDINATE DEFINITION

A rectangular element is considered having eight degrees of freedom, namely u_i and v_i at each of four corner nodes i. Any point P inside this element, as illustrated in Figure 7.3, can be conveniently defined by local normalised co-ordinates ξ and η. These co-ordinates which in general are curvilinear will be so determined as to give

$\eta = -1$ on side 12

$\eta = 1$ on side 43

$\xi = 1$ on side 23

$\xi = -1$ on side 14

The relationship between the Cartesian x-y co-ordinates and the curvilinear ξ - η co-ordinates can be written as

$$x = N_1 x_1 + N_2 x_2 + N_3 x_3 + N_4 x_4 = \{N\}^T \{x\}$$
$$y = N_1 y_1 + N_2 y_2 + N_3 y_3 + N_4 y_4 = \{N\}^T \{y\} \qquad (7.13)$$

where

$$N_1 = \frac{1}{4}(1-\xi)(1-\eta)$$

$$N_2 = \frac{1}{4}(1-\xi)(1+\eta)$$

$$N_3 = \frac{1}{4}(1+\xi)(1+\eta)$$

$$N_4 = \frac{1}{4}(1+\xi)(1-\eta)$$

or generally

$$N_i = \frac{1}{4}(1+\xi\xi_i)(1+\eta\eta_i) \qquad (7.14)$$

where ξ_i and η_i take their nodal values (-1, -1), (1, -1), (1, 1) and (-1, 1), while $\{x\}$ and $\{y\}$ lists the nodal Cartesian co-ordinates. Thus for any values of ξ and η the x and y co-ordinates can be found.

7.4.2. ISOPARAMETRIC SHAPE FUNCTIONS

In finite element analysis it is necessary to define the variation of displacement components u and v in terms of the nodal values of these functions. Suitable shape functions are generally written in term of Cartesian co-ordinates. Curvilinear co-ordinates will now be used and it will be assumed that the same functions N_1, N_2, N_3 and N_4 previously used can be again employed. Such shape functions are termed isoparametric. Thus

$$u(\xi,\eta) = N_1 u_1 + N_2 u_2 + N_3 u_3 + N_4 u_4 = \{N\}^T \{u\}$$
$$v(\xi,\eta) = N_1 v_1 + N_2 v_2 + N_3 v_3 + N_4 v_4 = \{N\}^T \{v\} \quad (7.15)$$

in which u_1, v_1, etc. represent the nodal values of displacements.

7.4.3. EVALUATION OF ELEMENT MATRICES IN CURVILINEAR CO-ORDINATES

In finite element analysis matrices defining element properties require evaluation of integrals of the form

$$I = \int_V [H]\, dV \quad (7.16)$$

where $[H]$ is a function of N or its derivatives with respect to Cartesian x-y co-ordinates. As an example of this the stiffness matrix of an axi-symmetric element is given by

$$[k] = 2\pi \int\int [B]^T [D] [B]\, x\, dx\, dy \quad (7.17)$$

in which

$$[B] = [B_1, B_2, \cdots]$$

with

$$[B_i] = \begin{bmatrix} \frac{\partial N_i}{\partial x} & 0 \\ 0 & \frac{\partial N_i}{\partial y} \\ \frac{\partial N_i}{\partial y} & \frac{\partial N_i}{\partial x} \\ \frac{N_i}{x} & 0 \end{bmatrix} \quad (7.18)$$

As N_i is defined in terms of the curvilinear $\xi-\eta$ system some transformations are necessary. In particular, derivatives $\frac{\partial N_i}{\partial x}$ and $\frac{\partial N_i}{\partial y}$ have to be determined in terms of $\frac{\partial N_i}{\partial \xi}$ and $\frac{\partial N_i}{\partial \eta}$ respectively. Noting that

$$\begin{Bmatrix} \frac{\partial N_i}{\partial \xi} \\ \frac{\partial N_i}{\partial \eta} \end{Bmatrix} = \begin{bmatrix} \frac{\partial x}{\partial \xi} & \frac{\partial y}{\partial \xi} \\ \frac{\partial x}{\partial \eta} & \frac{\partial y}{\partial \eta} \end{bmatrix} \begin{Bmatrix} \frac{\partial N_i}{\partial x} \\ \frac{\partial N_i}{\partial y} \end{Bmatrix} = \left[J\right] \begin{Bmatrix} \frac{\partial N_i}{\partial x} \\ \frac{\partial N_i}{\partial y} \end{Bmatrix} \tag{7.19}$$

in which $\left[J\right]$ is the Jacobian matrix which can easily be evaluated by numerical process, noting that from Equations (7.13) and (7.19) that

$$\left[J\right] = \begin{bmatrix} \frac{\partial N_1}{\partial \xi} & \frac{\partial N_2}{\partial \xi} & \cdots \\ \frac{\partial N_1}{\partial \eta} & \frac{\partial N_2}{\partial \eta} & \cdots \end{bmatrix} \begin{bmatrix} x_1 & y_1 \\ x_2 & y_2 \\ \vdots & \vdots \end{bmatrix} \tag{7.20}$$

To find the Cartesian derivatives we invert $\left[J\right]$ and then

$$\begin{Bmatrix} \frac{\partial N_i}{\partial x} \\ \frac{\partial N_i}{\partial y} \end{Bmatrix} = \left[J\right]^{-1} \begin{Bmatrix} \frac{\partial N_i}{\partial \xi} \\ \frac{\partial N_i}{\partial \eta} \end{Bmatrix} \tag{7.21}$$

and thus the expression for $\left[B_i\right]$ can be calculated.

The only further change which requires to be done for calculating the integrals given by Equations (7.16) and (7.17) is to transform the variables using the following standard expression

$$dx\ dy = \det\left[J\right].d\xi\ d\eta \qquad (7.22)$$

and change the limits of integration to -1 and 1 in both integrals.

Clearly, exact integration will in general be a tedious if not impossible matter and numerical integration is a necessary part of the process.

Load, mass, stress and other element matrices can be derived in an analogous manner.

7.4.4. SATISFACTION OF CONVERGENCE CRITERIA

The cutting up of the structure into finite elements introduces the approximation of reducing the infinite number of degrees of freedom to a finite. To ensure convergence to the correct solution by finer mesh subdivision the shape functions must satisfy the two criteria necessary for convergence of the finite element analysis, as given by Zienkiewicz (94). The first is that any required state of constant strain can be adequately reproduced on an element. A simple proof of this has been given by Irons (102). The second is that the displacement be continuous between adjacent elements; this condition is satisfied as can be seen by inspection of the shape functions used.

7.4.5. NUMERICAL INTEGRATION

There are many schemes for numerical evaluation of definite integrals. The Gauss quadrature (numerical integration) method will be outlined only, since it has proved most useful for finite element work (102, 103).

To evaluate the integral

$$\int_{-1}^{1} f(x)\, dx$$

by Gauss method, sets of discrete abscissae x_i and of the corresponding weight coefficients W_i are determined which may render the equation

$$\int_{-1}^{1} f(x)\, dx = \sum_{i=1}^{n} W_i\, f(x_i) \qquad (7.23)$$

exact for polynomials of a given degree. Gauss quadrature using n sampling points is exact if the integrand is a polynomial of degree (2n - 1) or less. Conversely, if the degree of f(x) is bigger then (2n - 1) then the Equation (7.23) is approximate for n sampling points; the error is of order $0(\Delta)^{2n}$.

Values of abscissae and weight coefficients of the Gaussian Quadrature are given for $n \leqslant 16$ by Kopal (104).

In two dimensions we obtain the quadrature formula by integrating first with respect to one co-ordinate and then with respect to the other:

$$I = \int_{-1}^{1}\int_{-1}^{1} f(x,y)\, dx\, dy = \int_{-1}^{1} \left[\sum_{i=1}^{n} W_i\, f(x_i,y)\right] dy$$

$$= \sum_{j=1}^{n} W_j \left[\sum_{i=1}^{n} W_i \, f(x_i, y_j) \right] = \sum_{j=1}^{n} \sum_{i=1}^{n} W_j \, W_i \, f(x_i, y_j) \qquad (7.24)$$

In the above the number of integrating points in each direction was assumed to be the same, but it is not essential to do so.

7.5. REPRESENTATION OF BOND AND LINKAGE ELEMENT STIFFNESS

The bond-slip characteristics of reinforced concrete members have been extensively investigated experimentally as described in section 6.2.2. This bond-slip behaviour is modelled in the present work by using closely spaced spring linkages, as suggested by Ngo and Scordelis (66) . Each bond linkage contains two springs one acting parallel to the bar axis and the other acting perpendicular to it. Such a linkage is shown conceptually in Figure 7.4. Each short segment of the bar is directly joined to the adjacent bar segments. In addition, it is connected to the adjacent concrete by longitudinal springs of stiffness k_h, and normal springs of stiffness k_v. The dimension of each spring may be reduced to zero without changing the concept. In practical cases it is usually convenient to specify one such linkage element at the top of a bar segment, and one at the bottom. The two springs in the linkage element are considered uncoupled, so that the longitudinal performance is independent of effects in the normal direction.

The bond linkage element is easily incorporated into a finite element idealization of a reinforced concrete member.

The steel elements are connected to the concrete elements through the linkage elements at nodal points. This is shown in Figure 7.5 where adjacent concrete and steel elements are shown separated for clarity. Actually the linkage elements have no physical dimensions at all, and only their mechanical properties are of importance. Thus for example linkage element (10) has its ends connected to concrete node 14 and the other end to steel node 13, however node 14 and node 13 actually occupy the same point in space.

To incorporate the linkage element into a finite element computer program, it is necessary to develop its stiffness matrix. Let the springs in the h and v directions have stiffness k_h and k_v, respectively. These stiffnesses can be obtained from experimental bond-slip curves, e.g.

$$k_h = \frac{du}{dd} A \qquad (7.25)$$

where u = local bond stress in h direction

d = local slip in h direction

$\frac{du}{dd}$ = slope of experimentally obtained bond-slip curves in h direction

A = bar surface area tributary to one spring, and given by

$$A = \frac{\pi D L}{2} \qquad (7.26)$$

where D = diameter of steel bar

L = spacing of springs

The factor 2 appears in the denominator if, as is usually convenient in two-dimensional idealisation, linkage elements are placed both at the top and at the bottom of the bar segment; however for the axi-symmetric case only one spring exists round the perimeter of the bar and the factor 2 disappears.

Hence from Equations (7.25) and (7.26) we have

$$k_h = \frac{du}{dd} \frac{\pi D L}{2} \qquad (7.27)$$

Let h and v axes define the orientation of the steel bar and be inclined at an angle θ with the x and y co-ordinate axes as shown in Figure 7.6. The matrix equation representing the uncoupled relationship between linkage force and spring deformation (local bond slip) is given by:

$$\begin{Bmatrix} F_h \\ F_v \end{Bmatrix} = \begin{bmatrix} k_h & 0 \\ 0 & k_v \end{bmatrix} \begin{Bmatrix} \delta_h \\ \delta_v \end{Bmatrix}$$

or

$$\{F_{hv}\} = [K_{hv}] \cdot \{\delta_{hv}\} \qquad (7.28)$$

The relationship between deformations in the h-v and x-y systems is given by :

$$\begin{Bmatrix} \delta_h \\ \delta_v \end{Bmatrix} = \begin{bmatrix} -\cos\theta & -\sin\theta & \cos\theta & \sin\theta \\ \sin\theta & -\cos\theta & -\sin\theta & \cos\theta \end{bmatrix} \begin{Bmatrix} \delta_{ix} \\ \delta_{iy} \\ \delta_{jx} \\ \delta_{jy} \end{Bmatrix}$$

or

$$\{\delta_{hv}\} = [TA] \cdot \{\delta_{xy}\} \tag{7.29}$$

Similarly the nodal forces in the x-y system are found by similar transformation :

$$\begin{Bmatrix} F_{ix} \\ F_{iy} \\ F_{jx} \\ F_{jy} \end{Bmatrix} = \begin{bmatrix} -\cos\theta & \sin\theta \\ -\sin\theta & -\cos\theta \\ \cos\theta & -\sin\theta \\ \sin\theta & \cos\theta \end{bmatrix} \begin{Bmatrix} F_h \\ F_v \end{Bmatrix}$$

or

$$\{F_{xy}\} = [TA]^T \cdot \{F_{hv}\} \tag{7.30}$$

Using Equations (7.28), (7.29) and (7.30) we get :

$$\begin{aligned} \{F_{xy}\} &= [TA]^T [K_{hv}] \{\delta_{hv}\} \\ &= [TA]^T [K_{hv}] [TA] \{\delta_{xy}\} \end{aligned} \tag{7.31}$$

The linkage element stiffness, in x-y co-ordinates, is therefore given by

$$[K_{xy}] = [TA]^T [K_{hv}] [TA] \tag{7.32}$$

Performing the indicated operations and letting $s = \sin\theta$ and $c = \cos\theta$, the complete stiffness matrix is obtained :

$$\left[K_{xy}\right] = \begin{bmatrix} k_h c^2+k_v s^2 & k_h sc-k_v sc & -k_h c^2-k_v s^2 & -k_h sc+k_v sc \\ k_h sc-k_v sc & k_h s^2+k_v c^2 & -k_h sc+k_v sc & -k_h s^2-k_v c^2 \\ -k_h c^2-k_v s^2 & -k_h sc+k_v sc & k_h c^2+k_v s^2 & k_h sc-k_v sc \\ -k_h sc+k_v sc & -k_h s^2-k_v c^2 & k_h sc-k_v sc & k_h s^2+k_v c^2 \end{bmatrix} \quad (7.33$$

For the particular case of h and v axes coinciding with the x and y axes respectively, i.e. $\theta = 0$, the above equation reduces to :

$$\left[K_{xy}\right] = \begin{bmatrix} k_h & 0 & -k_h & 0 \\ 0 & k_v & 0 & -k_v \\ -k_h & 0 & k_h & 0 \\ 0 & -k_v & 0 & k_v \end{bmatrix} \quad (7.34)$$

It is evident from Equation (7.25) that the stiffness of the linkage element is strictly non-linear. This was taken into account in the developed finite element program, using special non-linear techniques, described in section 7.10.

7.6. ASSEMBLY OF STRUCTURAL STIFFNESS MATRIX

The stiffness matrix of the complete structure can be obtained by the direct stiffness method superimposing appropriate stiffness contributions of all elements. This can be done by adding at each nodal point the appropriate stiffness contribution from every element meeting there. The structural stiffness term K_{ij} for the complete structure is the sum of all

forces acting on different elements meeting at nodal point i due to a unit displacement at nodal point j, and it exists only if i and j are connected by at least one element, of if i equals j, or i and j have been artificially connected to simulate some behaviour, otherwise K_{ij} is zero.

The assembly of the standard stiffness matrix can be programmed in the computer so that the terms of each element's stiffness matrix $[k]^e$ are put into the proper address of the structural stiffness matrix $[K]$ and all over-lapping terms from different elements are summed up. If the total number of kinematic degrees of freedom for the complete structure is n, a space of dimension (n x n) equal to the dimension of the $[K]$ matrix is cleared in the computer. A typical structural stiffness matrix is diagramatically shown in Figure 7.7, where it can be seen that it is symmetric and contains many zero terms and in particular there is a distance from the diagonal beyond which no terms exist. This is called banding of the matrix and the distance from the diagonal term to the last term in any row is called the semi-bandwidth.

The above method of storing the structural stiffness matrix in the computer is not the most economical since it contains a large number of zero terms. In practice the semi-bandwidth is usually less than $\frac{1}{10}$ of the matrix size. It is, therefore, usual to ignore most of the zero terms and to store $[K]$ in the form of band matrix. Also since $[K]$ is a symmetric matrix only the terms within the upper semi-bandwidth are stored into the computer as a one-dimensional array using a row-wise storage order. This is shown diagrammatically in Figure 7.7.

The band width of the structural stiffness matrix $[K]$ depends upon the degrees of freedom of each node and the largest difference of node numbers in all elements. By a judicious numbering of the nodal points the band width can be kept to a minimum.

7.7. INTRODUCTION OF BOUNDARY CONDITIONS

Prior to application of displacement boundary conditions, the structural stiffness matrix $[K]$ is singular, because it permits rigid body movements of the complete structure. Before $[K]$ can be inverted to determine the nodal displacements, it is necessary to provide sufficient kinematic restraints to the structure to prevent all rigid body movements. Also in some cases it may be desirable to prescribe some known displacements at some nodes.

There exist many methods of introducing boundary conditions, but some are not well adapted to computer programming, especially if the band storage format is adopted. Zienkiewicz (94) introduces boundary conditions by using an artifice due to Payne and Irons. This method has been adopted in this work and is explained below :

Assuming that we have a set of n equations

$$\begin{bmatrix} k_{11} & k_{12} & \cdots & k_{1m} & \cdots & k_{1n} \\ k_{21} & k_{22} & \cdots & k_{2m} & \cdots & k_{2n} \\ \vdots & \vdots & & \vdots & & \vdots \\ k_{m1} & k_{m2} & \cdots & k_{mm} & \cdots & k_{mn} \\ \vdots & \vdots & & \vdots & & \vdots \\ k_{n1} & k_{n2} & \cdots & k_{nm} & \cdots & k_{nn} \end{bmatrix} \begin{Bmatrix} u_1 \\ u_2 \\ \vdots \\ u_m \\ \vdots \\ u_n \end{Bmatrix} = \begin{Bmatrix} F_1 \\ F_2 \\ \vdots \\ F_m \\ \vdots \\ F_n \end{Bmatrix} \qquad (7.35)$$

we want to introduce the boundary condition $u_m = c$, where c is a constant prescribed displacement. This can be done by

(a) multiplying the diagonal coefficient of the above matrix $[K]$ at the point concerned, m, by a large number, say, 10^8 and

(b) replacing the term on the right hand side of the equation by the newly formed diagonal term multiplied by the prescribed displacement value c.

This has the effect of replacing the particular equation by one stating that the displacement in question is equal to the specified value, and retaining this equation in the system to be solved. This can be seen by considering the row in question, m, of the matrix $[K]$:

$$k_{m1}u_1 + k_{m2}u_2 + \ldots + k_{mm}u_m + \ldots + k_{mn}u_n = F_m$$

or

$$\sum_{i=1}^{m-1} k_{mi}u_i + k_{mm}u_m + \sum_{i=m+1}^{n} k_{mi}u_i = F_m \qquad (7.36)$$

and introducing the boundary condition we get :

$$\sum_{i=1}^{m-1} k_{mi}u_i + (k_{mm}\cdot 10^8)u_m + \sum_{i=m+1}^{n} k_{mi}u_i = (k_{mm}\cdot 10^8\cdot c) \qquad (7.37)$$

Considering the left hand side of the above equation it can be seen that the middle term is very much bigger than the other two terms, and thus we can write with a quite good approximation

that

$$(k_{mm} \cdot 10^8) u_m = k_{mm} \cdot 10^8 \cdot c$$

or

$$u_m = c \qquad (7.38)$$

which was to be proved.

The above method of introducing the boundary condition is very easy to program and can easily be applied to matrices which have been band stored.

7.8. SOLUTION OF EQUILIBRIUM EQUATIONS

A key factor in any finite element program is the subroutine for the solution of simultaneous equations. A very wide range of numerical methods exist for the solution of linear simultaneous equations and where a small number of equations is involved the method chosen is immaterial. For large numbers, however, it is important to choose the most economical in computer time and storage, and also the one best suited to take advantage of any special properties the equations may possess.

The two classes of solution method available are termed direct and indirect methods. In the former a single set of operations is carried out on the equations and the results are obtained, while in the latter, solution is attempted by a series of successive approximations. A set of operations, usually much shorter than with a direct method, is repeated several times while the results either converge towards a steady level

or show no definite trend. The only inaccuracy in the direct method is due to values being stored in the computer at each stage of the calculation to a limited number of decimal places, and fortunately structural problems are generally sufficiently well conditioned for this not to be a serious problem. The indirect methods, however, have the additional disadvantages that the rate of convergence may be slow, or the results may not converge at all, and for these reasons direct methods are to be preferred whenever possible.

A method which is particularly well suited to the solution of structural equations is Choleski's triangular decomposition method. This method was adopted in this work and was suitably modified to reduce demands on computer storage and time by taking advantage of the symmetry and banded nature of the structural stiffness matrix. This method is explained below :

Consider the structural stiffness equation

$$\left[K\right] \cdot \left\{\delta\right\} = \left\{F\right\} \qquad (7.39)$$

where $\left[K\right]$ = structural stiffness matrix
$\left\{\delta\right\}$ = nodal displacement vector
$\left\{F\right\}$ = nodal force vector

$\left[K\right]$ can be factored in the form

$$\left[K\right] = \left[L\right] \cdot \left[U\right] \qquad (7.40)$$

where $\left[L\right]$ and $\left[U\right]$ are lower and upper triangular matrices. Since $\left[K\right]$ is symmetric it can be arranged that

$$\left[L\right] = \left[U\right]^T \qquad (7.41)$$

and therefore

$$\left[K\right] = \left[U\right]^T \cdot \left[U\right] \tag{7.42}$$

Substituting Equation (7.42) in Equation (7.39),

$$\left[U\right]^T \cdot \left[U\right] \cdot \left\{\delta\right\} = \left\{F\right\} \tag{7.43}$$

Putting

$$\left[U\right] \cdot \left\{\delta\right\} = \left\{X\right\} \tag{7.44}$$

then

$$\left[U\right]^T \cdot \left\{X\right\} = \left\{F\right\} \tag{7.45}$$

Having found the upper triangular factor matrix $\left[U\right]$ from Equation (7.42), the process consists of solving Equation (7.45) for $\left\{X\right\}$ and then solving Equation (7.44) for $\left\{\delta\right\}$.

Since the structural stiffness matrix $\left[K\right]$ is a band matrix, of semi-band width B then it is not difficult to show that the factor matrices $\left[U\right]$ and $\left[U\right]^T$ are also band matrices with a semi-band width B. Thus Equation (7.42) has the form shown in Figure 7.8. The elements of the matrix $\left[U\right]$, and hence $\left[U\right]^T$, may be computed, using the rule for matrix multiplication, as follows :

$$\left\{\begin{array}{lll}
u_{11} = \sqrt{k_{11}} & & \\
u_{1i} = \dfrac{k_{1i}}{u_{11}} & & \\
u_{ii} = \sqrt{k_{ii} - \sum_{m=1}^{i-1} u_{mi}^2} \; ; & & (i>1) \\
u_{ij} = \dfrac{k_{ij} - \sum_{m=1}^{i-1} u_{mi}\, u_{mj}}{u_{ii}} \; ; & & (j>i) \\
u_{ij} = 0 \; ; & & (i>j)
\end{array}\right\} \tag{7.46}$$

and the elements of $[K]$ are overwritten by the elements of $[U]$ as they are calculated.

The evaluation of $\{X\}$ from Equation (7.45) can be carried out by forward substitution, starting with x_1, as follows :

$$\left.\begin{aligned} x_1 &= \frac{f_1}{u_{11}} \\ x_i &= \frac{f_i - \sum_{m=1}^{i-1} u_{mi}\, x_m}{u_{ii}} \; ; \qquad (i>1) \end{aligned}\right\} \qquad (7.47)$$

and the elements of $\{F\}$ are overwritten by the elements of $\{X\}$ as they are calculated.

The solutions $\{\delta\}$ are then found by backward substitution using Equation (7.44), commencing the process with the last equation, as follows :

$$\left.\begin{aligned} \delta_n &= \frac{x_n}{u_{nn}} \\ \delta_i &= \frac{x_i - \sum_{m=i+1}^{n} u_{im}\, \delta_m}{u_{ii}} \; ; \qquad (i<n) \end{aligned}\right\} \qquad (7.48)$$

The elements of $\{\delta\}$ as they are calculated they are stored in the vector $\{F\}$.

The Choleski method is a very efficient method of solving structural equations when advantage is taken of the

symmetry and banded form that they possess. By simply counting operations (105) one may conclude that computer execution time is approximately proportional to $\frac{nB^2}{2}$, as compared with approximately $\frac{n^3}{6}$ for a full symmetric matrix. In practice B is usually less than $\frac{n}{10}$, which means that execution time is only $3\frac{1}{2}$ % of that without taking advantage of banding.

7.9. MATERIAL PROPERTIES

7.9.1. CONCRETE STRESS-STRAIN RELATIONS

For many years a large number of experimental investigations have been carried out on the behaviour of concrete under multi-axial stresses. A variety of different shaped specimens, of different types of concrete, subjected to various loading and testing conditions have been tested. But still a consistent picture of behaviour has not been obtained.

Large differences have been found between the results of different investigations which are largely attributed to the difficulties in producing stress fields that are independent of machine and testing effects. Rigid platens or grips restraining the lateral movement of the end of specimens introduce complex and indefinable stress states. A number of investigations have been directed towards developing specimens free from this influence, so that results would represent fundamental properties of concrete. Finally, most tests, under multi-axial stresses, were primarily concerned with assessing strength characteristics to the exclusion of stress-strain relations.

In the present analytical study, because of the complex non-linear finite element techniques required to deal

with bond between concrete and steel and tensile cracking of the concrete elements, the simplifying assumption was made that concrete, prior to cracking, is a homogeneous, isotropic material. The modulus of elasticity and the Poisson's ratio of concrete were, therefore, taken to be constant and the same in all directions.

The adopted idealised stress-strain (σ-ε) relation for concrete in compression, as well as in tension, is shown in Figure 7.9. It's slope in compression was taken as equal to the slope at the origin of the experimentally determined σ-ε curve, shown in Figure 3.1. This was obtained from axially loaded cylinders, as described in section 3.1.1. The maximum compressive stress was taken as equal to 80 % of the 28-day cube strength (being approximately equal to the 28-day cylinder strength). A maximum compressive strain of 0.0035 was specified although no crushing of the concrete was expected in the specimens to be analysed. The σ-ε curve in tension was also taken as linear and having a slope equal to that in compression. The maximum tensile stress that concrete can carry was taken equal to the experimentally determined 28-day cylinder splitting strength.

7.9.2. STRENGTH CRITERIA FOR CONCRETE

There have been several proposals for concrete failure under complex states of stress, but there is still no satisfactory criterion which explains all aspects of failure. Nevertheless there is in general agreement about the definite existence of two types of failure. These are :

(i) Brittle or cleavage-type failure under predominantly tensile stresses.

(ii) Ductile or shear-type failure under compressive stresses.

In compression-tension regimes, there is a transition from one type to the other which depends to a large extent on the internal structure of concrete.

The above suggest that two independent concrete failure criteria are required : one for cleavage-type tensile failure and the other for shear-type compressive failure. In the specimens to be analysed in this work, concrete failure is restricted to the cleavage-type tensile case. This is so because in the tension specimens concrete is in tension, while the pull-out specimens were not loaded high enough to produce concrete compressive failure. Thus criteria for concrete failure in tension are only required in this work.

Two theories are commonly used to predict tensile cracking failure. In the maximum stress theory it is assumed that cracking occurs, under biaxial or triaxial stress, when the maximum tensile stress in any direction exceeds a limiting value of tensile stress. This is usually equal to the tensile stress producing failure in an axially loaded test specimen. In the maximum strain theory, it is assumed that cracking occurs when a maximum tensile strain reaches a limiting value. These two theories are very similar and in the particular case when $\nu = 0$ they are identical. The most commonly used theory of the two is the maximum stress theory. This was also the one adopted in the present investigation. The limiting value of tensile stress was taken equal to the tensile strength of a cylinder

in the standard split test.

7.9.3. STEEL STRESS-STRAIN RELATIONS

The stress-strain curve of the Welbond hot rolled deformed bar, used in the bond test programme, was determined as described in section 3.4, and shown in Figure 5.1. This is seen to be nearly linear up to 80 % of the characteristic strength of the bar. Since the maximum applied stress in the members to be analysed did not exceed this value, the adopted steel $\sigma - \varepsilon$ curve in the finite element program was taken as linear (Figure 7.9), with a modulus of elasticity equal to 200,000 N/mm^2, as determined experimentally.

7.10 NON-LINEAR SOLUTION METHODS

7.10.1. GENERAL

In the finite element formulation, described in the previous sections of this chapter, linear elastic behaviour was assumed. This was implied using

(a) a linear form of strain displacement relationships (see Equations (7.5) and (7.6)), and

(b) a linear form of stress-strain relationships (see Equation (7.7)).

But concrete, like most other materials, behaves non-elastically and non-linearly. Effects, which are of importance in the present study, such as the concrete's cracking and bond, all supersede the simple linear elasticity assumptions. Effects like these can be tackled by using non-linear solution methods, in which a series of linear problems are solved such

that at the final stage the appropriate non-linear conditions are satisfied. Thus the finite element method can still be used for analysing such problems.

A non-linear structural problem must obey the fundamental conditions of continuum mechanics, i.e. equilibrium, compatibility and the constitutive relations of the materials. As the Finite Element Method automatically satisfies the compatibility requirements at any stage, any solution process seeks to satisfy the given non-linear relationships whilst preserving equilibrium. At any stage, "out-of-balance" residual forces will generally exist due to departure from the linear behaviour, and these upset the equilibrium of the structure. The removal of these residuals by a succession of linear solutions is the basic step in all iterative solution processes.

Several methods have been developed for solving non-linear problems but none is general enough to cover all cases. In some non-linear problems the solution is not always unique and the solution achieved may not be the one required. It is important in this respect to have some physical insight into the nature of the problem and thus recognize an unacceptable solution. Iterative solution methods are most suitable in finite element analysis and are reviewed in the next section. The solution method adopted in this work is also given.

7.10.2. BASIC NON-LINEAR ITERATIVE SOLUTION METHODS

7.10.2.1. GENERAL EQUATIONS

Several iterative methods have been developed for the solution of the assembled stiffness equations of non-linear

problems, given by

$$\left[K\right]\left\{\delta\right\} - \left\{R\right\} = \left\{0\right\} \qquad (7.49)$$

and possessing a non-linear constitutive law of the form

$$f\left(\left\{\sigma\right\}, \left\{\varepsilon\right\}\right) = \left\{0\right\} \qquad (7.50)$$

This is done by replacing the non-linear constitutive law by an equivalent linear elastic (given by Equation (7.7)), i.e.

$$\left\{\sigma\right\} = \left[D\right]\left(\left\{\varepsilon\right\} - \left\{\varepsilon_o\right\}\right) + \left\{\sigma_o\right\} \qquad (7.51)$$

and by iterative means one or more of the parameters $\left[D\right]$, $\left\{\varepsilon_o\right\}$ or $\left\{\sigma_o\right\}$ are adjusted in this equation so that the final solution given by Equation (7.49) satisfies Equation (7.50).

Which of the three quantities mentioned above is to be adjusted in the iteration process depends on :

(a) the solution method used in the equivalent elastic problem,

(b) the nature of the physical law defining the stress-strain relation.

The various existing iteration processes can be broadly classified into two categories :

(a) The "variable stiffness" processes, in which the iteration is conducted by adjustment of the elasticity matrix $\left[D\right]$.

(b) The "constant stiffness" processes in which the iteration is conducted by adjustment of the initial strain matrix $\left\{\varepsilon_o\right\}$ or the initial stress matrix $\left\{\sigma_o\right\}$.

Combinations of the two basic procedures have also been used.

7.10.2.2. "VARIABLE STIFFNESS" METHODS

"Variable stiffness" methods are those in which the elasticity matrix $[D]$ is adjusted according to the stress or strain level reached. The problem is resolved for the same load with the new elastic constants and the process repeated until no further displacement occurs. In mathematical terms, as the elasticity matrix influences the final stiffness matrix $[K]$ of the assembly and

$$[D] = [D(\{\varepsilon\})] = [D(\{\delta\})] \qquad (7.52)$$

the problem reduces to the solution of

$$\{\psi\} = [K(\{\delta\})]\{\delta\} - \{R\} = \{0\} \qquad (7.53)$$

which can be obtained iteratively in different ways. Such a simple iterative scheme is as follows :

(a) Take $\{\delta\}_0 = 0$ and evaluate $[K(\{\delta\}_0)] = [K_0]$

(b) Solve Equation (7.53) for $\{\delta\}_1 = [K_0]^{-1} \cdot \{R\}$

(c) Repeat the process with

$$\{\delta\}_n = [K_{n-1}]^{-1} \cdot \{R\}$$

until no further displacement changes occur. It is usual to use a tangent stiffness value or a secant stiffness value for $[K_{n-1}]$. These two alternatives are illustrated in Figure 7.10 for a one-dimentional case.

A serious disadvantage of "variable stiffness" methods is that the required recalculation of the stiffness matrix $[K]$ of the assembly at each iteration is from the computational point of view an expensive operation. Therefore "constant

stiffness" processes are generally favoured.

7.10.2.3. "INITIAL STRAIN" METHOD

If $\{\varepsilon_o\}$ is adjusted, the process becomes the "initial strain" method, and is used when strains can be given in terms of stresses, i.e. Equation (7.50) takes the form

$$\{\varepsilon\} = f\left(\{\sigma\}\right) \qquad (7.54)$$

The elastic strains obtained at every stage are compared with those given by Equation (7.54) and the difference is used as an initial strain. These are then converted to equivalent nodal forces (given by Equation (7.11)), i.e.

$$\{R\}_o = \int_{vol} [B]^T [D] \{\varepsilon_o\} \, d(vol) \qquad (7.55)$$

and redistributed elastically. The iteration is repeated until $\{\varepsilon_o\}$ becomes sufficiently small. The details of the iterations are similar to those used in "initial stress" methods and described in the next section. The "initial strain" method is illustrated in Figure 7.11a for a one-dimensional case.

The advantage of "initial strain" methods is that at every stage of the iterations the same stiffness matrix $[K]$ of the assembly is used and if this is once inverted, each step can be accomplished in a fraction of time required for the first solution.

7.10.2.4. "INITIAL STRESS" METHOD

An alternative constant stiffness method is the "initial

stress" method, in which $\{\sigma_o\}$ is adjusted. This is useful when stresses are expressed in terms of strains, i.e.

$$\{\sigma\} = f(\{\varepsilon\}) \tag{7.56}$$

The problem is solved first elastically for a typical load increment $\Delta\{R\}$ using the original stiffness matrix $[K_o]$ and a first approximation is obtained, i.e.

$$\Delta\{\delta_o\} = [K_o]^{-1} \Delta\{R\} \tag{7.57}$$

The corresponding elastic stresses $\Delta\{\sigma_e\}$ are then calculated and compared with those given by Equation (7.56) and their difference is used as an initial stress which is redistributed elastically by calculating equivalent nodal forces (given by Equation (7.12)), i.e.

$$\Delta\{\sigma_o\} = \Delta\{\sigma_e\} - \Delta\{\sigma\} \tag{7.58}$$

and

$$\Delta\{R\}_o = \int_{vol} [B]^T \Delta\{\sigma_o\} \, d(vol) \tag{7.59}$$

A correction to the displacements is thus obtained and given by

$$\Delta\{\delta\}_1 = [K_o]^{-1} \Delta\{R\}_o \tag{7.60}$$

and the iteration continues using the recurrence relation

$$\Delta\{\delta\}_n = [K_o]^{-1} \Delta\{R\}_{n-1} \tag{7.61}$$

until $\Delta\{R\}_n$ is sufficiently small. The final displacement in this load increment is given by

$$\Delta\{\delta\} = \Delta\{\delta\}_o + \sum_{i=1}^{n} \Delta\{\delta\}_i \qquad (7.62)$$

The "initial stress" method is illustrated in Figure 7.11b for a one-dimensional case.

This method has the advantage of using the same stiffness matrix $[K]$ of the assembly during the iterations and also it has a distinct physical significance. The initial stresses are those released by the material no longer being able to sustain them and thus they are transferred to surrounding material in order to restore equilibrium. Indeed "stress transfer" was the name originally given to this process by Zienkiewicz et al (68) in the solution of "no-tension" problems.

The three non-linear solution methods described above are illustrated in Figure 7.12 for incremental loading of a member of a structure possessing a non-linear constitutive law.

7.10.2.5. COMBINATION OF VARIABLE AND CONSTANT STIFFNESS METHODS

As stated previously, "variable stiffness" methods suffer from the disadvantage that a complete reformulation of the stiffness matrix and a new solution of equations is required for each iteration. On the other hand, although the same stiffness matrix is used at every stage in "constant stiffness" methods and therefore an advantage in solution time per iteration is gained over the "variable stiffness" approach, good convergence cannot always be guarranteed. A compromise often used in such cases is to combine the two solution methods by updating the stiffness every so often.

7.10.3. NON-LINEAR SOLUTION METHOD ADOPTED IN THIS WORK

The non-linear solution method adopted in this work to deal with the non-linear stiffness of the bond linkage elements was a combination of "variable" and "initial stress" (constant stiffness) methods. At the end of each iteration of the "initial stress" process, convergence was checked and if the error in stress was more than 1 % of the total allowable stress, there were further iterations carried out. If convergence was not achieved within five iterations, the stiffness of the elements was updated and further iterations were carried out with the new stiffness until the percentage error in stress was less than 1 %.

7.11. CRACKING OF CONCRETE ELEMENTS

7.11.1. CRACK FORMATION

The formation and propagation of cracks have been based on the following assumptions :

(i) The maximum stress criterion is used, i.e. when a principal stress exceeds the limiting tensile stress, the material cracks in a plane normal to this principal stress. The crack formed passes through the centroid of the element.

(ii) Concrete is assumed to be homogeneous and isotropic prior to cracking, exhibiting a linear elastic tensile stress-tensile strain relation. However, the material becomes orthotropic as it undergoes fracture, because it is not capable of sustaining stresses normal to the direction of the crack. Therefore the modulus of elasticity normal to the crack is instantaneously reduced to zero and it is assumed that no interaction occurs

between this and the other directions. The assumed concrete tensile elastic-fracture model is shown in Figure 7.13. In addition, the tensile stresses developed in a concrete element at the time of appearance of the crack must be released and the stresses redistributed in the adjacent elements.

(iii) Since the element loses all the stiffness normal to the crack, stresses and strains have no meaning in that direction. But material parallel to the crack is still capable of carrying stress, given by new constitutive relationships. The cracking model used is shown in Figure 7.14.

(iv) On further loading, it is possible that new cracks will occur at some angle to the first crack.

(v) Also it is possible that on further loading a cracked element may experience a reversal of stresses and the crack may actually close. The element should then be capable of developing tensile stresses normal to the crack. But there is now a plane of weakness along the crack and the behaviour of the material becomes complicated. Thus in the absence of any relevant experimental data and for simplicity, no such possibility is envisaged in the present analysis.

7.11.2. SHEAR ON OPEN CRACKS

The surfaces of a typical cleavage crack are in general rough and irregular. When the opposite faces of a crack are subjected to parallel movement, there is aggregate interlocking restraining this movement. For a large enough crack width, the surfaces would completely separate and interlock would cease.

Aggregate interlocking is a complex phenomenon depending on many factors, which have not been adequately investigated so far. Nevertheless one of the most important effects of interlocking is that shear stress exists along a crack. In the present work, in the absence of more precise experimental information, interlocking is taken into account by assuming the shear stress to be a linear function of shear strain along the crack, i.e.

$$\tau^{*} = a\, G\, \gamma^{*} \qquad (7.63)$$

where τ^{*} = shear stress along crack

γ^{*} = shear strain along crack

G = modulus of rigidity of concrete

a = constant having values $0 \leqslant a \leqslant 1$

7.11.3. AXI-SYMMETRIC CONDITIONS

This work is concerned with axi-symmetric concrete members and therefore crack prediction is simpler than in the general three dimensional case described above. Since in axi-symmetric members hoop stresses and strains are principal quantities, cracks caused by these will always be in radial planes. All other cracks are similar to those in plane problems, with the exception that they are now circumferential. The different possible types of cracks in axi-symmetric members are shown in Figure 7.15, together with cracks in 2-dimensional members for comparison purposes.

7.11.4. CONSTITUTIVE RELATIONS

For uncracked, isotropic materials the incremental constitutive laws in global co-ordinates, in the axi-symmetric case are given by Equations (7.7) and (7.9), which could be also written in a slightly different form as :

$$\begin{Bmatrix} \Delta\sigma_r \\ \Delta\sigma_z \\ \Delta\tau_{rz} \\ \Delta\sigma_\theta \end{Bmatrix} = \frac{E(1-\nu)}{(1+\nu)(1-2\nu)} \begin{bmatrix} 1 & \frac{\nu}{1-\nu} & 0 & \frac{\nu}{1-\nu} \\ \frac{\nu}{1-\nu} & 1 & 0 & \frac{\nu}{1-\nu} \\ 0 & 0 & \frac{G(1+\nu)(1-2\nu)}{E(1-\nu)} & 0 \\ \frac{\nu}{1-\nu} & \frac{\nu}{1-\nu} & 0 & 1 \end{bmatrix} \begin{Bmatrix} \Delta\varepsilon_r \\ \Delta\varepsilon_z \\ \Delta\gamma_{rz} \\ \Delta\varepsilon_\theta \end{Bmatrix} \qquad (7.64)$$

Thus

$$\Delta\{\sigma\} = [D_T].\Delta\{\varepsilon\} \qquad (7.65)$$

where $[D_T]$ is the tangential elasticity matrix.

When an element cracks orthotropic conditions are produced and new incremental constitutive relations will apply for the material parallel to the cracks. Although no stresses exist across the crack, the form of the $[D_T]$ matrix is preserved by reducing the corresponding terms to zero. Also a shear term is introduced to account for any aggregate interlocking. For axi-symmetric problems, the incremental constitutive relations have one of the following forms depending on whether one or more of the three possible types of cracks (Figure 7.15) have formed :

(i) For one circumferential crack :

$$\begin{Bmatrix} \Delta\varepsilon_n^* \\ \Delta\varepsilon_t^* \\ \Delta\gamma^* \\ \Delta\varepsilon_\theta^* \end{Bmatrix} = \frac{1}{E} \begin{bmatrix} 0 & 0 & 0 & 0 \\ 0 & 1 & 0 & -\nu \\ 0 & 0 & \frac{E}{aG} & 0 \\ 0 & -\nu & 0 & 0 \end{bmatrix} \begin{Bmatrix} \Delta\sigma_n^* \\ \Delta\sigma_t^* \\ \Delta\tau^* \\ \Delta\sigma_\theta^* \end{Bmatrix}$$

and inverting we get

$$\begin{Bmatrix} \Delta\sigma_n^* \\ \Delta\sigma_t^* \\ \Delta\tau^* \\ \Delta\sigma_\theta^* \end{Bmatrix} = \begin{bmatrix} 0 & 0 & 0 & 0 \\ 0 & \frac{E}{1-\nu^2} & 0 & \frac{\nu E}{1-\nu^2} \\ 0 & 0 & aG & 0 \\ 0 & \frac{\nu E}{1-\nu^2} & 0 & \frac{E}{1-\nu^2} \end{bmatrix} \begin{Bmatrix} \Delta\varepsilon_n^* \\ \Delta\varepsilon_t^* \\ \Delta\gamma^* \\ \Delta\varepsilon_\theta^* \end{Bmatrix} \qquad (7.66)$$

where $*$ denotes stresses and strains in the local (crack) axes, which are defined as normal and tangential to a crack formed at an angle φ_c with the r-global axis, as shown in Figure 7.16.

(ii) For two circumferential cracks :

$$\begin{Bmatrix} \Delta\varepsilon_n^* \\ \Delta\varepsilon_t^* \\ \Delta\gamma^* \\ \Delta\varepsilon_\theta^* \end{Bmatrix} = \frac{1}{E} \begin{bmatrix} 0 & 0 & 0 & 0 \\ 0 & 0 & 0 & 0 \\ 0 & 0 & 0 & 0 \\ 0 & 0 & 0 & 1 \end{bmatrix} \begin{Bmatrix} \Delta\sigma_n^* \\ \Delta\sigma_t^* \\ \Delta\tau^* \\ \Delta\sigma_\theta^* \end{Bmatrix}$$

and inverting we get

$$\begin{Bmatrix} \Delta\sigma_n^* \\ \Delta\sigma_t^* \\ \Delta\tau^* \\ \Delta\sigma_\theta^* \end{Bmatrix} = \begin{bmatrix} 0 & 0 & 0 & 0 \\ 0 & 0 & 0 & 0 \\ 0 & 0 & 0 & 0 \\ 0 & 0 & 0 & E \end{bmatrix} \begin{Bmatrix} \Delta\varepsilon_n^* \\ \Delta\varepsilon_t^* \\ \Delta\gamma^* \\ \Delta\varepsilon_\theta^* \end{Bmatrix} \qquad (7.67)$$

(iii) For a radial crack :

$$\begin{Bmatrix} \Delta\varepsilon_n^* \\ \Delta\varepsilon_t^* \\ \Delta\gamma^* \\ \Delta\varepsilon_\theta^* \end{Bmatrix} = \frac{1}{E} \begin{bmatrix} 1 & -\nu & 0 & 0 \\ -\nu & 1 & 0 & 0 \\ 0 & 0 & \frac{E}{aG} & 0 \\ 0 & 0 & 0 & 0 \end{bmatrix} \begin{Bmatrix} \Delta\sigma_n^* \\ \Delta\sigma_t^* \\ \Delta\tau^* \\ \Delta\sigma_\theta^* \end{Bmatrix}$$

and inverting we get

$$\begin{Bmatrix} \Delta\sigma_n^* \\ \Delta\sigma_t^* \\ \Delta\tau^* \\ \Delta\sigma_\theta^* \end{Bmatrix} = \begin{bmatrix} \frac{E}{1-\nu^2} & \frac{\nu E}{1-\nu^2} & 0 & 0 \\ \frac{\nu E}{1-\nu^2} & \frac{E}{1-\nu^2} & 0 & 0 \\ 0 & 0 & aG & 0 \\ 0 & 0 & 0 & 0 \end{bmatrix} \begin{Bmatrix} \Delta\varepsilon_n^* \\ \Delta\varepsilon_t^* \\ \Delta\gamma^* \\ \Delta\varepsilon_\theta^* \end{Bmatrix} \qquad (7.68)$$

(iv) For one circumferential and one radial crack :

$$\begin{Bmatrix} \Delta\varepsilon_n^* \\ \Delta\varepsilon_t^* \\ \Delta\gamma^* \\ \Delta\varepsilon_\theta^* \end{Bmatrix} = \frac{1}{E} \begin{bmatrix} 0 & 0 & 0 & 0 \\ 0 & 1 & 0 & 0 \\ 0 & 0 & \frac{E}{aG} & 0 \\ 0 & 0 & 0 & 0 \end{bmatrix} \begin{Bmatrix} \Delta\sigma_n^* \\ \Delta\sigma_t^* \\ \Delta\tau^* \\ \Delta\sigma_\theta^* \end{Bmatrix}$$

and inverting we get

$$\begin{Bmatrix} \Delta\sigma_n^* \\ \Delta\sigma_t^* \\ \Delta\tau^* \\ \Delta\sigma_\theta^* \end{Bmatrix} = \begin{bmatrix} 0 & 0 & 0 & 0 \\ 0 & E & 0 & 0 \\ 0 & 0 & aG & 0 \\ 0 & 0 & 0 & 0 \end{bmatrix} \begin{Bmatrix} \Delta\varepsilon_n^* \\ \Delta\varepsilon_t^* \\ \Delta\gamma^* \\ \Delta\varepsilon_\theta^* \end{Bmatrix} \qquad (7.69)$$

(v) For two circumferential and one radial cracks :

$$\begin{Bmatrix} \Delta\sigma_n^* \\ \Delta\sigma_t^* \\ \Delta\tau^* \\ \Delta\sigma_\theta^* \end{Bmatrix} = \frac{1}{E} \begin{bmatrix} 0 & 0 & 0 & 0 \\ 0 & 0 & 0 & 0 \\ 0 & 0 & 0 & 0 \\ 0 & 0 & 0 & 0 \end{bmatrix} \begin{Bmatrix} \Delta\varepsilon_n^* \\ \Delta\varepsilon_t^* \\ \Delta\gamma^* \\ \Delta\varepsilon_\theta^* \end{Bmatrix} \qquad (7.70)$$

Thus for all the above cases

$$\Delta\{\sigma\}^* = [D_T]^* . \Delta\{\varepsilon\}^* \qquad (7.71)$$

where $[D_T]^*$ is the tangent elasticity matrix in crack directions.

As $[D_T]^*$ is constructed in a local co-ordinate system, it is necessary to transform it back into the global co-ordinate system for stiffness calculations. This is done as follows :

The two sets of strains in the two co-ordinate systems are related by the following well-known transformation rule (101), where $c=\cos\varphi_c$ and $s=\sin\varphi_c$

$$\begin{Bmatrix} \Delta\varepsilon_r^* \\ \Delta\varepsilon_z^* \\ \Delta\gamma_{rz}^* \\ \Delta\varepsilon_\theta^* \end{Bmatrix} = \begin{bmatrix} c^2 & s^2 & sc & 0 \\ s^2 & c^2 & -sc & 0 \\ -2sc & 2sc & c^2-s^2 & 0 \\ 0 & 0 & 0 & 1 \end{bmatrix} \begin{Bmatrix} \Delta\varepsilon_r \\ \Delta\varepsilon_z \\ \Delta\gamma_{rz} \\ \Delta\varepsilon_\theta \end{Bmatrix} \qquad (7.72)$$

i.e.

$$\Delta\{\varepsilon\}^* = [R] . \Delta\{\varepsilon\} \qquad (7.73)$$

Now since work done is independent of the co-ordinate system, then

$$\left(\Delta\{\varepsilon\}^*\right)^T . \Delta\{\sigma\}^* = \left(\Delta\{\varepsilon\}\right)^T . \Delta\{\sigma\} \qquad (7.74)$$

Substituting Equations (7.65), (7.71) and (7.73) into (7.74) we get :

$$\left[D_T\right] = \left[R\right]^T \cdot \left[D_T\right]^* \cdot \left[R\right] \qquad (7.75)$$

7.11.5. RELEASE OF TENSILE STRESSES IN CRACKED ELEMENTS

Fracture of a concrete element occurs when one or more of its principal stresses exceed the limiting tensile stress. Then two modifications are needed :

(i) The $\left[D_T\right]$ matrix of the uncracked element must be replaced by one taking account of cracking and of rotation of the axes, as described in the previous section, and

(ii) The tensile stresses developed in the element at the time of cracking cannot be supported by it since it is cracked and should therefore be released by redistributing them into the adjacent concrete elements. This is shown how it can be done in the following :

Let the principal stresses at the centroid of an element be given by

$$\left\{\sigma\right\}_p = \begin{Bmatrix} \sigma_1 \\ \sigma_2 \\ \tau_{12} \\ \sigma_\theta \end{Bmatrix}$$

where τ_{12} is equal to zero and σ_1 is the maximum principal stress. After cracking, i.e. when σ_1 exceeds the limiting tensile stress, the element cannot sustain the stress σ_1 normal to the crack. The stresses released are, therefore, given by

$$\{\sigma_{rel}\}_p = \begin{Bmatrix} \sigma_1 \\ 0 \\ 0 \\ 0 \end{Bmatrix}$$

which are defined in the principal local (or crack) co-ordinate system. The equivilent released stresses in the global r-z system can be found by using the following well-known transformation rule (101), where $c=\cos\varphi_c$ and $s=\sin\varphi_c$

$$\{\sigma_{rel}\}_r = [Q]^{-1} \{\sigma_{rel}\}_p \qquad (7.76)$$

where

$$[Q]^{-1} = \begin{bmatrix} c^2 & s^2 & -2sc & 0 \\ s^2 & c^2 & 2sc & 0 \\ sc & -sc & c^2-s^2 & 0 \\ 0 & 0 & 0 & 1 \end{bmatrix} \qquad (7.77)$$

Therefore from

$$\{\sigma_{rel}\}_r = \begin{Bmatrix} \sigma_1 . c^2 \\ \sigma_1 . s^2 \\ \sigma_1 . sc \\ 0 \end{Bmatrix} \qquad (7.78)$$

The released stresses given by Equation (7.78) can be used to find equivalent nodal forces, in the global system, to be applied at the nodes of the cracked element, so that the stresses normal to the crack are redistributed to the adjacent

concrete elements. These equivalent nodal forces can be calculated using Equation (7.78), i.e.

$$\left\{F_{rel}\right\}_r = 2\pi \int\int \left[B\right]^T \left\{\sigma_{rel}\right\}_r r \, dr \, dz \qquad (7.79)$$

where $\left[B\right]$ is the element strain matrix.

7.11.6. CRACKING PROCEDURE

The main steps of the cracking procedure are as follows :

(i) Analyse the structure for displacements, strains and stresses for each increment of load and at the end of each increment calculate the total displacements, strains and stresses.

(ii) Find the element or elements that crack at any stage of loading.

(iii) Calculate nodal forces equivalent to the tensile stresses to be released in the just cracked elements.

(iv) Modify the elasticity matrix $\left[D\right]$ of the just cracked elements, to take account of the loss of stiffness normal to cracks.

(v) Reanalyse the member with modified elasticity matrix and under equivalent nodal forces for displacements, strains and stresses.

(vi) Superimpose the results obtained at (v) on the values obtained at (i) and check again for further cracking. If no more elements crack, proceed with the next load stage, otherwise repeat steps (iii) to (vi).

(a) Structural Idealisation

Specify :
(i) Nodal co-ordinates and element topology
(ii) Material properties
(iii) Boundary conditions
(iv) Applied and initial nodal loads $\{F\}$
(v) Initial stresses $\{\sigma_o\}$ and strains $\{\varepsilon_o\}$

(b) Element Characteristics

Evaluate :
(i) Elasticity matrix $[D]$
(ii) Stress matrix $[DB]$
(iii) Stiffness matrix $[k]^e$

(c) Structure Stiffness Matrix $[K]$

Formulate :

$$[K_{ij}] = [k_{ij}]^e$$

(d) Boundary Conditions

Introduce :
(i) Prescribed nodal displacements
(ii) Kinematic restraints to prevent rigid body movements

(e) Equilibrium Equations

Solve :

$$[K]\{\delta\} = \{F\}$$

for nodal displacements $\{\delta\}$

(f) Element Stresses

Determine :

$$\{\sigma\} = [DB]\{\delta\}^e - [D]\{\varepsilon_o\} + \{\sigma_o\}$$

Table 7.1 The finite Element Analysis Procedure

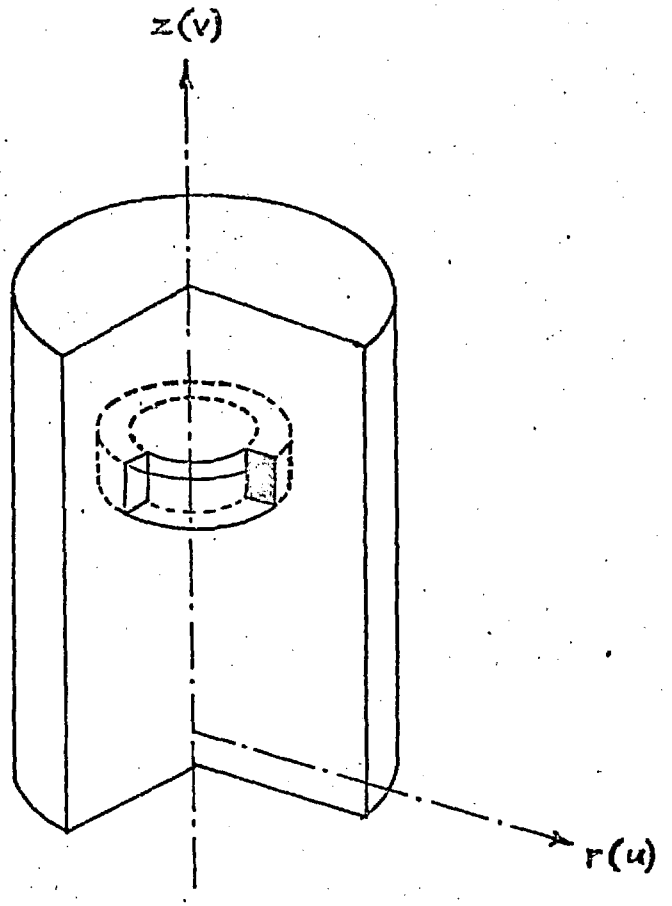


FIGURE 7.1 ELEMENT OF AN AXI-SYMMETRIC SOLID

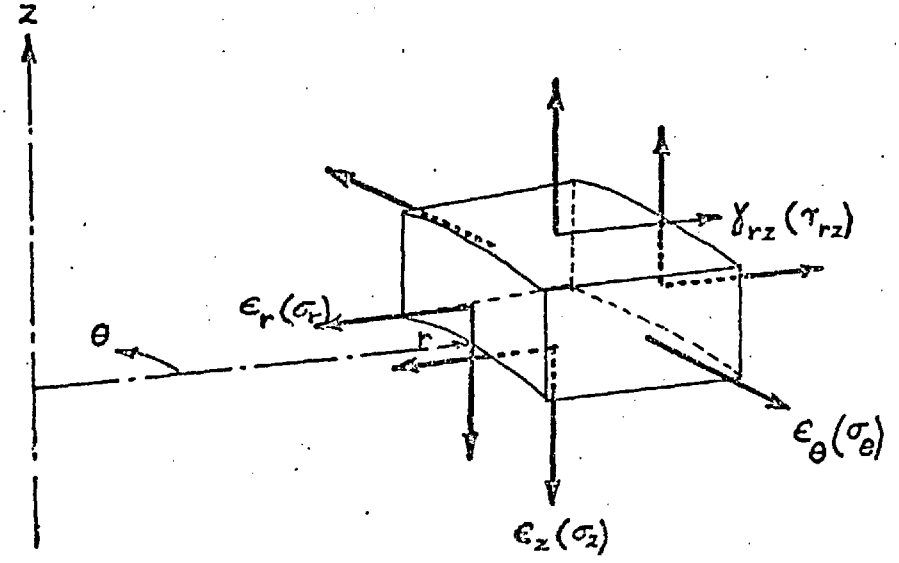


FIGURE 7.2 STRAINS AND STRESSES INVOLVED IN THE ANALYSIS OF AXI-SYMMETRIC SOLIDS

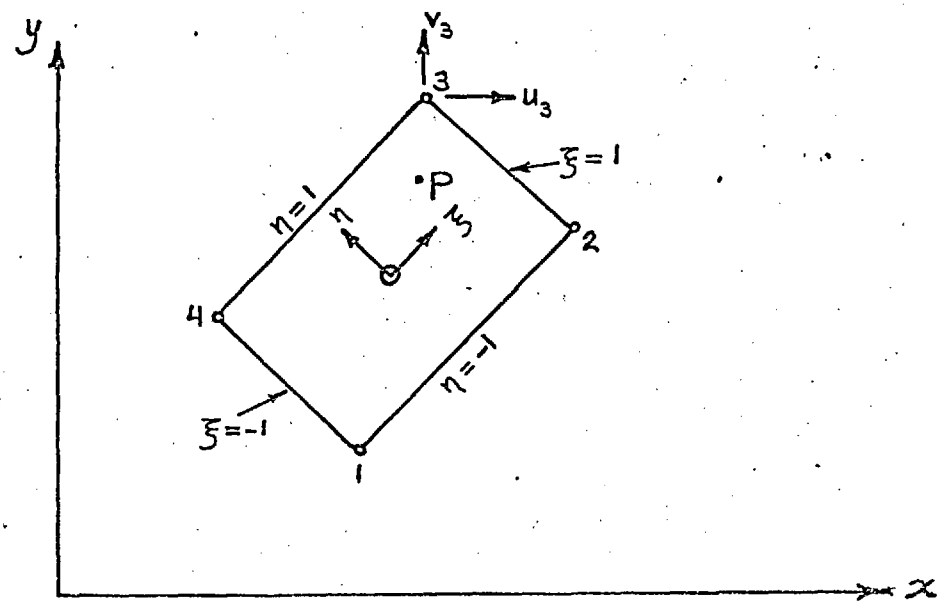
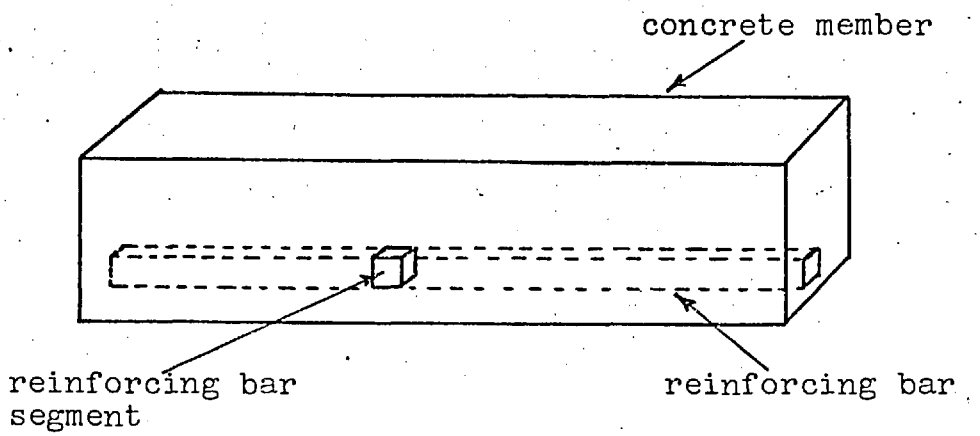
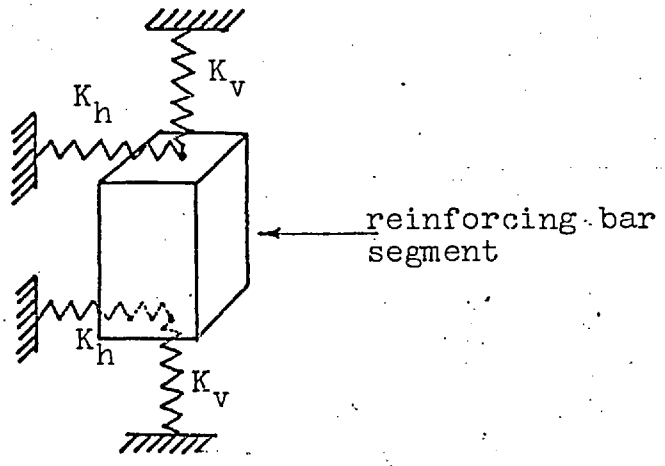


FIGURE 7.3 CURVILINEAR CO-ORDINATES FOR A RECTANGULAR ELEMENT

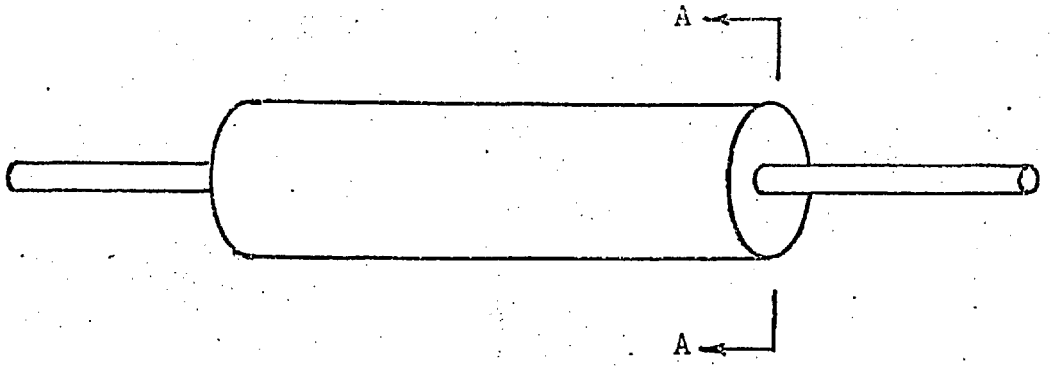


(a) Model of reinforced concrete member

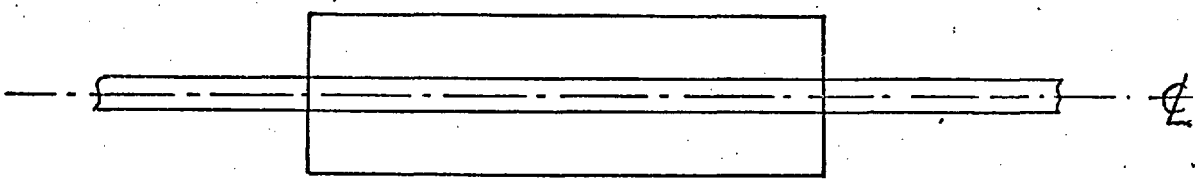


(b) Detail of bond linkage

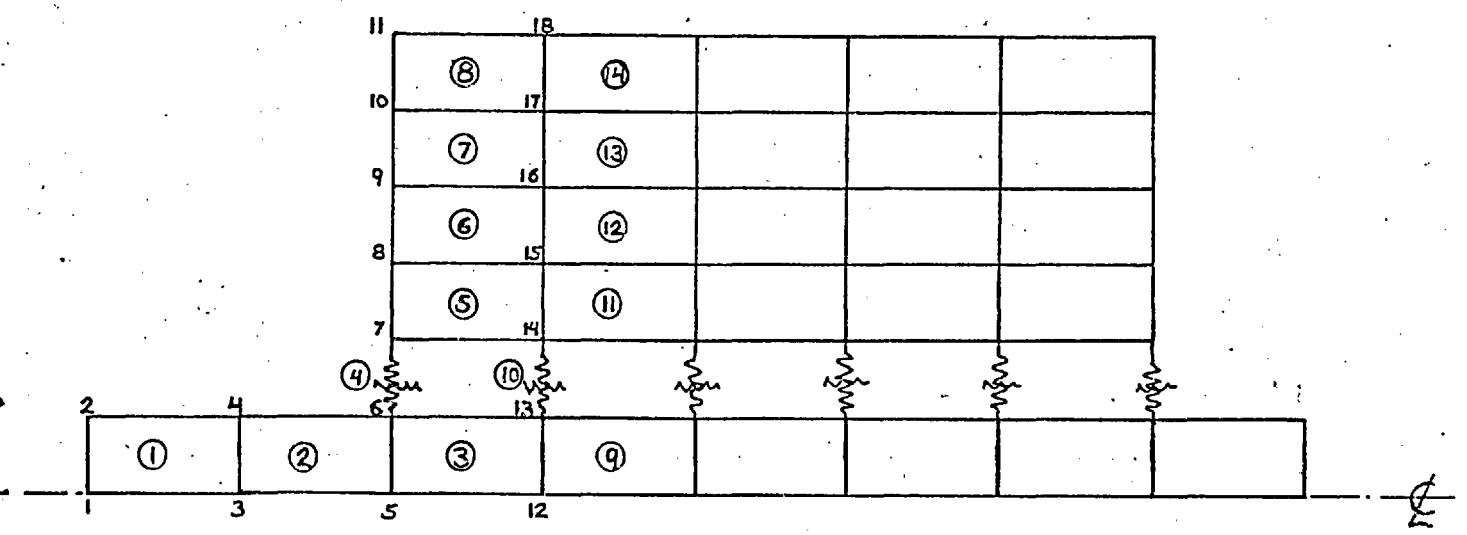
FIGURE 7.4 BOND REPRESENTATION



(a) Reinforced concrete member



(b) Section A-A of reinforced concrete member



(c) Finite element idealisation of upper half of (b)

FIGURE 7.5 FINITE ELEMENT IDEALISATION OF A REINFORCED CONCRETE MEMBER

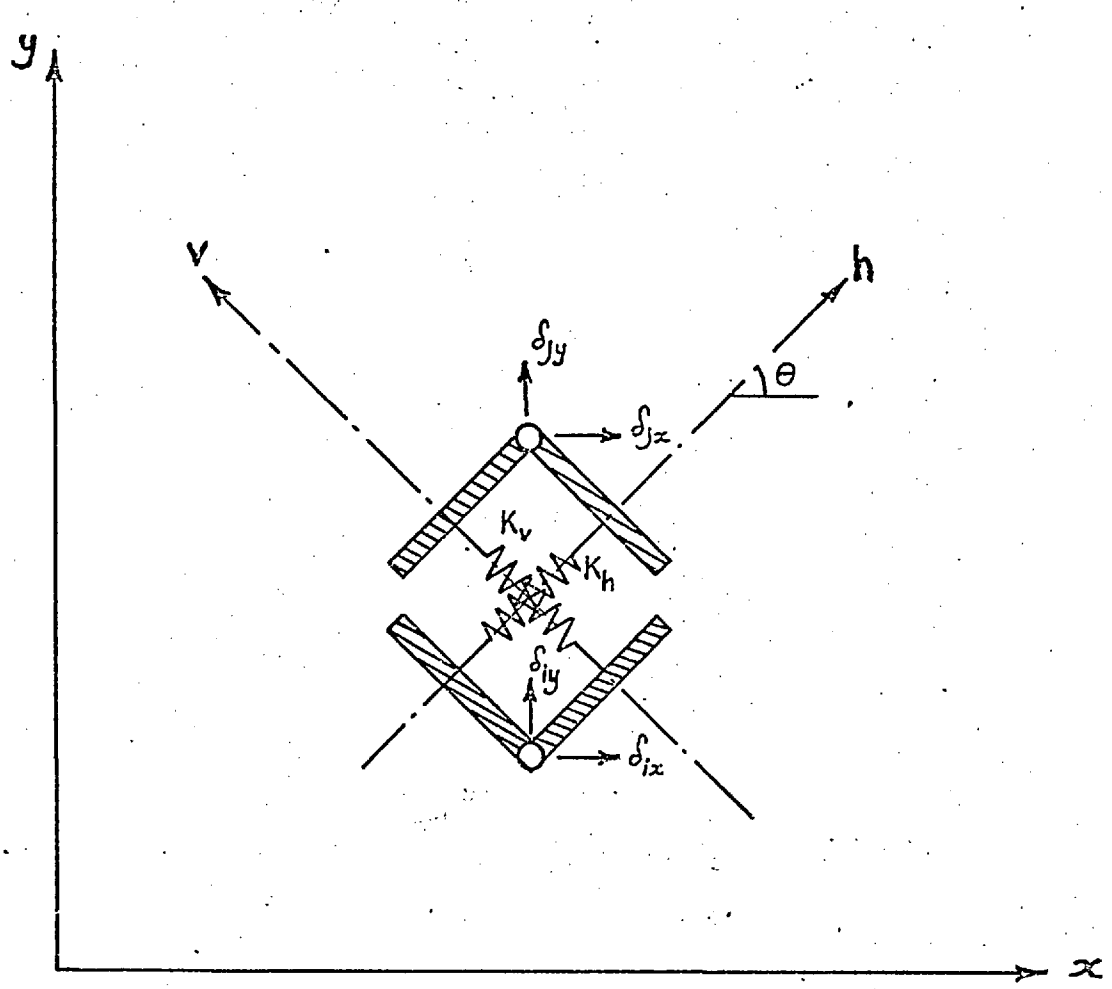
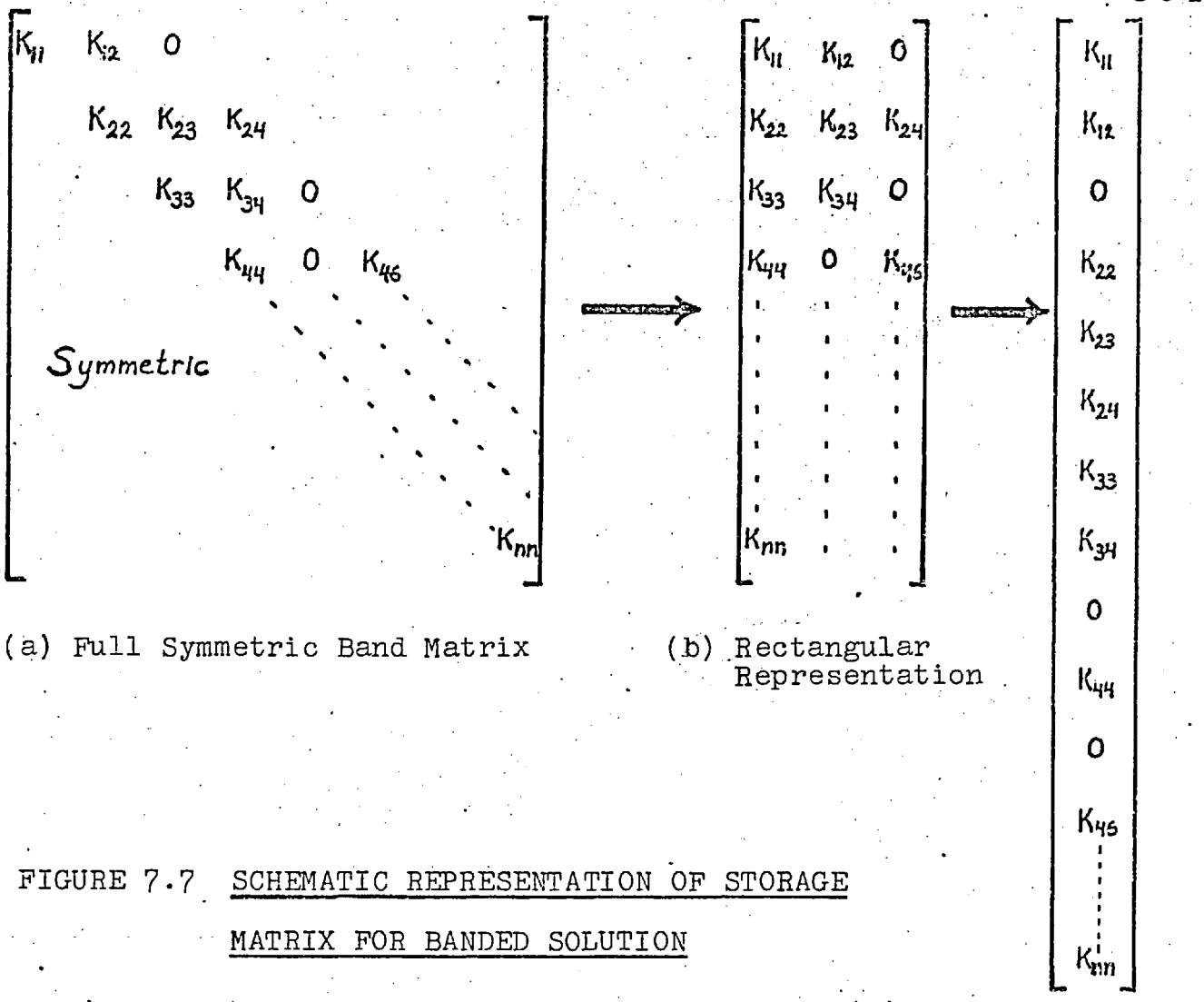


FIGURE 7.6 BOND LINKAGE ELEMENT



(a) Full Symmetric Band Matrix

(b) Rectangular Representation

(c) One-dimensional Computer Storage

FIGURE 7.7 SCHEMATIC REPRESENTATION OF STORAGE MATRIX FOR BANDED SOLUTION

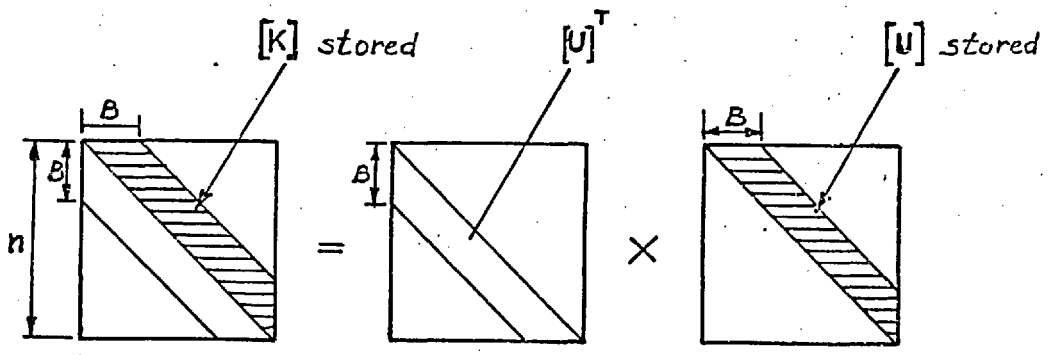
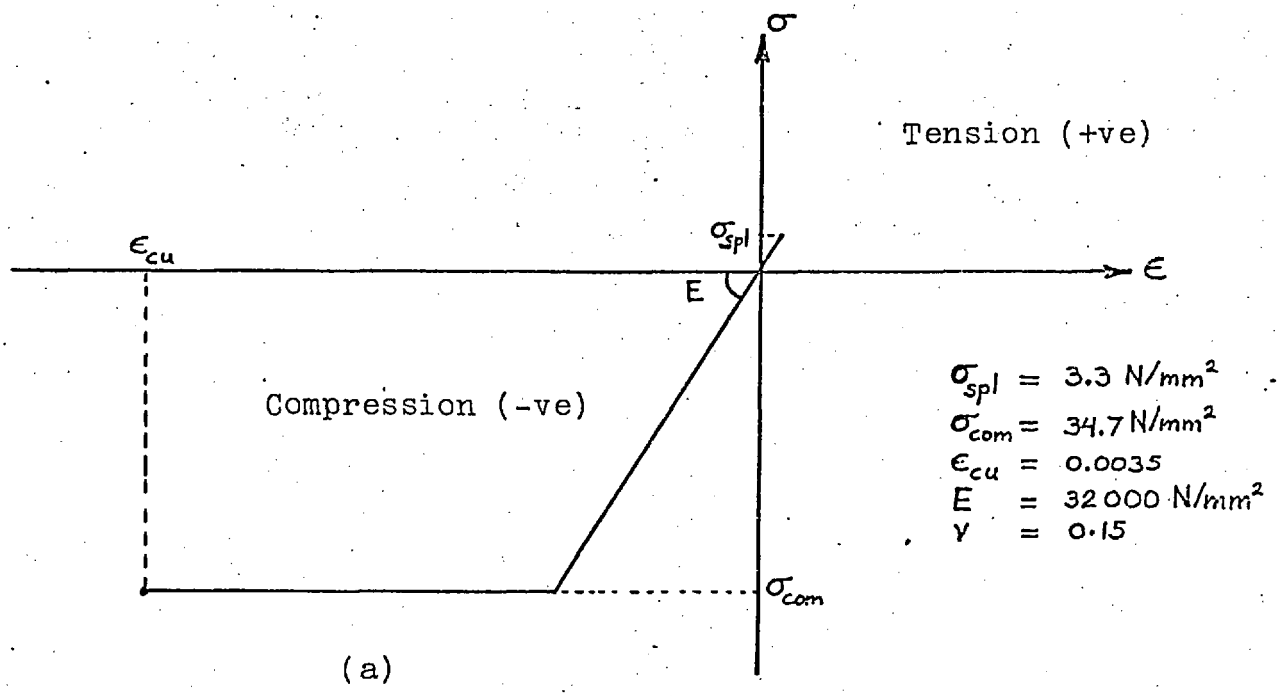
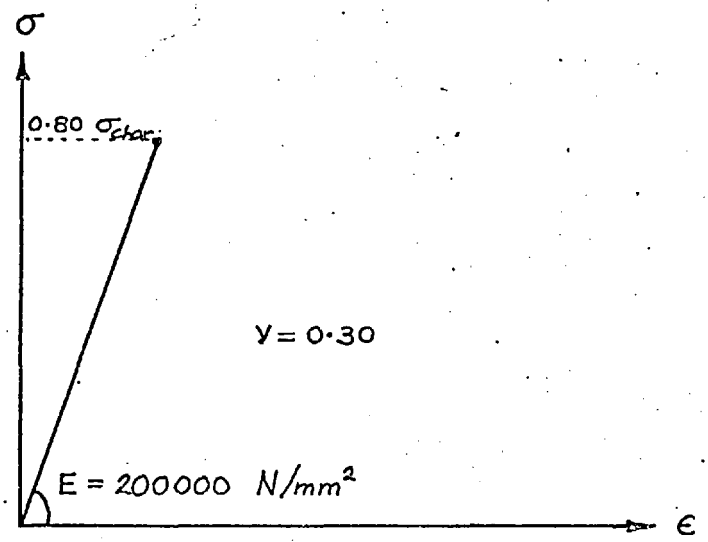


FIGURE 7.8 SCHEMATIC STORAGE ARRANGEMENT IN CHOLESKI METHOD



(a)

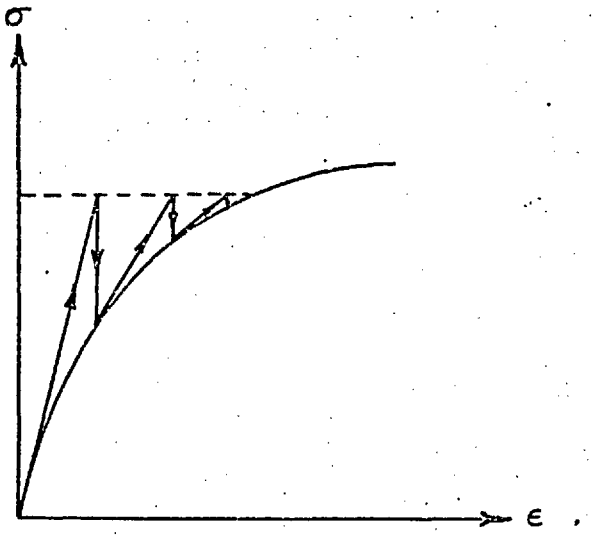


(b)

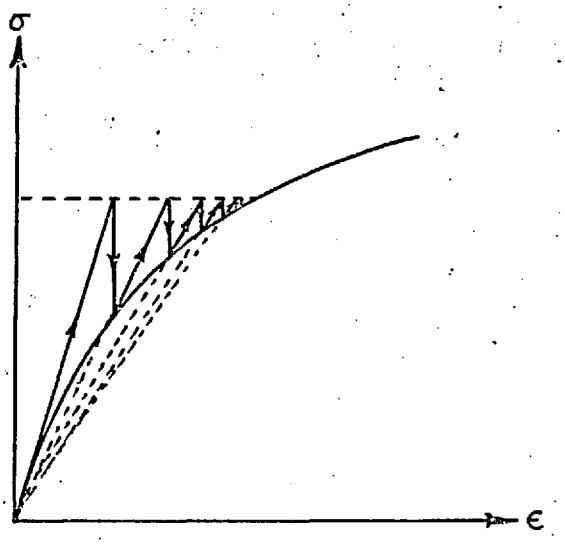
FIGURE 7.9 IDEALISED STRESS-STRAIN RELATIONS

(a) For steel

(b) For concrete



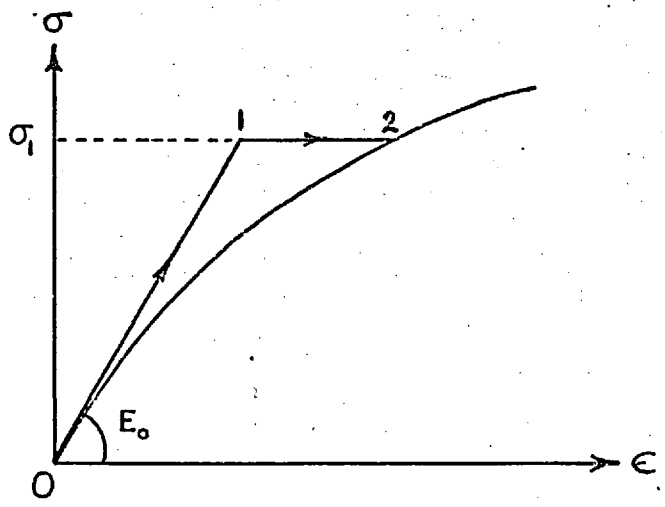
(a) Tangent Stiffness Approach



(b) Secant Stiffness Approach

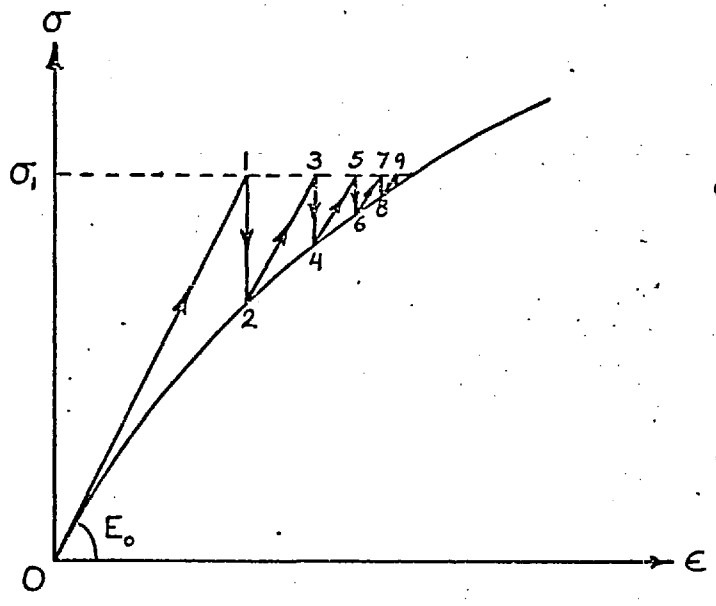
FIGURE 7.10 VARIABLE STIFFNESS SOLUTION METHODS FOR NON-LINEAR CONSTITUTIVE LAWS

(One dimentional case)



$\epsilon_1 - \epsilon_2$ = initial strain

(a) Initial Strain Approach



$\sigma_1 - \sigma_2$ = initial stress

(b) Initial Stress Approach

FIGURE 7.11 CONSTANT STIFFNESS SOLUTION METHODS FOR NON-LINEAR CONSTITUTIVE LAWS

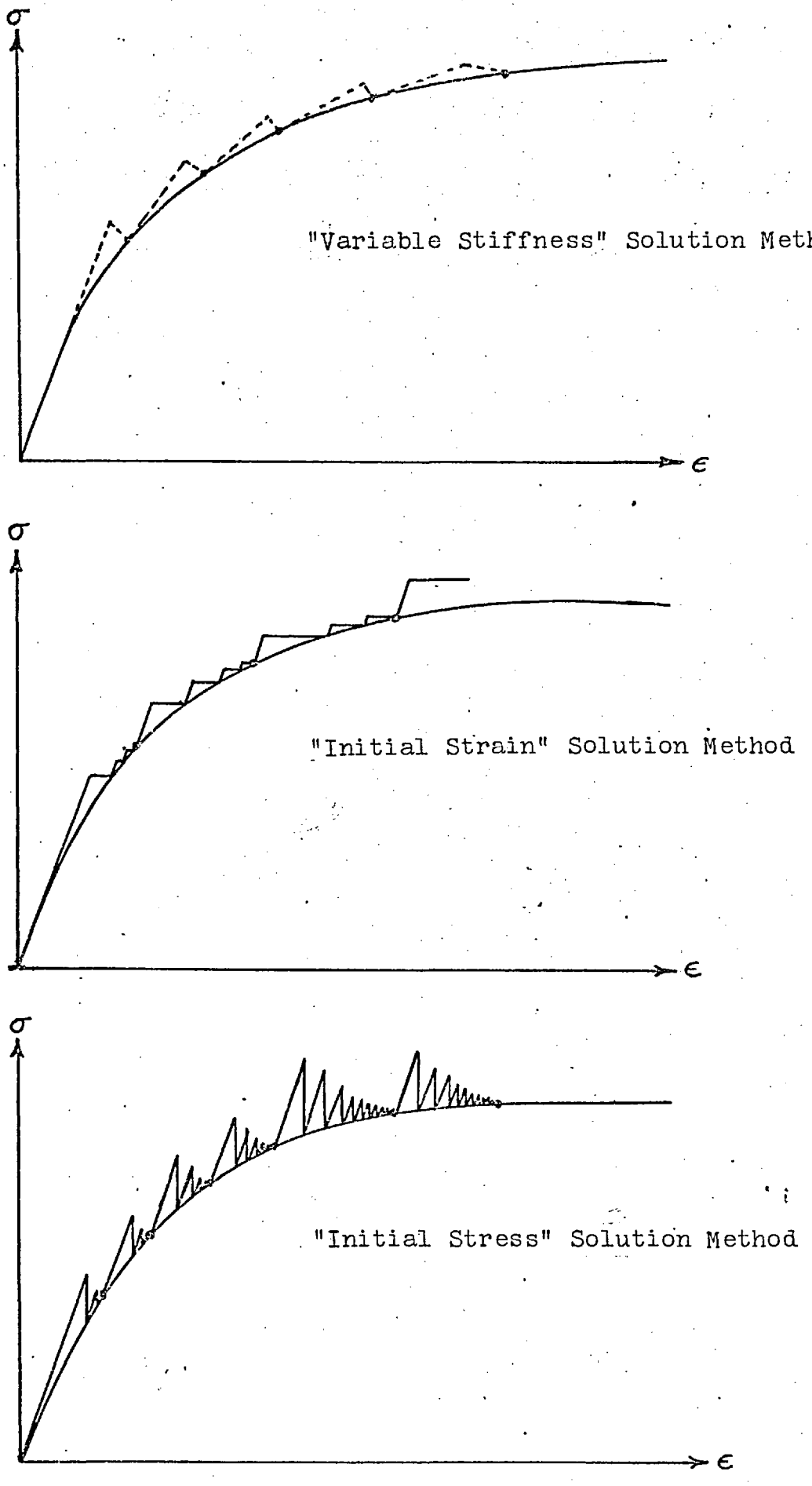


FIGURE 7.12 NON-LINEAR SOLUTION METHODS

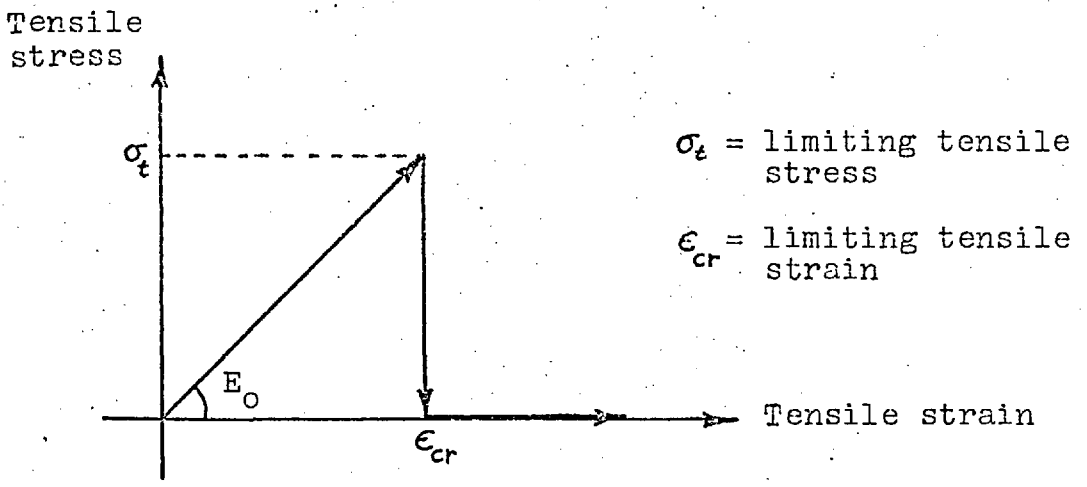
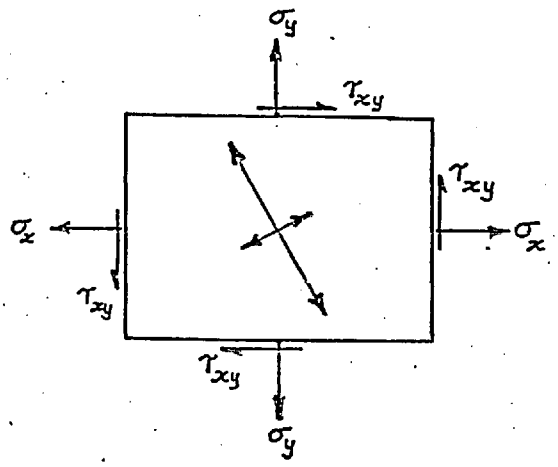
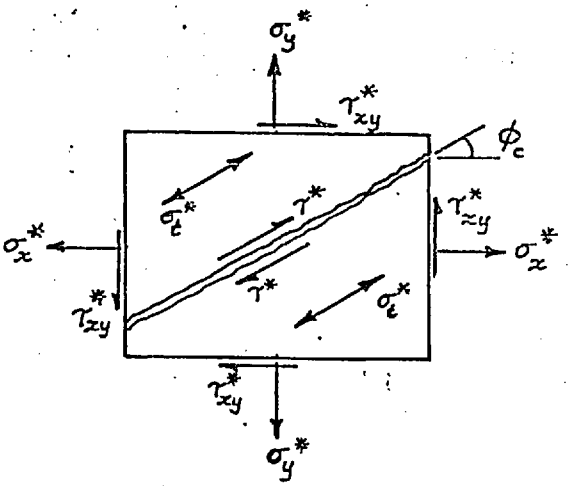


FIGURE 7.13 ASSUMED CONCRETE TENSILE ELASTIC-FRACTURE MODEL

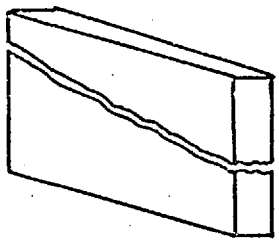


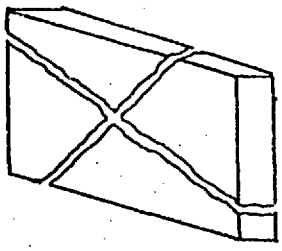
Stresses in concrete element before cracking



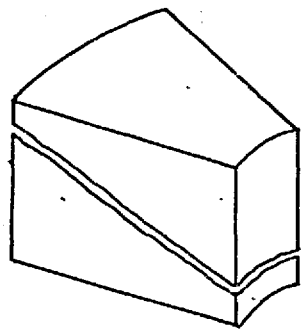
Stresses in concrete element after cracking

FIGURE 7.14 CRACKING MODEL

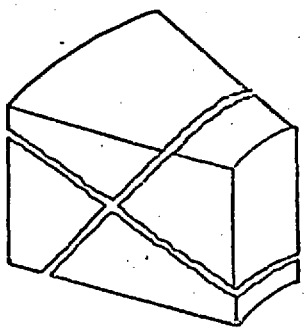




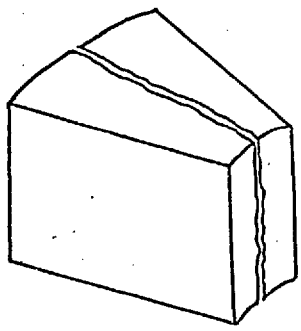
Cracks in two - dimensional cases



One circumferential crack



Two circumferential cracks



Radial crack

Cracks in axi-symmetric cases

FIGURE 7.15 TYPES OF CRACKS

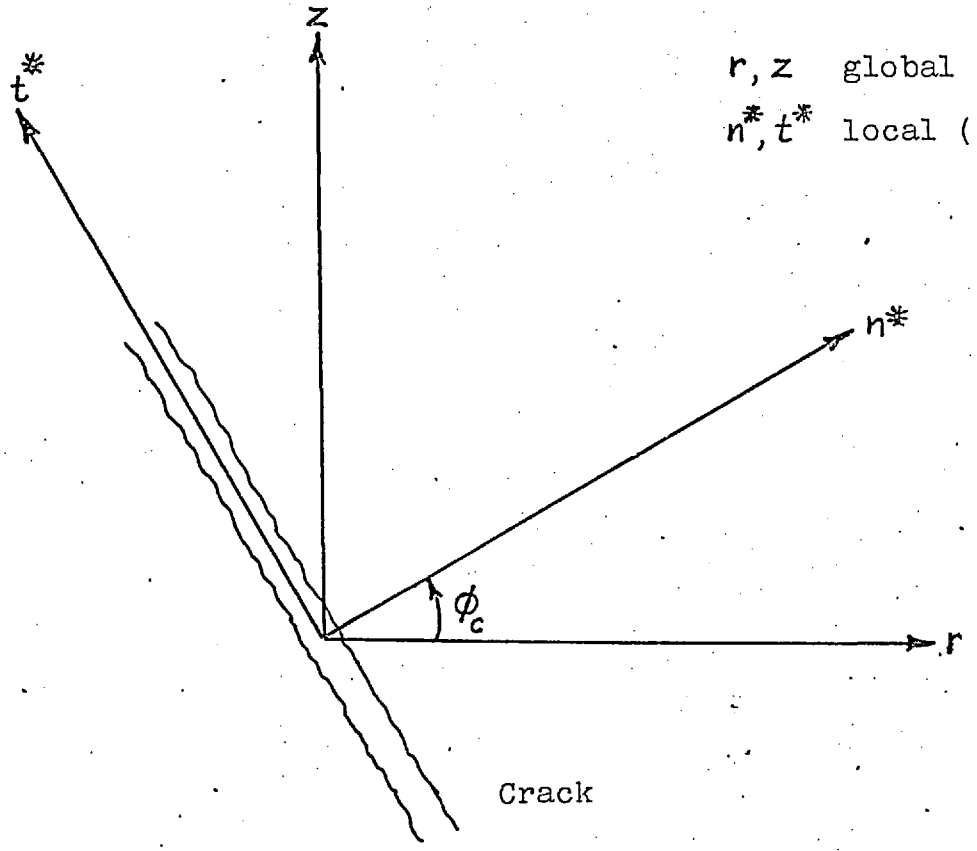


FIGURE 7.16. GLOBAL AND LOCAL AXES

CHAPTER 8

DESCRIPTION OF COMPUTER PROGRAM AND ANALYSIS OF REINFORCED CONCRETE TENSION MEMBER AND PULL-OUT SPECIMEN

8.1. GENERAL

In this chapter a description is given of the main features of the computer program developed during the course of this work, to deal with the non-linear response of reinforced concrete members under load. It represents the practical implementation of the theoretical modelling of reinforced concrete members, given in chapter 7, by means of special bond linkage elements and suitably adapted non-linear finite element techniques.

The second part of this chapter deals with the analysis of a concrete tension member and a pull-out specimen, axially reinforced with a deformed steel bar, and which have been tested as described in sections 6.4 and 6.5 respectively. The load-crack width characteristics of the tension member and the load-slip characteristics of the pull-out specimen, predicted by the non-linear finite element analysis are compared with those experimentally obtained.

8.2. DESCRIPTION OF NON-LINEAR FINITE ELEMENT COMPUTER PROGRAM

8.2.1. INTRODUCTION TO COMPUTER PROGRAM

The developed computer program has been based on the displacement-type finite element formulation and has been

written to analyse axi-symmetric concrete tension members and pull-out specimens, axially reinforced with a deformed steel bar. The concrete is in tension in the case of the tension members and in compression in the case of the pull-out specimens, while the steel bar is in tension in both.

The reinforced concrete members were modelled by rectangular concrete elements and rectangular steel elements. Bond between steel and concrete was modelled by non-linear linkage elements, connected between corresponding concrete and steel nodes. It is possible to trace the response of these members in terms of displacements, strains and stresses under gradually increasing load, while there is slip between the steel and concrete and cracks propagate through the concrete matrix. Load can be applied at any of the nodes and boundary conditions allow fixing of any node in one or more directions.

The program was coded in the Fortran IV language and has been run on a CDC 6400 computer. It requires a fast core storage of 40 K to analyse a system of 81 elements and 102 nodes. There is no restriction regarding the number of elements, nodes, nodal forces or restrained nodes and by suitable modification of the dimensions of relevant variables any size of problem can be tackled. Of course the maximum size system that can be analysed is governed by the size of the computer available. All members analysed in this work were easily within the limits of the CDC 6400 core memory.

A description of the program sequence of operations and functions of various modules and subroutines are given in section 8.2.2. The analysis of the reinforced concrete members

is given in section 8.3.

8.2.2. STRUCTURE OF PROGRAM

8.2.2.1. MODULES

The program consists of seven modules, each with a distinct operational function. Each module is composed of one or more subroutines. Some subroutines are used in more than one module. If there are more than one subroutine in a module, one of them is the main subroutine that controls the module's operations. The modules are controlled by the master driving segment, CONCMEB (Concrete Members), a description of which is given in section 8.2.2.2. The program sequence of operations is briefly given below and then a description of the modules follows.

The finite element program developed in this work consists of the master driving segment, CONCMEB, which by calling various modules it :

(a) Reads the input geometry and material data.

(b) Reads the applied loads.

(c) Assembles the structure stiffness matrix and introduces boundary conditions.

(d) Solves for nodal displacements.

(e) Finds strains and stresses for a particular load increment and calculates total displacements, strains and stresses.

(f) Checks all bond linkage elements to see if they satify their non-linear constitutive law, and if they don't, it redistributes the excessive stresses to adjacent elements and

sets up an iteration loop which it terminates when convergence has been achieved.

(g) Finds all concrete elements that develop tension in excess of the tensile strength of concrete, labels as cracked the most highly stressed of them, and calculates released nodal forces.

(h) Starts a crack formation loop, i.e. it modifies the stiffness of the structure due to the presence of the cracked element and re-analyses it under the released nodal forces. It repeats the loop until no more cracks are formed and then it prints final values of strains, stresses in local and principal directions and displacements.

(i) Repeats the above process for the next load increment.

The modules, schematically shown in Figure 8.1, are described with reference to their general functions as follows :

1. Geometry and Material Module

This is the first module called by the master segment CONCMEB, and is composed of one subroutine called GDATA. It handles input data describing the material properties and geometry of the structure to be solved. This module is used only once.

2. Loading Module

This is the second module entered and is composed of the subroutine LOAD. It reads and writes out the loads applied at each loaded node in every load increment.

3. Stiffness Module

This is the third module called by the master segment. It organises the stiffness calculations of the concrete, steel

and bond elements and assembles the global stiffness matrix of the system by suitably adding up corresponding stiffness components. The flow of operations in this module is governed by subroutine FORMSK. The subroutines associated with this module are shown in Figure 8.1.

Evaluation of stiffnesses, in the case of bond linkage elements, is made according to the strain state prevailing in the elements at the time of calculation, while in the case of concrete elements according to whether they are cracked or not in one or more directions. The stiffness matrix $[K]$, as well as element identification, elasticity (constitutive) matrix $[D]$ and strain matrix $[B]$ for each element, are permanently stored on to tapes, which can be retrieved when needed in the other modules.

4. Solution Module

This module consists of the subroutine SOLVE. It solves the simultaneous structural stiffness equations, using Choleski's triangular decomposition method, suitably adapted to take advantage of the symmetry and banded nature of the equations.

5. Stress Module

This module consists of the subroutine STRESS. It calculates incremental strains and stresses, as well as total displacements, strains and stresses for the bond linkage, the steel and concrete elements. Principal element stresses and their directions are also calculated.

This module is entered in every iteration immediately after the solution of the simultaneous equations in module SOLVE.

6. Bond Linkage Checking Module

This module consists of the subroutine BOND, and is entered after the stress module. It compares computed and allowable stresses for each bond linkage element and if their difference is larger than 1 % of the allowable stress, initial stress and equivalent nodal forces are calculated to be redistributed by the master segment, CONCMEB, to adjacent elements.

7. Crack Checking Module

This module is controlled by the subroutine CRACK and is entered after the Bond Linkage Checking Module. It finds the concrete elements in which one or more of the principal stresses exceed the tensile strength of concrete and the most highly stressed of these elements is considered to crack. This is achieved by releasing the appropriate principal stresses and calling the GAUSS and SHAPE subroutines to calculate equivalent nodal forces. These are used by the master segment to redistribute the released stresses to the adjacent elements.

8.2.2.2. CONTROL OF THE MODULES

The master segment CONCMEB first reads the job control parameters such as the number of nodes, number of elements, number of restrained nodes, number of load increments, maximum number of iterations, etc. CONCMEB also initialises the displacements, strains, stresses, the bond linkage iteration counter, the convergence flag and the crack formation flag. It then calls the Geometry and Material Module GDATA and calculates the size of the structural stiffness array. But the main purpose of the master segment CONCMEB is to control the

load increments and the iterations, as well as calling the appropriate modules at the right time. A flow chart of the sequence of operations is given in Figure 8.2, which is almost self explanatory, following the description of modules given in the previous section. Immediately after the BOND module there is a convergence flag inserted to check whether there are any excessive stresses to be released in the bond linkage elements. During the iterations the stiffness of the bond linkage elements is not recalculated, but the same one is used until the maximum allowable number of iterations is reached. This is taken equal to five in this work and when it is reached the stiffness of each bond linkage element is updated so that the iteration process is speeded up.

When convergence of bond linkage elements is satisfied the Crack Checking Module is called and this is followed by the crack formation flag. This starts a crack formation loop if the CRACK Module detects any elements in which the concrete failure criterion is exceeded, otherwise the master segment prints out total displacements, strains and stresses.

8.2.2.3. DESCRIPTION OF SUBROUTINES

A description of the main functions of each subroutine is given in the following :

GDATA

Its main function is to handle the input data defining the material properties and boundaries of all elements comprising a structure, i.e.

(i) Initial material properties (Young's modulus, Poisson's ratio, failure criteria for concrete,etc.) and a table of the non-linear bond stress-slip characteristics of the bond linkage elements (i.e. the co-ordinates of a few points defining the bond stress-slip relationship).
(ii) Node numbering of elements, nodal point co-ordinates and restrained boundary point data.

All the above information is written out for checking purposes.

LOAD

This subroutine handles the nodal loads applied in every load increment. The load vector for the whole structure, i.e. the one containing the two load components at each node, is first equalised to zero. Then it is modified to include the loads applied at particular nodes.

The two load components at each loaded node are then written out to facilitate error checking.

FORMSK

This subroutine controls the calculation of stiffness matrix and other characteristics of all types of elements. Each element is considered in the pre-determined sequence.

For each bond linkage element the LINK subroutine is called to evaluate its stiffness matrix according to the state of strain reached at the time of calculation. The stiffness matrix and element identification of each bond linkage element is stored on Tape 4. This data can be recalled when

needed in the other modules.

For each axi-symmetric rectangular steel and concrete element, the AXIRECT subroutine is called to evaluate its stiffness. For the steel elements the stiffness is independent of the level of stress, while for the concrete elements it is dependent on whether the element is cracked or not in one or more directions. The stiffness matrix $[K]$, elasticity matrix $[D]$, strain matrix $[B]$ and nodes of each concrete and steel element are stored on Tape 3. During constant stiffness iterations, the AXIRECT matrix is not called, but the data stored on Tape 3 is used.

The FORMSK subroutine also organises the assembly of the structure stiffness matrix. This is done by putting the terms of each element's stiffness matrix into the proper address of the structure stiffness matrix and adding up all over-lapping terms from different elements. This process is described in length in section 7.6.

The FORMSK subroutine finally introduces the displacement boundary conditions by modifying the structural stiffness matrix and load vector, as described in section 7.7.

LINK

This subroutine formulates the stiffness matrix and other characteristics of bond linkage elements. The allowable bond stress in each bond linkage element, corresponding to the reached slip value, is calculated by linearly interpolating in between the co-ordinates of points defining the bond stress-slip curve. The stiffness of the element is then proportional

to the slope of the curve at the point considered.

The stiffness matrix and node numbers of each bond linkage element are stored on Tape 4 and when this data is needed in other subroutines it can be retrieved from this tape.

AXIRECT

This subroutine formulates the stiffness matrix and other characteristic matrices of the axi-symmetric rectangular steel and concrete elements. These have been developed in section 7.3 and the isoparametric shape functions and numerical integration techniques in section 7.4.

The main steps in this subroutine are as follows :

(i) Evaluation of the current elasticity matrix $[D]$, according to whether the element is cracked or not and whether one or more cracks have formed. The different forms of $[D]$ are given in section 7.11.4.

(ii) Calculation of the co-ordinates of the Gauss integration points and the corresponding integration factors.

(iii) Formation of stiffness contribution from each integration point, as given in section 7.4.3. The isoparamatric shape functions, N, and their cartesian derivatives are supplied by calling subroutine SHAPE.

(iv) Calculation of the stiffness matrix, as given in section 7.4.5., i.e. by addition of the stiffness contributions from all the integration points, after being multiplied by the corresponding integration factors.

(v) Calculation of the strain matrix $[B]$ at the centroid of the element. This is required in subroutine CRACK to evaluate

forces due to released stresses (Equation (7.79)).

The stiffness matrix $[K]$, elasticity matrix $[D]$, strain matrix $[B]$ and nodes of each concrete and steel element are stored on Tape 3 and can be retrieved when needed in other modules.

GAUSS

This subroutine holds the numerical constants required for numerical integration by Gauss method, which is described in section 7.4.5. For each order of integration, the co-ordinates of the integration points, as well as the corresponding integration factors, are given.

SHAPE

This subroutine calculates a number of quantities required for the calculation of the stiffness and strain matrices of the axi-symmetric rectangular, isoparametric steel and concrete elements, as given in section 7.4.3. These quantities are evaluated at each Gauss integration point and are as follows :

(i) Shape functions and their first derivatives in the curvilinear (local) $\xi - \eta$ co-ordinate system.

(ii) Cartesian co-ordinates of present integration point.

(iii) The Jacobian matrix, its determinant and inverse.

(iv) The cartesian derivatives of the shape functions.

SOLVE

This subroutine solves the simultaneous structural

equations, using Choleski's triangular decomposition method, and thus finds the displacements of each node during each load increment. The solution method has been adapted to take advantage of the symmetry and banding of the structural stiffness matrix and thus both the computer storage and computer time required for the solution are reduced.

The structural stiffness matrix is first decomposed into a lower and an upper triangular matrix, in which the elements are easily determined, as explained in section 7.8. Then by forward and backward substitution using the calculated upper triangular matrix and the load vector, the displacement vector for all nodes of the structure is calculated.

If a new set of stiffnesses have been evaluated, SOLVE goes through all the above steps, whereas if there is only a new set of forces, SOLVE skips the first step and starts the forward substitution part of the solution process using the upper triangular matrix stored during the previous call of the SOLVE subroutine.

STRESS

This subroutine calculates total displacements, strains and stresses in the bond linkage and rectangular axi-symmetric steel and concrete elements.

STRESS calculates the incremental strains and stresses for each element using the incremental nodal displacements, determined by SOLVE, and reading the element matrices $[B]$ and $[D]$ from Tape 3 and 4. These values are used to calculate the total displacements, strains and stresses. Principal stresses

and their directions are also determined.

BOND

This subroutine calculates the allowable stress for each bond linkage element, corresponding to the strain computed by STRESS module, using the bond stress-slip characteristics specified in the GDATA module.

If in any bond linkage element the difference between the allowable stress and the one computed by the STRESS module is larger than 1 % of the allowable stress, then this difference is used as an initial stress and equivalent nodal forces are calculated, as given in section 7.10.2.4. These forces are used by the master segment to redistribute the initial stress to adjacent elements.

The computed strain and stress, the allowable stress, as well as the % stress error in each bond linkage element are printed out.

CRACK

This subroutine deals with concrete elements in which one or more of the principal stresses exceed the tensile strength of concrete. The relevent theory is given in section 7.11.

The most highly stressed of the above elements is considered to crack and since a cracked element is incapable of supporting any stresses perpendicular to the crack, equivalent nodal forces are calculated to be used by the master segment for redistributing the stresses to adjacent elements. These

forces are evaluated by first finding the released stresses in the global r - z co-ordinate system and then numerically integrating the expression given by Equation (7.79). The GAUSS subroutine is called to provide the integration points and integration factors and the SHAPE subroutine to privide the strain matrix $[B]$.

8.3. ANALYSIS OF REINFORCED CONCRETE TENSION MEMBER AND PULL-OUT SPECIMEN AND COMPARISON WITH EXPERIMENTAL DATA

8.3.1. BASIS OF THE ANALYSIS

The cylindrical concrete tension member and the pull-out specimen, axially reinforced with a deformed steel bar, were analysed using the developed non-linear axi-symmetric finite element program, described in section 8.2. This was based on the theory given in chapter 7. An incremental loading procedure was adopted and the response of the concrete members under load was followed as described in section 8.2.2.1.

The adopted idealised stress-strain relation for concrete in compression, as well as in tension, and the one for steel are shown in Figure 7.9. The values of different parameters have been determined experimentally.

The maximum stress theory was adopted for tensile concrete failure and the limiting value of tensile stress was taken equal to 3.3 N/mm^2, as determined from a number of standard cylinder split tests.

8.3.2. ANALYSIS OF REINFORCED CONCRETE TENSION MEMBER AND COMPARISON WITH EXPERIMENTAL DATA

8.3.2.1. DESCRIPTION OF MODEL AND FINITE ELEMENT IDEALISATION

Tests carried out on concrete tension members, 76 mm in diameter and 800 mm long, concentrically reinforced with a 16 mm diameter Welbond deformed bar are described in section 6.4. Eight or nine cracks formed along the concrete length under monotonically increasing bar load, and a typical member is shown in Figure 8.3(a). Plots of steel stress against average concrete surface strain, steel stress against crack spacing and steel stress against crack width are given in section 6.4. An average minimum crack spacing from all tested members was found equal to 87 mm.

The above behaviour of the long reinforced concrete tension members was studied analytically by considering a section bounded by two primary cracks, i.e. a 90 mm long concrete block was chosen since it was approximately equal to the measured average minimum crack spacing. Analysing this block, shown in Figure 8.3(b), by means of the developed non-linear finite element program, the formation and propagation of internal cracks under increasing loads could be followed and the end face displacements could be used to predict values of the crack widths measured in the long tension members. This block's displaced end faces are shown exaggerated in Figure 8.3(c) for illustration purposes.

The axi-symmetric finite element idealisation, of the tension specimen to be analysed, is shown in Figure 8.4. Concrete and steel were modelled by rectangular elements. The

concrete elements near the steel-concrete interface were chosen smaller than those away from it, since internal crack formation is initiated from this interface. Symmetry permitted the study of only one quarter of the member. It is evident that the displacement of the central point (used as the origin of co-ordinates) must be zero; points along the z-axis move only in the z direction, and points along the r-axis move only in the r direction. These boundary conditions are also shown in Figure 8.4.

Bond linkage elements joining concrete and steel are located at nodal points along the steel-concrete interface. These are shown diagrammatically in Figure 8.4 as springs joining separate corresponding steel and concrete nodal points. In the analysis, the nodal points joined by any spring occupy the same point in space, and the spring dimension shrinks to zero.

The calculation of stiffness of a linkage element requires the determination of tributary bar surface area, using Equation (7.26). For a typical interior linkage element :

$$A = \pi DL = \pi(16)(5) = 251.3 \text{ mm}^2$$

For the bond linkage element at the end face of the concrete, the tributary area is one-half this quantity, or 125.7 mm^2. The stiffness of each bond linkage element was obtained from Equation (7.25) and for the bond stress - slip curve given in Figure 8.5. This is a mean curve to those experimentally obtained (section 6.2) from short embedment basic specimens, of both small and big concrete covers since the tension members had a concrete cover equal to the average of the two

covers of the basic specimens.

To represent aggregate interlocking of the faces of a crack, an aggregate interlock constant of a = 0.5 was used in Equation (7.63) and introduced into the constitutive matrix of an element that just cracked.

Load was introduced into the analytical model in the same manner as for the long tension members, at the protruding ends of the reinforcing bar. For the model, load increments of 10,000 N or 49.7 N/mm^2 steel stress were used.

8.3.2.2. ANALYTICAL RESULTS AND COMPARISON WITH EXPERIMENTAL DATA

The development of internal cracking in the concrete tension specimen, predicted by the finite element program, is traced in Figures 8.6(a), (b), (c) and (d) for increasing free steel bar stresses, i.e. stresses in the bar outside the concrete member. Both transverse and radial cracks are formed that propagate through the concrete matrix under increasing bar loads. The first cracks are formed at a free bar stress of approximately 60 N/mm^2.

Most of the transverse internal cracks are formed at the steel-concrete interface. For small bar loads they are concentrated near the concrete end face and under increasing bar load they propagate more into the concrete while new cracks are formed further away from the concrete end face. All transverse cracks are at an angle of 40° to 60° to the bar axis and their width is very small. At the maximum applied steel stress of 348 N/mm^2 the maximum internal crack width was

not more than 0.012 mm at the steel-concrete interface. The predicted internal transverse cracking patterns, shown in Figures 8.6(a) to (d) are in very close agreement with the experimental internal cracking patterns obtained by Goto (38,39). He tested axially loaded concrete tension specimens and injected ink into the internal cracks and by splitting the specimens axially he observed internal cracks formed at an angle of 45° to 80° to the bar axis, as shown in Figure 2.6.

Radial cracks are also predicted, by the finite element analysis, to originate mostly at the steel-concrete interface and right next to the concrete end face. These are denoted in Figures 8.6(a) to (d) by a * since they form in a radial plane, i.e. parallel to that of the paper. The radial cracks propagate, at high bar loads, through the concrete to the surface of the concrete member and appear as short longitudinal cracks formed next to the concrete end face, which is considered to be a primary crack face. At even higher bar loads these cracks extend for a short distance along the concrete surface. Similar longitudinal cracks were observed to form at high bar load levels in the tested long tensile members, reported in section 6.4 and in addition also reported by Goto (38, 39).

The variation of steel stress with distance along the bar for three bar load levels is shown in Figure 8.7. The values plotted correspond to those calculated by the finite element analysis at the centroid of the rectangular steel elements. The steel stress is seen to decrease with distance

from the end face of the concrete member and to be minimum at its centre line. This decrease is biggest for the biggest free bar stress. However if it is expressed as a percentage of the free bar stress it is biggest for the smallest one. For example, the steel stress at the centre line of the concete member is 15, 30 and 38 N/mm^2 less than the 50, 199 and 348 N/mm^2 free bar stress respectively, or 30, 15 and 11 % less than the three corresponding free bar stress values. Similar results have been obtained by Bresler and Bertero (37). It should also be noted that no substantial modification of the steel stress was produced by the internal cracks initiated at the steel-concrete interface.

The bond stress curves of Figure 8.8 reflect the steel stress variation just described. At low free bar stress levels the maximum bond stress was obtained at the concrete member end face and the bond stress diminished rapidly, and almost linearly, with distance from it. Under increasing free bar stress internal cracking near this face had the effect of moving the peak bond stress inward. The maximum bond stress reached, at the highest applied steel stress of 348 N/mm^2, was only of the order of 30 % of the maximum bond stress of the bond stress - slip curve used in this analysis. No higher bond stresses could be developed because of internal cracks forming and releasing these stresses.

The area under a bond stress curve between the member end face and a point at a distance from it, represents the total bond force developed between these two points, which is equal to the corresponding drop in the bar load. Since this

area increases with increasing free bar stress (Figure 8.8), except very close to the end face, then this means that the drop in bar load increases with increasing free bar stress. This is in agreement with the calculated steel stress values mentioned above.

The extension of the embedded steel bar in the concrete tension specimen, computed by the finite element program for different load levels, was used to plot free bar steel stress against average embedded steel strain, as shown in Figure 8.9. In addition the stress-strain of a steel bar free in air is shown plotted with a dashed line for comparison purposes. The slope of the curve for the embedded steel bar, for stresses higher than 30 N/mm^2, is constant and approximately equal to that for the free steel bar. However for steel stresses up to 30 N/mm^2 the slope of the embedded steel bar is slightly bigger than that for higher stress values. This is in agreement with the general shape of the experimental steel stress versus average concrete surface strain curve reported in section 6.4 and with Broms' experimental findings (35).

The nodal displacements along the concrete end face, computed by the finite element program, have been used to plot the displacement of the tension member end face, which is shown in Figure 8.10 for various free bar stresses. The concrete displacement is maximum at the steel surface and decreases with distance from it. This decrease is steeper at higher bar loads. The displacement of the concrete outer surface is almost zero, except at a steel stress of 348 N/mm^2 a very slight compression of 0.001 mm is obtained. Similar results have been obtained

experimentally by Broms (35). This profile of the concrete end face is mainly due to the internal cracks in the concrete matrix originating from the steel surface. The extension of the concrete is only a small proportion of the concrete displacement, because if it is assumed that the average concrete strain along the 45 mm concrete length is 0.5 of its ultimate tensile strain, then the maximum concrete extension just before fracture, is equal to $45 \times 0.5 \times \varepsilon_{ult}$ or $45 \times 0.5 \times (100\ \mu\text{-strain})$ i.e. 0.002 mm, as compared to a concrete displacement at the bar surface of 0.038 mm.

Since the end face of the above tension member is an external crack face, the curves of Figure 8.10 represent the profile of a crack face for different bar load levels. The crack width at any point along the concrete end face, is then equal to twice the difference between the steel displacement ΔL and the concrete displacement ΔE at that particular point, as shown in Figure 8.3. Since ΔE is equal to zero at the outer concrete surface, the crack width is maximum on the concrete member's surface and equal to twice ΔL. The computed ΔL values, by the finite element program, for the different applied bar loads were thus used to calculate corresponding crack width values. These are shown plotted in Figure 8.11 together with the experimentally obtained crack width data from the 800 mm long reinforced concrete tension members, for comparison purposes. The predicted steel stress - mean crack width relation is linear and satisfactorily close to the corresponding experimentally obtained relation, taking into account that the sensitivity of the crack measuring device

was 0.02 mm/division and cracks were estimated to the nearest $\frac{1}{2}$ division. It should also be pointed out in this respect that the theoretical steel stress - mean crack width relation is based only on one bond stress - slip curve, shown in Figure 8.5, which is a mean curve to those experimentally obtained (section 6.2) from short embedment basic specimens. Further analytical studies could be carried out to establish the effect of the observed scatter in the obtained bond stress - slip curves on the steel stress - average crack width relation in tension members.

8.3.3. ANALYSIS OF CONCRETE PULL-OUT SPECIMEN AND COMPARISON WITH EXPERIMENTAL DATA

Tests carried out on pull-out specimens, 76 mm in diameter, with a concrete cover of 100 mm or 200 mm and with a 16 mm diameter Welbond deformed bar axially embedded in them, are described in section 6.5. Loaded end and free end slip readings were taken at a number of load stages and a pull-out specimen is shown in Plate 3.16. Plots of bar load against loaded end slip and bar load against free end slip are given in section 6.5.

The above load - slip characteristics of the pull-out specimens were studied analytically by considering the 100 mm long specimen. The axi-symmetric finite element idealisation of this specimen is shown in Figure 8.12. Concrete and steel were modelled by rectangular elements. The concrete elements near the steel concrete interface were chosen smaller than those away from it, since these affect the slipping of

the bar more than those away from this interface. Symmetry permitted the study of only one half of the specimen. Thus points on the z-axis move only in the z direction. Points on the specimen's loaded end face are considered to be fixed in the z direction, because this face was bearing on a fixed thick steel plate while load was applied to the bar, and also fixed in the r direction, because of the friction forces developed between the concrete and steel surfaces. These boundary conditions are also shown in Figure 8.12.

Bond linkage elements joining concrete and steel are located at nodal points along the steel - concrete interface. These are shown diagrammatically in Figure 8.12 as springs joining separate corresponding steel and concrete nodal points. In the analysis, the nodal points joined by any spring occupy the same point in space, and the spring dimension diminishes to zero.

The tributary bar surface area for a typical interior linkage element, given by Equation (7.26), is equal to :

$$A = \pi DL = \pi(16)(10) = 502.6 \text{ mm}^2$$

For the bond linkage elements at the two end faces of the concrete, the tributary area is one-half of this quantity, or 251.3 mm^2. This area is required for the calculation of the stiffness of a bond linkage element, which is given by Equation (7.25).

Two bond stress-slip curves were used in the computer program and are shown in Figure 8.13. The one denoted by M is a mean curve to those experimentally obtained (section 6.2) from short embedment basic specimens, of both small and big

concrete covers since the pull-out specimens had a concrete cover equal to the average of the two covers of the basic specimens. The other bond stress-slip curve denoted by S is one of a steep initial slope, but of the same maximum bond stress, which was used to investigate the effect on the load-end slip characteristics of the pull-out specimens of a different initial slope bond stress-slip curve.

Load was introduced into the analytical model in the same manner as for the pull-out specimens, i.e. at the protruding ends of the reinforcing bar. In contrast to the tension specimens, the concrete in pull-out specimens is in compression under applied tensile bar load.

The computed loaded end and free end slips, by the finite element program, for the different applied bar loads and for the two bond stress-slip curves, are shown plotted in Figures 8.14 and 8.15 respectively. The experimentally obtained corresponding load-end slip characteristics, given in section 6.5, are also shown plotted in these figures for ease of comparison. The predicted characteristics, using both bond stress-slip curves, are in satisfactory agreement with the corresponding actual ones. However, there is some difference between corresponding predicted curves using the two bond stress-slip curves, especially for the free end case. This difference is within the scatter of the experimentally determined curves. Since the loaded end slips are in excess of 0.10 mm, the maximum bond stress in the pull-out specimens nearly reached the maximum values obtained in the short embedment specimens, given in section 6.2. Further analytical

studies could be carried out to establish the effect of the observed scatter in the maximum bond stress and in the slope of the obtained bond stress-slip curves, on the load-end slip characteristics of pull-out specimens.

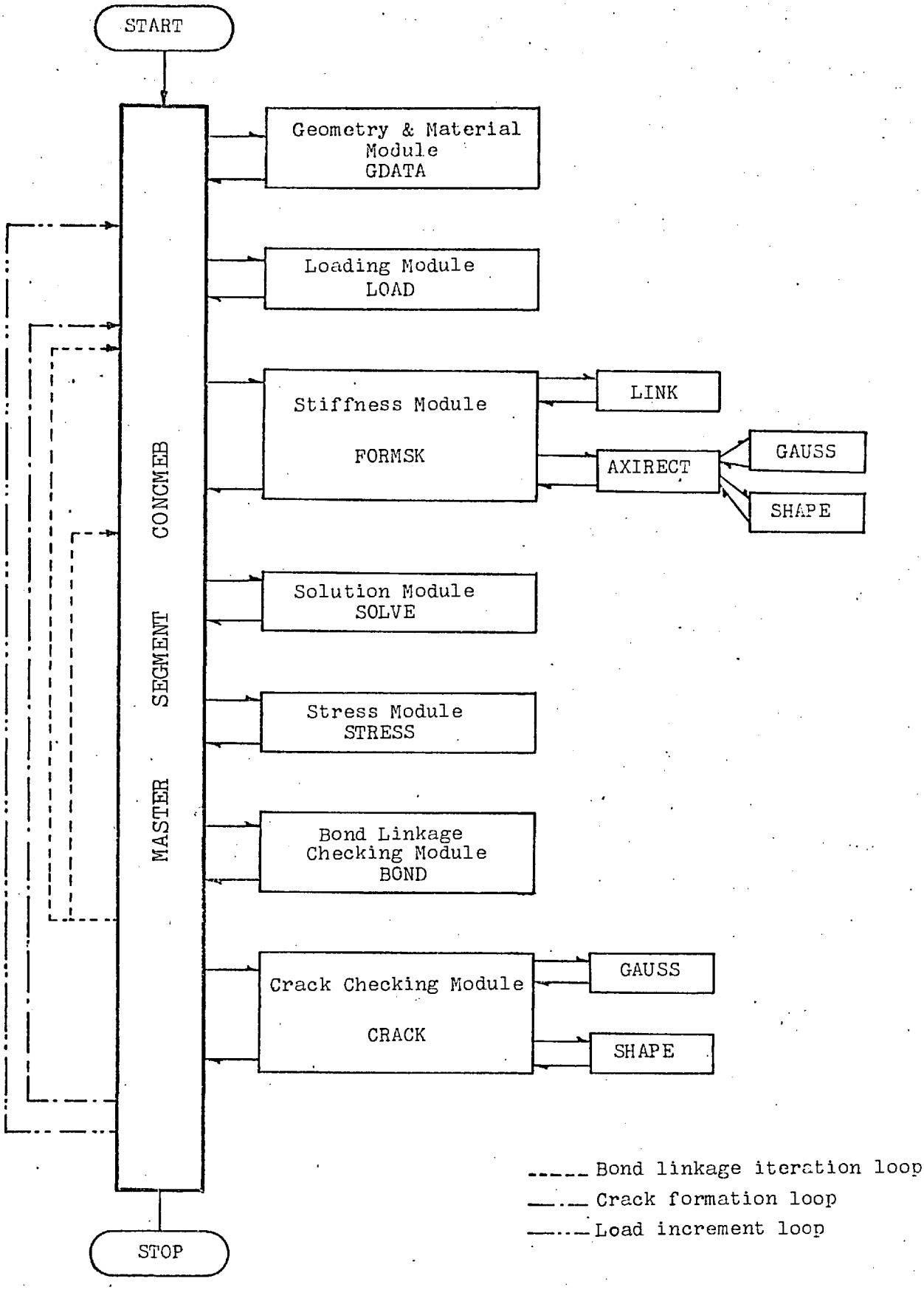
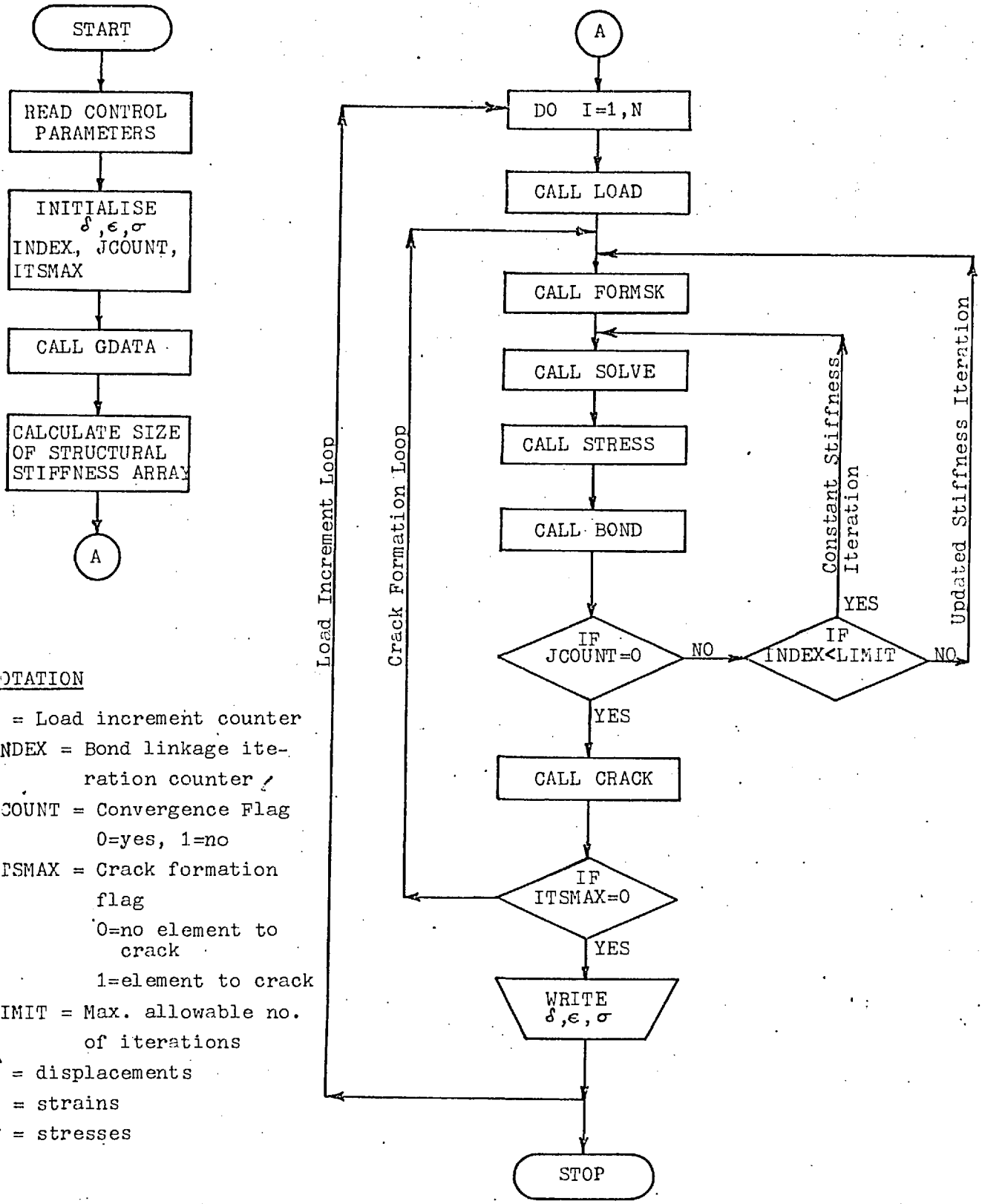


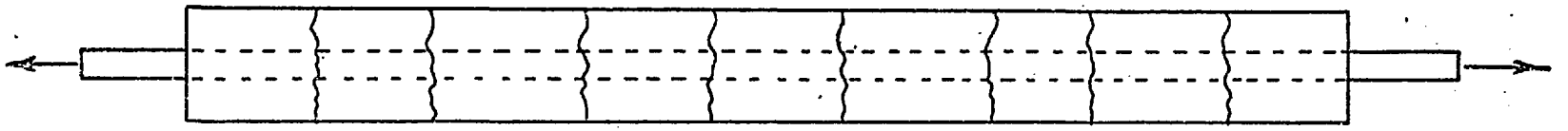
FIGURE 8.1 PROGRAM MODULES AND SUBROUTINES



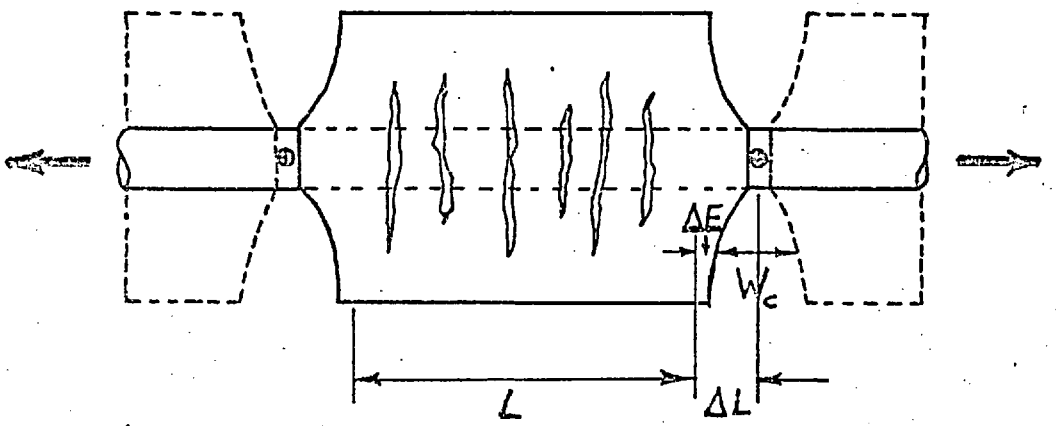
NOTATION

I = Load increment counter
INDEX = Bond linkage iteration counter
JCOUNT = Convergence Flag
0=yes, 1=no
ITSMAX = Crack formation flag
0=no element to crack
1=element to crack
LIMIT = Max. allowable no. of iterations
δ = displacements
ϵ = strains
σ = stresses

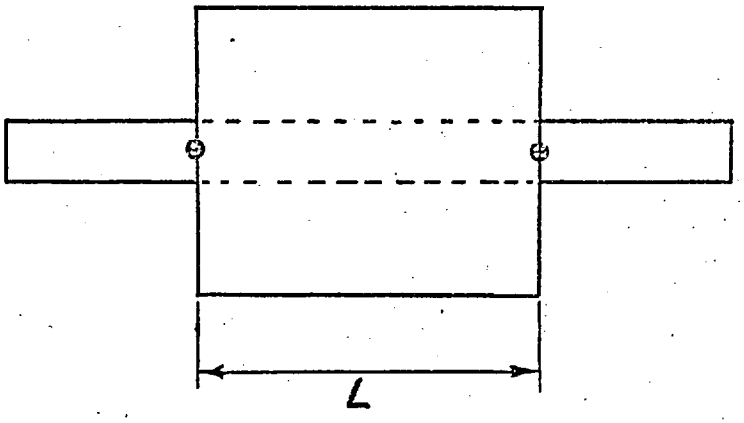
FIGURE 8.2 FLOWCHART FOR CONCMEB



(a) Long tension member



(c) Displaced end faces of (b) shown exaggerated



(b) Section bounded by two external cracks

W_c = External crack width
ΔL = Steel displacement
ΔE = Concrete displacement

$$W_c = 2(\Delta L - \Delta E)$$

FIGURE 8.3 DETERMINATION OF EXTERNAL CRACK WIDTH

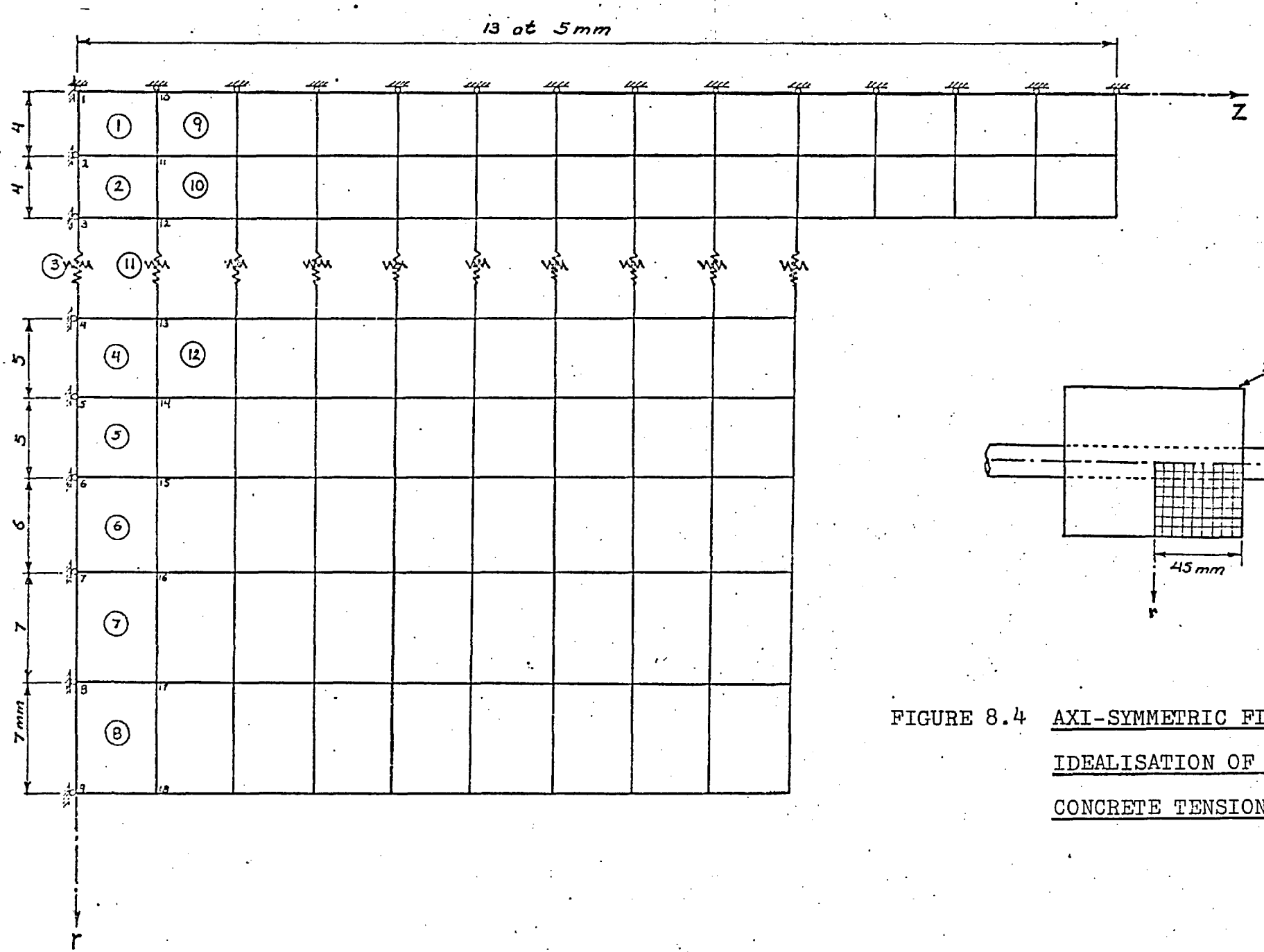


FIGURE 8.4 AXI-SYMMETRIC FINITE ELEMENT IDEALISATION OF A REINFORCED CONCRETE TENSION MEMBER

BOND-SLIP CURVES USED IN THE FINITE ELEMENT ANALYSIS

OF REINFORCED CONCRETE TENSION MEMBERS

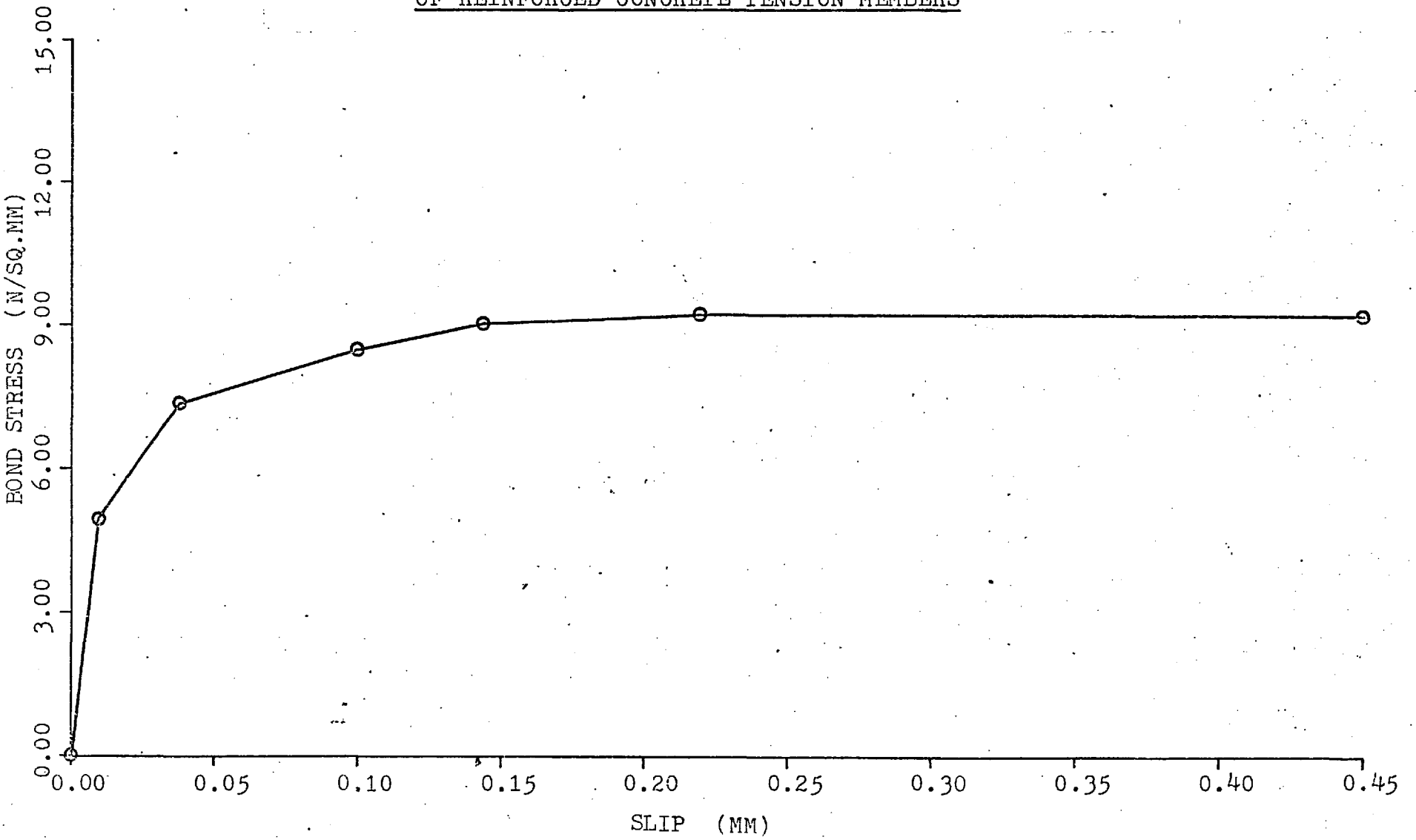


FIGURE 8.5

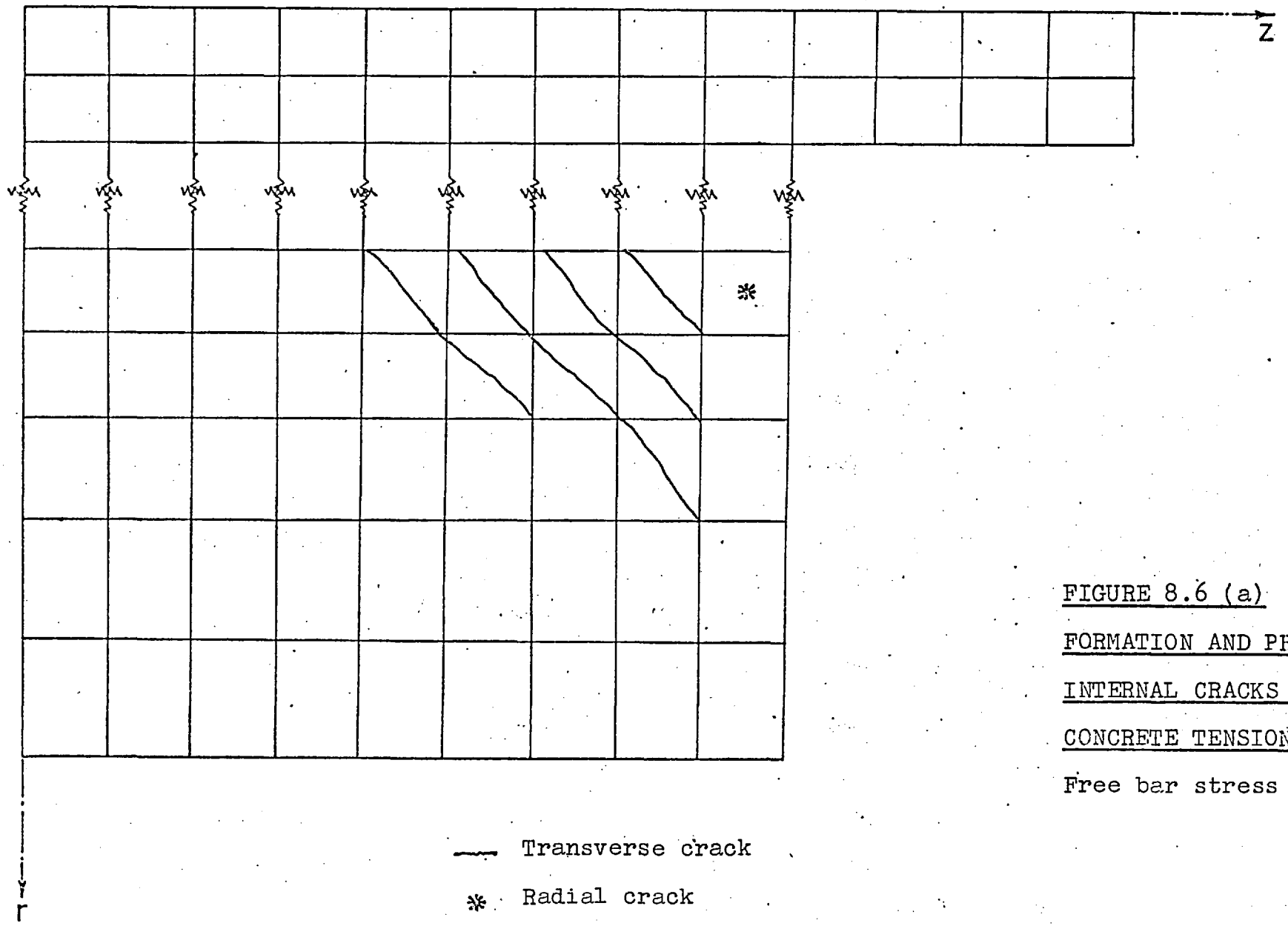


FIGURE 8.6 (a)

FORMATION AND PROPAGATION OF INTERNAL CRACKS IN REINFORCED CONCRETE TENSION SPECIMENS

Free bar stress = 99 N/mm^2

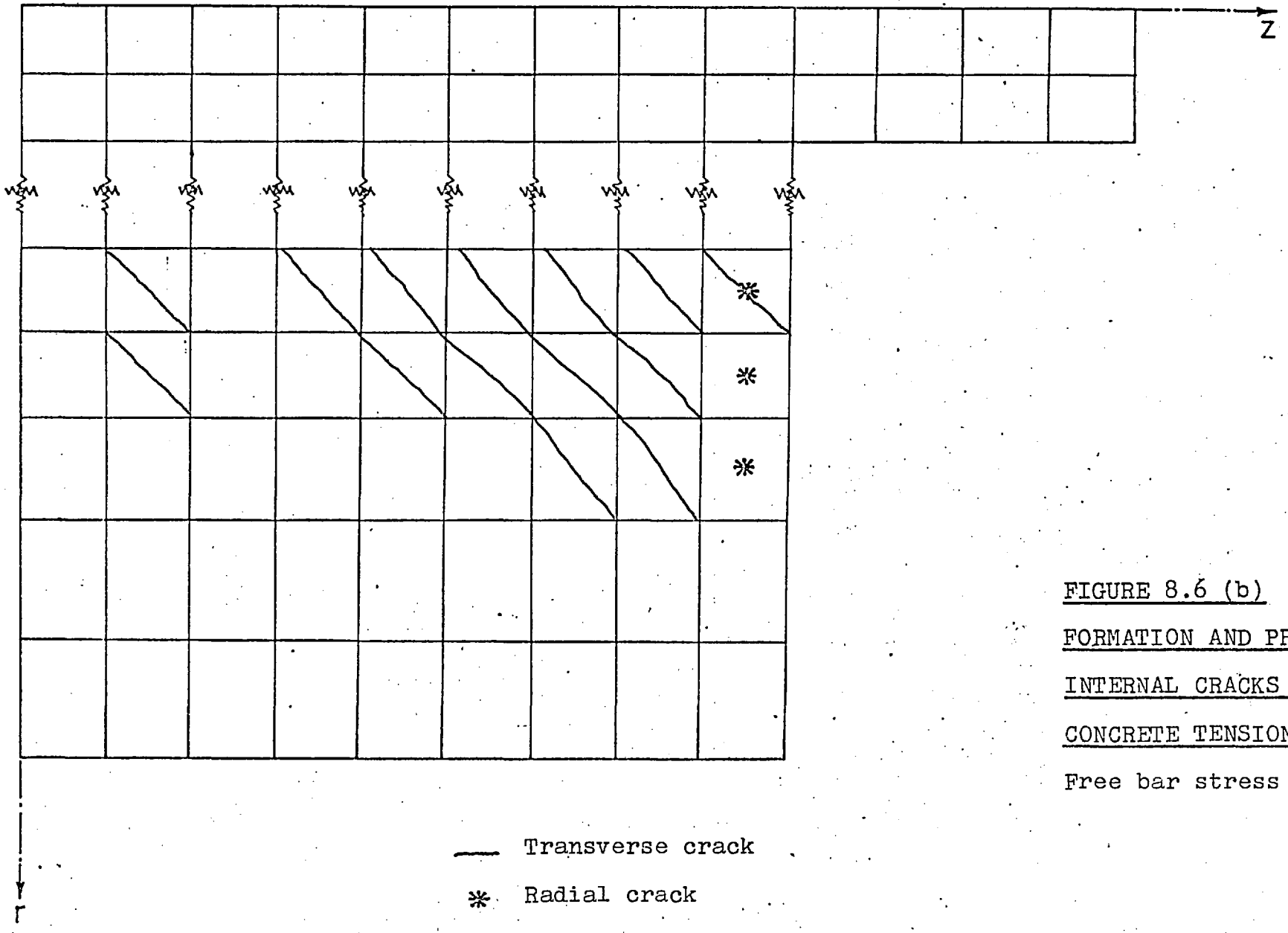


FIGURE 8.6 (b)

FORMATION AND PROPAGATION OF INTERNAL CRACKS IN REINFORCED CONCRETE TENSION SPECIMENS

Free bar stress = 149 N/mm^2

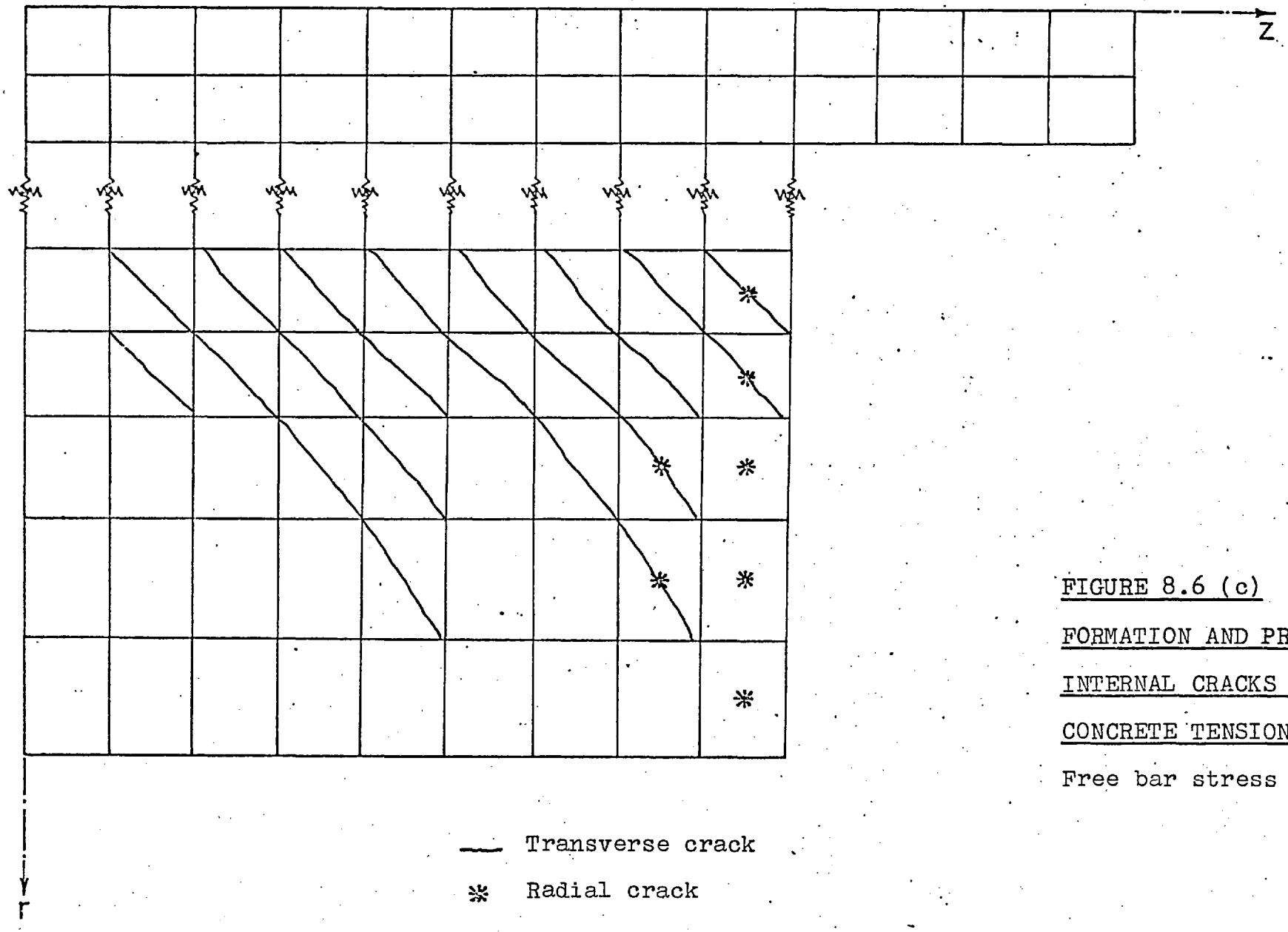


FIGURE 8.6 (c)

FORMATION AND PROPAGATION OF INTERNAL CRACKS IN REINFORCED CONCRETE TENSION MEMBERS

Free bar stress = 249 N/mm^2

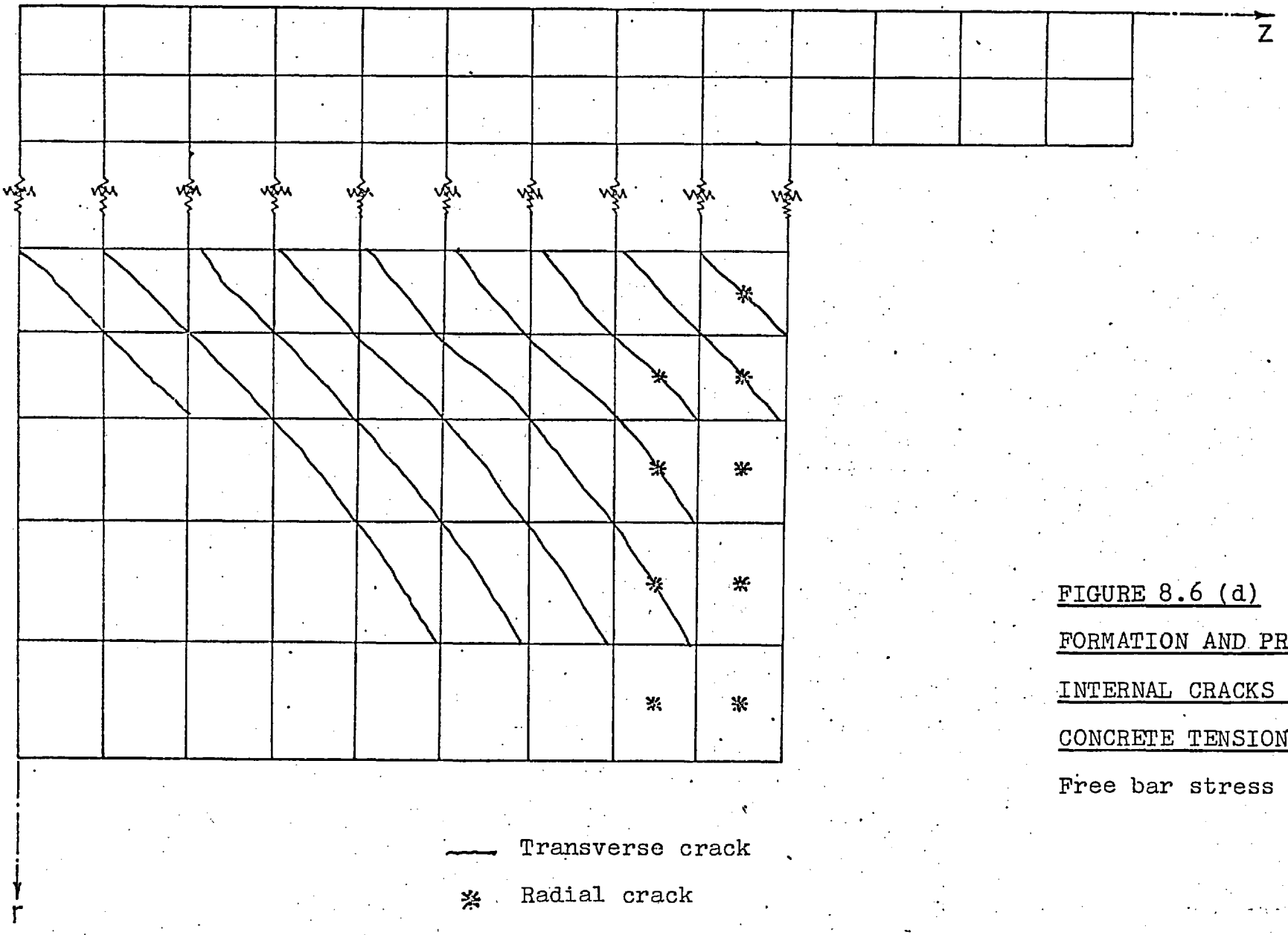


FIGURE 8.6 (d)

FORMATION AND PROPAGATION OF INTERNAL CRACKS IN REINFORCED CONCRETE TENSION MEMBERS

Free bar stress = 348 N/mm^2

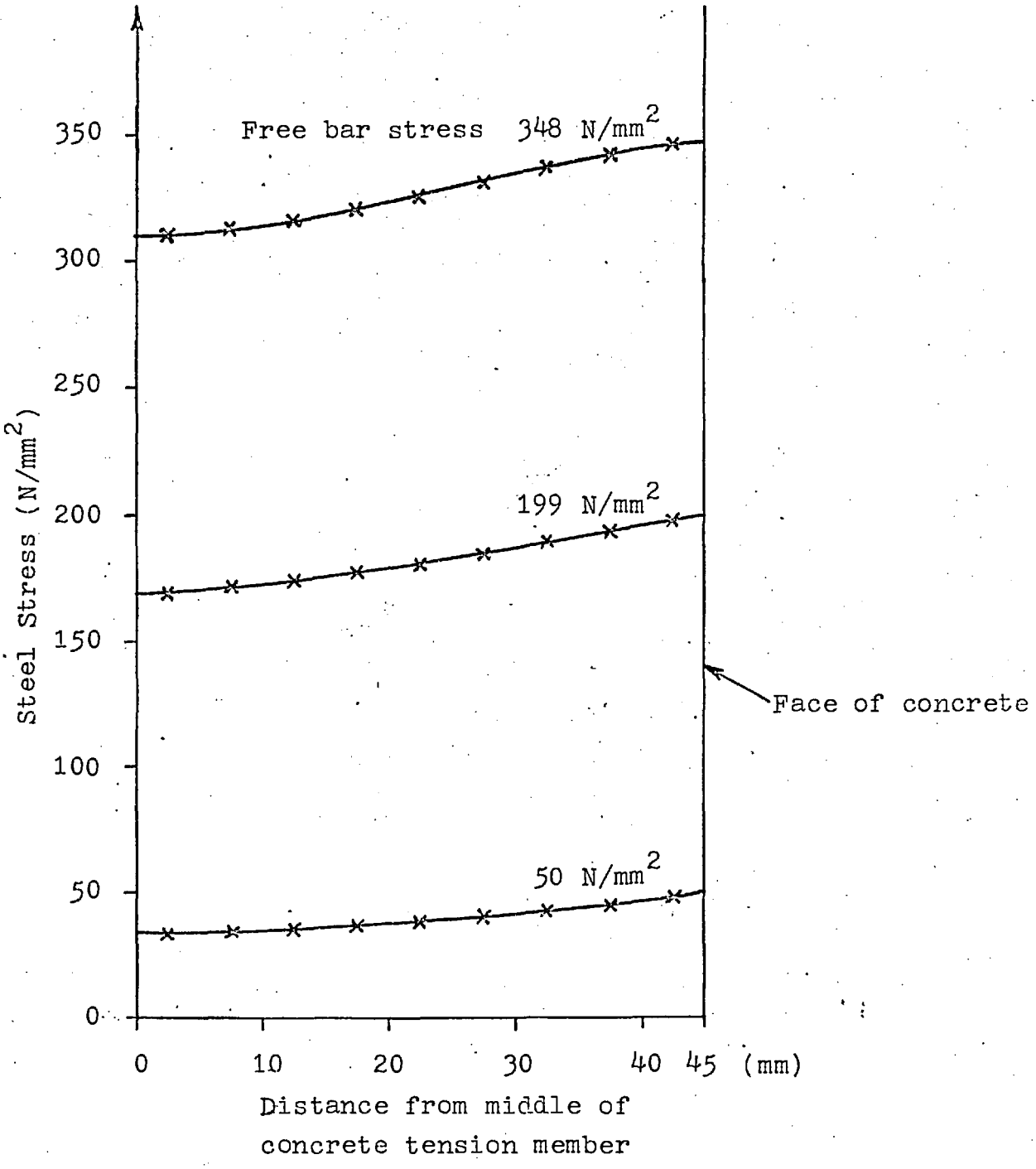


FIGURE 8.7 VARIATION OF STEEL STRESS WITH DISTANCE ALONG BAR EMBEDDED IN CONCRETE TENSION MEMBER

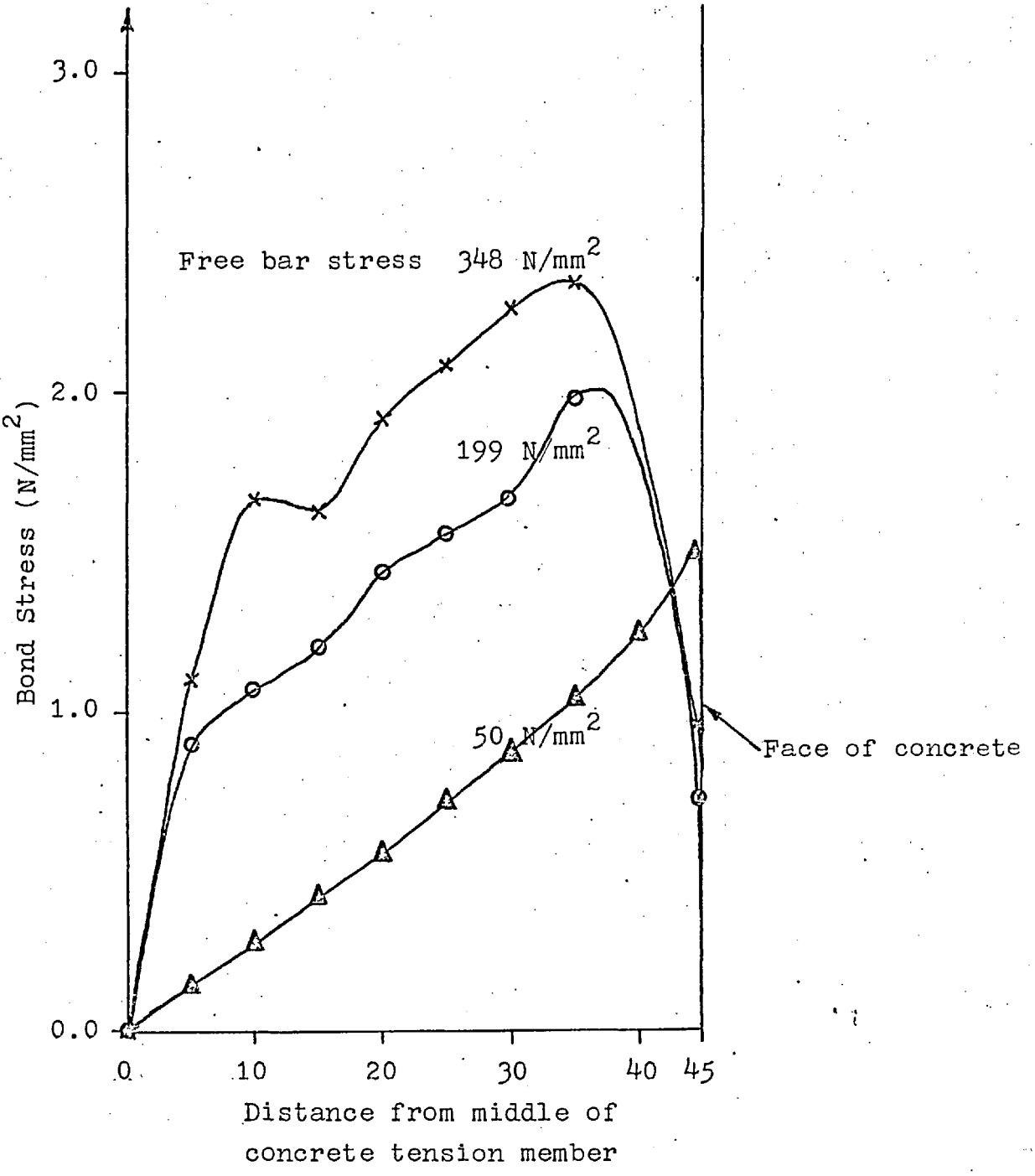


FIGURE 8.8 VARIATION OF BOND STRESS WITH DISTANCE ALONG BAR EMBEDDED IN CONCRETE TENSION MEMBER

FREE BAR STEEL STRESS - AVERAGE EMBEDDED STEEL STRAIN

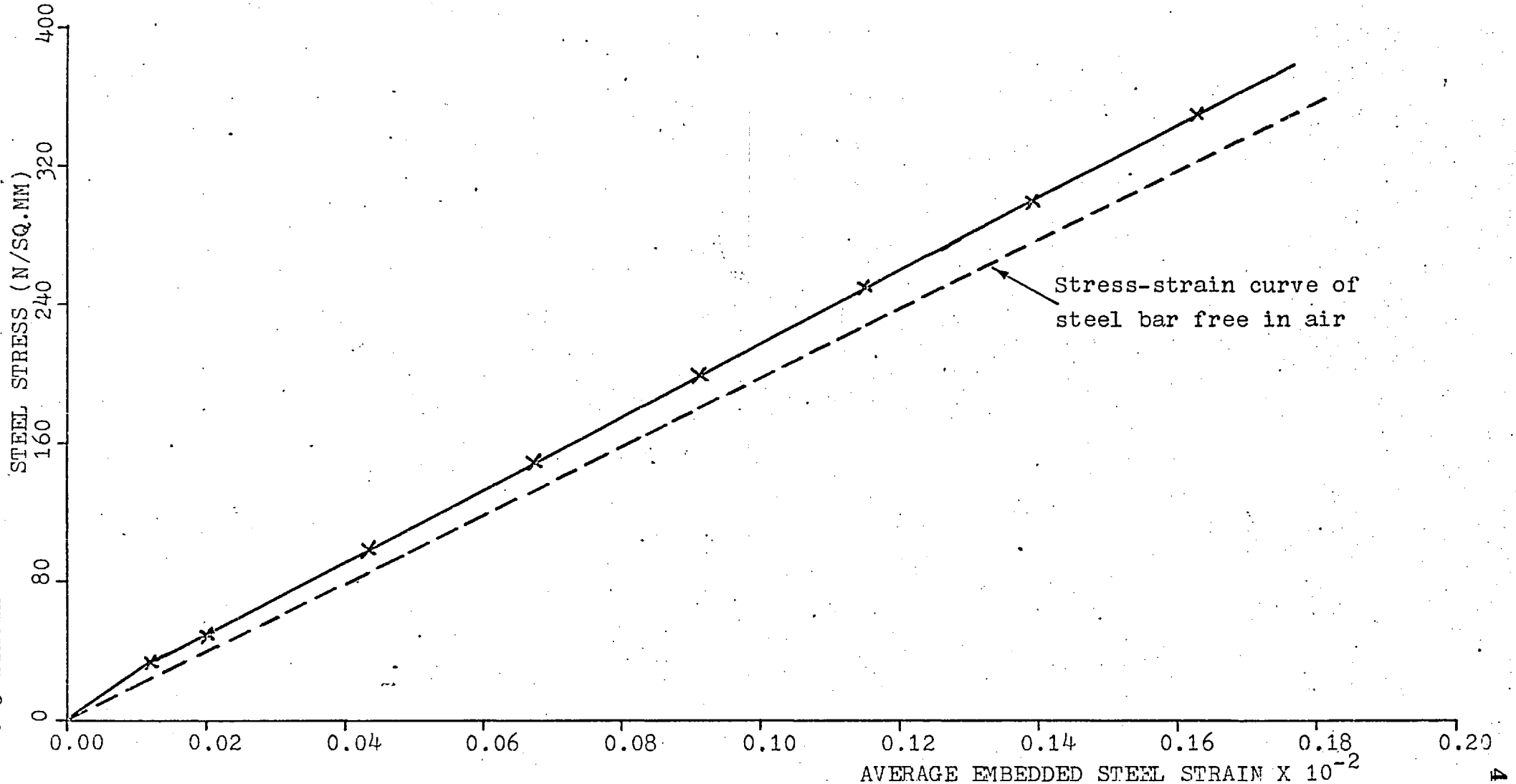


FIGURE 8.9

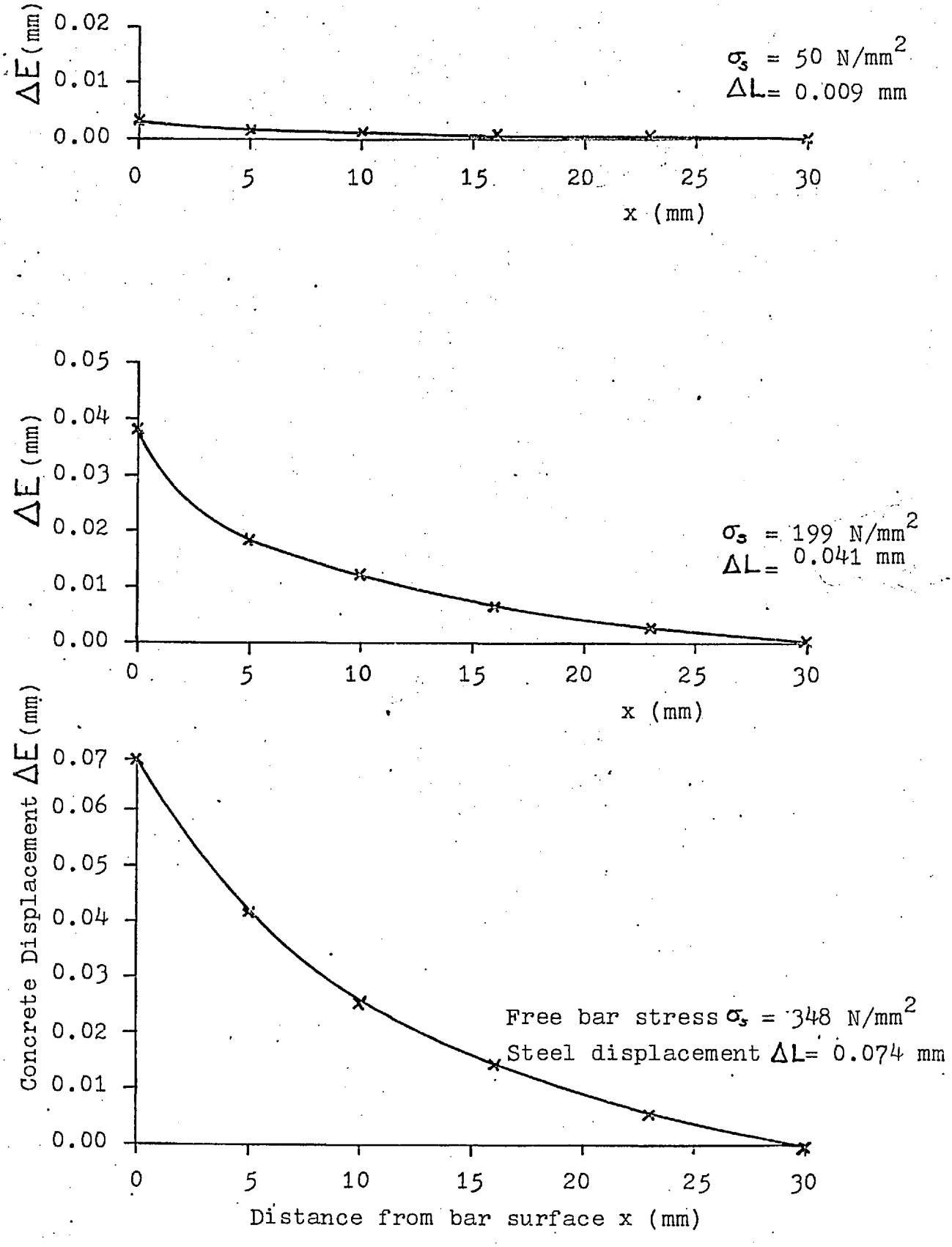


FIGURE 8.10 DISPLACEMENT OF END FACE OF REINFORCED CONCRETE TENSION MEMBER

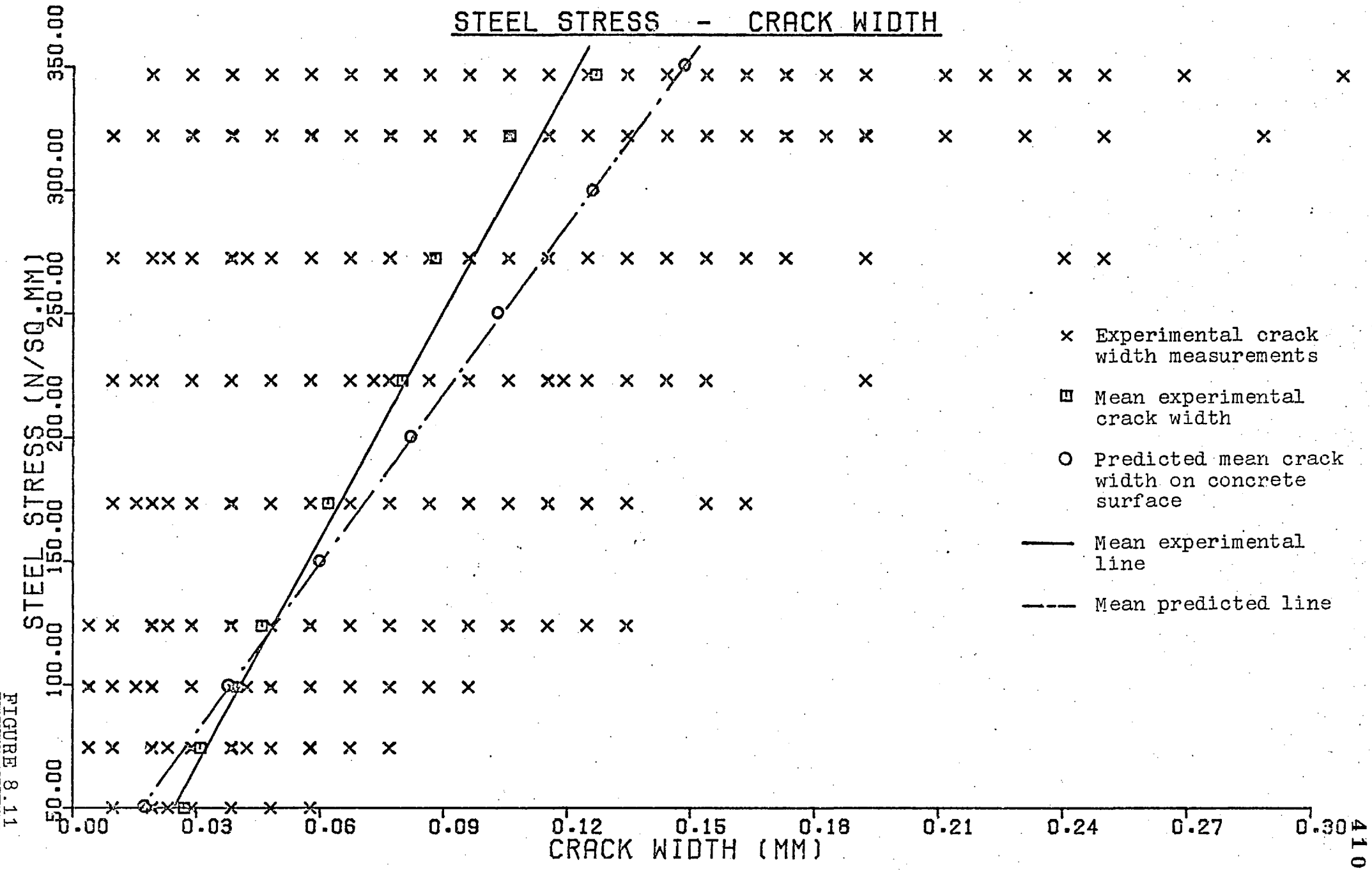

STEEL STRESS - CRACK WIDTH
STEEL STRESS (N/SQ.MM)
350.00
300.00
250.00
200.00
150.00
100.00
50.00
0.00
0.03
0.06
0.09
0.12
0.15
0.18
0.21
0.24
0.27
0.30
CRACK WIDTH (MM)
Experimental crack width measurements
Mean experimental crack width
Predicted mean crack width on concrete surface
Mean experimental line
Mean predicted line

FIGURE 8.11

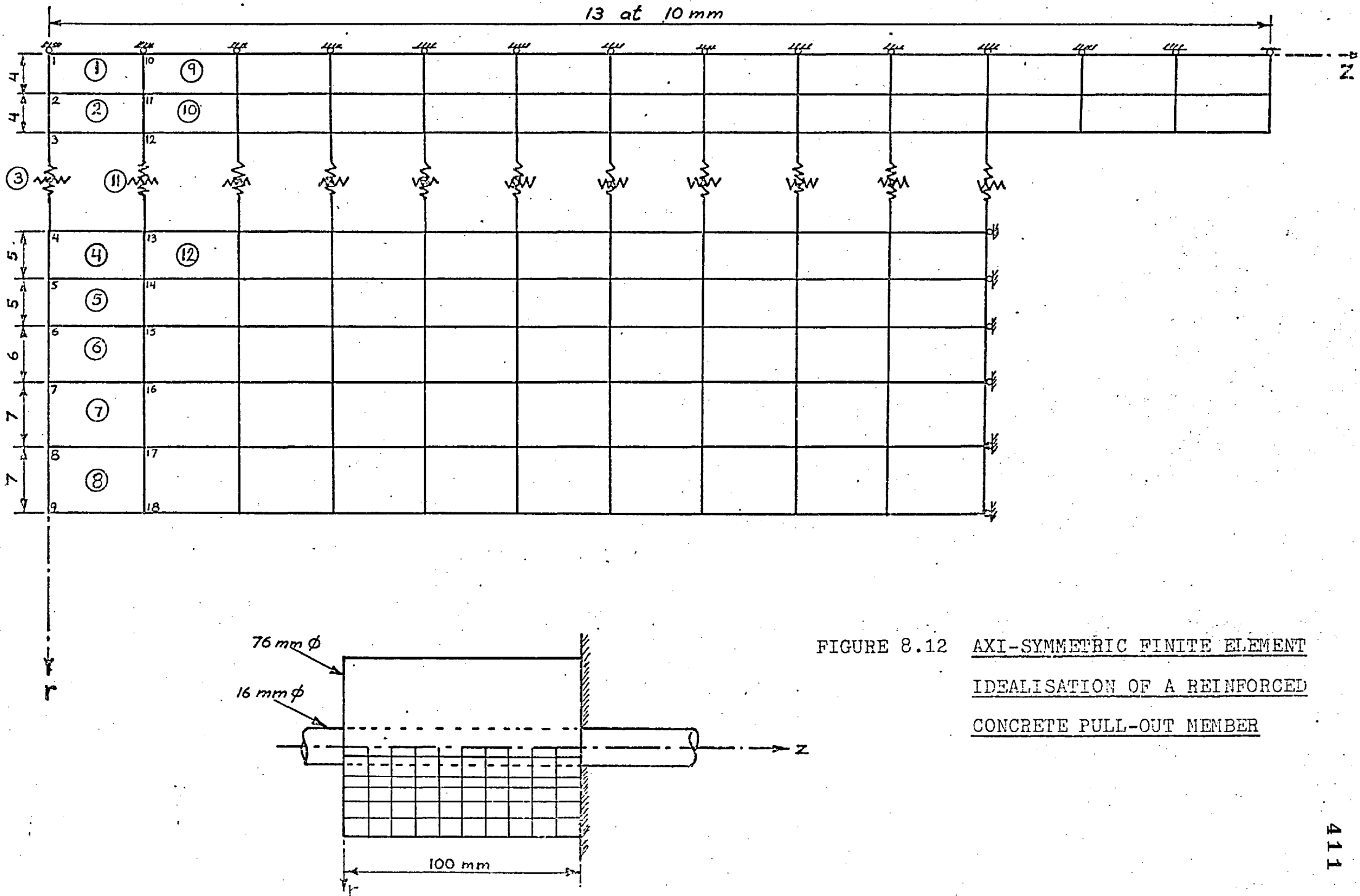


FIGURE 8.12 AXI-SYMMETRIC FINITE ELEMENT IDEALISATION OF A REINFORCED CONCRETE PULL-OUT MEMBER

BOND-SLIP CURVES USED IN THE FINITE ELEMENT ANALYSIS

OF REINFORCED CONCRETE PULL-OUT MEMBERS

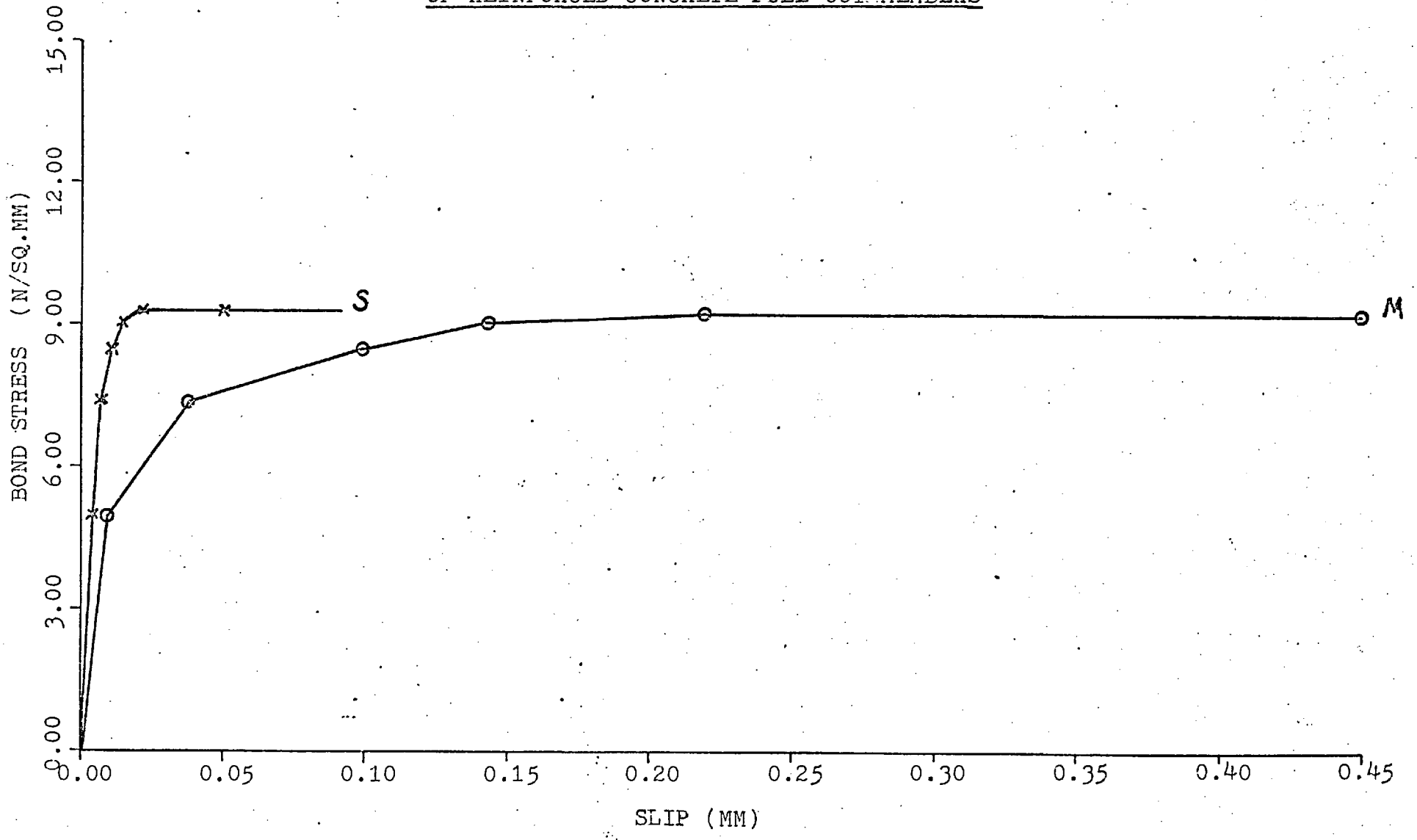


FIGURE 8.13

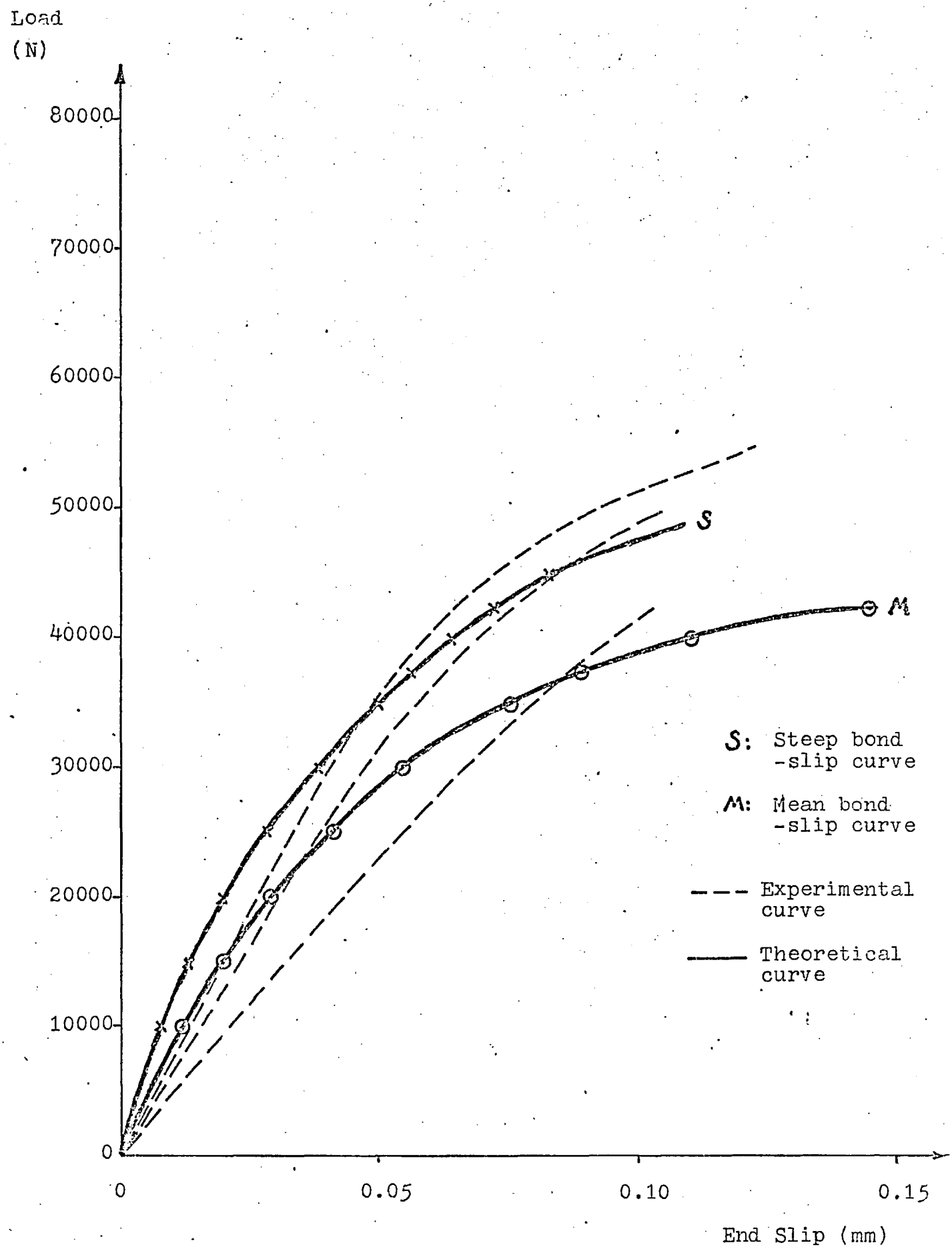


FIGURE 8.14 THEORETICAL AND EXPERIMENTAL LOAD VERSUS LOADED END SLIP CURVES FOR 100 MM LONG PULL-OUT SPECIMENS

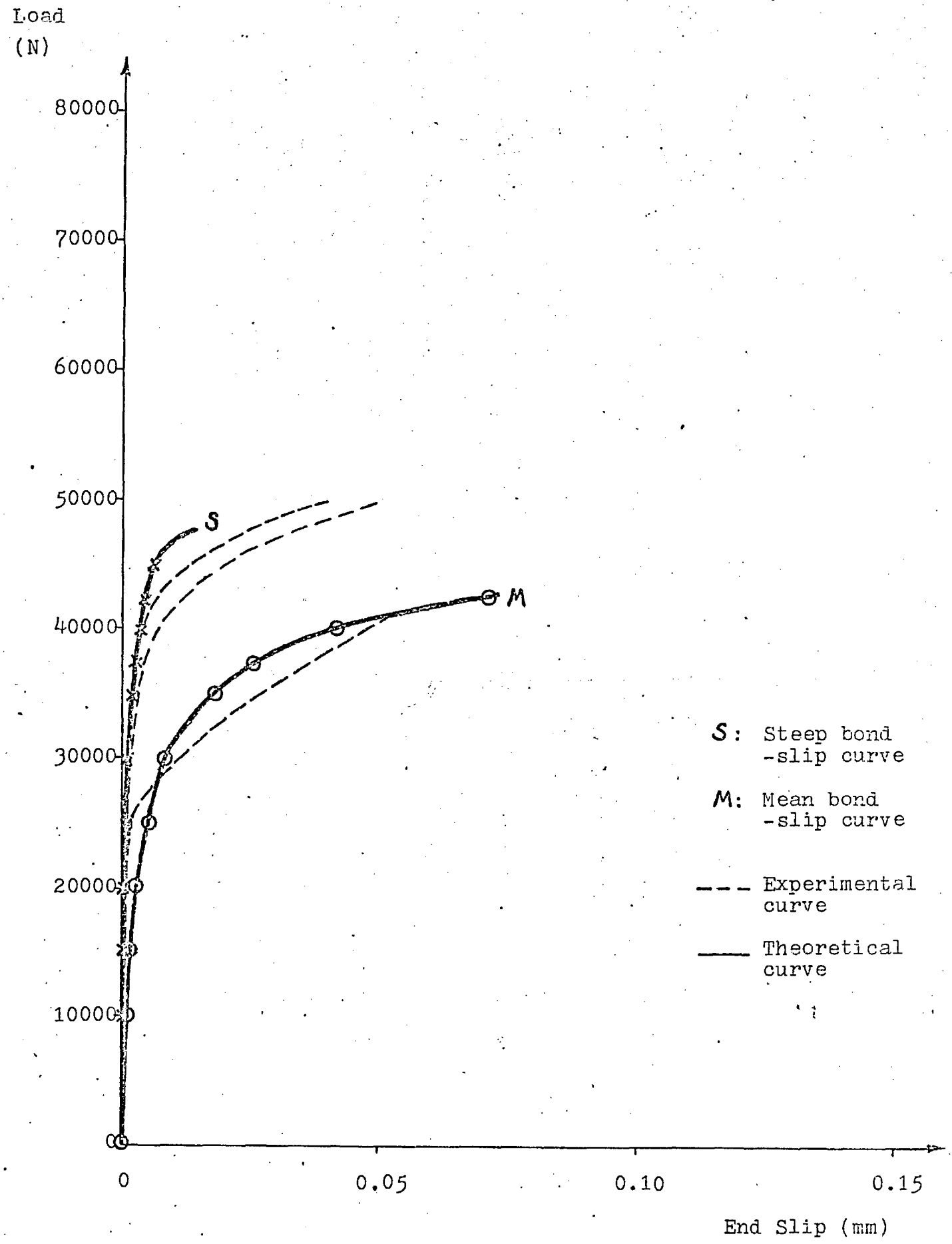


FIGURE 8.15 THEORETICAL AND EXPERIMENTAL LOAD VERSUS FREE END SLIP CURVES FOR 100 MM LONG PULL-OUT SPECIMENS

CHAPTER 9

MAIN CONCLUSIONS OF PRESENT INVESTIGATION AND SUGGESTIONS FOR FUTURE RESEARCH

9.1. MAIN CONCLUSIONS OF THE FATIGUE INVESTIGATION

In fatigue, the following conclusions can be drawn from the tests :

(a) A considerable scatter is present in fatigue data and thus a large number of tests are required to obtain a reliable estimate of the fatigue properties. Consequently statistical techniques are essential for obtaining and comparing mean stress range-number of cycles to failure (S - N) curves.

(b) The S - N curves of four different hot rolled deformed bars marketed in the United Kingdom differed widely when tested both with and without identification marks in the test length. With identification marks in the test length, the bar with the largest fatigue life is the Sheerness bar and the one with the shortest fatigue life the Welbond bar. The Sheerness bar is also the bar with the largest fatigue life, when no identification marks are present, and Unisteel the one with the shortest fatigue life.

(c) Identification marks on hot rolled deformed bars act as stress raisers. All bars with identification marks included in their test length fail at one of these marks, except for the Unisteel bar which has marks with a smooth

profile. There is an appreciable reduction in fatigue life due to the identification marks and its magnitude depends on their stress concentration factor. Suitable profiling of the identification marks can eliminate this effect.

(d) The fatigue life of hot rolled deformed bars is reduced when the test length increases.

(e) The stress concentration at a crack and the local fretting between steel and concrete in the vicinity of a crack would appear to produce a large reduction in fatigue life when compared to that of an appropriate length of steel tested free in air.

9.2. MAIN CONCLUSIONS OF THE BOND AND CRACKING INVESTIGATION

From the research reported on bond and cracking the following conclusions can be drawn :

(a) A considerable scatter is present in the bond stress - slip curves of hot rolled deformed and mild steel plain bars. Thus a sufficient number of test replications are necessary to obtain reliable estimates of the curves and to assess the effects of different factors statistically.

(b) There is no appreciable difference in the mean initial slope of bond stress - slip curves obtained from specimens of different concrete cover to steel, different bar back load values or different direction of bar pull relative to the direction of settlement of concrete.

(c) The maximum bond stress is not significantly affected by the magnitude of the bar back load and hence by inference by distance from a crack face, or a loaded end, in

a concrete member. The maximum bond stress nevertheless increases with increasing concrete cover. It also increases, but to a lesser extent, by pulling the bar in the opposite rection to that of casting as compared to pulling it in the same direction.

(d) The maximum bond stress developed by plain bars is only 1/2 to 1/3 of that of deformed bars and is reached at much smaller slips than those for the deformed bars.

(e) The bond stress - slip curves under repeated loading are characterised by residual slip at zero load and hysteresis loops formed by the loading and unloading paths. Every load cycle produces additional slip, at any load level, which tends to diminish for an increasing number of equal magnitude load repetitions and the hysteresis loops become more congested. However, the first cycle is the one which causes most of the bond destruction, i.e. additional slip, and the higher the peak load the larger the bond destruction is at the first cycle as well as at subsequent cycles.

(f) The non-linear finite element program, incorporating the bond stress - slip relations of hot rolled deformed bars forecast satisfactorily the experimentally obtained relation between bar load and end slip in pull-out specimens. The relation between steel stress at a crack and mean crack width in reinforced concrete tension members was also forecast satisfactorily and the program was also capable predicting the formation and propagation of internal cracks.

(g) Analytical results suggest that the maximum bond stress in the tensile specimens, at 80 % of the yield stress

of the bar, was only 30 % of the maximum stress obtained in the short length specimens. Conversely the maximum bond stress in the pull-out specimens reached the maximum values obtained in the short length specimens.

9.3. SUGGESTIONS FOR FUTURE RESEARCH

Lastly arises the question of suggestions for future research. In the present investigation fatigue tests were carried out on two test lengths of hot rolled deformed bars in air and one test length of deformed bars embedded in concrete tension members. It is suggested that more fatigue tests should be carried out with different lengths of both kinds of specimens to establish the separate effects of test length and stress concentration at a crack. It is also suggested that fatigue tests in the long life region of the S-N curves should be carried out, since the present investigation was limited to the finite life. Also another related area for further investigations is that of applying a spectrum of loading on reinforcing bars and try to predict their fatigue lives from the results of fatigue tests of constant amplitude.

Further tests with a statistical basis should be carried out on the short length pull-out specimens to establish the effect of repeated fluctuating and alternating loading on the bond characteristics, for various values of minimum stress amplitude. These characteristics and their statistical variation should then be used in conjunction with a similar finite element program as presented here to forecast crack widths of tension members under given load histories and these analytical

results should be compared to corresponding experimental studies. This suggested programme is thus aimed at establishing the effect of load history on the width of cracks in tension members.

REFERENCES

1. MADAYAG A.F. ''Metal fatigue: Theory and design''. John Wiley and Sons, New York, 1969.

2. FORREST P.G. ''Fatigue of metals''. Pergamon Press, New York, 1962.

3. HEYWOOD R.B. ''Designing against fatigue''. Chapman and Hall, London, 1962.

4. TETELMAN A.S. and McEVILY Jr. A.J. ''Fracture of structural materials''. John Wiley and Sons, 1967.

5. REHM G. ''Contributions to the problem of the fatigue strength of steel bars for concrete reinforcement''. Preliminary Publication, 6th Congress of the IABSE (Stockholm, 1960), International Association for Bridge and Structural Engineering, Zurich, 1960, pp. 35-46.

6. SORETZ S. ''Fatigue behaviour of high-yield steel reinforcement''. Concrete and Constructional Engineering (London), V. 60, No. 7, July 1965, pp. 272-280.

7. WASCHEIDT H. ''On the fatigue strength of embedded concrete reiforcing steel (Zur frage der dauerschwing-

festigkeit von betonstählen im einbetonierten zustand)''. Doctoral Thesis, Technical University of Aachen, Germany, 1965.

8. GORODNITSKY F.M. and KONEVSKY W.P. ''Investigation of the fatigue properties of steel reinforcement''. Steel for Prestressing, FIP Symposium (Madrid, June 1968), Theme 7.

9. BANNISTER J.L. ''The behaviour of reinforcing bars under fluctuating stress''. Concrete (London), October 1969, pp. 405-409.

10. SNOWDON L.C. ''The static and fatigue performance of concrete beams with high strength deformed bars''. Current Paper No. CP 7/71, Building Research Station, Garston, Watford, March 1971.

11. GRONQVIST N. ''Fatigue strength of reiforcing bars''. Second International Symposium on Concrete Bridge Design, SP-26, American Concrete Institute, Detroit, 1971, pp. 1011-1059.

12. PFISTER J.F. and HOGNESTAD E. ''High strength bars as concrete reinforcement, Part 6, Fatigue tests''. Journal of the PCA Research and Development Laboratories, V. 6, No. 1, January 1964, pp. 65-84.

13. BURTON K.T. ''Fatigue tests of reinforcing bars''. Jounal of the PCA Research and Development Laboratories, V. 7, No. 3, September 1965, pp. 13-23.

14. BURTON K.T. and HOGNESTAD E. ''Fatigue test of reinforcing bars- Tack welding of stirrups''. ACI Journal, Proceedings V. 64, No. 5, May 1967, pp. 244-252.

15. HANSON J.M., BURTON K.T. and HOGNESTAD E. ''Fatigue tests of reinforcing bars - Effect of deformation pattern''. Journal of the PCA Research and Development Laboratories, V. 10, No. 3, September 1968, pp. 2-13.

16. HANSON J.M., SOMES M.F. and HELGASON T. ''Investigation of design factors affecting fatigue strength of reinforcing bars-Test program''. Abeles Symposium on Fatigue of Concrete, SP-41, American Concrete Institute, Detroit, 1974, pp. 71-106.

17. HELGASON T. and HANSON J.M. ''Investigation of design factors affecting fatigue strength of reinforcing bars-Statistical analysis''. Abeles Symposium on Fatigue of Concrete, SP-41, American Concrete Institute, Detroit, 1974, pp. 107-138.

18. ACI COMMITTEE 215. ''Considerations for design of concrete structures subjected to fatigue loading''. ACI Journal, Proceedings V.71, No. 3, March 1974, pp. 97-121.

19. LASH S.D. ''Can high-strength reinforcement be used for highway bridges?''.
First International Symposium on Concrete Bridge Design, SP-22, American Concrete Institute, Detroit, 1969, pp. 283-299.

20. MACGREGOR J.C., JHAMB I.C. and NUTTALL N. ''Fatigue strength of hot- rolled reinforcing bars''.
ACI Journal, Procceedings V.68, No. 3, March 1971, pp. 169-179.

21. JHAMB I.C. and MACGREGOR J.C. ''Effect of surface characteristics on fatigue strength of reinforcing steel''.
Abeles Symposium on Fatigue of Concrete, SP-41, American Concrete Institute, Detroit, 1974, pp. 139-168.

22. JHAMB I.C. and MACGREGOR J.C. ''Stress concentrations caused by reinforcing bar deformations''.
Abeles Symposium on Fatigue of Concrete, SP-41, American Concrete Institute, Detroit, 1974, pp. 169-182.

23. KOKUBU M. and OKAMURA H. ''Fundamental study on fatigue behaviour of reinforced concrete beams using high strength deformed bars''.
Transactions, Japan Society of Civil Engineers (Tokyo), No. 122, October 1965, pp. 1-28 (in Japanese with English summary).

24. KOKUBU M., TADA Y., TACHIBANA I. and MATSUMOTO Y. ''Fatigue behaviour of reiforced concrete beams with high-strength deformed bars''. Transactions, Japan Society of Civil Engineers (Tokyo), No. 122, October 1965, pp. 29-42 (in Japanese with English summary).

25. NAKAYAMA N. ''Fatigue test on T-shaped concrete beams reinforced with deformed bars''. Transactions, Japan Society of Civil Engineers (Tokyo), No. 122, October 1965, pp. 43-50 (in Japanese with English summary).

26. KOKUBU M. and OKAMURA H. ''Fatigue behaviour of high strength deformed bars in reinforced concrete bridges''. First International Symposium on Concrete Bridge Design, SP-23, American Concrete Institute, Detroit, 1969, pp. 301-316.

27. WARNER R.F. and HULSBOS C.L. ''Probable fatigue life of prestressed concrete flexural members''. Report No. 223-24A, Fritz Engineering Laboratory, Lehigh University, July 1962.

28. BENNETT E.W. and BOGA R.K. ''Some fatigue tests of large diameter deformed hard drawn wire''. Civil Engineering and Public Works Review (London), V. 62, No. 726, January 1967, pp. 59-61.

29. BAUS R. and BRENNEISEN A. ''The fatigue strength of

prestressing steel''.
Steel for Prestressing, FIP Symposium (Madrid, June 1968), Cement and Concrete Association, London, 1969, pp. 95-117.

30. EDWARS A.D. and PRICE K.M. ''Fatigue characteristics of bonded post-tensioned concrete I-beams''.
Report CSTR 69-1, Concrete Structures and Technology, Imperial College, June 1969.

31. REUNION INTERNATIONAL DES LABORATOIRES D'ESSAI ET DE RECHERCHES SUR LES MATERIAUX ET LES CONSTRUCTIONS.
''Bond and crack formation in reinforced concrete''.
RILEM Symposium, Stockholm, 1957.

32. WATSTEIN D. and BRESLER B. ''Bond and cracking in reinforced concrete''.
Reinforced Concrete Engineering, Volume 1, John Wiley and Sons, 1974.

33. BROMS B. ''Technique for investigation of internal cracks in reinforced concrete members''.
ACI Journal, Proceedings V.62, No. 1, January 1965, pp. 35-43.

34. BROMS B. 'Stress distribution in reinforced concrete members with tension cracks''.
ACI Journal, Proceedings V.62, No.9, September 1965, pp. 1095-1108.

35. BROMS B. 'Crack width and crack spacing in reinforced concrete members''.
ACI Journal, Proceedings V.62, No. 10, October 1965, pp. 1237-1255. Also ACI Supplement.

36. BROMS B. and LUTZ L. ''Effect of arrangement of reinforcement on crack width and spacing in reinforced concrete members''.
ACI Journal, Proceedings V.62, No. 11, November 1965, pp. 1395-1409.

37. BRESLER B. and BERTERO V. ''Behaviour of reiforced concrete under repeated load''.
Journal of the Structural Division of ASCE, V.94, ST6, June 1968, pp. 1567-1590.

38. GOTO Y., UEDA S. and MAKI Y. ''Investigation on tension cracks in reinforced concrete members''.
(in Japanese) Japan Society of Civil Engineers, The Second Symposium on Deformed Bars, Concrete Library No. 14, Tokyo, December 1965.

39. GOTO Y. ''Cracks formed in concrete around deformed tension bars''.
ACI Journal, Proceedings V.68, No. 4, April 1971, pp. 244-251.

40. WATSTEIN D. ''Bond stress in concrete pull-out specimens''.
ACI Journal, Proceedings V. 13, No. 1, September 1941, pp.37-50.

41. WATSTEIN D. ''Distribution of bond stress in concrete pull-out specimens''.
ACI Journal, Proceedings V.18, No. 9, May 1947, pp. 1041-1052.

42. MAINS R.M. ''Measurement of the distribution of tensile stresses along reinforcing bars''.
ACI Journal, Proceedings V.23, No. 3, November 1951, pp. 225-252.

43. EVANS R.H. and WILLIAMS A. ''Bond stress in prestressed concrete from X-ray photographs''.
Proceedings ICE, Part 1, V.4, No. 2, March 1955, pp. 212-235.

44. EVANS R.H. and WILLIAMS A. ''Bond stress and crack width in beams reiforced with square grip reinforcement''.
RILEM Symposium on Bond and Crack Formation in Reinforced Concrete, V.I, Stockholm, 1957, pp. 105-116.

45. NILSON A.H. ''Bond stress-slip relations in reinforced concrete''.
Report No. 345, Department of Structural Engineering, Cornell University, New York, December 1971.

46. WAHLA M.I., SCOTT N.R. and NILSON A.H. ''Direct measurement of bond-slip in reinforced concrete''.
Proceedings of American Society of Agricultural engineers, 1969, paper 69-921.

47. NILSON A.H. ''Finite element analysis of reinfoced concrete''.
Ph.D. Thesis, University of California, Berkeley, June 1967, pp.192.

48. NILSON A.H. ''Non linear analysis of reinforced concrete by the finite element method''.
ACI Journal, Proceedings V. 65, No. 9, Sptember 1968, pp. 757-766.

49. BRESLER B. and BERTERO V. ''Influence of load history on cracking in reinforced concrete''.
Report to California Division of Highways, Department of Civil Engineering, Division of Structural Engineering and Structural Mechanics, University of California, Berkeley, 1966.

50. REHM G. ''The basic principles of the bond between steel and concrete''.
Cement and Concrete Association Translation No. 134, from the German Deutscher Ausschuss fur Stahlbeton No. 138: Uber die grundlagen des Verbundes zwischen stahl und beton, 1961.

51. LUTZ L.A. and GERGELY P. ''The mechanics of bond and slip of deformed reinforcing bars in concrete''.
Research Report No. 324, Department of Structural Engineering, Cornell University, 1966.

52. LUTZ L.A. and GERGELY P. ''Mechanics of bond and slip of deformed bars in concrete''.

ACI Journal, Proceedings V.64, No. 11, November 1967, pp. 711-721.

53. STOCKER M.F. and SOZEN M.A. ''Investigation of prestressed reinforced concrete for highway bridges, Part V: Bond characteristics of prestressing strand''. Bulletin No. 503, Engineering Experiment Station, College of Engineering, University of Illinois, 1970.

54. MORITA S. and KAKU T. ''Local bond stress-slip relationship under repeated loading''. IABE Symposium on the resistance and ultimate deformability of structures, Lisbon, 1973.

56. EDWARDS A.D. and PICARD A. ''The fatigue and bond characteristics of prestressing strand''. Report No. CSTR 71/8, Concrete Structures and Technology, Imperial Cllege, November 1971.

57. EDWARDS A.D. and PICARD A. ''Bonding properties of $\frac{1}{2}$ in. diameter strand''. ACI Journal, Proceedings V. 69, No. 11, November 1972, pp. 684-689.

58. REIS E.E. Jr., MOSER J.D., BIANCHINI A.C. and KESLER C.E. ''Causes and control of cracking in concrete reinforced with high-strength steel bars - Areview of research''. Bulletin No. 479, Engineering Experiment Station, University of Illinois, 1965.

59. ACI COMMITTEE 224. ''Control of cracking in concrete structures''.
ACI Journal, Proceedings V. 69, No. 12, December 1972, pp. 717-753.

60. ACI COMMITTEE 224. ''Causes, mechanism and control of cracking in concrete''.
ACI Bibliography, No. 9, 1971, pp. 92.

61. WATSTEIN D. and MATHEY R.G. ''Width of cracks in concrete at the surface of reinforcing steel evaluated by means of tensile bond specimens''.
ACI Journal, Proceedings V. 56, No. 7, 1959, pp. 47-56.

62. WATSTEIN D. and PARSONS D.E. ''Width and spacing of tensile cracks in axially reinforced concrete cylinders''.
Research Paper RP1545, U.S. Department of Commerce, National Bureau of standards, July 1943, pp. 24.

63. CEB COMMISSION IV. ''Report on cracking''.
Bulletin d'information No. 12, Paris, February 1959, pp. 28.

64. LUTZ L.A. ''Analysis of stresses in concrete near a reiforcing bar due to bond and transverse cracking''.
ACI Journal, Proceedings V. 67, No. 47, October 1970, pp. 778-787.

65. CATTLEY R.F. ''A review of research on the behaviour

of reinforced concrete beams and slabs''.
TRRL Supplementary Report 47 UC, Transport and Road Research Laboratory, Department of the Environment, Berkshire, 1974, pp. 22.

66. NGO D. and SCORDELIS A.C. ''Finite element analysis of reinforced concrete beams''.
ACI Journal, Proceedings V. 64, No. 3, March 1967, pp. 152-163.

67. NGO D, FRANKLIN H.A. and SCORDELIS A.C. ''Finite element study of reinforced concrete beams with diagonal tension cracks''.
Report No. UC SESM 70-19, Department of Civil Engineering, University of California, Berkeley, December 1970, pp. 88.

68. ZIENKIEWICZ O.C., VALLIAPPAN S. and KING I.P. ''Stress analysis of rock as a no tension material''.
Geothechnique V. 18, No. 1, March 1968, pp.56-66.

69. VALLIAPPAN S. and NATH P. ''Tensile crack propagation in reinforced concrete beams - finite element technique''.
International Conference on Shear, Torsion and Bond in Reinforced and Prestressed Concrete, India, January 1969.

70. VALLIAPPAN S. and DOOLAN T.F. ''Non linear stress analysis of reinforced concrete''.
Journal of Structural Division ASCE, V. 98, ST4,

April 1972, pp. 885-898.

71. ZIENKIEWICZ O.C., VALLIAPPAN S. and KING I.P. ''Elasto-plastic solutions of engineering problems, 'Initial stress' finite element approach''. International Journal of Numerical Methods in Engineering, V. 1, January 1969, pp. 75-100.

72. LOOV R.E. ''The determination of stresses and deformations of reinforced concrete after cracking''. International Conference on Structures, Solid Mechanics and Engineering Design, Southampton University, April 1969.

73. MÜHLENBRUCH C.W. ''The effect of repeated loading on the bond strength of concrete''. Proceedings ASTM, Part I, V. 45, 1945. Proceedings ASTM, Part II, V. 48, 1948.

74. PERRY E.S. and JUNDI N. ''Pull-out bond stress distribution under static and dynamic repeated loadings''. ACI Journal, Proceedings V. , No. 5, May 1969, pp. 377-380.

75. ISMAIL M.A. and JIRSA J.O. ''Bond deterioration in reinforced concrete subjected to low cycle loads''. ACI Journal, Proceedings V. 69, No. 6, June 1972, pp. 334-343.

76. SINGH H.N., FERSTLE K.H. and TULIN L.G. ''Shear strength of concrete beams under cyclic loading - A

liminary study''.
IABE Symposium on Resistance and Ultimate Deformability of Structures, Lisbon, 1973.

77. ROAD RESEARCH LABORATORY. ''Design of concrete mixes''. Road Research Note No. 4, 2nd Edition, HMSO, 1950, pp. 16.

78. McINTOSH J.D. ''Concrete mix design''. Cement and Concrete Association, London, 1964.

79. BRITISH STANDARDS INSTITUTION. ''Hot rolled steel bars for the reinforcement of concrete''. BS 4449 : 1969.

80. AMSLER MANUAL. Instruction No. 122/10, Alfred J. Amsler & Company, Schaffhausen, Switzerland.

81. BRITISH STANDARDS INSTITUTION. ''Methods for the load verification of testing machines''. BS 1610 : 1964.

82. BRITISH STANDARDS INSTITUTION. ''Dynamic foce calibration of axial load fatigue testing machines by means of a strain gauge technique''. Draft for Development, DD2 : 1971.

83. BRITISH STANDARDS INSTITUTION. ''Methods for fatigue testing''. BS 3518
Part 1. General principles, 1962.
Part 3. Direct stress fatigue tests, 1963.
Part 5. Guide to the application of statistics, 1966.

84. AMERICAN SOCIETY FOR TESTING MATERIALS. ''A guide for fatigue testig and the statistical analysis of fatigue data''.
ASTM Special Technical Publication, No. 91-A, Committee E-9, Philadelphia, 1963.

85. FIP COMMISSION ON STEEL FOR PRESTRESSING. ''Recommendations for the Approval, Supply and Acceptance of Steels for Prestressing Tendons''.
1974

86. HALD A. ''Statistical theory with engineering applications''.
John Wiley and Sons, New-York, 1952.

87. HALD A. ''Statistical tables and formulas''.
John Wiley and Sons, New-York, 1952.

88. PARSONS R. ''Statistical analysis: a decision making approah''.
Harper and Row, New-York, 1974.

89. DIXON W.J. and MSSEY F.J. ''Introduction to statistical analysis''
McGraw - Hill Book Company, New-York, 1962.

90. CROW E.L., DAVIS F.A. and MAXFIELD M.N. ''Statistics manual''.
Dover Publications Inc., New-York, 1960.

91. DRAPER N.R. and SMITH H. ''Applied regression analysis''.
Wiley, New-York, 1968.

92. BLOM G. ''Statistical estimates and transformed Beta variables''.
John Wiley and Sons, New-York, 1958.

93. KIMBALL B.F. ''On the choice of plotting positions on probability paper''.
Journal of the American Statistical Association, V. 55, 1960, pp. 546-560.

94. ZIENKIEWICZ O.C. ''The finite element method in engineering science''.
McGraw-Hill, London, 1971.

95. LIVESLEY R.K. ''Matrix methods of structural analysis''.
Pergamon Press, Oxford, 1964.

96. FRAEIJS DE VEUBEKE B. ''Displacement and equilibrium models in the finite element method''.
Chapter 9 in Stress Analysis, ed. Zienkiewicz O.C. and Holister G.S., Wiley, London, 1965.

97. MELOSH R.J. ''Basis for derivation of matrices for the direct stiffness method''.
AIAA Journal, V. 1, No. 7, 1963, pp. 1631-37.

98. IRONS B.M. and BARLOW J. Comment on ''Matrices for the direct stiffness method''.

AIAA Journal, V. 2, No. 2, 1964, pp. 403.

99. COOK R.D. ''Concepts and applications of finite element analysis''.
John Wiley, 1974.

100. ZIENKIEWICZ O.C. and CHEUNG Y.K. ''The finite element method in structural and continuum mechanics''.
McGraw-Hill, London, 1967.

101. TIMOSHENKO S. and GOODIER J.N. ''Theory of elasticity''.
2nd. ed., McGraw-Hill, 1951.

102. IRONS B.M. ''Engineering applications of numerical integration in stiffness method''.
AIAA Journal, No. 4, 1966, pp. 2035-2037.

103. IRONS B.M. ''Numerical integration applied to finite element methods''.
Conference on the use of digital computers in structural engineering, University of Newcastle, 1966.

104. KOPAL Z. ''Numerical analysis''
2nd. ed., Chapman & Hall, 1961.

105. FOX L. ''An introduction to numerical linear algebra''.
Oxford University Press, 1966.

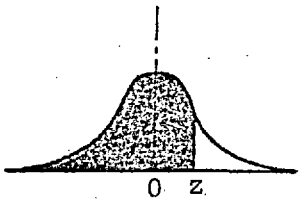
APPENDIX A

STATISTICAL TABLES

(From Ref. 87)

TABLE A.1

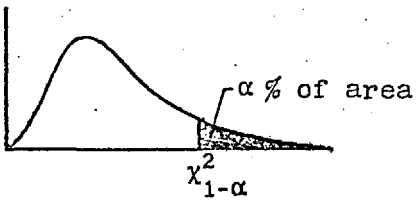
AREAS UNDER THE NORMAL CURVE



z	0.00	0.01	0.02	0.03	0.04	0.05	0.06	0.07	0.08	0.09
0.0	0.5000	0.5040	0.5080	0.5120	0.5160	0.5199	0.5239	0.5279	0.5319	0.5359
0.1	0.5398	0.5438	0.5478	0.5517	0.5557	0.5596	0.5636	0.5675	0.5714	0.5753
0.2	0.5793	0.5832	0.5871	0.5910	0.5948	0.5987	0.6026	0.6064	0.6103	0.6141
0.3	0.6179	0.6217	0.6255	0.6293	0.6331	0.6368	0.6406	0.6443	0.6480	0.6517
0.4	0.6554	0.6591	0.6628	0.6664	0.6700	0.6736	0.6772	0.6808	0.6844	0.6879
0.5	0.6915	0.6950	0.6985	0.7019	0.7054	0.7088	0.7123	0.7157	0.7190	0.7224
0.6	0.7257	0.7291	0.7324	0.7357	0.7389	0.7422	0.7454	0.7486	0.7518	0.7549
0.7	0.7580	0.7612	0.7642	0.7673	0.7704	0.7734	0.7764	0.7794	0.7823	0.7852
0.8	0.7881	0.7910	0.7939	0.7967	0.7995	0.8023	0.8051	0.8078	0.8106	0.8133
0.9	0.8159	0.8186	0.8212	0.8238	0.8264	0.8289	0.8315	0.8340	0.8365	0.8389
1.0	0.8413	0.8438	0.8461	0.8485	0.8508	0.8531	0.8554	0.8577	0.8599	0.8621
1.1	0.8643	0.8665	0.8686	0.8708	0.8729	0.8749	0.8770	0.8790	0.8810	0.8830
1.2	0.8849	0.8869	0.8888	0.8907	0.8925	0.8944	0.8962	0.8980	0.8997	0.9015
1.3	0.9032	0.9049	0.9066	0.9082	0.9099	0.9115	0.9131	0.9147	0.9162	0.9177
1.4	0.9192	0.9207	0.9222	0.9236	0.9251	0.9265	0.9279	0.9292	0.9306	0.9319
1.5	0.9332	0.9345	0.9357	0.9370	0.9382	0.9394	0.9406	0.9418	0.9429	0.9441
1.6	0.9452	0.9463	0.9474	0.9484	0.9495	0.9505	0.9515	0.9525	0.9535	0.9545
1.7	0.9554	0.9564	0.9573	0.9582	0.9591	0.9599	0.9608	0.9616	0.9625	0.9633
1.8	0.9641	0.9649	0.9656	0.9664	0.9671	0.9678	0.9686	0.9693	0.9699	0.9706
1.9	0.9713	0.9719	0.9726	0.9732	0.9738	0.9744	0.9750	0.9756	0.9761	0.9767
2.0	0.9772	0.9778	0.9783	0.9788	0.9793	0.9798	0.9803	0.9808	0.9812	0.9817
2.1	0.9821	0.9826	0.9830	0.9834	0.9838	0.9842	0.9846	0.9850	0.9854	0.9857
2.2	0.9861	0.9864	0.9868	0.9871	0.9875	0.9878	0.9881	0.9884	0.9887	0.9890
2.3	0.9893	0.9896	0.9898	0.9901	0.9904	0.9906	0.9909	0.9911	0.9913	0.9916
2.4	0.9918	0.9920	0.9922	0.9925	0.9927	0.9929	0.9931	0.9932	0.9934	0.9936
2.5	0.9938	0.9940	0.9941	0.9943	0.9945	0.9946	0.9948	0.9949	0.9951	0.9952
2.6	0.9953	0.9955	0.9956	0.9957	0.9959	0.9960	0.9961	0.9962	0.9963	0.9964
2.7	0.9965	0.9966	0.9967	0.9968	0.9969	0.9970	0.9971	0.9972	0.9973	0.9974
2.8	0.9974	0.9975	0.9976	0.9977	0.9977	0.9978	0.9979	0.9979	0.9980	0.9981
2.9	0.9981	0.9982	0.9982	0.9983	0.9984	0.9984	0.9985	0.9985	0.9986	0.9986
3.0	0.9986	0.9987	0.9987	0.9988	0.9988	0.9989	0.9989	0.9989	0.9990	0.9990
3.1	0.9990	0.9991	0.9991	0.9991	0.9992	0.9992	0.9992	0.9992	0.9993	0.9993
3.2	0.9993	0.9993	0.9994	0.9994	0.9994	0.9994	0.9994	0.9995	0.9995	0.9995
3.3	0.9995	0.9995	0.9995	0.9996	0.9996	0.9996	0.9996	0.9996	0.9996	0.9997
3.4	0.9997	0.9997	0.9997	0.9997	0.9997	0.9997	0.9997	0.9997	0.9998	0.9998
3.5	0.9998	0.9998	0.9998	0.9998	0.9998	0.9998	0.9998	0.9998	0.9998	0.9998
3.6	0.9998	0.9998	0.9999	0.9999	0.9999	0.9999	0.9999	0.9999	0.9999	0.9999
3.7	0.9999	0.9999	0.9999	0.9999	0.9999	0.9999	0.9999	0.9999	0.9999	0.9999
3.8	0.9999	0.9999	0.9999	0.9999	0.9999	0.9999	0.9999	1.0000	1.0000	1.0000
3.9	1.0000	1.0000	1.0000	1.0000	1.0000	1.0000	1.0000	1.0000	1.0000	1.0000

TABLE A.2

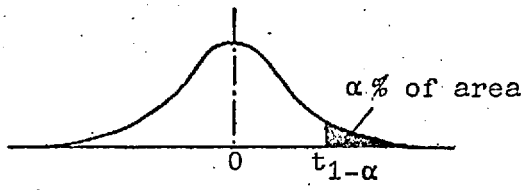
χ^2 DISTRIBUTION



φ \ (1-α)×100	2.5	5.0	10.0	90.0	95.0	97.5
1	0.00	0.00	0.02	2.71	3.84	5.02
2	0.05	0.10	0.21	4.61	5.99	7.38
3	0.22	0.35	0.58	6.25	7.82	9.35
4	0.48	0.71	1.06	7.78	9.49	11.14
5	0.83	1.15	1.61	9.24	11.07	12.83
6	1.24	1.64	2.20	10.65	12.59	14.45
7	1.69	2.17	2.83	12.02	14.07	16.01
8	2.18	2.73	3.49	13.36	15.51	17.54
9	2.70	3.33	4.17	14.68	16.92	19.02
10	3.25	3.94	4.87	15.99	18.31	20.48
11	3.82	4.58	5.58	17.28	19.68	21.92
12	4.40	5.53	6.30	18.55	21.03	23.34
13	5.01	5.89	7.04	19.81	22.36	24.74
14	5.63	6.57	7.79	21.06	23.69	26.12
15	6.26	7.26	8.55	22.31	25.00	27.49
16	6.91	7.96	9.31	23.54	26.30	28.85
17	7.56	8.67	10.09	24.77	27.59	30.19
18	8.23	9.39	10.87	25.99	28.87	31.53
19	8.91	10.12	11.65	27.20	30.14	32.85
20	9.59	10.85	12.44	28.41	31.41	34.17
30	16.79	18.49	20.60	40.26	43.77	46.98
40	24.43	26.51	29.05	51.81	55.76	59.34
50	32.36	34.76	37.69	63.17	67.51	71.42
60	40.48	43.19	46.46	74.40	79.08	83.30
70	48.76	51.74	55.33	85.53	90.53	95.02
80	57.15	60.39	64.28	96.58	101.88	106.63
90	65.65	69.13	73.29	107.57	113.15	118.14
100	74.22	77.93	82.36	118.50	118.50	129.56

TABLE A.3

t - DISTRIBUTION



d.f.	$t_{.90}$	$t_{.95}$	$t_{.975}$
1	3.078	6.314	12.706
2	1.886	2.920	4.303
3	1.638	2.353	3.182
4	1.533	2.132	2.776
5	1.476	2.015	2.571
6	1.440	1.943	2.447
7	1.415	1.895	2.365
8	1.397	1.860	2.306
9	1.383	1.833	2.262
10	1.372	1.812	2.228
11	1.363	1.796	2.201
12	1.356	1.782	2.179
13	1.350	1.771	2.160
14	1.345	1.761	2.145
15	1.341	1.753	2.131
16	1.337	1.746	2.120
17	1.333	1.740	2.110
18	1.330	1.734	2.101
19	1.328	1.729	2.093
20	1.325	1.725	2.086
30	1.310	1.697	2.042
40	1.303	1.684	2.021
50	1.298	1.676	2.009
60	1.296	1.671	2.000
80	1.292	1.664	1.990
100	1.290	1.660	1.984
200	1.286	1.653	1.972
500	1.283	1.648	1.965
∞	1.282	1.645	1.960

TABLE A.4

PERCENTAGE POINTS OF THE χ^2/d.f. DISTRIBUTION

φ \ α	2.5	5.0	10.0	90.0	95.0	97.5
1	0.00	0.00	0.02	2.71	3.84	5.02
2	0.03	0.05	0.11	2.30	3.00	3.69
3	0.07	0.12	0.20	2.08	2.60	3.12
4	0.12	0.18	0.27	1.94	2.37	2.79
5	0.17	0.23	0.32	1.85	2.21	2.57
6	0.21	0.27	0.37	1.77	2.10	2.41
7	0.24	0.31	0.41	1.72	2.01	2.29
8	0.27	0.34	0.44	1.67	1.94	2.19
9	0.30	0.37	0.46	1.63	1.88	2.11
10	0.33	0.39	0.49	1.60	1.83	2.05
11	0.35	0.42	0.51	1.57	1.79	1.99
12	0.37	0.44	0.53	1.55	1.75	1.94
13	0.39	0.45	0.54	1.52	1.72	1.90
14	0.40	0.47	0.56	1.50	1.69	1.87
15	0.42	0.48	0.57	1.49	1.67	1.83
16	0.43	0.50	0.58	1.47	1.64	1.80
17	0.45	0.51	0.59	1.46	1.62	1.78
18	0.46	0.52	0.60	1.44	1.60	1.75
19	0.47	0.53	0.61	1.43	1.59	1.73
20	0.48	0.54	0.62	1.42	1.57	1.71
30	0.56	0.62	0.69	1.34	1.46	1.57
40	0.61	0.66	0.73	1.30	1.39	1.48
50	0.65	0.70	0.75	1.26	1.35	1.43
60	0.68	0.72	0.77	1.24	1.32	1.39
80	0.71	0.76	0.80	1.21	1.27	1.33
100	0.74	0.78	0.82	1.18	1.24	1.30
200	0.81	0.84	0.87	1.13	1.17	1.21
500	0.88	0.90	0.92	1.08	1.11	1.13
∞	1.00	1.00	1.00	1.00	1.00	1.00

TABLE A.5 $F_{0.90}$ DISTRIBUTION

Degrees Of Freedom For The Denominator (φ_2)	Degrees Of Freedom For The Numerator (φ_1)																	
	1	2	3	4	5	6	7	8	9	10	15	20	30	50	100	200	500	∞
1	39.9	49.5	53.6	55.8	57.2	58.2	58.9	59.4	59.9	60.2	61.2	61.7	62.3	62.7	63.0	63.2	63.3	63.3
2	8.53	9.00	9.16	9.24	9.29	9.33	9.35	9.37	9.38	9.39	9.42	9.44	9.46	9.47	9.48	9.49	9.49	9.49
3	5.54	5.46	5.39	5.34	5.31	5.28	5.27	5.25	5.24	5.23	5.20	5.18	5.17	5.15	5.14	5.14	5.14	5.13
4	4.54	4.32	4.19	4.11	4.05	4.01	3.98	3.9	3.94	3.92	3.87	3.84	3.82	3.80	3.78	3.77	3.76	3.76
5	4.06	3.78	3.62	3.52	3.45	3.40	3.37	3.34	3.32	3.30	3.24	3.21	3.17	3.15	3.13	3.12	3.11	3.10
6	3.78	3.46	3.29	3.18	3.11	3.05	3.01	2.98	2.96	2.94	2.87	2.84	2.80	2.77	2.75	2.73	2.73	2.72
7	3.59	3.26	3.07	2.96	2.88	2.83	2.78	2.75	2.72	2.70	2.63	2.59	2.56	2.52	2.52	2.48	2.48	2.47
8	3.46	3.11	2.92	2.81	2.73	2.67	2.62	2.59	2.56	2.54	2.46	2.42	2.38	2.35	2.32	2.31	2.30	2.29
9	3.36	3.01	2.81	2.69	2.61	2.55	2.51	2.47	2.44	2.42	2.34	2.30	2.25	2.22	2.19	2.17	2.17	2.16
10	3.28	2.92	2.73	2.61	2.52	2.46	2.41	2.38	2.35	2.32	2.24	2.20	2.16	2.12	2.09	2.07	2.06	2.06
11	3.23	2.86	2.66	2.54	2.45	2.39	2.34	2.30	2.27	2.25	2.17	2.12	2.08	2.04	2.00	1.99	1.98	1.97
12	3.18	2.81	2.61	2.48	2.39	2.33	2.28	2.24	2.21	2.19	2.10	2.06	2.01	1.97	1.94	1.92	1.91	1.90
13	3.14	2.76	2.56	2.43	2.35	2.28	2.23	2.20	2.16	2.14	2.05	2.01	1.96	1.92	1.88	1.86	1.85	1.85
14	3.10	2.73	2.52	2.39	2.31	2.24	2.19	2.15	2.12	2.10	2.01	1.96	1.91	1.87	1.83	1.82	1.80	1.80
15	3.07	2.70	2.49	2.36	2.27	2.21	2.16	2.12	2.09	2.06	1.97	1.92	1.87	1.83	1.79	1.77	1.76	1.76
16	3.05	2.67	2.46	2.33	2.24	2.18	2.13	2.09	2.06	2.03	1.94	1.89	1.84	1.79	1.76	1.74	1.73	1.72
17	3.03	2.64	2.44	2.31	2.22	2.15	2.10	2.06	2.03	2.00	1.91	1.86	1.81	1.76	1.73	1.71	1.69	1.69
18	3.01	2.62	2.42	2.29	2. 0	2.13	2.08	2.04	2.00	1.98	1.89	1.84	1.78	1.74	1.70	1.68	1.67	1.66
19	2.99	2.61	2.40	2.27	2.18	2.11	2.06	2.02	1.98	1.96	1.86	1.81	1.76	1.71	1.67	1.65	1.64	1.63
20	2.97	2.59	2.38	2.25	2.16	2.09	2.04	2.00	1.96	1.94	1.84	1.79	1.74	1.69	1.65	1.63	1.62	1.61
22	2.95	2.56	2.35	2.22	2.13	2.06	2.01	1.97	1.93	1.90	1.81	1.76	1.70	1.65	1.61	1.59	1.58	1.57
24	2.93	2.54	2.33	2.19	2.10	2.04	1.98	1.94	1.91	1.88	1.78	1.73	1.67	1.62	1.58	1.56	1.54	1.53
26	2.91	2.52	2.31	2.17	2.08	2.01	1.96	1.92	1.88	1.86	1.76	1.71	1.65	1.59	1.55	1.53	1.51	1.50
28	2.89	2.50	2.29	2.16	2.06	2.00	1.94	1.90	1.87	1.84	1.74	1.69	1.63	1.57	1.53	1.50	1.49	1.48
30	2.88	2.49	2.28	2.14	2.05	1.98	1.93	1.88	1.85	1.82	1.72	1.67	1.61	1.55	1.51	1.48	1.47	1.46
40	2.84	2.44	2.23	2.09	2.00	1.93	1.87	1.83	1.79	1.76	1.66	1.61	1.54	1.48	1.43	1.41	1.39	1.38
50	2.81	2.41	2.20	2.06	1.97	1.90	1.84	1.80	1.76	1.73	1.63	1.57	1.50	1.44	1.39	1.36	1.34	1.33
60	2.79	2.39	2.18	2.04	1.95	1.87	1.82	1.77	1.74	1.71	1.60	1.54	1.48	1.41	1.36	1.33	1. 1	1.29
80	2.77	2.37	2.15	2.02	1.92	1.85	1.79	1.75	1.71	1. 8	1.57	1.51	1.44	1.38	1.32	1.28	1.26	1.24
100	2.76	2.36	2.14	2.00	1.91	1.83	1.78	1.73	1.70	1.66	1.56	1.49	1.42	1.35	1.29	1.26	1.23	1.21
200	2.73	2.33	2.11	1.97	1.88	1.80	1.75	1.70	1.66	1.63	1.52	1.46	1.38	1.31	1.24	1. 0	1.17	1.14
500	2.72	2.31	2.10	1.96	1.86	1.79	1.73	1.68	1.64	1.61	1.50	1.44	1.36	1.28	1.21	1.16	1.12	1.09
∞	2.71	2.30	2.08	1.94	1.85	1.77	1.72	1.67	1.63	1.60	1.49	1.42	1.34	1.26	1.18	1.13	1.08	1.00

TABLE A.5 $F_{0.95}$ DISTRIBUTION

Degrees Of Freedom For The Denominator (φ_2)	Degrees Of Freedom For The Numerator (φ_1)																	
	1	2	3	4	5	6	7	8	9	10	15	20	30	50	100	200	500	∞
1	161	200	216	225	230	234	237	239	241	242	246	248	250	252	253	254	254	254
2	18.5	19.0	19.2	19.2	19.3	19.3	19.4	19.4	19.4	19.4	19.4	19.4	19.5	19.5	19.5	19.5	19.5	19.5
3	10.1	9.55	9.28	9.12	9.01	8.94	8.89	8.85	8.81	8.79	8.70	8.66	8.62	8.58	8.55	8.54	8.53	8.53
4	7.71	6.94	6.59	6.39	6.26	6.16	6.09	6.04	6.00	5.96	5.86	5.80	5.75	5.70	5.66	5.65	5.64	5.63
5	6.61	5.79	5.41	5.19	5.05	4.95	4.88	4.82	4.77	4.74	4.62	4.56	4.50	4.44	4.41	4.39	4.37	4.37
6	5.99	5.14	4.76	4.53	4.39	4.28	4.21	4.15	4.10	4.06	3.94	3.87	3.81	3.75	3.71	3.69	3.68	3.67
7	5.59	4.74	4.35	4.12	3.97	3.87	3.79	3.73	3.68	3.64	3.51	3.44	3.38	3.32	3.27	3.25	3.24	3.23
8	5.32	4.46	4.07	3.84	3.69	3.58	3.50	3.44	3.39	3.35	3.22	3.15	3.08	3.02	2.97	2.95	2.94	2.93
9	5.12	4.26	3.8	3.63	3.48	3.37	3.29	3.23	3.18	3.14	3.01	2.94	2.86	2.80	2.76	2.73	2.72	2.71
10	4.96	4.10	3.71	3.48	3.33	3.22	3.14	3.07	3.02	2.98	2.85	2.77	2.70	2.64	2.59	2.56	2.55	2.54
11	4.84	3.98	3.59	3.36	3.20	3.09	3.01	2.95	2.90	2.85	2.72	2.65	2.57	2.51	2.46	2.43	2.42	2.40
12	4.75	3.89	3.49	3.26	3.11	3.00	2.91	2.85	2.80	2.75	2.62	2.54	2.47	2.40	2.35	2.32	2.31	2.30
13	4.67	3.81	3.41	3.18	3.03	2.92	2.83	2.77	2.71	2.67	2.53	2.46	2.38	2.31	2.26	2.23	2.22	2.21
14	4.60	3.74	3.34	3.11	2.96	2.85	2.76	2.70	2.65	2.60	2.46	2.39	2.31	2.24	2.19	2.16	2.14	2.13
15	4.54	3.68	3.29	3.06	2.90	2.79	2.71	2.64	2.59	2.54	2.40	2.33	2.25	2.18	2.12	2.10	2.08	2.07
16	4.49	3.63	3.24	3.01	2.85	2.74	2.66	2.59	2.54	2.49	2.35	2.28	2.19	2.12	2.07	2.04	2.02	2.01
17	4.45	3.59	3.20	2.96	2.81	2.70	2.61	2.55	2.49	2.45	2.31	2.23	2.15	2.08	2.02	1.99	1.97	1.96
18	4.41	3.55	3.16	2.93	2.77	2.66	2.58	2.51	2.46	2.41	2.27	2.19	2.11	2.04	1.98	1.95	1.93	1.92
19	4.38	3.52	3.13	2.90	2.74	2.63	2.54	2.48	2.42	2.38	2.23	2.16	2.07	2.00	1.94	1.91	1.89	1.88
20	4.35	3.49	3.10	2.87	2.71	2.60	2.51	2.45	2.39	2.35	2.20	2.12	2.04	1.97	1.91	1.88	1.86	1.84
22	4.30	3.44	3.05	2.82	2.66	2.55	2.46	2.40	2.34	2.30	2.15	2.07	1.98	1.91	1.85	1.82	1.80	1.78
24	4.26	3.40	3.01	2.78	2.62	2.51	2.42	2.36	2.30	2.25	2.11	2.03	1.94	1.86	1.80	1.77	1.75	1.73
26	4.23	3.37	2.98	2.74	2.59	2.47	2.39	2.32	2.27	2.22	2.07	1.99	1.90	1.82	1.76	1.73	1.71	1.69
28	4.20	3.34	2.95	2.71	2.56	2.45	2.36	2.29	2.24	2.19	2.04	1.96	1.87	1.79	1.73	1.69	1.67	1.65
30	4.17	3.32	2.92	2.69	2.53	2.42	2.33	2.27	2.21	2.16	2.03	1.94	1.85	1.77	1.71	1.67	1.65	1.64
40	4.08	3.23	2.84	2.61	2.45	2.34	2.25	2.18	2.12	2.08	1.92	1.84	1.74	1.66	1.59	1.55	1.53	1.51
50	4.03	3.18	2.79	2.56	2.40	2.29	2.20	2.13	2.07	2.03	1.87	1.78	1.69	1.60	1.52	1.48	1.46	1.44
60	4.00	3.15	2.76	2.53	2.37	2.25	2.17	2.10	2.04	1.99	1.86	1.75	1.65	1.56	1.48	1.44	1.41	1.39
80	3.96	3.11	2.72	2.49	2.33	2.21	2 13	2.06	2.00	1.95	1.79	1.70	1.60	1.51	1.43	1.38	1.35	1.32
100	3.94	3.09	2.70	2.46	2.31	2.19	2.10	2.03	1.97	1.93	1.77	1.68	1.57	1.48	1.39	1.34	1.31	1.28
200	3.89	3.04	2.65	2.42	2.26	2.14	2.06	1.98	1.93	1.88	1.72	1.62	1.52	1.41	1.32	1.26	1.22	1.19
500	3.86	3.01	2.62	2.39	2.23	2.12	2.03	1.96	1.90	1.85	1.69	1.59	1.48	1.38	1.28	1.21	1.16	1.11
∞	3.84	3.00	2.60	2.37	2.21	2.10	2.01	1.94	1.88	1.83	1.67	1.57	1.46	1.35	1.24	1.17	1.11	1.00

TABLE A.5 $F_{0.975}$ DISTRIBUTION

Degrees Of Freedom For The Denominator (φ_2)	Degrees Of Freedom For The Numerator (φ_1)																	
	1	2	3	4	5	6	7	8	9	10	15	20	30	50	100	200	500	∞
1	648	800	864	900	922	937	948	957	963	969	985	993	1001	1008	1013	1016	1017	1018
2	38.5	39.0	39.2	39.2	39.3	39.3	39.4	39.4	39.4	39.4	39.4	39.4	39.5	39.5	39.5	39.5	39.5	39.5
3	17.4	16.0	15.4	15.1	14.9	14.7	14.6	14.5	14.5	14.4	14.3	14.2	14.1	14.0	14.0	13.9	13.9	13.9
4	12.2	10.6	9.98	9.60	9.36	9.20	9.07	8.98	8.90	8.84	8.66	8.56	8.46	8.38	8.32	8.29	8.27	8.26
5	10.0	8.43	7.76	7.39	7.15	6.98	6.85	6.76	6.68	6.62	6.43	6.33	6.23	6.14	6.08	6.05	6.03	6.02
6	8.81	7.26	6.60	6.23	5.99	5.82	5.70	5.60	5.52	5.46	5.27	5.17	5.07	4.98	4.92	4.88	4.86	4.85
7	8.07	6.54	5.89	5.52	5.29	5.12	4.99	4.90	4.82	4.76	4.57	4.47	4.36	4.28	4.21	4.18	4.16	4.14
8	7.57	6.06	5.42	5.05	4.82	4.65	4.53	4.43	4.36	4.30	4.10	4.00	3.89	3.81	3.74	3.70	3.68	3.67
9	7.21	5.71	5.08	4.72	4.48	4.32	4.20	4.10	4.03	3.96	3.77	3.67	3.56	3.47	3.40	3.37	3.35	3.33
10	6.94	5.46	4.83	4.47	4.24	4.07	3.95	3.85	3.78	3.72	3.52	3.42	3.31	3.22	3.15	3.12	3.09	3.08
11	6.72	5.26	4.63	4.28	4.04	3.88	3.76	3.66	3.59	3.53	3.33	3.23	3.12	3.03	2.96	2.92	2.90	2.88
12	6.55	5.10	4.47	4.12	3.89	3.73	3.61	3.51	3.44	3.37	3.18	3.07	2.96	2.87	2.80	2.76	2.74	2.72
13	6.41	4.97	4.35	4.00	3.77	3.60	3.48	3.39	3.31	3.25	3.05	2.95	2.84	2.74	2.67	2.63	2.61	2.60
14	6.30	4.86	4.24	3.89	3.66	3.50	3.38	3.29	3.21	3.15	2.95	2.84	2.73	2.64	2.56	2.53	2.50	2.49
15	6.20	4.76	4.15	3.80	3.58	3.41	3.29	3.20	3.12	3.06	2.86	2.76	2.64	2.55	2.47	2.44	2.41	2.40
16	6.12	4.69	4.08	3.73	3.50	3.34	3.22	3.12	3.05	2.99	2.79	2.68	2.57	2.47	2.40	2.36	2.33	2.32
17	6.04	4.62	4.01	3.66	3.44	3.28	3.16	3.06	2.98	2.92	2.72	2.62	2.50	2.41	2.33	2.29	2.26	2.25
18	5.98	4.56	3.95	3.61	3.38	3.22	3.10	3.01	2.93	2.87	2.67	2.56	2.44	2.35	2.27	2.23	2.20	2.19
19	5.92	4.51	3.90	3.56	3.33	3.17	3.05	2.96	2.88	2.82	2.62	2.51	2.39	2.30	2.22	2.18	2.15	2.13
20	5.87	4.46	3.86	3.51	3.29	3.13	3.01	2.91	2.84	2.77	2.57	2.46	2.35	2.25	2.17	2.13	2.10	2.09
22	5.79	4.38	3.78	3.44	3.22	3.05	2.93	2.84	2.76	2.70	2.50	2.39	2.27	2.17	2.09	2.05	2.02	2.00
24	5.72	4.32	3.72	3.38	3.15	2.99	2.87	2.78	2.70	2.64	2.44	2.33	2.21	2.11	2.02	1.98	1.95	1.94
26	5.66	4.27	3.67	3.33	3.10	2.94	2.82	2.73	2.65	2.59	2.39	2.28	2.16	2.05	1.97	1.92	1.90	1.88
28	5.61	4.22	3.63	3.29	3.06	2.90	2.78	2.69	2.61	2.55	2.34	2.23	2.11	2.01	1.92	1.88	1.85	1.83
30	5.57	4.18	3.59	3.25	3.03	2.87	2.75	2.65	2.57	2.51	2.31	2.20	2.07	1.97	1.88	1.84	1.81	1.79
40	5.42	4.05	3.46	3.13	2.90	2.74	2.62	2.53	2.45	2.39	2.18	2.07	1.94	1.83	1.74	1.69	1.66	1.64
50	5.34	3.98	3.39	3.06	2.83	2.67	2.55	2.46	2.38	2.32	2.11	1.99	1.87	1.75	1.66	1.60	1.57	1.55
60	5.29	3.93	3.34	3.01	2.79	2.63	2.51	2.41	2.33	2.27	2.06	1.94	1.82	1.70	1.60	1.54	1.51	1.48
80	5.22	3.86	3.28	2.95	2.73	2.57	2.45	2.36	2.28	2.21	2.00	1.88	1.75	1.63	1.53	1.47	1.43	1.40
100	5.18	3.83	3.25	2.92	2.70	2.54	2.42	2.32	2.24	2.18	1.97	1.85	1.71	1.59	1.48	1.42	1.38	1.35
200	5.10	3.76	3.18	2.85	2.63	2.47	2.35	2.26	2.18	2.11	1.90	1.78	1.64	1.51	1.39	1.32	1.27	1.23
500	5.05	3.72	3.14	2.81	2.59	2.43	2.31	2.22	2.14	2.07	1.86	1.74	1.60	1.46	1.34	1.25	1.19	1.14
∞	5.02	3.69	3.12	2.79	2.57	2.41	2.29	2.19	2.11	2.05	1.83	1.71	1.57	1.43	1.30	1.21	1.13	1.00

APPENDIX B

FATIGUE DATA

TABLE B.1

RESULTS OF FATIGUE TESTS OF 900 mm LONG WELBOND SPECIMENS WITHOUT IDENTIFICATION MARKS - TESTED FREE IN AIR

MIN. STRESS = 20.0 PER CENT OF CHARACTERISTIC STRENGTH

STRESS RANGE = 70.0 PER CENT OF CHARACTERISTIC STRENGTH

FATIGUE LIVES	Z VALUES
265000.	-.690
266000.	-.645
266000.	-.645
271000.	-.417
294000.	.629
319000.	1.767

VALUE OF MEAN FATIGUE LIFE = 280167.

STANDARD DEVIATION = 21977.

LOG OF FATIGUE LIVES	Z VALUES
5.423	-.702
5.425	-.652
5.425	-.652
5.433	-.407
5.468	.668
5.504	1.745

VALUE OF MEAN OF LOG OF FATIGUE LIVES = 5.446

VARIANCE = .00108

STANDARD DEVIATION = .03292

MEAN FATIGUE LIFE = 279481.

TABLE B.2

RESULTS OF FATIGUE TESTS OF 900 MM LONG WELDOND SPECIMENS WITHOUT IDENTIFICATION MARKS - TESTED FREE IN AIR

MIN. STRESS = 20.0 PER CENT OF CHARACTERISTIC STRENGTH

STRESS RANGE = 65.0 PER CENT OF CHARACTERISTIC STRENGTH

FATIGUE LIVES	Z VALUES
338000.	-1.083
346000.	-.938
369000.	-.523
379000.	-.343
428000.	.541
435000.	.668
491000.	1.678

VALUE OF MEAN FATIGUE LIFE = 398000.

STANDARD DEVIATION = 55414.

LOG OF FATIGUE LIVES	Z VALUES
5.529	-1.141
5.539	-.969
5.567	-.496
5.579	-.300
5.631	.593
5.633	.712
5.691	1.601

VALUE OF MEAN OF LOG OF FATIGUE LIVES = 5.596

VARIANCE = .00350

STANDARD DEVIATION = .05914

MEAN FATIGUE LIFE = 394804.

TABLE B.3

RESULTS OF FATIGUE TESTS OF 900 MM LONG WELDED SPECIMENS WITHOUT IDENTIFICATION MARKS - TESTED FREE IN AIR

MIN. STRESS = 20.0 PER CENT OF CHARACTERISTIC STRENGTH

STRESS RANGE = 63.0 PER CENT OF CHARACTERISTIC STRENGTH

FATIGUE LIVES	Z VALUES
315000.	-1.538
396000.	-.370
404000.	-.255
421000.	-.010
484000.	.899
510000.	1.274

VALUE OF MEAN FATIGUE LIFE = 421667.

STANDARD DEVIATION = 69336.

LOG OF FATIGUE LIVES	Z VALUES
5.498	-1.642
5.598	-.299
5.606	-.182
5.624	.060
5.665	.678
5.708	1.185

VALUE OF MEAN OF LOG OF FATIGUE LIVES = 5.620

VARIANCE = .00548

STANDARD DEVIATION = .07400

MEAN FATIGUE LIFE = 416723.

TABLE B.4

RESULTS OF FATIGUE TESTS OF 900 MM LONG WELDED SPECIMENS WITHOUT IDENTIFICATION MARKS - TESTED FREE IN AIR

MIN. STRESS = 20.0 PER CENT OF CHARACTERISTIC STRENGTH

STRESS RANGE = 60.0 PER CENT OF CHARACTERISTIC STRENGTH

FATIGUE LIVES	Z VALUES
536000.	-.660
543000.	-.744
554000.	-.561
644000.	.934
662000.	1.233

VALUE OF MEAN FATIGUE LIFE = 587800.

STANDARD DEVIATION = 60201.

LOG OF FATIGUE LIVES	Z VALUES
5.729	-.674
5.735	-.745
5.744	-.546
5.809	.946
5.821	1.219

VALUE OF MEAN OF LOG OF FATIGUE LIVES = 5.767

VARIANCE = .00192

STANDARD DEVIATION = .04380

MEAN FATIGUE LIFE = 585388.

TABLE B.5

RESULTS OF FATIGUE TESTS OF 900 MM LONG WELBOND SPECIMENS
WITHOUT IDENTIFICATION MARKS - TESTED FREE IN AIR

MIN. STRESS = 20.0 PER CENT OF CHARACTERISTIC STRENGTH

STRESS RANGE = 70.0 PER CENT OF CHARACTERISTIC STRENGTH

FATIGUE LIVES	Z VALUES
224000.	-1.022
229000.	-.952
249000.	-.676
340000.	.583
355000.	.791
390000.	1.275

VALUE OF MEAN FATIGUE LIFE = 297833.

STANDARD DEVIATION = 72270.

LOG OF FATIGUE LIVES	Z VALUES
5.350	-1.062
5.360	-.972
5.396	-.630
5.531	.642
5.550	.819
5.591	1.203

VALUE OF MEAN OF LOG OF FATIGUE LIVES = 5.463

VARIANCE = .01130

STANDARD DEVIATION = .10632

MEAN FATIGUE LIFE = 290520.

TABLE B.6

RESULTS OF FATIGUE TESTS OF 900 MM LONG WELDOND SPECIMENS
WITHOUT IDENTIFICATION MARKS - TESTED FREE IN AIR

MIN. STRESS = 20.0 PER CENT OF CHARACTERISTIC STRENGTH

STRESS RANGE = 65.0 PER CENT OF CHARACTERISTIC STRENGTH

FATIGUE LIVES	Z VALUES
337000.	-1.323
375000.	-.725
398000.	-.362
430000.	.142
493000.	1.134
493000.	1.134

VALUE OF MEAN FATIGUE LIFE = 421000.

STANDARD DEVIATION = 63482.

LOG OF FATIGUE LIVES	Z VALUES
5.528	-1.399
5.574	-.697
5.600	-.306
5.633	.202
5.693	1.100
5.693	1.100

VALUE OF MEAN OF LOG OF FATIGUE LIVES = 5.620

VARIANCE = .00437

STANDARD DEVIATION = .06610

MEAN FATIGUE LIFE = 416982.

TABLE B.7

RESULTS OF FATIGUE TESTS OF 900 MM LONG WELBOND SPECIMENS WITHOUT IDENTIFICATION MARKS - TESTED FREE IN AIR

MIN. STRESS = 20.0 PER CENT OF CHARACTERISTIC STRENGTH

STRESS RANGE = 63.0 PER CENT OF CHARACTERISTIC STRENGTH

FATIGUE LIVES	Z VALUES
348000.	-1.305
399000.	-.592
423000.	-.256
456000.	.205
462000.	.289
560000.	1.660

VALUE OF MEAN FATIGUE LIFE = 441333.

STANDARD DEVIATION = 71503.

LOG OF FATIGUE LIVES	Z VALUES
5.542	-1.420
5.601	-.564
5.626	-.199
5.659	.272
5.665	.354
5.748	1.558

VALUE OF MEAN OF LOG OF FATIGUE LIVES = 5.640

VARIANCE = .00481

STANDARD DEVIATION = .06938

MEAN FATIGUE LIFE = 436631.

TABLE B.8

RESULTS OF FATIGUE TESTS OF 900 MM LONG WELBOND SPECIMENS
WITHOUT IDENTIFICATION MARKS - TESTED FREE IN AIR

MIN. STRESS = 20.0 PER CENT OF CHARACTERISTIC STRENGTH

STRESS RANGE = 60.0 PER CENT OF CHARACTERISTIC STRENGTH

FATIGUE LIVES	Z VALUES
541000.	-.992
556000.	-.909
600000.	-.666
768000.	.261
913000.	1.062
946000.	1.244

VALUE OF MEAN FATIGUE LIFE = 720667.

STANDARD DEVIATION = 181087.

LOG OF FATIGUE LIVES	Z VALUES
5.733	-1.041
5.745	-.932
5.778	-.628
5.885	.359
5.960	1.050
5.976	1.192

VALUE OF MEAN OF LOG OF FATIGUE LIVES = 5.846

VARIANCE = .01181

STANDARD DEVIATION = .10866

MEAN FATIGUE LIFE = 702033.

TABLE B.9

RESULTS OF FATIGUE TESTS OF 400 MM LONG WELDED SPECIMENS WITH IDENTIFICATION MARKS - TESTED FREE IN AIR

MIN. STRESS = 20.0 PER CENT OF CHARACTERISTIC STRENGTH

STRESS RANGE = 70.0 PER CENT OF CHARACTERISTIC STRENGTH

FATIGUE LIVES	Z VALUES
154000.	-1.186
160000.	-.791
162000.	-.659
180000.	.527
186000.	.922
190000.	1.186

VALUE OF MEAN FATIGUE LIFE = 172000.

STANDARD DEVIATION = 15179.

LOG OF FATIGUE LIVES	Z VALUES
5.188	-1.214
5.204	-.781
5.210	-.641
5.255	.551
5.270	.922
5.279	1.163

VALUE OF MEAN OF LOG OF FATIGUE LIVES = 5.234

VARIANCE = .00147

STANDARD DEVIATION = .03839

MEAN FATIGUE LIFE = 171441.

TABLE B.10

RESULTS OF FATIGUE TESTS OF 400 MM LONG WELDED SPECIMENS WITH IDENTIFICATION MARKS - TESTED FREE IN AIR

MIN. STRESS = 20.0 PER CENT OF CHARACTERISTIC STRENGTH

STRESS RANGE = 57.0 PER CENT OF CHARACTERISTIC STRENGTH

FATIGUE LIVES	Z VALUES
282000.	-1.674
321000.	.062
325000.	.240
328000.	.374
342000.	.997

VALUE OF MEAN FATIGUE LIFE = 319600.

STANDARD DEVIATION = 22457.

LOG OF FATIGUE LIVES	Z VALUES
5.451	-1.691
5.507	.088
5.512	.259
5.516	.385
5.534	.959

VALUE OF MEAN OF LOG OF FATIGUE LIVES = 5.504

VARIANCE = .00100

STANDARD DEVIATION = .03162

MEAN FATIGUE LIFE = 318939.

TABLE B.11

RESULTS OF FATIGUE TESTS OF 400 MM LONG WELDED SPECIMENS WITH IDENTIFICATION MARKS - TESTED FREE IN AIR

MIN. STRESS = 20.0 PER CENT OF CHARACTERISTIC STRENGTH

STRESS RANGE = 53.0 PER CENT OF CHARACTERISTIC STRENGTH

FATIGUE LIVES	Z VALUES
345000.	-.865
390000.	-.230
484000.	1.095

VALUE OF MEAN FATIGUE LIFE = 406333.

STANDARD DEVIATION = 70925.

LOG OF FATIGUE LIVES	Z VALUES
5.538	-.697
5.591	-.182
5.685	1.078

VALUE OF MEAN OF LOG OF FATIGUE LIVES = 5.605

VARIANCE = .00554

STANDARD DEVIATION = .07444

MEAN FATIGUE LIFE = 402324.

TABLE B.12

RESULTS OF FATIGUE TESTS OF 400 MM LONG WELDED SPECIMENS WITH IDENTIFICATION MARKS - TESTED FREE IN AIR

MIN. STRESS = 20.0 PER CENT OF CHARACTERISTIC STRENGTH

STRESS RANGE = 50.0 PER CENT OF CHARACTERISTIC STRENGTH

FATIGUE LIVES	Z VALUES
420000.	-.921
421000.	-.912
446000.	-.679
534000.	.141
633000.	1.064
659000.	1.306

VALUE OF MEAN FATIGUE LIFE = 516833.

STANDARD DEVIATION = 107289.

LOG OF FATIGUE LIVES	Z VALUES
5.623	-.953
5.624	-.941
5.649	-.658
5.728	.227
5.801	1.063
5.819	1.261

VALUE OF MEAN OF LOG OF FATIGUE LIVES = 5.707

VARIANCE = .00781

STANDARD DEVIATION = .08835

MEAN FATIGUE LIFE = 509858.

TABLE B.13

RESULTS OF FATIGUE TESTS OF 400 MM LONG WELDED SPECIMENS WITH IDENTIFICATION MARKS - TESTED FREE IN AIR

MIN. STRESS = 20.0 PER CENT OF CHARACTERISTIC STRENGTH

STRESS RANGE = 49.0 PER CENT OF CHARACTERISTIC STRENGTH

FATIGUE LIVES	Z VALUES
463000.	-1.624
516000.	-1.046
622000.	.104
633000.	.224
645000.	.354
684000.	.778
724000.	1.213

VALUE OF MEAN FATIGUE LIFE = 612429.

STANDARD DEVIATION = 91991.

LOG OF FATIGUE LIVES	Z VALUES
5.666	-1.697
5.713	-1.014
5.794	.163
5.801	.274
5.810	.392
5.835	.762
5.860	1.120

VALUE OF MEAN OF LOG OF FATIGUE LIVES = 5.783

VARIANCE = .00475

STANDARD DEVIATION = .06891

MEAN FATIGUE LIFE = 606094.

TABLE B.14

RESULTS OF FATIGUE TESTS OF 400 MM LONG WELDED SPECIMENS WITHOUT IDENTIFICATION MARKS - TESTED FREE IN AIR

MIN. STRESS = 20.0 PER CENT OF CHARACTERISTIC STRENGTH

STRESS RANGE = 70.0 PER CENT OF CHARACTERISTIC STRENGTH

FATIGUE LIVES	Z VALUES
279000.	-1.558
309000.	-.816
330000.	-.297
348000.	.148
353000.	.272
375000.	.816
400000.	1.434

VALUE OF MEAN FATIGUE LIFE = 342000.

STANDARD DEVIATION = 40439.

LOG OF FATIGUE LIVES	Z VALUES
5.446	-1.639
5.490	-.791
5.519	-.246
5.542	.195
5.549	.314
5.574	.816
5.602	1.351

VALUE OF MEAN OF LOG OF FATIGUE LIVES = 5.531

VARIANCE = .00274

STANDARD DEVIATION = .05232

MEAN FATIGUE LIFE = 339907.

TABLE B.15

RESULTS OF FATIGUE TESTS OF 400 MM LONG WELBOND SPECIMENS WITHOUT IDENTIFICATION MARKS - TESTED FREE IN AIR

MIN. STRESS = 20.0 PER CENT OF CHARACTERISTIC STRENGTH

STRESS RANGE = 67.0 PER CENT OF CHARACTERISTIC STRENGTH

FATIGUE LIVES	Z VALUES
377000.	-.926
389000.	-.611
400000.	-.267
402000.	-.210
413000.	.105
476000.	1.909

VALUE OF MEAN FATIGUE LIFE = 409333.

STANDARD DEVIATION = 34927.

LOG OF FATIGUE LIVES	Z VALUES
5.576	-.973
5.589	-.621
5.602	-.248
5.604	-.187
5.616	.144
5.678	1.884

VALUE OF MEAN OF LOG OF FATIGUE LIVES = 5.611

VARIANCE = .00126

STANDARD DEVIATION = .03544

MEAN FATIGUE LIFE = 408165.

TABLE B.16

RESULTS OF FATIGUE TESTS OF 400 MM LONG WELDOND SPECIMENS
WITHOUT IDENTIFICATION MARKS - TESTED FREE IN AIR

MIN. STRESS = 20.0 PER CENT OF CHARACTERISTIC STRENGTH

STRESS RANGE = 65.0 PER CENT OF CHARACTERISTIC STRENGTH

FATIGUE LIVES	Z VALUES
493000.	-1.225
510000.	-.952
543000.	-.423
603000.	.540
632000.	1.006
635000.	1.054

VALUE OF MEAN FATIGUE LIFE = 569333.

STANDARD DEVIATION = 62311.

LOG OF FATIGUE LIVES	Z VALUES
5.693	-1.257
5.708	-.950
5.735	-.383
5.780	.566
5.801	.991
5.803	1.034

VALUE OF MEAN OF LOG OF FATIGUE LIVES = 5.753

VARIANCE = .00230

STANDARD DEVIATION = .04799

MEAN FATIGUE LIFE = 566462.

TABLE B.17

RESULTS OF FATIGUE TESTS OF 400 MM LONG WELDED SPECIMENS WITHOUT IDENTIFICATION MARKS - TESTED FREE IN AIR

MIN. STRESS = 20.0 PER CENT OF CHARACTERISTIC STRENGTH

STRESS RANGE = 63.0 PER CENT OF CHARACTERISTIC STRENGTH

FATIGUE LIVES	Z VALUES
520000.	-.913
526000.	-.871
562000.	-.624
587000.	-.452
672000.	.132
824000.	1.176
879000.	1.554

VALUE OF MEAN FATIGUE LIFE = 652857.

STANDARD DEVIATION = 145564.

LOG OF FATIGUE LIVES	Z VALUES
5.716	-.973
5.721	-.919
5.750	-.608
5.769	-.404
5.827	.230
5.916	1.186
5.944	1.489

VALUE OF MEAN OF LOG OF FATIGUE LIVES = 5.806

VARIANCE = .00858

STANDARD DEVIATION = .09262

MEAN FATIGUE LIFE = 639871.

TABLE B.18

RESULTS OF FATIGUE TESTS OF 400 MM LONG JONES SPECIMENS WITH IDENTIFICATION MARKS - TESTED FREE IN AIR

MIN. STRESS = 20.0 PER CENT OF CHARACTERISTIC STRENGTH

STRESS RANGE = 70.0 PER CENT OF CHARACTERISTIC STRENGTH

FATIGUE LIVES	Z VALUES
233000.	-.855
239000.	-.658
246000.	-.428
257000.	-.066
262000.	.099
317000.	1.908

VALUE OF MEAN FATIGUE LIFE = 259000.

STANDARD DEVIATION = 30404.

LOG OF FATIGUE LIVES	Z VALUES
5.367	-.909
5.379	-.679
5.391	-.418
5.410	-.022
5.418	.152
5.501	1.875

VALUE OF MEAN OF LOG OF FATIGUE LIVES = 5.411

VARIANCE = .00231

STANDARD DEVIATION = .04803

MEAN FATIGUE LIFE = 257630.

TABLE B.19

RESULTS OF FATIGUE TESTS OF 400 MM LONG JONES SPECIMENS WITH IDENTIFICATION MARKS - TESTED FREE IN AIR

MIN. STRESS = 20.0 PER CENT OF CHARACTERISTIC STRENGTH

STRESS RANGE = 60.0 PER CENT OF CHARACTERISTIC STRENGTH

FATIGUE LIVES	Z VALUES
411000.	-1.260
417000.	-1.123
468000.	.042
484000.	.407
498000.	.727
519000.	1.207

VALUE OF MEAN FATIGUE LIFE = 466167.

STANDARD DEVIATION = 43768.

LOG OF FATIGUE LIVES	Z VALUES
5.614	-1.281
5.620	-1.129
5.670	.080
5.685	.433
5.697	.732
5.715	1.165

VALUE OF MEAN OF LOG OF FATIGUE LIVES = 5.667

VARIANCE = .00172

STANDARD DEVIATION = .04144

MEAN FATIGUE LIFE = 464420.

TABLE B.20

RESULTS OF FATIGUE TESTS OF 400 MM LONG JONES SPECIMENS
WITH IDENTIFICATION MARKS - TESTED FREE IN AIR

MIN. STRESS = 20.0 PER CENT OF CHARACTERISTIC STRENGTH

STRESS RANGE = 57.0 PER CENT OF CHARACTERISTIC STRENGTH

FATIGUE LIVES	Z VALUES
450000.	-1.162
499000.	-.362
500000.	-.346
503000.	-.297
545000.	.389
630000.	1.777

VALUE OF MEAN FATIGUE LIFE = 521167.

STANDARD DEVIATION = 61232.

LOG OF FATIGUE LIVES	Z VALUES
5.653	-1.247
5.699	-.335
5.699	-.319
5.702	-.265
5.736	.443
5.799	1.722

VALUE OF MEAN OF LOG OF FATIGUE LIVES = 5.715

VARIANCE = .00242

STANDARD DEVIATION = .04922

MEAN FATIGUE LIFE = 518320.

TABLE B.21

RESULTS OF FATIGUE TESTS OF 400 MM LONG JONES SPECIMENS
WITH IDENTIFICATION MARKS - TESTED FREE IN AIR

MIN. STRESS = 20.0 PER CENT OF CHARACTERISTIC STRENGTH

STRESS RANGE = 55.0 PER CENT OF CHARACTERISTIC STRENGTH

FATIGUE LIVES	Z VALUES
460000.	-.985
500000.	-.727
544000.	-.443
557000.	-.359
792000.	1.157
823000.	1.356

VALUE OF MEAN FATIGUE LIFE = 612667.

STANDARD DEVIATION = 155058.

LOG OF FATIGUE LIVES	Z VALUES
5.663	-1.074
5.699	-.771
5.736	-.385
5.746	-.287
5.699	1.163
5.915	1.318

VALUE OF MEAN OF LOG OF FATIGUE LIVES = 5.776

VARIANCE = .01116

STANDARD DEVIATION = .10563

MEAN FATIGUE LIFE = 597335.

TABLE B.22

RESULTS OF FATIGUE TESTS OF 450 MM LONG JONES SPECIMENS WITHOUT IDENTIFICATION MARKS - TESTED FREE IN AIR

MIN. STRESS = 20.0 PER CENT OF CHARACTERISTIC STRENGTH

STRESS RANGE = 70.0 PER CENT OF CHARACTERISTIC STRENGTH

FATIGUE LIVES	Z VALUES
360000.	-.698
369000.	-.610
419000.	-.321
511000.	.579
600000.	1.449

VALUE OF MEAN FATIGUE LIFE = 451600.

STANDARD DEVIATION = 102258.

LOG OF FATIGUE LIVES	Z VALUES
5.556	-.947
5.567	-.835
5.622	-.254
5.709	.652
5.778	1.365

VALUE OF MEAN OF LOG OF FATIGUE LIVES = 5.646

VARIANCE = .00905

STANDARD DEVIATION = .09514

MEAN FATIGUE LIFE = 443020.

TABLE B.23

RESULTS OF FATIGUE TESTS OF 400 MM LONG JONES SPECIMENS
WITHOUT IDENTIFICATION MARKS - TESTED FREE IN AIR

MIN. STRESS = 20.0 PER CENT OF CHARACTERISTIC STRENGTH

STRESS RANGE = 68.0 PER CENT OF CHARACTERISTIC STRENGTH

FATIGUE LIVES	Z VALUES
343000.	-1.632
456000.	.131
458000.	.162
462000.	.225
519000.	1.114

VALUE OF MEAN FATIGUE LIFE = 447600.

STANDARD DEVIATION = 64080.

LOG OF FATIGUE LIVES	Z VALUES
5.535	-1.676
5.659	.180
5.661	.208
5.665	.265
5.715	1.023

VALUE OF MEAN OF LOG OF FATIGUE LIVES = 5.647

VARIANCE = .00444

STANDARD DEVIATION = .06666

MEAN FATIGUE LIFE = 443595.

TABLE B.24

RESULTS OF FATIGUE TESTS OF 400 MM LONG JONES SPECIMENS
WITHOUT IDENTIFICATION MARKS - TESTED FREE IN AIR

MIN. STRESS = 20.0 PER CENT OF CHARACTERISTIC STRENGTH

STRESS RANGE = 65.0 PER CENT OF CHARACTERISTIC STRENGTH

FATIGUE LIVES	Z VALUES
384000.	-1.585
596000.	-.296
666000.	.250
768000.	.749
790000.	.882

VALUE OF MEAN FATIGUE LIFE = 644600.

STANDARD DEVIATION = 164536.

LOG OF FATIGUE LIVES	Z VALUES
5.584	-1.657
5.775	-.161
5.836	.312
5.885	.702
5.898	.795

VALUE OF MEAN OF LOG OF FATIGUE LIVES = 5.796

VARIANCE = .01629

STANDARD DEVIATION = .12765

MEAN FATIGUE LIFE = 624553.

TABLE B.25

RESULTS OF FATIGUE TESTS OF 400 mm LONG JONES SPECIMENS
WITHOUT IDENTIFICATION MARKS - TESTED FREE IN AIR

MIN. STRESS = 20.0 PER CENT OF CHARACTERISTIC STRENGTH

STRESS RANGE = 60.0 PER CENT OF CHARACTERISTIC STRENGTH

FATIGUE LIVES	Z VALUES
649000.	-1.201
699000.	-.765
793000.	.054
866000.	.696
927000.	1.222

VALUE OF MEAN FATIGUE LIFE = 786800.

STANDARD DEVIATION = 114744.

LOG OF FATIGUE LIVES	Z VALUES
5.812	-1.248
5.844	-.744
5.899	.112
5.938	.709
5.967	1.171

VALUE OF MEAN OF LOG OF FATIGUE LIVES = 5.892

VARIANCE = .00410

STANDARD DEVIATION = .06399

MEAN FATIGUE LIFE = 780043.

TABLE B.26

RESULTS OF FATIGUE TESTS OF 400 MM LONG SHEERNESS SPECIMENS WITH IDENTIFICATION MARKS - TESTED FREE IN AIR

MIN. STRESS = 20.0 PER CENT OF CHARACTERISTIC STRENGTH

STRESS RANGE = 73.0 PER CENT OF CHARACTERISTIC STRENGTH

FATIGUE LIVES	Z VALUES
240000.	-.975
253000.	-.676
270000.	-.285
300000.	.405
349000.	1.532

VALUE OF MEAN FATIGUE LIFE = 282400.

STANDARD DEVIATION = 43478.

LOG OF FATIGUE LIVES	Z VALUES
5.380	-1.032
5.403	-.678
5.431	-.241
5.477	.467
5.543	1.483

VALUE OF MEAN OF LOG OF FATIGUE LIVES = 5.447

VARIANCE = .00418

STANDARD DEVIATION = .06465

MEAN FATIGUE LIFE = 279852.

TABLE B.27

RESULTS OF FATIGUE TESTS OF 400 MM LONG SHEERNESS SPECIMENS WITH IDENTIFICATION MARKS - TESTED FREE IN AIR

MIN. STRESS = 20.0 PER CENT OF CHARACTERISTIC STRENGTH

STRESS RANGE = 70.0 PER CENT OF CHARACTERISTIC STRENGTH

FATIGUE LIVES	Z VALUES
286000.	-1.051
333000.	-.571
386000.	-.031
394000.	.051
546000.	1.602

VALUE OF MEAN FATIGUE LIFE = 389000.

STANDARD DEVIATION = 98015.

LOG OF FATIGUE LIVES	Z VALUES
5.456	-1.181
5.522	-.548
5.587	.067
5.595	.152
5.737	1.509

VALUE OF MEAN OF LOG OF FATIGUE LIVES = 5.580

VARIANCE = .01090

STANDARD DEVIATION = .10439

MEAN FATIGUE LIFE = 379855.

TABLE B.28

RESULTS OF FATIGUE TESTS OF 400 MM LONG SHEERNESS SPECIMENS WITH IDENTIFICATION MARKS - TESTED FREE IN AIR

MIN. STRESS = 20.0 PER CENT OF CHARACTERISTIC STRENGTH

STRESS RANGE = 68.0 PER CENT OF CHARACTERISTIC STRENGTH

FATIGUE LIVES	Z VALUES
441000.	-.973
450000.	-.800
460000.	-.627
500000.	.103
535000.	.742
580000.	1.563

VALUE OF MEAN FATIGUE LIFE = 494333.

STANDARD DEVIATION = 54797.

LOG OF FATIGUE LIVES	Z VALUES
5.644	-1.007
5.653	-.820
5.663	-.618
5.699	.151
5.728	.775
5.763	1.519

VALUE OF MEAN OF LOG OF FATIGUE LIVES = 5.692

VARIANCE = .00222

STANDARD DEVIATION = .04710

MEAN FATIGUE LIFE = 491881.

TABLE B.29

RESULTS OF FATIGUE TESTS OF 400 MM LONG SHEERNESS SPECIMENS WITH IDENTIFICATION MARKS - TESTED FREE IN AIR

MIN. STRESS = 20.0 PER CENT OF CHARACTERISTIC STRENGTH

STRESS RANGE = 65.0 PER CENT OF CHARACTERISTIC STRENGTH

FATIGUE LIVES	Z VALUES
625000.	-1.360
715000.	-.615
730000.	-.491
829000.	.328
887000.	.808
950000.	1.330

VALUE OF MEAN FATIGUE LIFE = 789333.

STANDARD DEVIATION = 120812.

LOG OF FATIGUE LIVES	Z VALUES
5.796	-1.442
5.854	-.574
5.863	-.440
5.919	.380
5.948	.817
5.978	1.259

VALUE OF MEAN OF LOG OF FATIGUE LIVES = 5.893

VARIANCE = .00453

STANDARD DEVIATION = .06732

MEAN FATIGUE LIFE = 781541.

TABLE B.30

RESULTS OF FATIGUE TESTS OF 400 MM LONG SHEERNESS SPECIMENS WITHOUT IDENTIFICATION MARKS - TESTED FREE IN AIR

MIN. STRESS = 20.0 PER CENT OF CHARACTERISTIC STRENGTH

STRESS RANGE = 73.0 PER CENT OF CHARACTERISTIC STRENGTH

FATIGUE LIVES	Z VALUES
255000.	-1.057
270000.	-.668
320000.	-.239
337000.	-.025
380000.	.516
472000.	1.674

VALUE OF MEAN FATIGUE LIFE = 339000.

STANDARD DEVIATION = 79438.

LOG OF FATIGUE LIVES	Z VALUES
5.407	-1.162
5.431	-.910
5.505	-.159
5.528	.070
5.580	.601
5.674	1.559

VALUE OF MEAN OF LOG OF FATIGUE LIVES = 5.521

VARIANCE = .00966

STANDARD DEVIATION = .09826

MEAN FATIGUE LIFE = 331692.

TABLE B.31

RESULTS OF FATIGUE TESTS OF 400 MM LONG SHEERNESS SPECIMENS
WITHOUT IDENTIFICATION MARKS - TESTED FREE IN AIR

MIN. STRESS = 20.0 PER CENT OF CHARACTERISTIC STRENGTH

STRESS RANGE = 70.0 PER CENT OF CHARACTERISTIC STRENGTH

FATIGUE LIVES	Z VALUES
370000.	-1.087
403000.	-.686
461000.	.012
481000.	.254
585000.	1.510

VALUE OF MEAN FATIGUE LIFE = 460000.

STANDARD DEVIATION = 82789.

LOG OF FATIGUE LIVES	Z VALUES
5.568	-1.166
5.605	-.680
5.664	.084
5.682	.325
5.767	1.437

VALUE OF MEAN OF LOG OF FATIGUE LIVES = 5.657

VARIANCE = .00584

STANDARD DEVIATION = .07643

MEAN FATIGUE LIFE = 454257.

TABLE B.32

RESULTS OF FATIGUE TESTS OF 400 MM LONG SHEERNESS SPECIMENS
WITHOUT IDENTIFICATION MARKS - TESTED FREE IN AIR

MIN. STRESS = 20.0 PER CENT OF CHARACTERISTIC STRENGTH

STRESS RANGE = 69.0 PER CENT OF CHARACTERISTIC STRENGTH

FATIGUE LIVES	Z VALUES
460000.	-.889
500000.	-.524
560000.	.023
710000.	1.391

VALUE OF MEAN FATIGUE LIFE = 557500.

STANDARD DEVIATION = 109659.

LOG OF FATIGUE LIVES	Z VALUES
5.663	-.947
5.699	-.505
5.748	.095
5.851	1.356

VALUE OF MEAN OF LOG OF FATIGUE LIVES = 5.740

VARIANCE = .00670

STANDARD DEVIATION = .08184

MEAN FATIGUE LIFE = 549912.

TABLE B.33

RESULTS OF FATIGUE TESTS OF 400 MM LONG SHEERNESS SPECIMENS WITHOUT IDENTIFICATION MARKS - TESTED FREE IN AIR

MIN. STRESS = 20.0 PER CENT OF CHARACTERISTIC STRENGTH

STRESS RANGE = 68.0 PER CENT OF CHARACTERISTIC STRENGTH

FATIGUE LIVES	Z VALUES
500000.	-1.391
560000.	-.758
599000.	-.346
670000.	.403
721000.	.940
741000.	1.151

VALUE OF MEAN FATIGUE LIFE = 631833.

STANDARD DEVIATION = 94808.

LOG OF FATIGUE LIVES	Z VALUES
5.699	-1.461
5.748	-.723
5.777	-.285
5.826	.445
5.859	.923
5.870	1.101

VALUE OF MEAN OF LOG OF FATIGUE LIVES = 5.796

VARIANCE = .00445

STANDARD DEVIATION = .06669

MEAN FATIGUE LIFE = 625752.

TABLE- B.34

RESULTS OF FATIGUE TESTS OF 400MM LONG UNISTEEL SPECIMENS WITH IDENTIFICATION MARKS - TESTED FREE IN AIR

MIN. STRESS = 20.0 PER CENT OF CHARACTERISTIC STRENGTH

STRESS RANGE = 68.0 PER CENT OF CHARACTERISTIC STRENGTH

FATIGUE LIVES	Z VALUES
308000.	-1.435
331000.	-.505
335000.	-.344
349000.	.222
358000.	.586
380000.	1.475

VALUE OF MEAN FATIGUE LIFE = 343500.

STANDARD DEVIATION = 24745.

LOG OF FATIGUE LIVES	Z VALUES
5.489	-1.482
5.523	-.484
5.525	-.317
5.543	.250
5.544	.603
5.580	1.430

VALUE OF MEAN OF LOG OF FATIGUE LIVES = 5.535

VARIANCE = .00098

STANDARD DEVIATION = .03134

MEAN FATIGUE LIFE = 342757.

TABLE B.35

RESULTS OF FATIGUE TESTS OF 400MM LONG UNISTEEL SPECIMENS WITH IDENTIFICATION MARKS - TESTED FREE IN AIR

MIN. STRESS = 20.0 PER CENT OF CHARACTERISTIC STRENGTH

STRESS RANGE = 67.0 PER CENT OF CHARACTERISTIC STRENGTH

FATIGUE LIVES	Z VALUES
365000.	-1.021
370000.	-.881
400000.	-.045
423000.	.597
450000.	1.350

VALUE OF MEAN FATIGUE LIFE = 401600.

STANDARD DEVIATION = 35851.

LOG OF FATIGUE LIVES	Z VALUES
5.562	-1.042
5.568	-.889
5.602	-.009
5.626	.621
5.653	1.319

VALUE OF MEAN OF LOG OF FATIGUE LIVES = 5.602

VARIANCE = .00148

STANDARD DEVIATION = .03851

MEAN FATIGUE LIFE = 400333.

TABLE B.36

RESULTS OF FATIGUE TESTS OF 460MM LONG UNISTEEL SPECIMENS WITH IDENTIFICATION MARKS - TESTED FREE IN AIR

MIN. STRESS = 20.0 PER CENT OF CHARACTERISTIC STRENGTH

STRESS RANGE = 65.0 PER CENT OF CHARACTERISTIC STRENGTH

FATIGUE LIVES	Z VALUES
390000.	-1.410
436000.	-.268
443000.	-.117
470000.	.542
500000.	1.273

VALUE OF MEAN FATIGUE LIFE = 447800.

STANDARD DEVIATION = 40990.

LOG OF FATIGUE LIVES	Z VALUES
5.591	-1.454
5.639	-.251
5.646	-.080
5.672	.559
5.699	1.226

VALUE OF MEAN OF LOG OF FATIGUE LIVES = 5.650

VARIANCE = .00162

STANDARD DEVIATION = .04026

MEAN FATIGUE LIFE = 446277.

TABLE B.37

RESULTS OF FATIGUE TESTS OF 400MM LONG UNISTEEL SPECIMENS WITH IDENTIFICATION MARKS - TESTED FREE IN AIR

MIN. STRESS = 20.0 PER CENT OF CHARACTERISTIC STRENGTH

STRESS RANGE = 64.0 PER CENT OF CHARACTERISTIC STRENGTH

FATIGUE LIVES	Z VALUES
430000.	-.956
450000.	-.667
470000.	-.378
531000.	.502
600000.	1.499

VALUE OF MEAN FATIGUE LIFE = 496200.

STANDARD DEVIATION = 69262.

LOG OF FATIGUE LIVES	Z VALUES
5.633	-1.092
5.653	-.666
5.672	-.345
5.725	.556
5.778	1.458

VALUE OF MEAN OF LOG OF FATIGUE LIVES = 5.692

VARIANCE = .00346

STANDARD DEVIATION = .05883

MEAN FATIGUE LIFE = 492499.

APPENDIX C

TYPICAL COMPARISON OF TWO REGRESSION LINES

APPENDIX C. TYPICAL COMPARISON OF TWO REGRESSION LINES

The regression lines of WEL-F-400-WI and JON-F-400-WI series of fatigue tests are compared below using the values given in Table 5.7 and in Appendix B.

(i) Check the equality of two variances about the regression lines :

$$F = \frac{s_{r_1}^2}{s_{r_2}^2} = \frac{0.00417}{0.00414} = 1.01$$

$$\phi_1 = N_1 - 1 = 27 - 1 = 26$$
$$\phi_2 = N_2 - 1 = 24 - 1 = 23$$

for $\alpha = 5\%$ $\quad F_{.975}(26,23) = 2.38$

$\alpha = 10\%$ $\quad F_{.950}(26,23) = 2.01$

Since $F < F_{.950} < F_{.975}$ the two variances are not significantly different.

Thus the average variance about the two regression lines, s_{rr}^2, is given by

$$s_{rr}^2 = \frac{(N_1 - 2)s_{r_1}^2 + (N_2 - 2)s_{r_2}^2}{N_1 + N_2 - 4} =$$

$$= \frac{(27-2)(0.00417) + (24-2)(0.00414)}{27 + 24 - 4} = 0.00416$$

$$\therefore \quad s_{rr}^2 = 0.06447$$

(ii) Comparison of slopes of two regression lines :

$$h_1 = \sum_{i=1}^{k} n_i (x_i - \bar{x}_1)^2 = \frac{s_{r_1}^2}{s_{b_1}^2} = \frac{0.00417}{0.04365} = 0.09553$$

$$h_2 = \sum_{i=1}^{k} n_i (x_i - \bar{x}_2)^2 = \frac{s_{r_2}^2}{s_{b_2}^2} = \frac{0.00414}{0.10786} = 0.03838$$

$$t = \frac{b_1 - b_2}{s_{rr}\left[\frac{1}{h_1} + \frac{1}{h_2}\right]^{\frac{1}{2}}} = \frac{-3.420 + 3.465}{0.06447\left[\frac{1}{0.09553} + \frac{1}{0.03838}\right]^{\frac{1}{2}}}$$

$$= 0.116$$

Degrees of freedom = $N_1+N_2-4 = 27+24-4 = 47$

$\therefore\ t_{.950} = 1.679$ and $t_{.975} = 2.014$

Since $t < t_{.950} < t_{.975}$ the slopes of the two lines are not significantly different.

(iii) Test the identity of the two regression lines :

$$B = \frac{a_1 - a_2}{\bar{x}_1 - \bar{x}_2} = \frac{5.573 - 5.642}{1.743 - 1.780} = 1.865$$

$$b = \frac{b_1 h_1 + b_2 h_2}{h_1 + h_2} = \frac{(-3.420)(0.09553) + (-3.465)(0.03838)}{0.09553 + 0.03838}$$

$$= -3.433$$

$$s = \left[\frac{(N_1 - 2)s_{r_1}^2 + (N_2 - 2)s_{r_2}^2 + \frac{(b_1 - b_2)^2}{\frac{1}{h_1} + \frac{1}{h_2}}}{N_1 + N_2 - 3}\right]^{\frac{1}{2}} =$$

$$= \left[\frac{(27-2)(0.00417) + (24-2)(0.00414) + \frac{(-3.420+3.465)^2}{\frac{1}{0.09553} + \frac{1}{0.03838}}}{27 + 24 - 3} \right]^{\frac{1}{2}}$$

$$= 0.063801$$

$$t = \frac{B - b}{s \left[\frac{1}{(\bar{x}_1 - \bar{x}_2)^2} \left(\frac{1}{N_1} + \frac{1}{N_2} \right) + \frac{1}{h_1 + h_2} \right]^{\frac{1}{2}}}$$

$$= \frac{1.865 + 3.433}{0.063801 \left[\frac{1}{(1.743-1.780)^2} \left(\frac{1}{27} + \frac{1}{24} \right) + \frac{1}{0.09553+0.03838} \right]^{\frac{1}{2}}}$$

$$= 10.3$$

Degrees of freedom = $N_1 + N_2 - 3 = 27 + 24 - 3 = 48$

$\therefore t_{.950} = 1.679$ and $t_{.975} = 2.011$

Since $t_{.950} < t_{.975} < t$ the two regression lines are significantly different.